Copyright

by

Catherine Grace Hovell

2011

The Dissertation Committee for Catherine Grace Hovell certifies that this is the approved version of the following dissertation:

Structural Performance of Texas U-Beams

at Prestress Transfer and Under Shear-Critical Loads

Committee:

_____
Oguzhan Bayrak, Co-Supervisor

_____
Sharon L. Wood, Co-Supervisor

_____
James O. Jirsa

_____
Eric B. Williamson

_____
Ofodike A. Ezekoye

Structural Performance of Texas U-Beams at Prestress Transfer and Under Shear-Critical Loads

by

Catherine Grace Hovell, B.S., M.S.E.

Dissertation

Presented to the Faculty of the Graduate School of

The University of Texas at Austin

in Partial Fulfillment

of the Requirements

for the Degree of

Doctor of Philosophy

The University of Texas at Austin

August 2011

To my family and friends,

for their love and support

Acknowledgements

The dissertation presented in the following pages benefited from the input and dedication of many more people than just the author. First and foremost, I would like to thank my advisor, Oguzhan Bayrak, whose dedication to his work and his students cannot be questioned. I am a better researcher and this dissertation is a better piece of work because of his efforts. The other members of my committee, James Jirsa, Sharon Wood, Eric Williamson, and Ofodike Ezekoye deserve recognition as well, for the feedback, insight, and encouragement they provided in the past four years. I would like to include John Breen in that list as well, as he was always available to discuss research, bridge design, or the best local golf courses.

I could not have achieved this goal without the efforts of Chip Dumais, Art Ruggieri, Roseanna Neupauer, Rodney Davis, Jose Gomez, and Mike Brown, who were there in my formative years.

The magnitude of this research project required the commitment of an army of students. The second PhD student on the project, Alejandro Avendaño, helped get the work done for sure, but was also a friend, confidant, proof-reader, and golf coach. The hours put in by Andy Moore and Dave Dunkman are countless and certainly eased my burden each day. Bryan Bindrich and Nancy Larson made sharing the elevated slab more… interesting, but they were also generous with their time when needed. The efforts of David Wald, Eisuke Nakamura, and Stephanie German are also appreciated. I feel confident that the work left to be done by David Langefeld to finish this project will be excellent, as has been his standard.

For the financial support which made this project possible, I thank the Texas Department of Transportation. Our Project Monitoring Committee – Dean Van Landuyt, John Holt, Amy Eskridge, and Graham Bettis – helped steer our progress and ensure that the work had use in the field. I appreciate their contributions.

Field fabrication of U-Beams required additional help and dedication beyond the everyday toils of laboratory work. I want to thank Jorge Hinojosa of Bexar Concrete Works, Steve Crim of Valley Prestress, and Bruce Williams of Texas Concrete for letting

us use their prestressing facilities and for helping me get my work done. Adam Kirk and Jose Gallardo of the University of Texas also deserve thanks for giving their time for field trips unrelated to their own studies.

The work performed for this research project could not have been completed without the help of the staff of the Ferguson Structural Engineering Laboratory. In particular, I would like to thank Blake Stasney, Dennis Fillip, Jessica Hanten, Scott Hammock, Eric Schell, Barbara Howard, and Mike Wason. Rising above and beyond this group is Andrew Valentine, who probably put as much blood, sweat, and tears into these U-Beams as I did.

Other friendships developed here deserve their own recognition, as these friends helped me maintain my sanity through the past four years. Kim Talley, office-mate and true friend, showed me how the process worked by going through it all before me. Jason Stith was always around to share a good story and listen when I needed an ear. Kerry Kreitman was my carpool buddy and kept me calm in the final months of writing, while James Kleineck was always around, making me feel less pathetic when working at midnight on a Friday. Jeremiah Fasl, an icon of Ferguson Lab dedication, is also an icon for friendship, always available to host a movie night, willing to drive the group to lunch, or organize the golf outing. You all have been excellent friends to me, and I will truly miss you.

To Mom, Dad, and John: thank you for supporting me as I fulfilled a lifelong goal. To Jay: you have been by my side through this entire process; I hope I can now help you achieve your dreams as fully as you've seen me through mine.

August, 2011

Structural Performance of Texas U-Beams at Prestress Transfer and Under Shear-Critical Loads

Catherine Grace Hovell, Ph.D.

The University of Texas at Austin, 2011

Supervisors: Oguzhan Bayrak, Sharon L. Wood

The Texas U-Beam standard designs were released in the 1990's and have been used increasingly in bridges across the state since. While prototypes of the 54-in. deep prestressed concrete beam were built during the design phase, no full-scale load tests were performed.

This study of the U-Beam had five goals: (i) determine the magnitude and location of stresses induced in reinforcing bars in the end region of the beam at prestress transfer, (ii) measure concrete curing temperatures in square and skewed end blocks, (iii) establish the vertical shear capacity of the standard section, (iv) evaluate interaction between behavior at prestress transfer and performance under shear-critical loads, and (v) identify design and detailing improvements and make recommendations. Eight full-scale Texas U54 prestressed concrete beams were fabricated to achieve these goals.

Load testing of the first four of these beams revealed a critical weakness along the bottom flange-to-web interface of the beam. The weakness caused failures that occurred at loads well below the calculated shear capacity. Given the horizontal sliding observed, the failure mode was called horizontal shear. The next two beams were fabricated to test three modifications to the end-region design, two of which were deemed successful. The

final two beam sections tested contained the recommended new standard reinforcement and concrete geometry.

A method to evaluate the horizontal shear demand on and capacity of the bottom flange-to-web interface of prestressed concrete beams was developed. The calculations were formulated using the theories of beam bending and shear friction. This method was calibrated and verified using the U-Beam test data, a series of small-scale specimens, and results of shear tests in the literature.

Stresses induced in reinforcing bars at prestress transfer met expectations set by existing codified equations. No modifications to the current U-Beam standard design are needed to manage these stresses. The induced stresses did not influence vertical shear behavior, and no interaction between the two is believed to exist for U-Beams.

This dissertation contains the specifics of the beams tested and the data collected, and provides the details of recommended changes to the Texas U-Beam standard drawings.

TABLE OF CONTENTS

List of Tables ..... **xvi**

List of Figures ..... **xix**

CHAPTER 1 Introduction **1**

1.1 Introduction 1
1.2 Texas U-Beam 1
1.3 Project Motivation 2
1.3.1 Bursting and Spalling Study 3
1.3.2 End-Region Detailing Improvements 4
1.3.3 Shear Study 5
1.4 Project Objectives 6
1.5 Outline of Dissertation 7

CHAPTER 2 Background **9**

2.1 Introduction 9
2.2 Texas U-Beam Design and Development 9
2.3 Research on U-Beams 13
2.3.1 Louetta Road Overpass (1994-1998) 13
2.3.1.1 Performance at Release (Barrios, 1994) 13
2.3.1.2 Effect of Curing Temperatures (Myers and Carrasquillo, 1998) 14
2.3.1.3 Structural Performance (Gross and Burns, 2000) 17
2.3.2 Huang and Shahawy (2005) 18
2.3.3 Summary of U-Beam Research 19
2.4 Beam Behavior at Prestress Transfer 20
2.5 University of Texas Prestressed Concrete Shear Database 24
2.5.1 Significant Recent Studies 24
2.5.1.1 NCHRP 579 / Nagle & Kuchma (2007) 24
2.5.1.2 Hamilton, Llanos, & Ross (2009) 28
2.5.1.3 Tx Girder Shear Study 29
2.5.1.4 Texas Box-Beam Shear Study 31
2.5.2 Collection, Filtered, and Evaluation Databases 36
2.5.3 Characteristics of Test Specimens in Literature 38
2.5.3.1 Beam Shape 38
2.5.3.2 Specimen Depth 39
2.5.3.3 Compressive Strength of Concrete 39
2.5.3.4 Shear Span-to-Depth Ratio 40
2.5.3.5 Shear Area 41
2.5.3.6 Reinforcement Ratio 43
2.5.3.7 Bottom Flange-to-Web Width Ratio 44
2.5.4 Evaluation of Shear Strength Calculation Methods 45

2.6 Shear Strength Calculation Methods 45
2.6.1 ACI Building Code 318-08 46
2.6.2 AASHTO LRFD Bridge Design Specifications: General Procedure 49
2.6.3 AASHTO LRFD Bridge Design Specifications: Segmental Procedure ... 53
2.6.4 Summary 56
2.7 Chapter Summary 58

CHAPTER 3 Experimental Program 59
3.1 Introduction.....59
3.2 Beam Fabrication 60
3.2.1 Texas U54 61
3.2.1.1 Prestressing Strands 62
3.2.1.2 Standard Reinforcing 66
3.2.2 Fabrication Process 67
3.2.3 Casting Procedure 69
3.2.4 Concrete Materials 72
3.3 Temperature Monitoring.....73
3.4 Observation at Prestress Transfer 74
3.5 Shear Testing 75
3.5.1 Shear Test Instrumentation 78
3.5.2 Loading Procedure 79
3.5.3 Definition of Shear Span..... 81
3.5.4 Definition of Failure Shear 82
3.5.5 Comparison to Calculated Shear Capacity 82
3.6 Test Variables 84
3.6.1 Beam Geometry and Skew..... 84
3.6.2 End Block Length 84
3.6.3 Reinforcing Bar Type 84
3.6.4 Bearing Condition..... 85
3.6.5 Amount of Prestressing..... 86
3.6.6 Reinforcing Bar Details 86
3.6.7 Web Width 87
3.6.8 Test Variable Summary 87
3.7 Chapter Summary 92

CHAPTER 4 Specimen Details & Test Observations: Phase I..... 94
4.1 Introduction.....94
4.2 Beam 0 95
4.2.1 Shear Testing 97
4.3 Beam 1 97
4.3.1 Early-Age Behavior 98
4.3.2 Shear Testing 99
4.4 Beam 2 100
4.4.1 Early-Age Behavior 102

4.4.2 Shear Testing 102
4.5 Intermediate Analysis 103
4.6 Beam 3 104
4.6.1 Early-Age Behavior 106
4.6.2 Shear Testing 106
4.7 Summary of Phase I Beam Tests 107
4.8 Phase I to Phase II Transition 109

CHAPTER 5 Specimen Details and Test Observations: Phase II 111
5.1 Introduction 111
5.2 Beam 4 112
5.2.1 Design Modifications 112
5.2.1.1 Web Walls 113
5.2.1.2 Shear Reinforcement 114
5.2.1.3 Confinement Reinforcing 114
5.2.1.4 Top Strands 115
5.2.1.5 Supplementary Reinforcement 116
5.2.2 Early-Age Behavior 118
5.2.3 Shear Testing 118
5.3 Beam 5 119
5.3.1 Design Modifications 119
5.3.1.1 Shear Reinforcement 120
5.3.1.2 Confinement 120
5.3.1.3 Supplementary Reinforcement 121
5.3.2 Shear Testing 121
5.4 Intermediate Analysis 122
5.4.1 Constructability 122
5.4.1.1 End Block Congestion 123
5.4.1.2 Cover Requirements 125
5.4.2 Serviceability 127
5.4.3 Recommendations 129
5.5 Beam 6 130
5.5.1 Design Modifications 131
5.5.1.1 Increased End Block Length 132
5.5.1.2 Confinement Steel 133
5.5.1.3 Supplementary Reinforcement 133
5.5.2 Shear Testing 133
5.6 Beam 7 134
5.6.1 Shear Testing 135
5.7 Summary of Phase II Testing 136
5.8 Horizontal Shear Performance 138
5.9 Chapter Summary 138

CHAPTER 6 Analysis of Results 138
6.1 Introduction 138
6.2 Stresses Induced in Reinforcing Bars at Prestress Transfer 140
6.2.1 Heavily-Prestressed Beams 140
6.2.2 Lightly-Prestressed Beam 144
6.2.3 U-Beam Behavior in Context 145
6.2.4 Summary 147
6.3 Curing Temperatures 147
6.4 Distribution of Load 152
6.5 Cracking Behavior 157
6.5.1 Crack Widths 158
6.5.2 Overall Vertical Strain 161
6.6 Demand on Tensile Reinforcement 163
6.7 Demand on Vertical Reinforcement 169
6.7.1 Shear Instrumentation Region 170
6.7.2 Bottom Flange-to-Web Interface Instrumentation Region 171
6.8 Vertical Shear Performance 173
6.8.1 Phase I Beam Performance 174
6.8.2 Phase II Beam Performance 177
6.8.3 Comparison to UTPCSDB 181
6.8.4 U-Beam Design Recommendations 182
6.9 Summary of Results 185

CHAPTER 7 Horizontal Shear Strength Evaluation 188
7.1 Introduction 188
7.1.1 Motivation 188
7.1.2 Chapter Organization 189
7.2 Mechanics of Horizontal Shear 190
7.3 Bending Induced Horizontal Shear Stresses 192
7.4 Theory of Shear Friction 196
7.5 Recommended Calculation Procedure 199
7.5.1 Horizontal Shear Ratio 200
7.5.2 Ultimate Evaluation Point 201
7.5.3 Calculation for Demand 202
7.5.4 Calculation for Capacity 206
7.6 Example Calculation 210
7.6.1 Example Specimen Properties 211
7.6.2 Example Calculation for Demand 212
7.6.3 Example Calculation for Capacity 213
7.6.4 Example Evaluation 215
7.7 Verification of Methodology 216
7.7.1 Formation of Evaluation Database 216
7.7.2 Database Composition 218
7.7.3 Accuracy of Horizontal Shear Calculations 221

7.8 Horizontal Shear in U-Beams 224
7.8.1 Initial Calculations 225
7.8.2 Push-Off Tests 226
7.8.3 Explanation of Behavior 232
7.8.4 Application of Findings 234
7.9 Recommendations for Use in Design 237
7.10 Summary 239

CHAPTER 8 Conclusions and Recommendations 240

8.1 Texas U-Beams 240
8.2 Project Motivation 240
8.3 Project Summary 241
8.4 Recommended New Standard Design 242
8.5 Conclusions 244
8.5.1 Behavior at Prestress Transfer 244
8.5.2 Vertical Shear Performance 245
8.5.3 Horizontal Shear Evaluation 246
8.6 Recommendations for Further Study 248
8.6.1 Existing U-Beam Analysis and Retrofit 248
8.6.2 Effect of Reinforcement Position on Shear-Friction Strength 248

APPENDIX A U-Beam Information and Drawings 250

A.1 2006 Prestressed Concrete U-Beams 250
A.2 1998 Edition of U-Beam Standards 256
A.3 U-Beam Geometry 259
A.4 U-Beam Reinforcing Bar Details 259
A.5 U-Beam End Block Reinforcement 261
A.6 Beam 0 Information and Drawings 262
A.7 Beam 1 Information and Drawings 266
A.8 Beam 2 Information and Drawings 271
A.9 Beam 3 Information and Drawings 276
A.10 Beam 4 Information and Drawings 281
A.11 Beam 5 Information and Drawings 288
A.12 Beam 6 Information and Drawings 293
A.13 Beam 7 Information and Drawings 299

APPENDIX B Collected Data 307
B.1 Overview 307
B.2 End-Region Stresses at Prestress Transfer 307
B.3 Curing Temperatures 311
B.4 Web Distortion 315
B.5 Load Distribution 317
B.6 Shear Test Cracks 320
B.7 Maximum Crack Widths 332
B.8 Vertical Strain in Webs 334
B.9 Strain in Reinforcing Bars 336
B.10 Shear-Deflection Plots 338

APPENDIX C Horizontal Shear Evaluation Database 342
C.1 Introduction 342
C.2 Notations 342
C.3 Table of General Properties 344
C.4 Table of Data for Demand Calculations 347
C.5 Table of Data for Capacity Calculations 350
C.6 Reinforcing Bar Locations 352
C.6.1 Texas U-Beams: Hovell (2011) 352
C.6.2 Alshegeir & Ramirez (1992) 354
C.6.3 Avendaño (2011) 356
C.6.4 Avendaño & Bayrak (2008) 359
C.6.5 Avendaño, et al. (unpublished) 359
C.6.6 Hamilton, Llanos, & Ross (2009) 361
C.6.7 Hawkins & Kuchma (2007) 361
C.6.8 Heckmann & Bayrak (2008) 362
C.6.9 Labonte & Hamilton (2005) 364
C.6.10 Naito, Parent, & Brunn (2005) 365
C.6.11 Ramirez & Aguilar (2005) 366
C.6.12 Runzell, Shield, and French (2007) 366
C.6.13 Shahawy, Robinson, and Batchelor (1993) 367
C.6.14 Tawfiq (1995) 369
C.7 References for HSED Data Points 371

APPENDIX D Vertical Shear Capacity Calculations 372
D.1 Notation 372
D.2 ACI Detailed Method (2008) 374
D.3 AASHTO LRFD General Procedure (2010) 375
D.4 AASHTO LRFD Segmental Procedure (2010) 376

APPENDIX E Fold-Up U-Beam 377
E.1 Instructions 377

References **380**

Vita **388**

LIST OF TABLES

Table 2-1: Cross-sectional properties of the Texas U54 and AASHTO Type IV beams. 10
Table 2-2: Web shear reinforcement in the Texas U-Beam per March 1998 and July 2003 drawings. 12
Table 2-3: Bottom flange-to-web width ratios for standard beam sections. 45
Table 2-4: Summary of shear performance data from UTPCSDB-2011 Evaluation Database-Level II (from Nakamura (2011)). 57
Table 3-1: Summary of beams fabricated for this research project. 59
Table 3-2: Composition of Type III cement concrete mixtures. 72
Table 3-3: Composition of Type I cement concrete mixtures. 73
Table 3-4: Basic geometric properties of the fabricated U-Beams. 88
Table 3-5: Concrete material properties for the U-Beam test specimens. 89
Table 3-6: Reinforcing bar locations and material properties for U-Beam test specimens. 90
Table 3-7: Details of prestressing used in U-Beam test specimens. 91
Table 3-8: Details of shear test setup for U-Beam test specimens. 92
Table 4-1: Summary of key features of Beam 0 and Phase I test regions. 95
Table 4-2: Debonding pattern for Beam 3. 105
Table 4-3: Summary of Phase I test beams and variables. 108
Table 5-1: Summary key features of Phase II test regions. 112
Table 5-2: Interface steel distribution in several beam sections. 117
Table 5-3: Summary of Phase II test variables. 137
Table 6-1: Summary of end regions involved in this research project. 139
Table 6-2: Summary of temperature data. 148
Table 6-3: TxDOT Standard Specifications regarding curing temperature (TxDOT, 2004). 149
Table 6-4: Summary of calculated and observed cracking loads and shears. 158
Table 6-5: General trends for the relationship between crack width and proximity to capacity. 160
Table 6-6: Summary of longitudinal demand calculations. 166
Table 6-7: Summary of calculated shear capacities for Phase II beams. 180
Table 7-1: Comparison of calculation methods at critical interface in a Tx28 beam. 204
Table 7-2: Non-linear and average shear stress comparisons for various beam types. 205
Table 7-3: Cohesion and friction coefficents for three calculation methods. 208
Table 7-4: Maximum shear stress limit factors for three calculation methods. 209
Table 7-5: Summary of horizontal shear example calculations. 215
Table 7-6: Filtering criteria used to form Evaluation Database – Level I (from Nakamura (2011)). 216

Table 7-7: Filtering criteria used to form the Horizontal Shear Evaluation Database. 217
Table 7-8: List of references used in the Horizontal Shear Evaluation Database.....218
Table 7-9: Statistics for the recommended horizontal shear evaluation method. 223
Table 7-10: Statistics for HSRs when using ACI (2008) calculation for capacity. 224
Table 7-11: Summary of modified push-off specimen results. 232
Table 7-12: Summary of average horizontal shear ratios using original and modified equations. 236
Table A-1: Standard and modified U54 beam section properties. 259
Table A-2: Summary of information about Beam 0. 263
Table A-3: Summary of information about Beam 1. 267
Table A-4: Summary of information about Beam 2. 272
Table A-5: Details of debonding pattern used in Beam 3. 276
Table A-6: Summary of information about Beam 3. 278
Table A-7: Summary of information about Beam 4. 282
Table A-8: Summary of information about Beam 5. 289
Table A-9: Summary of information about Beam 6. 294
Table A-10: Details of debonding pattern used in Beam 7. 299
Table A-11: Summary of information about Beam 7. 300
Table B-1: Temperature measurements in Beam 1 (cast October, 2008). 312
Table B-2: Temperature measurements in Beam 2 (cast February, 2009). 312
Table B-3: Temperature measurements in Beam 3 (cast July, 2009). 313
Table B-4: Temperature measurements in Beam 4 (cast October, 2009). 313
Table B-5: Temperature measurements in Beam 6 (cast November, 2010). 314
Table C-1: General properties of beams in the Horizontal Shear Evaluation Database. 344
Table C-2: Parameters for horizontal shear demand calculation. 347
Table C-3: Parameters for horizontal shear capacity calculation. 350
Table C-4: Reinforcing bar locations in specimens tested by Hovell (2011). 353
Table C-5: Reinforcing bar locations in specimens tested by Alshegeir and Ramirez (1992). 354
Table C-6: Reinforcing bar locations in specimens tested by Avendaño (2011). 356
Table C-7: Reinforcing bar locations in specimens tested by Avendaño and Bayrak (2008). 359
Table C-8: Reinforcing bar locations in specimens tested by Avendaño, et al. (unpublished). 360
Table C-9: Reinforcing bar locations in specimens tested by Hamilton, Llanos, and Ross (2009). 361
Table C-10: Reinforcing bar locations in specimens tested by Hawkins and Kuchma (2007). 362
Table C-11: Reinforcing bar locations in specimens tested by Heckmann and Bayrak (2008). 363
Table C-12: Reinforcing bar locations in specimens tested by Labonte and Hamilton (2005). 364

Table C-13: Reinforcing bar locations in specimens tested by Naito, Parent, and Brunn (2005). 365
Table C-14: Reinforcing bar locations in specimens tested by Ramirez and Aguilar (2005). 366
Table C-15: Reinforcing bar locations in specimens tested by Runzell, Shield, and French (2007). 367
Table C-16: Reinforcing bar locations in specimens tested by Shahawy, Robinson, and Batchelor (1993). 368
Table C-17: Reinforcing bar locations in specimens tested by Tawfiq (1995). 369
Table C-18: Author names, titles, and publication years for references included in the HSED. 371

LIST OF FIGURES

Figure 1-1: Cross section of the Texas U54. 2
Figure 1-2: Plan views of Texas U-Beam end block configurations: (A) standard end block with square internal void, and (B) optional end block with skewed internal void. 4
Figure 2-1: Cross-sectional dimensions of the Texas U54 U-Beam. 10
Figure 2-2: Cross section of U-Beam bridge, with standard web reinforcing bars highlighted. 10
Figure 2-3: Web shear reinforcement in the Texas U-Beam per (A) March 1998 and (B) July 2006 drawings. 12
Figure 2-4: Confinement scenarios tested by Barrios (1994). 14
Figure 2-5: Concrete strength at release and 56 days, as related to maximum temperature during hydration (Myers and Carrasquillo, 1998). 16
Figure 2-6: Concrete strength at release and 56 days, as related to temperature rise during hydration (Myers and Carrasquillo, 1998). 16
Figure 2-7: Live loading scheme used by Gross and Burns (2000) 18
Figure 2-8: Florida U-Beam, as studied by Huang and Shahawy (2005). 19
Figure 2-9: Spreading of near anchorage zone (from Nilson (1987)). 20
Figure 2-10: Bursting and spalling deformations (from Dunkman 2009). 21
Figure 2-11: Total transverse-bar force within $h/4$ vs. prestressing force measured in previous beam tests from the literature (from Dunkman (2009)). 22
Figure 2-12: Maximum transverse-bar stress compared with average stress within $h/4$ (from Dunkman (2009)). 23
Figure 2-13: Horizontal sliding failure mode seen in several of the BT-63 specimens tested by Nagle and Kuchma (2007). 25
Figure 2-14: End region of the beam model used by Nagle and Kuchma (2007) showing (A) dimension definitions and (B) location of horizontal shear stress. 26
Figure 2-15: Strut-and-tie model for beam with (A) fully bonded tendons and (B) significant numbers of unbounded tendons located beneath the web (from Hamilton, Llanos, and Ross, 2009). 28
Figure 2-16: Tx28 after shear testing, with horizontal failure crack highlighted. 29
Figure 2-17: Horizontal shear damage visible in specimens (A) Tx46-S and (B) Tx70-N. 30
Figure 2-18: Cross-sectional dimensions of the Texas 4B28 tested by Avendaño (2011). 31
Figure 2-19: Typical layout of Texas 4B28s in service. 32
Figure 2-20: 4B28 loading scenarios used by Avendaño (2011). 33
Figure 2-21: Geometry of 5B40 Texas Box-Beams tested by Avendaño, et al. (2011). 35
Figure 2-22: 5B40 loading scenarios used by Avendaño (2011). 35

Figure 2-23: (A) Failure of the end block of specimen 5B40-3-Q, as tested by Avendaño (2011), with longitudinal sliding visible (B). 36
Figure 2-24: Distribution of beam shapes in UTPCSDB-2011 Filtered Database. 38
Figure 2-25: Distribution of specimen size in the UTPCSDB-2011 Filtered Database. 39
Figure 2-26: Distribution of concrete compressive strength in the UTPCSDB-2011 Filtered Database. 40
Figure 2-27: Distribution of shear span-to-depth ratios in the UTPCSDB-2011 Filtered Database. 41
Figure 2-28: Distribution of shear area in the UTPCSDB-2011 Filtered Database. 42
Figure 2-29: Increase in shear area of tested specimens through time (from Nakamura (2011)). 42
Figure 2-30: Distribution of reinforcement ratios in the UTPCSDB-2011 Filtered Database. 43
Figure 2-31: Distribution of bottom flange-to-web width ratio in UTPCSDB-2011 Filtered Database. 44
Figure 2-32: Shear Performance Ratio calculated using the ACI Detailed Method (2008) for beam tests in the UTPCSDB-2011 Evaluation Database-Level II (from Nakamura (2011)). 49
Figure 2-33: Shear Performance Ratio calculated using the AASHTO General Procedure (2010) for beam tests in the UTPCSDB-2011 Evaluation Database-Level II (from Nakamura (2011)). 53
Figure 2-34: Shear Performance Ratio calculated using the AASHTO Segmental Procedure (2010) for beam tests in the UTPCSDB-2011 Evaluation Database-Level II (from Nakamura (2011)). 55
Figure 2-35: Shear Performance Ratio calculated using the AASHTO Segmental Procedure (2010) with no limit on K for beam tests in the UTPCSDB-2011 Evaluation Database-Level II (from Nakamura (2011)). 56
Figure 2-36: Summary of shear performance ratios across three calculation methods (from Nakamura (2011)). 57
Figure 3-1: Beam fabrication locations. 60
Figure 3-2: Geometry of the Texas U54 beam. 61
Figure 3-3: Plan view of end block options in skewed U-Beams: (A) square void with triangular end block, and (B) skewed void with square end block. 62
Figure 3-4: Strand positions in the Texas U54. 62
Figure 3-5: (A) Reaction plate at the live end of the prestressing bed at FSEL. (B) Strand layout for UT-fabricated U-Beams and (C) TxDOT standard strand layout. 63
Figure 3-6: Total number of prestressing strands in Texas U-Beams. 64
Figure 3-7: Prestressing force in typical Texas U-Beams at beam end and midspan. 65
Figure 3-8: Percentage of debonding in typical Texas U-Beams. 65

Figure 3-9: Standard web and confining reinforcing bar shapes used in this study. 67
Figure 3-10: Two-stage monolithic cast procedure. 70
Figure 3-11: Monolithic cast procedure. 71
Figure 3-12: Position of thermocouples used in temperature monitoring during curing. 74
Figure 3-13: Location of instrumentation monitored at prestress transfer. 75
Figure 3-14: Forces that develop in the U-Beam during loading. 76
Figure 3-15: Deck form system used, highlighting ¾" plywood. 76
Figure 3-16: Shear testing frame, with pictures of (A) strand slip and (B) shear deformation instrumentation shown. 77
Figure 3-17: Bearing conditions at the ends of the shear test specimen. 78
Figure 3-18: Typical locations for strand slip gauges during shear testing. 79
Figure 3-19: External post-tensioning system used to strengthen U-Beams during shear testing. 80
Figure 3-20: Schematic of how and when external post-tensioned clamps were used to aid in achieving a second failure within one beam. 81
Figure 3-21: Definition of the shear span, a, in a (A) squared and (B) skewed test region. 81
Figure 3-22: Explanation of the location and magnitude of V_{test}. 82
Figure 3-23: Explanation of comparison between calculated shear capacity and measured strength. 83
Figure 3-24: Typical stress-strain plots from material used in the tested U-Beams. 85
Figure 3-25: Comparison of (A) standard cross section to (B) cross section with widened web walls. 87
Figure 4-1: (i) Beam 0 elevation view, with reinforcing bar spacings indicated. 96
(ii) Standard cross section of Beam 0. 96
Figure 4-2: (i) Plan view of Beam 1. 98
(ii) Elevation view of Beam 1. 98
(iii) Standard cross section of Beam 1. 98
Figure 4-3: Test region B1S after failure of end region. 99
Figure 4-4: Test specimen B1N after failure of end region. 100
Figure 4-5: (i) Plan view of Beam 2. 101
(ii) Elevation view of Beam 2. 101
(iii) Standard cross section of Beam 2. 101
Figure 4-6: Test specimen B2N after failure of end region. 102
Figure 4-7: Horizontal crack along bottom flange-to-web interface in test specimen B2N. 103
Figure 4-8: Debonding pattern for Beam 3. 105
Figure 4-9: (i) Elevation view of Beam 3. 106
(ii) Standard cross section of Beam 3. 106
Figure 4-10: Damage to test specimen B3S after shear testing. 107
Figure 4-11: Failure shears of five Phase I test specimens. 109

Figure 5-1: (i) Elevation view of Beam 4. 113
(ii) Standard cross sections of Beam 4. 113
Figure 5-2: U-Beam cross section used in Beam 4, compared with the standard cross section. 114
Figure 5-3: Beam 4 cross-section detail, with new bars and geometry highlighted. 115
Figure 5-4: Generalized sketch of the increase in shear capacity towards the end of a full-length beam designed using the modified details used in the south (more heavily reinforced) end of Beam 4. 117
Figure 5-5: Failure of test region B4N. 119
Figure 5-6: (i) Elevation view of Beam 5. 120
(ii) Standard cross sections of Beam 5. 120
Figure 5-7: Cross sectional detail of Beam 5, with new bars highlighted. 121
Figure 5-8: Test region B5N after flexure-shear failure. 122
Figure 5-9: (A) End-region reinforcing in Beam 5; (B) six side-by-side bars (two #5s and four #4s) bundled together in the end block of Beam 5. 124
Figure 5-10: Workers using a 1.5 in. pry bar (outlined) to lift bottom strands; (B) resulting strand locations. 125
Figure 5-11: (A) Workers using a pry bar to move reinforcement away from void form (B). The cage was held back with tie wire and plastic chairs (C). 127
Figure 5-12: Extent of shear cracking in test regions B4S and B5N at the same shear load step relative to calculated shear capacity. 129
Figure 5-13: (i) Elevation view of Beam 6. 131
(ii) Standard cross sections of Beam 6. 131
Figure 5-14: Existing end block reinforcement compared with reinforcement used in Beam 6. 132
Figure 5-15: Test region B6S after flexure-shear failure. 134
Figure 5-16: (i) Plan view of Beam 7. 135
(ii) Elevation view of Beam 7. 135
(iii) Standard cross sections of Beam 7. 135
Figure 5-17: Test region B7N after shear failure. 136
Figure 5-18: Ratio of failure shear to calculated shear capacity for the five Phase II test specimens. 137
Figure 6-1: Location of widest crack observed in U-Beam end regions (B1S). Transverse stress measurements are represented by circles indicating stress magnitude and location of measurement. 142
Figure 6-2: Most significant bursting stresses measured within solid triangular end block of Beam 2. 143
Figure 6-3: Effect of supplemental transverse bars, through comparison of (A) B4N and (B) B4S. 144
Figure 6-4: Typical beam end region in beam with debonded strands (B3N). 145
Figure 6-5: Transverse bar force measured in specimens from this project and literature. 146

Figure 6-6: Comparison of measured maximum temperatures and maximum temperature differentials to the TxDOT limits. 150
Figure 6-7: Temperatures measured through the cross sections of the skewed end blocks of Beam 1 and Beam 2 at time of maximum temperature reading. 151
Figure 6-8: (A) Actual shape of a Texas U-Beam and (B) effective shape for calculations. 152
Figure 6-9: Linear potentiometers locations on web, for measuring distortion. 153
Figure 6-10: (A) Original orientation of linear potentiometers, (B) shape after applying load, and (C) definition of variables used in distortion calculation. 154
Figure 6-11: Typical distortion measured in the two webs of a rectangular and skewed beam. 154
Figure 6-12: Bearing conditions used in U-Beam load tests. 155
Figure 6-13: Ratio of load on west side load cell (short side of skewed beams) to total load at that end. 156
Figure 6-14: Maximum measured crack width plotted against the ratio of applied shear to failure shear. 159
Figure 6-15: Maximum measured crack widths for test specimens that failed in web-shear. 160
Figure 6-16: Comparison of cracking observed in the two test regions of Beam 4. 161
Figure 6-17: Vertical strain measured through the webs of Beam 4. 162
Figure 6-18: Vertical strain measured in B4N (wide web walls) and B3S (standard section). 162
Figure 6-19: Free-body diagram of the end region of a prestressed beam (from AASHTO (2010)). 164
Figure 6-20: Strand slip measured at 95% of failure load during shear testing. 165
Figure 6-21: Summary of longitudinal demand calculations. 166
Figure 6-22: Strand slip data gathered during shear tests B3N and B3S. 168
Figure 6-23: Bearing condition and monitored strand locations for B3N and B3S. 169
Figure 6-24: Locations of gauges monitored during shear testing. 169
Figure 6-25: Strain in reinforcing bars at maximum load. 170
Figure 6-26: Comparison of strains in B4S at maximum load to other test specimens at 67% of their failure load. 171
Figure 6-27: Measured strains in web reinforcing bars at bottom flange-to-web interface just before failure. 172
Figure 6-28: Comparison of measured strains in B4S at maximum load and the other test regions at 67% of maximum load. Gauges positioned at bottom flange-to-web interface. 173
Figure 6-29: Summary of Phase I U-Beam shear tests. 175
Figure 6-30: (A) Test region B3S after failure, with locations of pictures (B) and (C) shown. (B) Closer view of failure in B3S, showing kinking of reinforcing bars at bottom flange-to-web interface. (C) Original location of bar before failure. 176

Figure 6-31: Summary of Phase II U-Beam shear tests. 179
Figure 6-32: Texas U-Beam failure shear-to-calculated shear ratios (capacity calculated using ACI Detailed Method (2008)), compared to other UTPCSDB-2011 data points. 181
Figure 6-33: Texas U-Beam failure shear-to-calculated shear ratios (capacity calculated using AASHTO General Procedure (2010)), compared to other UTPCSDB-2011 data points. 182
Figure 6-34: Texas U-Beam failure shear-to-calculated shear ratios (capacity calculated using AASHTO Segmental Procedure (2010) with no limit on K), compared to other UTPCSDB-2011 data points. 182
Figure 6-35: Key reinforcing bars in the recommended new Texas U-Beam design. 184
Figure 6-36: Reinforcing bar changes in the end block. 184
Figure 6-37: Sectional view of (A) the existing U-Beam standard and (B) the recommended new U-Beam standard, highlighting added reinforcement and increased end block length. 185
Figure 7-1: Examples of horizontal shear damage observed in laboratory tests.....189
Figure 7-2: Examples of typical weB-shear failures (from Heckmann and Bayrak, 2008). 190
Figure 7-3: Example of horizontal shear failure. 191
Figure 7-4: Illustration of horizontal shear, using (A) unbonded and (B) bonded wood planks.....191
Figure 7-5: Horizontal shear schematic. 192
Figure 7-6: (A) Example beam, (B) shear diagram, and (C) moment diagram. 193
Figure 7-7: (A) Representative slice of beam, (B) considering only the area beneath the plane of interest (shaded), (C) stress resulting from the applied load. 194
Figure 7-8: Example calculations for shear stress using (A) rectangular and (B) I-shaped beams. 196
Figure 7-9: Shear friction hypothesis (from Birkeland and Birkeland, 1966). 197
Figure 7-10: Flexural member (A) just prior to and (B) just after exceeding the horizontal shear capacity of the bottom flange-to-web interface. (C) Free-body diagram drawn from failed shape. 200
Figure 7-11: Location of the Ultimate Evaluation Point. 201
Figure 7-12: Calculated shear stress in the example Tx28, using non-linear and linear sectional analyses, and an average shear stress calculation. 204
Figure 7-13: Area of concrete involved in resisting horizontal shear in beams in end blocks. 210
Figure 7-14: Cross-sectional properties of the example Tx28-I-D specimen. 211
Figure 7-15: Elevation view of test setup used by Avendaño and Bayrak (2008). 212
Figure 7-16: Reinforcing bar layout in specimen Tx28-I-D. 212
Figure 7-17: Tx28-I-D cracking observed at failure. 215
Figure 7-18: Beam shapes included in the Horizontal Shear Evaluation Database. 219
Figure 7-19: Distribution of concrete strength for specimens in the HSED. 220

Figure 7-20: Distribution of specimen size in the HSED. 220
Figure 7-21: Distribution of shear span-to-depth ratio used in tests in the HSED. 221
Figure 7-22: Distribution of vertical reinforcement ratio for specimens in the HSED. 221
Figure 7-23: Ratios of vertical and horizontal shear demand to capacity for specimens in the HSED. 223
Figure 7-24: HSR-SPR plot for specimens in the HSED with calculations for capacity performed using the ACI (2008) shear-friction equation. 224
Figure 7-25: Summary of comparison between horizontal and vertical shear demand and capacity for Texas U-Beams. 225
Figure 7-26: Typical push-off specimen as described in literature. 226
Figure 7-27: (A) Typical U-Beam and (B) I-Beam bottom flange-to-web interface and reinforcing. 227
Figure 7-28: Critical interface of push-off specimens based on the reinforcement of (A) a standard Texas U-Beam and (B) an I-Beam (Tx 46). 228
Figure 7-29: Steps taken to design the modified push-off specimens used. 229
Figure 7-30: Dimensions and interface reinforcing bar locations in modified push-off specimens. 230
Figure 7-31: Modified push-off specimen viewed from four corners. 230
Figure 7-32: Placement of reinforcing bars crossing critical plane in modified push-off specimens. 231
Figure 7-33: Elevation view of a beam and the shear-friction model. 232
Figure 7-34: Cross-sectional view of shear-friction specimens with (A) distributed and (B) asymmetrical reinforcement. 233
Figure 7-35: Observations of asymmetric opening of shear-friction interface. 234
Figure 7-36: Summary of comparison between horizontal and vertical shear demand and capacity for Texas U-Beams, with correction factor in horizontal shear capacity calculation. 235
Figure 7-37: Ratio of horizontal shear demand to capacity for all points in the HSED. 236
Figure 7-38: Typical vertical shear capacity plot. 237
Figure 8-1: Existing and recommended U-Beam standard reinforcement. 243
Figure 8-2: Existing and recommended U-Beam end-block geometry and reinforcement. 243
Figure 8-3: (A) Existing bottom flange-to-web interface reinforcement and (B) recommended new reinforcement. 244
Figure A-1: Geometry of supplementary and confining reinforcement used in Beams 4, 5, 6, and 7. 260
Figure A-2: Modified end-block reinforcing bars used in Beams 6 and 7. 260
Figure A-3: Key showing reinforcing bar appearance in elevation view. 261
Figure A-4: Prestressing strand positions for Beam 0. 262
Figure A-5: Beam 0 plan view, elevation view, and standard sections. 264
Figure A-6: Beam 0 end-region plan views and cross-sections. 265
Figure A-7: Prestressing strand positions for Beam 1. 266

Figure A-8: Beam 1 plan view, elevation view, and standard sections. 268
Figure A-9: Beam 1 north end-region plan view and cross-sections. 269
Figure A-10: Beam 1 south end-region plan view and cross-sections. 270
Figure A-11: Prestressing strand positions for Beam 2. 271
Figure A-12: Beam 2 plan view, elevation view, and standard sections. 273
Figure A-13: Beam 2 north end-region plan view and north and south cross-sections. 274
Figure A-14: Beam 2 south end region plan view and cross-sections 275
Figure A-15: Prestressing strand positions for Beam 3. 276
Figure A-16: Distance from beam end to point of bond for strands in Beam 3. 277
Figure A-17: Beam 3 plan view, elevation view, and standard sections. 279
Figure A-18: Beam 3 end-region plan views and cross-sections. 280
Figure A-19: Prestressing strand positions for Beam 4. 281
Figure A-20: Beam 4 plan view, elevation view, and sections showing standard reinforcement. 283
Figure A-21: Beam 4 plan view, elevation view, and sections showing supplementary reinforcement. 284
Figure A-22: Beam 4 north end-region plan views and cross-sections. 285
Figure A-23: Beam 4 south end region plan views and cross-sections. 286
Figure A-24: Cross-sectional dimensions of the modified U-Beam used in Beam 4. 287
Figure A-25: Prestressing strand positions for Beam 5. 288
Figure A-26: Beam 5 plan view, elevation view, and sections showing standard reinforcement. 290
Figure A-27: Beam 5 plan view, elevation view, and sections showing supplementary reinforcement. 291
Figure A-28: Beam 5 end-region plan views and cross-sections. 292
Figure A-29: Prestressing strand positions for Beam 6. 293
Figure A-30: Beam 6 plan view, elevation view, and sections showing standard reinforcement. 295
Figure A-31: Beam 6 plan view, elevation view, and sections showing supplementary reinforcement. 296
Figure A-32: Beam 6 end-region plan views and cross-sections (1 of 2). 297
Figure A-33: Prestressing strand positions for Beam 7. 299
Figure A-34: Beam 7 plan view, elevation view, and sections showing standard reinforcement. 301
Figure A-35: Beam 7 plan view, elevation view, and sections showing supplementary reinforcement. 302
Figure A-36: Beam 7 north end-region plan views and cross-sections (1 of 2). 303
Figure A-37: Beam 7 south end-region plan views and cross-sections (1 of 2). 305
Figure B-1: Magnitude and location of cracking and stresses induced in reinforcement at prestress transfer for Beam 1. 308
Figure B-2: Magnitude and location of cracking and stresses induced in reinforcement at prestress transfer for Beam 2. 309

Figure B-3: Magnitude and location of cracking and stresses induced in reinforcement at prestress transfer for Beam 3. 310
Figure B-4: Magnitude and location of cracking and stresses induced in reinforcement at prestress transfer for Beam 4. 311
Figure B-5: Distortion measured in the webs during loading of test specimen B3S. 315
Figure B-6: Distortion measured in the webs during loading of test specimens B4N and B4S. 316
Figure B-7: Distortion measured in the webs during loading of test specimens B5N and B6S. 316
Figure B-8: Distortion measured in the webs during loading of test specimen B7N. 316
Figure B-9: Bearing conditions used in U-Beam load tests. 317
Figure B-10: Distribution of load into two bearing pads during testing of specimens B0S and B1N. 318
Figure B-11: Distribution of load into two bearing pads during testing of specimens B1S and B2N. 318
Figure B-12: Distribution of load into two bearing pads during testing of specimens B3N and B3S. 318
Figure B-13: Distribution of load into two bearing pads during testing of specimens B4N and B4S. 319
Figure B-14: Distribution of load into two bearing pads during testing of specimens B5N and B6S. 319
Figure B-15: Distribution of load into two bearing pads during testing of specimen B7N. 319
Figure B-16: Cracks observed during testing of specimen B0S. 321
Figure B-17: Cracks observed during testing of specimen B1N. 322
Figure B-18: Cracks observed during testing of specimen B1S. 323
Figure B-19: Cracks observed during testing of specimen B2N. 324
Figure B-20: Cracks observed during testing of specimen B3N. 325
Figure B-21: Cracks observed during testing of specimen B3S. 326
Figure B-22: Cracks observed during testing of specimen B4N. 327
Figure B-23: Cracks observed during testing of specimen B4S. 328
Figure B-24: Cracks observed during testing of specimen B5N. 329
Figure B-25: Cracks observed during testing of specimen B6S. 330
Figure B-26: Cracks observed during testing of specimen B7N. 331
Figure B-27: Maximum crack widths measured in test specimens B0S and B1N. 332
Figure B-28: Maximum crack widths measured in test specimens B1S and B2N. 332
Figure B-29: Maximum crack widths measured in test specimens B3N and B3S. 333
Figure B-30: Maximum crack widths measured in test specimens B4N and B4S. 333
Figure B-31: Maximum crack widths measured in test specimens B5N and B6S. 333
Figure B-32: Maximum crack widths measured in test specimen B7N. 334
Figure B-33: Location of linear potentiometer used to measure vertical strain during loading. 334

Figure B-34: Vertical strains measured in the webs of test specimen B3S during loading. 335
Figure B-35: Vertical strains measured in the webs of test specimens B4N and B4S during loading. 335
Figure B-36: Vertical strains measured in the webs of test specimens B5N and B6S during loading. 335
Figure B-37: Vertical strains measured in the webs of test specimen B7N during loading. 336
Figure B-38: Strain measured in reinforcing bars during load-testing of specimen B1N. 336
Figure B-39: Strain measured in reinforcing bars during load-testing of specimen B2N. 337
Figure B-40: Strain measured in reinforcing bars during load-testing of specimen B3N. 337
Figure B-41: Strain measured in reinforcing bars during load-testing of specimen B3S. 337
Figure B-42: Strain measured in reinforcing bars during load-testing of specimen B4N. 338
Figure B-43: Strain measured in reinforcing bars during load-testing of specimen B4S. 338
Figure B-44: Shear-deflection plot for specimen B0S. 339
Figure B-45: Shear-deflection plot for specimens B1N and B1S. 339
Figure B-46: Shear-deflection plot for specimens B2N. 340
Figure B-47: Shear-deflection plot for specimens B3N and B3S. 340
Figure B-48: Shear-deflection plot for specimens B4N and B4S. 340
Figure B-49: Shear-deflection plot for specimens B5N and B6S. 341
Figure B-50: Shear-deflection plot for specimens B7N. 341
Figure E-1: Model of 30-ft Texas U54 with detailing matching current standard. 378
Figure E-2 Model of 30-ft Texas U54 with detailing following recommended design. 379

CHAPTER 1
Introduction

1.1 INTRODUCTION

A study on prestressed concrete Texas U-Beams is presented in this dissertation. The investigation contained three parts: (a) measuring stresses induced in reinforcing bars at prestress transfer, (b) monitoring temperatures during curing of the concrete, and (c) determining the vertical shear capacity through load-testing. These tests were performed as part of Texas Department of Transportation (TxDOT) Research Project 0-5831. Beams were fabricated at the Ferguson Structural Engineering Laboratory (FSEL) at the University of Texas at Austin and at three prestressed concrete beam fabrication plants in Texas. Load-testing was performed at FSEL. A description of the Texas U-Beam and the motivation behind this research study are presented in the following sections. Primary objectives are then summarized. The chapter concludes with an outline of the remainder of this dissertation.

1.2 TEXAS U-BEAM

The cross section and basic dimensions of the Texas U54 can be seen in Figure 1-1. The beam design was formally introduced to the TxDOT bridge standards in 1998 as an alternative to I-Beams in high-visibility intersections (Ralls, et al., 1993). The use of U-Beams in an overpass is considered more aesthetically pleasing than a comparable bridge of I-Beams as fewer beam lines are needed, improving the appearance as viewed from below.

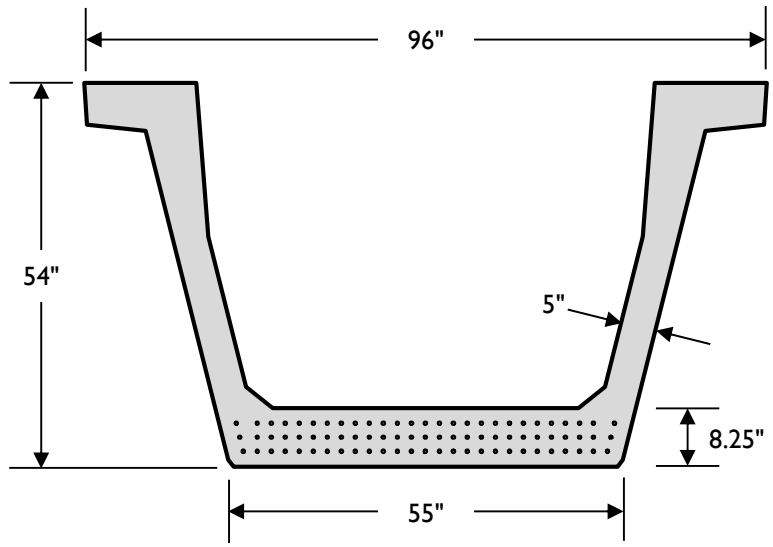

Figure 1-1: Cross section of the Texas U54.

The cross section of the U-Beam was optimized with regards to flexural capacity (Ralls, et al., 1993). The cross section has a large bottom flange that can hold a maximum of 81 prestressing strands, two 5-in. web walls, and an open top. The general dimensions came about through modifications to Houston Trapezoidal Girders, which were widely used in the state at the time. The major difference between the two designs is the lack of a monolithic top slab in the U-Beam; the open top of the U-Beam design allows for the use of reusable steel void forms that are removed after casting.

While a handful of studies performed in the 1990's investigated some aspects of the Texas U-Beam behavior (Barrios, 1994; Myers and Carrasquillo, 1998; Gross and Burns, 2000), the shear strength of the beam was never studied experimentally.

1.3 PROJECT MOTIVATION

TxDOT initiated this study to investigate the behavior of Texas U- and Box-Beams. The project goals included evaluating current design details with regard to behavior at prestress transfer, establishing the shear strength given any stresses induced at prestress transfer, and providing recommendations for improvement of structural behavior and constructability of the end regions. In the process of improving the reinforcing bar detailing and design, it was desired to reduce the amount of concrete

needed in the end blocks to control curing temperatures and hence improve the durability of the concrete.

The findings obtained in several research projects motivated the funding of this project by TxDOT. First, a study of a new Texas I-Beam standard shape (Tx Girders) by O'Callaghan and Bayrak (2007) found that reinforcing bars installed to resist shear forces some distance into the beam were highly stressed at prestress transfer. Second, material damage observed on Houston Trapezoidal Box Beams cast in 1995 and never put into service indicated a potential mass concrete-related problem in the solid end regions of two-webbed beams (Larson, et al., 2010).

The following sections provide brief summaries of the driving concerns in this project. The discussion from here will be limited to the U-Beam half of the study; the Box-Beam study is presented in Avendaño (2011).

1.3.1 Bursting and Spalling Study

Bursting and spalling stresses are transverse tensile stresses that develop as prestressing force is transferred into a concrete beam. These stresses cause cracking in the end regions of pretensioned girders. Crack width and length are typically controlled by ordinary reinforcement.

During design development of the Tx Girder sections, experimental research on the behavior of the new sections' end regions at prestress transfer was conducted at the University of Texas at Austin (O'Callaghan and Bayrak, 2007). At prestress transfer, the cracking observed in the Tx Girders was not limited to the very end of the beam, as had typically been seen in laboratory tests and in field-fabricated beams. Instead, longitudinal cracks up to 0.010 in. in width formed, extending more than three feet ($h/2$ to $3h/2$, where h is the total height of the beam) from beam end into the main span. From strain gauges mounted on end-region reinforcement, transverse stresses were found to be in excess of the maximum design stress (20 ksi) recommended by the AASHTO LRFD Bridge Design Specifications (2010 Interim Revisions).

The high transverse stresses and extensive cracking observed in Tx Girders indicated that the pretensioned Tx Girders could benefit from additional reinforcement

provided specifically to resist stresses induced at prestress transfer. Based on the findings of the project, TxDOT design standards were revised to include additional transverse steel in the prestress transfer zone. Given these findings, detailed study of bursting and spalling in other TxDOT-standard pretensioned beams was desired to ensure acceptable end-region serviceability. A study of transverse stresses in U-Beams was thus a key issue in the development of this project.

1.3.2 End-Region Detailing Improvements

The end blocks present in U-Beams serve as diaphragms connecting the independent webs at the points of bearing. In beams with skewed ends, two alternative details shown on TxDOT standard drawings (reproduced in simplified form in Figure 1-2) impact the shape of the interior void. In one case, (A), the interior void end is perpendicular to the beam webs, leaving a large, triangular end block. For the other, (B), the interior void is skewed, significantly reducing the volume of concrete in the region.

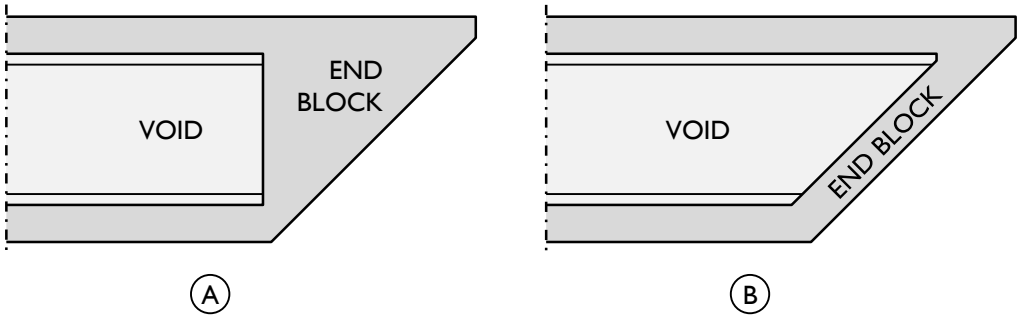

Figure 1-2: Plan views of Texas U-Beam end block configurations: (A) standard end block with square internal void, and (B) optional end block with skewed internal void.

For U-Beams, the square internal void geometry, which can result in a very large end block in highly-skewed beams, is universally chosen by precast concrete fabricators as it eliminates the need for custom internal void forms. While theoretically easier to fabricate, the large end block that comes with a squared internal void means more concrete in the end region. Large masses of concrete cause high curing temperatures. Temperatures in excess of 158°F (70°C) increase vulnerability to delayed ettringite formation (DEF). This durability problem can cause significant cracking (orders of magnitude more than would be seen at prestress transfer). One regulation set by TxDOT

in the Standard Specification (2004) to avoid this deleterious reaction is a limit on maximum temperature allowed during curing: 150°F for beams containing a straight-cement mixture, and 170°F for beams with 25% replacement of cement with fly ash. To avoid thermal cracking, which can also occur across a large block of concrete, a maximum temperature differential of 35°F is mandated in mass placements of concrete as well.

With the goal of reducing the volume of concrete used in the end region and thus reducing the curing temperatures, this project was designed to test the two current allowable internal void standards, as well as any other appropriate geometries, to confirm that reducing concrete in the end block would not negatively impact the structural performance at prestress transfer or under shear loading.

1.3.3 Shear Study

Several equations for approximating the shear capacity of a prestressed beam exist in both the ACI 318 Building Code (2008) and the AASHTO LRFD Bridge Design Specifications (2010). These equations were calibrated using the results of small-scale tests on single-webbed rectangular or I-shape beams. Prior to load-testing, it was not clear whether the strength of the Texas U-Beam, a 54-in. deep beam with two disconnected webs, could be calculated conservatively using these equations.

In current design practice, it is assumed that the two webs of the U-Beam act as one; the width of the shear area, b_w, is taken as two times the width of a single web. The flow of forces from the load point to the bearing pads is not intuitively obvious, especially in beams with significant skew. This project was designed to better understand the mechanisms of load-transfer in the U-Beam, evaluate the distribution of load between the two webs and, most importantly, confirm that the measured strength of the standard beam was in excess of calculated capacity.

1.4 PROJECT OBJECTIVES

The primary objectives of this study were as follows:

1. Determine the magnitude and extent of stresses induced in reinforcing bars at prestress transfer.

   Current provisions in the AASHTO LRFD Bridge Design Specifications (2010) state that the bars within $h/4$ of the beam end must be able to resist 4% of the prestressing force without being stressed beyond 20 ksi. While the reinforcing bar design used in each end of the eight Tx Girders tested by O'Callaghan and Bayrak (2007) came close to or met this requirement by calculation, measured stresses were much higher and extended much further into the beam. The first objective of this study was thus to determine the magnitude and extent of stresses in reinforcing bars in the end region of the Texas U54 beam.

2. Measure concrete curing temperatures in standard and skewed end blocks.

   Higher heats of hydration are expected in large masses of concrete as compared to smaller sections. It is also expected that a large mass of concrete can better resist forces caused by prestress transfer and during load-testing than a small one. By monitoring the temperature of the standard U-Beam end block and the optional skewed end block, the thermal benefit of the end block can be quantified and considered when evaluating proposed changes to the standard end block geometry.

3. Establish the vertical shear capacity of the Texas U-Beam.

   In design, the vertical shear capacity is estimated following one of several codified equations that have generally been calibrated using small, single-webbed rectangular or I-shaped beam specimens. The third objective of this research project was to measure the shear capacity of the U-Beam section and compare it to the calculated strength. These tests were designed to evaluate the effect of skew, end block geometry, and bearing condition on shear strength, as none of these variables are considered in design calculations.

4. Evaluate interaction between behavior at prestress transfer and under shear loads.
   Calculations for shear capacity assume that all anchored reinforcing bars placed between bearing point and load point can be stressed to their full yield strength, f_y. At prestress transfer, bars near beam end (theoretically, within $h/4$) will be stressed to resist the transverse force that results from the longitudinal prestressing. Depending on the location and magnitude of the stresses induced at prestress transfer, the available capacity of the reinforcing bars to resist shear loads may be decreased from f_y. By studying the Texas U-Beams at prestress transfer and while loaded until shear failure, any effects of prestress transfer on shear capacity could be evaluated.
5. Identify design and detailing improvements and recommend changes as needed.
   The final objective of this project was to present recommendations to TxDOT regarding the standard design of the U-Beam, with the goal of improving constructability, durability, and performance at prestress transfer and under loads. Of greatest benefit to this goal was the in-house fabrication of beams, which allowed the project researchers to observe potential problems and test improvements first-hand.

These five objectives were met through the fabrication and testing of eight full-scale Texas U-Beams. The details of the fabricated beams, the results gathered, and the conclusions drawn are described in this dissertation.

1.5 OUTLINE OF DISSERTATION

The details of this study on Texas U-Beams are presented in the remainder of this dissertation. To begin, relevant background on prestressed concrete U-Beams, behavior at prestress transfer, and shear testing is presented in Chapter 2. A database of specimens monitored at prestress transfer and reported in the literature and The University of Texas Prestressed Concrete Shear Database (UTPCSDB-2011) (Nakamura, 2011) are introduced and used as a basis for expected behavior at prestress transfer and under shear loads. The experimental procedures used in each phase of this study are presented in Chapter 3. The details of the beams fabricated as part of Phase I of testing are given in Chapter 4, with Phase II beams discussed in Chapter 5.

Summaries of the U-Beam test results with regard to prestress transfer, curing temperatures, and shear performance are presented in Chapter 6. A method for calculating the horizontal shear demand on and capacity of the bottom flange-to-web interface in prestressed beams is presented in Chapter 7. The method is verified using data from the literature. This dissertation finishes with Chapter 8, in which conclusions and final recommendations are given.

CHAPTER 2
Background

2.1 INTRODUCTION

An experimental test program was performed to evaluate the behavior of Texas U-Beams at prestress transfer and under shear loads. Prior to initiating the test program, relevant literature was studied, as presented here.

To begin, a brief introduction to the Texas U-Beam with details of the design and development process is given. Following is a review of the existing literature on U-shaped prestressed concrete beams. A primer on the cause of transverse stresses in the end region of a prestress beam due to prestress transfer follows; data from the literature have been gathered into a database representing typical behavior. The University of Texas Prestressed Concrete Shear Database (UTPCSDB) is introduced, and recent shear studies of interest are summarized. Three codified shear strength calculation methods are presented, with their accuracy evaluated using a subset of the data from the 2011 publication of the UTPCSDB (UTPCSDB-2011). With the knowledge gained through existing studies, a clear expectation of U-Beam behavior at prestress transfer and under shear-critical loads can be formed, which will later be compared to experimental observations.

2.2 TEXAS U-BEAM DESIGN AND DEVELOPMENT

The cross-sectional dimensions of the Texas U54 beam can be seen in Figure 2-1. The area, moment of inertia, weight, and location of neutral axis area summarized in Table 2-1. The corresponding values for the AASHTO Type IV I-Beam, a single-webbed, 54-in. deep standard highway girder, are also given. The TxDOT standard drawings for the Texas U-Beam can be found in Appendix A. The main web reinforcing consists of a single U-shaped #4 reinforcing bar that runs through each web and terminates after a 180° hook that would be embedded into a composite deck (Figure 2-2).

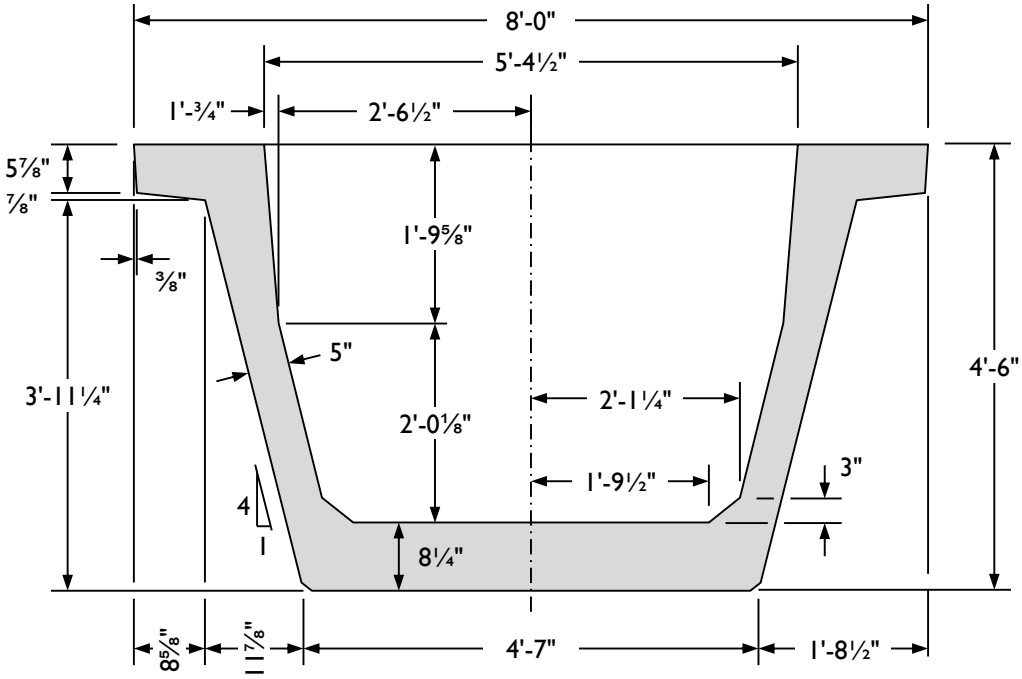

Figure 2-1: Cross-sectional dimensions of the Texas U54 U-Beam.

Table 2-1: Cross-sectional properties of the Texas U54 and AASHTO Type IV beams.

Property		Texas U54	AASHTO Type IV
Area	[in.^{2}]	1120	788
Moment of Inertia	[in.^{4}]	403,020	260,403
Distance to Neutral Axis from:			
Bottom	[in.]	22.36	24.75
Top	[in.]	31.58	29.25
Weight	[lb/ft]	1167	821

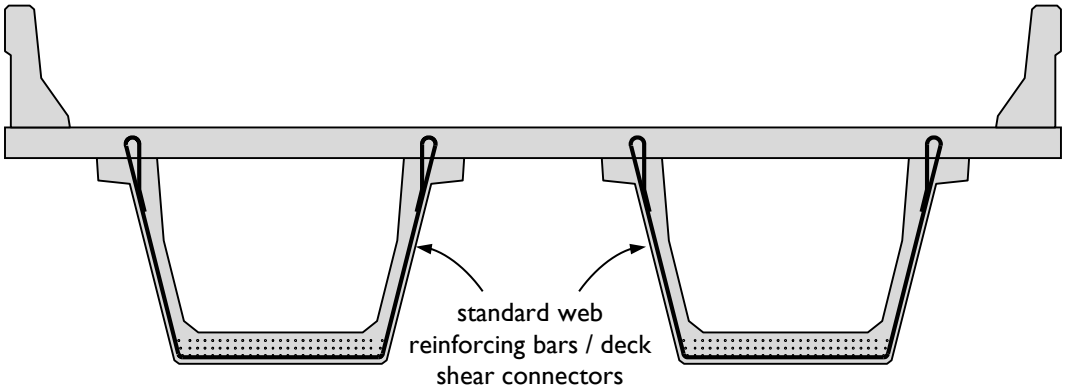

Figure 2-2: Cross section of U-Beam bridge, with standard web reinforcing bars highlighted.

The Texas U-Beam was designed with aesthetics and economy in mind (Ralls, et al., 1993). The two-webbed beam was meant to replace two I-shaped bridge girders in highly-visible settings where aesthetics are highly valued. The beam type was declared more attractive than I-Beams through the use of fewer beam lines. In terms of economy, using one beam instead of two would reduce fabrication, shipping, and erection efforts. In practice, Texas U-Beam typically replace 1.3 to 1.5 AASHTO Type IV beams (Holt, 2010).

The designers also computed the structural efficiency of the Texas U-Beam as compared to the AASHTO Type IV. Structural efficiency is defined by Guyon (1953) as:

$$\rho = \frac{I}{A y_b y_t} \qquad \textbf{Equation 2-1}$$

where

ρ = efficiency factor of section [dimensionless]

I = moment of inertia of section [in.^{4}]

A = area of cross section [in.^{2}]

y_b = distance from centroid of section to bottom fiber [in.]

y_t = distance from centroid of section to top fiber [in.]

A higher efficiency factor indicates a more efficient cross-sectional design. A rectangular section has an efficiency factor of 0.333. Given the cross-sectional properties provided in Table 2-1, the efficiency factor of a Texas U54 is 0.510 while the efficiency factor for a Type IV is 0.456. The significant size of the top and bottom flanges of the U54 increase the moment of inertia and thus the structural efficiency of the section.

In their paper, Ralls, et al. (1993) indicated that finite element analyses were performed on squared-end and skewed-end U-Beams to evaluate transportation and erection stresses. The study concluded that stresses in U-Beams were similar to those seen in I-Beam bridge girders, and no special handling was needed for this beam type. The authors also studied bearing pad options, considering using either three or four bearing pads. The three-pad design was ultimately selected, as reflected in the standard drawings.

The standard web reinforcing layout used in the Texas U-Beam was changed once since the first issuing of the drawings. A comparison of bar locations can be found in Figure 2-3 and Table 2-2. In the March 1998 plans, shear reinforcement ("R-bars") were spaced at 4 in. for almost 7 ft, at 12 in. for the next 6 ft, then at 18 in. through midspan. In the July 2006 standard drawings, the R-bars are spaced at tighter intervals further into the beam. With 3 in. between the beam end and the first stirrups, the bars are placed at 4 in. for 6 ft, at 6 in. for the next 9 ft, at 8 in. for the next 16 ft, and at 18 in. through midspan. In a 120-ft squared-end beam, the 2006 reinforcing bar layout results in the use of 160 stirrups, while the 1998 plans would use 116 stirrups.

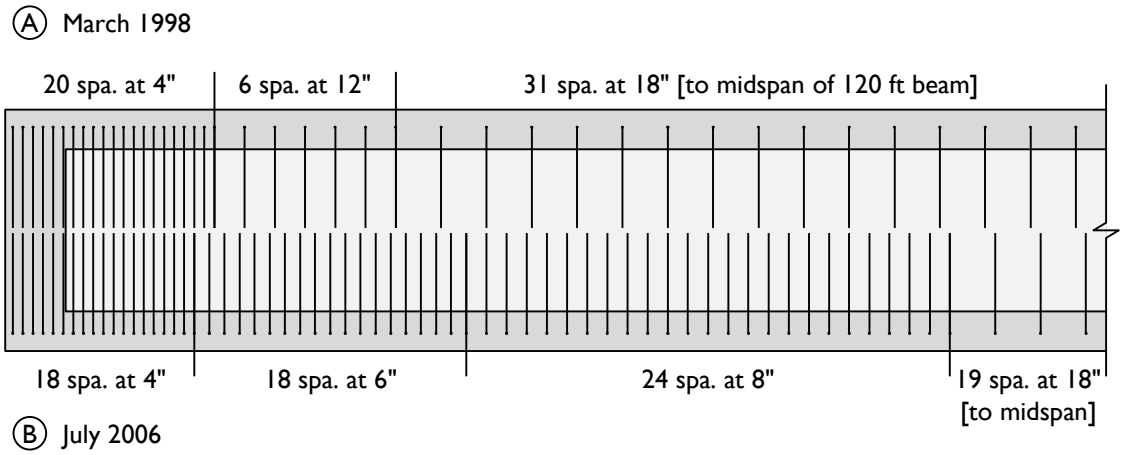

Figure 2-3: Web shear reinforcement in the Texas U-Beam per (A) March 1998 and (B) July 2006 drawings.

Table 2-2: Web shear reinforcement in the Texas U-Beam per March 1998 and July 2003 drawings.

	March 1998		July 2006	
Spacing	Distance	Number	Distance	Number
4 in.	7'-1"	21	6'-3"	19
6 in.	–	–	9'-0"	18
8 in.	–	–	16'-0"	24
12 in.	6'-0"	6	–	–
18 in.	47'-2"	31	29'-9"	19
ALL	120'-0"	116	120'-0"	160

2.3 RESEARCH ON U-BEAMS

No shear tests of full-scale U-Beams existed in the literature prior to those completed as part of this study. However, the beam type was involved in other research studies, which are described briefly here.

2.3.1 Louetta Road Overpass (1994-1998)

Soon after the Texas U-Beam standard design was introduced, two three-span bridges were built outside Houston, TX. The Louetta Road Overpass crossing Texas State Highway 249 was instrumented heavily and studied during the fabrication, erection, and early service life stages. Several aspects of the U-Beams were studied by a series of students at the University of Texas at Austin. The research projects investigated the use of High Performance Concrete (HPC) and 0.6-in. prestressing strands, the details of acceptable debonding practice in U-Beams, and the material properties of the concrete used in the beams. This final study considered the effect of hydration temperature in the large (skewed) end blocks of the bridge girders. The conclusions from these TxDOT studies are presented here.

2.3.1.1 Performance at Release (Barrios, 1994)

Barrios (1994) fabricated two full-scale U54 U-Beams specimens that were not to be put in service. These specimens were used to evaluate the behavior of the beams at prestress transfer. The variables included the debonding pattern and the presence of confinement reinforcing.

The test specimens were fabricated with seventy-two 0.6-in. prestressing strands. To reduce end-region stresses, top flange strands were included, and some of the bottom flange strands were debonded. Two confinement scenarios were used: one in which the confinement came solely from the standard web reinforcing bars (Figure 2-4(A)), and the second in which additional bars were placed to confine the strands located in the bottom flange (Figure 2-4(B)).

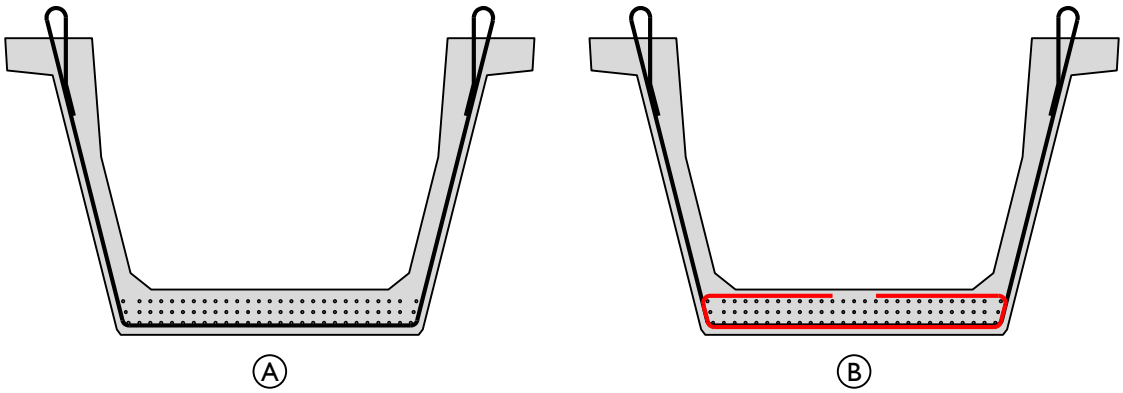

Figure 2-4: Confinement scenarios tested by Barrios (1994).

After prestress transfer, no cracking was seen in the bursting region (near the centroid of the prestressing), and very small cracks were observed in the spalling region (located just below the top flange-to-web interface). It was assumed that the stress in the extra confining reinforcement was low, and the author recommended that beams be built solely with the stirrups and without confining reinforcement in the end regions. This recommendation was accepted by TxDOT and is reflected in the current standard.

The study by Barrios did not include any load testing of the U-Beams. While confinement reinforcing was not seen to be necessary at prestress transfer, the bars could positively affect behavior during shear loading by confining the strands and delaying bond failure. When testing I-Beam specimens, Shahawy, Robinson, and Batchelor (1993) measured 10 to 20% higher failure shears in beams with confining reinforcement.

2.3.1.2 Effect of Curing Temperatures (Myers and Carrasquillo, 1998)

During fabrication of the beams used in the Louetta Road Overpass, Myers and Carrasquillo (1998) installed thermocouples in the end blocks of U-Beams, which recorded temperatures during curing. The data were used to find the maximum hydration temperature, the temperature gain during hydration, and the maximum temperature differential across a region of concrete. Further study was then conducted to determine the effect of these temperatures on concrete material properties, including concrete compressive strength.

Given the layout of the overpass in Houston, the fabricated U-Beams were significantly skewed, with skew angles between 32.6 and 39.4°. While the fabricator was given the option of building the beams with a skewed internal void (resulting in the small end block shown in Figure 1-3), the use of a square internal void was preferred and used. The resulting end blocks were quite large, and the hydration temperatures were measured to exceed 200°F in several beams, with one measuring 206°F. The temperature rise during hydration in these beams exceeded 90°F, with one measuring 110°F.

High temperatures during hydration are typically discouraged due to the association between curing temperatures and the initiation of the deleterious chemical mechanism Delayed Ettringite Formation (DEF). Ettringite, a byproduct of the hydration of cement, is not deleterious in its primary, natural state and does not pose a risk to concrete durability. Damage is caused when the temperature of the fresh (non-hardened) concrete exceeds 158°F (70°C), as at that point the ettringite dissolves into its component phases, which are trapped within the cement matrix (Bauer, et al., 2001). Over time and in the presence of water, the component parts come together to reform ettringite. As the solid ettringite is larger in volume than the component parts in solution, the reformation of the solid creates expansive forces within the concrete, and significant cracking can occur.

After observing the high hydration temperatures in the Louetta Road U-Beams, Myers and Carrasquillo (1998) measured the compressive strength of cylinders cured under varying temperature profiles. As shown in Figures 2-5 and 2-6, Myers and Carrasquillo concluded that high concrete curing temperatures and high temperature gains during curing reduced early-age and long-term compressive strength.

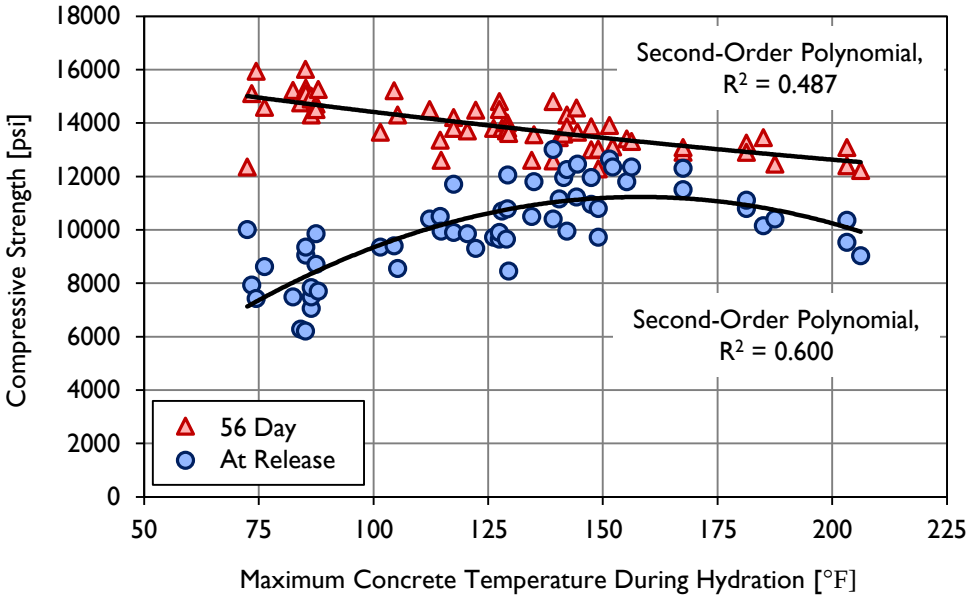

Figure 2-5: Concrete strength at release and 56 days, as related to maximum temperature during hydration (Myers and Carrasquillo, 1998).

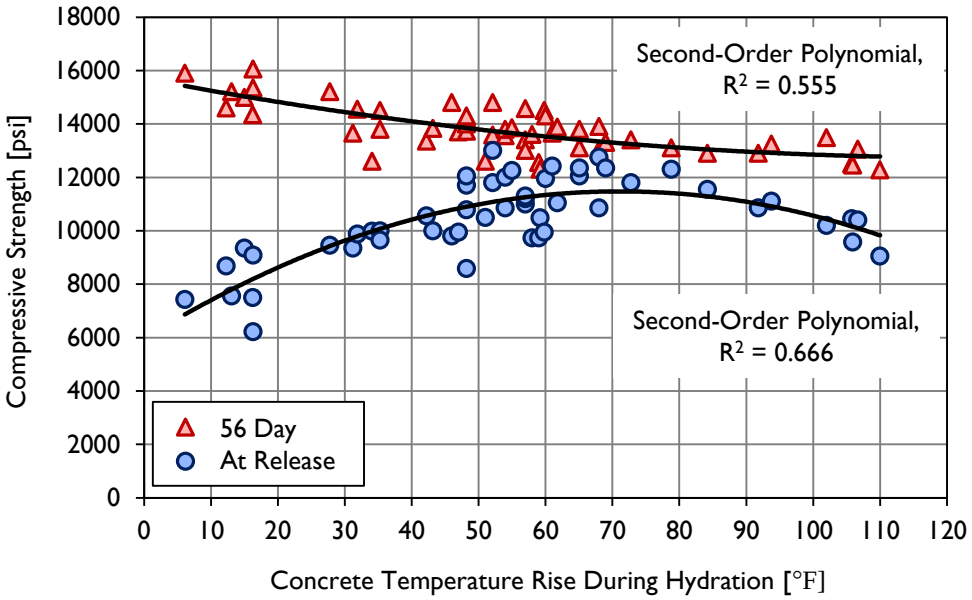

Figure 2-6: Concrete strength at release and 56 days, as related to temperature rise during hydration (Myers and Carrasquillo, 1998).

The concrete mixtures used in the Louetta Road Overpass U-Beams are very similar to those used in practice at the time of this study of U-Beams, with approximately 700 lb cement and 300 lb Class C Fly Ash used per cubic yard of concrete (Myers and

Carrasquillo, 1998). The temperature readings in the skewed end blocks should be considered typical for U-Beam fabrication, and the effect on compressive strength in the short and long term should be recognized.

2.3.1.3 Structural Performance (Gross and Burns, 2000)

The Louetta Road Overpass was studied to evaluate the performance of the new Texas U-Beam design, especially in comparison with another bridge built at the same time using AASHTO Type IV girders. Gross and Burns (2000) used the original discussion on efficiency presented in Ralls, et al. (1993) as a starting point for highlighting the benefits of the design. With a cross section larger than a typical I-Beam or Bulb-T beam of the same depth, a U-Beam can be subjected to a greater prestressing force without exceeding stress limits needed for release. This advantage was increased when High Performance Concrete was used.

A study of the stability of the U-Beam as compared to I-Beams was also presented, in which the benefit of the wide bottom flange was highlighted. Whereas rollover during transport or erection is a serious concern with I-Beams, the U-Beam is very stable.

Prior to the opening of the Louetta bridge, Gross and Burns (2000) performed a series of static live load tests using two dump trucks, positioned to replicate a single AASHTO HS20-44 truck load (Figure 2-7). The authors observed that the bridge was very stiff; deflection measurements were small enough to be close to the range of thermal noise and measurement error. Few conclusions were drawn about the performance of the beams from these tests. Similarly, Gross and Burns hesitated to use the results from the live load tests to evaluate the distribution of load between adjacent U-Beams. Observations indicated that load did not spread far from the point of application, but it was theorized that the bridge design, which included skewed beam ends, wide beam spacing, and splayed beam lines, could have influenced this behavior.

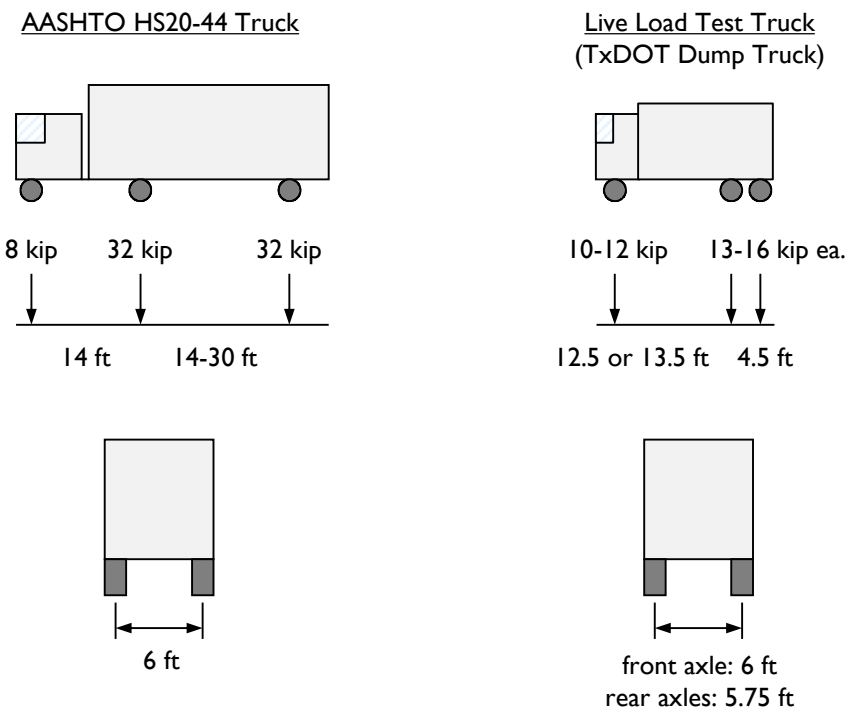

Figure 2-7: Live loading scheme used by Gross and Burns (2000).

At the end of the Louetta Road Overpass construction and the related studies, the researchers concluded that the Texas U-Beam was an efficient section ideal for use in standard highway bridges. The use of High Performance Concrete and 0.6-in. prestressing strands further increased the benefits that could be seen by using the section in lieu of standard I-Beams.

2.3.2 Huang and Shahawy (2005)

The state of Florida introduced a standard U-Beam design in 2000. The design is similar to the Texas U-Beam. During the construction of the first Florida U-Beam bridge (Figure 2-8), significant diagonal cracks were seen in the webs of the beams. Huang and Shahawy (2005) performed an analysis to identify the cause of the cracks and made recommendations for improved end-region details.

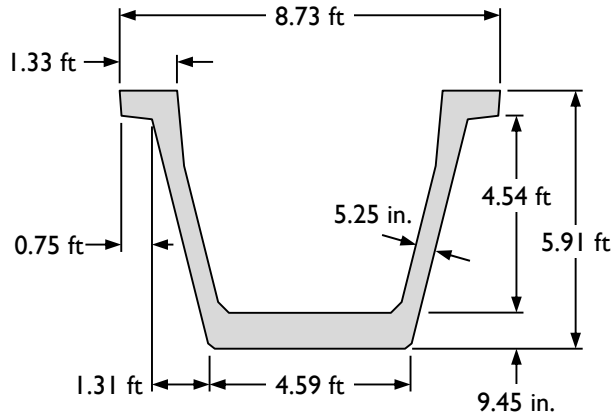

Figure 2-8: Florida U-Beam, as studied by Huang and Shahawy (2005).

The results of the analytical study corresponded well with observed crack patterns. The authors concluded that the cracks were formed by the stresses caused at prestress transfer. The recommendation was that supplementary stirrups be required in the end region to resist release forces, rather than allow those placed for live and dead load shear strength to be used for both purposes.

It is important to note that the reinforcement used in the Florida U-Beam is slightly different than in the Texas version: while the standard Texas U-Beam has #4 reinforcing bars spaced at 4 in. in the end region, this Florida beam had #5 reinforcing bars spaced at 6 in. on center. The total shear reinforcement per linear foot is approximately the same (1.24 in.^{2}/ft in Florida vs. 1.20 in.^{2}/ft in Texas).

2.3.3 Summary of U-Beam Research

Several studies in the literature have considered the performance of the Texas U-Beam. More specifically, the behavior at prestress transfer was studied during the early stages of U-Beam development by Barrios (1994). The structural behavior of one of the first U-Beam bridges in Texas was evaluated by Gross and Burns (2000); the frist U-Beam bridge built in Florida was analyzed by Huang and Shahawy (2005) after diagonal cracks were observed during fabrication. Myers and Carrasquillo (1998) took temperature measurements in the end blocks of skewed U-Beams and evaluated the effect of the temperatures on concrete compressive strength. There are no reported shear tests

of U-Beams in the literature. At the conclusion of the summarized studies, it was believed that the Texas U-Beam design was an efficient, structurally sound design that was well-suited to handle the loads (prestressing and service) for which it would be used.

2.4 BEAM BEHAVIOR AT PRESTRESS TRANSFER

Four of the Texas U-Beams fabricated as part of this research were monitored at prestress transfer to assess the magnitude and location of the induced transverse stresses. A description of the causes of these stresses and a summary of the effectiveness of codified equations as verified using data from studies in the literature is given herein.

The transfer of prestressing force into young concrete results in a complex state of stress in the end region of the beam (Figure 2-9). In typical highway beams, the prestressing force is concentrated in the bottom of the cross section. In the end region of the beam, transverse forces develop through the spreading of the longitudinal prestressing force into the full cross section. These transverse forces stress the end-region reinforcing bars and can cause cracking in regions where the tensile strength of the concrete is exceeded. More importantly for shear strength, the stress induced in the vertical reinforcing bars can reduce the capacity available for resisting vertical loads.

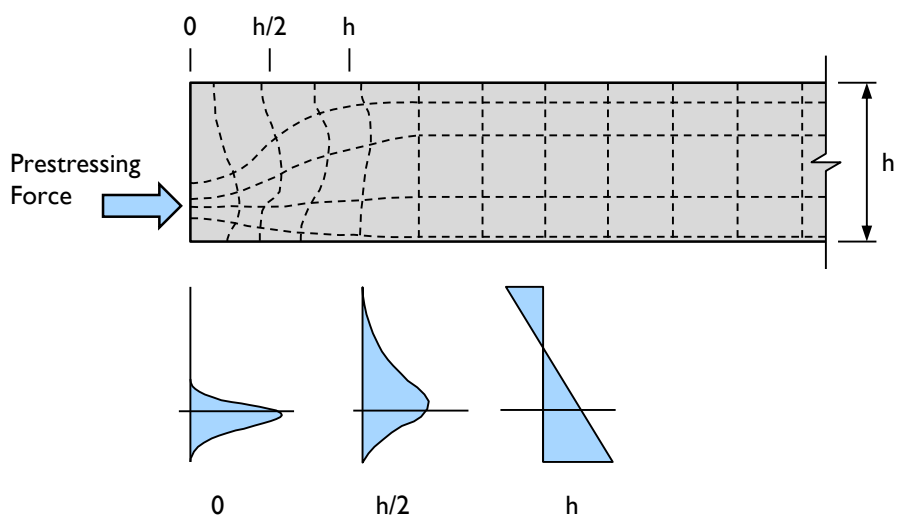

Figure 2-9: Spreading of near anchorage zone (from Nilson (1987)).

The transverse tensile stresses that are caused by prestress transfer fall into two categories: bursting and spalling stresses. The visible effect of these stresses (i.e., longitudinal cracking), are shown in Figure 2-10, with highly exaggerated deformations.

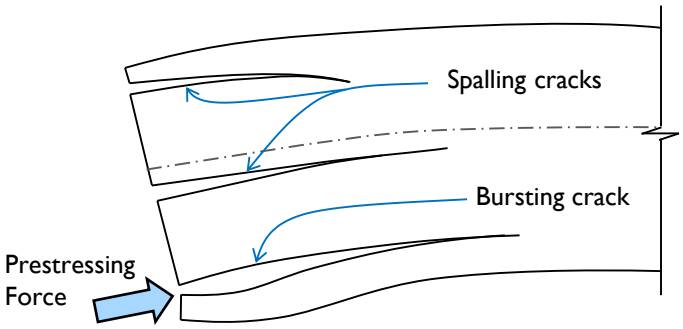

Figure 2-10: Bursting and spalling deformations (from Dunkman 2009).

Bursting stresses occur along the line of action of the prestressing force, as the prestressing force spreads from the centroid of the strands through the depth of the cross section. Spalling stresses occur away from the prestressing, primarily due to continuity. Regions of the cross section not in direct compression (e.g., near the top flange of typical highway girders) are forced to deform to remain with the stressed regions. When the bursting or spalling stresses exceed the tensile strength of the concrete, cracking results.

Codified practices regarding the transfer of prestressing in the end region of highway beams prescribe an amount of reinforcing required. The AASHTO LRFD Specifications (2010) state that 4% of the prestressing force shall be resisted by the reinforcing bars located within $h/4$ from the end of the beam, without stressing the bars beyond 20 ksi.

In 2007, O'Callaghan and Bayrak published results from a study on Tx Girders in which significant stresses were measured in reinforcing bars located well beyond $h/4$ from beam end. The study was performed on 28, 46, and 70 in.-deep Texas I-shaped beams with reinforcing bars instrumented through a distance h from each end. Strains associated with stresses greater than 20 ksi were seen in seven of the eight end regions tested, with stresses of 10 ksi being measured 36 in. or further from beam end.

As part of TxDOT Project 0-5831, Dunkman (2009) compiled a database of experimental studies on stresses induced in the end regions of prestressed beams at

transfer. The results from five studies were included in the database (Marshall and Mattock, 1962; Itani and Galbraith, 1986; Tuan et al., 2004; Crispino, 2007; and O'Callaghan and Bayrak, 2007), totaling 45 I-Beam sections and 8 inverted-T sections. The full details of these tests and the measurements made can be found in Dunkman (2009).

The data from the literature were used to evaluate the total bursting and spalling force induced in the transverse bars, as compared to the prestressing force on the section (Figure 2-11). The total force in the reinforcing bars was calculated using the maximum stress (converted from measured strain) recorded in one bar, multiplied by the area of all the bars located the same distance from the end of the beam, through $h/4$. As can be seen in Figure 2-11, several studies confirm that the requirement to resist 4% of the prestressing force is reasonable.

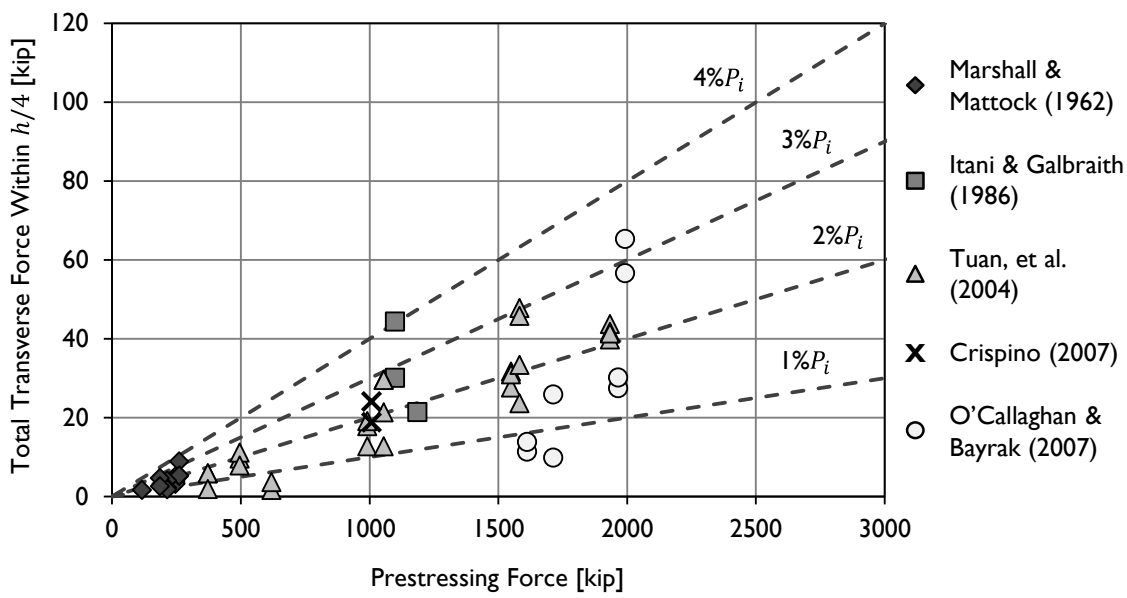

Figure 2-11: Total transverse-bar force within $h/4$ vs. prestressing force measured in previous beam tests from the literature (from Dunkman (2009)).

The total force in the end-region bars of the test specimens in the literature is shown in Figure 2-11. It should be noted that, given the calculation method, equal total forces could be found in a beam end region with very few bars, each highly stressed (poor end-region behavior) and a beam end region with many bars, each lightly stressed

(good end-region behavior). The latter case is preferred as narrower cracks are expected, reducing the possibility of serviceability problems.

In the AASHTO Specifications, there is no differentiation between average and maximum stress, indicating a linear stress profile through the end region of the beam. It was suggested by Marshall and Mattock (1962) that typical end-region behavior consists of a linearly decaying stress profile, in which the transverse stresses are a maximum at the end of the beam and decay to zero at $h/4$. In Figure 2-12, maximum and average end-region stresses are plotted and compared to three lines: the AASHTO stress limit of 20 ksi, the 1:1 ratio of a constant stress profile, and the 2:1 ratio of a stress profile associated with the linear decay model.

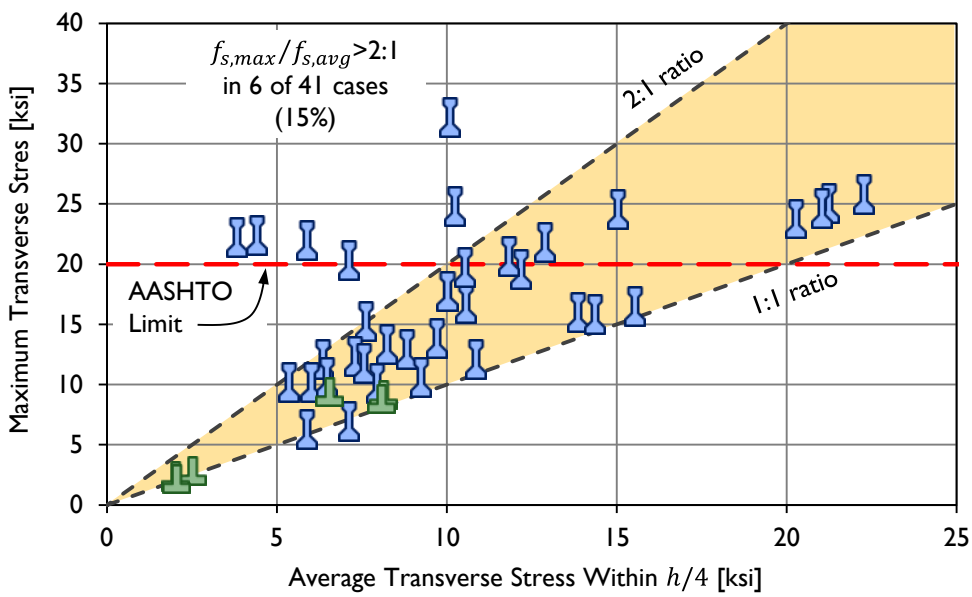

Figure 2-12: Maximum transverse-bar stress compared with average stress within $h/4$ (from Dunkman (2009)).

The majority of the specimens (85%) fall within the range defined by the 1:1 and 2:1 maximum-to-average stress ratios, implying that the true stress profile also falls between the two idealized scenarios. Maximum stresses in excess of 20 ksi were recorded in 13 of the 41 test regions (32%). At the onset of this study, it was expected that the U-Beam behavior at prestress transfer would be similar to that seen in these other studied beams.

2.5 UNIVERSITY OF TEXAS PRESTRESSED CONCRETE SHEAR DATABASE

The University of Texas Prestressed Concrete Shear Database (UTPCSDB) is a database of prestressed beam tests, collected from literature dating from 1954 to 2010, compiled by Avendaño and Bayrak (2008) and expanded by Nakamura (2011). There are currently a total of 1688 data points from studies conducted in the United States, Europe, and Japan[1]. The Database has been used to evaluate the accuracy of prestressed concrete shear strength calculation methods. It is expected that the accuracy of these equations, when applied to the Texas U-Beams, would fall within the ranges seen through the existing tests in the literature. The plots in this section were prepared using the data from the UTPCSDB-2011.

2.5.1 Significant Recent Studies

Four of the studies in the UTPCSDB-2011 are of particular relevance to the U-Beam research at hand, and are described briefly in this section.

2.5.1.1 NCHRP 579 / Nagle & Kuchma (2007)

As part of a National Cooperative Highway Research Program (NCHRP) series of projects, twenty shear tests were completed on ten 63-in. AASHTO/PCI Bulb-T beams at the University of Illinois. The primary goal of the NCHRP study was to evaluate the use of high-strength concrete in shear calculations, in which f'_c is currently limited to 10 ksi. The 52-ft long beams were decked prior to shear testing and loaded through a series of hydraulic actuators placed to represent a distributed loading scenario.

Using the same data, Nagle and Kuchma further studied the NCHRP beams, and presented their conclusions separately from the full NCHRP report. The 2007 paper discussed here is focused on understanding the observed behavior in the end regions of the tested beams, where sectional shear calculations ($V_c + V_s$) were deemed inappropriate.

[1] Nakamura (2011) reports 1696 data points; this number includes eight U-Beam shear tests that will not be considered in this chapter and have thus been excluded from the discussion. The subset databases have been similarly modified.

The shear failures of the bulb-T beams showed one or more of the following six characteristics: (i) diagonal crushing without yielding shear reinforcement, (ii) diagonal crushing with yielding of shear reinforcement, (iii) yielding and rupture of shear reinforcement, (iv) distributed diagonal crushing, (v) shear failure at the web/bulb interface, and (vi) strand slip. Of particular interest to this study are the beam specimens that failed at the web/bulb interface, referred to by Nagle and Kuchma as shear compression failures due to observed crushing of the web near the top of the bulb at failure. In several cases, significant sliding of the web relative to the bottom flange (on the order of two to six inches) was observed, as pictured in Figure 2-13.

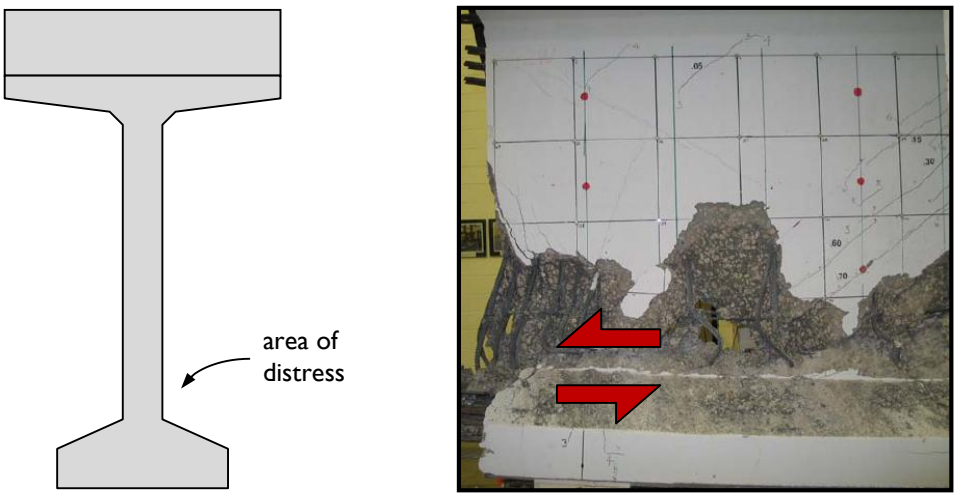

Figure 2-13: Horizontal sliding failure mode seen in several of the BT-63 specimens tested by Nagle and Kuchma (2007).

The authors proposed a method, based on the mechanics of strut-and-tie theory in the end region of a beam, for determining the strength of the bottom flange-to-web interface in prestressed highway beams. The calculation compares the horizontal shear demand in the end region to the capacity of the longitudinal reinforcement available to resist the horizontal loading.

To begin, consider the end region of the beam, as illustrated in Figure 2-14(A). The authors assumed that a direct strut came in to the support at an angle α, taken as 40° for the NCHRP beam tests. The angle α is related to the orientation of the principal compressive strain originating from the support. The magnitude of horizontal shear force

on the bottom flange-to-web interface is equal to the horizontal component of the diagonal force C, where the vertical component is equal to the reaction force.

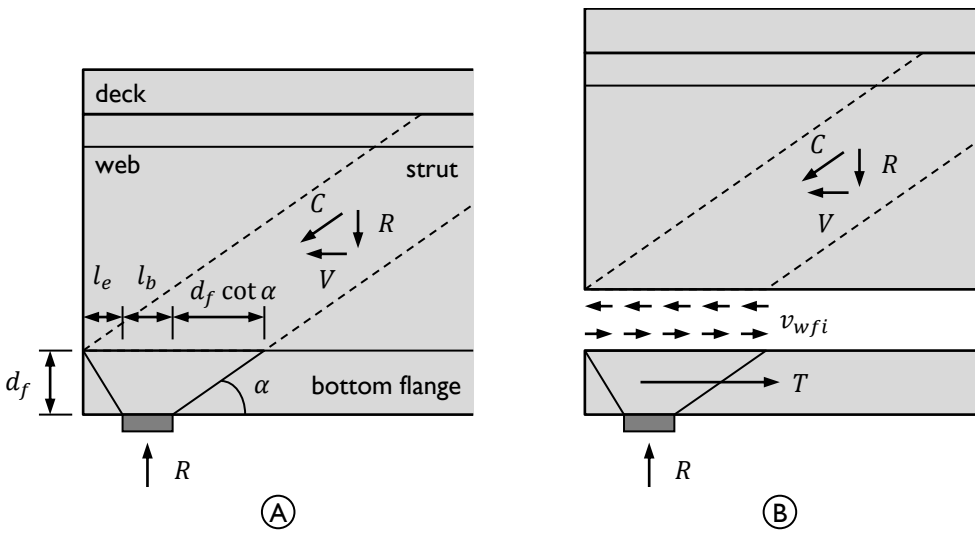

Figure 2-14: End region of the beam model used by Nagle and Kuchma (2007) showing (A) dimension definitions and (B) location of horizontal shear stress.

Nagle and Kuchma (2007) calculated the horizontal shear stress acting along the bottom flange-to-web interface (shown in Figure 2-14(B)) as:

$$v_{wfi} = \frac{R \cot\alpha}{t_w s}$$ **Equation 2-2**

where

v_{wfi} = horizontal shear stress along web-flange interface [ksi]

R = reaction force (shear load) [kip]

α = angle of principal compressive stress, taken as 40°

t_w = thickness of the web [in.]

s = length of the strut along a line parallel to the longitudinal direction of the girder, at the web-flange interface over the support, as shown in Figure 2-14 [in.]

= $l_e + l_b + d_f \cot\alpha$

l_e = distance from beam end to the back face of the bearing pad [in.]

l_b = length of the bearing pad [in.]

d_f = distance from tension flange to critical interface [in.]

The authors stated that if v_{wfi} is below 30% of f'_c, a shear compression failure is unlikely. In cases where the horizontal stress exceeds 30% of the concrete compressive strength, further calculations should be performed.

To begin, the horizontal shear demand is translated from a stress (v_{wfi}) to a force (V_{wfi}) by multiplying by the area, $t_w s$:

$$V_{wfi} = R \cot \alpha \qquad \textbf{Equation 2-3}$$

This horizontal force must be resisted by the reinforcing bars and prestressing strand in the bottom flange of the beam (Figure 2-14(B)). The tensile capacity is defined as:

$$T = A_{psf} f_{se} + A_{st} f_y \qquad \textbf{Equation 2-4}$$

where

T = capacity of the longitudinal tensile reinforcement [kip]

A_{psf} = total area of fully bonded prestressing strands located in the bottom flange [in.^{2}]

f_{se} = effective prestress, after consideration of all losses [ksi]

A_{st} = total area of horizontal reinforcement located in the bottom flange and anchored over the support [in.^{2}]

f_y = yield stress of horizontal reinforcement [ksi]

When the horizontal shear demand exceeds the tensile capacity, a strand slip failure is expected. When the tensile capacity of the longitudinal reinforcement exceeds the horizontal shear demand, the likelihood of a shear compression failure increases.

The final step performed by Nagle and Kuchma was a calculation of the remaining capacity in the bottom flange-to-web interface, which was found by determining the distance from the support to the first flexural crack. The authors compared their calculations for the location of that crack to observations during testing to confirm the accuracy of their method.

It should be noted that the success of this calculation method is highly contingent on the selection of the angle of principal compressive strain, α. It was stated by the

authors that a change of two degrees can change the calculated stress by 8%. The angle used in their study was so chosen from the results of high-level analyses performed during testing. As these computations are not available in all laboratory tests, nor in design, it is difficult to use this same method in generalized manner as would be needed for codification or even confirmation of other laboratory tests.

2.5.1.2 Hamilton, Llanos, & Ross (2009)

This study involved three types of prestressed bridge girders: AASHTO Type IV, AASHTO Type III, and post-tensioned girders from the 1950s. The first test group is relevant to the discussion at hand.

The AASHTO Type IV girders are of interest due to the unique failure mode observed at ultimate load. Many strands under the web of these beams were debonded at the end of the beam. The authors concluded that the debonding pattern forced a transverse spreading of load in the bearing region, causing the sides of the girder to crack and spall at failure. A simple strut-and-tie model of the end region of the beam illustrates how the transverse force formed above the bearing (Figure 2-15).

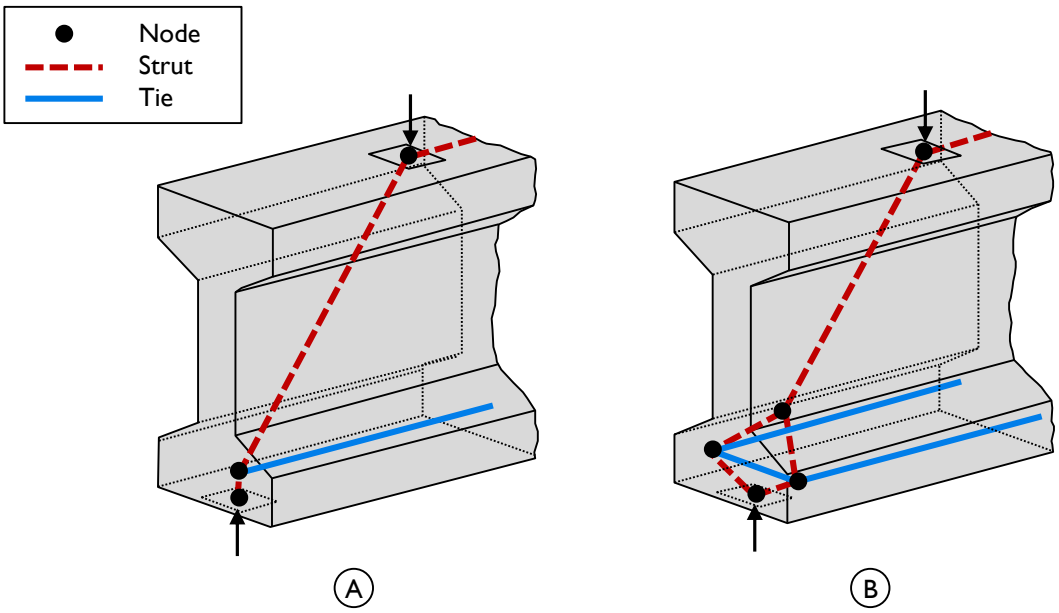

Figure 2-15: Strut-and-tie model for beam with (A) fully bonded tendons and (B) significant numbers of unbounded tendons located beneath the web (from Hamilton, Llanos, and Ross, 2009).

Unlike in I-Beams and Bulb-T beams, the strands in U-Beams cannot be harped to reduce the stresses at time of prestress transfer. To prevent significant cracking in the end regions, strand debonding is typically used by TxDOT. Up to 75% of the strands bonded at the midspan of a U-Beam can be debonded at the end. Current state debonding practice, however, requires that the strands in column 2 (the second column from the outside, closest to the webs) be debonded prior to the innermost strands. The work presented by Hamilton, Llanos, and Ross indicated that the transverse forces required to transfer load from the web to the bonded strands in the end region could be seen in Texas U-Beams with debonded strands, as well.

2.5.1.3 Tx Girder Shear Study

In 2008, Avendaño and Bayrak published the results of four shear tests on Tx28 I-Beams. The test specimens, loaded with a single point load at a shear span-to-depth ratio of 2.9 or 3.8, were able to support shear loads well in excess of the calculated vertical shear capacity for the section. However, the observed failure mode of these test specimens was not typical web-shear. Instead, the failure crack ran horizontally along the bottom flange-to-web interface, in a similar manner to that seen in the Nagle and Kuchma (2007) study, but with significantly less damage to the section (Figure 2-16). These failures suggest that a horizontal shear failure can occur along the bottom flange-to-web interface without the significant crushing seen by Nagle and Kuchma.

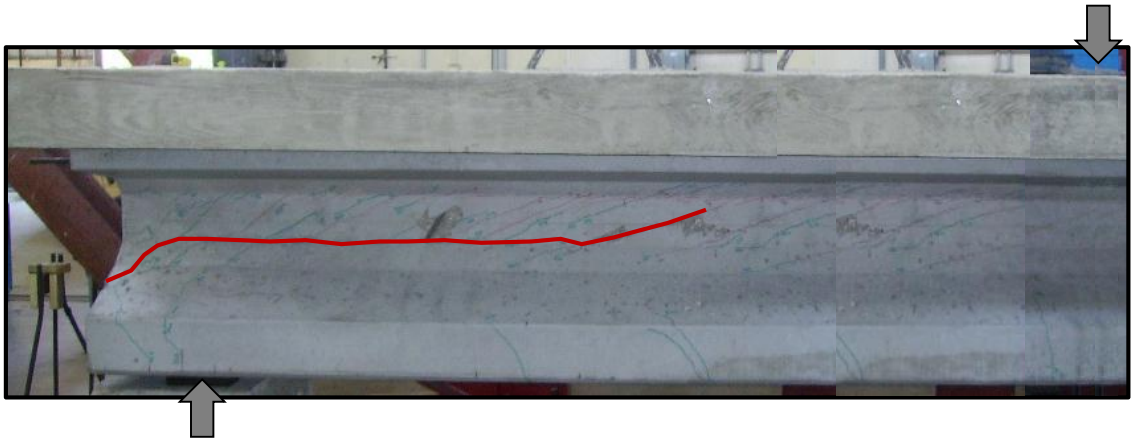

Figure 2-16: Tx28 after shear testing, with horizontal failure crack highlighted.

Three additional shear tests were performed on two Tx Girders (46- and 70-in. deep) in 2010 at Ferguson Structural Engineering Laboratory. These beam sections also failed at shear loads in excess of the shear capacity, calculated using the AASHTO LRFD General Method (2010). The failure mode observed was similar to that seen in the Tx28 test specimens: horizontal cracking along the bottom flange-to-web interface and sliding of the web relative to the bottom flange, visible at the ends of test specimens Tx46-S and Tx70-N (Figure 2-17).

Figure 2-17: Horizontal shear damage visible in specimens (A) Tx46-S and (B) Tx70-N.

The Tx Girder study was initiated to confirm the web-shear strength of this relatively new family of bridge girders. The data were also used to better understand the demands on the bottom flange-to-web interface and estimate the strength of that joint, as is discussed in detail in Chapter 7 of this dissertation.

In Chapter 7, it is explained that the amount of steel crossing the bottom flange-to-web interface (ρ_{int}) is directly correlated to the strength of the interface. The Tx Girders designs that were tested in 2008 and 2010 have approximately 5.0 in.^{2} of transverse reinforcing bars per linear foot of beam in the end region (ρ_{int} = 6%). The Texas U-Beam standard design has 1.2 in.^{2} of reinforcement per foot (ρ_{int} = 1%). Given the results of these Tx Girder tests, the chance of a horizontal sliding shear failure in Texas U-Beams is high.

2.5.1.4 Texas Box-Beam Shear Study

Two series of tests on Texas Box-Beams were conducted concurrently with the Texas U-Beam study presented in this dissertation. In the first, ten Texas 4B28 two-webbed box-beam girders were fabricated and tested, resulting in twenty individual shear tests (Avendaño, 2011). The standard beam cross section can be seen in Figure 2-18.

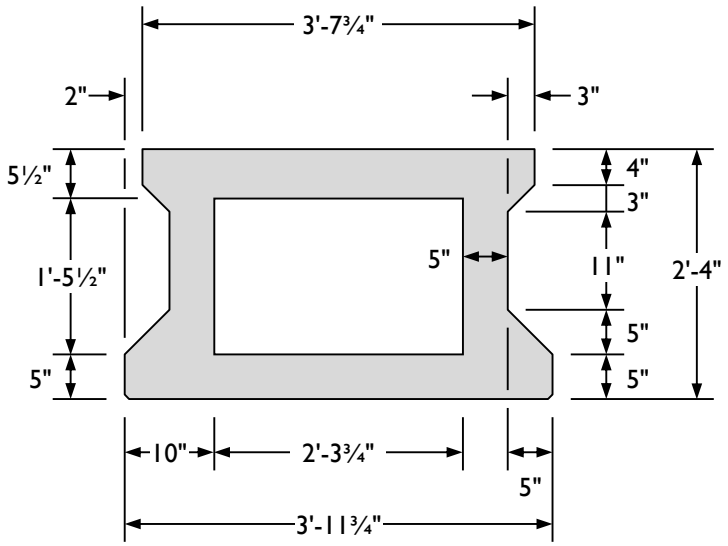

Figure 2-18: Cross-sectional dimensions of the Texas 4B28 tested by Avendaño (2011).

Like the Texas U-Beam, the Texas Box-Beam design has two webs that are considered to act as one integral web for the purposes of shear strength calculations. The webs are actually only connected at discrete points along the length, the most substantial for shear design being at the beam end, where the standards call for an end block at least 16 in. in length. Unlike the U-Beam, these beams are most commonly used side-by-side, with transverse post-tensioning and grout filling the space between the beams (Figure 2-19).

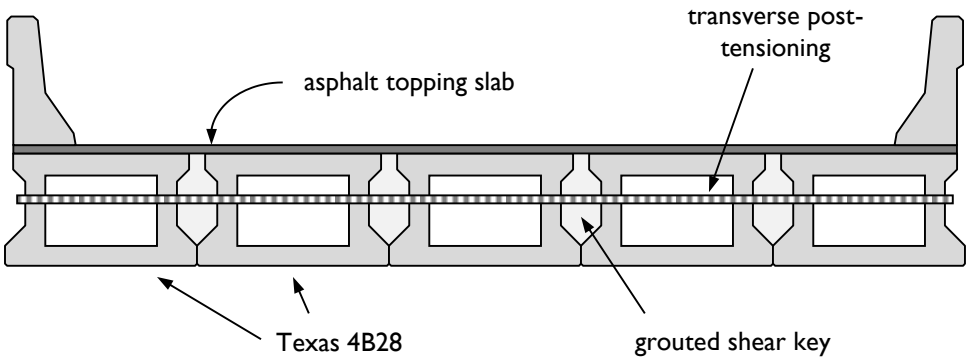

Figure 2-19: Typical layout of Texas 4B28s in service.

These beams were fabricated with the goal of studying the same variables in consideration for the U-Beam study. One end of each beam was skewed to 30° while the other was squared. The shear span-to-depth ratio was 2.9 or 3.4. Besides skew angle, the test variables included geometry of the internal void of the box beam (squared, skewed, or combined half-skew / half-square), the bearing condition (one or two bearing pads), and the type of concrete used (conventional concrete or self-consolidating concrete, each made with river gravel or crushed limestone). Plan views of the four end regions tested are given in Figure 2-20.

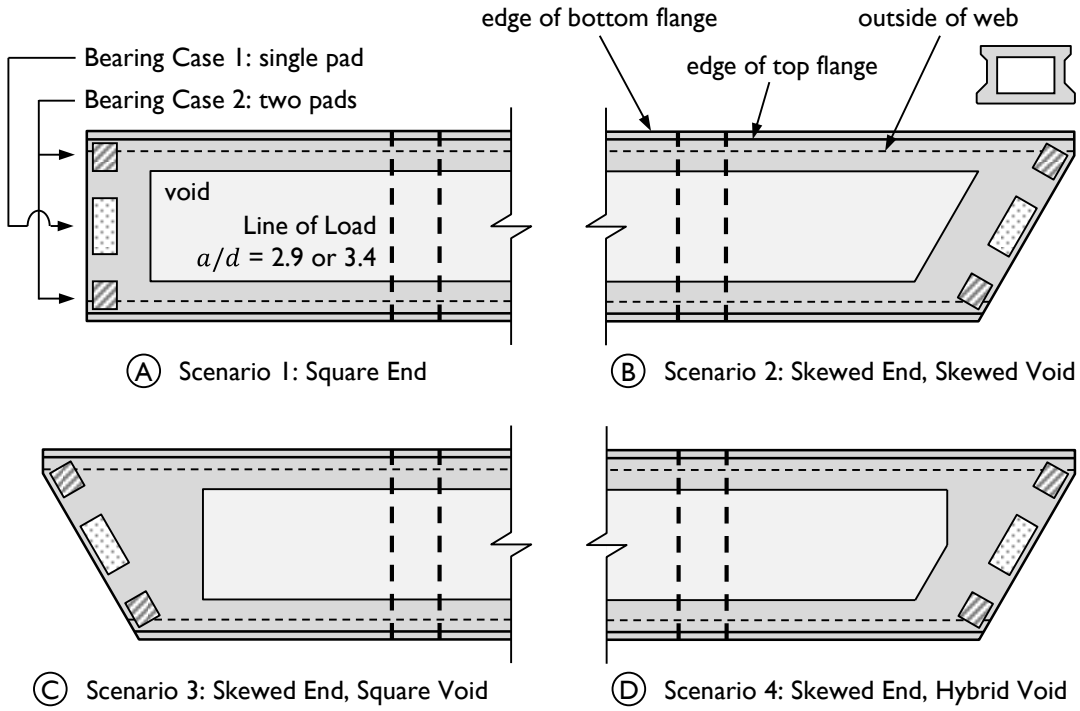

Figure 2-20: 4B28 loading scenarios used by Avendaño (2011).

Across all twenty shear tests, the failure shear exceeded the calculated shear capacity using shear capacity calculation methods provided in the ACI 318 Building Code (2008) and the AASHTO LRFD Bridge Design Specifications (2010). The failure mode was described by the authors as combination of one or more of three phenomena: (i) crushing of the diagonal compressive strut, (ii) yielding of the shear reinforcement, and (iii) straightening of a bent web reinforcing bar that was in tension, causing significant spalling in the web. The variables that influenced the failure shear the most were the concrete mixture design and aggregate type.

Several conclusions were made by the authors; those of particular importance to this study are summarized here:

- Bearing condition did not influence shear strength. The test specimens supported on a single bearing pad and those supported on two bearing pads did not show significant differences in measured strength. As the calculations for capacity do not consider this detail of bearing condition, the shear performance metric (V_{test}/V_n) was not significantly different either.

- The strength of two webs was appropriately estimated by combining the width in calculations. In shear calculations, the magnitude of b_w in two-webbed beams was found by adding the widths of the webs and treating the beam like an I-shaped section. During testing, the applied load distributed through the two webs, and ultimately one web failed while the other remained relatively undamaged. Treating the two webs like one in calculations consistently yielded conservative estimates for shear strength of the 4B28 beams tested.
- The shape of the interior void in the skewed ends did not influence strength. Three interior void shapes were tested, and as with the varied bearing condition, no significant difference was seen in measured strength when comparing the different test groups.

It is reasonable to assume these same conclusions would apply to other two-webbed beams, such as the Texas U-Beam.

Avendaño (2011) also tested four larger box-beams, Texas 5B40s (Figure 2-21). These beams were also fabricated and tested under the same test program from which this U-Beam study was funded. The major test variables were the same as those intended for the U-Beam study and considered with the Texas 4B28 beams: bearing condition, skew, and interior void geometry (Figure 2-22).

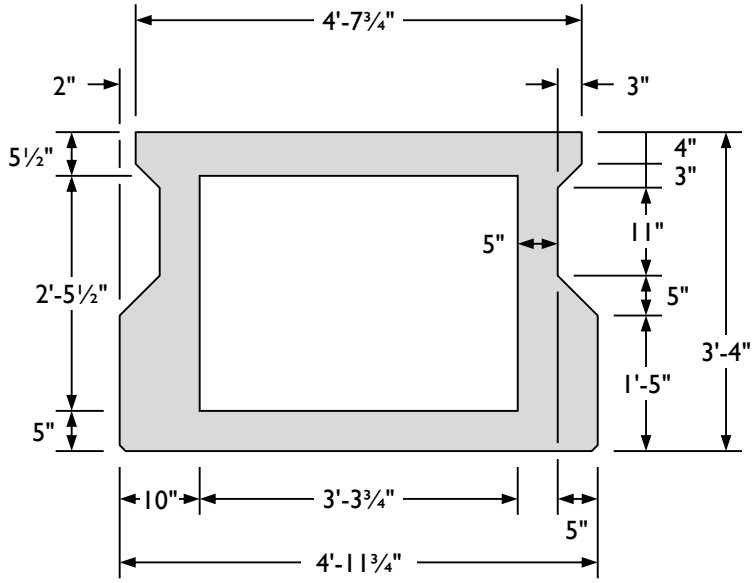

Figure 2-21: Geometry of 5B40 Texas Box-Beams tested by Avendaño, et al. (2011).

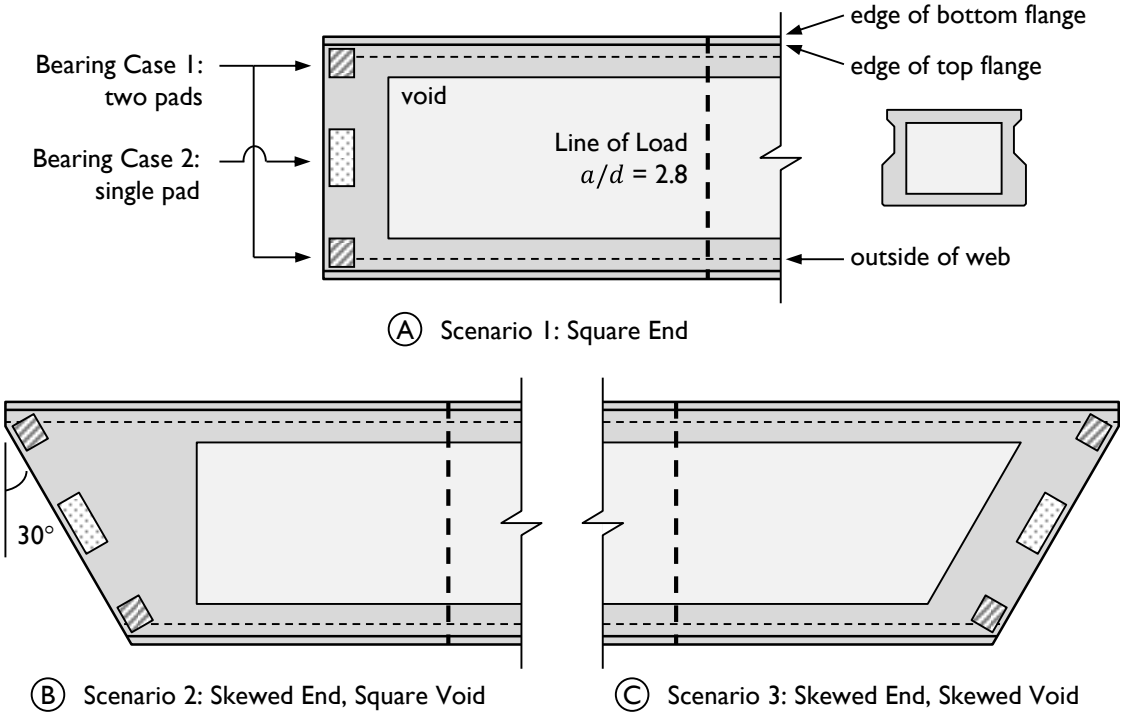

Figure 2-22: 5B40 loading scenarios used by Avendaño (2011).

The detailed results of this box beam study can be found in Avendaño (2011). The relevant conclusions available at publishing of this dissertation match those found in

the 4B28 study: bearing condition, internal void geometry, and the presence of two webs did not significantly affect the observed shear strength of the test specimens.

It should be noted that some horizontal shear damage was seen at failure of the 5B40 test specimens. While the beam failure was driven by a weakness in the end region, minor horizontal sliding was seen between beam end and load point (Figure 2-23). More significant to beam behavior, however, was the observed web crushing and, in one test specimen, bottom flange shearing. As in the study of Texas 4B28 beams, the failures occurred in one web. Damage to the end block of the 5B40s showed how one web moved longitudinally with respect to the rest of the beam (Figure 2-23).

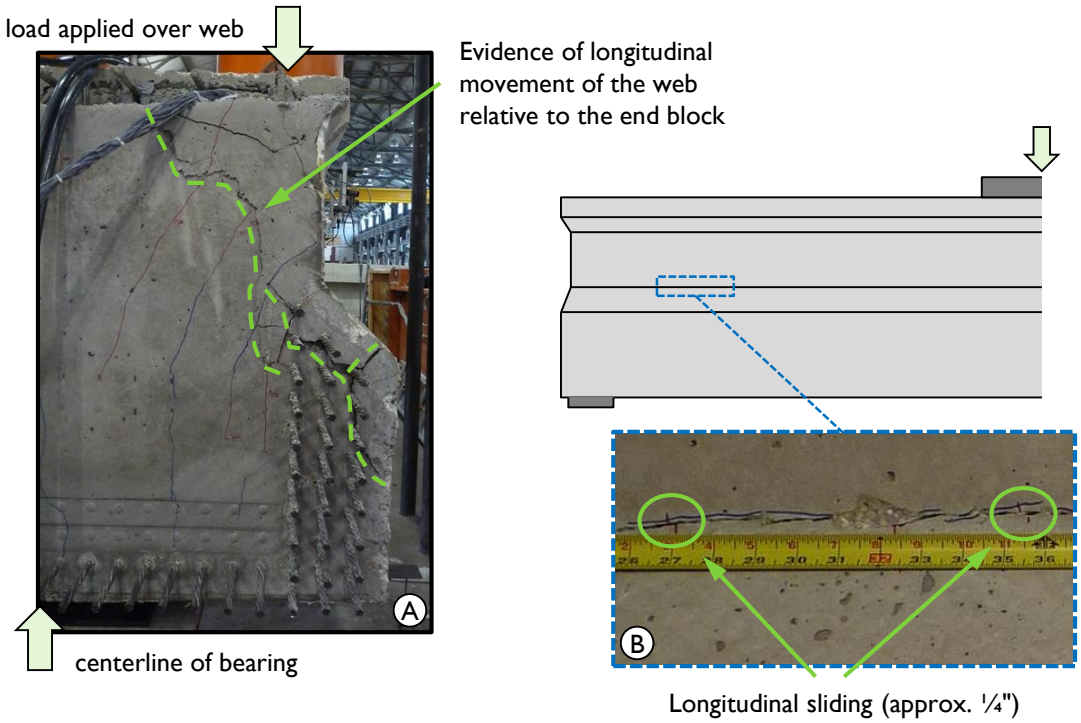

Figure 2-23: (A) Failure of the end block of specimen 5B40-3-Q, as tested by Avendaño (2011), with longitudinal sliding visible (B).

2.5.2 Collection, Filtered, and Evaluation Databases

Four databases made from the UTPCSDB-2011 were prepared by Nakamura and are used for analysis and discussion here. The first is the full Collection Database, which includes all 1688 data points. The Collection Database was reduced to 1146 data points (the Filtered Database) by removing tests with (i) incomplete test information available,

(ii) initial defects in the member, (iii) moving loads, (iv) no prestressing, and (v) observed failure modes not consistent with shear failure.

The Evaluation Database-Level I was formed by including tests points only when the following additional conditions were met:

- member depth greater than 12 in.,
- made from conventional concrete with a 28-day strength greater than 4.0 ksi,
- tested at a shear span-to-depth ratio greater than 2.0,
- contained at least the minimum shear reinforcement per ACI (2008) and AASHTO (2010) requirements,
- simply supported beams (no segmental sections), and
- prestressed or post-tensioned internally.

The Evaluation Database-Level I consists of 216 data points. These data points were chosen for use in evaluating the accuracy of the various existing design provisions. Each of these test points failed in one or more of the following seven ways: (i) shear failure, (ii) flexural-shear failure, (iii) web-crushing failure, (iv) shear-compression failure, (v) shear-tension failure, (vi) shear failure with signs of horizontal shear damage, and (vii) shear failure with signs of anchorage zone distress. Further description and pictures of these failure modes can be seen in Nakamura (2011).

The first five failure modes are considered traditional, well-understood shear failure modes, for which the design equations were written and calibrated. The final two failure modes – shear with signs of horizontal shear damage and with signs of anchorage zone distress – are not as well understood, and the author of the database was unsure if the code equations were appropriate for use in these specimens.

To remove this uncertainty, one final subset was made: the Evaluation Database-Level II, in which each specimen failed in a traditional shear-failure mode (Nakamura, 2011). A total of forty-six tests were removed from the Level I database: 30 that showed signs of anchorage zone distress, and 16 that had signs of horizontal shear distress. The remaining 170 tests constitute the UTPCSDB-2011 Evaluation Database-Level II.

2.5.3 Characteristics of Test Specimens in Literature

The characteristics of the reported prestressed shear test specimens can be studied using the Filtered Database from the UTPCSDB-2011. Presented characteristics include beam shape, specimen depth, compressive strength of concrete, shear span-to-depth ratio, shear area, reinforcement ratio, and bottom flange-to-web width ratio.

2.5.3.1 Beam Shape

The distribution of tested beam shapes in the literature is given in Figure 2-24. In the 1138 relevant tests found in the literature, not a single shear test was performed on a U-Beam bridge girder. Nineteen of the 23 tests on box-beams, the only two-webbed beams in the database, were performed at the University of Texas in conjunction with this study on U-Beams.

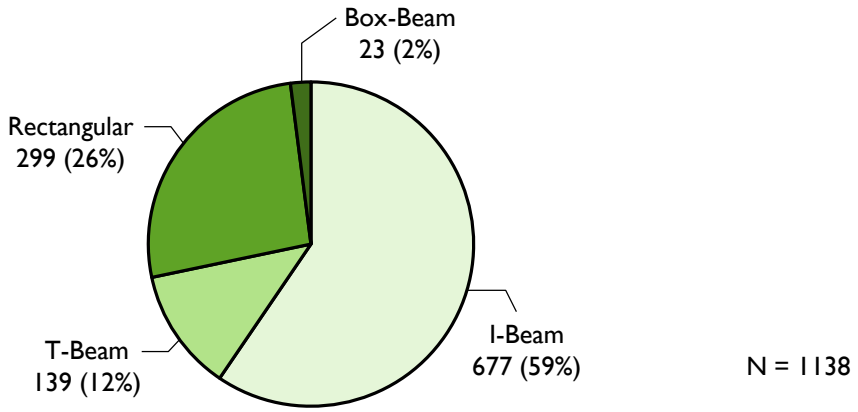

Figure 2-24: Distribution of beam shapes in UTPCSDB-2011 Filtered Database.

Given the number of bridges with U-Beam girders in service in Texas, and the increased use of the same or similar beam shapes across the country, it is necessary to confirm the capacity of these bridge girders is as expected (i.e., in excess of calculated capacities).

2.5.3.2 Specimen Depth

The distribution of specimen depth as found in the literature is shown in Figure 2-25; 50% of the test specimens in the Filtered Database are less than or equal to 12 in. deep.

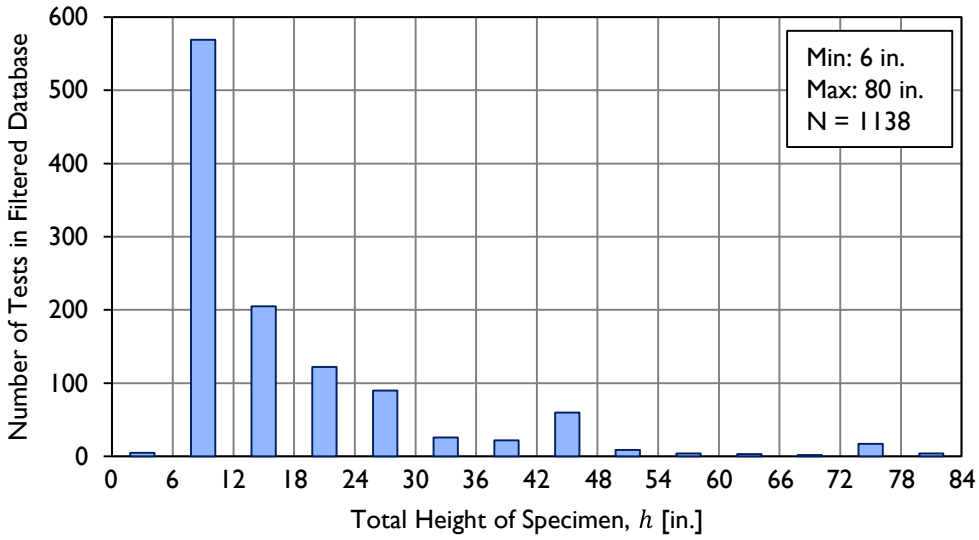

Figure 2-25: Distribution of specimen size in the UTPCSDB-2011 Filtered Database.

The Texas U-Beams tested in this study are 54 in. deep, and were decked as in the field with an 8-in. cast-in-place deck. The specimens studied herein will represent some of the largest beams reported in the literature; less than 3% of the tests in the UTPCSDB-2011 are greater in depth than 62 in.

2.5.3.3 Compressive Strength of Concrete

When the current prestressed concrete shear equations were developed in the 1950s, typical concrete strengths were less than 6.0 ksi. Since then, high performance, high-strength concretes have become commonplace, as these concrete mixtures allow for higher prestressing forces in beams and increase the flexural and shear capacities. The distribution of concrete strengths used in beams in literature is given in Figure 2-26.

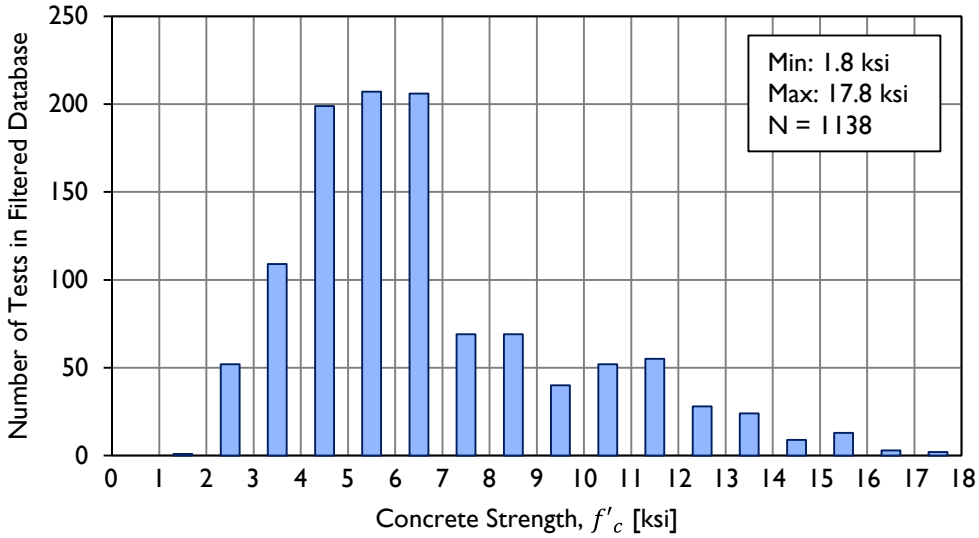

Figure 2-26: Distribution of concrete compressive strength in the UTPCSDB-2011 Filtered Database.

A study of production drawings for eighty Texas U-Beam designs used in beams currently in service indicated that typical design 28-day strengths are in the range of 5 to 10 ksi. The beams fabricated in this study had compressive strengths in excess of 11.0 ksi at the time of shear testing.

2.5.3.4 Shear Span-to-Depth Ratio

Shear behavior in prestressed concrete beams is highly related to the distance between the load point and the support. This metric is quantified using the shear span-to-depth ratio (a/d); the distribution of shear span-to-depth ratios found in the literature can be seen in Figure 2-27.

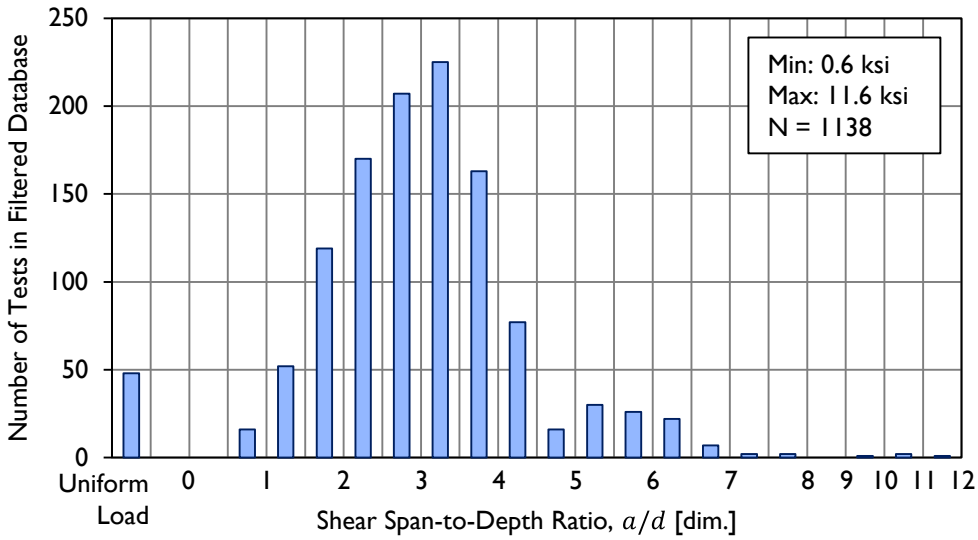

Figure 2-27: Distribution of shear span-to-depth ratios in the UTPCSDB-2011 Filtered Database.

Sectional design methods are intended for use when planar behavior is expected, generally defined to be beyond $2.5d$ from the support ($a/d \geq 2.5$). The shear span-to-depth ratios used during this U-Beam test program were 2.6 and 3.0.

2.5.3.5 Shear Area

In each shear capacity equation discussed in the next section of this chapter, there is a direct correlation between the shear area ($b_w d$) and the calculated shear capacity of the section. As previously stated, these design equations were validated using primarily small-scale specimens, which have small depths and narrow web widths, resulting in a low shear area. Given that many design equations were verified at a time when only small specimens were available, there is a possibility that the equations for shear will not appropriately estimate strength of larger beam members.

The large number of specimens with small shear area that exist in the literature can be seen in Figure 2-28. Almost 60% of the reported specimens have a shear area less than 50 in.^{2}.

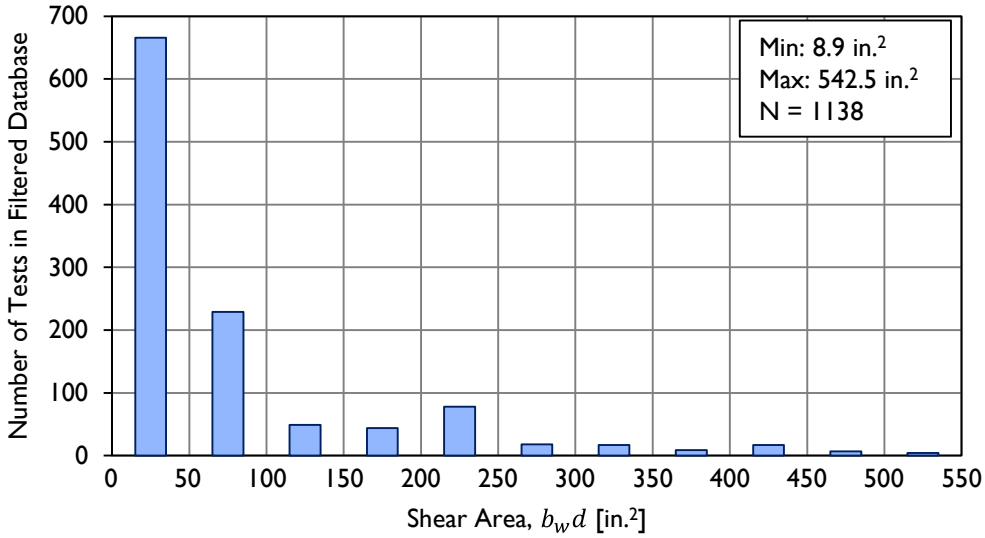

Figure 2-28: Distribution of shear area in the UTPCSDB-2011 Filtered Database.

The data presented in Figure 2-28 are repeated in Figure 2-29, with the average and maximum shear areas found plotted against the year in which the data were published. In the past two decades, the size of specimens has increased significantly, with the majority of tests being run on full-scale prestressed beam girders.

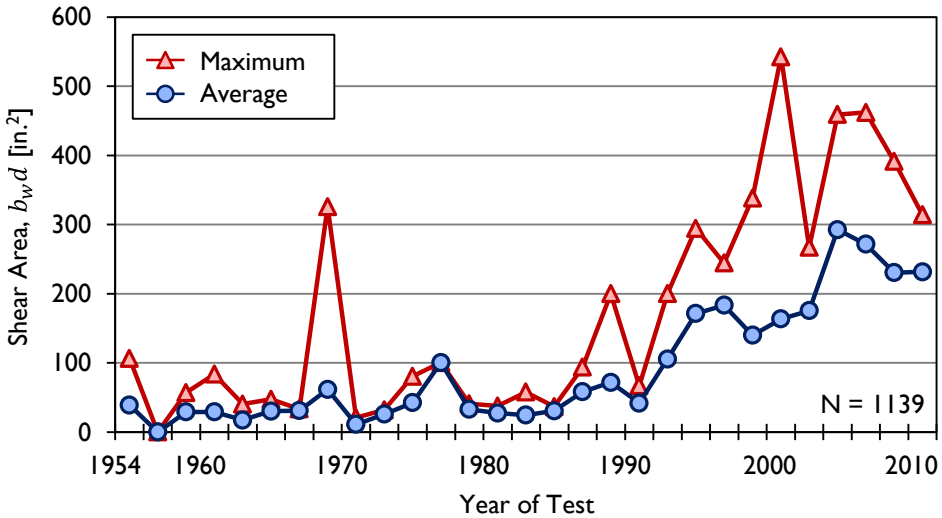

Figure 2-29: Increase in shear area of tested specimens through time (from Nakamura (2011)).

Even with the recent increase in shear area of typical beam tests, the Texas U-Beams involved in this study have a larger shear area than any other test found in

literature. The standard beam section, with three full rows of ½-in. prestressing strands in the bottom flange, has a shear area of 605 in.^{2}. One beam was fabricated with wider web walls, and the resulting test specimens (B4N and B4S) have shear areas of 940 in.^{2}, almost 75% larger than any other specimen in the literature.

2.5.3.6 Reinforcement Ratio

The amount of shear reinforcement in a prestressed concrete beam has a direct influence on the calculated strength of a beam and the expected behavior. While there are 1138 reported prestressed concrete shear tests in the literature considered in the Filtered Database, about half of those test specimens do not contain any shear reinforcing (Figure 2-30). Of the specimens that remain, 31% have a reinforcement ratio ($\rho_v f_y$) less than 0.25 ksi.

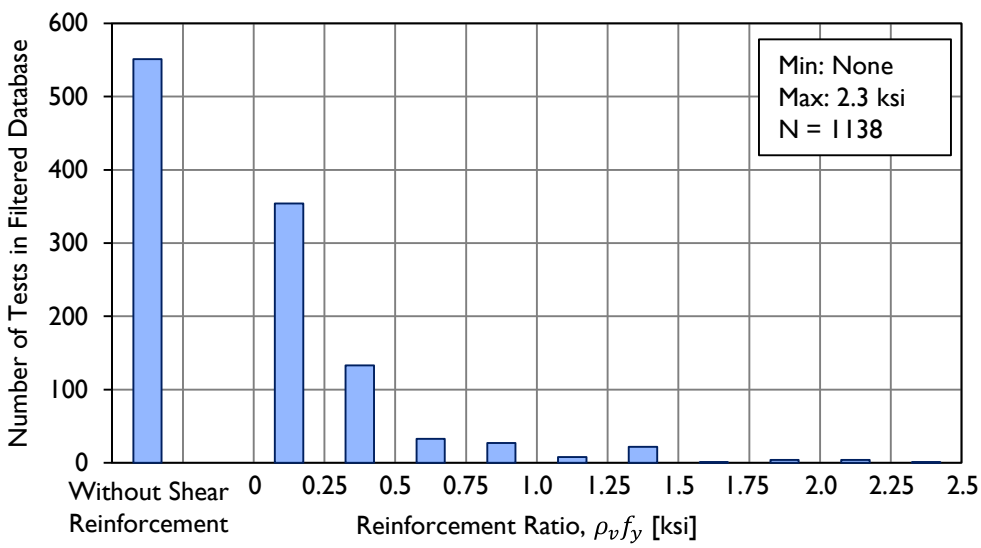

Figure 2-30: Distribution of reinforcement ratios in the UTPCSDB-2011 Filtered Database.

Using the existing standards for the Texas U-Beam, with Grade 60 reinforcing bars spaced at four inches, the reinforcement ratio ($\rho_v f_y$) is 0.6 ksi. The maximum shear reinforcement ratio tested in this study was just over 0.9 ksi.

2.5.3.7 Bottom Flange-to-Web Width Ratio

In Section 2.2, the efficiency factors of the Texas U-Beam and an AASHTO Type IV beam were computed. A section will have a high efficiency factor when a significant cross-sectional area is located away from the centroid of the section. In highway beams, efficiency is increased using a narrow web and large top and bottom flanges. However, in order to fully appreciate the benefit of the large bottom flange in a prestressed beam, it is necessary that the applied load is able to spread from the web to the extremities of the bottom flange, where the prestressing strands are located. The larger the bottom flange width is with respect to the web width, the more bottom flange depth is required to spread the load into the entire bottom flange.

The ratios of bottom flange-to-web width of the points in the UTPCSDB Filtered Database are given in Figure 2-31. All data points located in the 0.5 to 1.0 bin (458 tests, or 40%) are rectangular sections with an efficiency factor of 0.333.

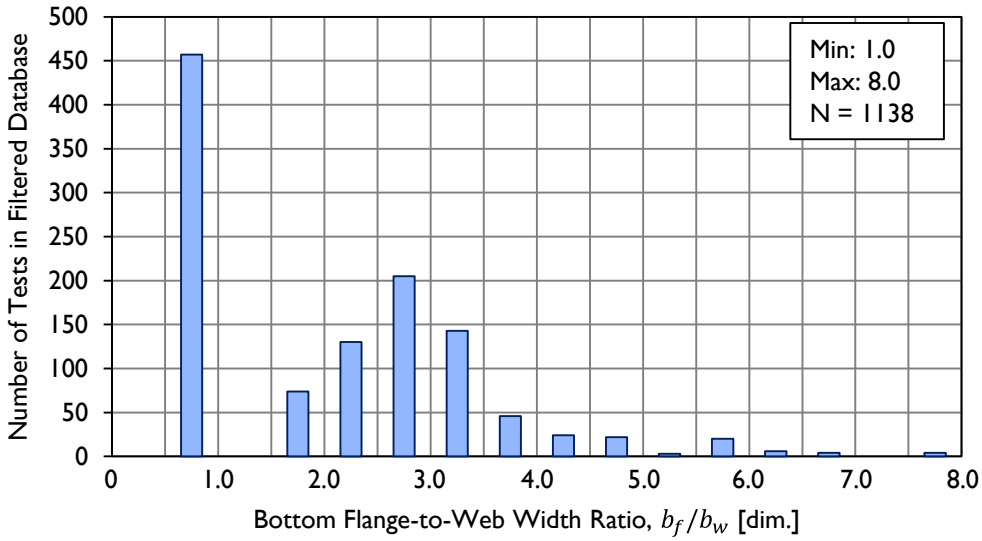

Figure 2-31: Distribution of bottom flange-to-web width ratio in UTPCSDB-2011 Filtered Database.

The bottom flange-to-web width ratio for a selection of typical standard highway beam sections is given in Table 2-3. The Texas U-Beam, with a bottom flange-to-web width ratio of 5.5, has one of the largest bottom flange-to-web width ratios in the literature. The majority of test specimens in the UTPCSDB with higher bottom flange-to-web width ratios than the Texas U-Beam were non-standard cross sections. One

standard cross section included was the NU1000, a bulb-T section developed in Nebraska with bottom flange-to-web ratios of 6.5 (Geren and Tadros, 1994; Ma, Tadros, and Baishya, 2000).

Table 2-3: Bottom flange-to-web width ratios for standard beam sections.

Beam Type	Ratio
AASHTO Type II	3.0
AASHTO Type III	3.1
AASHTO Type IV	3.3
Tx 46 (bulb-T)	4.6
PCI 72 (bulb-T)	4.3
Tx U54	5.5
NU 1000	6.5

2.5.4 Evaluation of Shear Strength Calculation Methods

Using the Evaluation Set of the UTPCSDB-2011 as described in Section 2.5.1, the accuracy and conservativeness of existing shear strength calculation methods can be evaluated. While the Texas U-Beams tested in this study are at the higher end of the data set with regard to member depth, shear area, and concrete compressive strength, it is reasonable to expect that the accuracy and conservativeness of existing shear capacity calculation methods for other beam sections will be similar to the accuracy for the Texas U-Beams.

Brief evaluations of the shear calculation methods considered in this dissertation are provided with the explanation of the calculation, in Section 2.6.

2.6 SHEAR STRENGTH CALCULATION METHODS

Three methods for calculating vertical shear resistance are considered in this study. The first is the Detailed Method from the ACI Building Code 318-08. The second is the General Procedure from the AASHTO LRFD Bridge Design Specifications (2007, with consideration of 2008, 2009, and 2010 Interim Revisions). The final calculation is referred to as the Segmental Procedure, also from the AASHTO LRFD Bridge Design Specifications (2010). The process for calculating shear strength using each method is

described briefly here. For further understanding, the reader is encouraged to refer directly to the source documents.

2.6.1 ACI Building Code 318-08

The first shear strength calculation method presented is the ACI 318-08 Detailed Method, as found in Section 11.3.3 of the ACI 318-08 Building Code (hereafter referred to as ACI (2008)). The calculation for shear strength consists of two components, that coming from concrete and that coming from reinforcing steel:

$$V_n = V_c + V_s \qquad \textbf{Equation 2-5}$$

where

V_n = nominal shear strength [lb]

V_c = nominal shear strength provided by concrete [lb]

V_s = nominal shear strength provided by shear reinforcement [lb]

The contribution from concrete as defined by ACI is the lesser of two shears: that needed to form a diagonal tension crack in the web (V_{cw}) and that needed to turn a flexural crack into a diagonal crack (V_{ci}). For normal-weight concrete, the equations for V_{ci} and V_{cw} are as follows.

$$V_{ci} = 0.6\sqrt{f_c'}\,b_w d_p + V_d + \frac{V_i M_{cre}}{M_{max}} \qquad \textbf{Equation 2-6(a)}$$

where

V_{ci} = nominal shear strength provided by concrete when diagonal cracking results from combined shear and moment [lb]

f_c' = specified compressive strength of concrete [psi]

b_w = web width [in.]

d_p = distance from extreme compression fiber to centroid of prestressing steel [in.]

V_d = shear force at section due to unfactored dead load [lb]

V_i = factored shear force at section due to externally applied loads occurring simultaneously with M_{max} [lb]

M_{cre} = moment causing flexural cracking at section due to

externally applied loads [lb-in.]

$$= \frac{I}{y_t}\left[6\sqrt{f'_c} + f_{pe} - f_d\right]$$

M_{max} = maximum factored moment at section due to externally applied loads [lb-in.]

I = moment of inertia of section resisting externally applied loads [in.^{4}]

y_t = distance from centroidal axis of section resisting externally applied loads to tension face [in.]

f_{pe} = compressive stress in concrete due to effective prestress forces only (after allowance for all prestress losses) at extreme tensile fiber [psi]

f_d = stress due to unfactored dead load at extreme tensile fiber [psi]

and

$$V_{cw} = \left[3.5\sqrt{f'_c} + 0.3f_{pc}\right] b_w d_p + V_p \qquad \textbf{Equation 2-6(b)}$$

where

f_{pc} = compressive stress in concrete (after allowance for all prestress losses) at centroid of cross section resisting externally applied loads [psi]

V_p = vertical component of effective prestress force at section [lb]

The concrete contribution to shear strength need not be taken to be less than $1.7\sqrt{f'_c}b_w d_p$.

The contribution from steel is based on Ritter's 1899 truss model for shear resistance. The load passing through the diagonal compression struts is lifted with vertically-oriented reinforcing bars. The assumed angle of the compression strut is 45°. The contribution of steel to the shear strength is related to the number of bars crossing an inclined shear crack, and can be found as:

$$V_s = \frac{A_v f_{yt} d}{s} \qquad \textbf{Equation 2-7}$$

where

A_v = area of vertical shear reinforcement at spacing s [in.^{2}]

f_{yt} = specified yield strength f_y of transverse reinforcement [psi]

d = distance from extreme compression fiber to centroid of longitudinal tension reinforcement [in.]

s = center-to-center spacing of reinforcement [in.]

The steel contribution to shear strength is limited to $8\sqrt{f'_c}b_w d$.

The ACI Detailed Method was first added to the ACI Building Code in the 1963 edition. At that time, the extent of prestressed concrete shear testing was limited; the data points available with which to confirm this method consisted of members 6 to 12 in. in depth, with concrete strengths less than 6000 psi (Avendaño and Bayrak, 2008). Even so, the method returns a conservative calculation for shear strength, regardless of specimen height or the compressive strength of the constitutive concrete. A histogram of shear strength ratios (test failure shear divided by calculated capacity) for the specimens in the UTPCSDB Evaluation Database-Level II, with V_n calculated using the ACI 318 Detailed Method is given in Figure 2-32. The maximum, minimum, average, and coefficient of variation (COV) are given on the graph. These numbers are repeated and compared to those from the other shear capacity calculation methods, along with the number and percent of unconservative test casts, in Table 2-4.

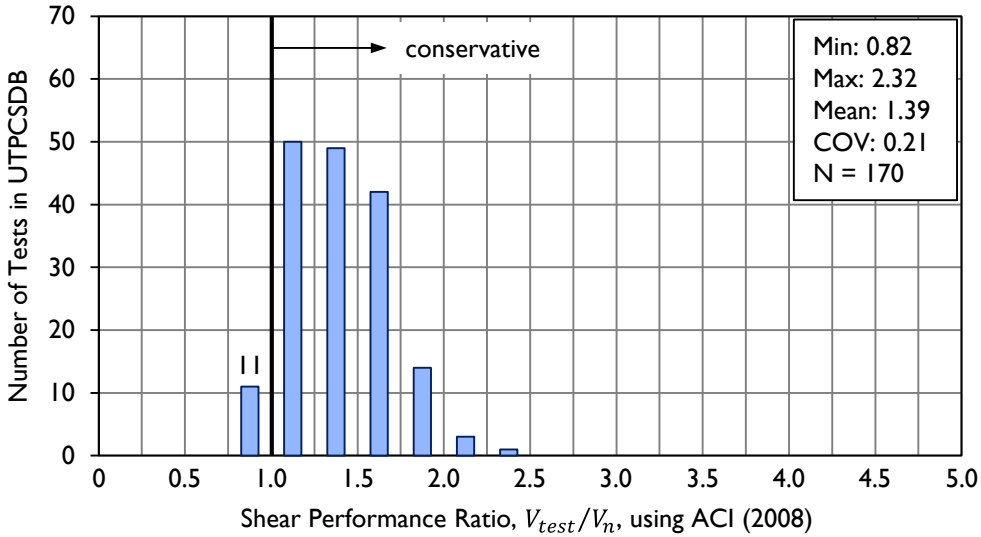

Figure 2-32: Shear Performance Ratio calculated using the ACI Detailed Method (2008) for beam tests in the UTPCSDB-2011 Evaluation Database-Level II (from Nakamura (2011)).

2.6.2 AASHTO LRFD Bridge Design Specifications: General Procedure

The second shear calculation method is from the AASHTO LRFD Bridge Design Specifications. The 4th Edition of the Specifications was published in 2007. Major changes to the General Procedure for calculating shear strength were published in the 2008 Interim Revisions. The details of the 2008 version are presented here, with applicable revisions from 2009 and 2010. This document will be referred to from here on as AASHTO (2010). The shear calculations used in this study follow the process detailed in §5.8.3.4.2: General Procedure.

The General Procedure given in AASHTO is based in the Modified Compression Field Theory (MCFT), introduced by Vecchio and Collins in 1986. The MCFT is a model that estimates the response of cracked concrete to shear and normal loads. Given the complexity of the model, simplifications have been made to use the theory in design equations. Specifically, the non-uniform shear stresses calculated by a sectional analysis are approximated with a uniform shear stress distributed over an area b_v wide by d_v deep. The direction of the principal compressive stresses is assumed to remain constant through that same depth.

This MCFT-based design procedure was introduced into the AASHTO Specifications in 1994. The determination of certain parameters (β and θ) required the use of extensive charts. In the 2008 Interim Revisions, equations for these parameters were introduced following the work of Bentz et al. (2006). This calculation method is now quite similar to that used in the Canadian design code (CSA, 2010).

As with the ACI 2008 calculation, the shear strength is found by combining the contributions from concrete and steel. The AASHTO calculation also gives credit to the vertical component of prestressing force:

$$V_n = V_c + V_s + V_p \leq 0.25 f_c' b_v d_v + V_p \qquad \textbf{Equation 2-8}$$

where

V_n = nominal shear resistance [kip]

V_c = nominal shear resistance provided by tensile stresses in the concrete [kip]

V_s = shear resistance provided by shear reinforcement [kip]

V_p = component in the direction of the applied shear of the effective prestressing force [kip]

f_c' = specified compressive strength of concrete [ksi]

b_v = effective web width taken as the minimum web width with the depth d_v [in.]

d_v = effective shear depth [in.]

The upper limit on V_n is set to help ensure a ductile failure: crushing of the concrete in the web of the beam will not occur prior to reinforcing bar yield.

The calculation for concrete contribution is:

$$V_c = 0.0316 \beta \sqrt{f'_c} b_v d_v \qquad \textbf{Equation 2-9}$$

where

β = factor indicating ability of diagonally cracked concrete to transmit tension and shear

The beta factor, which is found to reflect the ability of cracked concrete to carry shear, is calculated using the following equation:

$$\beta = \frac{4.8}{(1 + 750\varepsilon_s)}$$ **Equation 2-9(a)**

where the longitudinal strain ε_s is defined as:

$$\varepsilon_s = \frac{\frac{|M_u|}{d_v} + 0.5N_u + |V_u - V_p| - A_{ps}f_{po}}{E_sA_s + E_pA_{ps}}$$ **Equation 2-9(b)**

where

M_u = factored moment, not to be taken less than $(V_u - V_p)d_v$ [kip-in]

N_u = factored axial force, taken as positive if tensile and negative if compressive [kip]

V_u = factored shear force [kip]

A_{ps} = area of prestressing steel on the flexural tension side of the member [in.^{2}]

f_{po} = locked-in stress differential between prestressing strands and the surrounding concrete, equal to $0.7f_{pu}$ for typical levels of prestressing [ksi]

E_s = modulus of elasticity of longitudinal reinforcing bars [ksi]

A_s = area of non-prestressed steel on the flexural tension side of the member [in.^{2}]

E_p = modulus of elasticity of prestressing tendons [ksi]

If the calculation for ε_s returns a negative value, it can be taken to be equal to zero, or the denominator can be replaced with $(E_sA_s + E_PA_{ps} + E_cA_{ct})$, where E_c is the modulus of elasticity of concrete and $A_{ct}$is the area of concrete in tension. The value of ε_s should not be taken to be less than -0.40×10^{-3}.

The calculation for steel contribution is:

$$V_s = \frac{A_vf_yd_v \cot\theta}{s}$$ **Equation 2-10**

where

A_v = area of shear reinforcement within a distance s [in.^{2}]

f_y = specified minimum yield strength of reinforcing bars [ksi]

s = spacing of stirrups [in.]

θ = angle of inclination of diagonal compressive stresses [°]

The angle of inclination θ is found using the following equation:

$$\theta = 29 + 3500\varepsilon_s \qquad \textbf{Equation 2-10(a)}$$

and ε_s is as defined above in Equation 2-9(b).

It should be noted that the calculation for shear capacity presented here is dependent on the applied moment and shear (M_u and V_u). The inclusion of these terms reflects the influence of applied loads on the ability of the cracked concrete to carry further load. To calculate capacity, a known applied shear (and resulting moment) is needed; underestimating the applied shear will overestimate the concrete contribution to strength, and overestimating the applied shear will underestimate the concrete contribution to strength. In the calculations used in this dissertation, an iterative process was used such that the applied shear used in calculations is equal to ϕV_n.

Using the Evaluation Database-Level II of the UTPCSDB-2011, the accuracy of the AASHTO General Procedure (2010) was evaluated by Nakamura (2011). A histogram of shear strength ratios (test failure shear divided by calculated capacity) for this Procedure is given in Figure 2-33. The average shear strength ratio, coefficient of variation, and number and percent of unconservative test cases ($V_{test}/V_n < 1.0$) are given in Table 2-4.

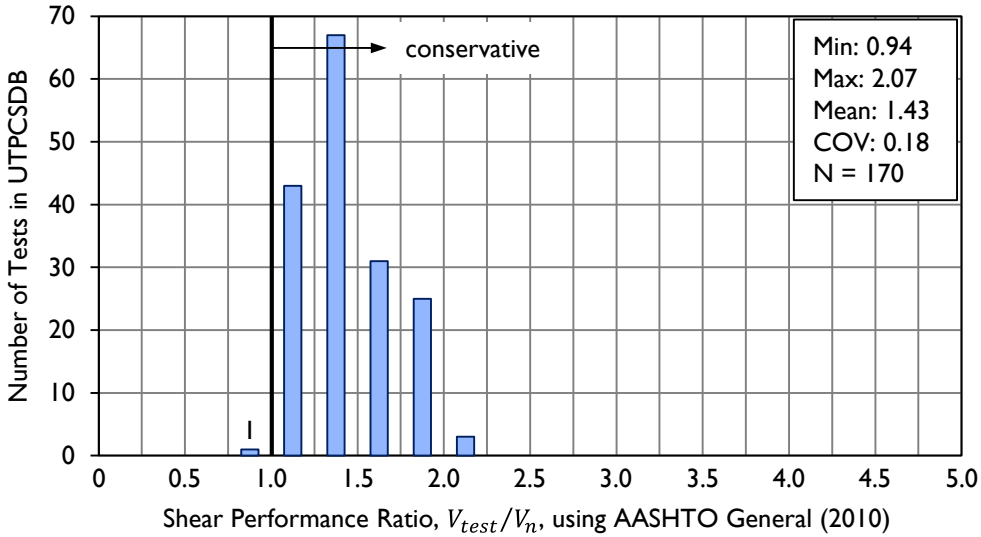

Figure 2-33: Shear Performance Ratio calculated using the AASHTO General Procedure (2010) for beam tests in the UTPCSDB-2011 Evaluation Database-Level II (from Nakamura (2011)).

2.6.3 AASHTO LRFD Bridge Design Specifications: Segmental Procedure

The third shear capacity calculation considered in this study is based on the provisions for segmental beams as specified in §5.8.6 of AASHTO (2010), referred to herein as the AASHTO Segmental Procedure. While the Texas U-Beams studied in this project are not segmental beam sections, the ease of use of this method as noted by Avendaño and Bayrak (2008) makes is appealing. It is thus important to verify that this method is accurate and conservative when used for shear calculations in Texas U-Beams.

The Segmental Procedure for calculating shear strength defines the nominal shear capacity as:

$$V_n = V_c + V_s \leq 12\sqrt{f_c'}b_v d_v$$ **Equation 2-11**

with

$$V_c = 2K\sqrt{f'_c}b_v d_v$$ **Equation 2-12**

and

$$V_s = \frac{A_v f_y d_v}{s}$$ **Equation 2-13**

In these calculations, the following notation is used:

V_n = nominal shear resistance [kip]

V_c = nominal shear resistance provided by tensile stresses in the concrete [kip]

V_s = shear resistance provided by shear reinforcement [kip]

f_c' = specified compressive strength of concrete [ksi]

b_v = effective web width taken as the minimum web width with the depth d_v [in.]

d_v = effective shear depth [in.]

K = stress variable [dim.]

A_v = area of shear reinforcement within a distance s [in.^{2}]

f_y = specified minimum yield strength of reinforcing bars [ksi]

s = spacing of stirrups [in.]

The dimensionless "stress variable" K used in Equation 2-12 is defined as

$$K = \sqrt{1 + \frac{f_{pc}}{2\sqrt{f'_c}}} \leq 2.0 \qquad \textbf{Equation 2-12(a)}$$

with

f_{pc} = unfactored compressive stress at centroid of the cross section resisting applied loads, after accounting for all prestress losses [ksi]

The variable K is used to increase the concrete contribution V_c with consideration to the prestressing force. The magnitude of K is derived from a Mohr's circle of an element located at the neutral axis of the prestressed beam, that considers initial compression from prestressing (f_{pc}) and the shear stress needed to cause diagonal cracking in the web of the member, $2\sqrt{f_c'}$. In an unprestressed (reinforced) concrete beam, K would equal 1.0 and the equation for V_c would match that for a reinforced beam, $V_c = 2\sqrt{f'_c}b_v d_v$. The value for K is limited to 1.0 when flexural tensile cracking has occurred, as is expected when the stress at the extreme tensile fiber exceeds $6\sqrt{f'_c}$. Further explanation as to the origination of the K factor can be found in Ramirez and Breen (1983).

While the equation for V_s used in this calculation procedure matches that in ACI 318, there is no upper limit on V_s explicitly stated. However, it can be noted that when K equals 1.0, V_s can be as large as $10\sqrt{f'_c}b_v d_v$. When K equals 2.0, the effective limit on V_s is $8\sqrt{f'_c}b_v d_v$, as in ACI 318.

Using the Evaluation Database-Level II of the UTPCSDB-2011, the accuracy of the AASHTO Segmental Procedure (2010) was evaluated by Nakamura (2011). A histogram of shear strength ratios for this Procedure is given in Figure 2-34. The average shear strength ratio, coefficient of variation, and number and percent of unconservative test cases are provided in Table 2-4.

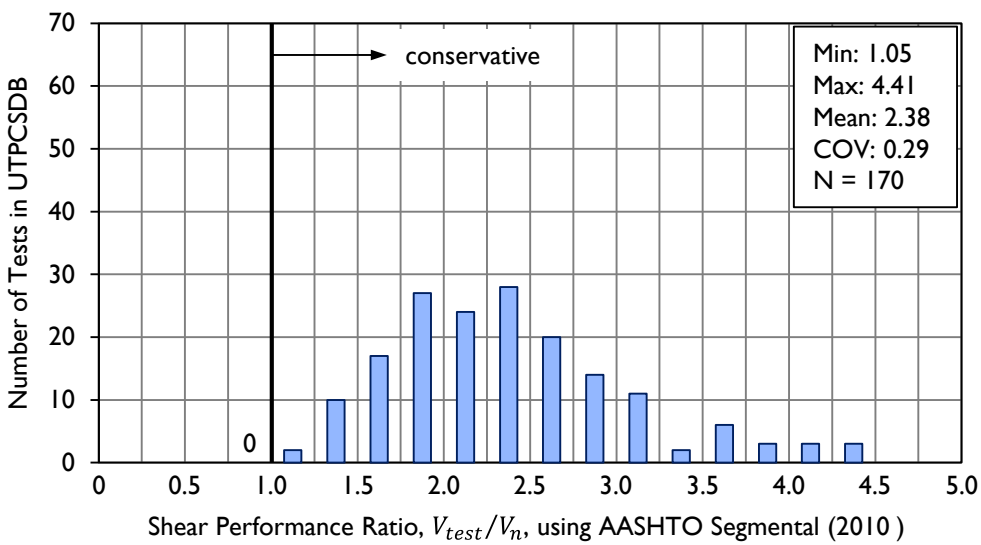

Figure 2-34: Shear Performance Ratio calculated using the AASHTO Segmental Procedure (2010) for beam tests in the UTPCSDB-2011 Evaluation Database-Level II (from Nakamura (2011)).

At the first publication of the UTPCSDB (by Avendaño and Bayrak in 2008) it was noted that removing the limit on K improved the accuracy of the AASHTO Segmental Procedure without creating any unconservative cases. The additional data gathered by Nakamura (2011) agreed with this observation (Figure 2-35), though two unconservative cases were found. In this dissertation, the Segmental Procedure will be used without the limit on K.

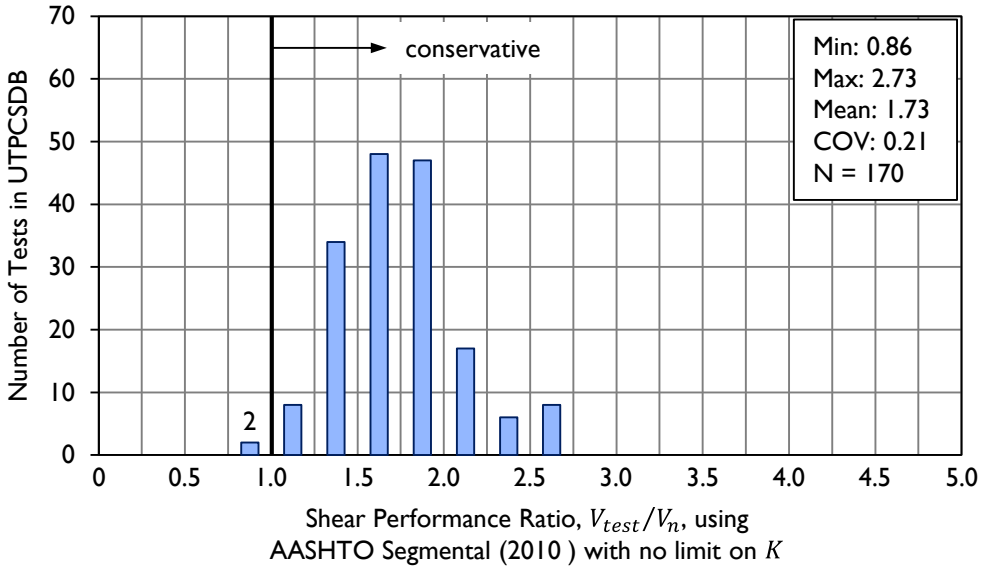

Figure 2-35: Shear Performance Ratio calculated using the AASHTO Segmental Procedure (2010) with no limit on *K* for beam tests in the UTPCSDB-2011 Evaluation Database-Level II (from Nakamura (2011)).

2.6.4 Summary

Three shear capacity calculation methods are presented in this section, and used in this dissertation. The UTPCSDB-2011 has been used to evaluate the accuracy of these methods, as summarized in Table 2-4 and Figure 2-36. When the AASHTO Segmental Procedure is used without a limit on K, the three vertical shear strength calculation methods return similar values for variance and conservatism. The calculations for strength found using the AASHTO General Procedure (2010) best balanced accuracy and conservatism, with little variation seen across data points.

Table 2-4: Summary of shear performance data from UTPCSDB-2011 Evaluation Database-Level II (from Nakamura (2011)).

Property	ACI Detailed Method (2008)	AASHTO General Procedure (2010)	AASHTO Segmental Procedure (2010)	AASHTO Segmental Procedure (2010) [no K limit]
Minimum	0.82	0.94	1.05	0.86
Maximum	2.32	2.07	4.41	2.73
Average	1.39	1.43	2.38	1.73
Coefficient of Variation	0.207	0.180	0.293	0.21
No. of Unconservative Tests	11	1	0	2
% Unconservative Tests	6.4%	0.6%	0.0%	1.2%

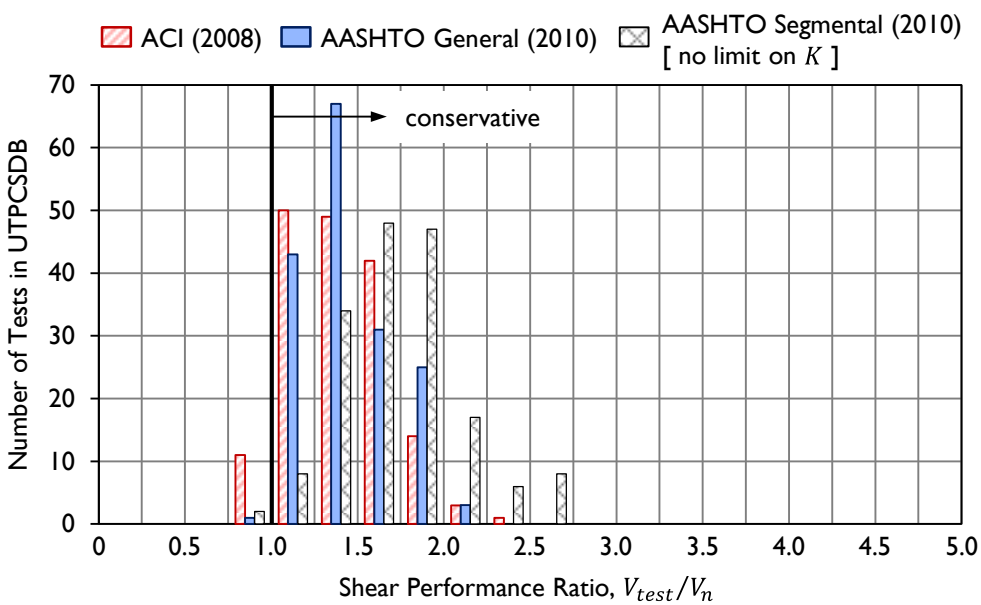

Figure 2-36: Summary of shear performance ratios across three calculation methods (from Nakamura (2011)).

Across a wide range of cross sections, prestressing force, reinforcement level, and concrete strength, all three methods for calculating vertical shear strength discussed here are generally conservative with regards to measured shear strengths. At the onset of this study, it was expected that the Texas U-Beams tested would perform similarly to the previous beam types tested, with measured shear strength exceeding the calculated strength by thirty to fifty percent.

2.7 CHAPTER SUMMARY

A review of the literature relevant to this study on the Texas U-Beam standard design was presented in this chapter. Details of the original U-Beam design and development were presented, along with the conclusions from known studies of the U-Beam. A summary of previously-collected data in prestressed beams at prestress transfer was given, to confirm the accuracy of AASHTO (2010) design equations for use in predicting beam behavior, and to provide a range of response expected during testing of the U-Beam.

The University of Texas Prestressed Concrete Shear Database was presented. The Database was used to confirm the accuracy of three methods for calculating shear strength in prestressed concrete beams: the ACI Detailed Method (2008), AASHTO General Procedure (2010), and AASHTO Segmental Procedure (2010).

There is a lack of test data on prestressed concrete U-Beams in the literature; the majority of data from beams monitored at prestress transfer and under applied loads come from tests on rectangular or I-shaped beams. These same beams were used to calibrate the design equations currently used. The large size of the Texas U-Beam, high typical levels of prestressing, and slanted webs combine to form a unique girder, the behavior of which may not be captured accurately with existing design equations. The appropriateness of applying equations for stresses induced at prestress transfer and vertical shear strength to Texas U-Beams can best be assessed through full-scale testing of these beams. At the completion of the tests conducted in this study, the knowledge gained will fill the existing gap in the literature. As more U-Beams are constructed in Texas and the design is used in exact or modified form in other states, the need for confidence in the appropriateness of the design equations grows.

The existing procedures for estimating the magnitude of stresses induced in reinforcing bars at prestress transfer and the vertical shear capacity have been shown to be conservative across existing data in the literature. It is expected that the equations will work similarly well for the Texas U-Beam. The following chapters detail the test program performed on Texas U-Beams to confirm this expectation.

CHAPTER 3
Experimental Program

3.1 INTRODUCTION

A total of eight 54-in. Texas U-Beam prestressed bridge girders were fabricated as part of this research project (Table 3-1). Four of these beams were built by the research team, at the Ferguson Structural Engineering Laboratory (FSEL). The remaining four beams were built at three prestressed fabrication yards in Texas. The beams fabricated in-house were monitored extensively at prestress transfer, resulting in eight test regions with regard to early-age behavior. Eleven shear load tests were performed (out of a maximum of sixteen available) on the ends of the eight beams. Plan views of each beam, along with nomenclature, fabrication date and location, and use in the study are given in Table 3-1.

Table 3-1: Summary of beams fabricated for this research project.

Beam	Beam Geometry [plan view]	Fabrication Date	Fabrication Location	Included in Study: at Prestress Transfer	Included in Study: under Shear-Critical Loads
0		01/29/2008	Fabricator A		X
1		11/18/2008	FSEL	X	X
2		02/26/2009	FSEL	X	X
3		07/16/2009	FSEL	X	X
4	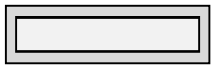	10/27/2009	FSEL	X	X
5		11/17/2009	Fabricator A		X
6		11/11/2010	Fabricator B		X
7		04/27/2011	Fabricator C		X

Details of fabrication, instrumentation, prestress transfer data collection, and shear load testing are provided in this chapter. A description of the major variables under study is given, along with tables summarizing all relevant beam and test properties. The specific details of the eight beams will be presented further in Chapters 4 and 5.

3.2 BEAM FABRICATION

The Texas U-Beams tested within this research program were fabricated at four different locations. At the Ferguson Structural Engineering Laboratory, U-Beam specimens were constructed by the research team. This in-house fabrication procedure allowed for the placement of extensive internal instrumentation, as will be described in the following sections. The research team was also able to closely observe areas of congestion or difficult reinforcing bar placement, from a constructability perspective.

The other three fabrication locations were commercial precast yards, businesses oriented around building high-quality products in short time. At these locations, the research team observed the reinforcing cage tying and concrete placement procedures, taking note of difficulties due to reinforcing bar congestion or design. No internal instrumentation was installed on reinforcing bars in the beams built outside the laboratory. The three fabrication yards will be referred to as Fabricators A, B, and C, and are located within Texas as shown in Figure 3-1. The general details of the Texas U54 beam are provided in the following section.

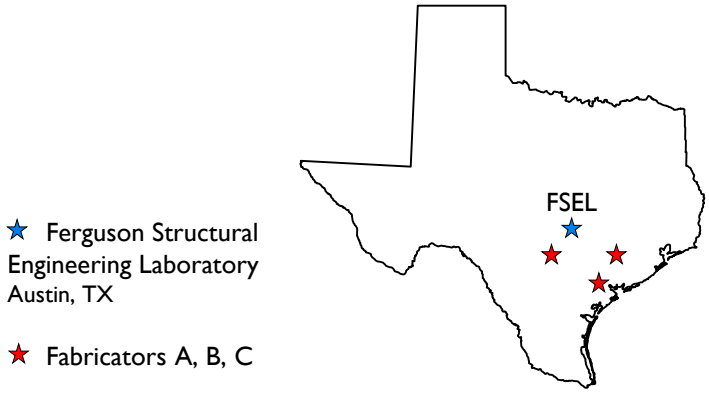

Figure 3-1: Beam fabrication locations.

3.2.1 Texas U54

The geometric details of the Texas U54 cross section are shown in Figure 3-2. The beam is 54 in. deep and 8 ft wide at the top flange. The web walls have approximately a 4:1 ratio of rise to run. The beam was originally designed using metric conventions, but the U.S. unit conversions are primarily used in design at the present time. The TxDOT standard drawings for the U-Beam are provided in Appendix A.

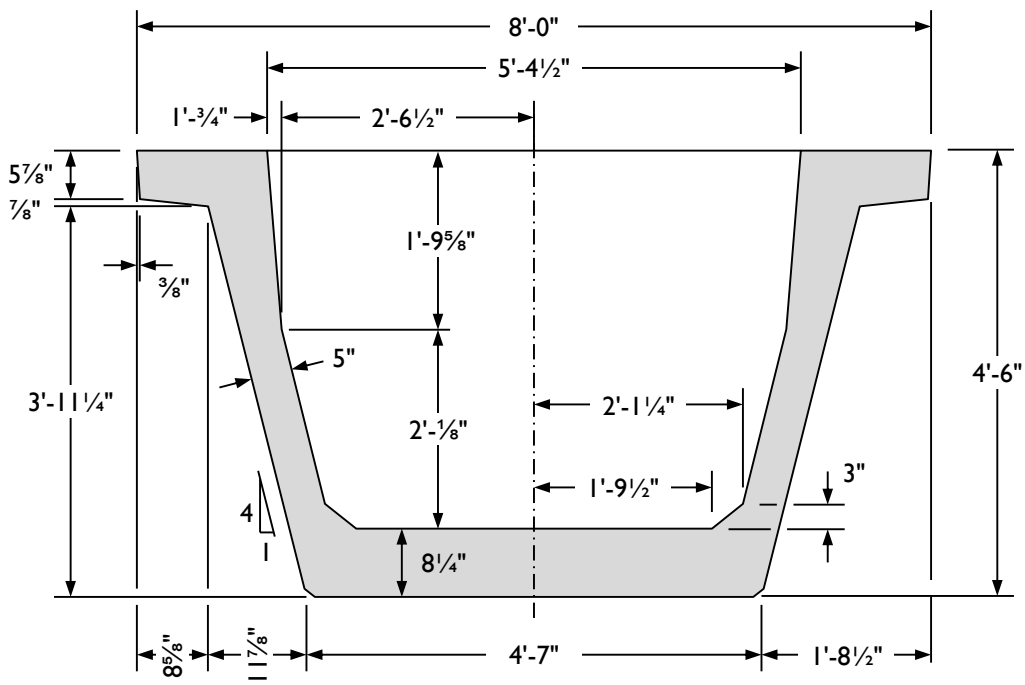

Figure 3-2: Geometry of the Texas U54 beam.

The two web walls of the Texas U-Beam are connected at discrete points along the length of the beam. At a minimum, the end of each beam has a solid diaphragm, between 18 and 24 inches in length. Intermediate diaphragms are placed no further than 13 ft from the centerline of the beam (and thus are only used in beams longer than approximately 30 ft).

Following the most recent release of the Texas U-Beam design standard drawings (2006), the end block of skewed beams can be dimensioned one of two ways. First, the internal void can be rectangular, as on squared-end beams, resulting in a triangular end block (Figure 3-3(A)). Alternatively, the internal void can be skewed to parallel the

exterior face of the beam, resulting in an end block of constant thickness. These two options are illustrated in Figure 3-3.

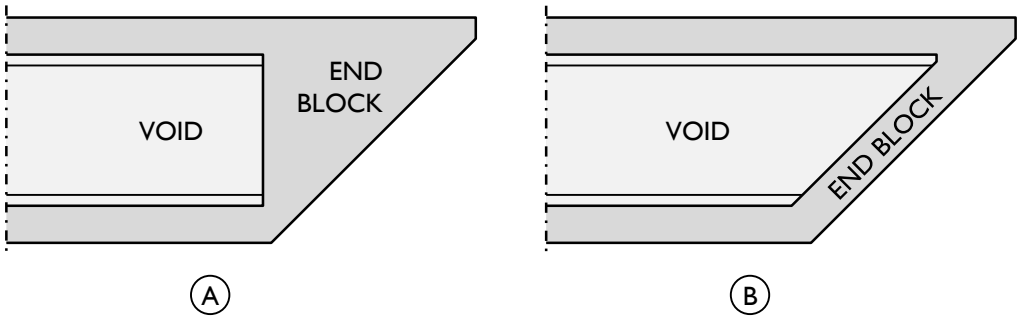

Figure 3-3: Plan view of end block options in skewed U-Beams: (A) square void with triangular end block, and (B) skewed void with square end block.

3.2.1.1 Prestressing Strands

The Texas U-Beam standard allows for up to 99 prestressing strands, spaced on a 1.97 in. (50 mm) grid, as shown in Figure 3-4. The use of more than 81 strands (three full rows) is uncommon in practice, as will be discussed later in this section. Unlike in an I-Beam, very few strands are positioned directly beneath the webs.

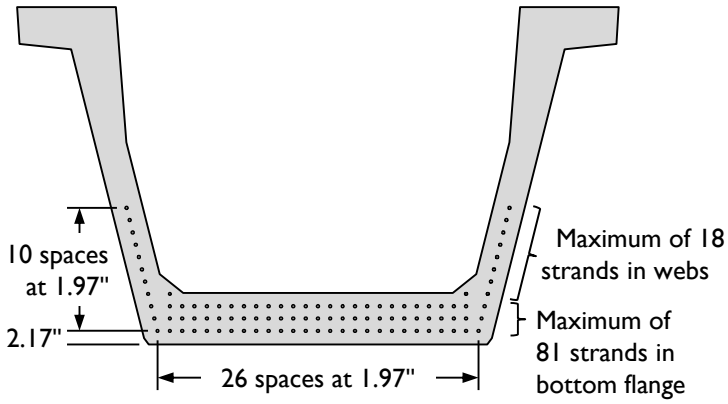

Figure 3-4: Strand positions in the Texas U54.

In the four beams fabricated in-house, four minor modifications were made from the standard U-Beam strand pattern. These changes were made so that the reaction plate used in the prestressing bed at FSEL could be used for both U-Beam and Box-Beam fabrication. The influence of these changes on the behavior of the U-Beams being tested is believed to be insignificant. The changes are as follows:

- Twenty-six strands were used in each row, rather than twenty-seven, with a space on center rather than a strand.
- The bottom row of strands was positioned at 2 in. from the bottom soffit to strand centerline, rather than 2.17 in.
- The strands were placed at 2 in. spacing on center (horizontally and vertically) rather than the designed 1.97 in.
- The outermost columns of strands, which typically follow the angle of the web wall rather than aligning vertically, were placed in line vertically (Figure 3-5).

The Texas Box Beams feature rows of twenty-eight strands, spaced at 2 in., with no angled strand patterns, with a space on center.

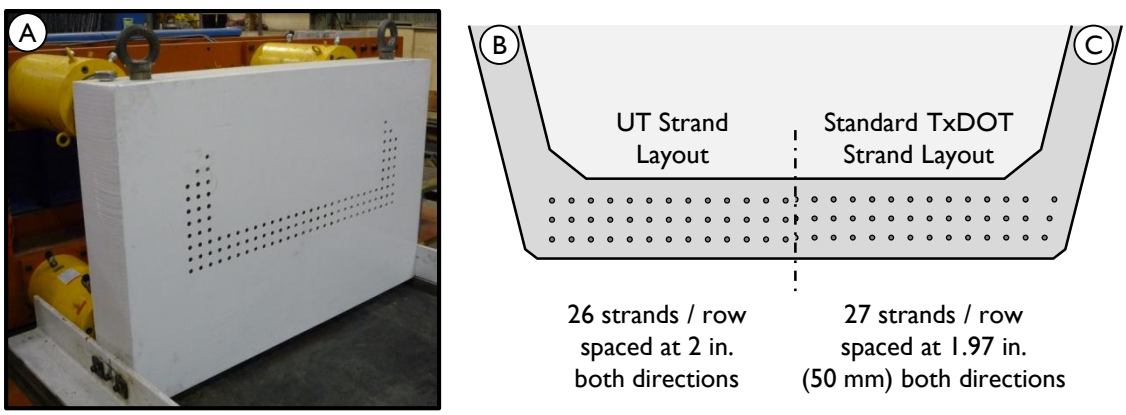

Figure 3-5: (A) Reaction plate at the live end of the prestressing bed at FSEL. (B) Strand layout for UT-fabricated U-Beams and (C) TxDOT standard strand layout.

A survey of existing U-Beams was performed by TxDOT to establish typical practice with regard to number of prestressing strands, size of prestressing strands, and amount of debonding used through the length of the beam. The results of that survey are presented here. A total of eighty Texas U40 and U54 beams designed between 2000 and 2009 were considered. Typical girder lengths were 100 to 150 ft. These beams are considered to be a representative sample of the Texas U-Beams in service today.

The total number of prestressing strands used in the survey set varied between 20 and 93, with both 0.5-in. and 0.6-in. diameter strands in use (Figure 3-6). The majority of

the included beams (80%) had between 50 and 80 prestressed strands. In this study, the first seven U-Beams fabricated contained between 64 and 78 0.5-in. diameter prestressing strands; the final beam contained 58 0.6-in. diameter prestressing strands.

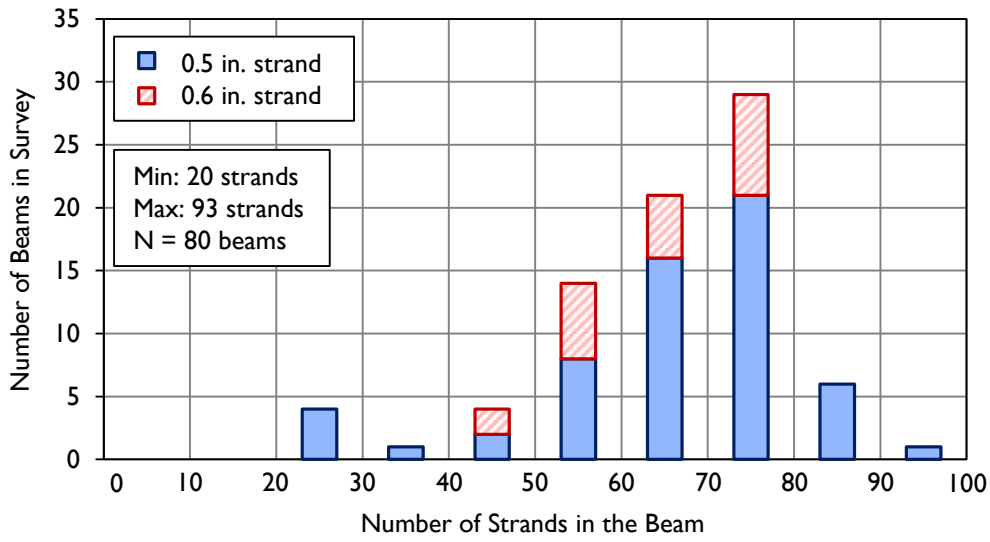

Figure 3-6: Total number of prestressing strands in Texas U-Beams.

It was mentioned in Chapter 2 that debonding of strands is used in Texas to control maximum stresses at prestress transfer. While AASHTO (2010) limits the percentage of strands debonded at beam end as compared to midspan to 25%, TxDOT allows for up to 75% of strands to be debonded (TxDOT, 2004). In U-Beams, where draped strands are not possible due to the inclined webs, debonding is typically used to a great extent. The relationship between prestressing force at beam end and beam midspan in the beams included in the survey is shown in Figure 3-7.

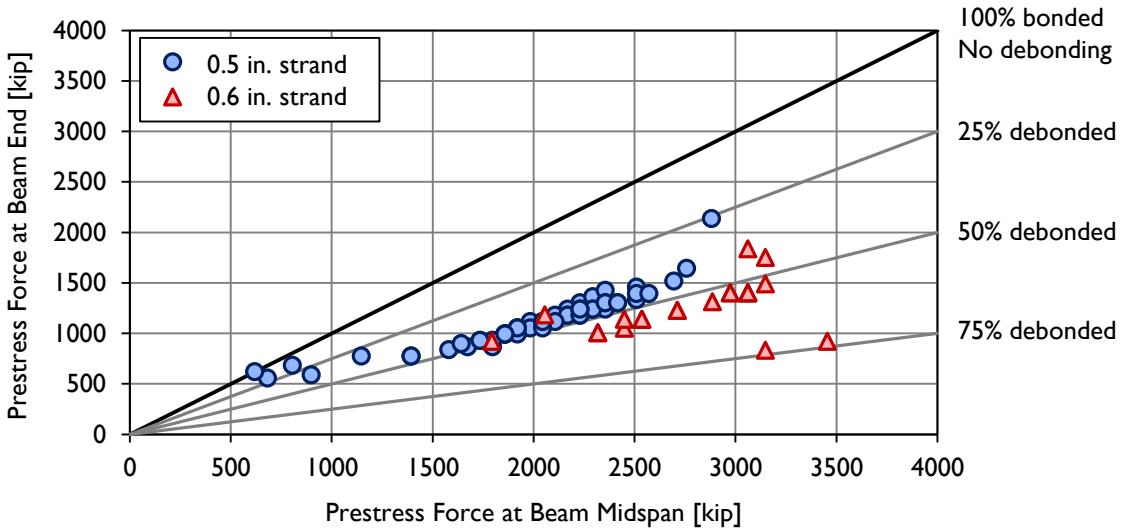

Figure 3-7: Prestressing force in typical Texas U-Beams at beam end and midspan.

Ninety-six percent of the beams included in this representative sample (77 of 80) have more than 25% of the strands debonded at beam end, violating the AASHTO limit for debonding of prestressing strands. Sixty-nine percent of the beams (55 of 80) considered in this survey had between 40 and 50% of the strands at midspan debonded at beam end, and another 20% (16 of 80) fell between 50 and 60% debonding (Figure 3-8). Two beams included in the sample had 73 and 74% debonding.

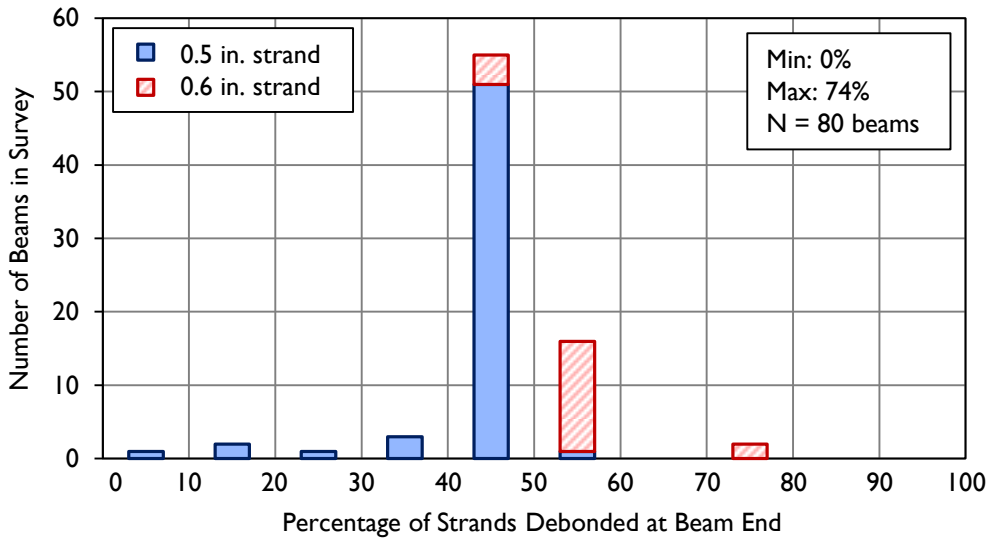

Figure 3-8: Percentage of debonding in typical Texas U-Beams.

As part of this study, two U-Beams fabricated included debonded strands. The first (Beam 3) was designed to test the effect of debonding on shear capacity and had 46% of the strands debonded at beam end. The second (Beam 7) had 9% of the strands debonded to satisfy a request by the fabricator to reduce the required strength at release. The effect of debonded strands on U-Beam behavior at prestress transfer and under shear loading was not a primary research variable in this study.

3.2.1.2 Standard Reinforcing

A total of twelve different reinforcing bar shapes are used in the Texas U-Beams. The reinforcing bars of particular interest to this shear study are shown in Figure 3-9. The shape and location of the other bars, which are primarily used only in the end blocks of the U-Beams, can be seen in Appendix A. Main shear reinforcing bars (R-bars) were positioned in the beams at one or more constant spacings from beam end to load point (e.g., 4 in. and 6 in.).

Standard Web Reinforcing: R-bar [#4, #5 for Beam 5]

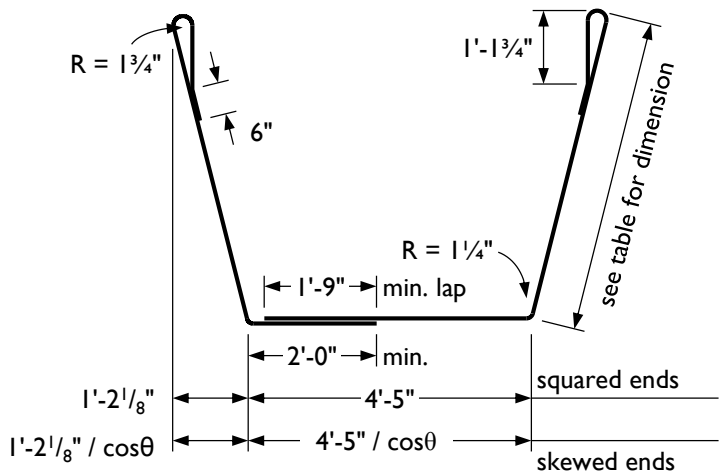

Skew Angle	Dimension
0° through 15°	4'-11½"
15° through 30°	5'-0"
30° through 45°	5'-1"

Supplementary Web Reinforcing: L-bar [see table for size]

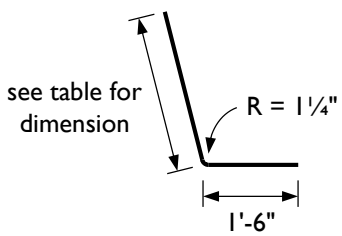

Beam	Bar Size	Dimension
0, 1, 2, 3	[not used]	
4	#5	2'-5"
5	#6	3'-10"
6, 7	#5	2'-5"

Confinement Reinforcing: C-bar [#4]

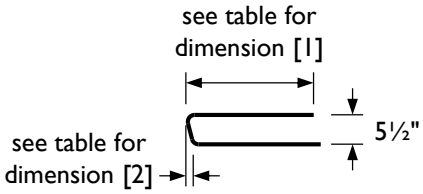

Beam	Dimension	
	[1]	[2]
0, 1, 2, 3	[not used]	
4	2'-0"	0"
5	3'-3"	1⅜"
6, 7	2'-0"	1⅜"

Figure 3-9: Standard web and confining reinforcing bar shapes used in this study.

3.2.2 Fabrication Process

The major steps followed in the U-Beam fabrication process are described in this section. As slightly different procedures are followed in commercial fabrication yards as opposed to at FSEL, the process will be described using typical commercial methods with the differences for in-house fabrication highlighted.

- Strand installation and stressing

  To begin, prestressing strands were strung the length of the fabrication line (generally 300-500 ft at a fabrication yard, approximately 55 ft at FSEL). Both in fabrication plants and at FSEL, the slack in the strands was removed using a monostrand jack, generally by applying one to two kips of load. The strands were then tensioned to their jacking stress (202.5 ksi) either using a monostrand jack (one strand stressed at a time) or a series of hydraulic rams (all strands stressed in unison). Both stressing methods are used in Texas prestressed beam fabrication plants; beams fabricated at FSEL were gang-stresssed, using rams to stress all strands at once. Beam end-face forms (or "headers") were positioned to define the length of the beam.

- Reinforcing bar placement

  Starting in the endblocks, reinforcing bars were positioned, often tied directly to the prestressing strands. The order of bar placement was critical: adding or removing a bar in the end block once the end block cage was complete generally means untying the entire end block.

- Side form assembly

  Once the rebar cage was finalized, the side forms were placed to the outside of the web reinforcing. Plastic chairs were used to ensure proper cover between the bars and the exterior face of the beam. The side forms were secured to the bottom soffit and to the headers which were placed earlier.

- Beam casting

  There are two typical casting processes for U-Beams in the state of Texas: a two-stage monolithic cast and a typical monolithic cast. The details of each are given in Section 3.2.3.

Two factors forced changing the process slightly for beams fabricated at FSEL: to begin, due to space constraints in the prestressing bed at FSEL, it was easiest to place the side forms prior to reinforcing bar placement. Second, installation of internal instrumentation took significant time and it was not desired to keep the prestressing

strands fully stressed during that process. As a result, the first three beams were fabricated in the following steps: (i) placement of the side forms and (ii) reinforcing bars, (iii) stringing and de-slacking the prestressing strands, (iv) installing internal instrumentation, (v) positioning the headers, and (vi) fully tensioning the prestressing strands. This final step was generally performed the morning of the concrete placement.

The more complex reinforcing bar layout used in the fourth beam fabricated in-house required the side forms not be in place until after the reinforcing cage was complete. As the side forms were previously used to support the cage until it was self-standing, it was necessary to string the prestressing strands first to ease construction. For this beam, the following order was followed: (i) stringing and de-slacking the strands, (ii) tying the reinforcing bars, (iii) installing internal instrumentation, (iv) placing the side forms and headers, and (v) full tensioning of the strands. It is not believed that the different procedures followed had any effect on performance at prestress transfer or under shear loads.

3.2.3 Casting Procedure

Two methods for handling the internal void of the U-Beam during casting are currently used in the state of Texas. In the first, the internal void is secured after concrete has been placed in the bottom slab of the U-Beam. This method results in a two-stage monolithic cast. In the second, the internal void is positioned prior to any concrete placement, resulting in a monolithic cast. Each method has its benefits and drawbacks, as described herein.

In the two-stage cast (Figure 3-10), it is necessary to secure the void under time constraints, in order not to form a cold joint at the bottom flange-to-web interface. Difficulties that arise during void placement (generally from interference between the reinforcing bars and the void) can slow the process and render the beam unusable. It is also possible to overfill the bottom flange, requiring concrete be removed prior to void placement (which is time-consuming and labor-intensive), or risk beam rejection due to the thickened bottom slab. However, good consolidation through the bottom slab

concrete can be easily achieved using internal vibrators, and significant air voids are uncommon.

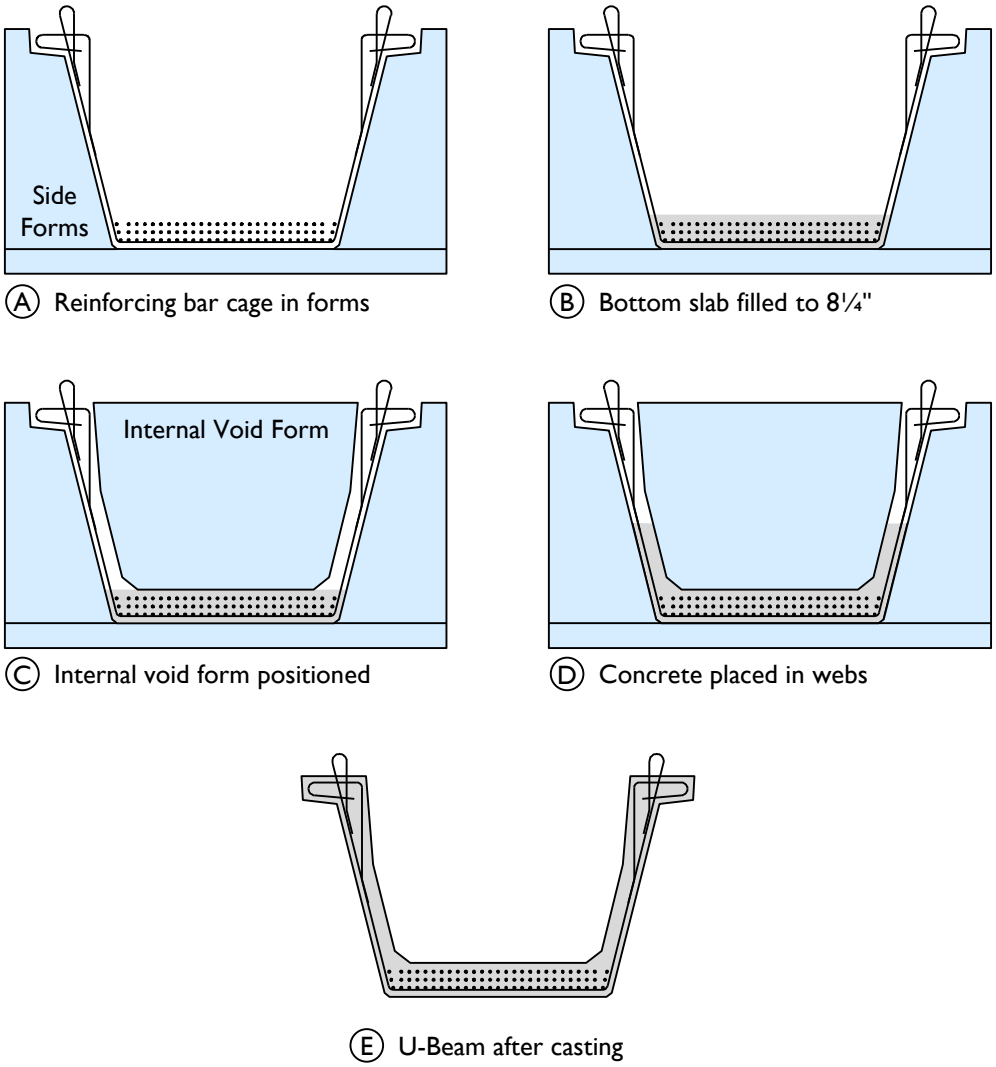

Figure 3-10: Two-stage monolithic cast procedure.

In the monolithic cast (Figure 3-11), the void is secured before any concrete has been placed. When the pour begins, concrete is placed into the forms from one side of the void. The concrete mixture must flow well enough to cross through the bottom flange without the aid of internal vibrators in the bottom flange. Once the concrete has flowed up the second web a significant distance (generally about half the web height), concrete is placed into both webs directly. The benefit of this method comes from the ease of void

form placement and the reduction of the possibility of "running out of time". However, the concrete mixture design must be well-made and appropriate for this use; a bad concrete mixture can cause the beam to be rejected by leaving voids through the bottom flange, segregating as it passes through the effective sieve of reinforcing bars and prestressing strands, and/or failing to flow through to the second web. Concrete cannot be placed in the second web before it has flowed up from the bottom without significant danger of trapping a large air void unfilled beneath the void form. This fabrication method is only allowed in U-Beams (not Texas Box-Beams) because the internal void is removed after casting, allowing inspection of both the bottom and the top of the bottom flange.

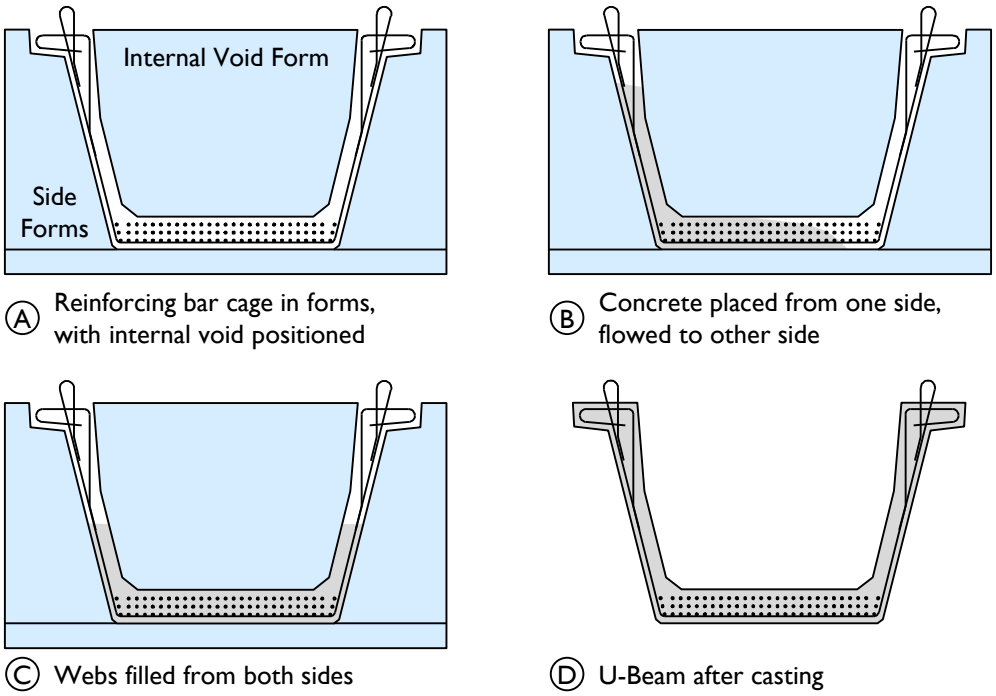

Figure 3-11: Monolithic cast procedure.

Both casting methods presented here were used during fabrication of the beams in this study. The first seven beams fabricated – four at FSEL, the two cast by Fabricator A, and the one cast by Fabricator B – were cast using the two-stage monolithic process. The final beam (made by Fabricator C) was made using the monolithic casting procedure. The monolithic cast has become more popular recently with the increased use of self-

consolidating concrete (SCC), and is expected to become the predominant casting method in the state in the coming years.

3.2.4 Concrete Materials

A total of eight different concrete mixtures were used during this research study. The eight beams were fabricated using five different mixture designs (two at the Ferguson Laboratory and a different design at each of the three fabrication yards). Three additional mixtures were used for the decks of the eight beams. The mixture proportions and identifying labels are provided in Tables 3-1 and 3-2. Type III cement was used in each beam (Table 3-2), the decks were built with Type I cement (Table 3-3). The aggregate quantities are based on saturated surface dry conditions. The differences in the concrete mixtures were not believed to influence the structural behavior of the beams.

Table 3-2: Composition of Type III cement concrete mixtures.

Material		Details	Quantity					
			Mixture Designation					Units
			III-A	III-B	III-C	III-D	III-E	
Cementitious Material		Type III Cement	611	599	611	600	673	lb/yd^3 concrete
		Type F Fly Ash		200	204	200	224	
Coarse Aggregate		¾" Crushed Limestone ½" Crushed Limestone 1" River Gravel ¾" River Gravel	1600	1821	1855	1734	1937	lb/yd^3 concrete
Fine Aggregate		Sand	1379	1152	1124	1318	948	lb/yd^3 concrete
Water		–	202	252	167	205	230	lb/yd^3 concrete
Water/CM		–	0.33	0.32	0.21	0.26	0.26	–
Admixtures	Superplasticizer	Sika Viscocrete 2100 Sika Viscocrete 2110	13.3	6.8	4.8	7.0		oz./hundred weight cementitious material
	Retarder	Sika Plastiment BASF Pozzolith 300R	5.1	3.8	1.8	1.5	3.0	
	Water Reducer	Sika Sikament 686 Sika Plastocrete 161 BASF Glenium 7700	24.9	8.3			7.0	

Table 3-3: Composition of Type I cement concrete mixtures.

Material		Details	Quantity			
			Mixture Designation			Units
			I-F	I-G	I-H	
Cementitious Material		Type I Cement	526	592	658	lb/yd^3 concrete
		Type F Fly Ash	178	200	231	
Coarse Aggregate		1" River Rock ⅜" Crushed Dolomite	1795	1719	1690	lb/yd^3 concrete
Fine Aggregate		Sand	1296	1441	1410	lb/yd^3 concrete
Water		–	253	238	240	lb/yd^3 concrete
Water/CM		–	0.36	0.30	0.27	–
Admixtures	Superplasticizer	Sika Viscocrete 2100	5.5	7.0		oz./hundred weight cementitious material
	Retarder	Sika Plastiment ES	0-2.5	0-2.0	2.0	
	Water Reducer	Sika Sikaplast 500		6.0	6.9	

Concrete samples were taken during casting of each beam and deck. The 4"×8" cylinders were tested regularly to determine the compressive strength gain of the concrete through time. Beam and deck cylinder strength was measured on the day of specimen testing; these strengths were used in final calculations for capacity of the test specimen. It is not believed that the variation in concrete strengths between specimens effected the performance of the beams.

3.3 TEMPERATURE MONITORING

In the four beams fabricated at the Ferguson Laboratory, a series of thermocouples were placed throughout the beam to measure curing temperatures in the first twenty-four hours after concrete placement. The thermocouples were located as shown in Figure 3-12. These gauges were primarily used to measure the temperature profile through the end block of the U-Beams during hydration. Symmetric locations in the cross section were assumed to have equal temperatures, requiring fewer thermocouples in each end block. One additional thermocouple, positioned at the bottom, outermost strand eight feet from the end of the beam, was used to determine the appropriate time to release the prestressed strands, through matching the temperature at that point to cylinders that could be tested for compressive strength by using a temperature match-curing system.

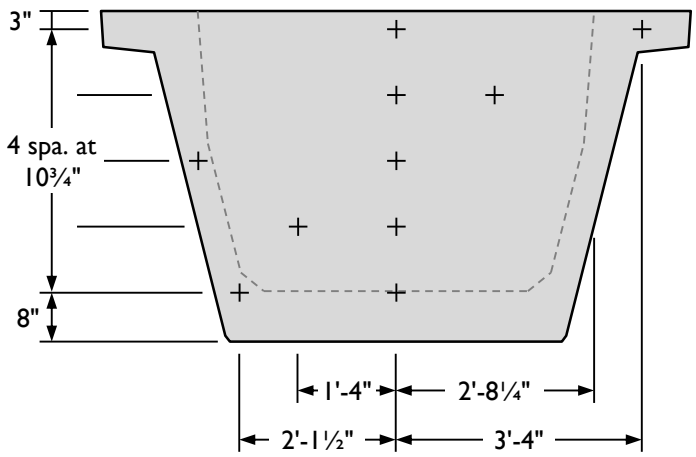

Figure 3-12: Position of thermocouples used in temperature monitoring during curing.

The thermocouples were positioned in an effort to capture the hottest and coolest points across the end block cross section. Longitudinally, the panel of gauges was placed halfway between beam end and the end face of the void in squared test regions, and through the centroid of the end block in skewed test regions.

A single thermocouple was placed at the perceived hot-spot (located at the centroid) of five of the eight U-Beam end blocks cast at local fabrication yards. The remaining three end blocks were not monitored during curing. In several cases, the thermocouples placed in the field were damaged during casting and did not return viable data.

3.4 OBSERVATION AT PRESTRESS TRANSFER

Two additional types of internal instrumentation were used in the Texas U54s fabricated at the Ferguson Laboratory during this study. These gauges were affixed to the reinforcing bars and to the prestressing strand (Figure 3-13). As the bars elongated or contracted, the electrical resistance across the gauge changed; the change in resistance was then converted to strain. The strain was then multiplied by an assumed modulus of elasticity for the reinforcing bars of 29,000 ksi to return a stress value; the term "measured stress" will be used from here on to refer to the gathered and processed data.

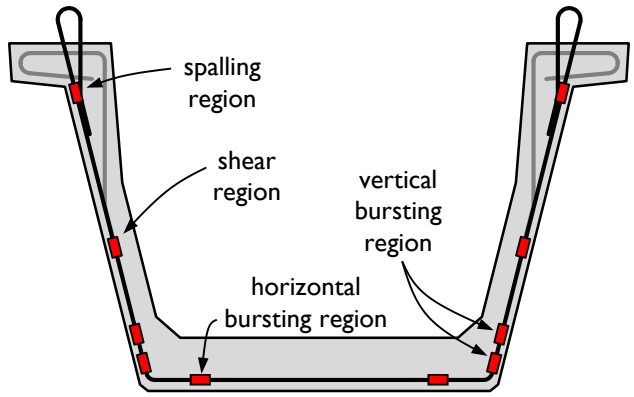

Figure 3-13: Location of instrumentation monitored at prestress transfer.

These gauges were monitored while and after the prestressing strands were released, to evaluate the magnitude and location of stresses in the section at prestress transfer.

3.5 SHEAR TESTING

Shear tests were performed at the Ferguson Laboratory at the University of Texas at Austin. Prior to testing the U-Beams, an 8-in. deep deck was cast with standard reinforcing bars. The deck served two purposes: first, given the inclined webs of the U-Beam, forces transferred through the webs have both a horizontal and vertical component (Figure 3-14). The deck provides the necessary horizontal restoring force that limits rotation of the slanted webs under vertical loads. Second, the flexural capacity of the beam system was significantly increased through the addition of the deck, thus helping ensure a shear failure would occur before flexural failure. The deck was made with high early-strength concretes ($f_c' > 7.5$ ksi at testing, which often occurred within a week of deck placement). The strength of the deck concrete, which was higher than is typically used in U-Beam bridges in the state, was not thought to influence the shear behavior of the beams. The width of the deck was 8 ft; there was no overhang.

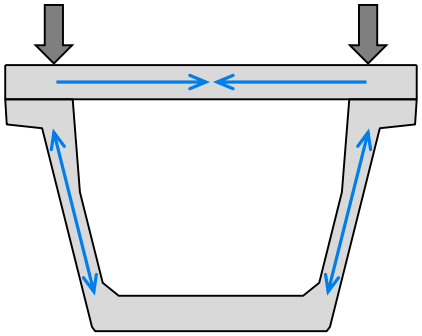

Figure 3-14: Forces that develop in the U-Beam during loading.

The total depth of the beam with cast-in-place deck was 62.75 in. While the deck concrete was only 8 in. thick, the forms spanning the interior void consisted of a sheet of ¾ in. plywood resting on the inside edges of the top flange (Figure 3-15). The U-Beam cross section is drawn through this dissertation without differentiation between plywood and concrete. Calculations performed consider an 8 in. deck with a centroid located 58.75 in. from the bottom of the U-Beam.

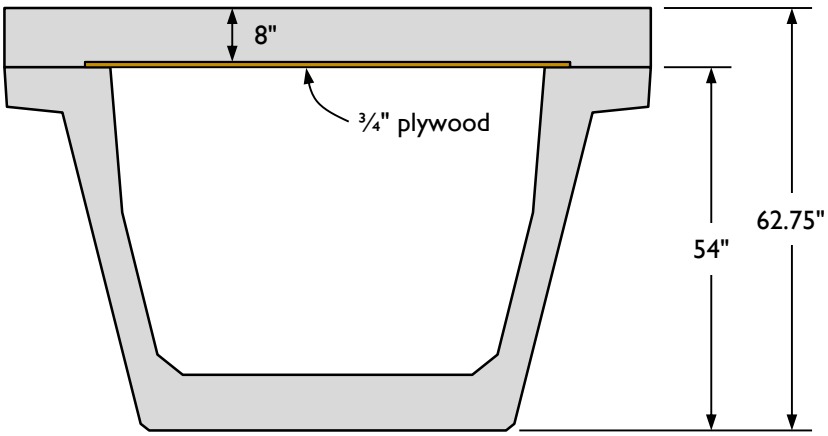

Figure 3-15: Deck form system used, highlighting ¾" plywood.

A shear testing frame (Figure 3-16) was built to react against a strong floor in FSEL. Two rams, each with a 2,000 kip capacity, were placed above the webs of the beam being tested. The rams reacted against a steel beam supported by two smaller spreader beams. The smaller beams distributed the load to six 3.5-in. rods, which were anchored to the strong floor. The frame was designed to resist an applied load of 4,000 kip.

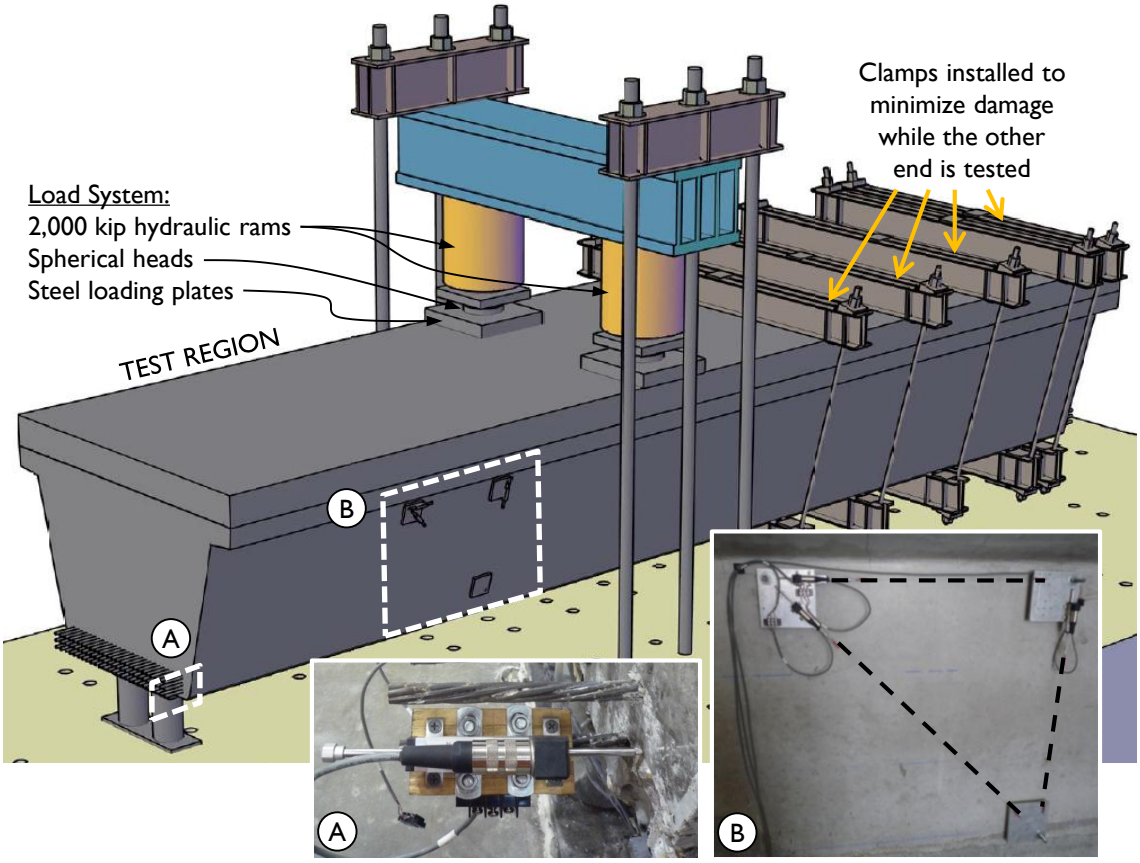

Figure 3-16: Shear testing frame, with pictures of (A) strand slip and (B) shear deformation instrumentation shown.

The U-Beams were supported on three bearing pads, per TxDOT standard practice. At one end, a single bearing pad measuring 32 in. wide by 9 in. in the longitudinal direction, was used beneath the centerline of the beam a distance 6 in. from beam end to bearing centerline. At the other end, two bearing pads (16 in. wide by 9 in. long) were placed 13.5 in. off centerline, again 6 in. from beam end. These bearing conditions are shown in Figure 3-17.

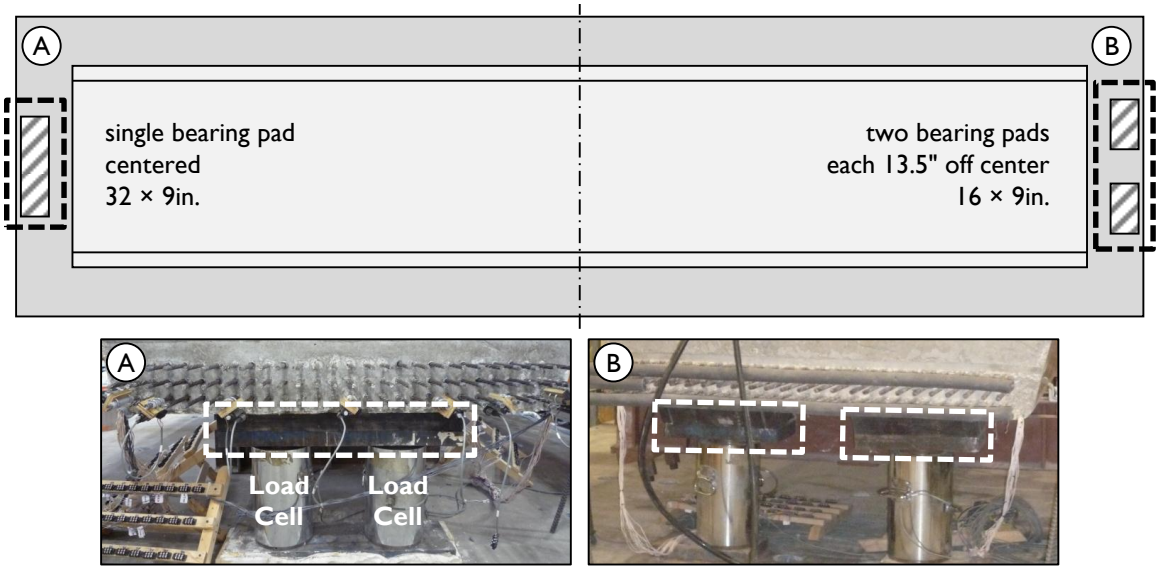

Figure 3-17: Bearing conditions at the ends of the shear test specimen.

Two 24×26×4 in. steel plates, positioned directly above the two webs, were used between the loading rams and the deck of the beam to distribute load (Figure 3-16). The load plates were oriented with the 24 in. dimension in the longitudinal direction.

3.5.1 Shear Test Instrumentation

In addition to the strain gauges described in Section 3.2.2, load cells, a pressure transducer, and linear potentiometers were used as is detailed in the following paragraphs.

The load passing through the beam to the bearing pads was measured in two locations. First, a pressure transducer was attached to the hydraulic pump connected to the two rams, measuring the total pressure applied. Second, four 1,000-kip load cells were placed beneath the bearing pads to measure reaction forces. The load cells are visible beneath the bearing pads in Figure 3-17.

Six linear potentiometers were used to measure vertical deflections at either end and under the load, on each side of the beam, as load was applied. Potentiometers were placed on both sides of the beam in order to capture any rotation that might occur. The linear potentiometers at either end of the beam were placed at the longitudinal centerline

of the bearing pads to measure the deflection associated with compression of the bearing pads.

Strand slip was also monitored during loading using additional linear potentiometers. These gauges were clamped to individual strands, with the plunger against the beam surface. If the strand slipped inwards under load, the gauge would move while the beam face would not, thus providing a measurement of the slip. These potentiometers were usually placed on the bottom row of strands, with more towards the outermost strands, as these strands were taking the most load and thus would be the first to slip. A strand slip gauge is shown in Figure 3-16(A). Typical strand slip gauge locations are shown in Figure 3-18; as the bottom row is stressed the most by flexural loading, gauges were only placed on strands in that row.

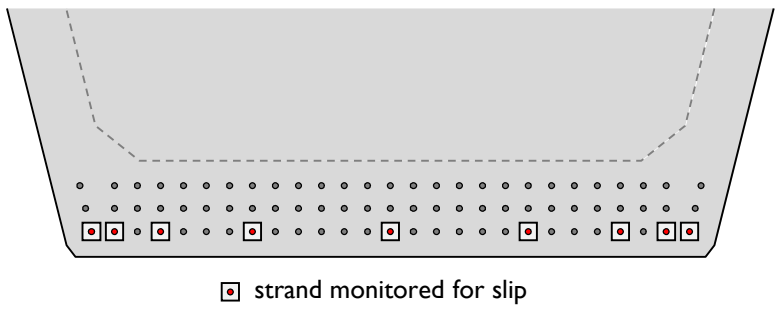

Figure 3-18: Typical locations for strand slip gauges during shear testing.

A series of linear potentiometers, positioned halfway between the load point and the bearing point, were used to measure web shear distortion occurring within the webs. The three gauges were oriented as shown in Figure 3-16(B). Using geometry, the displacements measured by each of those potentiometers were used to calculate the shear distortion. The threaded rods which held the potentiometers were adhered in the web walls using epoxy, to a depth of at least 3 in.

3.5.2 Loading Procedure

With the exception of one beam (Beam 0), the U-Beams tested in this study were loaded 154 in. from the centerline of the support, resulting in a span-to-depth ratio of 2.6. Beam 0 was loaded at midspan of the beam, at a shear span-to-depth ratio of 3.0.

Each beam was designed to be tested twice in shear, with one test at each end of the beam. The shear test regions are referred to by number and beam end (N and S for North and South, respectively). External post-tensioned clamps were used to strengthen the beam end not being tested. In testing the first three beams, the clamps were used only during the second test on one beam, to strengthen the end that failed in the first test. In the later tests, the clamps were also used during the first test to minimize damage to the end to be tested later. The clamps are shown in Figure 3-19, with a schematic of how they were used during testing provided in Figure 3-20. Despite all efforts, five beams were severely damaged in the first test to the extent that conducting a second test on the same beam was not possible, despite the strengthening system.

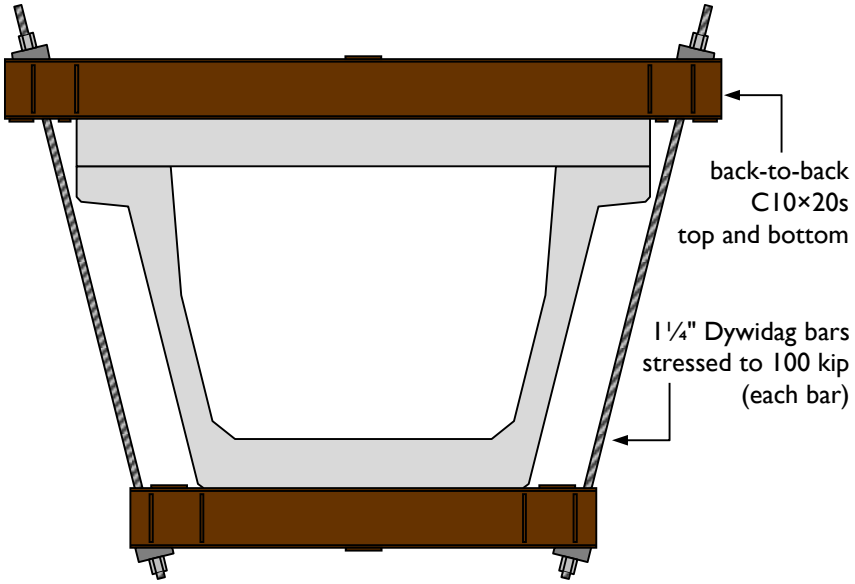

Figure 3-19: External post-tensioning system used to strengthen U-Beams during shear testing.

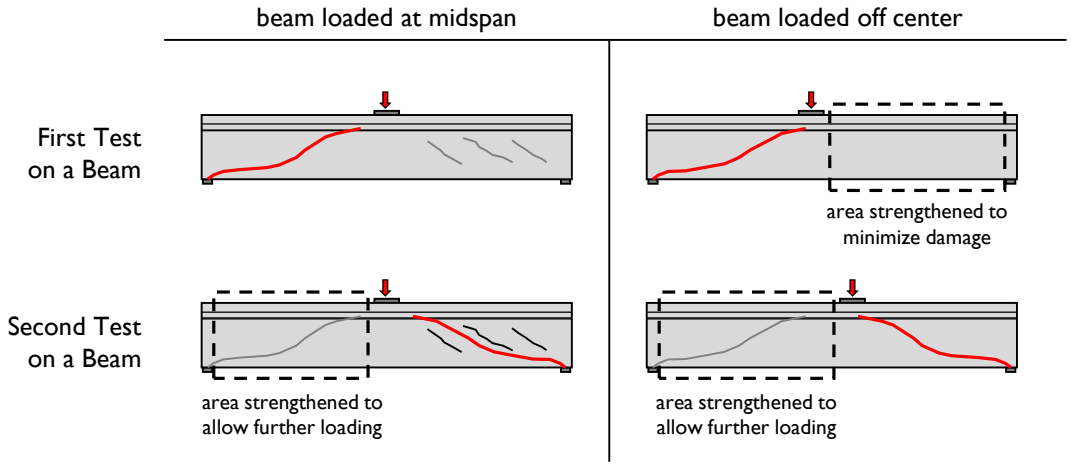

Figure 3-20: Schematic of how and when external post-tensioned clamps were used to aid in achieving a second failure within one beam.

A three-dimensional drawing of the complete shear test setup, highlighting the use of the linear potentiometers and the external post-tensioning clamps, is shown in Figure 3-16.

3.5.3 Definition of Shear Span

The shear span was defined as the distance along the beam centerline from the point of load to the centerline of the bearing pad, as shown in Figure 3-21. When a skewed beam was supported on two bearing pads, this definition resulted in one bearing pad being positioned almost two feet closer to and one bearing pad two feet further from the load than the shear span suggests.

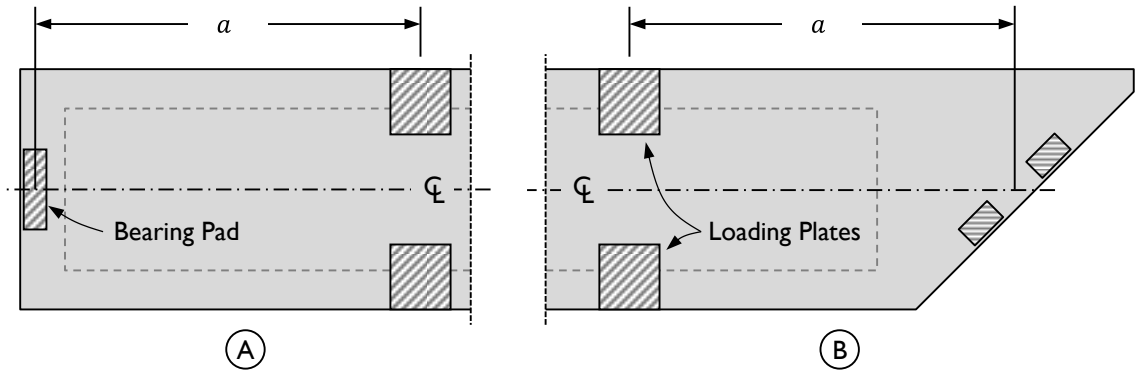

Figure 3-21: Definition of the shear span, *a*, in a (A) squared and (B) skewed test region.

3.5.4 Definition of Failure Shear

The failure shear was defined to be the applied load carried by the two load cells supporting the test region during the test, plus the dead load shear expected halfway through the shear span (Figure 3-22). The dead loads came from the beam, the cast-in-place deck, and the test frame, and typically exceeded 90 kips (thus contributing approximately 25 kip shear to V_{test}). At failure, the difference in between the dead load shear included in V_{test} and the dead load shear near the support or near the load point was less than 3% of V_{test}.

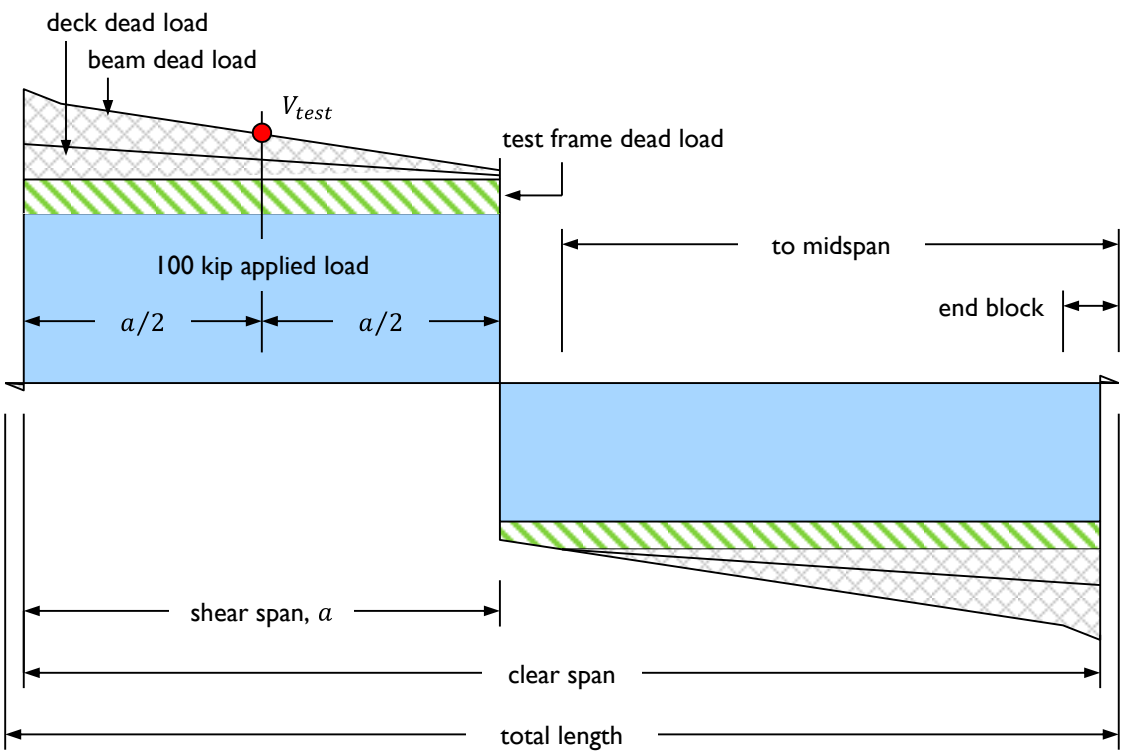

Figure 3-22: Explanation of the location and magnitude of V_{test}.

3.5.5 Comparison to Calculated Shear Capacity

The shear capacity of each test region was calculated from beam end to load point following the AASHTO General Procedure (2010) presented in Chapter 2. For most test specimens, the capacity was calculated twice: near beam end, where the reinforcing bars

were spaced at 4 in., and near load point, where the reinforcing bars were spaced at 6 in. A typical shear capacity plot, made from these calculations, can be seen in Figure 3-23. Also plotted is the applied shear, which varied from beam end to load point due to the dead load. As shown in Figure 3-22, V_{test} was defined to be on this line, halfway between load point and support.

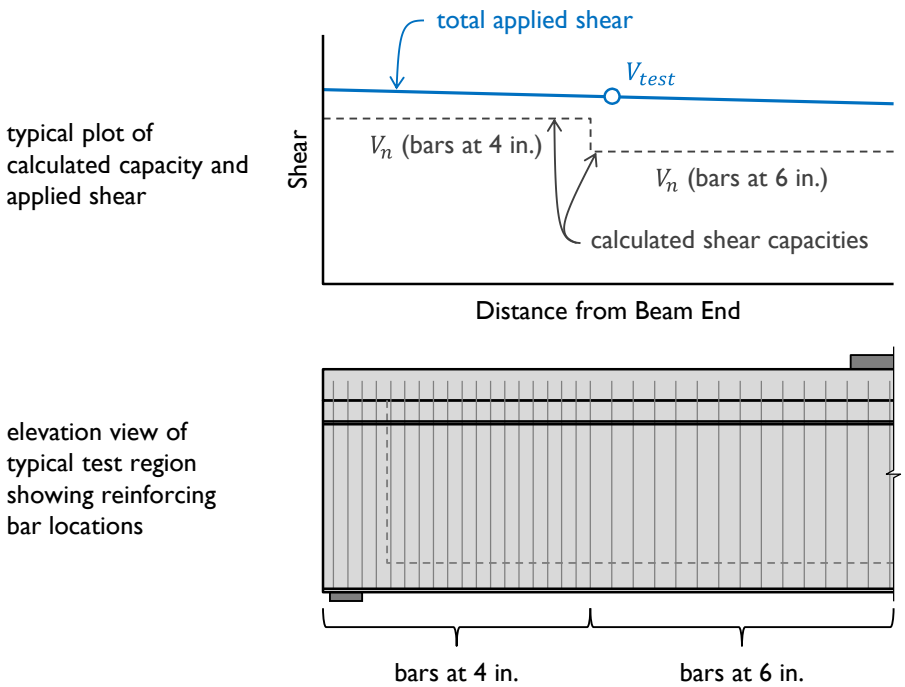

Figure 3-23: Explanation of comparison between calculated shear capacity and measured strength.

The failure shear (V_{test}) was compared to each of the calculated shear capacities (typically, V_n found using a bar spacing of 4 in. and V_n found using a bar spacing of 6 in.) to get the shear performance ratio, or the ratio of failure shear to calculated shear capacity (V_{test}/V_n). A singular shear performance ratio was chosen by considering the location of the failure: when failure was observed within the 4-in. spacing region, the shear performance ratio was defined to be that found using the calculated shear capacity with a 4-in. bar spacing; when failure was observed within the 6-in. spacing region, the shear performance ratio was defined to be that found using the calculated shear capacity with a 4-in. bar spacing.

3.6 TEST VARIABLES

Brief descriptions of seven of the variables tested in this study are presented in the following sections. Tables summarizing the use of these variables in the test specimens is provided in Section 3.6.8. Further details of the test specimens are given in the following two chapters.

3.6.1 Beam Geometry and Skew

As described in previous chapters, the original intent of this study was to investigate the influence of internal void geometry on beam response at prestress transfer and shear strength. Three beams were fabricated with an external skew of 45°. Beams 2 and 7 had a square internal void (Figure 3-3(A)), while Beam 1 was built with an internal void parallel to the external skew (Figure 3-3(B)).

3.6.2 End Block Length

The current TxDOT standard dictates the length of the end block in a beam with low levels of skew (less than 30°) be between 18 and 24 in. In beams with significant skew (30 to 45°), the end block is limited to 24 to 30 inches in length, measured along the edge of the bottom flange.

Beams 1 through 5 had end blocks set at the minimum allowable dimension (18 in. for squared ends, 24 in. for skewed ends). The tested ends of Beams 6 and 7 (B6S and B7N) were fabricated with 30 and 36 in. end blocks, respectively.

3.6.3 Reinforcing Bar Type

Two test regions were fabricated using welded-wire reinforcement (WWR) as opposed to standard Grade 60 reinforcing bars. The wire mesh used was an equal-area replacement to the standard bars. Wire mesh typically has a higher yield strength than standard reinforcing bars, with a much less well-defined yield plateau.

Material samples were tested to determine the yield strength of the bars used in the test specimens. Typical stress-strain plots from the material testing program for welded-wire reinforcement and Grade 60 reinforcement can be seen in Figure 3-24. The

WWR has a greater yield strength (approximately 85 ksi vs. 65 ksi), but the standard reinforcing bars show much more ductility after yield. The yield strength of the WWR was determined by fitting two tangents to the upper and lower sections of the curve and finding their intersection.

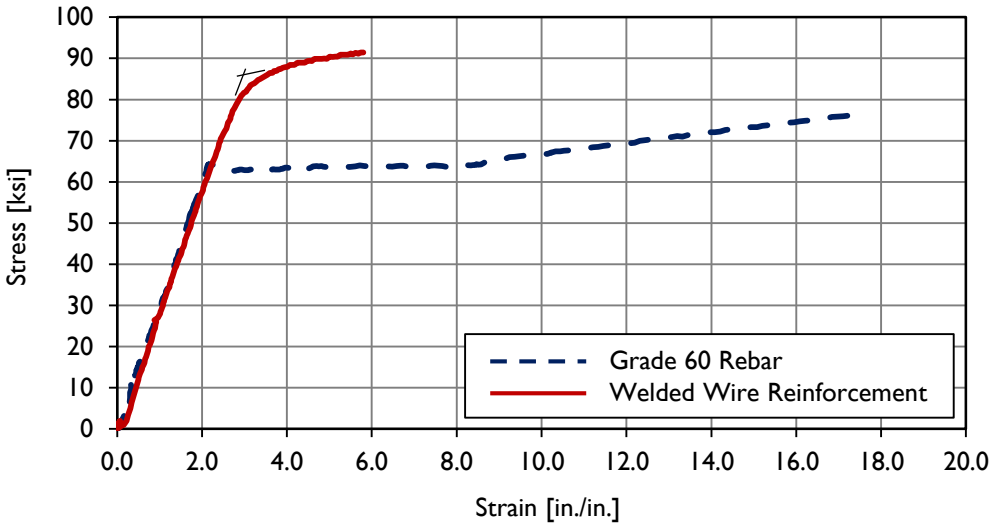

Figure 3-24: Typical stress-strain plots from material used in the tested U-Beams.

TxDOT allows welded-wire reinforcement to be used in an equal-area replacement in Texas U-Beams. At least one fabricator in the state typically uses this material. In calculating shear capacity, ACI 318 (2008) limits the yield strength of standard reinforcing bars to 60 ksi and the yield strength of welded-wire reinforcement to 80 ksi, while AASHTO LRFD (2010) allows for 75 ksi to be used for WWR. As is typical in any comprehensive shear research program, actual material properties were used in strength calculations in this study as opposed to design values.

3.6.4 Bearing Condition

As described in Section 3.2.4, Texas U-Beams are supported on three bearing pads. As a result, test specimens were tested with either a single- or double-bearing pad configuration, as shown in Figure 3-17.

3.6.5 Amount of Prestressing

Test specimens were fabricated using 0.5- or 0.6-inch diameter Grade 270 low-relaxation prestressing tendons stressed to 202.5 ksi. The number of strands used varied from 58 to 78. The strand layout for each test section can be found with the beam descriptions in Chapters 4 and 5.

The amount of prestressing has two effects on shear behavior. First, at prestress transfer, the bars in the end region of the beam are stressed, as was described in Section 2.4. The reinforcing bar details in the end region of the Texas U-Beam are not dependent on the number of strands bonded within the beam. As a result, the reinforcing bars in the end region of beams with a higher number of prestressing strands were expected to be more heavily stressed prior to shear testing than the bars in beams with fewer strands. Second, the magnitude of the prestressing affects the shear capacity, as recognized in the calculations presented in Chapter 2.

With two exceptions, the prestressing strands were fully bonded through the length of the beam. In Beam 3, significant amounts of debonding was used to investigate the effect of sheathed strands and decreased prestressing force on shear strength. In Beam 7, at the request of the fabricator, five (of 58) strands were debonded the full length of the beam to reduce the required strength for release.

In Beam 4, three 0.5-in. strands were also included in each of the two top flanges of the beam. These strands were included to test an alternative to debonding of bottom flange prestressing strands for purposes of controlling stresses at prestress transfer. The strands were stressed to 150 ksi.

3.6.6 Reinforcing Bar Details

The U-Beam test specimens described in the next two chapters are split into two groups: Phase I and Phase II beams. The Phase I beams were designed following existing TxDOT practice with regards to reinforcing bar and geometric details. The Phase II beams contained reinforcing bar and geometric details not in the standard.

The size and location of the main shear reinforcing bars, supplementary bars that were used in Phase II beams, and confinement steel are of particular interest. The

reinforcement details (size, number, and spacing of bars) are provided with the beam descriptions in the following chapters.

3.6.7 Web Width

In Beam 4, the cross-sectional geometry of the U-Beam was altered to increase the amount of concrete available to contribute to the strength of the beam. The two cross sections are shown in Figure 3-25. The perpendicular dimension of each web was increased from 5.0 in. to 7.75 in. The area of the beam increased from 1120 in.^{2} to 1381 in.^{2}, and the moment of inertia increased from 403,020 in.^{4} to 464,790 in.^{4}. All dimensions of the modified cross section can be found in Appendix A.

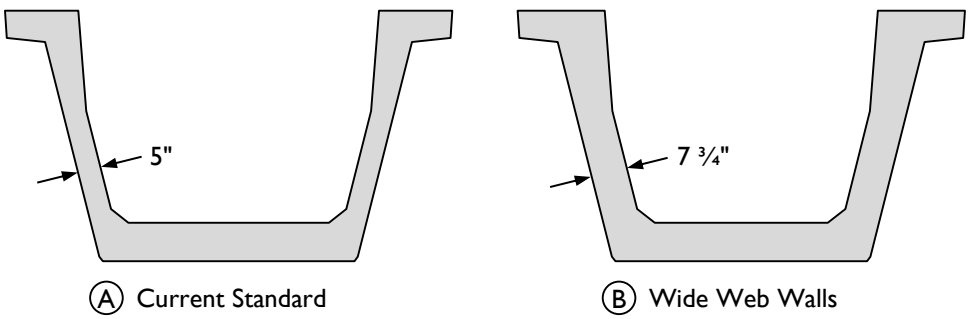

Figure 3-25: Comparison of (A) standard cross section to (B) cross section with widened web walls.

In order to fabricate a beam with wider web walls, a new internal void form was needed. The form was fabricated at FSEL out of wood, as purchasing a steel internal void for one beam was not economical.

3.6.8 Test Variable Summary

All design data pertinent to this study are presented here in five tables. The tables include information on geometry (Table 3-4), concrete material properties (Table 3-5), reinforcing bar layout and strength (Table 3-6), prestress strand positioning (Table 3-7), and shear test set-up (Table 3-8). The specific constituent materials in each concrete mixture design are provided in Tables 3-1 and 3-2.

Table 3-4: Basic geometric properties of the fabricated U-Beams.

Basic Geometric Properties													
Beam ID		Fabrication Date	Fabrication Location	Centerline Length, L_{CL} [ft]	Total Length, L [ft]	Exterior Skew Angle, θ_{ext} [°]	Interior Void Skew Angle, θ_{void} [°]	Length of End Block, l_{eb} [in.]	Gross Beam Area, A_b [in.^{2}]	Total Web Width, b_w [in.]	Height of Beam Centroid, y_{bot} [in.]	Beam Weight [kip]
	B0N	01/29/2008	Fabricator A	30	30	0.0	90.0	29	1120	10.0	22.36	43.4
	B0S					0.0	90.0	22				
PHASE I	B1N	11/18/2008	FSEL	26.75	30	0.0	90.0	18.0				39.9
	B1S					45.0	45.0	24.0				
	B2N	02/26/2009	FSEL	26.75	30	0.0	90.0	18.0				47.3
	B2S					45.0	90.0	24.0				
	B3N	07/16/2009	FSEL	30	30	0.0	90.0	18.0				43.4
	B3S					0.0	90.0	18.0				
PHASE II	B4N	10/27/2009	FSEL	30	30	0.0	90.0	18.0	1381	16.0	24.02	50.7
	B4S					0.0	90.0	18.0				
	B5N	11/17/2009	Fabricator A	30	30	0.0	90.0	18.0	1120	10.0	22.36	43.4
	B5S					0.0	90.0	18.0				
	B6N	11/11/2010	Fabricator B	30	30	0.0	90.0	36.0				50.4
	B6S					0.0	90.0	30.0				
	B7N	04/27/2011	Fabricator C	31.75	35	0.0	90.0	36.0				62.9
	B7S					45.0	90.0	30.0				

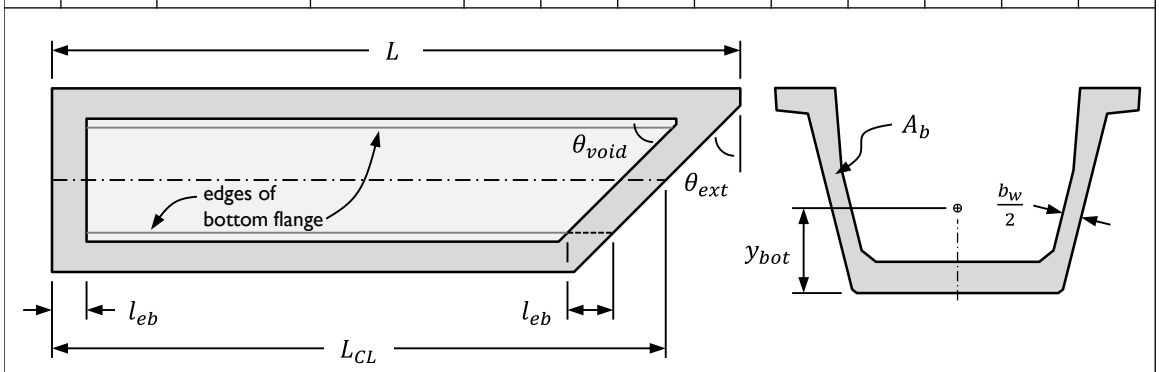

Table 3-5: Concrete material properties for the U-Beam test specimens.

Concrete Material Properties									
Beam ID		Beam Concrete Mixture Design ID	Release Strength [ksi]	Release Factor	28-day Compressive Strength of Beam [ksi]	Compressive Strength of Beam at Shear Testing [ksi]	Deck Concrete Mixture Design ID	28-day Compressive Strength of Deck [ksi]	Compressive Strength of Deck at Shear Testing [ksi]
	B0S	[unknown]				12.90	III-A	10.5	10.8
PHASE I	B1N	III-A	6.4	0.66	11.7	11.96	I-F	10.5	10.5
	B1S					11.96			10.5
	B2N	III-A	6.7	0.64	10.3	11.48	I-F	10.0	8.6
	B2S					[not tested]			[not tested]
	B3N	III-B	5.9	0.62	11.3	11.31	I-F	10.3	8.5
	B3S					12.10			10.7
PHASE II	B4N	III-B	6.4	0.66	10.3	11.44	I-F	7.5	7.5
	B4S					11.44			7.5
	B5N	III-C	5.6	0.65	12.4	13.23	I-G		7.6
	B6S	III-D	5.4	0.66	11.4	12.02	I-H	10.0	10.7
	B7N	III-E	7.9	0.55	12.4	12.45	I-G		9.6

Table 3-6: Reinforcing bar locations and material properties for U-Beam test specimens.

Transverse Reinforcing Bar Details and Material Properties													
			Reinforcing Bar Spacing[1]										
			Region 1			Region 2			Region 3				
	Beam ID	Reinforcing Bar Type	Size	Spacing	Distance	Size	Spacing	Distance	Size	Spacing	Distance	Yield Strength [ksi]	Bar Spacing Used in Calculations [in.]
	B0N	Gr. 60	2-#4	8 in.	15'-0"	[no second region]			[no third region]			60.0 [nominal]	8.0
	B0S	Gr. 60	2-#4	18 in.	15'-0"	[no second region]			[no third region]				18.0
PHASE I	B1N	Gr. 60	2-#4	4 in.	6'-3"	2-#4	6 in.	8'-9"	[no third region]			65.8	4.0
PHASE I	B1S[2]	Gr. 60	2-#4	4 in.	6'-3"	2-#4	6 in.	3'-2½"	[no third region]			65.8	4.0
PHASE I	B2N	WWM	2-#4	4 in.	6'-3"	2-#4	6 in.	8'-9"	[no third region]			85.2	4.0
PHASE I	B2S[2]	Gr. 60	2-#4	4 in.	6'-3"	2-#4	6 in.	3'-2½"	[no third region]			65.8	4.0
PHASE I	B3N	Gr. 60	2-#4	4 in.	6'-3"	2-#4	6 in.	8'-9"	[no third region]			65.3	4.0
PHASE I	B3S	Gr. 60	2-#4	4 in.	6'-3"	2-#4	6 in.	8'-9"	[no third region]			65.3	4.0
PHASE II	B4N	Gr. 60	2-#4	3 in.	5'-0"	2-#4	4 in.	5'-0"	2-#4	6 in.	5'-0"	63.0	3.0
PHASE II	B4S	Gr. 60	2-#4 6-#5	3 in.	5'-0"	2-#4 6-#5	4 in. 4 in.	5'-0" 2'-8"	2-#4	6 in.	5'-0"	63.0 60.6	6.0
PHASE II	B5N	Gr. 60	2-#5 2-#6	4 in.	8'-3"	2-#5	6 in.	6'-9"	[no third region]			63.8 69.8	6.0
PHASE II	B6S	WWM	2-D20 4-#5	4 in.	8'-3"	2-D20	6 in.	6'-9"	[no third region]			85.0	6.0
PHASE II	B7N	Gr. 60	2-#4 4-#5	4 in.	8'-3"	2-#4	6 in.	3'-6½"	[no third region]			62.5 63.3	6.0

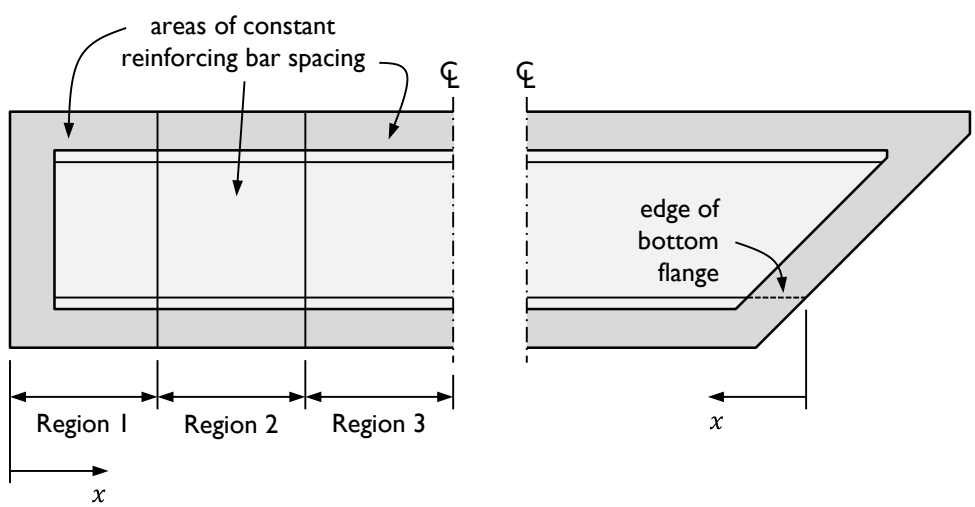

[1] Bar positions defined through midspan.
[2] Reinforcing bars in skewed ends measured along bottom flange, with 0'-0" positioned at obtuse angle.

Table 3-7: Details of prestressing used in U-Beam test specimens.

Prestressing Details																	
		Strand		Total			Row 1			Row 2			Row 3			Top Strand	
	Beam ID	Diameter [in.]	Area [in.^{2}]	Number	Height, y [in.]	Area Bonded at Beam End[1] [in.^{2}]	Number	Height, y [in.]	Debonded[2]	Number	Height, y [in.]	Debonded[2]	Number	Height, y [in.]	Debonded[2]	Number	Height, y [in.]
	B0S	0.5	0.153	68	3.76	10.404	27	2.17	none	27	4.14	none	14	6.11	none	none used	
PHASE I	B1N	0.5	0.153	78	4.00	11.934	26	2.0	none	26	4.0	none	26	6.0	none	none used	
	B1S																
	B2N	0.5	0.153	78	4.00	11.934	26	2.0	none	26	4.0	none	26	6.0	none	none used	
	B2S																
	B3N	0.5	0.153	42	4.19	6.426	12	2.0	14	14	4.0	12	16	6.0	10	none used	
	B3S																
PHASE II	B4N	0.5	0.153	84	7.43	12.852	26	2.0	none	26	4.0	none	26	6.0	none	6	52.0
	B4S																
	B5N	0.5	0.153	66	3.69	10.098	27	2.17	none	27	4.14	none	12	6.11	none	none used	
	B6S	0.5	0.153	64	3.62	9.792	27	2.17	none	27	4.14	none	10	6.11	none	none used	
	B7N	0.6	0.220	52	3.29	11.66	27	2.17	none	27	4.14	5	4	6.11	none	none used	

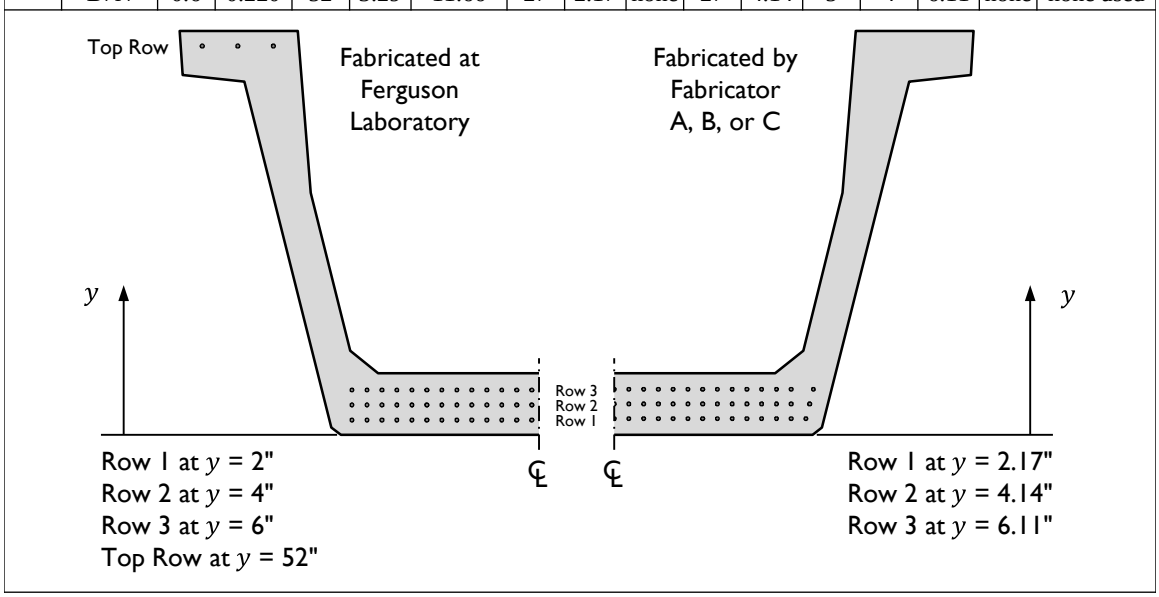

[1] Equal to area used in shear capacity calculations, as no strands gained bond between beam end and $a/2$.
[2] Number of debonded strands in the row.

Table 3-8: Details of shear test setup for U-Beam test specimens.

Details of Shear Test Setup										
	Beam ID	Clear Span, L_{cl} [in.]	Shear Span, a [in.]	Depth to Tensile Reinforcement, d [in.]	Shear Span-to-Depth Ratio, a/d	Number of Bearing Pads	Depth of CIP Deck, h_{deck} [in.]	Length of Bearing Pad, l_{LP} [in.]	Length of Load Plate, l_{LP} [in.]	Beam Overhang, oh [in.]
	B0S	348	174	59.0	3.0	2	8.0[1]	9.0	24.0	6.0
PHASE I	B1N	303	154	58.8	2.6	1				
	B1S	303	154	58.8	2.6	2				
	B2N	303	154	58.8	2.6	1				
	B3N	348	154	58.5	2.6	1				
	B3S	348	154	58.6	2.6	2				
PHASE II	B4N	348	154	58.8	2.6	1				
	B4S	348	154	58.8	2.6	1				
	B5N	348	154	59.1	2.6	1				
	B6S	348	154	59.1	2.6	1				
	B7N	369	154	59.5	2.6	1				

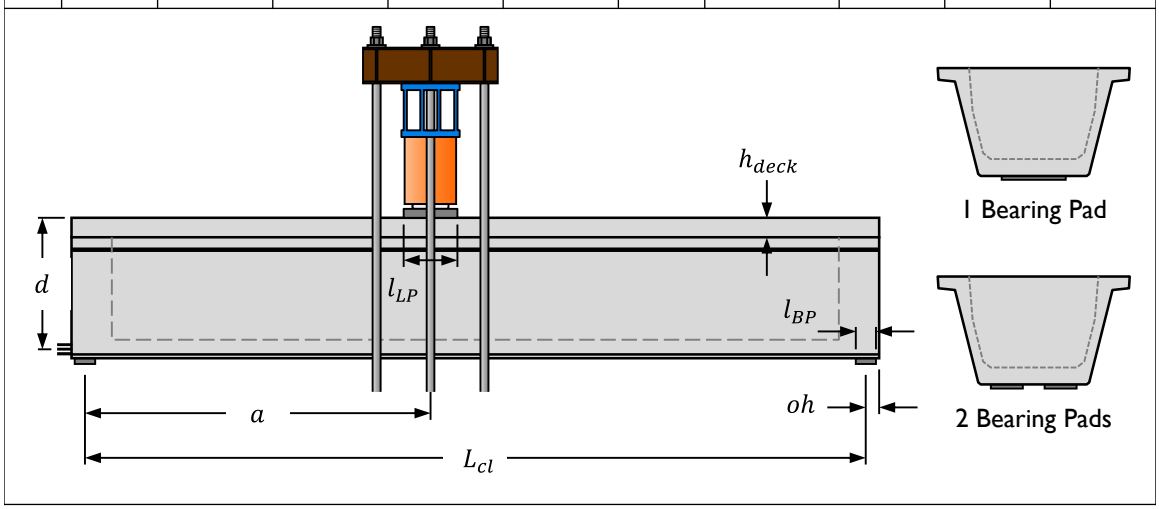

[1] Plywood forms raise the centroid of the deck and increase the total height by ¾ in., as seen in Figure 3-15.

3.7 CHAPTER SUMMARY

An experimental testing program was performed on a series of eight Texas U54 prestressed concrete bridge girders fabricated at the Ferguson Laboratory in Austin, TX and at three Texas fabrication plants. Eight end regions were studied at prestress transfer, nine end regions were thermally monitored during curing, and eleven end regions were shear load-tested. The details of the testing program, with regard to test set-up and

instrumentation were presented in this chapter. The primary test variables considered during this study were discussed, and all geometric and material properties were presented in a series of tables. The following two chapters will present a more thorough description of each beam fabricated.

CHAPTER 4

Specimen Details & Test Observations: Phase I

4.1 INTRODUCTION

Eight prestressed concrete Texas U-Beams were tested at the Ferguson Laboratory. Of the eight beams, four were built by the research team and four were built at local prestressed concrete beam fabrication yards. Eight end regions were analyzed at prestress transfer and eleven shear tests were performed. The design of each beam was developed with the information gathered from testing the preceding beam.

The 54-in. deep U-Beams tested have been subdivided into three groups: (i) Beam 0, which was designed to test a specific reinforcing bar detail; (ii) Phase I beams (numbered 1, 2, and 3), the design of which followed current TxDOT standard practice; and (iii) Phase II beams (numbered 4, 5, 6, and 7), each of which incorporated design modifications intended to improve the standard design. The details of Beam 0 and the Phase I test specimens are given in this chapter. The details of the Phase II test specimens are given in the following chapter. A summary of the key features of each test region discussed in this chapter is given in Table 4-1, along with whether the beam end region was tested at prestress transfer, under shear loads, or both.

Table 4-1: Summary of key features of Beam 0 and Phase I test regions.

Beam ID	End Geometry	Beam End Tested: At Prestress Transfer	Beam End Tested: Under Shear Loading	Key Feature of Test Region
B0S			X	18 in. reinforcing bar spacing
B1N		X	X	Standard squared end region
B1S	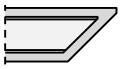	X	X	Skewed internal void
B2N		X	X	Welded-wire reinforcement
B2S	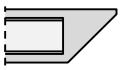	X		Standard skewed end region
B3N		X	X	46% of strands debonded
B3S		X	X	46% of strands debonded

Limited results (specifically, maximum release stresses and shear performance values) are presented in this chapter; in-depth discussion of these results and analysis of other collected data can be found in Chapter 6. These selected test results are presented in this chapter to help the reader understand the logic with which each test successive specimen was designed. For simplicity, in this chapter and the next, the shears causing failure are compared only to the shear capacities calculated using the AASHTO LRFD General Procedure (2010), as described in Chapter 2; comparisons to the two other calculation methods previously discussed are made in Chapter 6.

4.2 BEAM 0

Near the beginning of this research project, TxDOT engineers raised concern about older (pre-2006) U-beams, which were designed with a wider stirrup spacing near beam end than is currently allowed. The original U-Beam standard design allowed stirrups spaced at 18 in. within 13 ft of the beam end, as was shown in Figure 2-3. The concerns expressed by TxDOT was focused on the shear capacity of U-Beam bridges under super-heavy loads. As a shear testing frame was already being set up, it was

requested that the research team test a beam featuring the current standard spacing (i.e., 8 in.) at one end and an 18 in. spacing at the other end.

The beam was constructed by Fabricator A and was then delivered to the Ferguson Laboratory. Elevation and cross-sectional views of the beam are shown in Figure 4-1. The reinforcing bar spacings indicated are for stirrups only; end block reinforcement has been removed for clarity. The end blocks in Beam 0 and all Phase I beams were constructed following standard plans (provided in Appendix A). The total length of this and each subsequent Phase I beam was 30'-0". Beam 0 contained 68 0.5-in. diameter prestressing strands. The shear test performed on Beam 0 was used to verify the strength of beams with 18 in. reinforcing bar spacing near the end of the span and to establish the testing methods that would be used for subsequent beams.

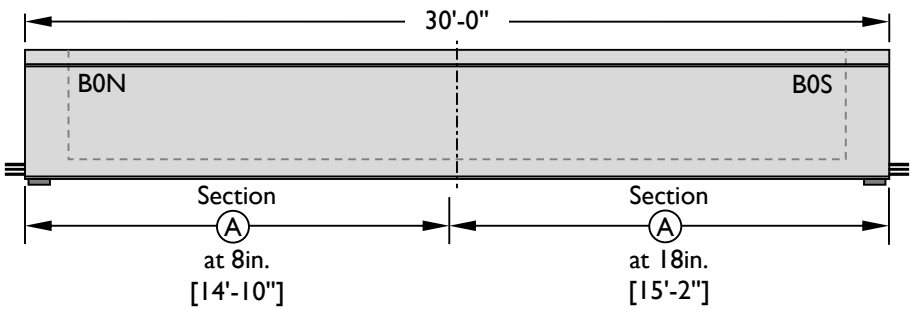

Figure 4-1: (i) Beam 0 elevation view, with reinforcing bar spacings indicated.

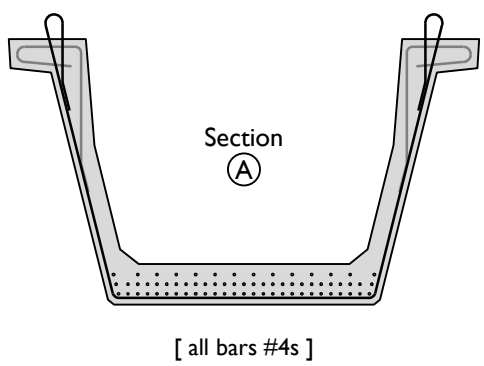

Figure 4-1: (ii) Standard cross section of Beam 0.

As Beam 0 was fabricated outside of Ferguson Laboratory, strain gauges were not installed on the reinforcing bars and data were not gathered regarding initial straining due to prestress transfer.

4.2.1 Shear Testing

After an 8-in. deck was cast as discussed in Chapter 3, and allowed to cure sufficiently, Beam 0 was loaded at midspan (a/d = 3.0). By loading at midspan, the shear in each beam end was the same. No strengthening system was used during this beam test, resulting in both ends of the beam being tested simultaneously. The south end, with 18-in. reinforcing bar spacing, failed first, in a web-crushing manner. The failure shear was 491 kip. The shear capacity was calculated with a constant stirrup spacing of 18 in.; the details of this and all subsequent shear capacity calculations can be found in Appendix D. The shear performance ratio (V_{test}/V_n) was 1.04, indicating 4% conservatism in the AASHTO General Procedure (2010) shear strength calculation for this test region.

After strengthening the failed end with post-tensioned clamps, the beam was loaded again in order to determine the strength of the end with 8-in. reinforcement spacing. Failure of the second test region (B0N) could not be achieved due to the heavy damage caused by the first test. Beyond confirmed that the shear strength of this U-Beam with 18-in. stirrup spacing was above the calculated shear capacity, few conclusions regarding U-Beam behavior were made using this beam.

4.3 BEAM 1

Phase I of this study included beams with designs following current practice. The three beams tested in Phase I used standard reinforcing bar placement along the length, with end-region geometries constructed as specified on the TxDOT U-Beam standard drawings.

The north end of Beam 1 was designed as a typical U-Beam section, as is currently fabricated and put into service through the state of Texas. This test region, B1N, was squared and contained standard reinforcing bar and geometric detailing. The south end of Beam 1 was fabricated to test the most extreme skewed beam end allowed by TxDOT. This test region, B1S, had a 45-degree exterior skew angle with a parallel 45-degree interior void skew angle. As mentioned in Chapter 3, this geometric detail is

allowed by TxDOT standard plans, but is rarely, if ever, used in field fabrication. The plan view, elevation view, and standard cross section of Beam 1 are given in Figure 4-2.

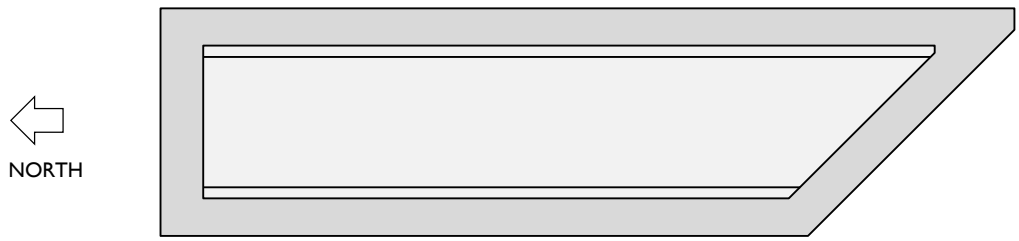

Figure 4-2: (i) Plan view of Beam 1.

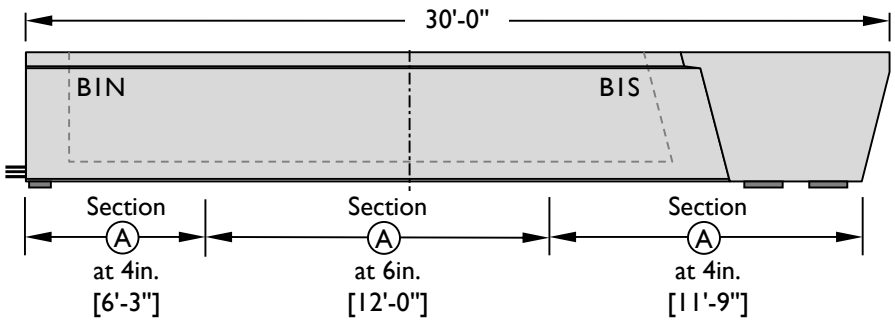

Figure 4-2: (ii) Elevation view of Beam 1.

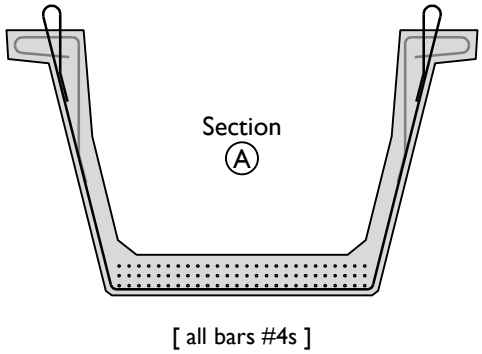

Figure 4-2: (iii) Standard cross section of Beam 1.

4.3.1 Early-Age Behavior

As discussed in Chapter 3, each of the beams fabricated in-house was instrumented heavily to evaluate the stresses induced in reinforcing bars at prestress transfer. A detailed discussion of the stresses measured in the four beams fabricated at the Ferguson Laboratory, including comparisons with stresses reported in the literature, is presented in Chapter 6. Within this chapter, maximum and average stresses measured are

reported, as it was theorized that reinforcing bar stresses caused by prestress transfer could negatively influence shear performance. The maximum stress seen in the end regions of Beam 1 due to the application of the prestressing force was 26 ksi, while most gauges read strains associated with stresses below 5 ksi.

4.3.2 Shear Testing

After a deck was cast on Beam 1, the beam was load tested. The load was applied at midspan along the centerline of the beam, resulting in a shear span-to-depth ratio of 2.6 in each test region. This ratio was held constant for the remainder of the beams tested. As with Beam 0, both shear regions were tested simultaneously.

The beam failed first in the south, skewed end of the beam, at a shear of 612 kip. As was typical during this study, the failure was concentrated on one side of the beam. The majority of damage was located near the bottom flange-to-web interface at beam end, in the region of the beam with 4-in. stirrup spacing (Figure 4-3). Given this failure location, evaluation of the ratio of failure shear to calculated capacity was made using V_n calculated with stirrups spaced at 4 in. The failure shear was 34% below that calculated shear capacity.

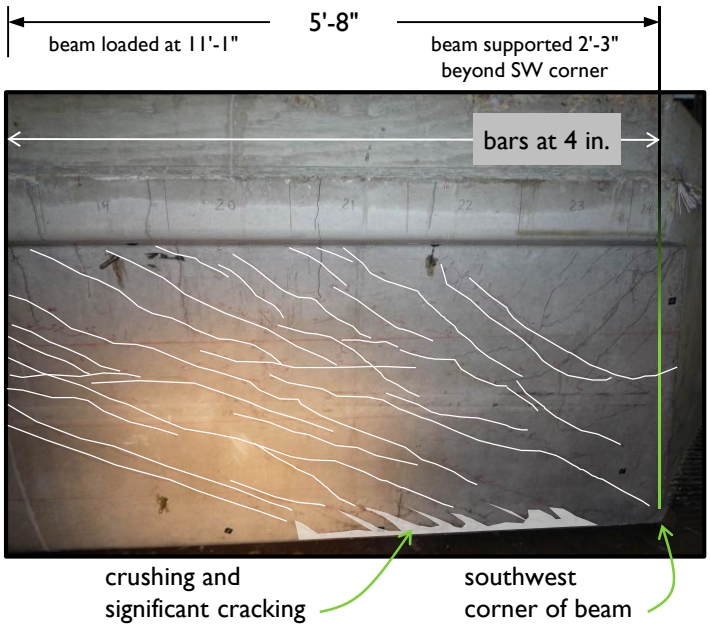

Figure 4-3: Test region B1S after failure of end region.

After strengthening the south end with external post-tensioned clamps, the north, squared end was tested. It should be noted that the calculated capacity for both the squared and skewed ends of Beam 1 were the same. The squared end failed at a shear load of 659 kip, again in the end region near the support (Figure 4-4). The ratio of failure shear to calculated shear strength for test region B1N was 0.71.

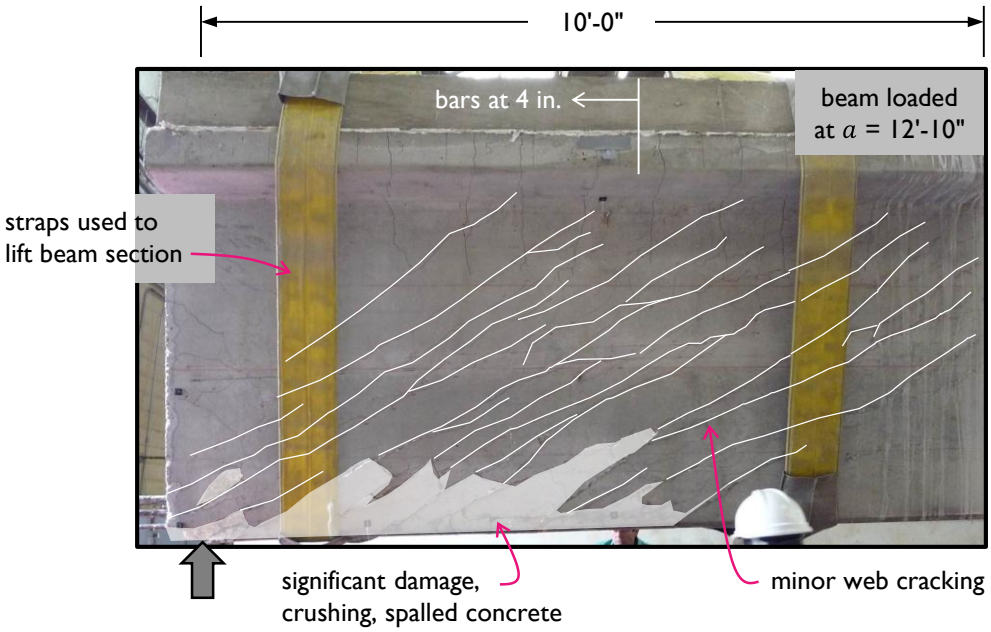

Figure 4-4: Test specimen B1N after failure of end region.

After examination of shear tests in the literature, as described in Chapter 2, the calculated shear capacities of the U-Beams tested were expected to be 40 to 50% conservative with respect to the measured strengths. This expectation was not met with either test region of Beam 1.

4.4 BEAM 2

While the shears carried by each end of Beam 1 were lower than expected, the initial plan to test a second skewed design matching current practice was still followed. A plan view of Beam 2 can be seen in Figure 4-5(i), with elevation and cross-sectional views following.

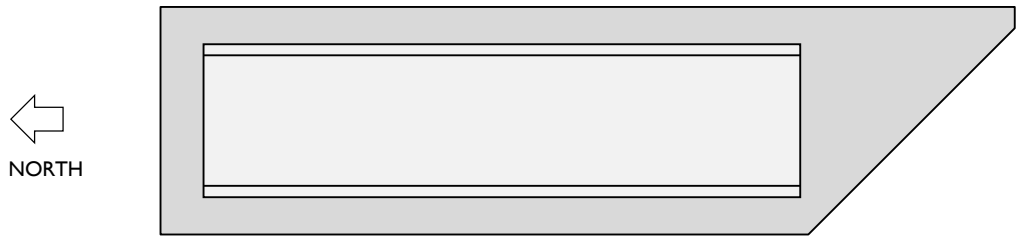

Figure 4-5: (i) Plan view of Beam 2.

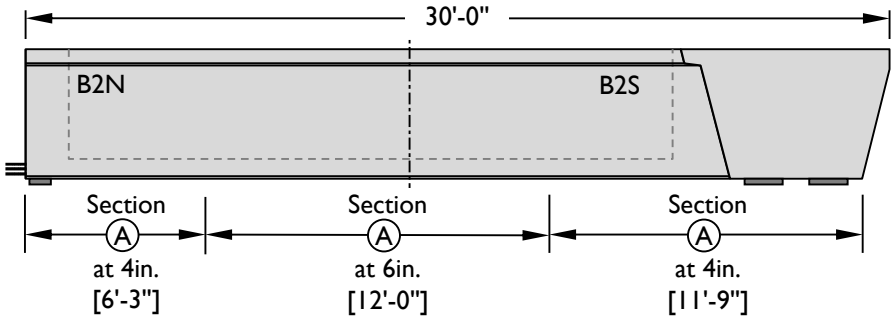

Figure 4-5: (ii) Elevation view of Beam 2.

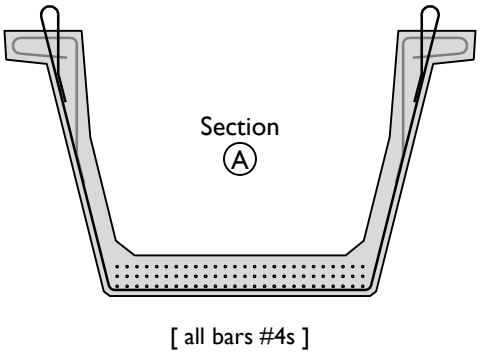

Figure 4-5: (iii) Standard cross section of Beam 2.

Beam 2 was built with two variables to compare against Beam 1. At the squared end, the stirrups were constructed using welded-wire reinforcement. All other properties matched the squared end of Beam 1. At the south, skewed end of Beam 2, the interior void form was rectangular, resulting in a solid triangular end block, rather than the narrow end block of Beam 1. This end block detail is the one predominantly used by fabricators during construction of beams with skewed ends.

4.4.1 Early-Age Behavior

As with Beam 1, Beam 2 was instrumented heavily. At prestress transfer, the maximum stresses seen in the reinforcing bars within the end region was 29 ksi, with most strain gauges reading strains associated with stresses below 5 ksi.

4.4.2 Shear Testing

Beam 2 was tested in shear in the same fashion as Beam 1: after casting a deck, the beam was loaded at midspan (a/d = 2.6) until first failure. The north, squared end failed at a shear of 610 kip, again in the region with reinforcing bars spaced at 4 in. (Figure 4-6). This failure shear was 44% below the calculated strength for that section. While the calculations for strength take advantage of the higher yield stress associated with welded-wire reinforcing, the shear load sustained by the beam did not indicate that the welded wire improved the shear performance of the beam.

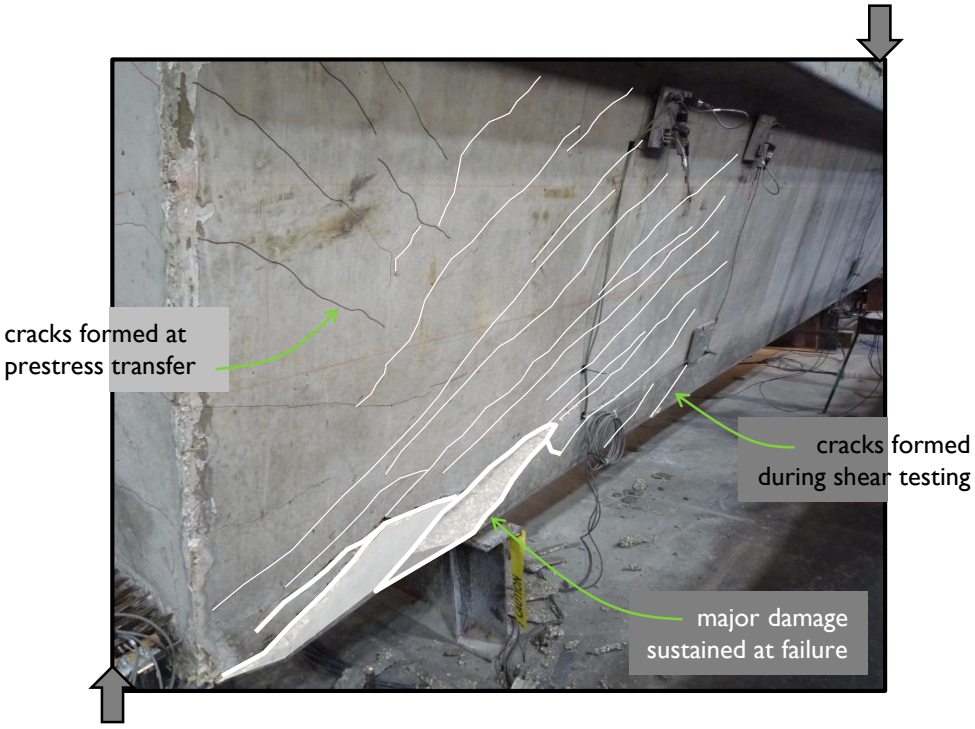

Figure 4-6: Test specimen B2N after failure of end region.

Attempts to induce a shear failure in test region B2S (the skewed end of the beam) were not successful, as there was too much damage to test region B2N to allow for

further loading. Prior to removing the beam from the laboratory, it was cut into two pieces. Once the cut was made, the damage sustained on the interior of the beam was examined. A horizontal crack was observed along the interface between the bottom flange and the web of the beam (Figure 4-7).

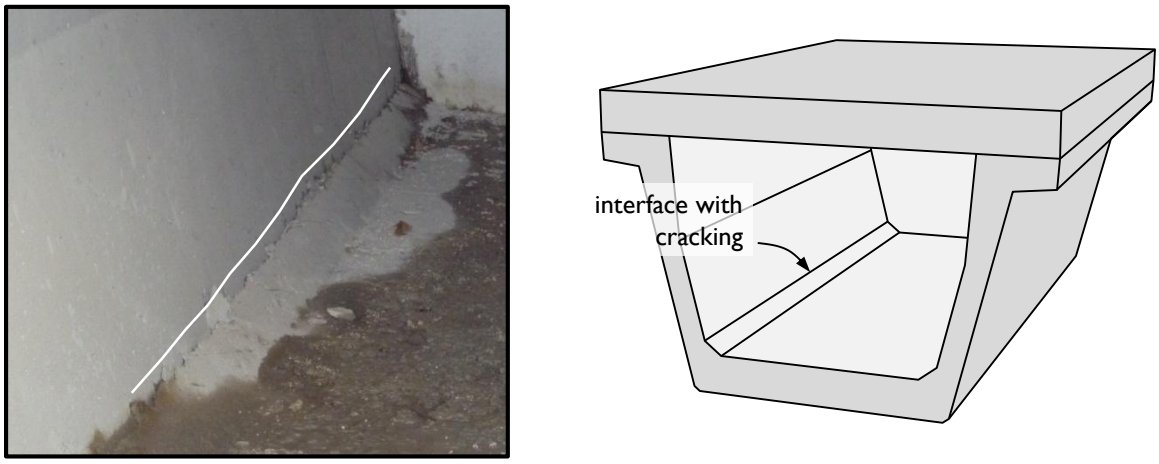

Figure 4-7: Horizontal crack along bottom flange-to-web interface in test specimen B2N.

4.5 INTERMEDIATE ANALYSIS

Having conducted shear tests on four test regions, with three failing significantly below the calculated shear capacity, the research team met with the TxDOT Project Monitoring Committee (PMC) to discuss the results. Prior to the start of the testing program, it had been expected that high stresses induced at prestress transfer might cause low shear failures. In the testing of Beams 1 and 2, shear failures occurred 29 to 44% below the calculated shear capacity, though no high stresses were measured in the shear instrumentation region after prestress transfer. While failure was expected in the web near load point, the observed damage at failure was most significant near the interface between the bottom flange and the web of the beam at beam end.

Discussion with the PMC indicated that a new variable should be considered: debonding of prestressing strands. While the project had been driven by the worst-case scenario regarding release stresses (including as many strands as possible), beams in the field have as many as 75% of the strands debonded in the end region of the beam for control of top-fiber tensile stresses, as presented in Chapter 3 (Van Landuyt, 2009).

Debonding strands was perceived to have two potential effects on the shear capacity of the beam. First, by reducing the number of strands and thus the prestressing force in the end region, the associated transverse transfer stresses would be reduced, thereby reducing the negative impact these stresses might have on shear performance. Second, shielding strands through the bearing region of the beam would reduce the area of steel available to act as a longitudinal tie, and reduce the shear capacity available.

4.6 BEAM 3

Beam 3 was designed to determine the effects of debonding on shear performance and to represent a more typical design (with respect to end-region stresses) into the series of U-Beams tested. The original project goals of evaluating the influence of skew, end block geometry, and bearing condition were put on hold until the failure of the standard section was better understood.

The standard TxDOT drawings regarding geometry and reinforcing bar layout were used for Beam 3. The debonding plan was formed after studying eighty Texas U-Beams designed between 2000 and 2008, as presented in Chapter 3. That study revealed that significant debonding (40-60%) is typical practice in Texas despite the AASHTO LRFD Bridge Design Specifications maximum limit of 25% debonded strands (AASHTO §5.11.4.3).

Debonding strands reduces the flexural capacity of the beam section. Calculations performed during the design of Beam 3 indicated that debonding more than 38 strands (of 78 at midspan) would likely result in a flexural failure of the beam, rather than the desired shear failure. To avoid this scenario, 36 strands (46%) were debonded at the end of the beam. Table 4-2 and Figure 4-8 contain the details of the debonding pattern.

Table 4-2: Debonding pattern for Beam 3.

STRUCTURE	DEBONDED STRAND PATTERN PER ROW							
	DIST FROM BOTTOM (in.)	NO. OF STRANDS		NUMBER OF STRANDS DEBONDED TO (ft from end)				
		TOTAL	DE-BOND	3	6	9	12	15
UT U-Beam 3	2.0	26	14		4	4	4	2
	4.0	26	12		4	2	4	2
	6.0	26	10		2	2		6

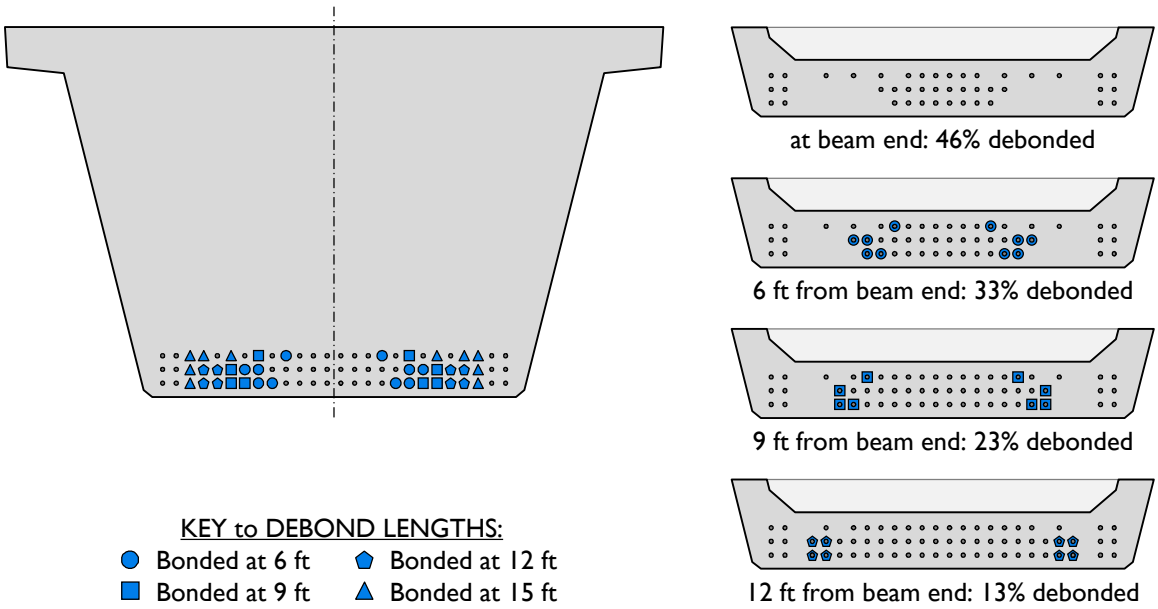

Figure 4-8: Debonding pattern for Beam 3.

The reinforcing bar layout of Beam 3, which was the same as standard practice (and the squared ends of both Beam 1 and Beam 2), is shown in Figure 4-9. The north and south ends of Beam 3 are identical and squared (no skew).

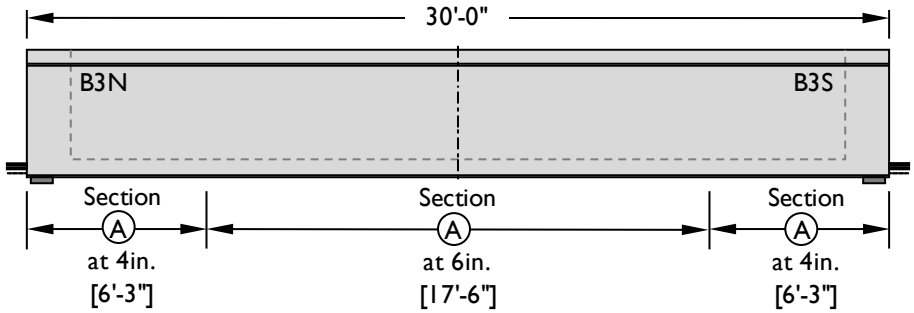

Figure 4-9: (i) Elevation view of Beam 3.

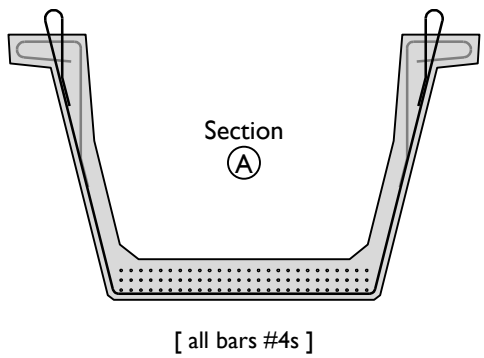

Figure 4-9: (ii) Standard cross section of Beam 3.

4.6.1 Early-Age Behavior

Debonding the strands significantly reduced the effects of prestress transfer: the maximum stress seen in the end-region reinforcing of the beam was 6 ksi, and most gauges read strains associated with reinforcing bar stresses below 2 ksi.

4.6.2 Shear Testing

Beam 3 was loaded with a shear span-to-depth ratio consistent with the previously tested Phase I beams (equal to 2.6). As the centerline length was longer in Beam 3 than in Beams 1 and 2, the load was placed 1'-8" from the midspan of the beam to create the same shear span. Prior to initial loading, the longer span was strengthened using external post-tensioned clamps to minimize damage to that section during the first test. After the first test, the beam was repositioned beneath the load and the clamps moved to strengthen the damaged end during the testing of the second end (as illustrated in Figure 3-20).

The two ends of Beam 3 failed at 655 and 663 kip shear, or 3 and 4% below the calculated shear capacity given a 4-in. reinforcing bar spacing. The failure shears and failure mode in both shear test regions was consistent with that seen in Beams 1 and 2, with major damage concentrated in the bottom flange near the end of the beam. The damage caused at the failure of test specimen B3S is pictured in Figure 4-10.

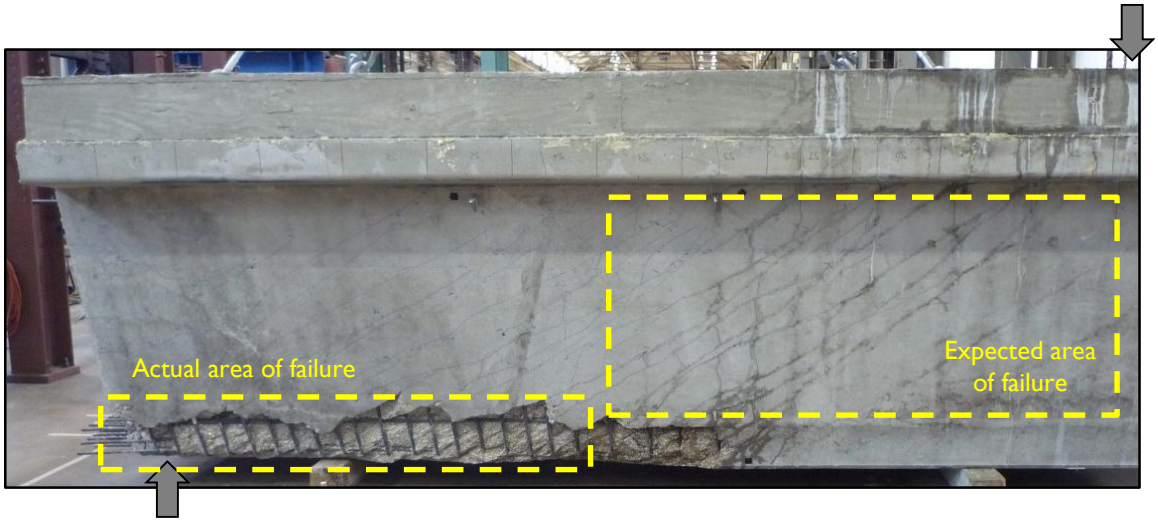

Figure 4-10: Damage to test specimen B3S after shear testing.

4.7 SUMMARY OF PHASE I BEAM TESTS

Five test regions were loaded to failure during Phase I of this project. A summary of the variables studied is presented in Table 4-3. Test specimen B1N was a "typical" beam, with no skew and fabricated with conventional reinforcing bars and fully bonded strands. B2N had the same geometric properties as B1N, but contained welded wire reinforcing. The two test specimens in Beam 3 (B3N and B3S) were geometrically identical to B1N and contained the same reinforcement. At midspan, the prestressing was the same as in B1N as well, but in the two Beam 3 test specimens, 46% of the strands bonded at midspan were sheathed at beam end. Test specimens B1S and B2S were skewed beams with varied internal void geometries. Specimen B2S could not be loaded to failure due to the extensive damage in the beam caused by testing specimen B2N. The calculated shear capacity did not account for the internal or external skew.

Table 4-3: Summary of Phase I test beams and variables.

Beam	End Geometry	Bearing Condition	Type of Reinforcing	Number of 0.5 in. Prestressed Strands Bonded at Beam End	Failure Mode	$\frac{V_{test}}{V_n}$
B1N		single pad	Grade 60	78	horizontal shear	0.71
B1S	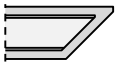	double pad	Grade 60	78	horizontal shear	0.66
B2N		single pad	welded wire mesh	78	horizontal shear	0.54
B2S	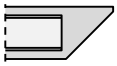	--	Grade 60	78	--	--
B3N		single pad	Grade 60	42 (46% of 78)	horizontal shear	0.96
B3S		double pad	Grade 60	42 (46% of 78)	horizontal shear	0.97

When the ratio of failure shear to calculated shear capacity is considered (as in Table 4-3), the performance of the test specimens seems to vary from one another, with V_{test}/V_n ranging from 0.56 to 0.97. When the failure shear is plotted instead, without normalization to the calculated capacity (Figure 4-11), it can be seen that the failure shears are very similar, within 10% of one another. While the calculated shear capacity (V_n) increased or decreased, respectively, due to the influence of higher reinforcing bar strength (B2N) or smaller contribution from prestressing (B3N, B3S), the measured capacity (V_{test}) did not change. The lack of variability in the failure shears indicated independence between beam behavior and multiple critical variables that contributed to calculations for shear capacity. Given this observation and the location and magnitude of sustained damage at failure, it was concluded that these beams were not failing in a typical web-shear failure mode. Further discussion will be presented in Chapters 6 and 7 regarding the observed behavior at failure of the Phase I test specimens.

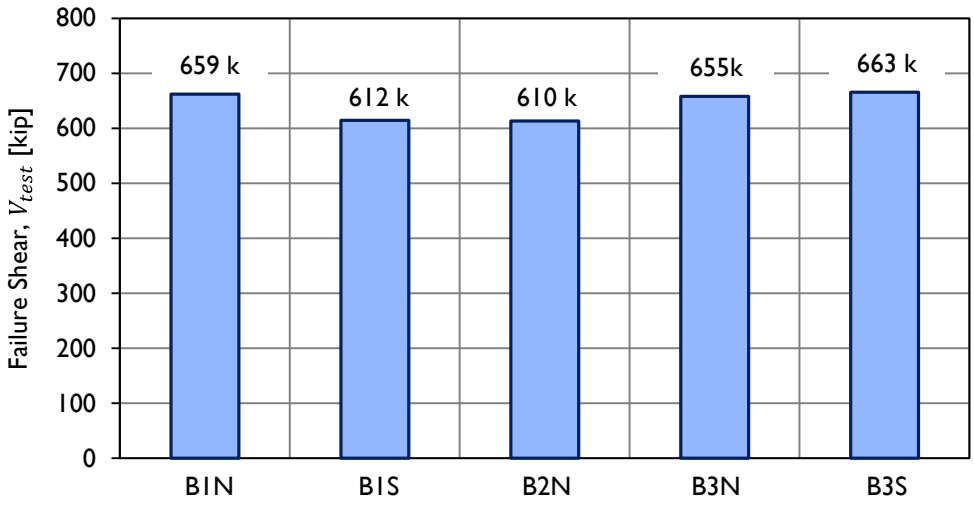

Figure 4-11: Failure shears of five Phase I test specimens.

4.8 PHASE I TO PHASE II TRANSITION

The beams built as part of Phase I of testing were designed using current standards, with the intention of considering variables including skew, interior void geometry, bearing condition, reinforcement type, and debonding. Despite the wide range of differing properties under which each beam section was constructed and tested, the resulting strengths were within 10% of one another. More importantly, the damage observed at failure was concentrated in the bottom flange – not the web – in the theoretically strongest region of the shear span, where reinforcing bars were spaced at 4 in. No significant damage was seen in the beam webs, where typical shear failures occur.

Observations of the failure crack patterns and associated damage indicated that the beams were failing due to an unforeseen weakness at the bottom flange-to-web interface. Given the horizontal shear failure mechanism observed, comparisons to the vertical web-shear capacities calculated using the ACI Detailed Method, the AASHTO General Procedure, or the AASHTO Segmental Procedure are inappropriate.

Driven by the need to improve the performance of the Texas U54 design, two new goals were set by the TxDOT PMC and the research team. First, it was desired that mechanics of beam bending be used to explain the observed failure, and a method for

calculating the capacity of a prestressed beam at the bottom flange-to-web joint be presented. The details of this study can be found in Chapter 7.

The second and more important goal was to increase the strength of the bottom flange-to-web interface in the Texas U54 in order to prevent horizontal shear failure from occurring at loads below the calculated vertical shear capacity. Four U-Beams were fabricated with details not currently in the U-Beam standard, then load-tested to confirm the behavior at failure was as desired. The reinforcement and geometric details and shear performance of these beams are discussed in the next chapter.

CHAPTER 5

Specimen Details and Test Observations: Phase II

5.1 INTRODUCTION

All five test regions that were loaded to failure as part of Phase I of this study failed by sliding of the web against the bottom flange. This failure mode is known as horizontal shear, the mechanics of which are described in Chapter 7.

Detailing a new standard U-Beam design capable of controlling horizontal shear in Texas U-Beams, to a point where horizontal shear does not occur prior to exceeding the calculated vertical shear capacity, was the focus of the second phase of this study. A total of four beams were fabricated, one at the Ferguson Laboratory and one at each of three prestressed concrete beam fabrication plants. The beam fabricated at FSEL provided two end regions for study at prestress transfer. Five shear tests were performed on the eight beam end regions; in three cases, the damage caused by the test to one end of the beam prevented the load-testing of the other end.

Two different cross sections and three reinforcing layouts were used in the first three regions designed and tested. At the conclusion of those tests (after testing region B5N), a final recommended design was detailed by the research team. This design was tested in two test specimens: a squared-end beam (B6S) and a highly skewed-end beam (B7N). A summary of the key features of the Phase II test specimens is given in Table 5-1. Also noted is whether the beam was tested at prestress transfer, under shear loads, or both.

Table 5-1: Summary key features of Phase II test regions.

Beam ID	End Geometry	Beam End Tested: At Prestress Transfer	Beam End Tested: Under Shear Loading	Key Feature of Test Region
B4N	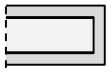	X	X	Wide web walls, no supplementary reinforcement
B4S	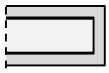	X	X	Wide web walls, 3-#5 supplementary reinforcement paired with R-bars
B5N			X	#5 R-bar, #6 supplementary reinforcement
B6S	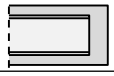		X	Recommended design, squared end
B7N	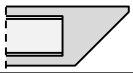		X	Recommended design, skewed end

Reinforcing details of the tested designs and the observed failures are presented in this chapter. The ratios of failure shear to calculated shear capacity are given, along with a summary of the data gathered at prestress transfer for Beam 4, the only Phase II beam fabricated with internal instrumentation. As with the Phase I tests, for simplicity, only the shear capacity calculated using the AASHTO General Method (2010) is given in this chapter. Further data analysis is presented in Chapter 6.

5.2 BEAM 4

Beam 4 was built at the Ferguson Laboratory. The beam was 30 ft long and was squared at both ends. Seventy-eight 0.5-in. diameter prestressing strands were used in the bottom flange of the beam.

5.2.1 Design Modifications

The two ends of Beam 4 were designed with identical geometry but different internal reinforcement design. The most significant difference between Beam 4 and the other beams fabricated in this study was the use of a different cross section, with wider web walls than the current standard. Both ends of Beam 4 contained more reinforcing steel than the existing TxDOT standard U-Beam design. The major changes to the basic U-beam design are detailed in this section. A summary of the reinforcing bar layout is

given in Figure 5-1. The bar spacings indicated refer to the placement of the stirrups (R-bars); end block reinforcement has been removed for clarity but can be seen in Appendix A.

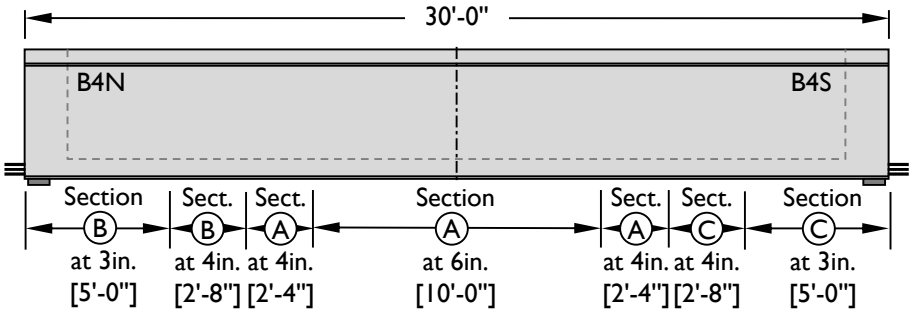

Figure 5-1: (i) Elevation view of Beam 4.

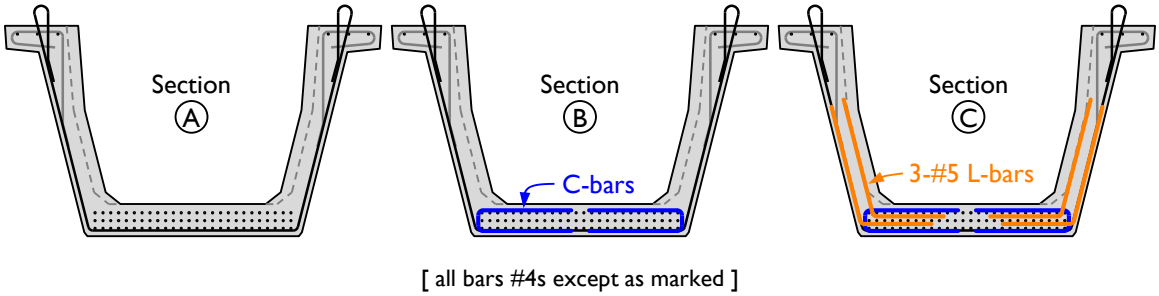

Figure 5-1: (ii) Standard cross sections of Beam 4.

5.2.1.1 Web Walls

The web walls in Beam 4 were increased from the standard 5.0 in. to 7.75 in., increasing the web width by 55% through the full beam length (Figure 5-2). The Texas U-Beam was originally intended to be a replacement for two AASHTO Type IV girders with 8 in. webs (b_w = 16 in.) (Ralls, et al., 1993), yet was designed with narrower webs. While increasing the web width increases V_c (and thus V_n) calculations, the research team believed this change would strengthen the bottom flange-to-web interface to prevent horizontal shear from controlling the failure, and improve serviceability of the beam. The increased web width would also allow for easier placement of additional reinforcing bars towards the inside web wall without violating cover requirements. All dimensions of this modified cross section are provided in Appendix A.

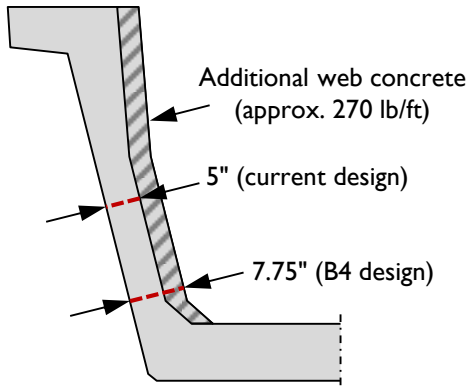

Figure 5-2: U-Beam cross section used in Beam 4, compared with the standard cross section.

As widening the web walls increases the unit weight of the section by 23%, this design was intended to be implemented with a transition zone located fifteen feet into the beam from either end, at which point the web width would decrease to the current standard design. With the extra dead load acting only at the beam ends, the dead load moment at midspan of a 120-ft long U-Beam would increase by only 1.5%.

5.2.1.2 Shear Reinforcement

Stirrup (R-bar) spacing was reduced from 4 in. to 3 in. for the first 5'-0" of the beam. The bars were spaced at four inches for the next 5'-0", then at six inches for the remainder of the beam (see Figure 5-1). A full-length beam would follow the remaining TxDOT standards, beginning with an 8-in. spacing at 15'-0".

5.2.1.3 Confinement Reinforcing

Confinement reinforcing was included around the prestressing strands for a distance 7'-8" from beam end ("C-bars"), following AASHTO (2010) specification §5.10.10.2 that states:

> *For the distance of 1.5d from the end of the beams other than box beams, reinforcement shall be placed to confine the prestressing steel in the bottom flange. The reinforcement shall not be less than No. 3 deformed bars, with spacing not exceeding 6.0 in. and shaped to enclose the strands. (pg 5-158)*

The existing standard U-Beam design does not include any confinement to the prestressing strands other than what is provided by the bend of the stirrup. This design

was implemented following the research of Barrios (1994), who studied the response of Texas U54s with and without confinement steel at prestress transfer. As no cracks were found in the lower region of the beam at prestress transfer, the recommendation at the time was to use the design without confining reinforcement. Those beams were not load tested.

The C-bars used in Beam 4 (Figure 5-3) were designed to not overlap, as excessive congestion of reinforcement beneath the strands, especially in the end regions, could be detrimental to quality of construction. This geometry was possible given the large width of the bottom flange and the minimal benefit that comes from the leg of the confinement as compared to the corners.

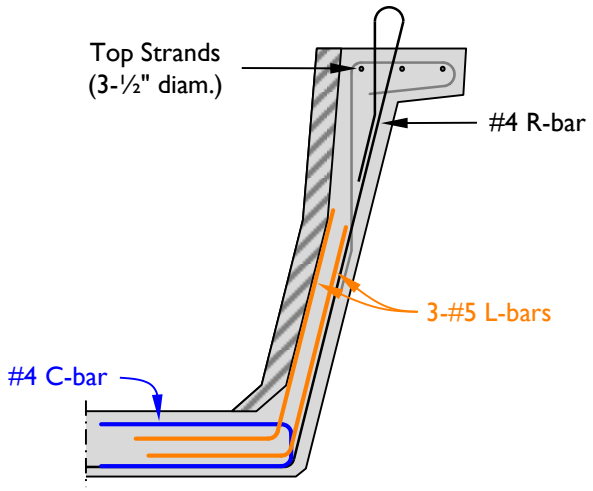

Figure 5-3: Beam 4 cross-section detail, with new bars and geometry highlighted.

5.2.1.4 Top Strands

Top strands were included (three per flange) to limit top flange stresses without needing to debond strands (Figure 5-3). Calculations regarding moment capacity were performed with and without the strands, and the difference was found to be negligible, due to the location of the top strands relative to the neutral axis of the decked beam. The top strands were stressed to 150 ksi.

5.2.1.5 Supplementary Reinforcement

Special reinforcing bars ("L-bars") were used at one end of the beam (test section B4S) for a distance 7'-8" from beam end. Three #5 bars were placed at each R-bar location in each web. One bar was bundled with the R-bar in the web, with the steel passing between Rows 1 and 2 of prestressing strands (Figure 5-3). The other two bars were bundled together towards the interior face of the beam, akin to the P-bars of the current standard. The length of the upper leg of the bar was determined by establishing the length necessary to develop the bar fully at the bottom flange-to-web interface. By terminating the bar mid-height in the web, the steel was not intended for use in web-shear reinforcement consideration.

The amount of steel crossing the bottom flange-to-web interface was decided upon using two criteria: constructability and existing designs for which horizontal shear was not an issue. Constructability was achieved by maintaining the size of the R-bars at #4s so as to maximize cover, and through the design of the confinement bars to not overlap.

The final amount of steel to be used was determined by studying the recently-released Tx Girder design. The Tx Girders (28 to 70 in. in depth), designed and tested in 2006 and implemented in 2007, are constructed with a reinforcement ratio ($A_s/(b_w s)$) of 6.1% for a distance 3'-2½" (0.55 to 1.38h) from beam end.

By comparison, the standard Texas U-Beam design uses 1.0% steel in the first 6'-3" (1.4h) of the beam. Beam 4 was built with 1.3% for the first 5'-0" (1.1h) at one end (B4N) and 4.7% for the first 5'-0" of the other end (B4S). These reinforcing distributions are summarized along with the information from Beams 5, 6, and 7 in Table 5-2. Several values are given for each end of Beam 4; the interface steel distribution in these test regions is given out to the point where the bar spacing increases to 6 in.

Table 5-2: Interface steel distribution in several beam sections.

	Interface Steel Reinforcement Ratio [%]	Distance [ft]	Relative distance [–]
Tx Girder	6.1	3'-2½"	0.55 to 1.38h
Standard U54 [Beams 1-3]	1.0	6'-3"	1.4h
Beam 4 North	1.3 1.0	5'-0" to 10'-0"	1.1h 2.2h
Beam 4 South	4.7 3.5 1.0	5'-0" to 7'-8" to 10'-0"	1.1h 1.7h 2.2h
Beam 5	3.8	8'-3"	1.8h
Beam 6 Beam 7	4.1	8'-3"	1.8h

The relative shear capacity along the length of a U-Beam, designed with the same end-region reinforcing bar layout as B4S, is shown in Figure 5-4. The calculated shear strength would be highest at beam end, where the reinforcing bars are spaced at 3 in., and would decrease at each point of bar spacing change. Fifteen feet from beam end, the cross section would transition to the standard shape with narrow web walls. The confinement bars and the supplementary bottom flange-to-web interface reinforcement do not contribute to vertical shear capacity.

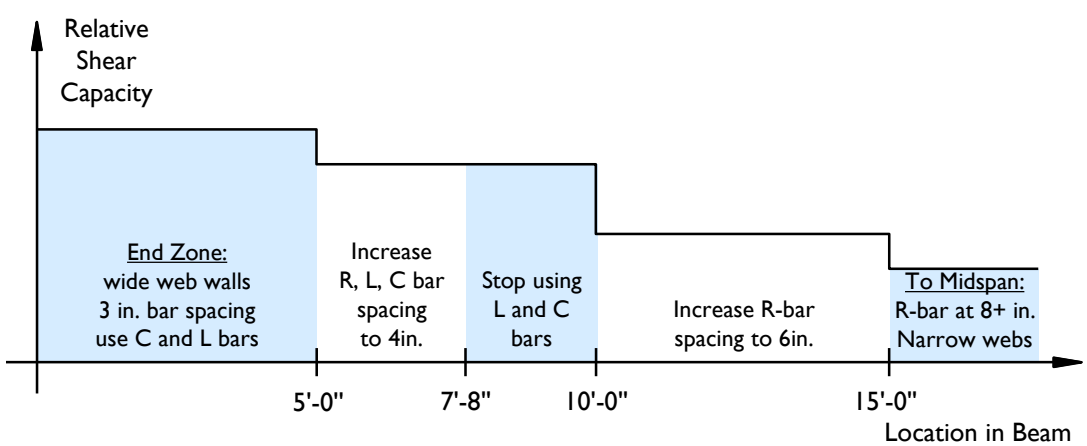

Figure 5-4: Generalized sketch of the increase in shear capacity towards the end of a full-length beam designed using the modified details used in the south (more heavily reinforced) end of Beam 4.

5.2.2 Early-Age Behavior

The maximum stress observed in reinforcing bars at prestress transfer was 30 ksi. Reinforcing bar stresses inferred from measured strains were typically below 5 ksi. The higher stresses were located very close to beam end (< $h/4$).

5.2.3 Shear Testing

Two shear tests were performed on Beam 4. The first was in test region B4S, the end of the beam that included the three #5 L-bars at each R-bar location. The test was stopped at 1191 kip applied shear, prior to the failure of the test region. The applied shear was 5% above the shear strength calculated following the AASHTO General Procedure (2010) using a 3-in. stirrup spacing, and 37% above the shear strength calculated using a 6-in. stirrup spacing. Instrumentation on reinforcing bars showed strains at approximately 50% of yield when the test was halted, significantly lower than the strains measured near failure in previously tested beams. While it cannot be guaranteed that this test specimen would have failed without signs of horizontal shear distress, it is known that the shear at failure would have exceeded the calculated shear capacity through the length.

By stopping the test of specimen B4S before failure, the modified design used on the other end of the beam, B4N, with wider web walls and confining reinforcement, could be tested. No special reinforcing was included in specimen B4N. B4N failed at a shear of 973 kip, 14% below the calculated strength for a section with 3-in. reinforcing bar spacing, where failure was observed.

The failure mode of test region B4N was web-crushing, with significant horizontal shear damage along the bottom flange-to-web interface. The test region is pictured in Figure 5-5. Crushing was observed through the width of the web. Damage along the bottom flange-to-web interface was seen only on the interior of the beam, where a horizontal crack was visible extending 10 ft from the end block into the beam. This horizontal cracking was similar to that seen in the Phase I test regions.

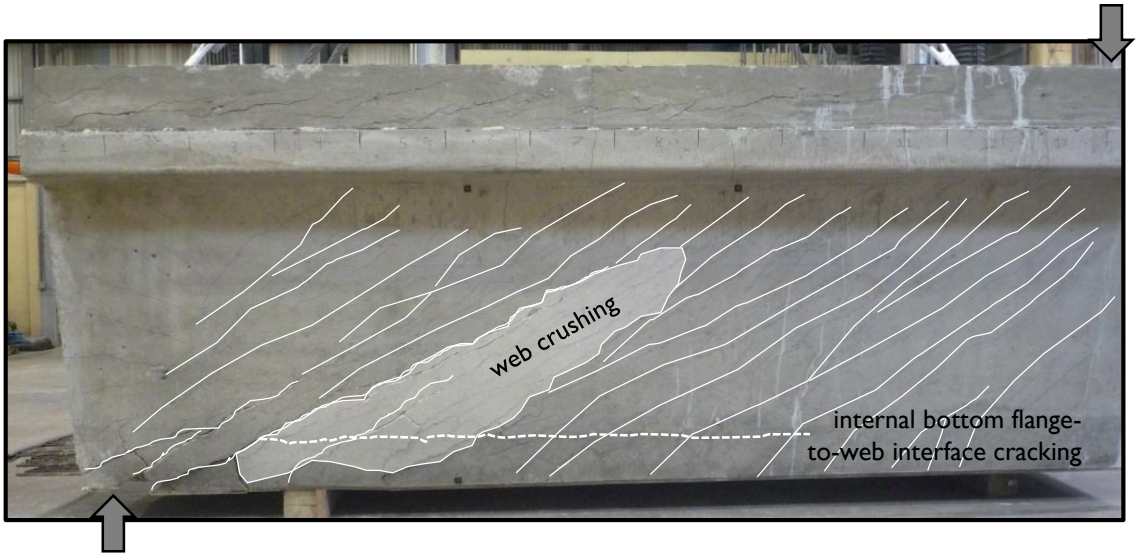

Figure 5-5: Failure of test region B4N.

5.3 BEAM 5

Beam 5 was 30 ft long and was squared at both ends (no skew). The beam was fabricated by Fabricator A, and no internal instrumentation was installed. Sixty-six 0.5-in. diameter prestressing strands were used in Beam 5, all of which were fully bonded through the length of the beam. The two ends of the beam were identical.

5.3.1 Design Modifications

Beam 5 used the standard cross-sectional geometry, with 5-in. web walls. However, like in Beam 4, several modifications to the standard reinforcement were incorporated, as described in the following sections. These changes are summarized graphically in Figure 5-6. This design was proposed by the TxDOT Project Monitoring Committee.

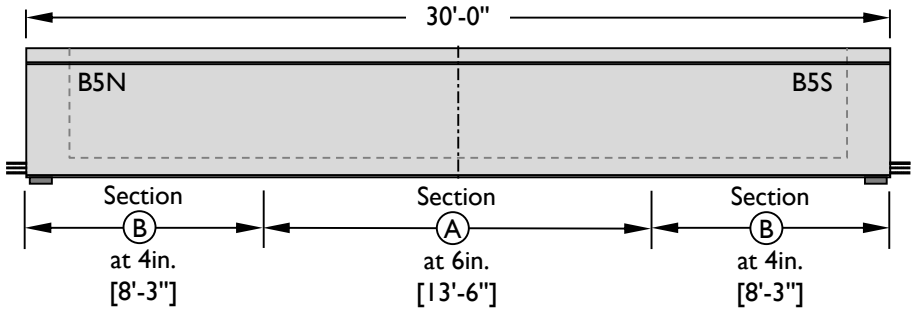

Figure 5-6: (i) Elevation view of Beam 5.

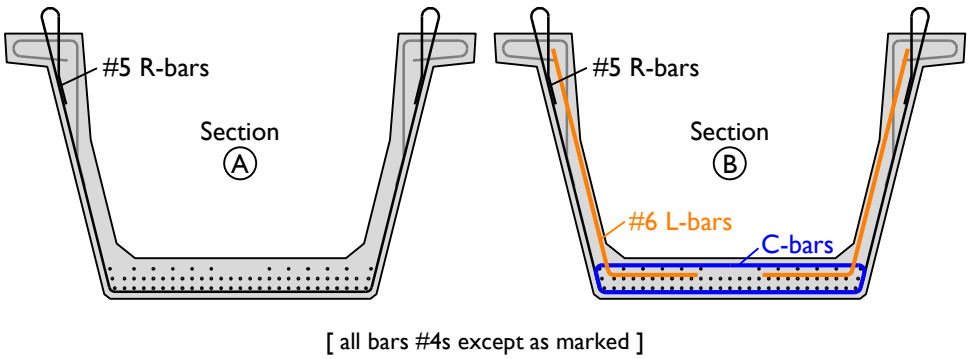

Figure 5-6: (ii) Standard cross sections of Beam 5.

5.3.1.1 Shear Reinforcement

The size of the stirrups (R-bars) was increased from the current standard #4 to a #5. A minimum clear cover of 1 in. was specified in the bottom of the beam and on both sides of the web face. The reinforcing bars were placed at slightly different intervals from the current standard: 4 in. for 8'-3" (increased from 6'-3"), then at 6 in. through midspan.

5.3.1.2 Confinement

Following the previously-referenced AASHTO (2010) specification, confining reinforcing bars (C-bars) were added in the end regions of the beam (through 8'-3" from beam end). Unlike in Beam 4, the hairpin-shaped bars overlapped by two feet at the middle of the beam. The location of the confinement reinforcing is shown in Figure 5-7.

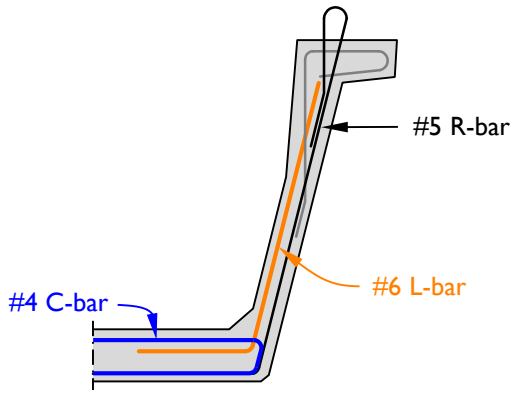

Figure 5-7: Cross sectional detail of Beam 5, with new bars highlighted.

5.3.1.3 Supplementary Reinforcement

Additional bottom flange-to-web reinforcing bars were also used in Beam 5. Rather than using several small bars as was done in B4S, a single #6 was used with each R-bar (Figure 5-7). Like the bars in Beam 4, these bars (L-bars) were placed where P-bars typical are located in the cross section. The bars extended through the entire web region and into the top flange of the beam. The design built in Beam 5 contained 3.8% steel crossing the bottom flange-to-web interface for 8'-3" (1.8h) from beam end.

An elevation view and typical cross sections of Beam 5 are shown in Figure 5-6. As compared to the standard section, the "end-region" reinforcing steel extends further into the beam, confinement bars are included, the R-bars are #5s instead of #4s, and the #6 L-bar has been added.

Like the L-bars used in Beam 4, the supplementary bars used in Beam 5 were not included in calculations for shear capacity, as they are not fully anchored to resist load in the web of the beam.

5.3.2 Shear Testing

The north end of Beam 5 (B5N) failed at a shear of 1030 kip, in a flexure-shear mode (see Figure 5-8), at a load 11% above the calculated shear capacity, as calculated using the AASHTO General Procedure (2010) with a stirrup spacing of 6 in. The failure shear is compared to the capacity with the wider bar spacing as the failure occurred near midspan, where reinforcing bars were placed at 6 in. and no supplementary bars were

provided. Unlike in previous tests, the failure of this beam section occurred as expected, at the location where the theoretical strength was lowest.

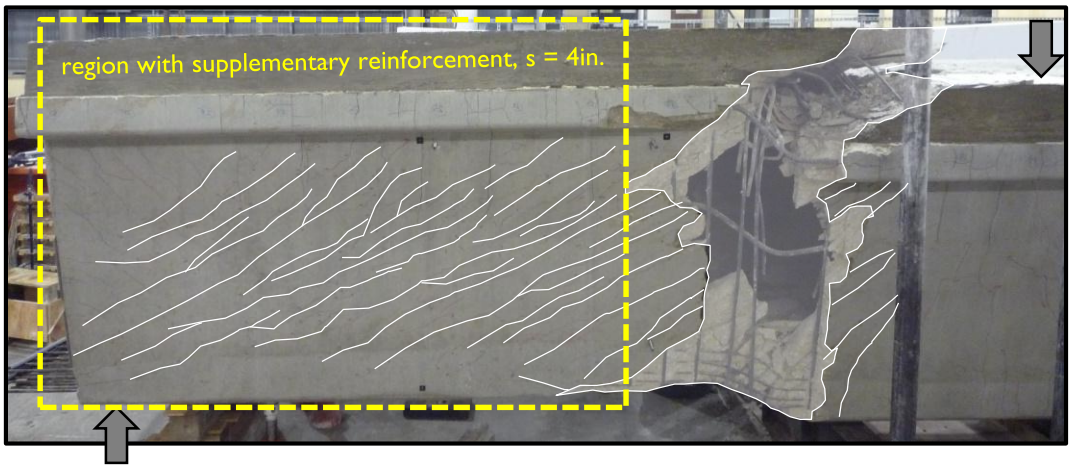

Figure 5-8: Test region B5N after flexure-shear failure.

As with Beams 0 and 2, a second test could not be performed at the other end of the beam due to the extensive damage caused by the first test.

5.4 INTERMEDIATE ANALYSIS

Beams 4 and 5 contained three modified designs of the Texas U-Beam end region. The three shear tests performed (on test sections B4N, B4S, and B5N) confirmed that two of the designs (those used in B4S and B5N) increased the strength of the bottom flange-to-web interface sufficiently to prevent horizontal shear from controlling the failure strength. The design used in B4N did not result in an acceptable failure, and was not considered further for implementation.

The constructability and serviceability of the designs used in B4S and B5N are discussed here, as the observations and conclusions helped to determine the final recommended new design, which was then implemented in Beams 6 and 7.

5.4.1 Constructability

Beam 4 was designed and fabricated by the research team without time constraints, which allowed the design to be modified as needed when constructability issues arose. The as-built design presented in Section 5.2 did not have any significant

problems with congestion, low cover, or interference of bars. Beam 5, which was fabricated in a single day at a prestress fabrication yard, did not have the same time allowance. During the fabrication of Beam 5, research team members observed the process and measured critical values such as clearance of the bars and location of the strands. While the design could not be modified for use in that test specimen, the observations were used to influence decisions for designs moving forward. This section highlights the two major issues seen: congestion of reinforcing bars in the end blocks, and trouble maintaining proper cover on the reinforcement.

5.4.1.1 End Block Congestion

The existing standard end block design in the Texas U-Beam is congested. With R-bars spaced at four inches and lapped across the bottom flange, and two U-shaped bars (V-bars) potentially next to the lapped R-bars, the maximum clear space between bars is less than two inches. Adding confinement reinforcement in this region caused further congestion. Beam 4 was designed with confinement bars that did not overlap, thus reducing the number of bars that could be grouped together in the end block.

In Beam 5, the confinement bars overlapped by nearly two feet. Because of this, beneath the bottom row of strand, there were up to six bars side-by-side (totaling more than three inches of steel) (see Figure 5-9). With shear reinforcing bars spaced at 4 in., one inch of clear space was available, through which ¾ in. aggregate had to pass. This congestion created several possible problems: (i) segregation of the concrete, with only cement paste existing beneath the strands; (ii) delamination of the concrete beneath the mat of reinforcing, creating a falling hazard for a beam in service; and (iii) poor transfer of prestressing force into the surrounding concrete.

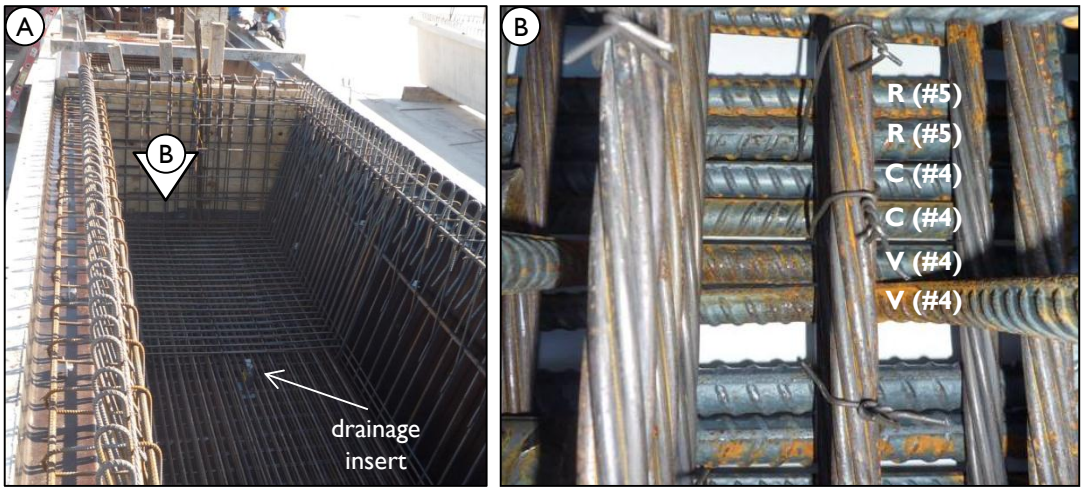

Figure 5-9: (A) End-region reinforcing in Beam 5; (B) six side-by-side bars (two #5s and four #4s) bundled together in the end block of Beam 5.

Lapping the confinement steel also prevented the placement of the drainage insert just beyond the end block (1'-6" to 2'-0" from beam end), as is standard practice. The insert was too wide to fit in the space between R- and C-bars below the strand: previous spacing was 3 in. and had been reduced to 2 in. The insert was moved to just beyond the C-bars, as shown in Figure 5-9(A). A smaller drainage insert, C-bars that did not overlap, or the removal of one pair of C-bars would have allowed for proper placement of the drainage insert. Otherwise, significant water could stagnate in the end of the beams.

The supplementary reinforcing bars that were added at the south end of Beam 4 were positioned for ease of construction. The outer bar was paired with an R-bar and ran between the first and second row of strands. The inner two bars, while somewhat more difficult to place, were located in the same position as the current P-bars, with the belief that construction of beams with the L-bars would be akin to construction of a fascia girder with current standards. The difficult region for bar placement was again within the end blocks, where P-bars are not currently used. With the R-bar spacing decreased in the end region, a smaller drainage insert would have been needed even without overlapping C-bars. This conflict was not noticed during fabrication as drainage inserts were not needed and thus not installed in these beams which were built and kept indoors.

5.4.1.2 Cover Requirements

Prior to beam fabrication, the Beam 5 reinforcing bars were drawn to scale in cross section. It was found that with the location of the bottom row of prestressing strand, the size of the R-bars, and the required bend radius of those bars, clearances would likely be less than 1.0 in. below the strand, 1.3 in. on the outer webs, and 0.4 in. on the inner web. In the field, the desired clearances were forced by the fabricator using 1.5 in. riser chairs below the strands and to the outside of the bars, as is standard practice at that fabrication plant.

To get these large chairs underneath the transverse leg of the R-bar (maximum design clearance is 1.30 in., given location of strand, optimal placement of bars, and ignoring deformations on the bars), a 1.5 in. pry bar was used to lift the reinforcement and place the chairs (see Figure 5-10(A)). By inserting these chairs, the clearance below the R-bar was set to 1.5 in. However, this clearance was achieved by shifting the location of the bottom row of strands, as is shown in Figure 5-10(B).

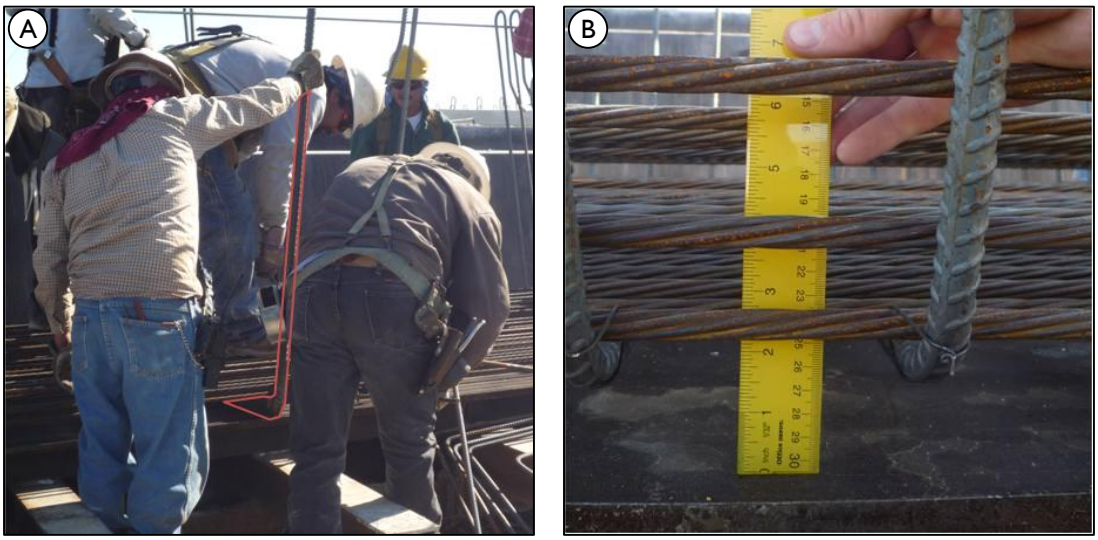

Figure 5-10: Workers using a 1.5 in. pry bar (outlined) to lift bottom strands; (B) resulting strand locations.

In the field, prestressed beam reinforcing cages are built without the beam side forms in place. Chairs are tied to the outside of the transverse bars, ensuring a proper standoff (clear cover) between the bar and the face of the beam. While TxDOT drawings

require only a 1 in. clear cover, the fabricator again used 1.5 in. chairs. Prior to casting, the spacing between the reinforcing bars and the side form wall was measured at between 1.25 and 2.25 in. However, putting the side forms on required a slight bending inwards of the reinforcing bar cage, as the original bar placement would not have allowed for such clearance off the forms.

The problem associated with flexing the cage inwards was not apparent until the bottom flange had been poured, at which point there was not time to make major changes. Upon lowering and securing the interior void form in place, it was realized that the X-bars, with a vertical section meant to be parallel to the interior face of the web wall, were touching the void throughout the length (see Figure 5-11(B)). This problem was again solved using a pry bar, this time forcing the cage outwards enough to fit 1.5 in. chairs between the cage and the void (Figure 5-11(A)). While not difficult to manage on the first side (as the void could shift slightly to the unbraced side), the second side took nearly thirty minutes to relocate, as chairs that were placed frequently broke upon release of the pry bar. Supplementary support methods were also used, as shown in Figure 5-11(C), where tie wire was used to hold the cage back against the side forms, thus reducing side form cover but increasing cover on the side of the void.

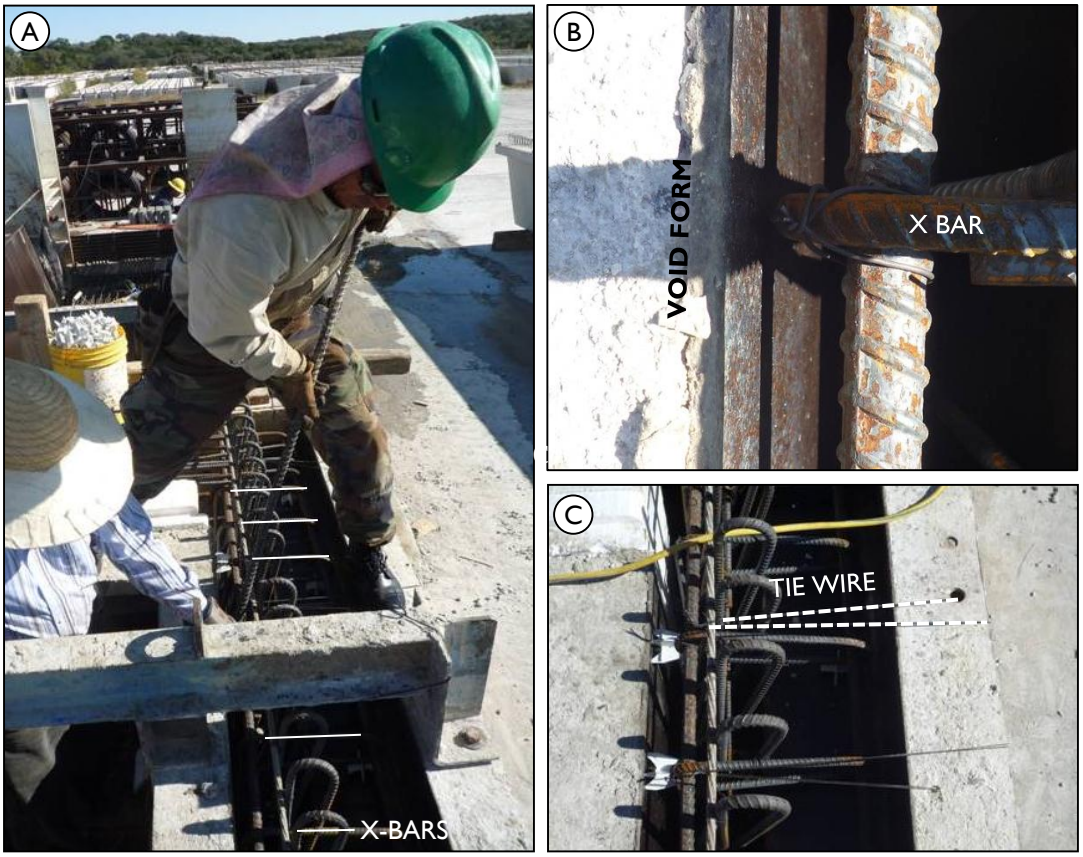

Figure 5-11: (A) Workers using a pry bar to move reinforcement away from void form (B). The cage was held back with tie wire and plastic chairs (C).

The designs implemented in Beam 4 and Beam 5 both feature the use of new bars – confinement (C-bars) and L-shaped shear-interface bars (L-bars). However, Beam 4 design minimized congestion of bars, in particular below the bottom row of strands, where shear reinforcing and multiple end block bars already wrap. Additionally, by continuing to use #4 bars for the primary shear steel, the current cover standards are maintained without adding to the difficultly of placing the void mid-cast. The observations made during the fabrication of Beam 5 were used in making recommendations for final design changes, as presented in Section 5.4.3.

5.4.2 Serviceability

The data gathered and presented in Avendaño and Bayrak (2008) indicate that for best serviceability performance, the contributions to shear strength from concrete and

from steel should be well proportioned. The authors of that study recommended limiting V_s/V_c to less than 1.5, with V_s and V_c calculations made using the ACI 318-08 Detailed Method.

In the standard Texas U-Beam design with Grade 60 reinforcing stirrups spaced at six inches (as seen in the midspan of the beams), the ratio of V_s/V_c is 0.8. In the Beam 4 design, with increased concrete area (and thus V_c) and very little new steel that would contribute to V_s, the ratio decreased to 0.4. In the Beam 5 design, where significant amounts of steel were added without increasing the concrete contribution, the ratio increased to 1.2. With the strength of the section so reliant on steel, the likelihood of diagonal cracking under service loads was increased.

The extent of diagonal cracks seen in B4S and B5N at three points in the loading are shown in Figure 5-12. As the calculated capacities (using the AASHTO General Method (2010)) of the two sections are very similar, the cracking shown is occurring with almost the same shear in each section. While diagonal cracks were first observed in test region B5N at 27% of the calculated strength of the section, B4S did not show web cracking until 61% of the calculated strength. At higher loads, the diagonal crack widths observed were also significantly smaller in B4S than in B5N (e.g., 0.010 in. in B4S at V_n vs. 0.025 in. in B5N). It should be noted that the service shear that could be expected in this region of the span due to a HL-93 truck loading plus the dead load of a 140-ft beam with no skew is approximately 275 kip (just above 30% of the calculated capacity of these sections).

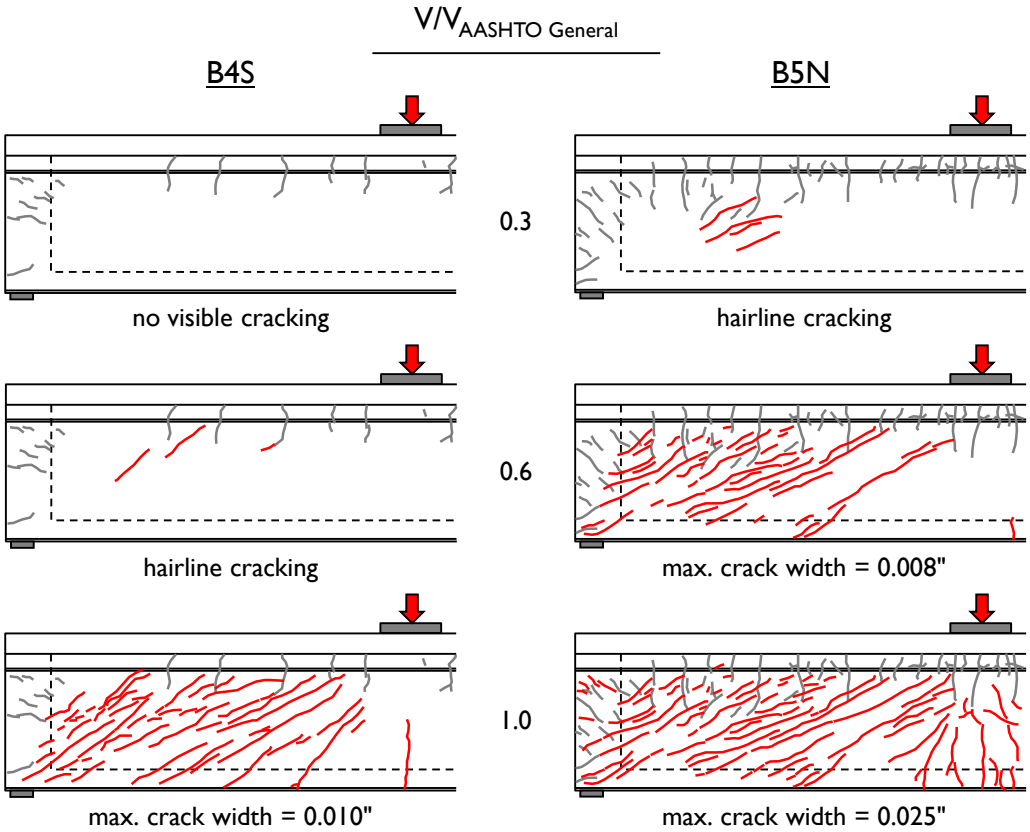

Figure 5-12: Extent of shear cracking in test regions B4S and B5N at the same shear load step relative to calculated shear capacity.

When diagonal cracks are present, water ingress increases and reinforcing bar and strand corrosion become more likely, posing a threat to the durability of the U-Beam. It is believed that in a beam with a 1 in. cover requirement that is used in coastal areas, diagonal cracking should be minimized or avoided.

5.4.3 Recommendations

The final recommended design was influenced by the observations during fabrication and testing, as discussed in the previous pages, and through discussion with the TxDOT Project Monitoring Committee. The following points shaped the new design:

- <u>Maintain size of stirrups</u>

  Several of the constructability issues encountered with Beam 5 (reduced cover, wide bends, limited clear space between bars) could be alleviated by

maintaining the current size of the stirrup reinforcing bar. The addition of steel at the bottom flange-to-web interface in the new design would have to be achieved without increasing the size of the stirrup.

- Maintain web width

  While the cracking performance of Beam 4 was significantly better than Beam 5, and the B4S reinforcing design sufficiently increased the bottom flange-to-web interface strength, the cost to fabricators for new internal void forms was deemed to be excessive and thus not an option. The new design would have to strengthen the standard without adding width to the web walls.

- Discount increased curing temperatures

  While this project began with the intention of decreasing the size of the end blocks in the standard design, it also began prior to the introduction of a requirement for the use of fly ash in prestressed girders built for TxDOT. With the 25% replacement of cement by fly ash now typical in these beams, the perceived susceptibility to ASR/DEF was decreased. The associated concern with high curing temperatures was also decreased. The new design was allowed to increase strength by maintaining or even increasing the length of the end blocks in the standard.

The resulting recommended design was implemented in Beams 6 and 7, as described in the following sections.

5.5 BEAM 6

The Beam 6 design was proposed by the research team as the final recommended design to increase the strength of the bottom flange-to-web boundary and prevent horizontal shear from controlling strength, while not sacrificing constructability or practicality with regard to cost to fabricators. The beam was fabricated by Fabricator B. No internal reinforcing bar instrumentation (i.e., strain gauges) were used in this beam. A total of 64 0.5-in. diameter prestressing strands were included, fully bonded through

the length of the beam. As is standard practice by Fabricator B, welded-wire reinforcement was used for the main web reinforcing bars.

5.5.1 Design Modifications

Both test specimens B4S (widened web walls, supplementary reinforcing steel) and B5N (supplementary steel only) successfully strengthened the bottom flange-to-web interface so that a horizontal shear failure did not occur before the calculated shear capacity was met. In terms of serviceability, the additional concrete present in the webs of Beam 4 significantly improved the cracking performance. However, with the request by TxDOT to maintain the existing cross section, the design of Beam 6 combines the best structural solution with practical realities of mass production. The beam elevation and cross sections can be seen in Figure 5-13.

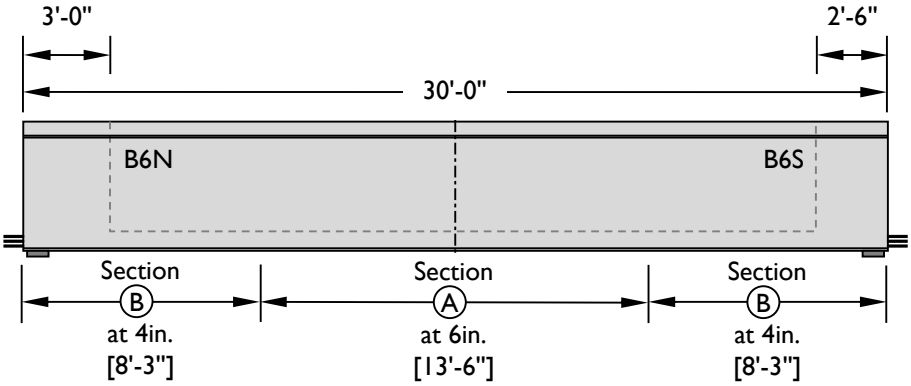

Figure 5-13: (i) Elevation view of Beam 6.

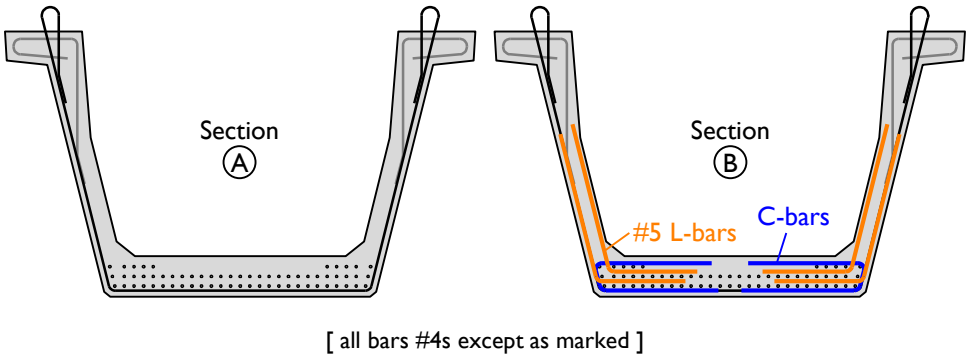

Figure 5-13: (ii) Standard cross sections of Beam 6.

5.5.1.1 Increased End Block Length

The design of Beam 6 incorporated additional concrete in the end region through a longer end block rather than wider webs. Despite the higher curing temperatures that are expected with such a change, TxDOT engineers and the Project Monitoring Committee believed that the required use of fly ash and the common practice use of cooling water pipes in the end blocks would sufficiently control maximum temperatures and prevent deleterious material reactions (TxDOT, 2010).

The recommendation for use in the new Texas U-Beam standard is an end block between 2'-6" and 3'-0" for beams with less than 30° skew. Beam 6 was fabricated with one end block of each length; the larger end block was expected to be a worst-case scenario with respect to high curing temperatures while the small end block was the worst-case scenario for horizontal shear strength and overall shear performance. Further discussion on measured temperatures is given in Chapter 6.

To reinforce the larger end blocks, and better tie the webs to the end block and to each other, the longitudinally-oriented legs of the D and DS bars of the current standard were increased from 1'-0" and 3'-6" to 2'-0" and 5'-6" (Figure 5-14). Bars DE and a second plane of bars F were added. The details of these bars are given in Appendix A.

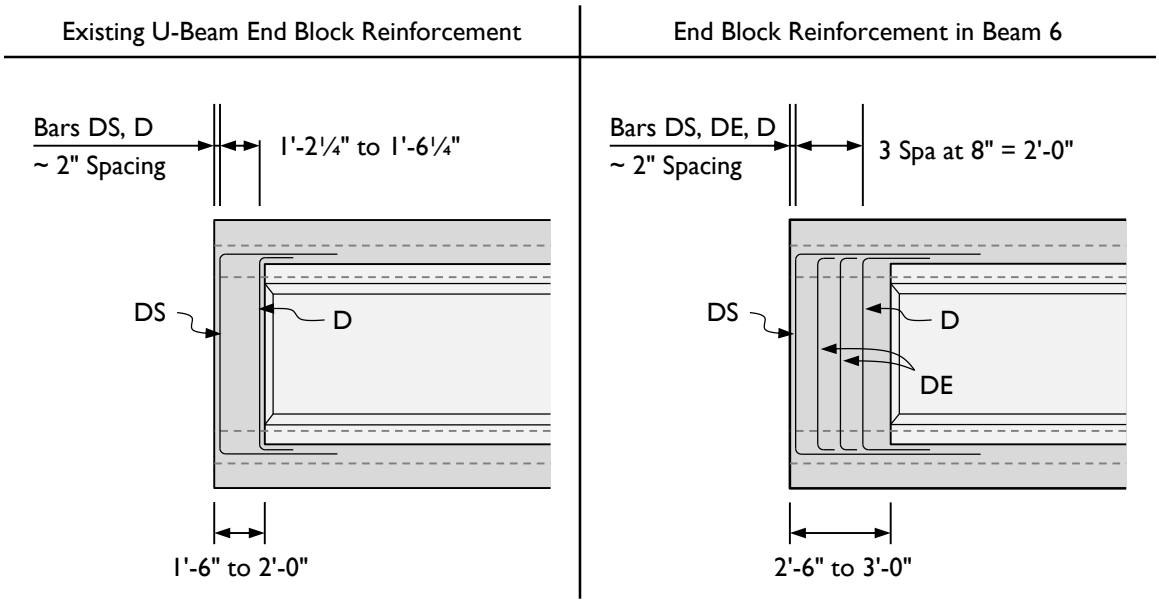

Figure 5-14: Existing end block reinforcement compared with reinforcement used in Beam 6.

5.5.1.2 Confinement Steel

Given the construction complications and congestion seen with the confinement steel of Beam 5, that were not seen with Beam 4, the design of confinement steel used in Beam 4 was used in Beam 6. The hairpin bars do not overlap in the center, but provide confinement to the outermost strands. The bars are used for a distance 8'-3" from beam end ($1.8h$).

5.5.1.3 Supplementary Reinforcement

As shown in Table 5-2, the amount of steel crossing the bottom flange-to-web interface in test region B4S was significantly more than in B5N. Both beams, however, were able to carry the calculated shear capacity without sustaining damage to the bottom flange-to-web interface. The shear performance of B5N showed that the amount of steel crossing the bottom flange-to-web interface used in that beam was adequate for a beam with the standard cross section. Beam 6 was fabricated with two #5 bars at each stirrup in each web rather than a single #6 so that bar could be developed quicker and the required bend radius be smaller, but the area of reinforcing at the bottom flange-to-web interface was at least that used in B5N. The geometry of the bar used in Beam 6 matched that used in Beam 4 (Figure 5-13(ii)), with the bar terminating in the mid-web. Both ends of Beam 6 contained the same reinforcement.

5.5.2 Shear Testing

Beam 6 was loaded as in previous tests, at a shear span-to-depth ratio of 2.6. The test region B6N failed in flexure-shear at a shear load of 1054 kip (Figure 5-15). This shear load exceeded the calculated shear capacity for a beam with stirrups spaced at 6 in. by 27%. As with Beam 5, no significant damage was seen in the end region of the beam, where the supplementary bars were located. No evidence of horizontal shear distress was seen.

Figure 5-15: Test region B6S after flexure-shear failure.

5.6 BEAM 7

Beam 7 was fabricated for the purposes of confirming that the shear performance of the recommended design was satisfactory in a beam with significant skew. The beam was built with one end skewed to the maximum allowable angle, 45°. The recommendation for use in the Texas U-Beam standard is an end block between 3'-0" and 3'-6" (measured at the bottom flange) for beams with a skew of 30 to 45°.

In the previously-tested skewed-end test specimens (Beams 1 and 2), the load was placed at midspan of the centerline, resulting in an a/d = 2.6. This load configuration resulted in approximately equal shear in each end and forced the testing of both ends of the beam simultaneously. In order to have higher shear forces in the skewed end of the beam, Beam 7 was 35 ft long (31'-9" along the centerline), allowing for the same shear span-to-depth ratio as in previous tests, with the load offset from the centerline by over two feet.

The beam was fabricated with 0.6-in. diameter prestressing strands, stressed to 202.5 ksi. In order to minimize required release strength, as requested by the fabricator (Fabricator C), five of the 58 prestressing strands were debonded the full length of the beam. The area of 53 0.6-in. strands is approximately equivalent to 75 0.5-in. prestressing strands. Elevation, plan, and cross-sectional views of the beam are given in Figure 5-16. No internal gauges were used on reinforcing bars in Beam 7.

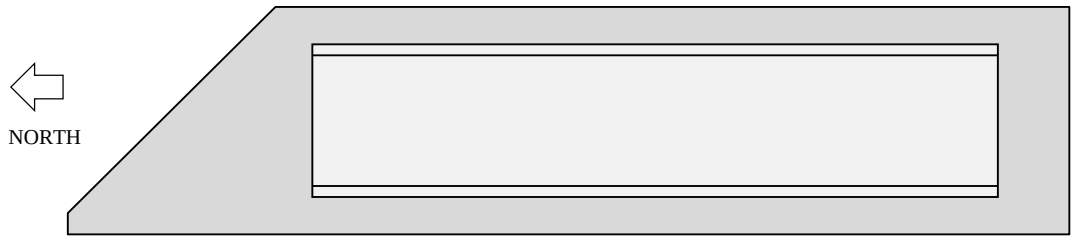

Figure 5-16: (i) Plan view of Beam 7.

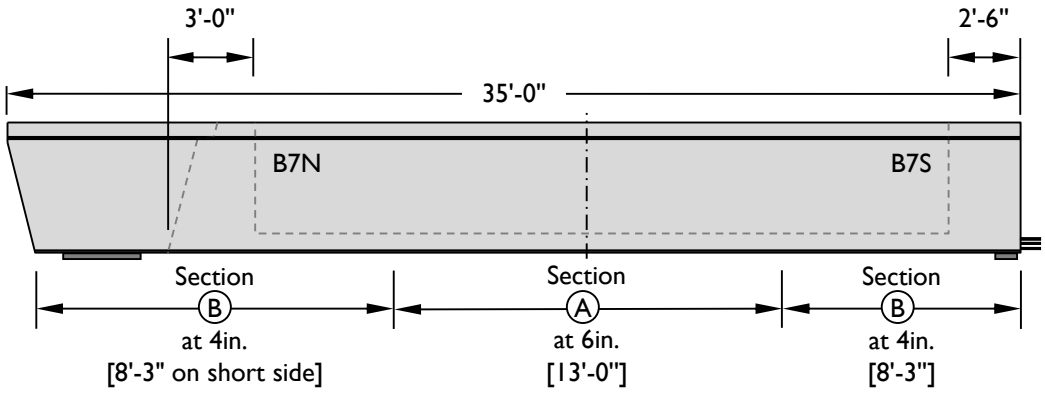

Figure 5-16: (ii) Elevation view of Beam 7.

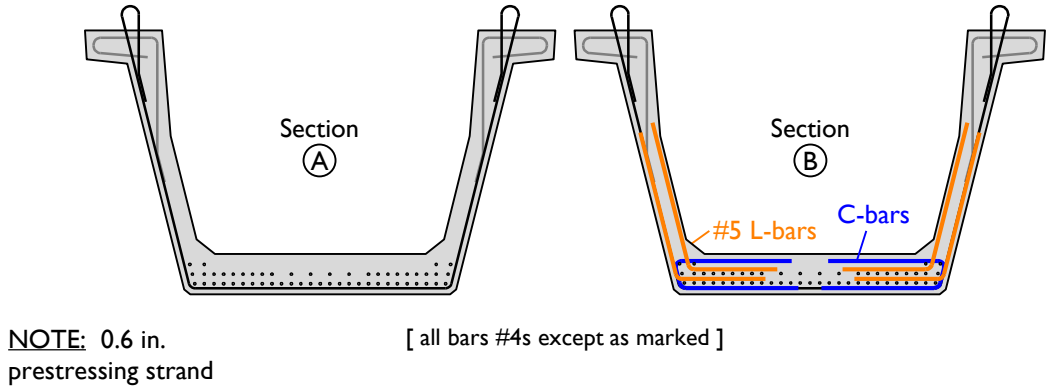

Figure 5-16: (iii) Standard cross sections of Beam 7.

5.6.1 Shear Testing

Test region B7N failed in web-crushing at a shear of 1210 kip (Figure 5-17). This shear was 65% in excess of the calculated shear capacity for a beam with reinforcing bars spaced at 6 in. Damage extended through the region with reinforcement spaced at 6 in. into the region with reinforcement spaced at 4 in., likely because of the proximity of the load point to the spacing change (approximately 2 ft in this test region). The failure shear

was 33% in excess of the calculated capacity when using a reinforcing bar spacing equal to 4 in. No signs of distress were observed along the bottom flange-to-web interface.

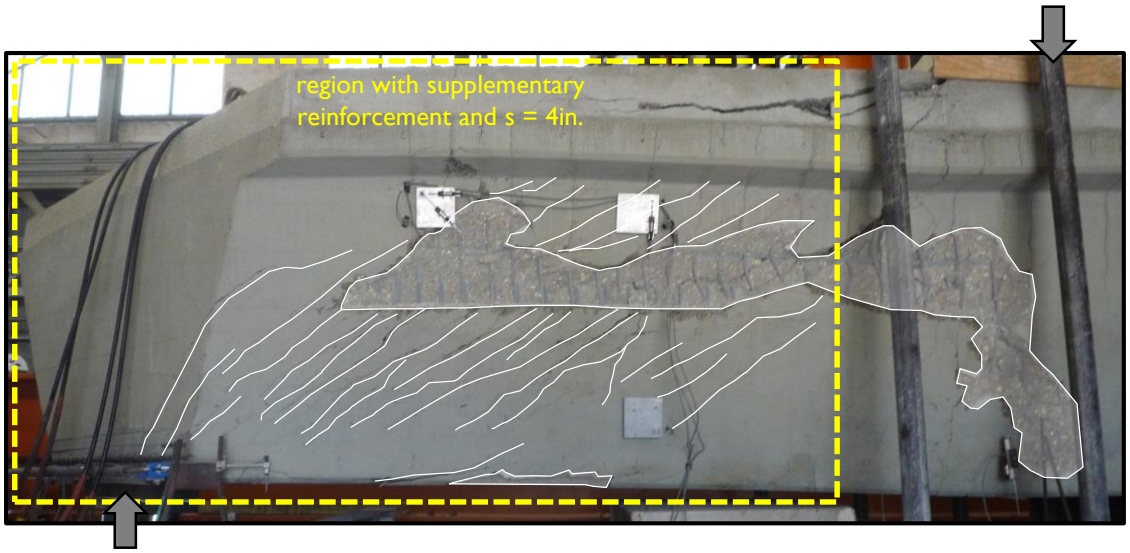

Figure 5-17: Test region B7N after shear failure.

5.7 SUMMARY OF PHASE II TESTING

Five shear tests were performed in Phase II of this study. Four different designs were tested, with a straight and skewed beam containing the recommended new reinforcing bars being the duplicate design. A summary of the Phase II test variables studied is presented in Table 5-3. Span-to-depth ratio (2.6) was held constant in all tests. Each test region was supported on a single central bearing pad, as that bearing configuration was seen to be more critical for load transfer. All beams included confinement reinforcement.

Table 5-3: Summary of Phase II test variables.

Beam	End Geometry	Supplementary Reinforcement [added to R-bars]	Type of Reinforcing	Number of 0.5" Prestressing Strands Bonded at Beam End	Length of End Block [in.]	Failure Mode
B4N	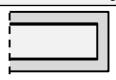	None	Grade 60	78, plus 6 in top flange	18.0	web crushing and horizontal shear
B4S	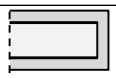	6-#5 S-bars	Grade 60	78, plus 6 in top flange	18.0	test halted prior to failure
B5N	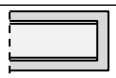	#5 R-bars* 2-#6 L-bars	Grade 60	66	18.0	flexure-shear
B6S	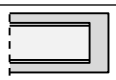	4-#5 bars	WWM	64	30.0	flexure-shear
B7N	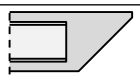	4-#5 bars	Grade 60	53 (0.6 in.)	36.0	web crushing

* size increase from standard #4 R-bar

The ratio of failure shear to the calculated shear capacity using the AASHTO General Procedure (2010) for the Phase II beam tests are plotted in Figure 5-18. Four of the five beam test regions failed at shear loads greater than the calculated capacity for the region of failure. Test specimen B4N, the only test specimen that did not carry more load than the calculated strength, was also the only test region to show signs of horizontal shear distress.

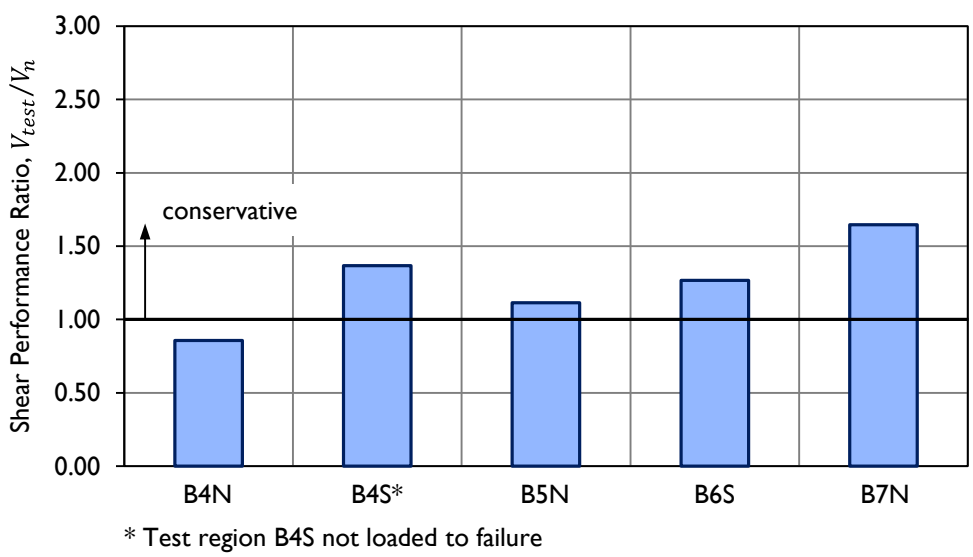

Figure 5-18: Ratio of failure shear to calculated shear capacity for the five Phase II test specimens.

5.8 HORIZONTAL SHEAR PERFORMANCE

The Phase II beams fabricated, tested, and described in this chapter were built to test modified end-region reinforcing bar designs detailed to increase the strength of the bottom flange-to-web interface to a point where horizontal shear in this region would not control the shear capacity. The reinforcing bar layouts were chosen after studying existing beam designs with favorable performance, with consideration given to constructability, serviceability, and practicality for application. The horizontal shear strength of the bottom flange-to-web interface was not calculated theoretically prior to the start of Phase II beam fabrication and testing.

Parallel to the laboratory testing being performed, a study was conducted in an effort to explain the mechanics of horizontal shear and provide a conservative, simple method for estimating the horizontal shear demand on and capacity of the bottom flange-to-web interface of prestressed bridge girders. The results and recommendations from that study are presented in Chapter 7 of this dissertation.

5.9 CHAPTER SUMMARY

Beams 6 and 7, designed with the recommended new U-Beam standard design, demonstrated excellent shear performance with regard to horizontal shear capacity and conservatism with regard to vertical shear capacity calculations. Two beams using the new design were fabricated in the field with very few issues during construction, and it is expected that the small problems that arose will be eased with time and increased familiarity.

CHAPTER 6
Analysis of Results

6.1 INTRODUCTION

In previous chapters, the U-Beams tested in this study have been presented individually. The reinforcement and geometric details of the beams were given in Chapters 4 and 5. Basic shear performance data were included, as the failure behavior and the conservatism between measured shear capacity and that calculated using codified equations for each test region helped guide the design of the next specimen. In this chapter, additional collected data are presented. The data will be discussed in the context of the other tested U-Beams and other tested beams from the literature. A complete presentation of the data gathered from each test region can be found in Appendix B.

Table 6-1 is provided for reference regarding which beam ends were used in each of the three major studies completed during this research project. The studies are of (i) strains gathered at prestress transfer, (ii) temperatures recorded during curing, and (iii) shear capacities measured through load-testing. Each beam end listed was involved in one, two, or all three of these studies. Only beam specimens fabricated at the Ferguson Laboratory were monitored at prestress transfer, resulting in eight test regions for this study. These same beams, plus two field-fabricated beams, contained thermocouples, returning ten test regions in which curing temperatures were recorded. Upon shear testing, three of the eight beams were tested at both ends; the other five beams were too heavily damaged during the first test to allow for a second test.

Table 6-1: Summary of end regions involved in this research project.

Beam ID	End Geometry	Data Gathered: Strains at Prestress Transfer	Data Gathered: Temperature During Curing	Data Gathered: Capacity Under Shear Loading	Key Features of Test Region
B0S				X	18-in. reinforcing bar spacing
B1N		X	X	X	Standard square end region
B1S	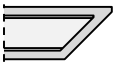	X	X	X	Skewed internal void
B2N		X	X	X	Welded-wire reinforcement
B2S	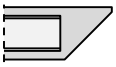	X	X		Standard skewed end region
B3N		X	X	X	46% of strands debonded, loaded on a single bearing pad
B3S		X	X	X	46% of strands debonded, loaded on two bearing pads
B4N		X	X	X	Wide web walls, top strands, no supplementary reinforcement
B4S		X	X	X	Wide web walls, top strands, 3-#5s paired with R-bars
B5N				X	#5 R-bar, #6 supplementary reinforcement
B6S			X	X	Recommended design, squared end, 30-in. end block
B7N	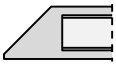			X	Recommended design, skewed end, 36-in. end block
B7S			X		New standard, squared end, 30-in. end block
TOTAL:		8 test regions	10 test regions	11 test regions	

The discussion in this chapter focuses most heavily on the observations and conclusions from shear testing. Following the presentation of the results from prestress transfer and beam curing are several sections on data gathered during shear testing. Specifically, discussion is provided on load distribution, shear and flexural cracking capacity as compared to calculation, and demand on vertical and longitudinal reinforcement, prior to presentation of the vertical shear capacities in context with

calculations and data from the literature. Discussions on horizontal shear capacity and demand calculations are presented in Chapter 7.

6.2 STRESSES INDUCED IN REINFORCING BARS AT PRESTRESS TRANSFER

The collected data from the eight U-Beam end regions tested in this study are summarized here. The recorded transverse (bursting and spalling) stresses and cracking for all eight beam test regions are compiled in Appendix B. In this section, key observations are highlighted, and the data are compared to previously tested beams reported in the literature, as were presented in Chapter 2. Of primary interest to this study is the effect of stresses induced at prestress transfer on the structural performance of the beam. There are two principal concerns: (i) magnitude of reinforcing bar stress caused by prestress transfer in end- and shear-region bars, and (ii) widths of cracks formed at prestress transfer.

The discussion of the eight U-Beam end regions is broken into two sections: to begin, the data from the end regions without debonded strands (both ends of Beams 1, 2, and 4) are presented. Following, the data from the two end regions with some debonding (both ends of Beam 3) are presented. The heavily prestressed (fully-bonded) beams were designed to be the worst-case scenarios for the transverse forces that occur at prestress transfer. The prestressing force in the end region of Beam 3 represents more typical practice within Texas, as the majority of beams designed in the state have 40 to 60% of the strands debonded in the end region to control top-fiber stresses near beam end at prestress transfer.

6.2.1 Heavily-Prestressed Beams

At prestress transfer, cracks developed in both the bursting (near the centroid of prestressing) and spalling (near the top flange-to-web interface) zones of these beam end regions. Each region typically had one or two cracks of hairline width that extended a distance less than $h/4$ from beam end. For the U54, with a height of 54 in., $h/4$ is equal

to 13.5 in. and is entirely contained within the solid end block of the beam (set in the standard at 18 in., minimum).

As discussed in Chapter 3, stresses from prestress transfer were obtained by measuring strains from strain gauges affixed to the reinforcing bars within the beam. The data were collected immediately before transfer and one hour after; the difference was defined to be the strain caused by the transfer of the prestressing force into the beam. The majority of recorded stresses were on the order of 2 to 3 ksi. Stresses in excess of the 20 ksi design limit stated by the AASHTO Specifications (2010) were observed in as many as four strain gauges per beam end region. From over three hundred monitored gauges, one measured stress in excess of 30 ksi.

The data collected at prestress transfer for Beams 1, 2, 3, and 4 were summarized in "bubble plots", or elevation views of each end of each beam with colored circles representing the magnitude of stress measured in gauges cast within the beam. Larger circles indicate higher measured stresses. Circles representing stresses below 10 ksi are blue, circles representing stresses between 10 and 20 ksi are green, and circles representing stresses above 20 ksi are red. Cracking visible after prestress transfer (within 3 days of concrete placement) are also shown. Bubble plots for each side of the eight beam end regions can be seen in Appendix B. The bubble plot for certain end regions are presented in this section as examples of typical behavior, and to highlight differences and key observations.

The bubble plot for the southwest corner of Beam 1 is given in Figure 6-1. The widest cracking seen in this study was observed in the spalling zone of the short side of the skewed test regions of Beam 1 and Beam 2. These cracks extended two feet into the beam, wrapped around onto the end face of the beam, and measured up to 0.025 in. wide. The large skew is likely to have contributed to the presence of this crack, as there is a disparity in the strand development across the beam in the transverse direction. As these beams were skewed to the maximum allowable angle (45°), they are expected to represent a worst-case scenario for this cracking pattern. As can be seen in Figure 6-1, while the cracking is not insignificant, the resulting stresses measured in bars near the

crack are small, with the exception of one measurement, from the bar located closest to the end face of the beam. Stresses in bars beyond $h/4$ from beam end were also small (less than 10 ksi). No cracks wider than 0.013 in. were measured in the thirteen rectangular end regions of beams fabricated for this project.

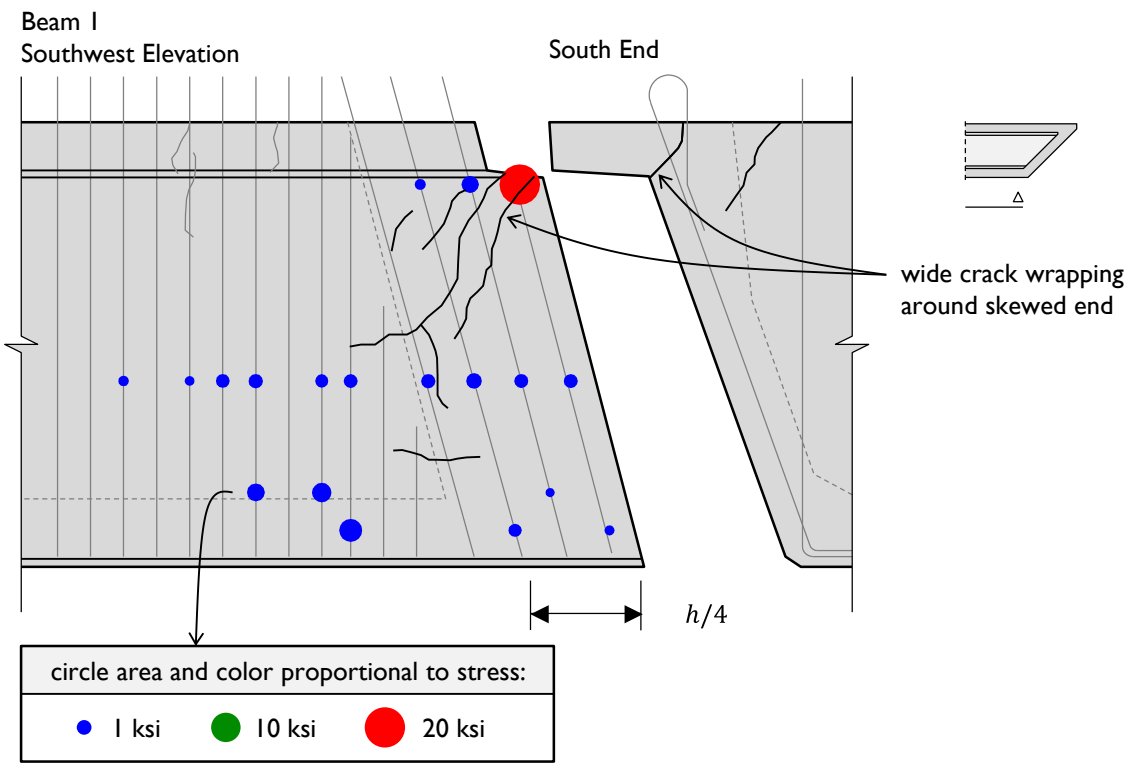

Figure 6-1: Location of widest crack observed in U-Beam end regions (B1S). Transverse stress measurements are represented by circles indicating stress magnitude and location of measurement.

With two exceptions, the maximum stresses seen in reinforcing bars in the end region was measured in the bar closest to the end of the beam. In both ends of Beam 2, greater stresses were measured in the bars away from the end face than in the first bar. The bubble plot for the southeast elevation of Beam are shown in Figure 6-2. In this end region, bursting stresses peaked at 29 ksi on the third bar from the end face. These stresses were recorded within the solid end block of the beam (which, given the skew of the beam, extended 7.5 ft into the beam).

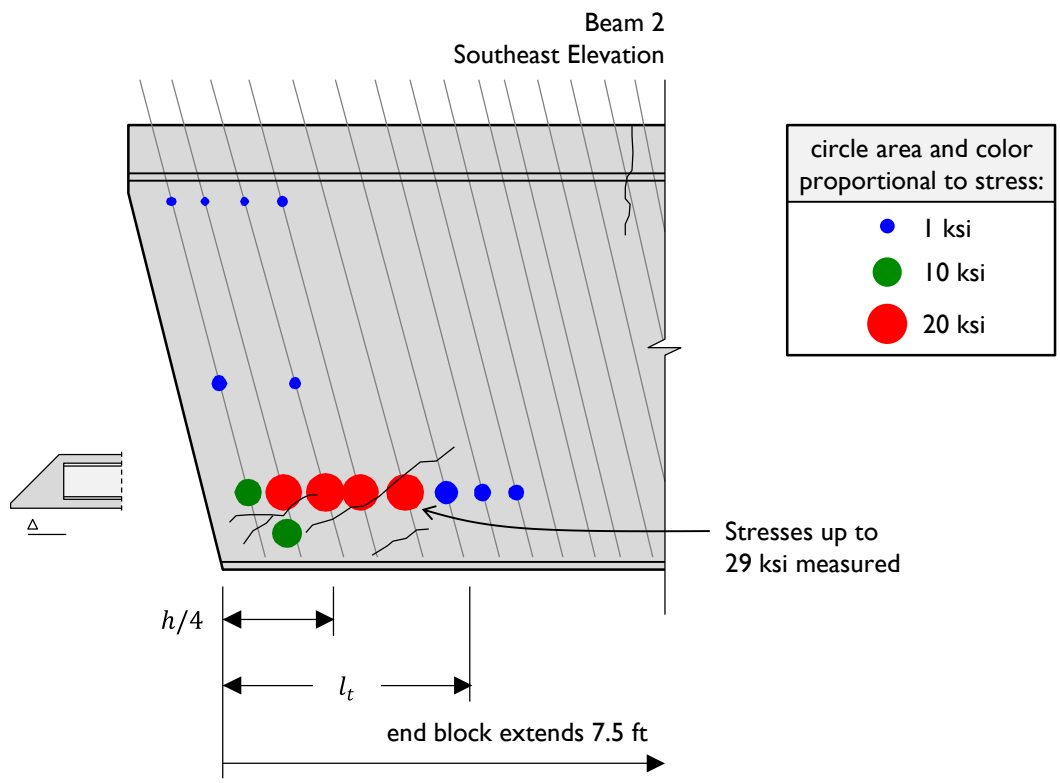

Figure 6-2: Most significant bursting stresses measured within solid triangular end block of Beam 2.

As presented in Chapter 5, one end of Beam 4 included additional reinforcing bars (L-bars) crossing the bottom flange-to-web interface, near the point where bursting stresses are expected. With all other variables the same, the behavior of the two ends, with and without the additional bars, can be compared to evaluate the influence of those bars on behavior at prestress transfer.

As can be seen in Figure 6-3, the maximum observed stress was not reduced through the inclusion of the L-bars; in fact, higher individual readings were seen in the end containing the supplementary steel, even with the additional steel present. However, in that same end, stresses of non-negligible magnitude (> 10 ksi) were seen through the first four bars, while similar stresses were recorded only in the first bar when the L-bar was included. As in the previously-discussed beams, no significant stresses were measured beyond the end block on either end of the beam. It is reasonable to conclude that the addition of bars across the bottom flange-to-web interface improved the bursting performance of the beam at prestress transfer. The L-bars, which were terminated

halfway up the beam web, were not able to aid in resisting the spalling stresses at the top of the web. Stresses of up to 30 ksi were measured in this region.

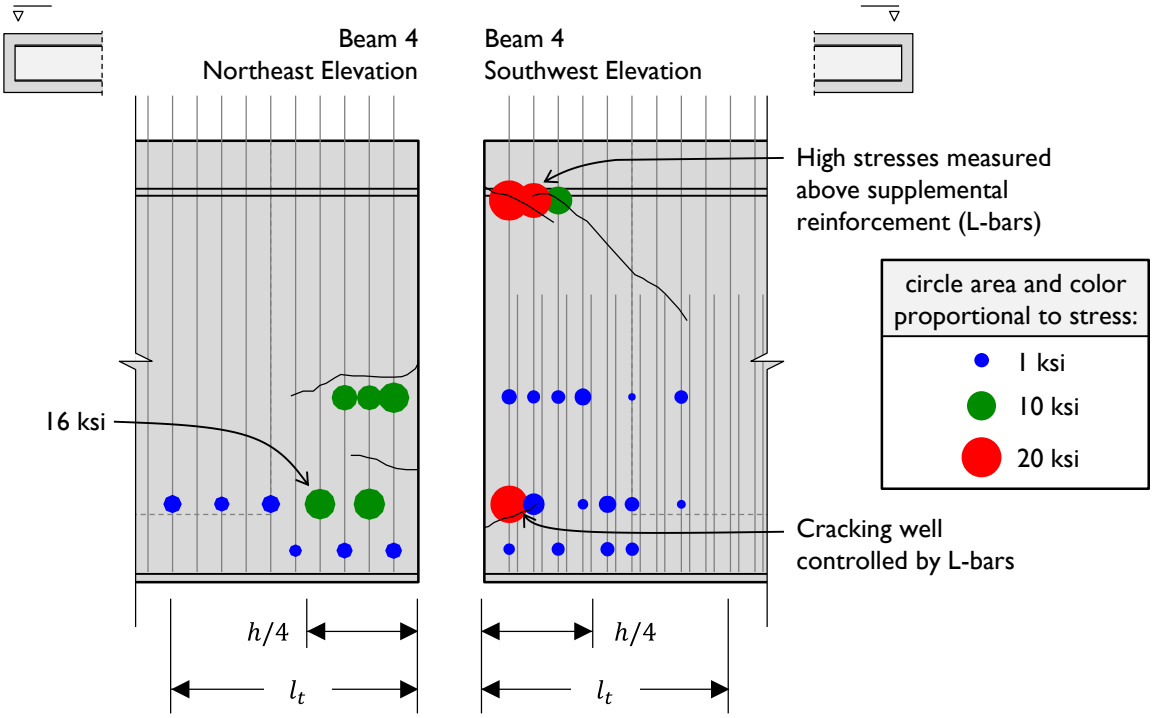

Figure 6-3: Effect of supplemental transverse bars, through comparison of (A) B4N and (B) B4S.

6.2.2 Lightly-Prestressed Beam

With a significantly reduced prestressing force at beam end, it was expected that the stresses observed in Beam 3 at prestress transfer would be less than those seen in Beams 1, 2, and 4. Indeed, stresses were much lower than in the other three beams, with no gauge reading values exceeding 6 ksi, as shown in Figure 6-4. No bursting or spalling cracks were observed in test regions B3N and B3S. Gauges installed near the points away from beam end where strands first became bonded also read low stresses, a reasonable observation given the small number (8 or 10) of strands that were bonded at any one point.

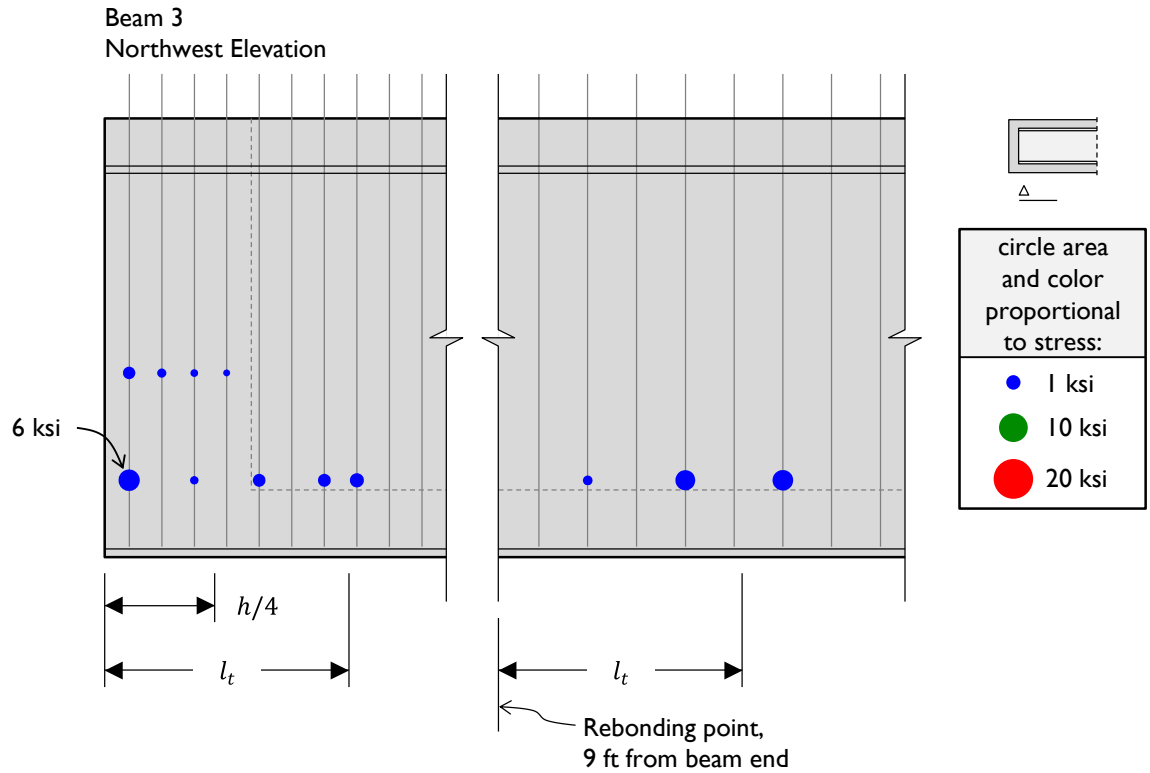

Figure 6-4: Typical beam end region in beam with debonded strands (B3N).

6.2.3 U-Beam Behavior in Context

The significance of the stresses measured in these U-Beams is best understood by comparing the measured values with those reported in the literature. In Chapter 2, a summary of the data gathered from existing literature was provided (from Dunkman (2009)). The stresses measured in the U-Beam end regions are plotted with the results of past studies on transverse reinforcing stresses in Figure 6-5. The total transverse force measured within $h/4$ from beam end is plotted on the vertical axis. The total transverse force was calculated by assuming that all bars positioned a given distance from beam end are stressed to the same level as the most heavily-stressed bar positioned at that distance from beam end (as determined through instrumentation). Stress was transformed into a force using the total area of bars at that distance from beam end. For a U-Beam, this calculation resulted in the assumption that all end-block reinforcement were as heavily-stressed as the web reinforcing bars. Instrumentation mounted on the end-block

reinforcement indicated this assumption was conservative. The AASHTO Specification (2010) procedure for detailing the end region of prestressed beams assumes that the force in the end region caused by prestress transfer is equal to 4% of the prestressing force. This design force is shown in Figure 6-5, as is the average value of total transverse force measured in previous studies (2% P_i).

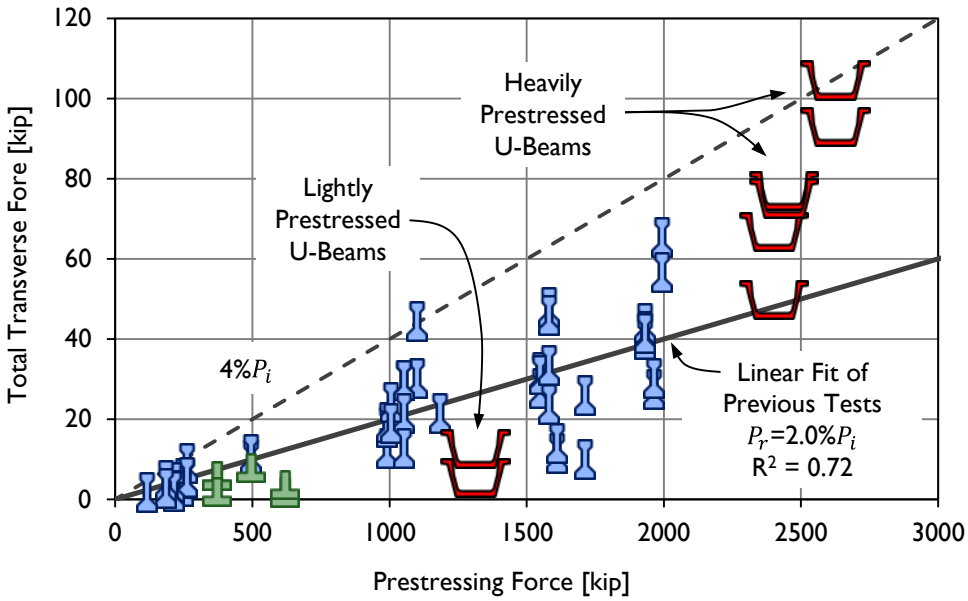

Figure 6-5: Transverse bar force measured in specimens from this project and literature.

The U-Beam end regions with debonded strands were subjected to less transverse force than the average specimen in the literature, and much less force than that assumed by the AASHTO design procedure. While the fully-bonded U-Beams contained more prestressing force than any of the other specimens found in the literature, the assumption presented in AASHTO – that 4% of the prestressing force would be transferred to the reinforcing bars – was still conservative.

The design provisions in the AASHTO Specifications assume that end-region reinforcement resisting prestress transfer will not be stressed beyond 20 ksi. This limitation is set to minimize the width of cracks that form. In five of the eight U-Beam end regions studied, stresses greater than 20 ksi were measured in at least one reinforcing bar. When the high stresses measured in the handful of bars is averaged across all the

bars within $h/4$, the average stress observed is less than 20 ksi. While certain bars were more heavily stressed than desired, the observed cracked did not introduce concerns regarding serviceability or beam performance.

6.2.4 Summary

Stresses were measured at prestress transfer in eight U-Beam end regions. Six of the beam end regions contained 78 fully-bonded 0.5-in. prestressing strands (two with six additional top strands) and two containing 42 fully-bonded strands and 36 strands that became bonded between 6 and 15 feet from beam end. Transverse stresses exceeded the AASHTO Specification design value of 20 ksi in five of the eight test regions, but the majority of readings from the embedded gauges returned stresses of only 2 to 3 ksi.

The impetus to study the behavior of U-Beams at prestress transfer was largely driven by the results of O'Callghan and Bayrak (2007), in which significant transverse stresses (greater than 20 ksi) were measured two to three feet from beam end in Tx Girders. Compared to Tx Girders, the stresses measured in the U-Beams in this study were insignificant. In the eight U-Beam end regions, only one developed significant stresses beyond $h/4$ from beam end. These stresses were seen within the beam end block, a solid mass of concrete with great structural redundancy. The end regions of the more lightly-prestressed beam did not crack, nor were significant stresses measured in reinforcing bars in the bursting or spalling zones. As most U-Beams fabricated do not contain as many as 78 fully-bonded strands at beam end, no significant problems with end region serviceability due to prestress transfer are expected in beams fabricated following the existing standard. Given the results from this study of behavior at prestress transfer, no changes are needed in the U-Beam standard to control the stress level in transverse reinforcement.

6.3 CURING TEMPERATURES

Temperatures were measured in multiple locations in each end block in the four beams fabricated at FSEL (Beams 1 through 4). Several beams fabricated outside the

laboratory also contained thermocouples placed in the end blocks, but in multiple cases, the data were lost due to a failure of the thermocouple or the datalogger. The maximum temperature measured in each monitored beam end during curing, along with the maximum temperature differential, ambient temperature, length of time from batching of concrete to prestress transfer, and amount of cementitious material in the concrete mixture design are given in Table 6-2.

Table 6-2: Summary of temperature data.

Test Region		Maximum Temperature Recorded	Maximum Temperature Differential	Ambient Temperature Range	Time of Release	Cementicious Materials
B0S		No Temperature Data Recorded				
B1N		137°F	38°F	71-77°F	17 hours	600 lb cement / yd^3
B1S	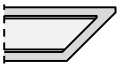	139°F	28°F			
B2N		142°F	34°F	73-84°F	18 hours	600 lb cement / yd^3
B2S	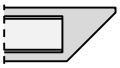	160°F	55°F			
B3N		165°F	52°F	93-105°F	20 hours	600 lb cement, 200 lb fly ash per yd^3
B3S		184°F	47°F			
B4N	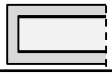	131°F	45°F	62-78°F	37 hours	600 lb cement, 200 lb fly ash per yd^3
B4S	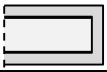	139°F	34°F			
B5N		No Temperature Data Recorded		39-68°F	27 hours	600 lb cement, 200 lb fly ash per yd^3
B6S	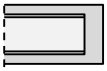	164°F	53°F	65-84°F	not known	600 lb cement, 200 lb fly ash per yd^3
B7N	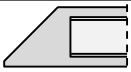	Temperature Data Lost		70-97°F	17 hours	675 lb cement, 225 lb fly ash per yd^3
B7S	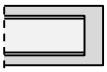	>173°F	Not Recorded			

The TxDOT Standard Specifications (2004) set two relevant limits on curing temperatures of prestressed beams, summarized in Table 6-3. The first limit is the maximum allowable temperature, equal to 150°F for concrete mixtures that do not include fly ash, and 170°F for mixtures containing fly ash. The second limit is the maximum allowable temperature differential across a cross section, set to 35°F. While the temperature differential regulation technically applies to mass concrete (defined as sections with a minimum dimension of 5 ft), it is reasonable that slightly smaller concrete sections such as the U-Beam end block should also be similarly constrained. The core temperature of mass concrete is also required to remain below 160°F, but only the beam maximum temperature requirements are considered here.

Table 6-3: TxDOT Standard Specifications regarding curing temperature (TxDOT, 2004).

	Straight-Cement Concrete	Concrete Containing 25% Fly Ash
Maximum Temperature (§424.3.B.7)	150°F	170°F
Temperature Differential (§420.4.G.14)	35°F	

The maximum temperatures and temperature differentials are compared to the appropriate TxDOT limit in Figure 6-6. While very high temperatures were recorded in some beams, these beams tended to contain fly ash and thus the temperatures were not above the TxDOT limit by more than 10%. More significant violations of the Specification were seen in the maximum temperature differentials. This requirement is set to reduce the chance of thermal cracking in mass of concrete. While no such cracking was observed in the U-Beams fabricated, the possibility of these high temperature differentials should not be ignored.

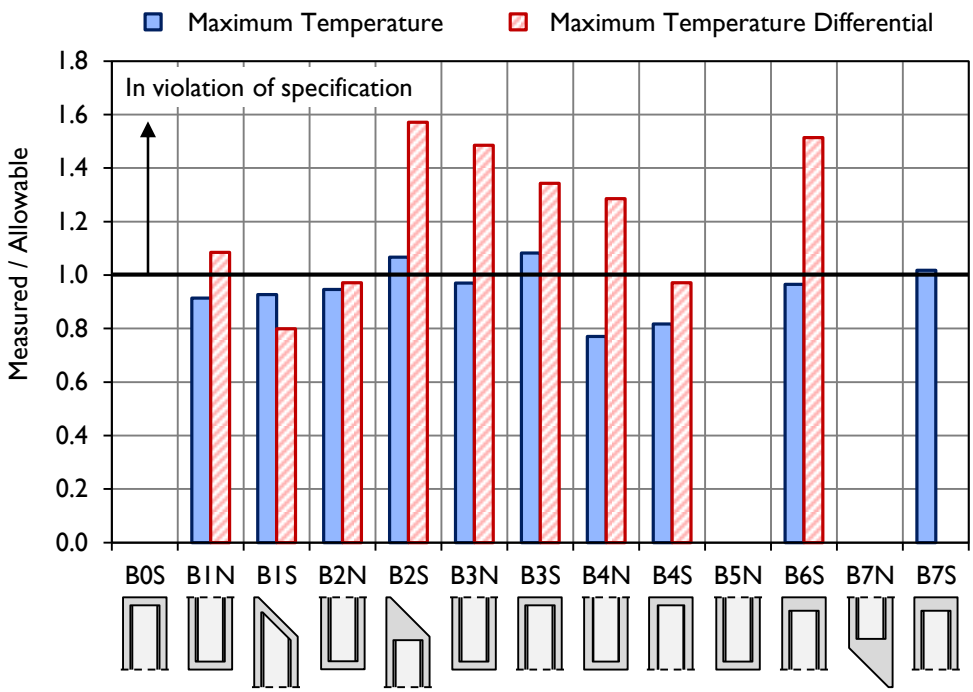

Figure 6-6: Comparison of measured maximum temperatures and maximum temperature differentials to the TxDOT limits.

Prior to the initiation of this project, it was known that reducing the size of the U-Beam end block would reduce the curing temperatures within. The study of curing temperatures was performed in part to determine how much change would be observed. The skewed end blocks of Beams 1 and 2, built, respectively, with a skewed internal void and a square internal void, provide an answer. As can be seen in Table 6-2, the ambient temperatures and concrete mixture designs were similar for the two beams. The maximum recorded temperatures and temperature differentials were very different. The temperature profile of each beam end, plotted on the same scale, is shown in Figure 6-7. Regarding TxDOT Specification compliance, test region B1S met both specifications, while B2S met neither and recorded the highest temperature differential of any beam end region studied.

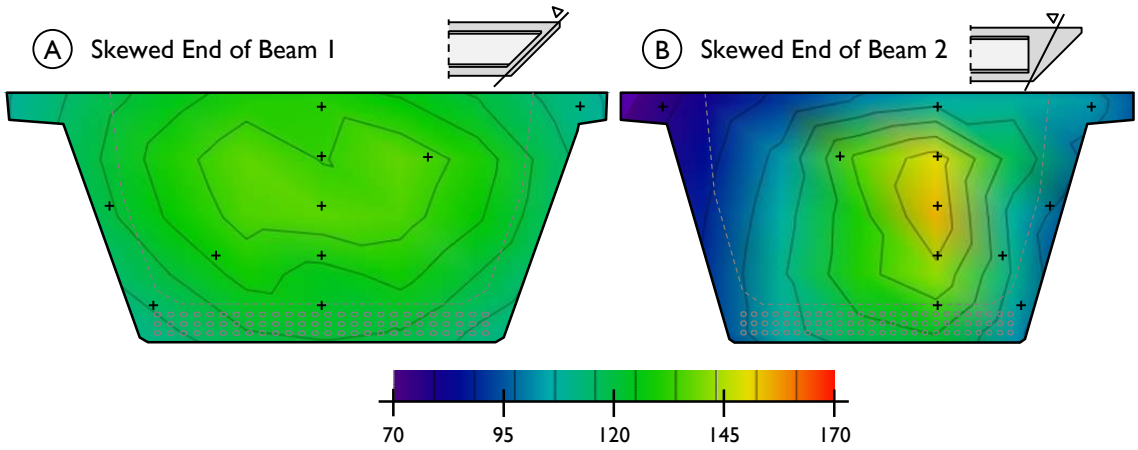

Figure 6-7: Temperatures measured through the cross sections of the skewed end blocks of Beam 1 and Beam 2 at time of maximum temperature reading.

More important than the end regions of Beams 1 and 2, however, are the end regions of Beam 7. This beam was fabricated using the recommended new standard design, which includes increasing the length of the end block. The curing temperature of Beam 7 was only recorded in the rectangular end; the thermocouple in the skewed end failed during casting. The temperature measured in the rectangular end of Beam 7 exceeded the existing TxDOT limit of 170°F for concrete with fly ash, indicating that the much larger skewed end block would likely have exceeded this limit as well.

There are two points to be highlighted prior to becoming concerned. First, no significant or special cooling methods were used during the curing of these beams. Some fabricators use water pipes through the end blocks, constantly flushed with cold water, during curing. No such pipes were used in the monitored beams. Secondly, with the stringent requirement for the inclusion of 25% fly ash in prestressed concrete mixtures (TxDOT, 2004), the chances of ASR and DEF-related problems are significantly reduced, thus decreasing the importance of the temperature limit (set for purposes of preventing DEF) (TxDOT, 2010).

Especially in a warm-weather climate as exists in Texas, in the absence of temperature-controlling mechanisms like water pipes, high curing temperatures are inevitable in large blocks of concrete. In light of the compressive strength data gathered by Myers and Carrasquillo (1998) (presented in Chapter 2), even if material reactions like

ASR are not of concern, it is beneficial for structural performance that curing temperatures be minimized.

6.4 DISTRIBUTION OF LOAD

The calculations for the concrete contribution (V_c) to vertical shear capacity presented in Chapter 2 are directly proportioned to the web width of the section. In this study and in practice, the web width of a U-Beam is defined assuming the two separated webs act integrally with one another. For purposes of calculations, a Texas U-Beam (Figure 6-8(A)) has the cross section shown in Figure 6-8(B).

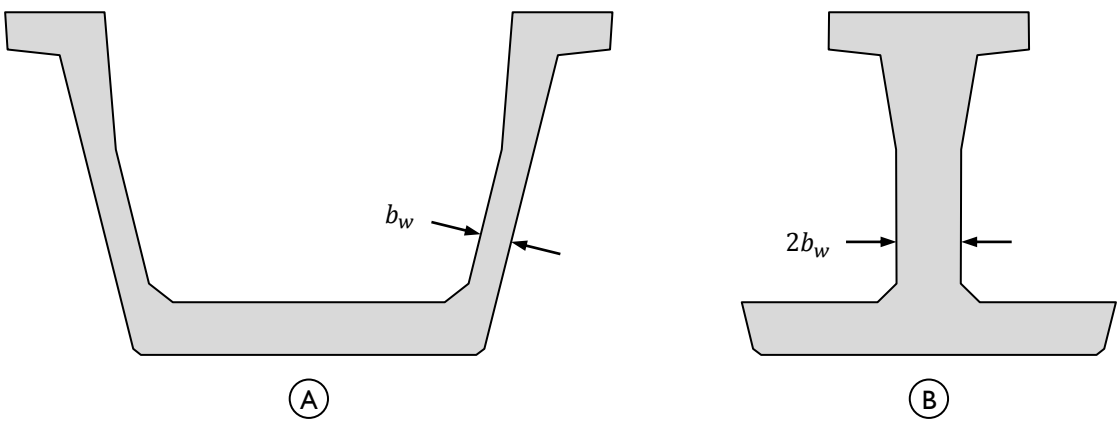

Figure 6-8: (A) Actual shape of a Texas U-Beam and (B) effective shape for calculations.

For satisfactory structural performance, it is necessary that load actually distribute somewhat evenly between the two webs of a typical U-Beam. The amount and proportion of load carried in each web of the test specimens in this study was estimated through two methods: linear potentiometers mounted on the beam webs and load cells supporting the beam ends.

The linear potentiometers were used to measure the amount of distortion in each web through the loading process. Three potentiometers were attached to the beam with threaded rods embedded into the web to form a triangle, as shown in Figure 6-9. Distortion was defined as the change in angle ϕ away from 90° (Figure 6-10(A)). The angle at any point during the loading, when the triangle would appear distorted as in Figure 6-10(B), was found using the Law of Cosines, which states that:

$$c^2 = a^2 + b^2 - 2ab\cos\phi$$ **Equation 6-1(a)**

where a, b, and c are the lengths of the triangle sides, positioned relative to ϕ as shown in Figure 6-10(C). The equation is rearranged to solve for ϕ, in radians:

$$\phi = \cos^{-1}\left[\frac{a^2 + b^2 - c^2}{2ab}\right]$$ **Equation 6-1(b)**

The angle ϕ was converted from radians to degrees, and the distortion at any shear was calculated to be:

$$distortion(V) = \phi(V)\frac{180°}{2\pi} - 90°$$ **Equation 6-2**

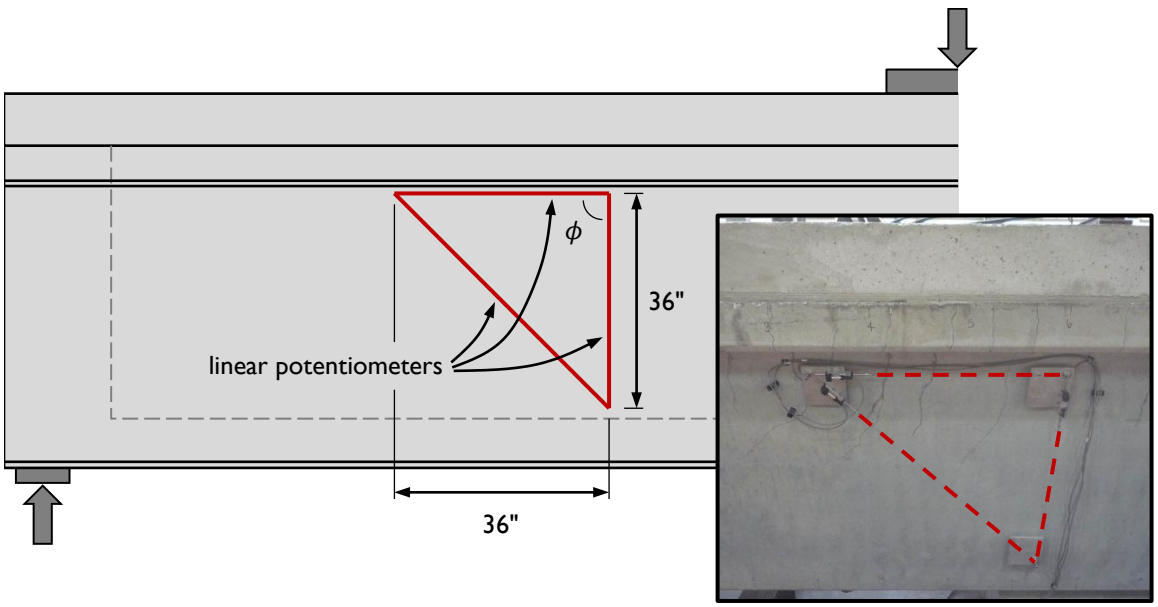

Figure 6-9: Linear potentiometers locations on web, for measuring distortion.

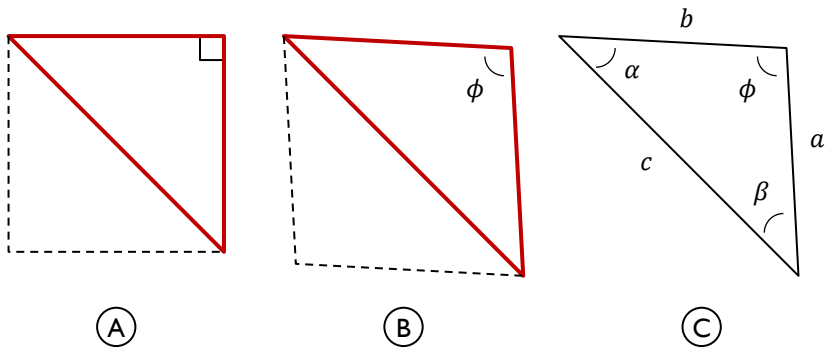

Figure 6-10: (A) Original orientation of linear potentiometers, (B) shape after applying load, and (C) definition of variables used in distortion calculation.

Especially in rectangular beams, if the distortion in the two webs were similar at the same moment in time, it stands to reason that the load carried by each web was also similar. A typical plot of distortion against percentage of failure load for a rectangular beam is shown in Figure 6-11(A) (data from test specimen B5N). The calculated vertical shear strength (found using the AASHTO General Method (2010)) is also shown. The difference in distortion between the two webs was less than 0.10° in all rectangular beams, with the maximum difference typically occurring just prior to failure. The distortion plots for each shear test during which this measurement was made can be found in Appendix B.

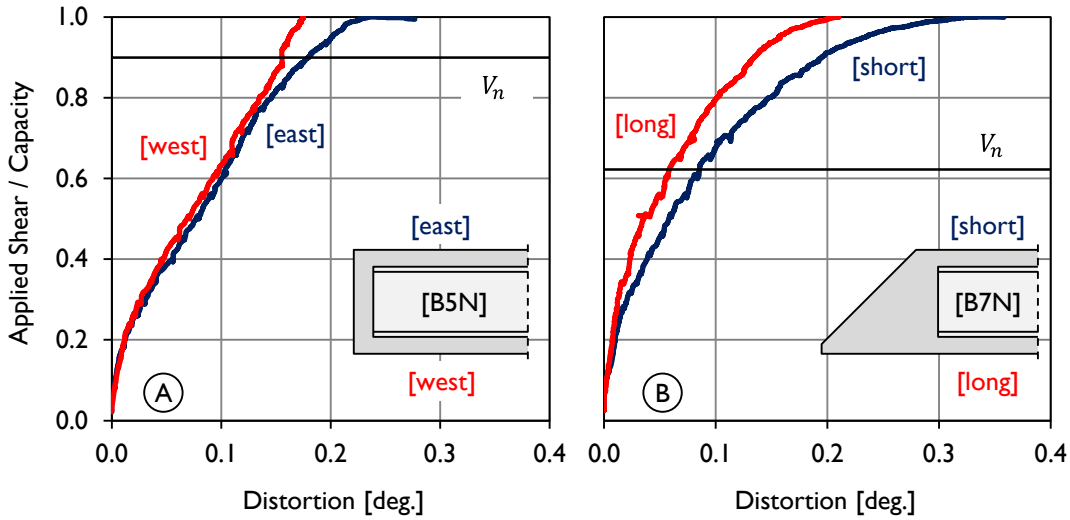

Figure 6-11: Typical distortion measured in the two webs of a rectangular and skewed beam.

Web distortion was measured in one of the two skewed test specimens (B7N). A greater difference in distortion was calculated (though still less than 0.15°), as seen in Figure 6-11(B). It is still reasonable to assume the two webs are close to equally distressed through the application of load, with the short side taking slightly more of the load. While the load distribution might not be exactly equal, the load is definitely being carried by both webs, as opposed to primarily by just one.

The second method used to estimate the division of load in the two webs of the U-Beams were the load cells positioned beneath the supports of the beam. Texas U-Beams are supported on three bearing pads: one central pad (measuring 32 in. wide) at one end and two smaller pads (16 in. wide) at the other. This bearing configuration provides more stability than the two pads used for I-Beams, which are much narrower. During shear testing, support reactions were measured using load cells placed beneath the bearing pads, as was described in Chapter 3. The loads measured at the end of the beam resting on two bearing pads were believed to be adequate estimations of the load in the respective webs (Figure 6-12(A)); the same assumption was not made for load cells positioned underneath a single bearing pad (Figure 6-12(B)).

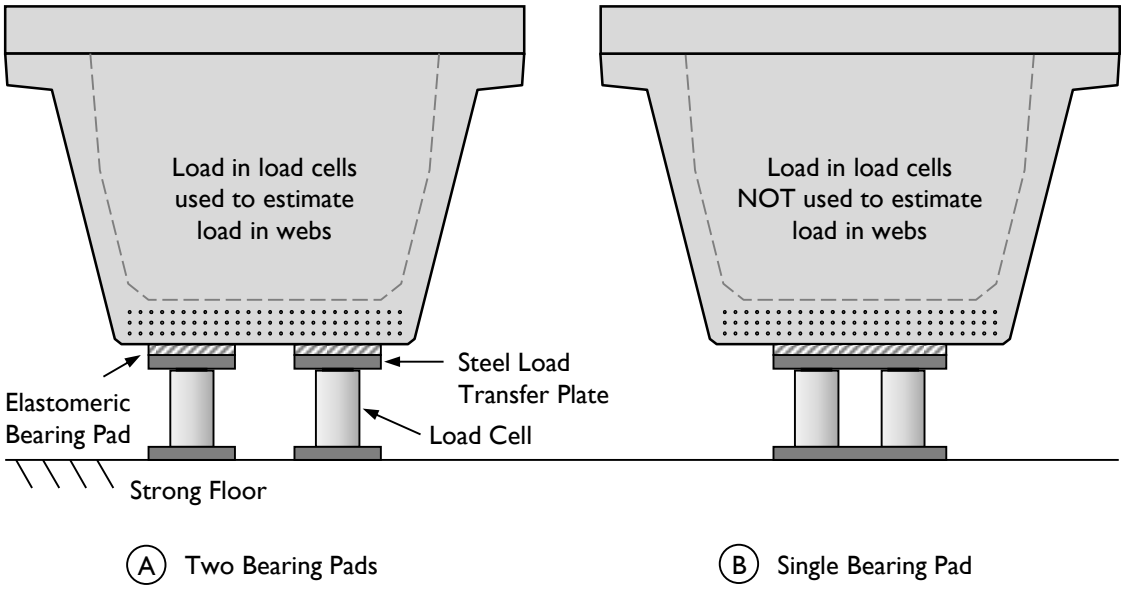

Figure 6-12: Bearing conditions used in U-Beam load tests.

The division of load between the two webs was estimated by calculating the ratio of load in one load cell to the total load carried by that end. For consistency, the load cell under the west side of the beam was used as the reference point (in skewed Beams 1 and 2, the west side is the shorter side of the skew; in Beam 7, the west side is the longer side of the skew). To summarize the results, two ratios from rectangular beams (B3S and B5N) and two ratios from skewed beams (B1S and the south end of Beam 2 during B2N shear test) are shown in Figure 6-13(A) and (B), respectively. The data gathered during other shear tests are given in Appendix B. The load cell data confirms the observations made from the distortion plots. In rectangular beams, load was distributed evenly between the two bearing points (and thus, presumably, the webs), with one bearing pad taking no more than 5% more or less than half the load at that end. In the skewed beams, the bearing closer to the short web carried 55 to 60% of the load.

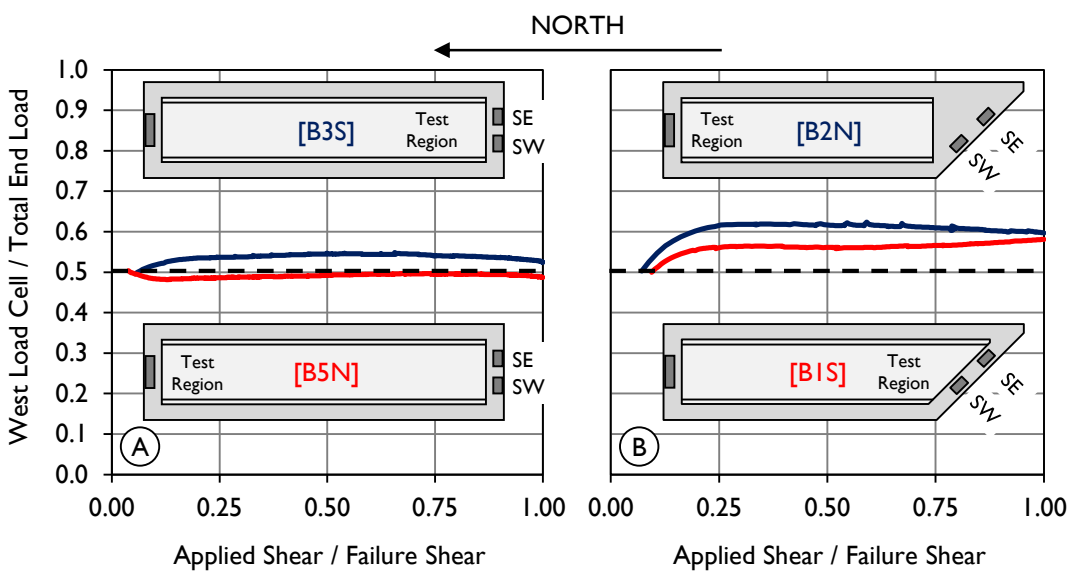

Figure 6-13: Ratio of load on west side load cell (short side of skewed beams) to total load at that end.

It is important that the combined web-wall theory provide a conservative estimation of shear strength with b_w equal to two times the width of a single web. As will be discussed further in Section 6.8, in test regions that failed in web-shear, an acceptable level of conservatism was seen. While the Texas U-Beam contains two webs that are not connected to one another away from the end block, performing calculations

as if the cross section were as shown in Figure 6-8(B) is reasonable. While there is evidence from this study that, in skewed ends, the shorter web takes slightly more load, this effect is likely to diminish as the load is placed further from the end of the beam, as the relative difference in web lengths will decrease.

6.5 CRACKING BEHAVIOR

The shear required to cause diagonal web-shear and flexure-shear cracking was recorded during testing. In three cases, the load required to cause flexural cracking was also recorded (flexural cracking was not observed in seven tests; in the final case, the exact load causing cracking was not noted). Loading was halted at increments of 25 to 100 kips to allow for visual observation and measurement of the cracking. The occurrence of cracking was confirmed using data collected from internal strain gauges and the external shear-deformation set-up, when available. Crack widths were measured in fractions of an inch using a plastic comparator.

The cracking shears observed were compared to calculated values found using the ACI 318-08 Detailed Method (Equations 11-10 and 11-12 of ACI 318-08, or Equations 2-6(a) and 2-6(b) of this dissertation) for, respectively, flexure-shear and web-shear cracks. These equations were presented in Chapter 2. The flexural cracking capacity was found as the load required to exceed the tensile capacity of the bottom fiber of the beam. Comparisons of recorded cracking shears and loads for the test specimens to the calculated cracking capacities (for web-shear, flexure-shear, and flexural cracking) are given in Table 6-4. All three types of cracks were not seen in every specimen; in many beams, the failure shear was well below the calculated flexure-shear and flexural cracking shears. In test region B7N, flexural and flexure-shear cracks were observed from a distance, but the exact loads causing the cracks were not recorded due to the large amount of shear on the test specimen with respect to calculated capacity.

Table 6-4: Summary of calculated and observed cracking loads and shears.

Test ID	Web-Shear Cracking (V_{cw})			Flexural Cracking (P_{flex})			Flexure-Shear Cracking (V_{ci})		
	Calculated [kip]	Observed [kip]	Ratio	Calculated [kip]	Observed [kip]	Ratio	Calculated [kip]	Observed [kip]	Ratio
B0S	314	233	0.74	[not observed]			[not observed]		
B1N	317	398	1.04	[not observed]			[not observed]		
B1S	317	331	0.65	[not observed]			[not observed]		
B2N	323	217	0.67	[not observed]			[not observed]		
B3N	269	247	0.92	[not observed]			585	554	0.95
B3S	cracked during test of B3N[1]			[not observed]			593	580	0.98
B4N	cracked during test of B4S[1]			[not observed]			955	749	0.78
B4S	558	525	0.94	1255	1479	1.14	955	800	0.84
B5N	335	247	0.74	1130	1491	1.27	850	636	0.75
B6S	296	389	1.31	1125	1497	1.28	846	806	0.95
B7N	324	341	1.05	shear not recorded[2]			shear not recorded[2]		
Average			0.96			1.23			0.87
COV			0.23			0.06			0.11

[1] Diagonal cracking first observed while test region was strengthened with post-tensioned clamps, during testing of the other end of the beam (see Figure 3-20).

[2] Flexural, flexure-shear cracking observed from a distance but exact shear causing cracking could not be recorded due to the large amount of shear on the beam with respect to calculated capacity.

6.5.1 Crack Widths

Crack widths can be used to compare beams existing in the field to those tested in the laboratory. If, upon inspection, diagonal cracks are found in a Texas U-Beam, it would be desirable to use the width of the crack to approximate how much load that beam is carrying relative to the failure load. In Figure 6-14, the measured diagonal crack widths in the U-Beam specimens are plotted against the ratio of applied shear to failure shear. The failure mode of the test specimen is also indicated. The widest diagonal cracks measured were 0.040 in., seen at applied loads very close to failure. No diagonal cracking was seen in any test region loaded to less than 20% of the capacity.

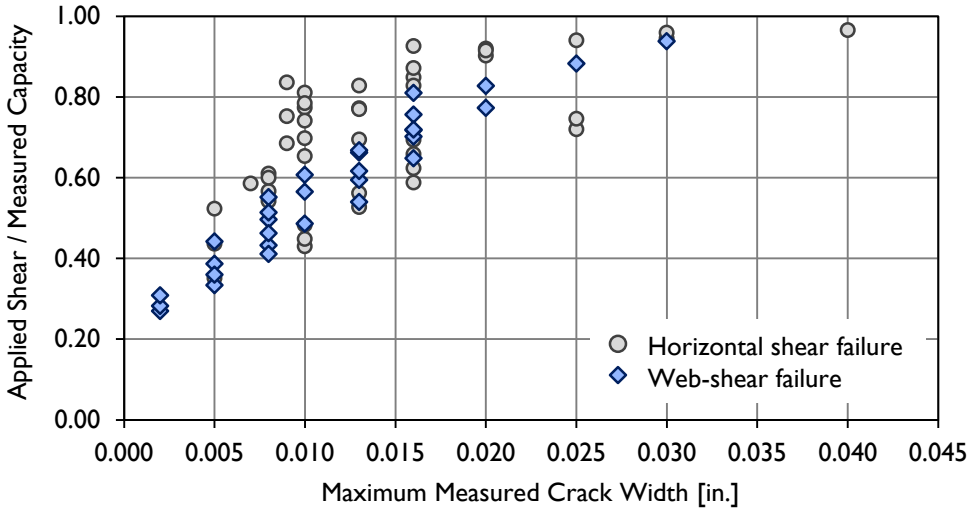

Figure 6-14: Maximum measured crack width plotted against the ratio of applied shear to failure shear.

Nine of the eleven test specimens are included in Figure 6-14 (test specimen B4S, which was not loaded to failure, was omitted, as was B0S, for which crack width data were not collected). By considering only certain specimens at a time, further observations can be made. To begin, the diagonal crack widths measured for only the test specimens that failed in web-shear (B5N, B6S, and B7N) are plotted in Figure 6-15. The scatter in crack widths is much smaller through these tests than through all the tests. Wider diagonal cracks (larger than 0.030 in.) were observed but not recorded, as the test specimens were loaded above the calculated shear capacity and a hands-on investigation was not deemed to be acceptably safe.

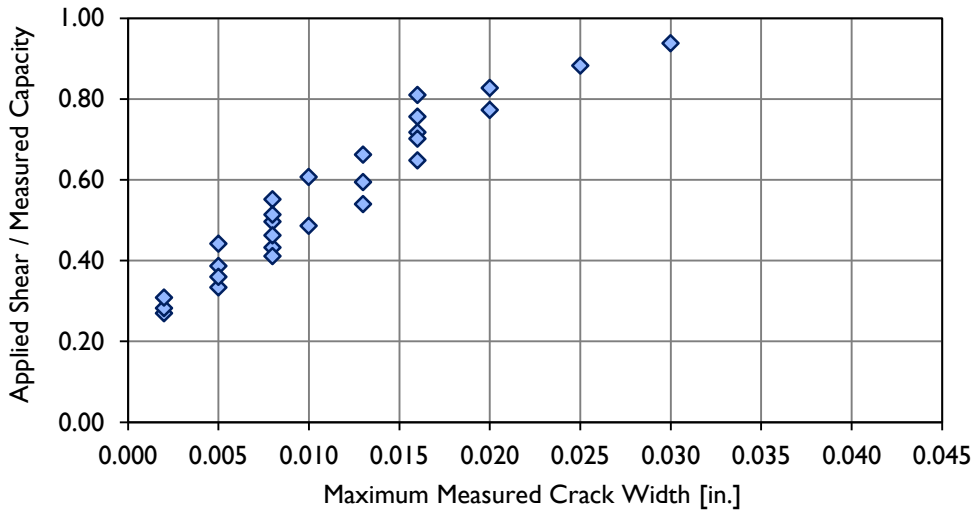

Figure 6-15: Maximum measured crack widths for test specimens that failed in web-shear.

The crack width data presented in the previous two graphs are summarized in general terms in Table 6-5. Crack widths of 0.010 in. were observed in beams loaded to approximately 40% of their capacity when both the current design details and the recommended new details were used. Wider cracks were observed at lower loads in test specimens with the current reinforcing details. It should be noted that these general conclusions are made using data from beams fabricated with conventional concrete and reinforced with Grade 60 bars or 85-ksi welded wire fabric. Beams utilizing alternate materials may not behave similarly.

Table 6-5: General trends for the relationship between crack width and proximity to capacity.

Maximum Crack Width [in.]	Percentage of Failure Load	
	Existing Details	Recommended Details
0.010	40%	40%
0.020	60%	70%
0.030	80%	90%

The reinforcing details of Beam 4 present an interesting side-by-side comparison of the effect of adding the supplementary reinforcing on cracking behavior (Figure 6-16). As the failure shear of B4S was not reached, the crack widths are plotted against applied shear. While the L-bars, which terminated at mid-height of the web, were installed in

B4S to increase the strength of the bottom flange-to-web interface and are not used in calculations for web-shear capacity, the crack widths observed in B4S are narrower than those seen B4N at the same shear. The inclusion of the L-bars reduced crack widths in test region B4S as the amount of steel crossing the cracks was increased in the bottom half of the web.

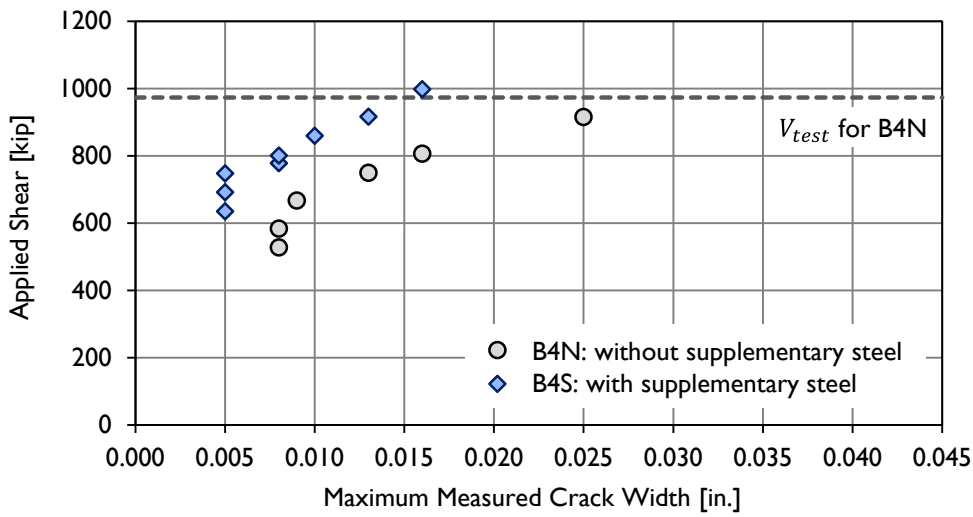

Figure 6-16: Comparison of cracking observed in the two test regions of Beam 4.

6.5.2 Overall Vertical Strain

Using the linear potentiometers mounted vertically on the web walls as described in Chapter 3 and shown in Figure 6-9, the overall strain in the webs of B4S and B4N at equal shear loads can be compared (Figure 6-17). These data are in agreement with the maximum crack widths: the addition of the L-bars reduced the magnitude of straining at equal shear in test region B4S as compared to B4N. The data gathered from instruments mounted on the second web of these specimens and on the gauged webs of other beam end regions during testing can be found in Appendix B.

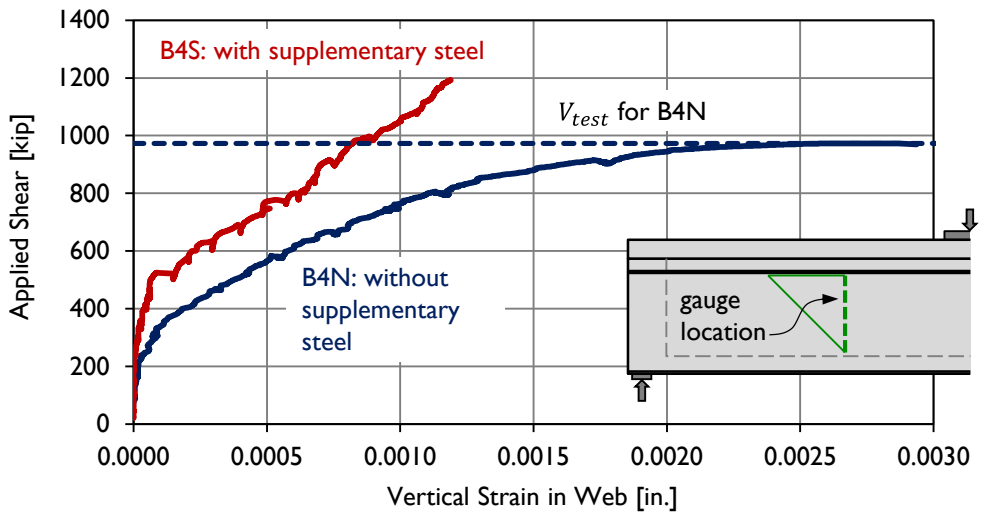

Figure 6-17: Vertical strain measured through the webs of Beam 4.

Prior to concluding that the expansion seen in B4S was less than in the other test specimens, it was necessary to compare these results to the expansion of the test regions built with the standard cross section. In Figure 6-18, the vertical strain in the web of B4N is compared with that of B3S. Unlike in the comparison to B4S, there is very little difference in behavior between B4N and B3S. While the additional reinforcing steel used in B4S reduced strain (even without extending full-depth), the thicker web walls of B4N did not alter the behavior.

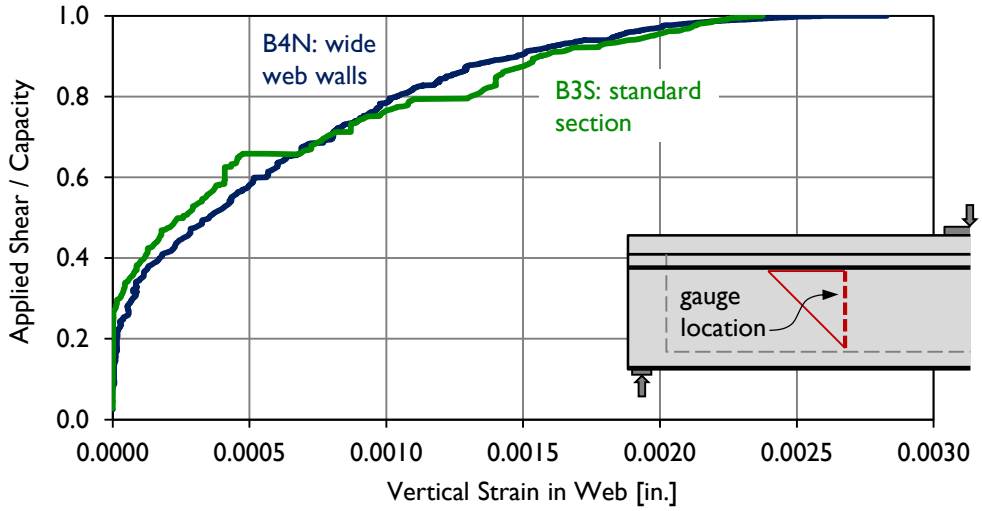

Figure 6-18: Vertical strain measured in B4N (wide web walls) and B3S (standard section).

6.6 DEMAND ON TENSILE REINFORCEMENT

Using nearly 1700 shear tests reported in the literature, Nakamura (2011) compiled a database of 223 points with which to evaluate codified shear provisions. He concluded that the AASHTO General Procedure (2010) was accurate and conservative, except in two cases: when beams failed with signs of horizontal shear damage, or with signs of anchorage zone distress. Horizontal shear distress was observed during six of the U-Beam shear tests performed during this study; the mechanics of this behavior are discussed in Chapter 7.

While significant strand slip was not observed in this study and was not a major focus for the research team, brief calculations were carried out following existing equations. The likelihood of prestressing strand slip was approximated following AASHTO Equation 5.8.3.5-1. Simplified for the U-Beam case at hand, the equation states:

$$T_n \geq T_{max} \qquad \textbf{Equation 6-3(a)}$$

$$A_{ps}f_{ps} + A_s f_y \geq \frac{|M_u|}{\phi_f d_v} + \left(\frac{|V_u|}{\phi_v} - 0.5V_s\right)\cot\theta \qquad \textbf{Equation 6-3(b)}$$

where

T_n = tensile capacity of the longitudinal reinforcement on the flexural tension side of the member [kip]

T_{max} = maximum tensile demand on longitudinal reinforcement [kip]

A_{ps} = area of bonded prestressing strands [in.^{2}]

f_{ps} = average stress in prestressing steel [ksi]

A_s = area of bonded longitudinal mild reinforcement [in.^{2}]

f_y = yield stress of mild reinforcement [ksi]

M_u = moment at the section [kip-in.]

d_v = effective shear depth [in.]

V_u = shear at the section [kip]

ϕ_f, ϕ_v = resistance factors

V_s = shear resistance provided by the transverse reinforcement

(found using AASHTO General Procedure (2010)) [kip]

θ = angle of inclination of diagonal compressive stresses (found using AASHTO General Procedure (2010)) [°]

This equation was derived by considering the free-body diagram shown in Figure 6-19. The demand on the longitudinal reinforcement (T_{max}) is found by summing moments about Point O. The aggregate interlock force (V_{agg}) is assumed to have a negligible moment about Point O. It should be noted that the equation for capacity does not consider the effects of bearing condition, confining reinforcement, end blocks, or skew. For this study, the demand on the longitudinal reinforcement was calculated at two points: at the front face of the bearing pad, where bending moment was zero but the prestressing strands were not completely developed, and a distance d_v from the load point, chosen as a point of high moment and high shear.

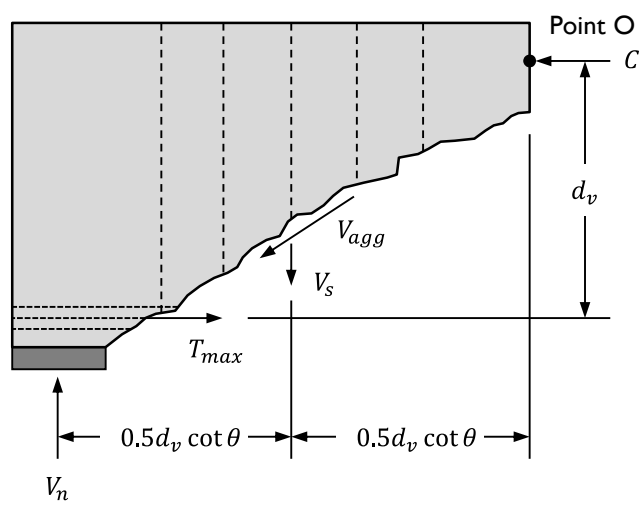

Figure 6-19: Free-body diagram of the end region of a prestressed beam (from AASHTO (2010)).

The calculated demand was compared to the capacity available in the longitudinal reinforcement at the two points studied. In U-Beam test specimens, the longitudinal reinforcement consisted of prestressing tendons and, at beam end, six U-shaped reinforcing bars (W-bars, shown in Appendix A). Given the proximity of the bearing to the beam end, the average available stress in the prestressing tendons near beam end was found to be around 90 ksi; for test region B7N, which contained 0.6-in. diameter strands, the available stress was 73 ksi.

Strand slip was monitored using linear potentiometers secured to the prestressing strands. The tip of the potentiometer rested on the beam; any change in reading during loading was attributed to the strand slipping into the beam with respect to the beam face. Between one and nine strands were monitored during eight of the eleven shear tests. Other than in the first use of this gauge (B2N), all gauges were attached to strands in the bottom row (located 2.0 or 2.17 in. from the bottom of the beam). A gauge was always placed on the outermost strand; this strand always slipped more than other monitored strands. For Beam 3, in which 36 strands were debonded at beam end, gauges were placed on fully bonded strands as well as on strands that became bonded at 6, 9, 12, and 15 ft from beam end. In this discussion, only the slip of fully-bonded strands will be considered. In an effort to differentiate between slip that occurred as a consequence of shear failure, and slip associated with loading, the presence of slip was evaluated at 95% of the failure shear. The maximum reading at $0.95V_{test}$ in the gauges used for each test is summarized in Figure 6-20. Significant slip was seen in two test regions: B2N and B3N. No slip was seen in the five test regions that contained confining reinforcement.

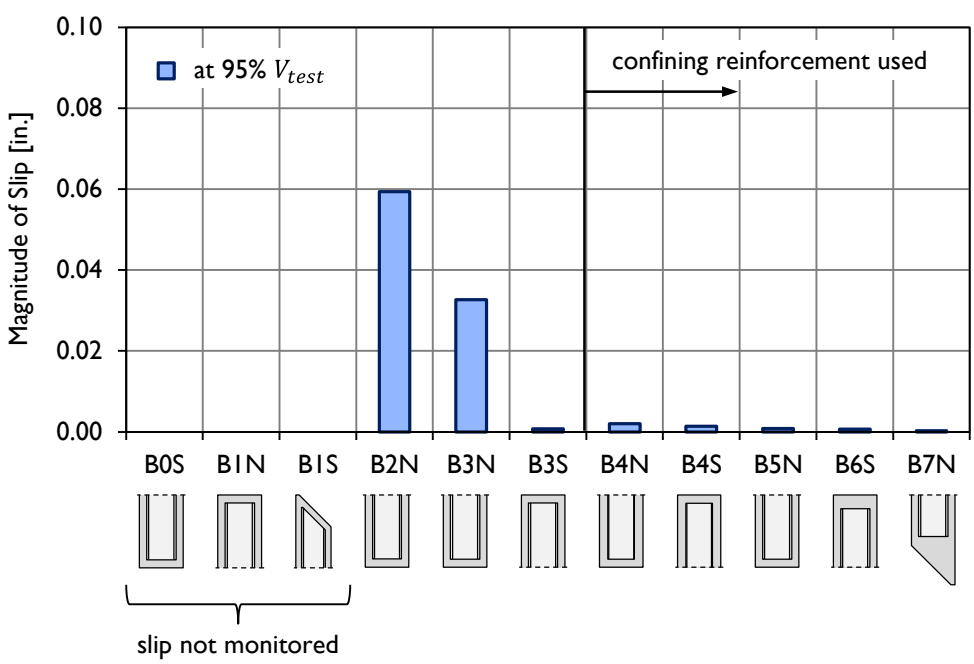

Figure 6-20: Strand slip measured at 95% of failure load during shear testing.

A summary of the demand and capacity calculated at the face of the bearing pad and near the load point is given in Figure 6-21 and Table 6-6. While in eight of the eleven test regions, slip was expected per the AASHTO equation, slip was observed during only two of the eight tests that utilized slip instrumentation, B2N and B3N.

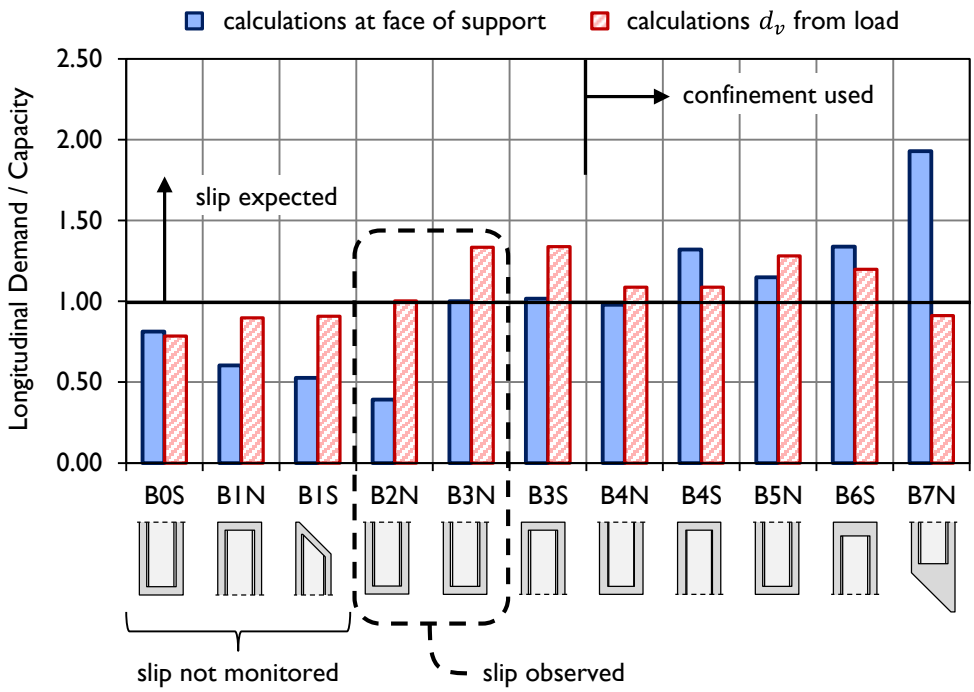

Figure 6-21: Summary of longitudinal demand calculations.

Table 6-6: Summary of longitudinal demand calculations.

Test ID	[at the face of the support]			[d_v from the load]			Slip Observed?
	T_{max} [kip]	T_n [kip]	$\frac{T_{max}}{T_n}$	T_{max} [kip]	T_n [kip]	$\frac{T_{max}}{T_n}$	
B0S	892	1096	0.81	2045	2601	0.79	not monitored
B1N	758	1256	0.60	2683	2984	0.90	not monitored
B1S	661	1255	0.53	2711	2984	0.91	not monitored
B2N	490	1251	0.39	2994	2984	1.00	Yes
B3N	715	715	1.00	2145	1607	1.34	Yes
B3S	727	714	1.02	2152	1607	1.34	No
B4N	1208	1234	0.98	3247	2984	1.09	No
B4S	1629	1234	1.32	3247	2984	1.09	No
B5N	1165	1014	1.15	3236	2525	1.28	No
B6S	1329	994	1.34	2932	2448	1.20	No
B7N	1894	982	1.93	2660	2915	0.91	No

While the underestimation of strength (or overestimation of demand) seen in the calculations for most test cases (slip calculated to be a problem but not seen to occur) is not ideal, it is at least conservative. Further research into the use of this equation would be beneficial for purposes of better predicting demand and capacity to reduce the unnecessary levels of conservatism.

The end regions of B2N and B3N, where slip was observed, were studied to understand when and how slip began. After the failure of test region B2N, a longitudinal crack was observed on the underside of the beam, near the position of the strand being monitored. It is possible that this crack formed during loading, which would then reduce the bond of the concrete to the strand and allow the strand to slip prior to beam failure.

When considering test region B3N, the discrepancy in recorded slip between the two ends of Beam 3 was of most interest. With identical reinforcing bar details and prestressing, the same constitutive concrete, and a similar loading scheme, it is surprising that the instrumentation indicated slip during testing of one end but not the other. To better understand these tests, the slip gauge data from both ends are presented in Figure 6-22. During each test, the strand in the bottom row, outermost position on either side was monitored. The data collected from the debonded strands are included as well, as those points illustrate how the general behavior of the two ends was similar. However, during testing of the north end (Figure 6-22(A)), the fully-bonded monitored strands began to slip at 70% of the failure shear, and steadily slipped until failure. During testing of the south end, those same two strands did not slip through the entire loading process.

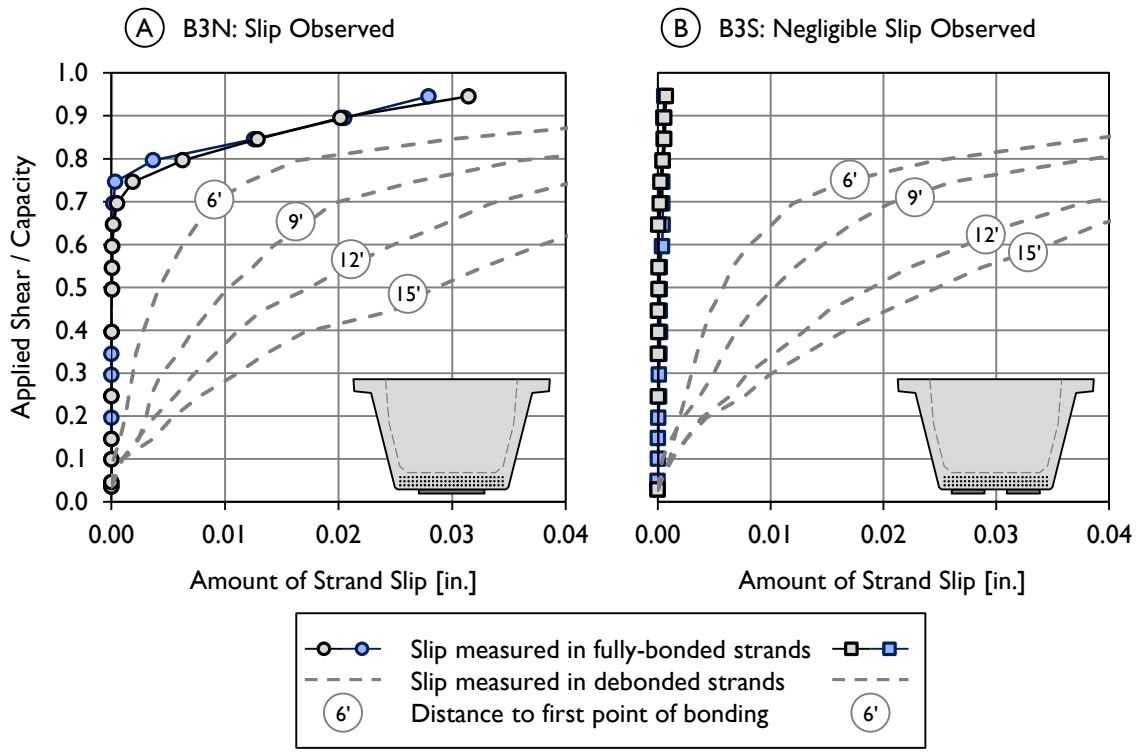

Figure 6-22: Strand slip data gathered during shear tests B3N and B3S.

It should be noted that the bearing conditions of B3N and B3S were different: while B3N was supported on one bearing pad, B3S was supported on two, as seen in Figure 6-23. In neither case is the monitored strand directly above the bearing pad, but in B3S the strands are much closer (3.5 in. vs. 9 in.) to the bearing pad. It is possible that the compression induced above the bearing pad helped to anchor the strands in B3S and prevent slip. Without more data, it is difficult to make conclusions on the effect of bearing placement relative to the web wall on strand anchorage. In a test series in which slip is expected or seen, this could be a variable for consideration. The observation of slip in the single-bearing pad condition indicated that bearing on a single pad was a more critical loading scenario than when two pads were used.

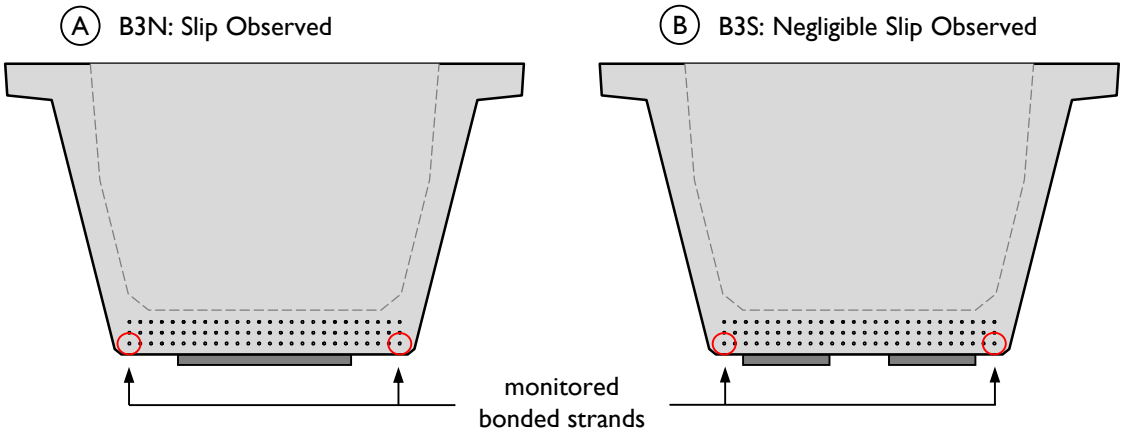

Figure 6-23: Bearing condition and monitored strand locations for B3N and B3S.

6.7 DEMAND ON VERTICAL REINFORCEMENT

Seven of the eight end regions containing strain gauges affixed to reinforcing bars were load-tested. The strain gauges were monitored during the test, in order to determine the magnitude of strains caused by loading. Gauges were located at mid-web, near the middle of the shear span (the shear instrumentation region), and at the bottom flange-to-web interface near the beam end (the bottom flange-to-web interface instrumentation region), as shown in Figure 6-24.

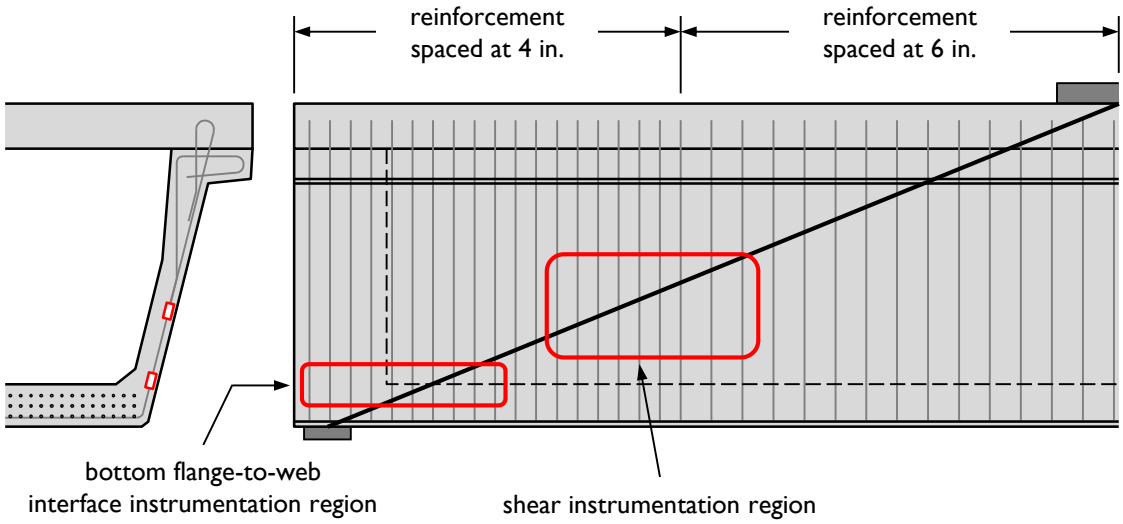

Figure 6-24: Locations of gauges monitored during shear testing.

6.7.1 Shear Instrumentation Region

Of the seven gauged and tested end regions, six failed along the bottom flange-to-web interface near beam end; while diagonal cracking was present in the webs of the beams, major damage was not sustained in this region. The magnitude of strain measured in the reinforcing bars, however, indicated that at failure, significant load was being carried by the bars, as seen in Figure 6-25. Gauges that measured strain values greater than 0.003 in./in. at failure are plotted at 0.003. Very few gauges read strains below the yield strain at failure. The gauges installed in the shear region of test specimen B4S (the loading of which was halted prior to failure) indicated strains in the reinforcing bars equal to less than half of the yield strain when the test was stopped.

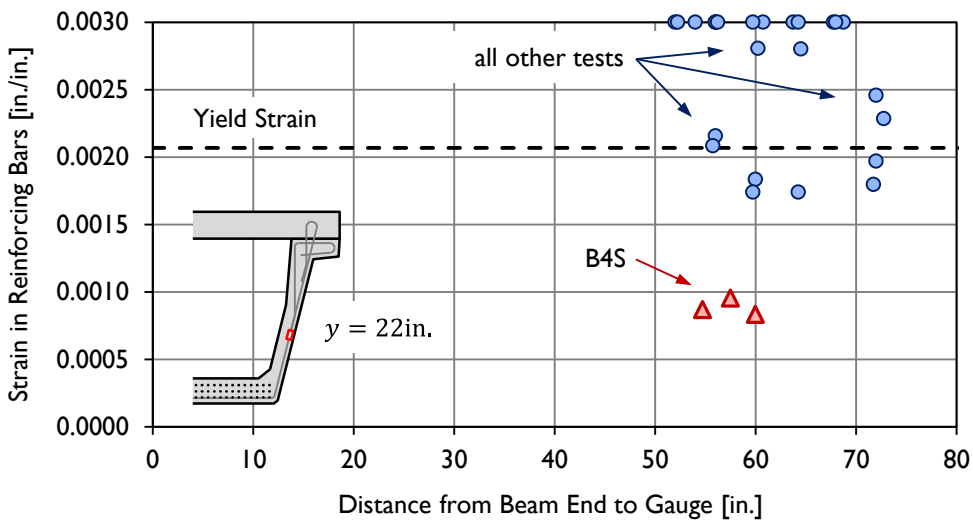

Figure 6-25: Strain in reinforcing bars at maximum load.

In an effort to estimate the remaining capacity in test specimen B4S, the strains at maximum load were compared to the strains in the other test specimens at V/V_{test} values below 1.0. The strains measured at maximum load for B4S and at approximately 67% of V_{test} for the other test specimens are plotted in Figure 6-26. While the strains measured in B4S at V_{max} were similar to those seen in the other test specimens at 67% of V_{test}, the assumption that B4S had an additional 50% reserve capacity is not ideal for several reasons. First, B4S contained significantly different reinforcement than any other gauged test specimen (as L-bars were included), and might have failed prior to the stirrups

reaching the strain levels seen in earlier beams. Second, the test region was expected to fail in a typical web-shear failure mode rather than the horizontal shear failure mode seen with the previous six test specimens; this failure mode may not have induced the same strains in the web reinforcing bars as the horizontal shear failure mode did. However, given the observed crack widths presented earlier, the overall vertical strains, and the strains measured in the reinforcing bars, it can be stated with some confidence that test specimen B4S was capable of carrying 10 to 20% more load than when the test was halted. Given the flexural capacity of the beam, load of that magnitude would likely cause a flexure-shear or flexural failure.

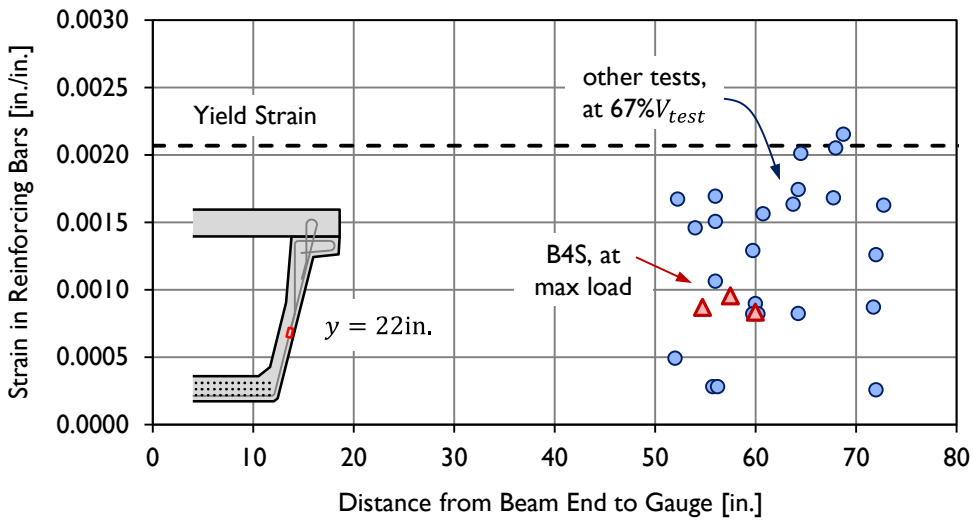

Figure 6-26:Comparison of strains in B4S at maximum load to other test specimens at 67% of their failure load.

6.7.2 Bottom Flange-to-Web Interface Instrumentation Region

The shear-friction theory from which the horizontal shear capacity calculation presented in Chapter 7 was derived is based on the assumption that when two sections of concrete slide against one another, the reinforcing bars crossing the slip plane are stressed and provide a clamping force on the interface. The internal instrumentation installed in the U-Beams tested in this study was used to determine whether this assumption is correct. The strains measured just before failure in the bottom flange-to-web interface gauges are plotted in Figure 6-27. The gauges in B4S are separated into two groups –

those on the main web reinforcing bars (R-bars) and those on the supplementary steel (L-bars).

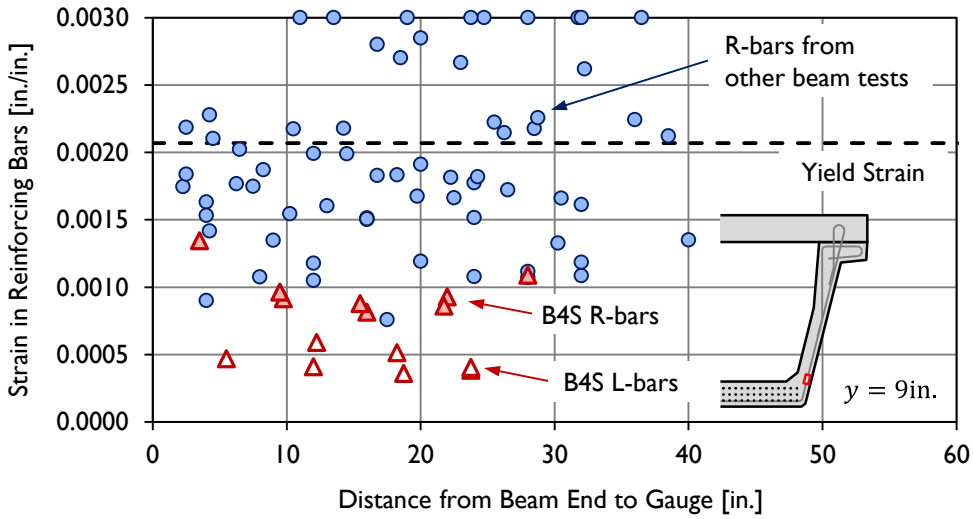

Figure 6-27: Measured strains in web reinforcing bars at bottom flange-to-web interface just before failure.

Compared to the strains measured in the shear instrumentation region, there is significantly more scatter in the data at the end of the beam. Even with the scatter, it can be seen that each gauge recorded positive strain readings, indicating tension existed across the bottom flange-to-web interface near failure. The strains in this region may have been higher in the monitored beams (Beams 1-4) than in the beams tested later in the program (Beams 5-7) due to the failure location, which was in the immediate vicinity of these gauges. The strains in B4S were generally below those measured in the other beams, but, as in the shear instrumentation region, this discrepancy may be due to the additional capacity of the section. When the B4S maximum load data are plotted with the other test data at 67% of the maximum load carried, the data points again fit with the others (Figure 6-28).

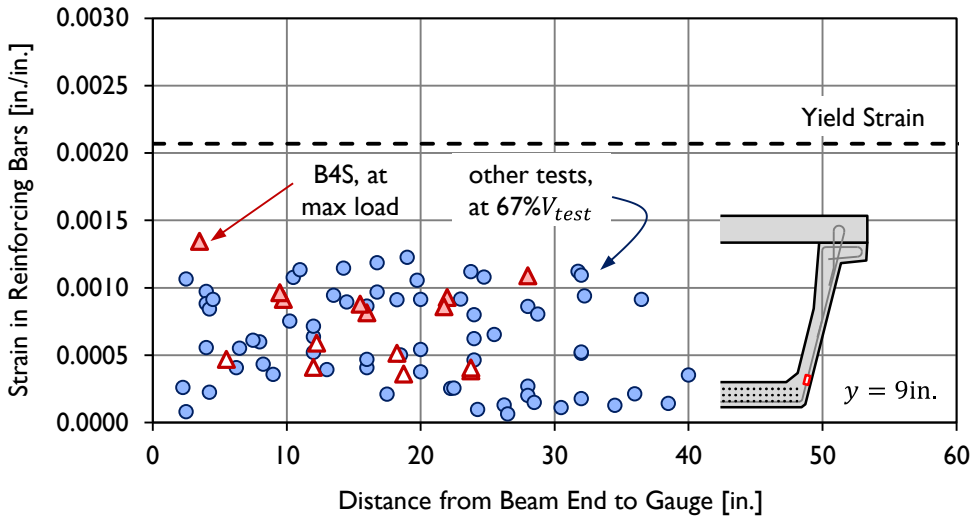

Figure 6-28: Comparison of measured strains in B4S at maximum load and the other test regions at 67% of maximum load. Gauges positioned at bottom flange-to-web interface.

Without testing B4S to failure, the maximum strains induced in the bars at failure cannot be definitively ascertained. As all other gauged beams failed in horizontal shear, it also cannot be determined from these data whether a beam that did not fail in horizontal shear would also show yielding of bars in the end region. However, given the multitude of data points showing tension in the reinforcing bars at the bottom flange-to-web interface near failure, the theory of shear-friction can be used with confidence to estimate the horizontal shear capacity of the section.

6.8 VERTICAL SHEAR PERFORMANCE

Having confirmed the assumption of load distribution in the two webs (Section 6.4), compared applied shears to expected cracking shears (Section 6.5), and established the demand on the longitudinal and transverse reinforcement (Sections 6.6 and 6.7), the vertical shear capacities measured are discussed here. While the previous discussions provide interesting insight into the behavior of U-Beams under load, it is ultimately necessary that the capacity of these beams be conservatively estimated using existing design equations that have been proven to work through hundreds of previous tests, as shown by Nakamura (2011). Basic comparisons of failure shear to capacity calculated using the AASHTO General Procedure (2010) were provided in Chapters 4 and 5. In this

section, the horizontal shear failure mode seen in the Phase I beams will be discussed further, the maximum shear carried by the Phase II beams that failed in web-shear will be compared with the other calculation methods and to tests from the literature, and final recommendations will be provided regarding improving the standard design of the Texas U-Beam.

6.8.1 Phase I Beam Performance

Two capacity calculations were made for each Phase I beam, first using a 6-in. stirrup spacing and then using a 4-in. stirrup spacing. Prior to testing, it was expected that the failure of the test region would occur within the weaker section of the beam, nearer to the load point, where stirrups were spaced at 6 in.

For the Phase I beam sections, failure was not observed at that location. Instead of failing at the expected weak point of the beam, where the stirrup spacing was wider, the failure occurred near the support. The major cracks observed were horizontal, along the bottom flange-to-web interface. When using a single calculation for strength to evaluate performance, the applied shear was compared with the calculated shear capacity of the beam region where the failure occurred (s = 4 in).

The calculated capacity for each test specimen with stirrups spaced at 4 and 6 in. are plotted in Figure 6-29 (with the capacity calculated using the AASHTO General Procedure (2010)). The applied shear at failure, reinforcing bar positions, and significant failure cracks are also shown. The applied shear varies from bearing point to load point due to the distribution of dead load along the beam length. The test shear value (V_{test}) provided equals the applied shear plus the dead load shear at the middle of the shear span, as described in Chapter 3.

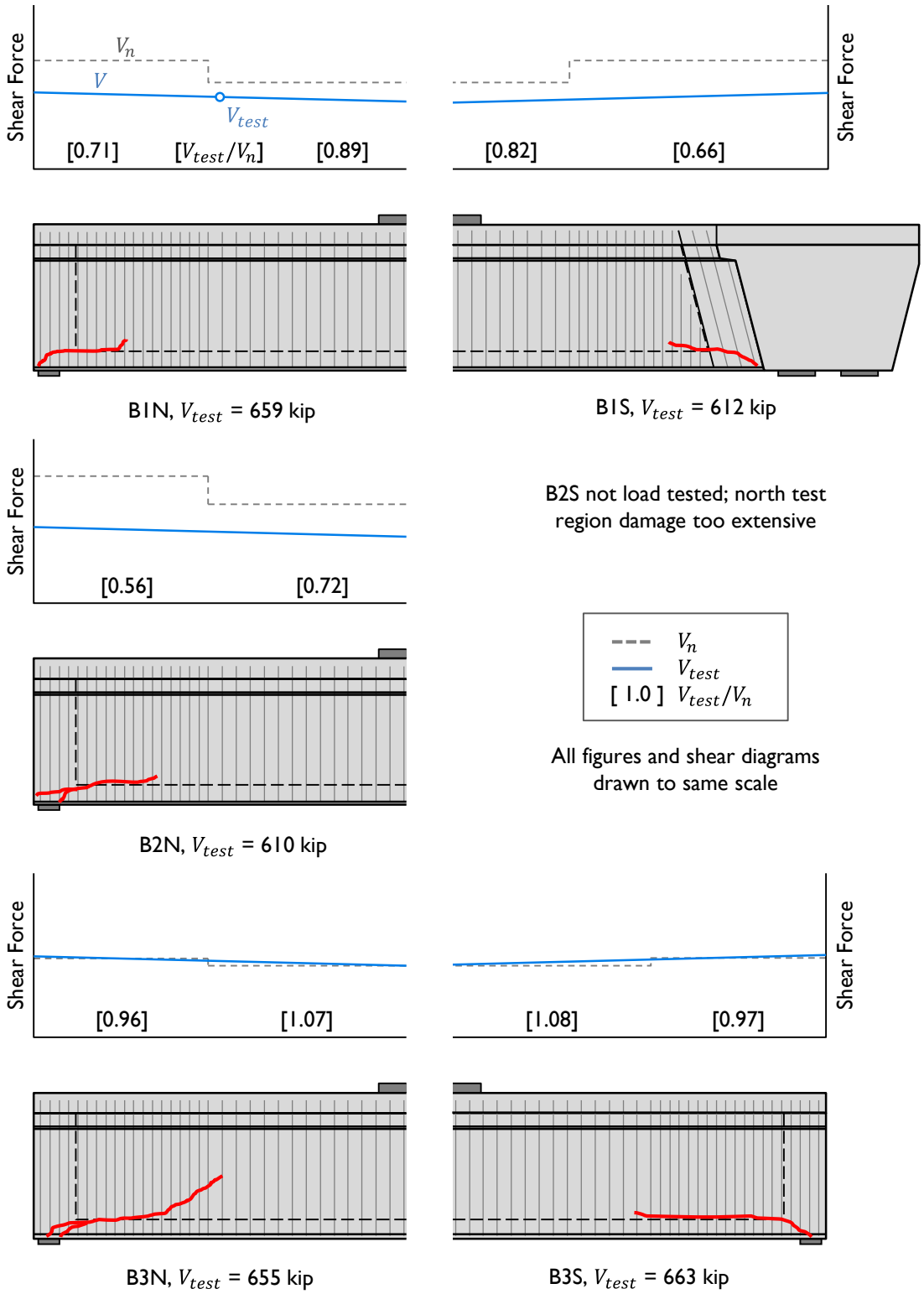

Figure 6-29: Summary of Phase I U-Beam shear tests.

Although distress was seen in the web regions where failure was expected, critical damage occurred along the bottom flange-to-web interface near the end of the beam, as shown in Figure 6-29. This damage was most evident in test region B3S, which is pictured in Figure 6-30. At failure, a large amount of concrete spalled, revealing the reinforcing bars crossing the web-to-flange interface. Each of the bars in the end region was kinked at the interface, indicating significant relative movement between the web and bottom flange.

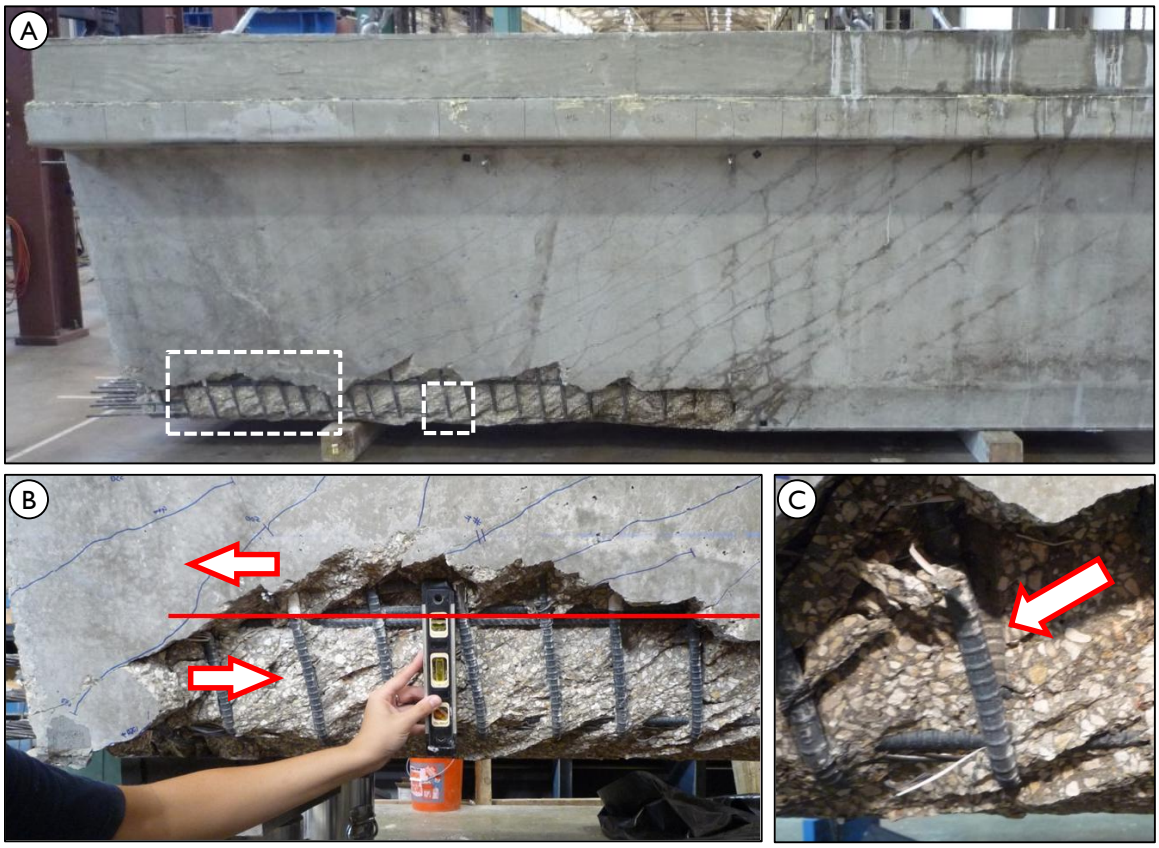

Figure 6-30: (A) Test region B3S after failure, with locations of pictures (B) and (C) shown. (B) Closer view of failure in B3S, showing kinking of reinforcing bars at bottom flange-to-web interface. (C) Original location of bar before failure.

This failure, referred to as a horizontal shear failure, occurred when the strength of the bottom flange-to-web interface was exceeded by the horizontal loads induced on the interface from the vertically-applied load. The mechanics of horizontal shear are

explained in Chapter 7, along with a discussion of the horizontal shear capacity of the Texas U-Beams tested in this study.

Given the location and type of failure seen in the Phase I test regions, it is not appropriate to assess the performance of the U-Beams against the expected shear capacity calculated using the web-shear calculation methods presented in Chapter 2. These estimations of strength were developed considering the load-carrying capacity of the web concrete and reinforcement. Since the failure does not occur in the web of the beam, the equations for shear capacity are not applicable for this failure mode.

The Phase I beams were originally designed to evaluate the influence of bearing condition, external skew, internal void geometry, reinforcing type, and amount of debonding on shear capacity. Given that the five Phase I U-Beam test regions did not fail in web-shear, the effect of these variables on the web-shear capacity cannot be evaluated using the data from these tests.

6.8.2 Phase II Beam Performance

The calculated capacities and applied shear forces for the five Phase II tests are shown in Figure 6-31. As with the Phase I beams, the capacities were calculated in multiple sections along the beam, each with a constant reinforcing bar spacing. The ratio of failure shear to the capacity (calculated using the AASHTO General Procedure) of each region is also provided. The failure modes of the five test regions are summarized here, with a description of the test region:

- B4N (wide web walls, no supplementary reinforcing): combination of web crushing and bottom flange-to-web interface failure.
- B4S (wide web walls, three #5 reinforcing bars paired with each stirrup): was not loaded to failure. Internal instrumentation and measured crack widths indicated loading was halted near 80% of V_u. No distress was seen at the bottom flange-to-web interface.
- B5N (#5 reinforcing bars used for stirrups, #6 supplementary reinforcing bar paired with each stirrup): flexure-shear failure in the web of the beam where reinforcing bars were spaced at 6 in.

- B6S (standard stirrups, two #4 reinforcing bars used as supplementary reinforcing with each stirrup, 30 in. end block): flexure-shear failure in the web of the beam where reinforcing bars were spaced at 6 in.
- B7N (reinforcing the same as B6S, 36 in. end block; beam skewed to 45°): web crushing in the six inch reinforcing bar spacing region; crushing and spalling of concrete in the four inch spacing region.

Significant cross-sectional damage was observed in the beam tests that failed in web-shear; pictures of these failures were provided in Chapter 5.

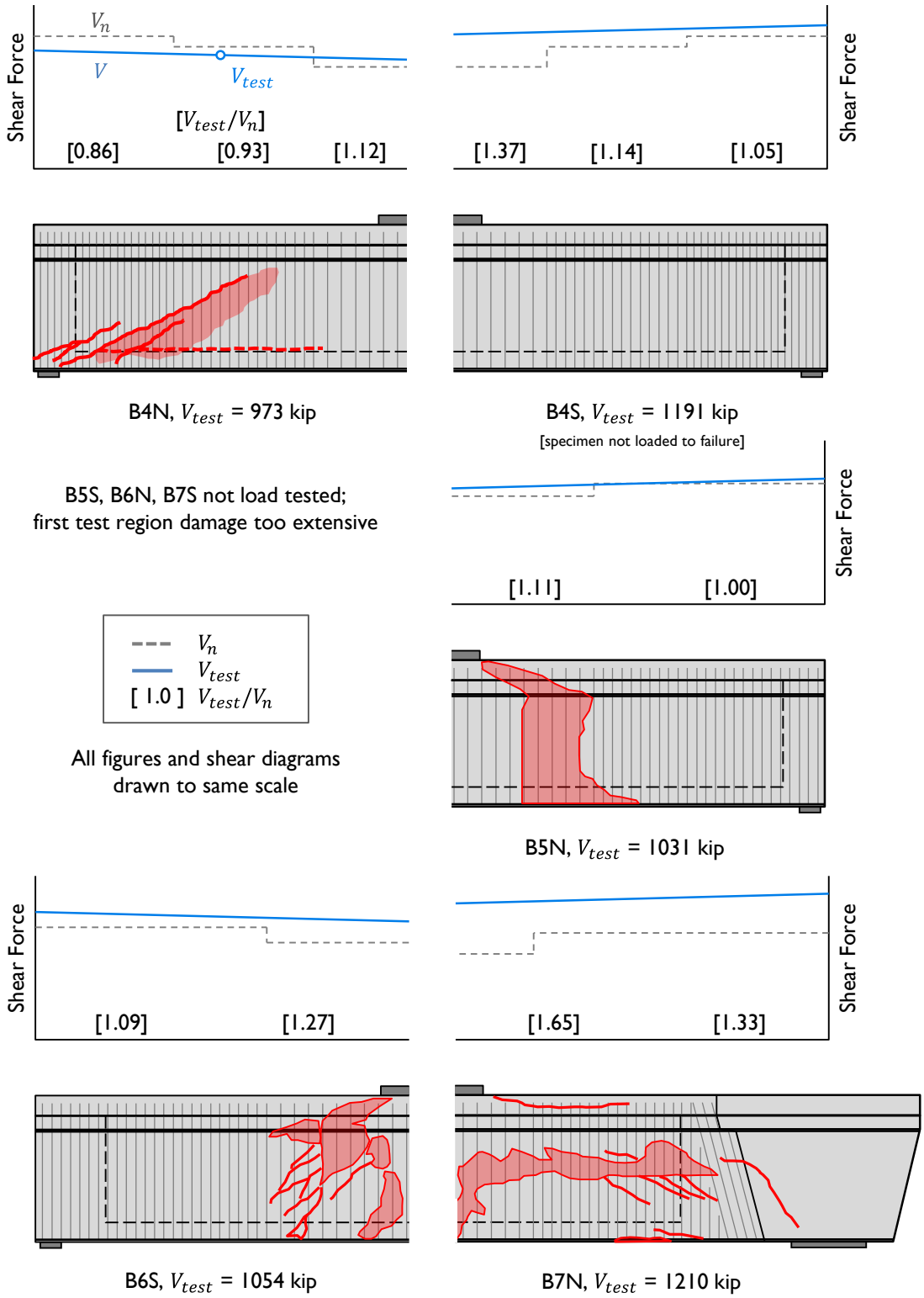

Figure 6-31: Summary of Phase II U-Beam shear tests.

The recommended new design (used in test regions B6S and B7N) allowed the beam to carry shear beyond the calculated capacity. The failures observed occurred in the theoretically weakest part of the beam, where reinforcing bars were spaced the widest. No distress was seen at the bottom flange-to-web interface during or after testing.

A total of three methods for calculating vertical shear capacity were presented in Chapter 2. The failure shears for each Phase II test specimen that failed in web-shear (all but B4N) are compared to the calculated capacity using each of these methods in Table 6-7. With so few test specimens failing in web-shear (three: B5N, B6S, and B7N), few comments can be made regarding the three shear methods used to estimate the strength. The failure shears computed for Beams 5, 6, and 7, using all three methods for calculation, were conservative. The AASHTO General Procedure was the most accurate while the AASHTO Segmental Procedure was overly conservative. The coefficient of variation for the three methods was essentially the same.

Table 6-7: Summary of calculated shear capacities for Phase II beams.

Test ID	Failure Shear [kip]	Bar Spacing [in.]	ACI Detailed Method		AASHTO General Procedure		AASHTO Segmental Procedure	
			Calc.	Ratio	Calc.	Ratio	Calc.	Ratio
B4N 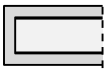	973	3.0			1134	0.86		
B4S 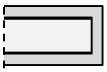	1191+	3.0 6.0	1051 804	1.13+ 1.48+	1134 871	1.05+ 1.37+	896 649	1.33+ 1.84+
B5N	1031	6.0	724	1.42	925	1.11	639	1.61
B6S 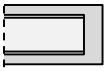	1054	6.0	631	1.67	832	1.27	551	1.91
B7N 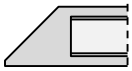	1210	6.0	572	2.12	735	1.65	489	2.47
Average[1]				1.74		1.34		2.00
COV[1]				0.20		0.20		0.22

[1] B4N (horizontal shear failure) and B4S (no failure reached) excluded

+ B4S was not loaded to failure, so the failure shear and ratios of failure shear to calculated capacities exceed the values presented here.

6.8.3 Comparison to UTPCSDB

The University of Texas Prestressed Concrete Shear Database (UTPCSDB-2011) was presented in Chapter 2. Nakamura (2011) used a subset of the database – the Evaluation Database-Level II – to evaluate the accuracy and conservatism of various calculation methods, including the three presented here. One requirement for inclusion to this subset was a typical web-shear failure. Test regions B5N, B6S, and B7N can be added to this evaluation set. The ratio of failure shear to calculated capacity (calculated using the ACI Detailed Method (2008), AASHTO General Procedure (2010), and AASHTO Segmental Procedure (2010)) for all the points in Nakamura's Evaluation Database-Level II, along with the three U-Beam tests, are shown in Figures 6-32, 6-33, and 6-34. The other eight U-Beam tests – six of which resulted in horizontal shear failures (B1N, B1S, B2N, B3N, B3S, and B4N), one of which was not taken to failure (B4S), and one of which did not meet the ACI requirement for minimum shear reinforcement (B0S) – are not plotted. Once the bottom flange-to-web interface was strengthened through the addition of reinforcing bars across the interface, as in specimens B5N, B6S, and B7N, the behavior of the beams was as anticipated and as desired.

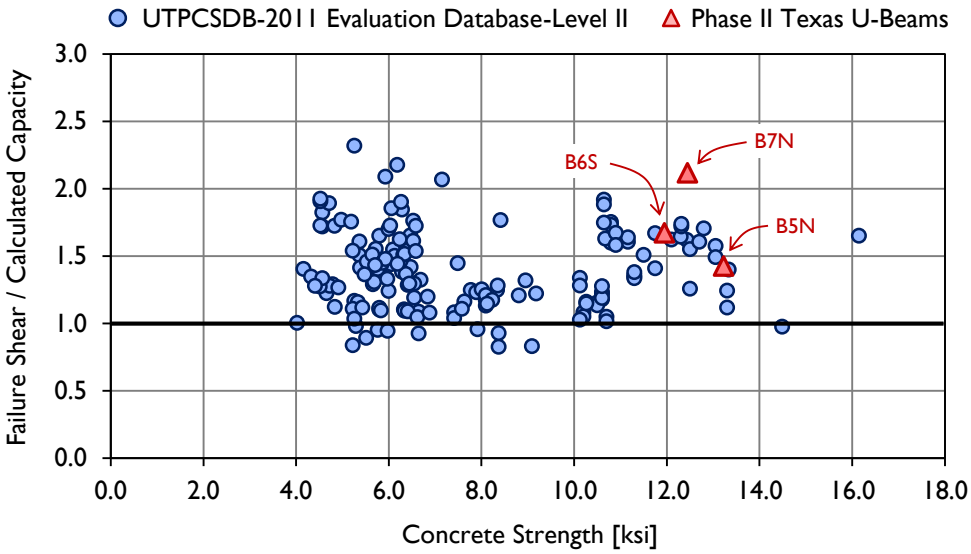

Figure 6-32: Texas U-Beam failure shear-to-calculated shear ratios (capacity calculated using ACI Detailed Method (2008)), compared to other UTPCSDB-2011 data points.

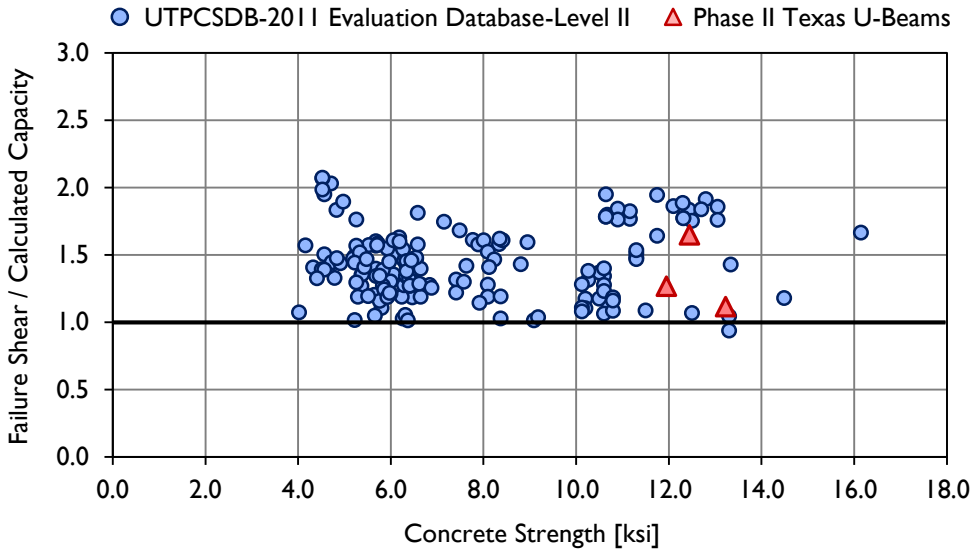

Figure 6-33: Texas U-Beam failure shear-to-calculated shear ratios (capacity calculated using AASHTO General Procedure (2010)), compared to other UTPCSDB-2011 data points.

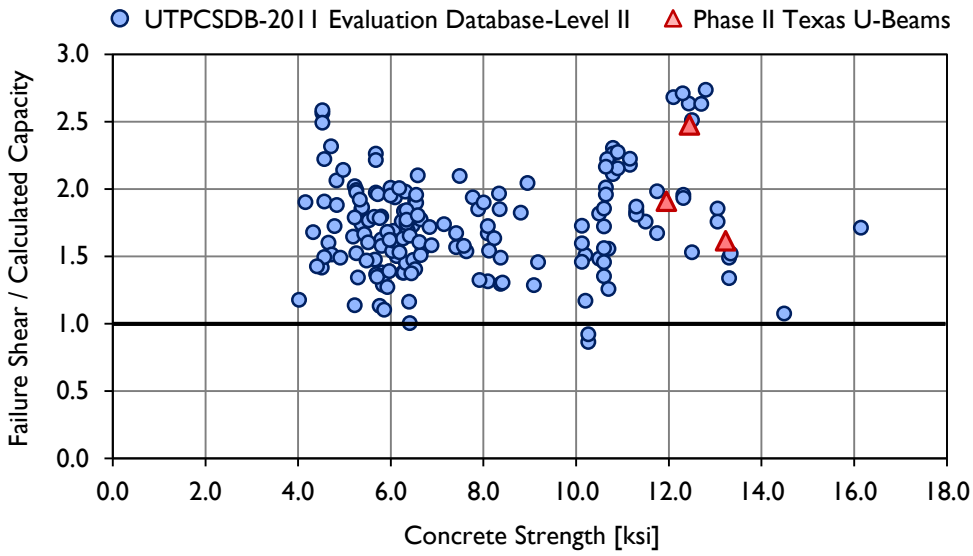

Figure 6-34: Texas U-Beam failure shear-to-calculated shear ratios (capacity calculated using the AASHTO Segmental Procedure (2010) with no limit on *K*), compared to other UTPCSDB-2011 data points.

6.8.4 U-Beam Design Recommendations

Modifications to the TxDOT U-Beam standard bridge drawings were proposed after the testing of the various details used in the end regions B4N, B4S, and B5N. The acceptability of the design modifications was confirmed through the fabrication and

testing of Beams 6 and 7. Given the favorable failure mode of the two end regions tested, and the conservatism seen with regard to capacity, the design used in Beams 6 and 7 is recommended for use in the bridge standard.

The complete reinforcing bar layouts used in Beams 6 and 7 are provided in Appendix A. The major features of the design are summarized here, with the reinforcing bar changes highlighted in Figures 6-35 and 6-36.

- Stirrups

  Maintain current use of #4 R-bars for web reinforcement. Use 4 in. bar spacing for an additional two feet from beam end (to 8'-3").

- Supplementary Steel

  Add two #5 L-bars in each web at each R-bar location through the reinforcing bar spacing change at 8'-3". Bundle one bar with R-bar on exterior web wall, with bottom leg passing between Rows 1 and 2 of the prestressing strands. Position the second bar on the interior web wall, with the hook inside the first column of strands and the bottom leg passing between Rows 2 and 3 of the prestressing strands.

- Confinement

  Add #4 confining reinforcement (C-bars), paired with R-bars, through reinforcing bar spacing change at 8'-3".

- End Blocks

  Increase the range of lengths for a standard end block from [1'-6" to 2'-0"] to [2'-6" to 3'-0"]. In beams with an exterior skew greater than 30°, another six inches should be added to the end block length, as in the current standard. Increase the length of the longitudinally-oriented legs of Bars D from 1'-0" to 2'-0" and of Bars DS from 3'-6" to 5'-6". Add bars DE and a second plane of bars F..

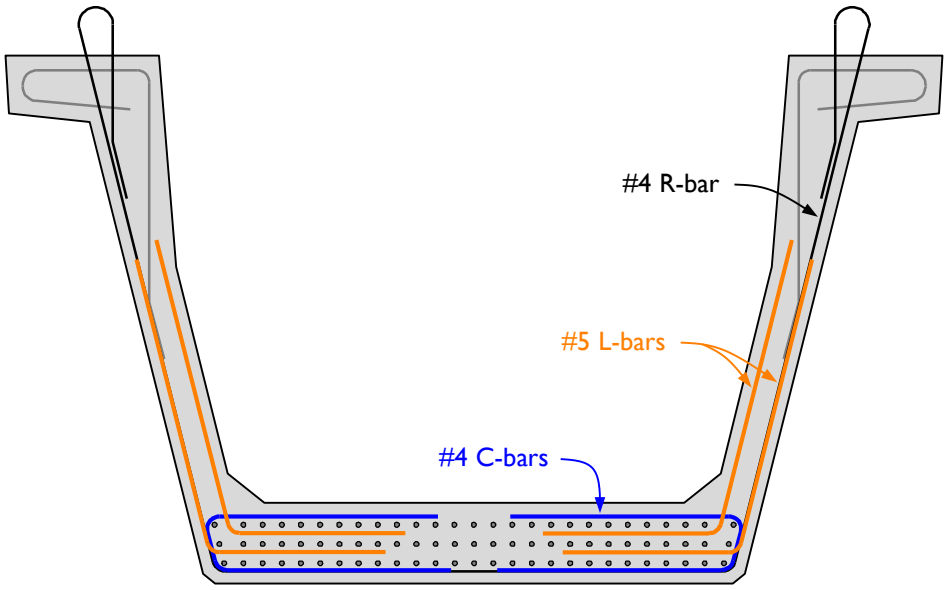

Figure 6-35: Key reinforcing bars in the recommended new Texas U-Beam design.

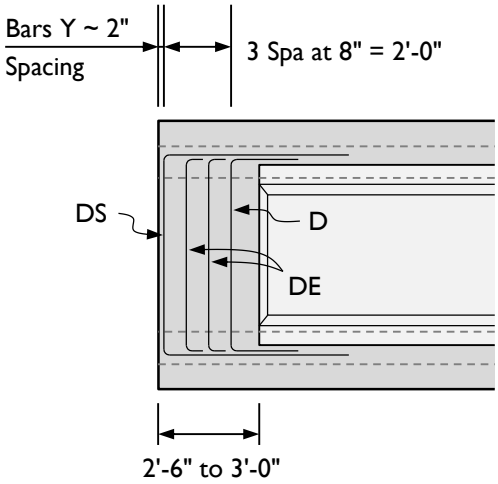

Figure 6-36: Reinforcing bar changes in the end block.

A section of the old and new design, cut horizontally along the bottom flange-to-web interface, is given in Figure 6-37. Two key changes to the standard that aided in preventing horizontal shear failure – increased end block length and addition of L-bars – are shown.

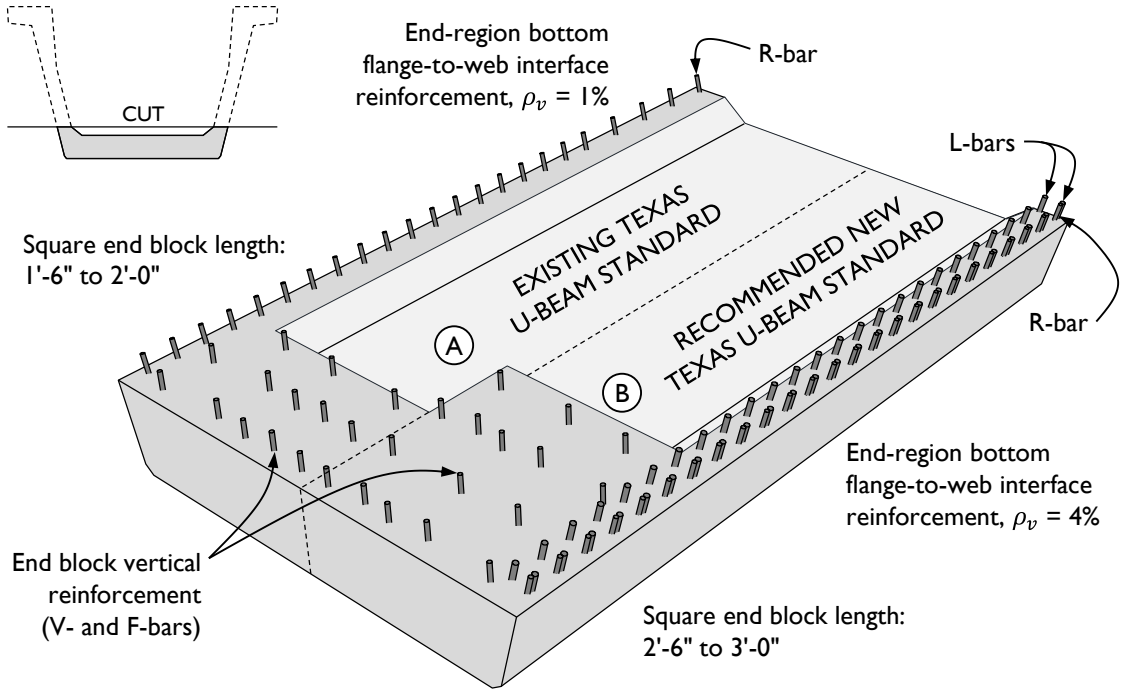

Figure 6-37: Sectional view of (A) the existing U-Beam standard and (B) the recommended new U-Beam standard, highlighting added reinforcement and increased end block length.

Given the failures seen in test regions B6S and B7N, it is expected that implementation of this design will lessen the likelihood that horizontal shear failures will occur.

6.9 SUMMARY OF RESULTS

Eight prestressed Texas U-Beams were built during the course of this research, resulting in eight test regions studied at prestress transfer, nine test regions temperature-monitored during curing, and eleven test regions load-tested to failure. The data from these three studies were presented in this chapter and are summarized here.

Given the generally low stresses induced in the transverse reinforcing bars at prestress transfer, it is not necessary to modify the end-region design of the Texas U-Beam to reduce reinforcing bar stresses or cracking. Observed cracks were typically short and narrow, with the worst cases occurring in the beams skewed to 45°, an extreme case rarely used in Texas. One monitored beam contained debonded strands, resulting in

a smaller prestressing force at the beam end. The measured internal stresses were very low, and no cracking was observed.

Without using cooling systems during curing, heats of hydration in excess of the TxDOT limits were observed in the large end blocks of the U-Beams fabricated. Curing temperatures were lower in beams with narrower end blocks and cooler ambient temperatures during curing. High thermal differentials were also recorded across the cross section, but no thermal cracking was observed. With the increased end block length recommended in the new beam design, monitoring and limiting temperatures should remain a key concern.

Upon load-testing the beams, a critical weakness was found at the bottom flange-to-web interface. Beam test specimens fabricated following the existing U-Beam standard design failed in horizontal shear in the end region of the beam, at shears well below the calculated capacity for the section. Beams were fabricated using alternate reinforcement, then load-tested to confirm that the calculated strength could be met. The final recommended design was tested in a rectangular beam and a highly skewed beam, with both failing well above the calculated capacity, with one failing in flexure-shear and the other by web crushing.

CHAPTER 7
Horizontal Shear Strength Evaluation

7.1 INTRODUCTION

Horizontal shear failure is defined here as the breakdown of the bottom flange-to-web interface of a prestressed beam under the application of vertical loads. Distinctive characteristics of this failure mode include measureable displacement of the web relative to the bottom flange and damage concentrated at the bottom flange-to-web interface rather than at mid-height of the beam web. Reinforcing bars exposed after failure are typically bent sharply at the bottom flange-to-web interface. This failure mode was studied after it was observed to occur in Texas U-Beams at shears up to 44% below the calculated shear capacity of the section.

In order to evaluate the likelihood of a horizontal shear failure in a prestressed concrete beam, it is necessary to compute the demand on and the strength of the bottom flange-to-web interface. The primary objective of this chapter is to present a verified method for these calculations. The chapter concludes with a focused analysis of horizontal shear in Texas U-Beams.

In this discussion, shear along the bottom flange-to-web interface of prestressed beams is referred to as “horizontal shear”. For clarity, the term “vertical shear” is used to refer to typical web-shear loads.

7.1.1 Motivation

Flexural optimization of highway bridge girders has led many states to begin using I-Beams with narrow webs and large bottom flanges (sometimes referred to as Bulb-T beams). In several research studies on shear strength of these optimized beams (Hawkins and Kuchma, 2007; Avendaño and Bayrak, 2008; Avendaño, et al., unpublished), the observed failures were marked by sliding between the web and bottom flange of the beams, rather than typical shear failure mechanisms in the beam web.

Examples of these failures, along with the failure seen in test specimen B3N in this study, are given in Figure 7-1.

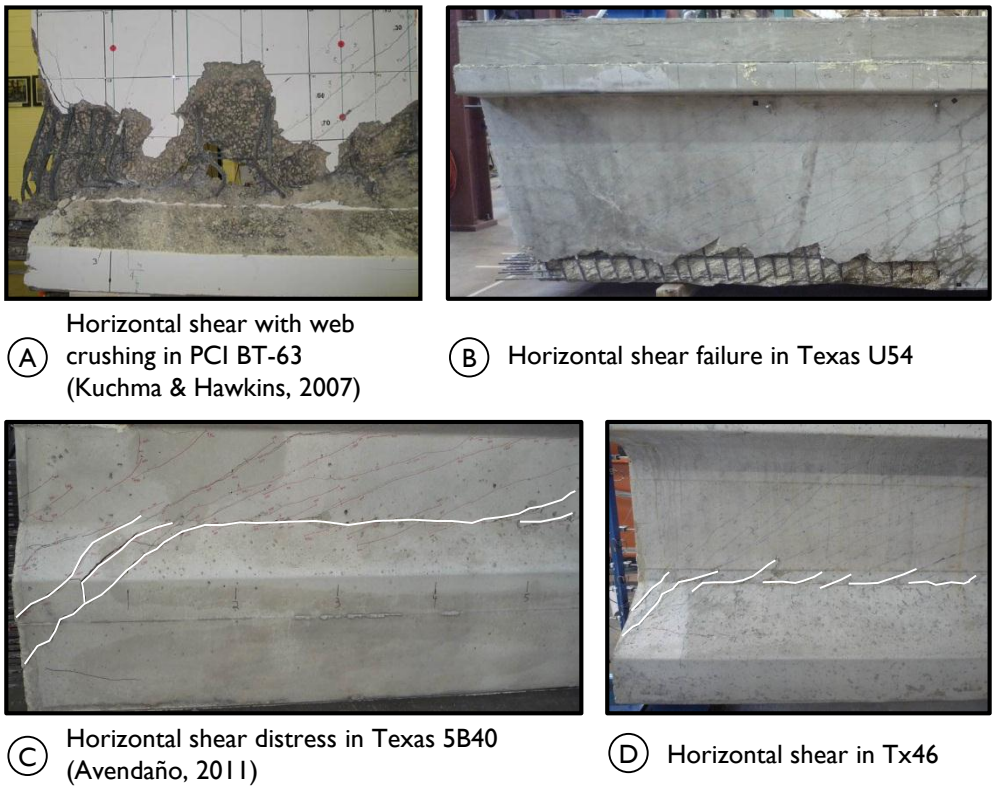

Figure 7-1: Examples of horizontal shear damage observed in laboratory tests.

Clear guidelines for calculating the strength of the bottom flange-to-web interface in prestressed concrete girders are not provided in either the ACI 318 Building Code (2008) or the AASHTO LRFD Bridge Design Specifications (2010). Given the increased use of these optimized beams and the observations of horizontal shear controlling failure of the sections, a thorough understanding of this failure mode is needed.

7.1.2 Chapter Organization

This chapter begins with a brief explanation of what is meant by a "horizontal shear failure" or "horizontal shear damage". Examples from the literature are provided. The theoretical bases for the proposed calculations for horizontal shear demand and horizontal shear capacity are reviewed in the sections following.

The proposed method for evaluating horizontal shear susceptibility that was derived is presented in Section 7.5; an example problem is given in Section 7.6. The evaluation method was verified using a subset of the University of Texas Prestressed Concrete Shear Database (UTPCSDB-2011), the results of which are described in Section 7.7. Recommendations for use in design are provided.

7.2 MECHANICS OF HORIZONTAL SHEAR

To illustrate the characteristic behavior of vertical shear and horizontal shear failures, four beam failure images are provided in Figure 7-2 and B-3. In Figure 7-2(A), a beam that has failed in shear-tension is pictured: the vertical force carried by the reinforcing bars exceeded the capacity of those bars, causing the bars to yield and then rupture. In Figure 7-2(B), a similar beam is pictured after failing in shear-compression: the compressive force in a diagonal strut has exceeded the compressive strength of the concrete, causing the concrete to crush.

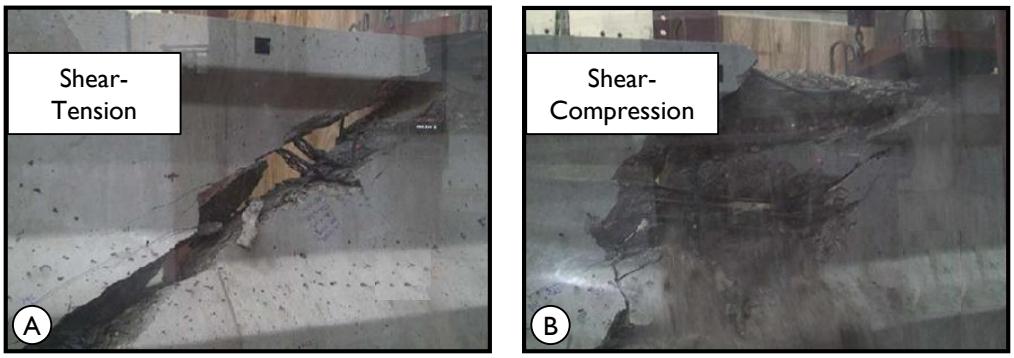

Figure 7-2: Examples of typical web-shear failures (from Heckmann and Bayrak, 2008).

Two beam end regions that failed in horizontal shear are pictured in Figure 7-3. In picture (A), very little damage is visible in the web, aside from minor diagonal cracking (the maximum diagonal crack width was 0.02 in.). The primary failure crack is located along the bottom flange-to-web interface, extending from the point where diagonal cracks first intersect the interface near the load point to the end of the beam. In picture (B), the longitudinal movement of the web with respect to the bottom flange can be seen.

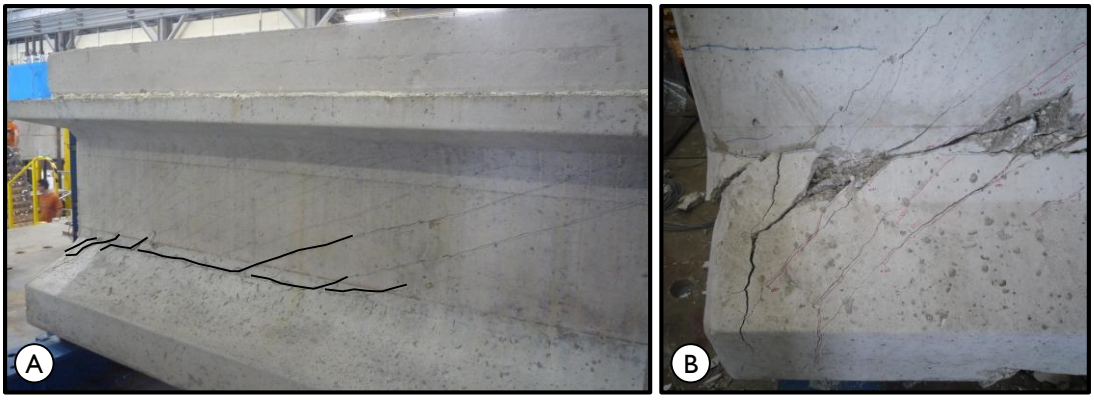

Figure 7-3: Example of horizontal shear failure.

The effect of vertical loads in the horizontal direction can be visualized in a simplistic manner by considering a series of boards stacked together, as shown in Figure 7-4. In Figure 7-4(A), the boards are not attached to each other, and as they flex under the applied load, the boards slip horizontally along the length, as seen at the beam ends. In Figure 7-4(B), the boards are bonded, and they deflect as a composite unit, with no visible slip at the ends.

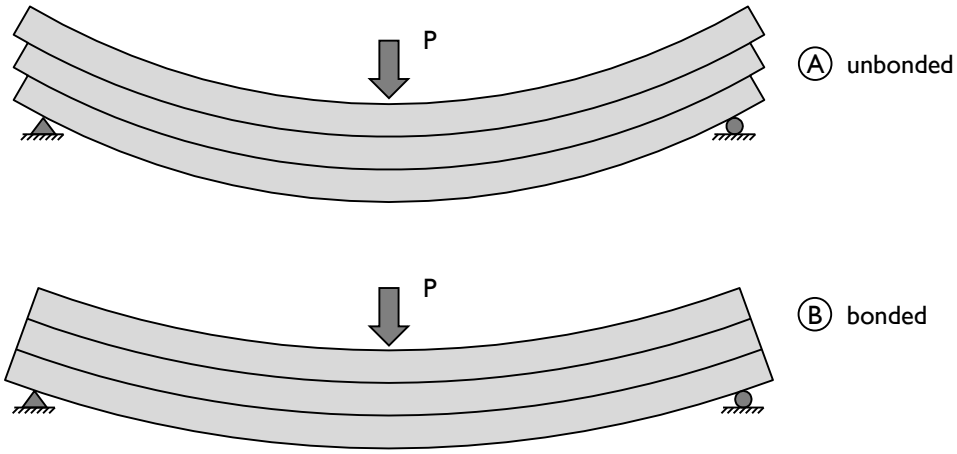

Figure 7-4: Illustration of horizontal shear, using (A) unbonded and (B) bonded wood planks.

The concept of stacked boards can be used to represent the upper and lower sections of a prestressed concrete beam, as is shown in Figure 7-5. In calculating the vertical capacity of this I-Beam, it is assumed that the cross section remains integral, with significant capacity to transfer loads from the web to the bottom flange. However, the interface between the bottom flange and the web has finite capacity that may be exceeded

under the application of external loads. When the capacity of the interface is exceeded, as shown in Figure 7-5(B), the two sections act individually and horizontal slip is observed. In this research, this failure is referred to as a horizontal shear failure, and the associated damage is called horizontal shear damage.

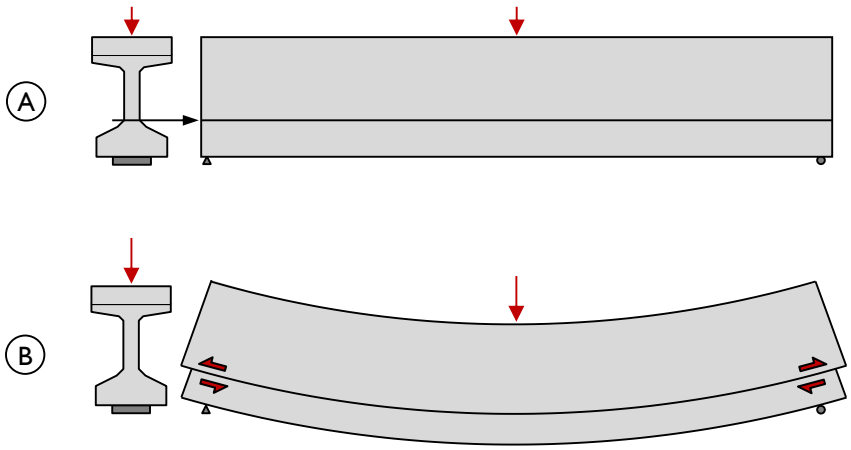

Figure 7-5: Horizontal shear schematic.

7.3 BENDING INDUCED HORIZONTAL SHEAR STRESSES

A brief primer for calculating horizontal shear stress at any point in the depth of a beam is provided in this section for the convenience of the reader. This derivation assumes simple beam theory. More detail can be found in typical mechanics of materials books; the information presented here was adapted from Hibbeler (2003). The calculations have been tailored for a simply-supported beam with a single point load, as illustrated in Figure 7-6. To begin the derivation, the shear and moment diagrams were drawn. A slice of beam with width dx is highlighted for use in further calculations.

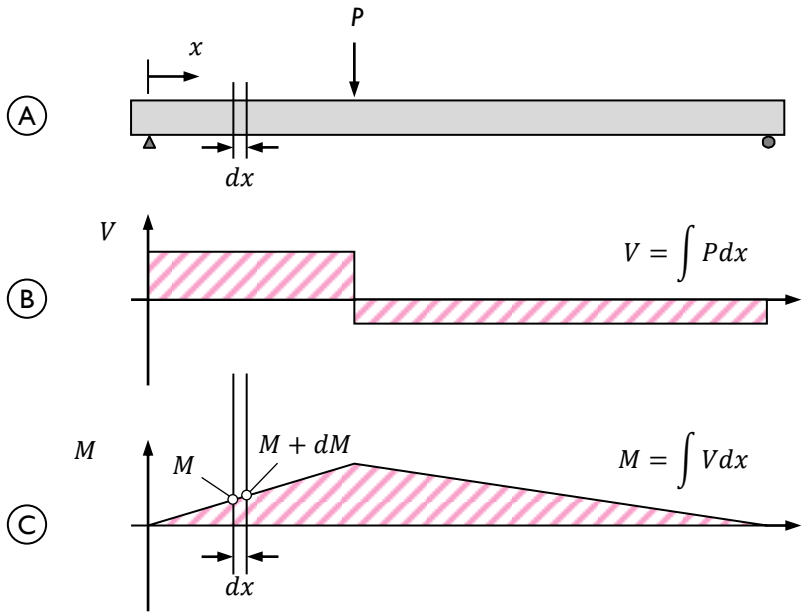

Figure 7-6: (A) Example beam, (B) shear diagram, and (C) moment diagram.

The slice dx has been isolated in Figure 7-7(A). To find the horizontal stress along the bottom flange-to-web interface, the beam is sliced again parallel to the neutral axis, at the height of interest (Figure 7-7(B)). The distribution of stresses on either side of the slice caused by the applied load are as shown in Figure 7-7(C). The slight difference in moment between one side of the slice and the other causes an imbalance in stress that is compensated for by the horizontal stress along the top surface of the slice. For a beam loaded under constant shear, the change in stress across a width dx is constant, as the slope of the moment diagram is constant. The representative slice shown in Figure 7-7(A) could be located at any point between the support and the load and the calculated shear stress τ would be the same.

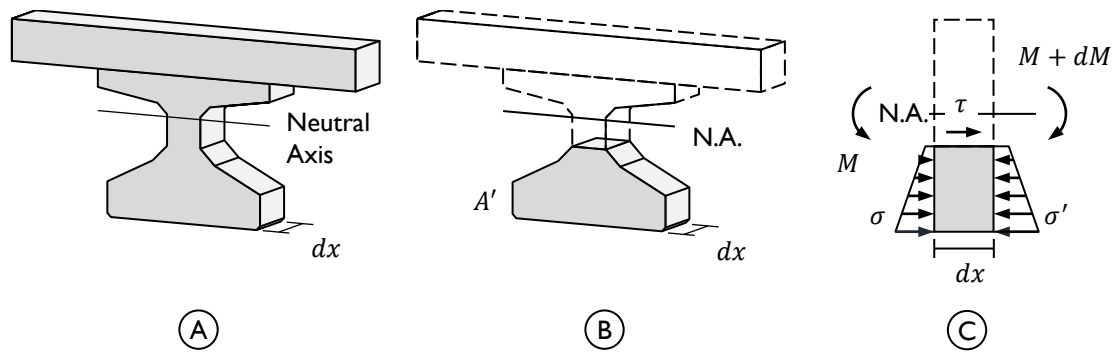

Figure 7-7: (A) Representative slice of beam, (B) considering only the area beneath the plane of interest (shaded), (C) stress resulting from the applied load.

The magnitude of the shear stress τ is computed using equilibrium of the section shown in Figure 7-7(C). As the sum of forces in the longitudinal direction (horizontal, with respect to the page) must equal zero, the following can be stated:

$$\int_{A'} \sigma' \, dA - \int_{A'} \sigma \, dA - \tau(t \, dx) = 0 \qquad \textbf{Equation 7-1(a)}$$

where

σ = longitudinal stress at a distance y from the neutral axis [ksi]

t = width of the cross section at the location of the cut (b_w in this example) [in.]

A' = area of the section below the cut [in.]

Given that the normal stress at any point in the height of the beam is defined as

$$\sigma = \frac{My}{I} \qquad \textbf{Equation 7-2}$$

where

M = applied moment [kip-in]

y = distance to the point of interest from the neutral axis [in.]

I = moment of inertia of the full cross section [in.^{4}]

Equation 7-1(a) can be expanded to

$$\int_{A'} \left(\frac{M + dM}{I}\right) y \, dA - \int_{A'} \left(\frac{M}{I}\right) y \, dA - \tau(t \, dx) = 0 \qquad \textbf{Equation 7-1(b)}$$

or

$$\left(\frac{dM}{I}\right)\int_{A'} y\,dA = \tau(t\,dx)$$ **Equation 7-1(c)**

Solving for τ, knowing that $V = dM/dx$, results in

$$\tau = \frac{V}{It}\int_{A'} y\,dA$$ **Equation 7-3(a)**

The integral in Equation 7-3(a) is the definition for the first moment of the area A' about the neutral axis, often referred to by the letter Q. This definition allows the equation for shear stress to simplify to

$$\tau = \frac{VQ}{It}$$ **Equation 7-3(b)**

The first moment of the area about the neutral axis of a rectangular cross section (i.e., a beam with constant width t) is

$$Q(y) = t\int_0^h y dy = \left[\frac{ty^2}{2}\right]_0^h$$ **Equation 7-4**

and the shear stress can be written as

$$\tau(y) = \frac{Vy^2}{2I}$$ **Equation 7-3(c)**

The variation in Q results in a parabolic distribution of shear stress through the depth of the section, as shown in Figure 7-8(A). By comparison, an I-Beam has a variable width through the depth, meaning the thickness term cannot be factored from the equation for Q. Of particular importance is the discontinuity that occurs at the interface between the bottom flange and the web of the beam. The shear stress is small at the top surface of the bottom flange (due to the large value for t), and large at the bottom of the web (where t is small), as shown in Figure 7-8(B).

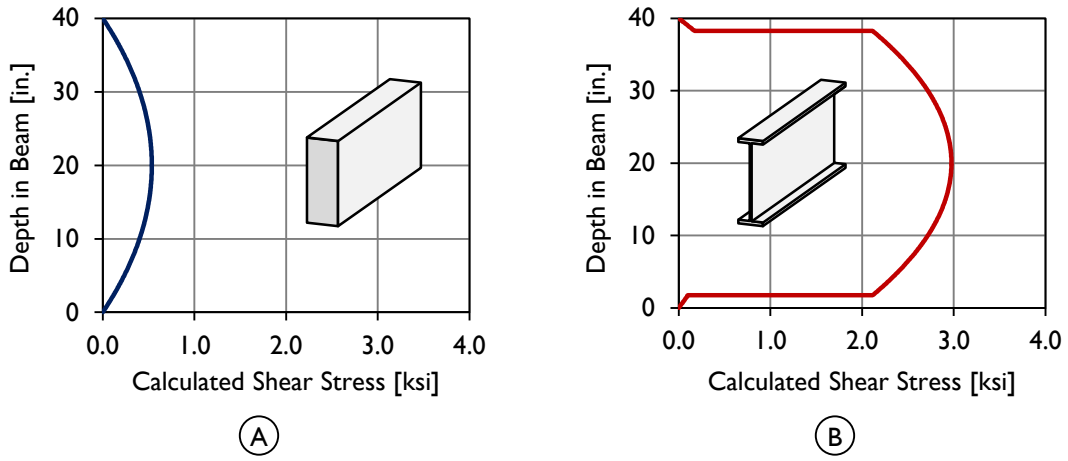

Figure 7-8: Example calculations for shear stress using (A) rectangular and (B) I-shaped beams.

Using Equation 7-3(b), the horizontal stress at any point through the depth due to a vertical load can be calculated. It is now necessary to evaluate the ability of a beam to resist these loads.

7.4 THEORY OF SHEAR FRICTION

The first theory of shear friction was presented in 1966 by Birkeland and Birkeland. The paper was written to aid in detailing the interface between reinforced concrete elements, such as corbels attached to columns. The authors proposed the hypothesis that as two sections of concrete begin to slide relative to one another, imperfections in the surface will cause them to separate, as shown in Figure 7-9. Reinforcing bars crossing the plane of the separation become stressed by the displacement, and the induced stresses create a clamping force on the section: a normal force for friction calculations. The maximum clamping force is related to the area and yield strength of the reinforcing bars, and the friction force is related to the roughness of the sliding plane.

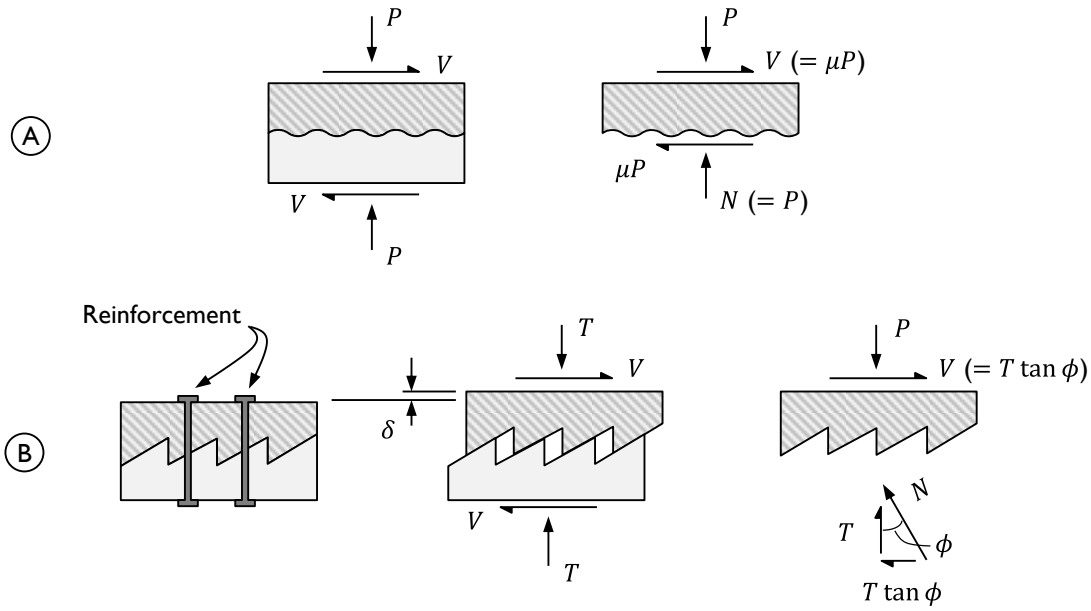

Figure 7-9: Shear friction hypothesis (from Birkeland and Birkeland, 1966).

Based on their theory, Birkeland and Birkeland proposed the following equations for evaluating the interface between two sections of concrete:

$$V_u = A_s f_y \tan\phi \qquad \textbf{Equation 7-5}$$

$$v_u = \rho f_y \tan\phi \leq 0.8\text{ksi} \qquad \textbf{Equation 7-6}$$

where

V_u	=	total ultimate shear force [kip]
A_s	=	total cross-sectional area of reinforcing across interface [in.^{2}]
f_y	=	yield strength of reinforcing (≤ 60 ksi) [ksi]
$tan\,\phi$	=	1.7 for monolithic concrete
v_u	=	ultimate shear stress on gross area (≤ 0.8 ksi) [ksi]
ρ	=	steel ratio, A_s/A_g
A_g	=	gross area of interface [in.^{2}]

The limit on allowable shear stress was included to estimate at what load the imperfections along the interface would crush.

The equation for the shear strength of an interface in the ACI 318-08 Building Code (referred to as ACI (2008)) is almost identical to the Birkeland and Birkeland equation. ACI (2008) Equation 11-25 states that interface strength is

$$V_n = A_{vf} f_y \mu \qquad \textbf{Equation 7-7}$$

with

V_n = nominal shear strength [lb]

A_{vf} = area of reinforcement crossing the interface [in.^{2}]

μ = coefficient of friction, defined as 1.4 for normal-weight concrete placed monolithically [psi]

Additional capacity can be gained through applying a permanent net compressive force across the interface, the magnitude of which is added to $A_{vf} f_y$. The maximum allowable shear stress associated with this equation is more complex than the hard 800 psi limit set by Birkeland and Birkeland and is not discussed here, but has a similar effect on calculations for capacity.

When designing the interface of brackets, corbels, or ledges (structures with vertically-aligned shear planes), the shear-friction equation in the 2010 AASHTO LRFD Bridge Design Specifications (referred to as AASHTO (2010)) is the same as in ACI (2008). AASHTO (2010) Equation 5.8.4.1-3 states:

$$V_{ni} = \mu\left(A_{vf} f_y + P_c\right) \qquad \textbf{Equation 7-8(a)}$$

where

V_{ni} = nominal shear resistance of the interface plane [kip]

μ = friction factor [dim.], equal to 1.4 for monolithically-placed concrete

A_{vf} = area of interface shear reinforcement crossing the shear plane [in.^{2}]

f_y = specified yield strength of reinforcement [ksi], limited to 60 ksi

P_c = permanent net compressive force normal to the shear plane [kip]

The maximum allowable shear stress is the lesser of 1.5 ksi and $0.25f_c'$ for monolithically-placed concrete.

The AASHTO (2010) shear-friction equation for horizontal interfaces (such as the interface between the top flange of a highway girder and a cast-in-place concrete deck) has a second term, meant to account for cohesion between the two concrete surfaces. Including this term, Equation 7-8(a) becomes:

$$V_{ni} = cA_{cv} + \mu\left(A_{vf}f_y + P_c\right) \qquad \textbf{Equation 7-8(b)}$$

where

c = cohesion factor [ksi], equal to 0.4 ksi for monolithically-placed concrete

A_{cv} = area of concrete considered to be engaged in interface shear transfer [in.^{2}]

The contribution of this cohesion term to calculations for bottom flange-to-web interface capacity will be discussed later in this chapter.

7.5 RECOMMENDED CALCULATION PROCEDURE

The recommended method for evaluating the horizontal shear demand on and strength of the bottom flange-to-web interface of a prestressed concrete beam is presented in this section. The calculations for horizontal shear demand and horizontal shear strength are based on the theories on beam bending and shear friction, respectively, that were presented in the previous two sections.

This evaluation method was derived using observations from laboratory testing. A beam loaded some distance from the support deformed as shown in Figure 7-10(A). Prior to failure, no signs of distress could be seen along the bottom flange-to-web interface. At failure, the reinforcing bars crossing the interface were bent, and the web had moved relative to the bottom flange (Figure 7-10(B)). From the failed shape, a free-body diagram was drawn to highlight the forces in the plane of and perpendicular to the critical interface (Figure 7-10(C)). Forces acting along the diagonal crack were omitted for simplicity.

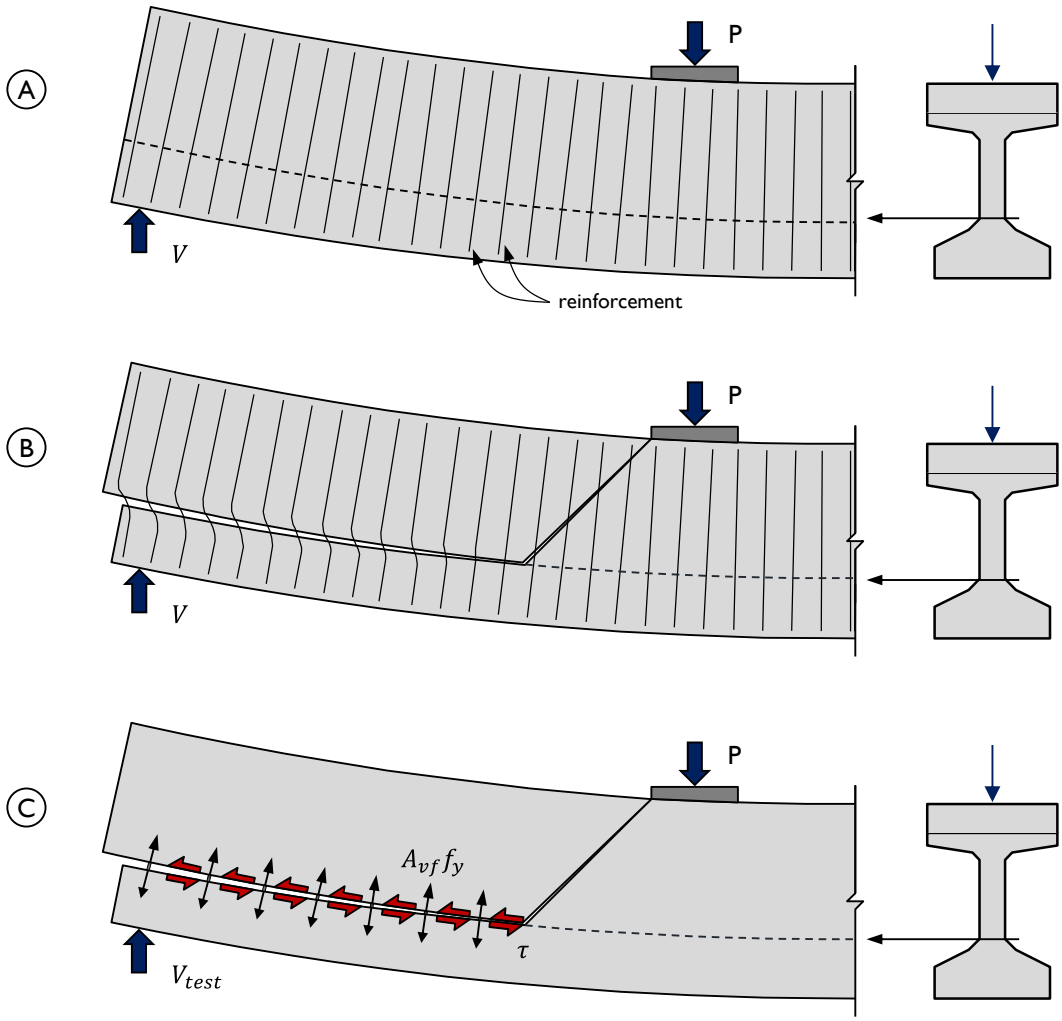

Figure 7-10: Flexural member (A) just prior to and (B) just after exceeding the horizontal shear capacity of the bottom flange-to-web interface. (C) Free-body diagram drawn from failed shape.

7.5.1 Horizontal Shear Ratio

Through the rest of this chapter, comparisons between demand and capacity will be made at discrete points using the Horizontal Shear Ratio (HSR), defined as:

$$\text{HSR} = \frac{demand}{capacity} \qquad \textbf{Equation 7-9}$$

When the HSR is equal to 1.0, the calculated demand equals the calculated capacity. A value greater than 1.0 implies that the demand is greater than the capacity and a

horizontal shear failure is probable. Conversely, a value less than 1.0 indicates that horizontal shear failure is unlikely.

7.5.2 Ultimate Evaluation Point

Study of laboratory tests that resulted in horizontal shear failure show a common pattern of distress. While diagonal cracks are seen in the webs, the primary failure crack begins at the bottom flange-to-web interface near the load. The point where a diagonal crack oriented at 45° intersects the bottom flange-to-web interface is defined as the Ultimate Evaluation Point (UEP) (Figure 7-11).

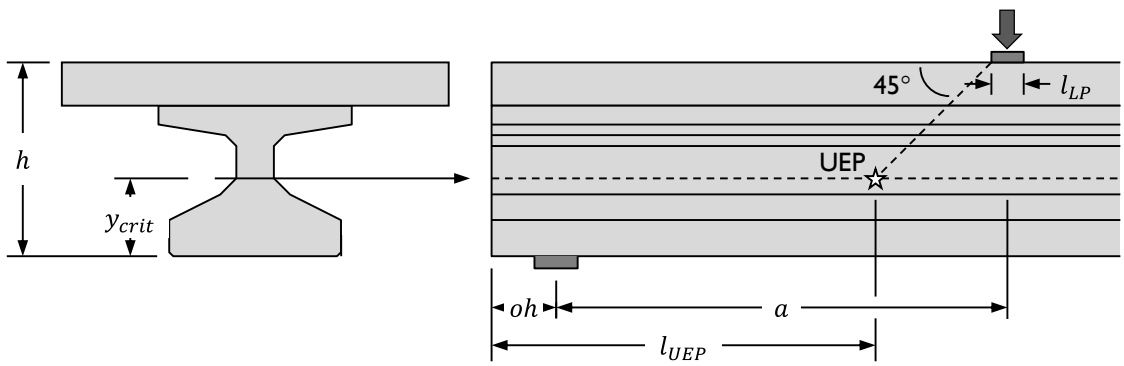

Figure 7-11: Location of the Ultimate Evaluation Point.

When presenting the results of laboratory tests in this chapter, a single metric for evaluation will be used: the Horizontal Shear Ratio calculated at the Ultimate Evaluation Point. The location of the UEP can be seen in Figure 7-11; the distance from beam end to the UEP is defined as:

$$l_{UEP} = a + oh - \frac{l_{LP}}{2} - h + y_{crit}$$ **Equation 7-10**

where

l_{UEP} = distance from beam end to the UEP [in.]

a = shear span [in.]

oh = beam overhang, from centerline of bearing pad to beam end [in.] (see Figure 7-11)

l_{LP} = length of the load plate [in.]

h = total depth of the composite section [in.]

y_{crit} = height of critical interface, measured from the bottom [in.]

7.5.3 Calculation for Demand

The recommended calculation for horizontal shear demand has two parts. To begin, the horizontal shear stress at the bottom flange-to-web interface must be found. Then, that stress is converted into a force for comparison to the capacity.

7.5.3.1 Horizontal Shear Stress Estimation

While it is possible, as shown in Section 7.3, to calculate the horizontal shear stress at any height within a beam member, it is very computationally expensive. The time and processing power required to perform that calculation, especially when non-linear aspects such as beam cracking are considered, limits the accessibility of the method for use in a simple design process. In an effort to reduce the computational effort without sacrificing an acceptable level of accuracy, three calculation methods to find horizontal shear stresses were considered and compared for a series of beam shapes.

The first, meant to be the most accurate (but also most computationally expensive) method was a non-linear sectional analysis. A non-linear sectional analysis accounts for the cracking of the concrete, the contribution of the prestressing strands, and the differing material properties between the beam and the deck. The results of this analysis are sensitive to the magnitude and location of the applied load.

There are cases where the accuracy afforded by a non-linear analysis is worth the increased computational effort. One such case could be when designing a section that will be used over and over, for which one very accurate analysis can possibly save on material and labor through all the fabricated beams, thus being worth the time required. For more routine bridge design checks, a simpler method that retains accuracy is desired. For this study, the non-linear analysis was performed to provide a “correct” answer that a simpler method would have to be able to predict in order to be deemed acceptable.

The second calculation, a linear sectional analysis, was performed as presented in Section 7.3. Material properties were assumed to be linear. The cost of the calculation was limited to the (non-trivial) derivation of Q at each point of interest through the depth.

The third calculation was the simplest, in which average vertical shear stress was used to estimate average horizontal shear stress. Unlike the sectional analyses (linear or non-linear), a single computation is used to approximate the shear stress that exists through the whole depth of the cross section. Through the depth, the average shear stress will overestimate the actual shear stress in some locations, and underestimate it in others. Average shear stress is defined as:

$$v_{avg} = \frac{V_{applied}}{b_w d} \qquad \textbf{Equation 7-11}$$

where:

v_{avg} = average shear stress through the depth of the section [ksi]

$V_{applied}$ = applied shear force on the section [kip]

d = distance from extreme compression fiber to centroid of tensile reinforcement [in.]

The calculation for average shear stress is simple and independent of many variables that otherwise complicate the process.

The results of the three sets of calculations, as performed on a Texas Tx28 I-Beam, are shown in Figure 7-12. For the layered sectional analyses, the horizontal shear stress was calculated at regular intervals 0.25 in. through the height of the beam. There is significant variation in the calculated stress through the depth. The average shear stress was calculated once, and is plotted as a constant value.

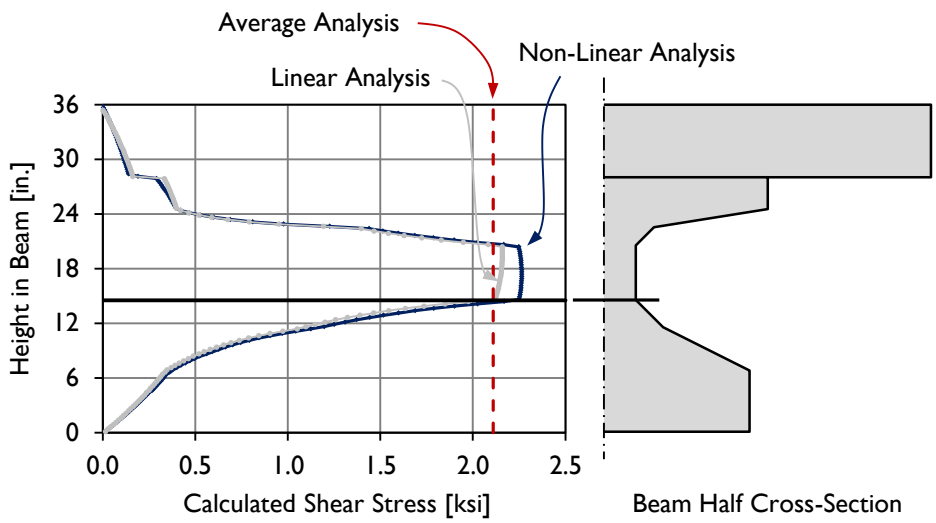

Figure 7-12: Calculated shear stress in the example Tx28, using non-linear and linear sectional analyses, and an average shear stress calculation.

Of particular importance to this study is the calculated shear stress at the joint between the bottom flange and web of the studied prestressed beams. The location of this interface in the Tx28 is marked in Figure 7-12 with a solid horizontal line (at a height of 14.5 in.). A comparison of the three calculation methods is provided in Table 7-1, with the layered sectional analyses methods being summarized by the value calculated at that critical interface.

Table 7-1: Comparison of calculation methods at critical interface in a Tx28 beam.

Calculation Method	Value [ksi]
Non-Linear Sectional	2.17
Linear Sectional	2.12
Average	2.11

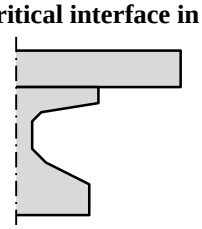

Specimen Tx28-I-D
V_{test} = 417 kip
b_w = 7 in.
d = 28.3 in.
Ref: Avendaño & Bayrak (2008)

For the Tx28 beam, the shear stress found using the linear section analysis and the averages stress calculation was within 3% of the stress found using a non-linear sectional analysis. Before concluding that the average shear stress is an acceptable estimation, these same calculations were performed for other standard beam geometries: the Texas Tx46 (I-Beam), 4B28 (Box-Beam), and U54 (U-Beam). The resulting shear stress value

comparisons are provided in Table 7-2. The average shear stress was within 10% of the shear stress found using a non-linear sectional analysis for each of these standard beams.

Table 7-2: Non-linear and average shear stress comparisons for various beam types.

Beam Type	Non-Linear / Average Shear Stress at Critical Interface
Tx28	1.03
Tx46	1.10
4B28	1.08
TxU54	0.99

Given the ease of the average shear stress calculation as compared to the sectional analysis, the average shear stress is recommended for use in horizontal shear demand calculations:

$$v_{hs} = \frac{V_{applied}}{b_w d}$$ **Equation 7-12**

where:

v_{hs} = horizontal shear stress caused by an applied load [ksi]

If a more precise understanding of the horizontal shear behavior is desired, a layered sectional analysis can be performed to find the shear stress at any location in the beam and at any point in the loading history. It should be noted that in a non-linear analysis, maximum horizontal stresses will be calculated at an applied load just below that which would cause flexural cracking; once cracking occurs, the stress on the interface drops significantly. If flexural cracking is found to occur, the load applied in the calculation should be decreased to find the maximum horizontal shear stress on the interface.

7.5.3.2 Horizontal Shear Force

To compare horizontal shear demand to capacity, the demand must be transformed from a stress to a force. This transformation is completed by multiplying the shear stress with the length over which it acts:

$$V_{u_{hs}} = v_{hs} b_w l_{crit}$$ **Equation 7-13**

where:

$V_{u_{hs}}$ = horizontal shear demand [kip]

l_{crit} = length of demand [in.]

The horizontal shear force was assumed to act between beam end and the Ultimate Evaluation Point. It should be noted that from the centerline of the bearing pad to the beam end, the applied shear is zero and thus does not add to the demand.

7.5.4 Calculation for Capacity

The recommended method for calculating horizontal shear capacity is based on the theory of shear friction. As was presented in Section 7.4, several codified equations exist for calculating the strength of interfaces. The specifics of the recommended calculation method were chosen after verification of the accuracy of the various methods using data from the literature (as will be presented in Section 7.7).

The recommended calculation contains four significant terms, as follows:

- <u>Steel clamping, $\mu A_{vf} f_y$</u>

  This calculation, equivalent to a simple friction calculation (μN), was originally suggested by Birkeland and Birkeland in 1966 to account for the total capacity of a shear interface. It is the primary term in the shear friction equation present in ACI (2008), and is also present in the shear friction equation given in AASHTO (2010).

- <u>Concrete cohesion, cA_{cv}</u>

  This term is included in the AASHTO (2010) equation for the capacity of horizontal interfaces (5.8.4.1-3 in AASHTO, or Equation 7-8(b) in this dissertation), but is not in the ACI (2008) equation. The AASHTO (2010) equation is used in typical highway girder-to-deck interface design.

- <u>Prestress transfer reduction, $\mu(0.04P_{PS})$</u>

  Following the AASHTO Specifications regarding end-region reinforcement (§5.10.10.1) and the results of O'Callaghan and Bayrak (2007), within the greater of the transfer length ($60d_b$, where d_b is equal to the diameter of the strand) and 36 in., it can be assumed that the reinforcing bars transverse to the line of prestressing are stressed to resist 4% of the prestressing force. This stress induced at prestress transfer reduces the ability of those same bars to be further stressed to resist horizontal sliding.

- <u>Beam shape / reinforcement detailing factor, k_d</u>

  This reduction factor was included to account for the effect of asymmetry in reinforcement placement across the interface, as was found to be a concern through capacity calculations for U-Beams and testing of modified push-off specimens during this project. The specifics of this study are presented in Section 7.8.

Combining these four terms, the recommended calculation for horizontal shear capacity of the bottom flange-to-web interface of prestressed concrete beams is:

$$V_{ni} = k_d\left[cA_{cv} + \mu(A_{vf}f_y - 0.04P_{PS})\right] \qquad \textbf{Equation 7-14}$$

where

V_{ni} = nominal shear resistance of the interface plane [kip]

k_d = beam shape / reinforcement detailing factor, equal to 1.0 for I-Beams, Box-Beams, and U-Beams with distributed reinforcement, and 0.8 for U-Beams with reinforcement following the existing standard [see Section 7.8]

c = cohesion coefficient [ksi], equal to 0.4 ksi

A_{cv} = area of concrete considered to be engaged in interface shear transfer [in.^{2}]

μ = friction coefficient [dim.], equal to 1.4

A_{vf} = area of interface shear reinforcement crossing the shear plane within the area A_{cv} [in.^{2}]

f_y = specified yield strength of reinforcement [ksi],

limited to 60 ksi

P_{PS} = force of prestressing transferred to the beam within the region of interest [kip]

The coefficients c and μ are defined following Article 5.8.4.3 in AASHTO (2010). This study only considered beams in which the concrete across the interface was placed monolithically, for which the AASHTO (2010) coefficients were found to be appropriate. These coefficients are not expected to be appropriate for beams with alternate concrete placement methods (e.g., with a cold joint). The coefficients for the recommended calculation, the shear-friction equation in ACI (2008), and the original equation by Birkeland and Birkeland (1966) are presented in Table 7-3.

Table 7-3: Cohesion and friction coefficents for three calculation methods.

Source of Coefficients	Cohesion and Friction Coefficients	
	c	μ
AASHTO (2010): normal-weight concrete placed monolithically[1]	0.40 ksi[1]	1.4[1]
ACI (2008): normal-weight concrete placed monolithically	0.0 ksi	1.4
Birkeland and Birkeland equivalents	0.0 ksi	1.7

[1] Recommended coefficients

The recommended capacity calculation has two limit states, both of which place a maximum on the horizontal shear stress that an interface surface can carry. These limits are as presented in AASHTO (2010). The limit states are:

$$V_{ni} \leq K_1 f_c' A_{cv}$$ **Equation 7-14(a)**

and

$$V_{ni} \leq K_2 A_{cv}$$ **Equation 7-14(b)**

Equation 7-14(a) restricts the horizontal shear stress to a percentage of the compressive strength of the concrete; Equation 7-14(b) places an absolute maximum on the horizontal shear stress. As with the limit in the original Birkeland and Birkeland equation, these limit states exist as an estimation for the load that would cause the imperfections along the shear interface to crush. The values of K_1 and K_2, like those of the cohesion and

friction coefficients, depend on the material and geometric properties of the interface in question. The values for three calculation methods (recommended (from Article 5.8.4.3 of AASHTO (2010)), ACI (2008), and Birkeland and Birkeland (1966)), are presented in Table 7-4. For normal-weight concrete placed monolithically, when the compressive strength of the concrete exceeds 6 ksi, the recommended second limit state (maximum horizontal shear stress of 1.5 ksi) will always control.

Table 7-4: Maximum shear stress limit factors for three calculation methods.

Source of Limit Factors	Limit Factors	
	K_1	K_2
AASHTO (2010): normal-weight concrete placed monolithically[1]	0.25[1]	1.5 ksi[1]
ACI (2008): normal-weight concrete placed monolithically	0.20	1.6 ksi
Birkeland and Birkeland equivalents	None	0.8 ksi

[1] Recommended limit factors

The capacity calculation must be performed across multiple intervals from beam end to Ultimate Evaluation Point to properly account for the effects of prestress transfer and to ensure the horizontal shear stress limits are not being exceeded. The intervals are defined by changes in prestressing, reinforcing bar layout, and geometry. The points bounding the regions of interest include:

- beam end, where capacity is equal to zero,
- a distance equal to the larger of the transfer length ($60d_b$) or 36 in. from any point of prestress application (most commonly the beam end),
- at points of reinforcing bar spacing change, and
- at points of web width change (e.g., end blocks).

Capacity calculated across these regions should be compared to the maximums set by Equation 7-14(a) and (b). Failing to perform multiple calculations across varying reinforcing bar spacing regions will overestimate the maximum available capacity; a single calculation that ignores an increase in web width will underestimate the maximum available capacity.

7.5.4.1 Effect of an End Block

The most obvious instance of a change in web width occurs in beams with solid end blocks. The beneficial effect of an end block can be included in capacity calculations by considering the increased area that can resist horizontal shear forces. Following the assumption for the spread of load used in strut-and-tie modeling (ACI, 2008), it is recommended that load be assumed to spread at a ratio of 2:1 (26.5°) (Figure 7-13). The additional concrete contributes to A_{cv} in the original capacity calculation, and when computing maximum allowable horizontal shear forces.

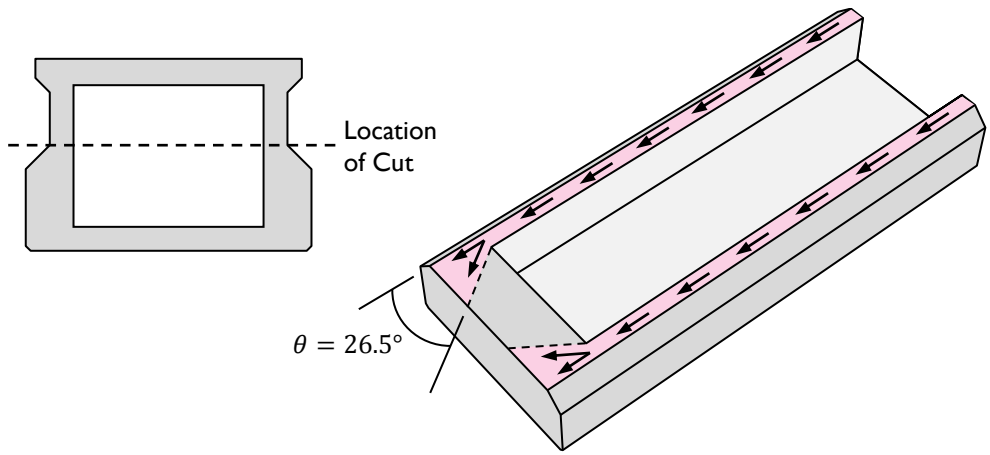

Figure 7-13: Area of concrete involved in resisting horizontal shear in beams in end blocks.

7.5.4.2 Permanent Clamping

The effect of permanent clamping on the horizontal shear capacity of the bottom flange-to-web interface was not considered in this study due to a lack of test data. It is hypothesized that permanent clamping (as may be attainable through the use of draped strands) will increase the capacity of the interface to resist horizontal sliding.

7.6 EXAMPLE CALCULATION

The procedure for calculating horizontal shear demand and capacity, as presented in the preceding section, will be demonstrated using a Tx28 specimen (Tx28-I-D) tested by Avendaño and Bayrak (2008). This beam was fabricated and load-tested prior to being added to the TxDOT state bridge standards (O'Callaghan and Bayrak, 2007;

Avendaño and Bayrak, 2008). The dimensions are similar to many optimized I-Beam and Bulb-T beam sections used around the country (e.g., the Virginia PCBT-29, New England NEBT-1000, or Nebraska NU750).

7.6.1 Example Specimen Properties

The cross-sectional properties and dimensions of the decked Tx28 beam specimen that was tested are given in Figure 7-14. The beam was prestressed with 36 0.6-in. diameter prestressing stands, which were stressed to 202.5 ksi before release. Prior to shear testing, an 8-in. thick, 6 ft wide cast-in-place deck was added to the beam. The beam concrete had a compressive strength of 13.8 ksi at time of testing.

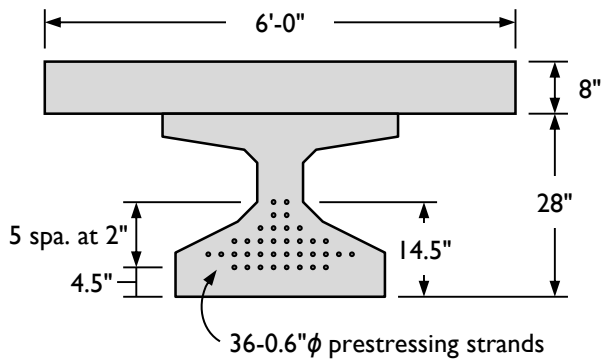

Figure 7-14: Cross-sectional properties of the example Tx28-I-D specimen.

The beam specimen, Tx28-I-D, was load-tested under the conditions shown in Figure 7-15. The shear span was 84 in., resulting in a span-to-depth ratio of 3.0. The distance from centerline of bearing pad to beam end was 12 in. The test specimen failed at a shear load of 417 kip, with horizontal shear damage along the web-to-flange interface. The calculated vertical shear capacity, found using the AASHTO General Procedure (2010), was 221 kip.

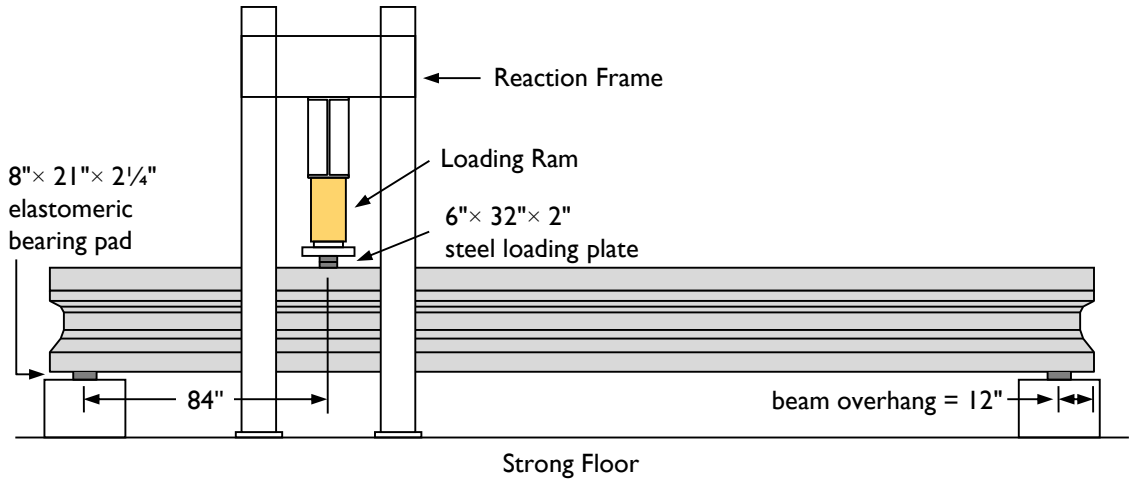

Figure 7-15: Elevation view of test setup used by Avendaño and Bayrak (2008).

The reinforcing bar layout for the specimen Tx28-I-D is given in Figure 7-16. The typical web reinforcement consisted of a two-legged #4 bar spaced at 4 in. near beam end (to 50.5 in.) and at 12 in. through the load point. Given the distributed reinforcement and symmetric cross section of this beam (typical to I-Beams), k_d is equal to 1.0. A #6 bar was bundled with each leg of the first two stirrups near beam end.

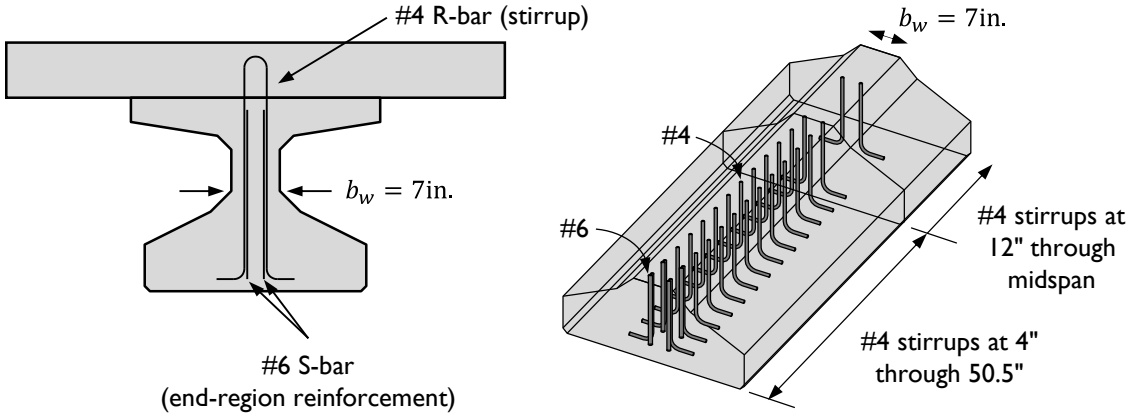

Figure 7-16: Reinforcing bar layout in specimen Tx28-I-D.

7.6.2 Example Calculation for Demand

The horizontal shear demand is found by first calculating the horizontal shear stress caused by the vertical load at failure. The horizontal shear stress between the centerline of the bearing pad and the UEP is estimated to be 2.11 ksi:

$$v_{hs} = \frac{V_{applied}}{b_w d} = \frac{417\text{kip}}{(7\text{in.})(28.3\text{in.})} = 2.11\text{ksi}$$

The horizontal shear demand is found by multiplying the horizontal shear stress by the length over which it acts, defined as from centerline of bearing pad to the Ultimate Evaluation Point. The location of UEP is found following Equation 7-10:

$$l_{UEP} = a + oh - \frac{l_{LP}}{2} - h + y_{crit}$$ **Equation 7-10**

$$l_{UEP} = 84\text{in.} + 12\text{in.} - \frac{6\text{in.}}{2} - 36\text{in.} + 14.5\text{in.} = 71.5\text{in.}$$

which means the critical length for demand calculations is $(l_{UEP} - oh)$, or 59.5 in. The horizontal shear demand is then calculated to be 877 kip:

$$V_{u_{hs}} = v_{hs} b_w l_{crit}$$ **Equation 7-13**

$$V_{u_{hs}} = (2.11\text{ksi})(7\text{in.})(59.5\text{in.}) = 877\text{kip}$$

The next step is to calculate the horizontal shear capacity.

7.6.3 Example Calculation for Capacity

The horizontal shear capacity calculation starts by defining the regions of interest. Following the guidelines given in Section 7.5.4 regarding defining regions of interest for capacity calculations, three regions can be found:

- Region 1 (Transfer Region): from beam end to the end of the transfer length, at 36 in.
- Region 2: from 36 in. to the reinforcing bar spacing change at 50.5 in.
- Region 3: from 50.5 in. to the Ultimate Evaluation Point at 71.5 in.

The capacity calculation (Equation 7-14) must be performed across each of these regions, ensuring that the horizontal shear stress does not exceed the limits set in Equation 7-14(a)

and (b). The capacity at the UEP that will be compared to the demand is found by summing the capacity of the three regions.

The equation for capacity is:

$$V_{ni} = k_d\left[cA_{cv} + \mu(A_{vf}f_y + P_c - 0.04P_{PS})\right] \qquad \textbf{Equation 7-14}$$

For the first region of specimen Tx28-I-D,

$$A_{cv} = (b_w)(l_1) = (7\text{in.})(36\text{in.}) = 252\text{in.}^2$$

$$A_{vf} = (4)(0.44\text{in.}^2) + (9)(2)(0.20\text{in.}^2) = 5.36\text{in.}^2$$

$$P_{PS} = (36)(0.216\text{in.}^2)(157\text{ksi}) = 1232\text{kip}$$

which results in a capacity of 482 kip:

$$V_{ni1} = (1.0)\left[0.4(252\text{in.}^2) + 1.4[(5.36\text{in.}^2)(60\text{ksi}) - 0.04(1232\text{kip})]\right]$$

$$V_{ni1} = 482\text{kip}$$

As the compressive strength of the concrete in the Tx Girder is 13.8 ksi, well above 6 ksi, it is necessary only to check the second limit state (Equation 7-14(b)):

$$V_{ni1\max} = K_1A_{cv} = 1.5(252\text{in.}^2) = 378\text{kip}$$

The original calculation for capacity (482 kip) exceeds the maximum allowable capacity for the region. The limited capacity, 378 kip, will be assigned to the region. The calculations presented here are summarized in Table 7-5, along with the corresponding calculations for Regions 2 and 3.

Table 7-5: Summary of horizontal shear example calculations.

Region	Length [in.]	Concrete Area [in.^{2}]	Steel Area [in.^{2}]	Prestress Force [kip]	Raw Capacity [kip]	Limit (b) [kip]	Capacity [kip]
1	36.0	252.0	5.36	1232	482	378*	378
2	14.5	101.5	1.60	0	175	152*	152
3	21.0	147.0	0.40	0	92*	221	92
TOTAL							623

* controls capacity

7.6.4 Example Evaluation

The evaluation of horizontal shear susceptibility in this example beam is completed by computing the ratio of horizontal shear demand to capacity (Equation 7-9):

$$HSR_{Tx28} = \frac{V_{u_{hs}}}{V_{n1}} = \frac{877\text{kip}}{623\text{kip}} = 1.41$$

As the HSR is greater than 1.0, evidence of horizontal shear distress is expected at failure. The test specimen is pictured in Figure 7-17; the most prominent crack at failure was at the interface between the bottom flange and web of the beam, near beam end. No evidence of web crushing or reinforcing bar yield was seen at failure. The calculation and observation are in good agreement: at the given loads, horizontal shear damage was expected and was seen. The calculation had 41% excess conservatism when applied to this example.

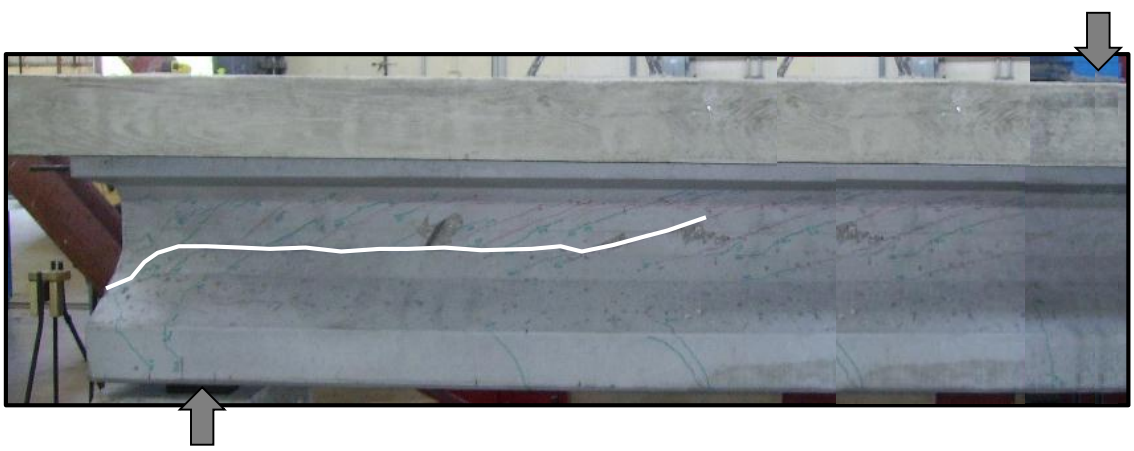

Figure 7-17: Tx28-I-D cracking observed at failure.

7.7 VERIFICATION OF METHODOLOGY

To confirm the accuracy of the recommended evaluation method, a verification database was formed using a subset of tests previously recorded in the University of Texas Prestressed Concrete Shear Database (UTPCSDB-2011) (Nakamura, 2011). The Horizontal Shear Evaluation Database (HSED) is presented in this section, and is used to observe trends in the calculation method proposed. Complete details of the test specimens included in this database, and the calculations performed, can be found in Appendix C.

7.7.1 Formation of Evaluation Database

The UTPCSDB-2011 consists of 1696 tests from 99 references published between 1954 and 2010. Nakamura (2011) presents a subset of these 1696 tests, referred to as the Evaluation Database – Level I, that consists only of "shear tests deemed useful for the evaluation of the shear design provisions". The filtering criteria and effect on number of tests considered are given in Table 7-6.

Table 7-6: Filtering criteria used to form Evaluation Database – Level I (from Nakamura (2011)).

Collection Database		1696 tests
Filtering Criteria: remove tests irrelevant to the shear behavior of prestressed concrete members	Failure modes other than shear failure (flexural, bond, bearing)	- 417 tests
	Nonprestressed member	- 156 tests
	Missing applied load at failure	- 6 tests
	With initial defects	- 4 tests
	Subjected to moving loads	- 7 tests
Filtering Criteria: remove tests not deemed useful for the evaluation of the shear design provisions	Concrete strength < 4 ksi	- 162 tests
	Concrete types other than normal concrete	- 59 tests
	Member height < 12.0 in.	- 337 tests
	Shear span-to-depth ratio < 2.0 (concentrated loads)	- 119 tests
	Insufficient amount of shear reinforcement (per ACI 318-08) (per AASHTO LRFD 2010)	 - 644 tests - 631 tests
	Continuous beams	- 37 tests
	Segmental specimens	- 18 tests
	Externally post-tensioned specimens	- 35 tests
Evaluation Database – Level I		223 tests

The Horizontal Shear Evaluation Database (HSED) is a subset of the Level I Evaluation Database, with certain additional criteria added, as summarized in Table 7-7. A total of 69 test specimens from 14 references were included in the HSED. Eight of these specimens are not included in the 2011 publication of the UTPCSDB, as the results were not available at that time. Eight of the nine squared-end U-Beam test regions described in this dissertation are included. Test region B0S was not considered in this study as insufficient information regarding bottom flange-to-web reinforcement and end block length was known. The fourteen references included in the HSED are listed in Table 7-8, with the sources of the sixteen new tests highlighted.

Table 7-7: Filtering criteria used to form the Horizontal Shear Evaluation Database.

Evaluation Database – Level I (Nakamura, 2011)		223 tests
Filtering Criteria: remove tests not deemed useful for the evaluation of the horizontal shear demand and capacity calculations	Post-tensioned specimen	- 67 tests
	Rectangular, U-, or T-shaped section	- 63 tests
	Non-standard beam section	- 146 tests
	Skewed beam specimen	- 9 tests
	Insufficient information regarding geometry of loading, reinforcement, or beam beyond bearing pad	- 159 tests
Include beam tests performed after UTPCSDB-2011 publication		+ 8 tests
Include squared-end U-Beam test specimens		+ 8 tests
Horizontal Shear Evaluation Database		69 tests

Table 7-8: List of references used in the Horizontal Shear Evaluation Database.

No.	Authors	Year	Number of Tests	Beam Type
1	Alshegeir & Ramirez	1992	3	AASHTO Type I, II
2	Avendaño & Bayrak	2008	4	Texas Tx28
3	Hamilton, Llanos, & Ross	2009	2	AASHTO Type III
4	Hawkins & Kuchma	2007	7	PCI BT-63
5	Heckmann & Bayrak	2008	6	Texas Type C
6	Avendaño	2011	10 (5)	Texas 4B28, 5B40, 5XB40
7	Labonte & Hamilton	2005	1	AASHTO Type II
8	Naito, Parent, Brunn, & Tate	2005	1	PCEF-45
9	Ramirez & Aguilar	2005	2	AASHTO Type I
10	Runzell, Shield, & French	2007	2	Minnesota MnType54
11	Shahawy, Robinson, & Batchelor	1993	8	AASHTO Type II
12	Tawfiq	1995	12	AASHTO Type II
13	Avendaño, et al. [unpublished]		3 (3)	Texas Tx46, Tx70
14	Hovell [this study]	2011	8 (8)	Texas U54, modified U54
TOTAL			69 (16)	10 I-Beam shapes 3 Box-Beam shapes 2 U-Beam shapes

7.7.2 Database Composition

As listed in Table 7-8 and shown in Figure 7-18, fifteen different standard beam shapes are included in the HSED, resulting in seventeen studied cross sections (two beam shapes were tested with and without a deck). The database contains ten I-Beam shapes (AASHTO Type I, II, and III; Texas Type C, Tx28, Tx46, and Tx70; PCI BT-63; PCEF-45; and Minnesota MnType54), three Box-Beam shapes (Texas 4B28, 5B40, 5XB40), and two U-Beam shapes (Texas U54 and modified U54). Twenty-two beam test specimens failed in horizontal shear or with signs of horizontal shear distress. Included in this subset are all three Tx Girders shapes, the Texas 5B40 Box-Beam, the PCI BT-63, and both Texas U-Beams. The remaining 47 tests failed in typical web-shear modes.

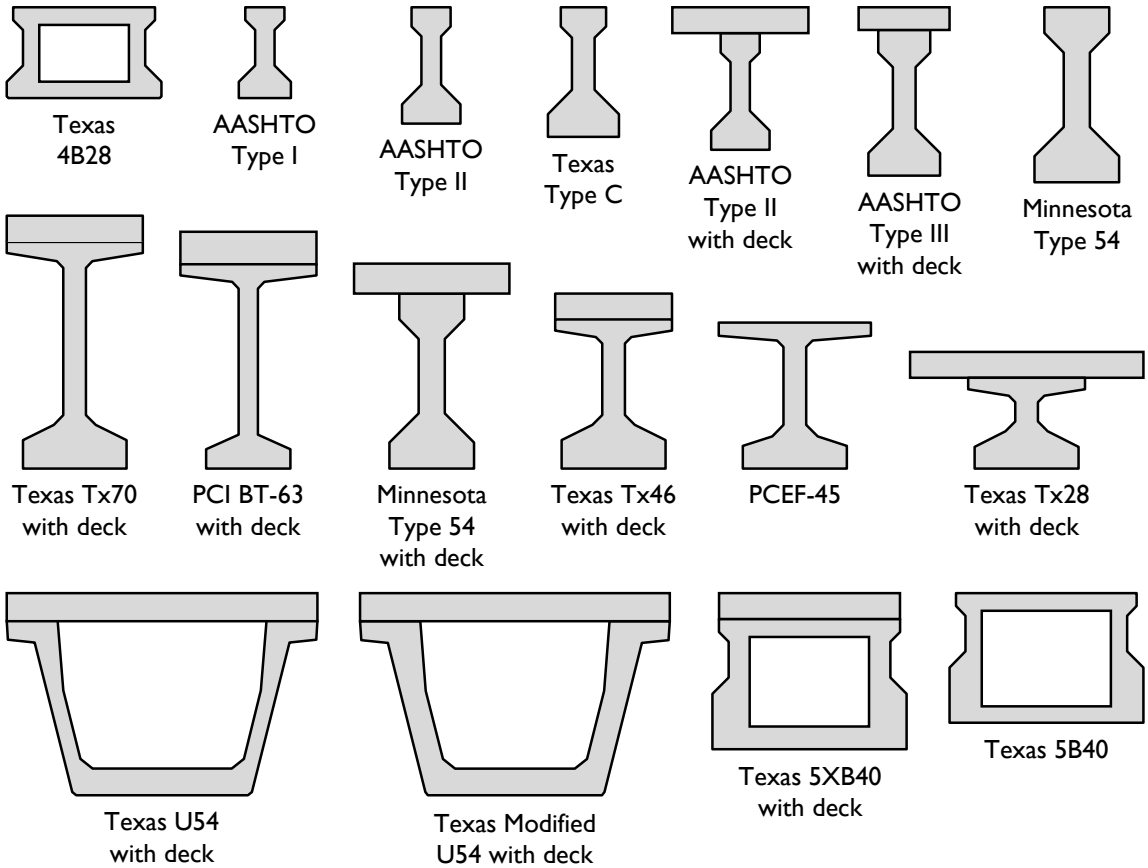

Figure 7-18: Beam shapes included in the Horizontal Shear Evaluation Database.

To better provide a description of the distribution of properties of the beam test specimens included in the Evaluation Database, four histograms are provided: concrete strength (Figure 7-19), total depth of section (Figure 7-20), shear span-to-depth ratio (Figure 7-21), and shear span reinforcement ratio (Figure 7-22).

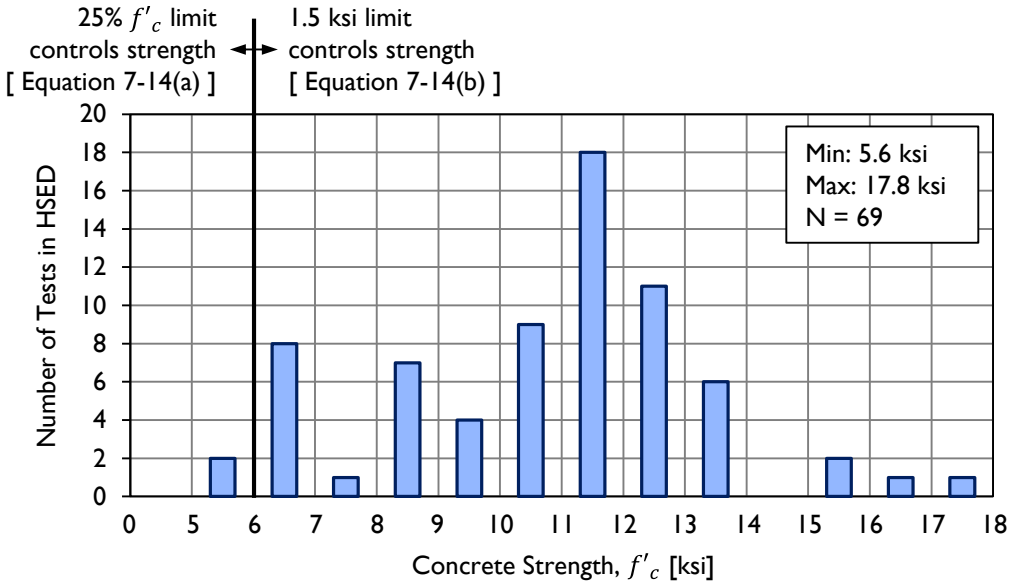

Figure 7-19: Distribution of concrete strength for specimens in the HSED.

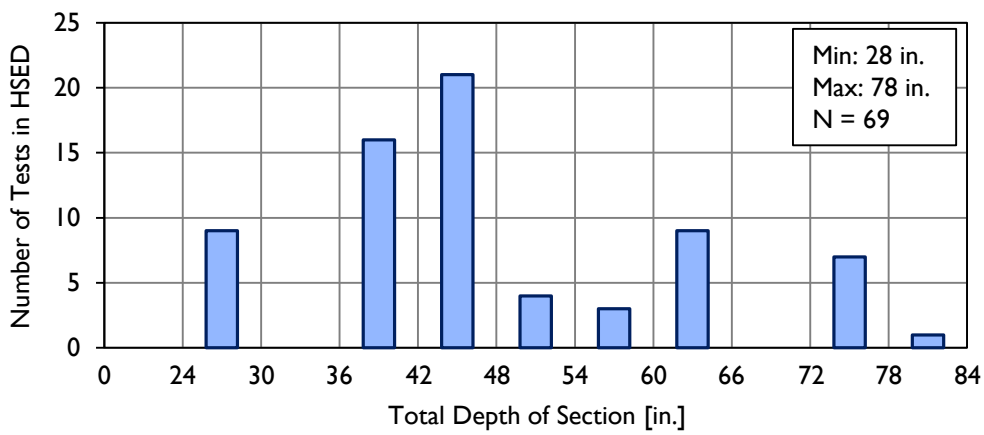

Figure 7-20: Distribution of specimen size in the HSED.

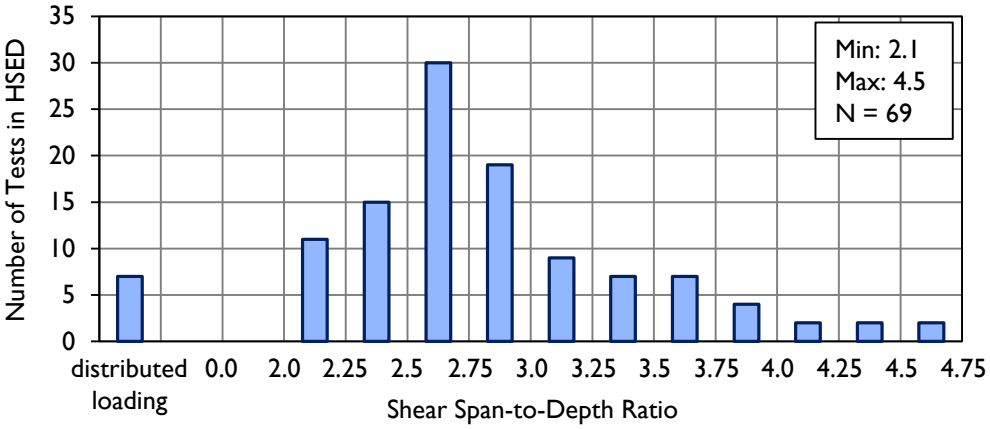

Figure 7-21: Distribution of shear span-to-depth ratio used in tests in the HSED.

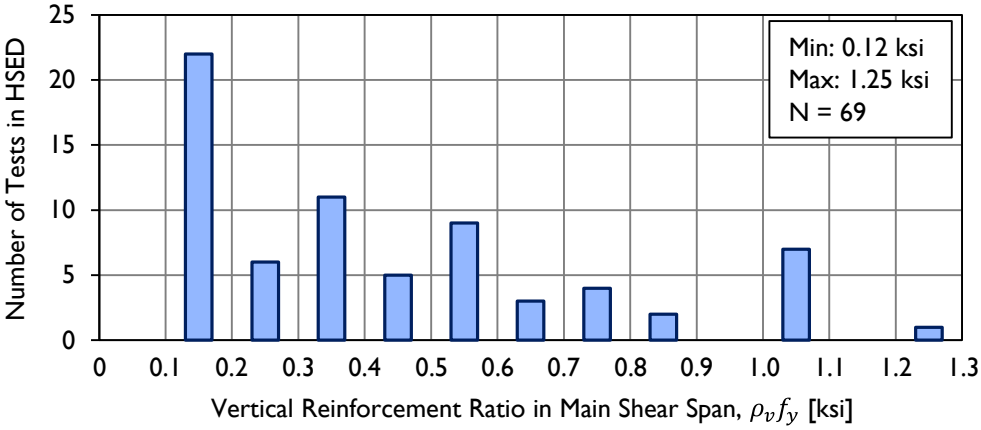

Figure 7-22: Distribution of vertical reinforcement ratio for specimens in the HSED.

As can be seen in the histograms, the data points in the Horizontal Shear Evaluation Database are primarily high-strength concrete beams with significant amounts of reinforcing, tested at a span where sectional analysis is appropriate. No specimens under 28 in. in depth were included; the maximum specimen depth was 78 in.

7.7.3 Accuracy of Horizontal Shear Calculations

Two metrics were calculated for each beam test in the Horizontal Shear Evaluation Database. The first is the Horizontal Shear Ratio, defined by Equation 7-9. The second is the Shear Performance Ratio (SPR), defined as:

$$SPR = \frac{V_{test}}{V_n}$$ **Equation 7-15**

where:

V_{test} = failure shear for a laboratory beam test specimen [kip]

V_n = vertical shear capacity calculated using the AASHTO General Procedure (2010) [kip]

Using these two values, a standard plot (HSR-SPR plot) was made: on the horizontal axis is the SPR; a value greater than 1.0 indicates conservatism in the AASHTO General Procedure web-shear strength calculation. On the vertical axis is the HSR; a value greater than 1.0 indicates that horizontal shear demand exceeds capacity, and horizontal shear damage is expected. Most beam tests in the literature should fall in the bottom right quadrant, with a measured capacity greater than calculations (SPR > 1.0) and horizontal shear demand less than capacity (HSR < 1.0).

The goal of this study on horizontal shear is to provide a metric can be used to accurately predict when the demand on the bottom flange-to-web interface exceeds the horizontal shear capacity of that interface. When looking at a database of test points, an acceptable method will show a clear demarcation between test points with horizontal shear damage and cases without. This difference can be seen visually in the HSR-SPR plot, or numerically by comparing the average HSR for specimens with observed horizontal shear damage and the average without. The coefficient of variation for each data set was also found to evaluate the scatter in the calculations. It was considered acceptable for the method to be over-conservative (i.e., an expectation of horizontal shear damage that is not seen), but not unconservative (i.e., an expectation of adequate horizontal shear strength when it is not present).

The HSR-SPR plot given in Figure 7-23 was made after the calculation method presented in Section 7.5 was followed for each of the sixty-nine data points in the HSED. The horizontal shear failure subset has an accuracy of 22/22: each of the twenty-two tests that failed in horizontal shear or with signs of horizontal shear distress have a calculated HSR greater than 1.0. The average, coefficient of variation, and accuracy for the typical

shear failure dataset and the horizontal shear failure dataset are provided in Table 7-9. While nine tests indicated that a horizontal shear failure was likely but was not observed, this conservatism is deemed acceptable.

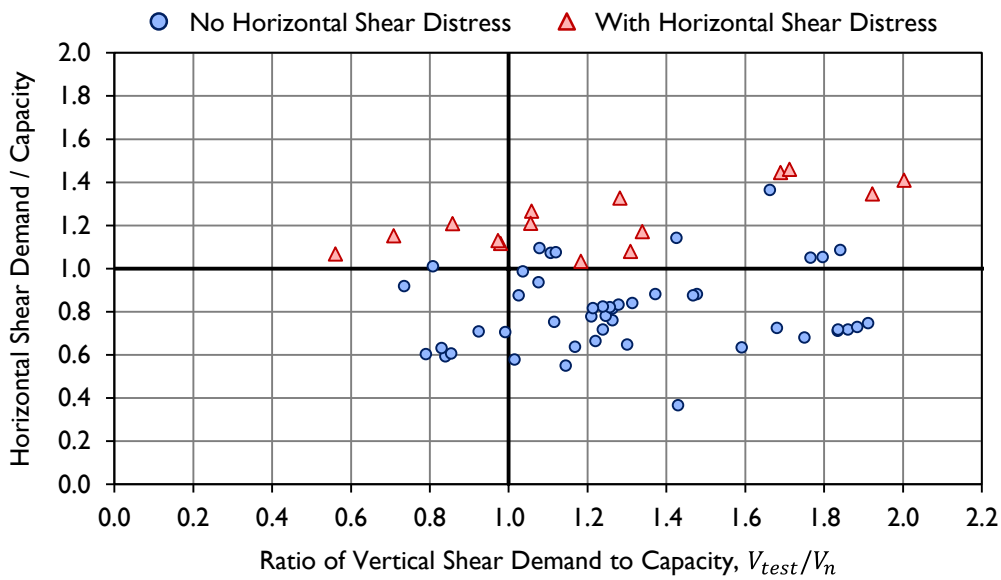

Figure 7-23: Ratios of vertical and horizontal shear demand to capacity for specimens in the HSED.

Table 7-9: Statistics for the recommended horizontal shear evaluation method.

No Horizontal Shear Distress		With Horizontal Shear Distress
0.81	Mean	1.27
0.23	COV	0.12
38/47	Accuracy	22/22

The horizontal shear capacity for each point in the HSED was also calculated using the ACI (2008) shear-friction equation. The HSR-SPR plot that resulted can be seen in Figure 7-24, with statistics on the data given in Table 7-10. Using this equation and coefficients resulted in excessively conservative calculations for horizontal shear strength. There was no clear demarcation between the two data sets (tests with and tests without horizontal shear distress). For these reasons, the ACI (2008) calculation method was not considered to be appropriate for use in estimating the horizontal shear capacity of the bottom flange-to-web interface of prestressed beams.

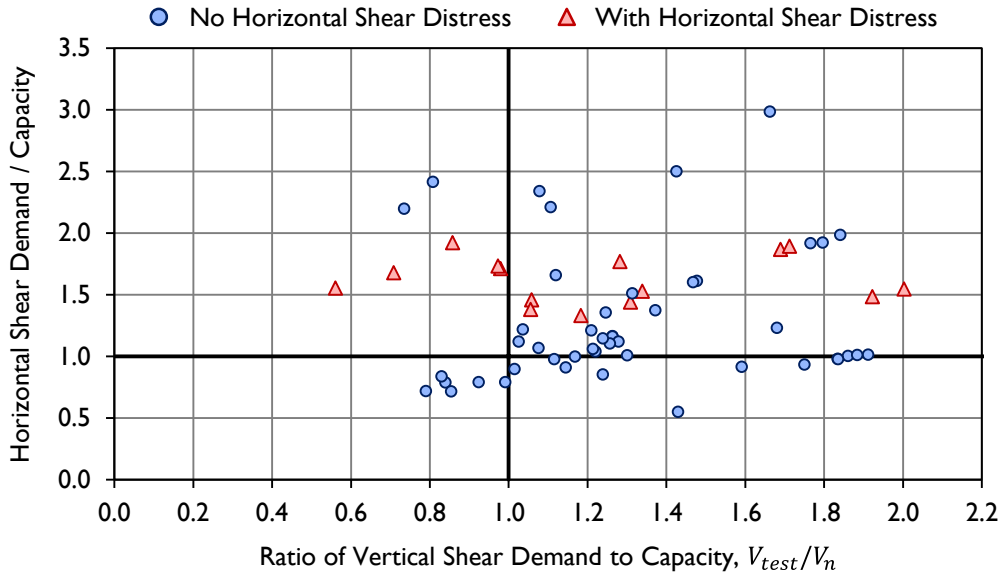

Figure 7-24: HSR-SPR plot for specimens in the HSED with calculations for capacity performed using the ACI (2008) shear-friction equation.

Table 7-10: Statistics for HSRs when using ACI (2008) calculation for capacity.

No Horizontal Shear Distress		With Horizontal Shear Distress
1.29	Mean	1.62
0.43	COV	0.12
16/47	Accuracy	22/22

7.8 HORIZONTAL SHEAR IN U-BEAMS

The calculation for horizontal shear capacity of the bottom flange-to-web interface of prestressed concrete beams presented in Section 7.5.4 included a beam shape / reinforcement detailing factor, k_d. For most beam shapes in the Horizontal Shear Evaluation Database, k_d was set to 1.0. However, it was recommended that 0.8 be used in capacity calculations for U-Beams with reinforcement details following the existing standard. This section includes a presentation of the rationale behind the inclusion of a reduction factor, and the testing performed to determine an appropriate value.

7.8.1 Initial Calculations

The horizontal shear demand on and capacity of the bottom flange-to-web interface of eight of the Texas U-Beam test regions studied in this project were calculated following Equations 7-13 and 7-14, respectively. The beam shape / reinforcing distribution factor, k_d, was set to 1.0.

The Horizontal Shear Ratios for the eight U-Beams considered in this study are plotted in Figure 7-25 against the Shear Performance Ratios, V_{test}/V_n, with the calculation for V_n made using the AASHTO General Procedure (2010). As described in Section 7.5.1, an HSR ratio below 1.0 indicates that at the given load, the demand on the horizontal bottom flange-to-web interface is less than the calculated capacity across the same region. Test specimens with an HSR below 1.0 are not expected to show signs of horizontal shear distress at failure. It can be seen in Figure 7-25 that the five test regions that did fail with significant horizontal shear distress and minor web distress had a calculated HSR below 1.0; the calculations are in conflict with observations.

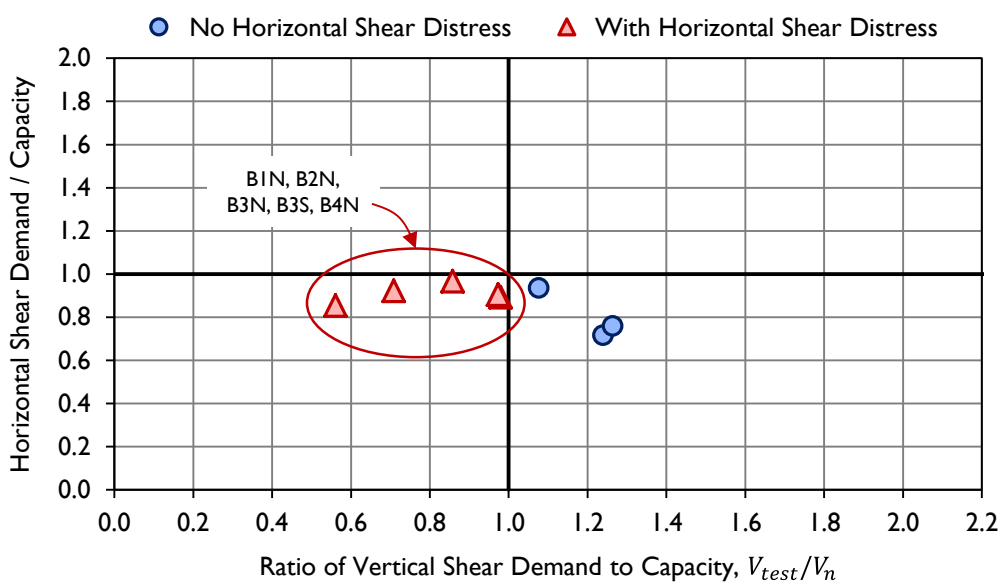

Figure 7-25: Summary of comparison between horizontal and vertical shear demand and capacity for Texas U-Beams.

Given the success of this calculation method in predicting the likelihood of horizontal shear distress in Box-Beams and I-Beams, the U-Beam was studied further to determine the cause of the atypically unconservative calculations.

7.8.2 Push-Off Tests

The shear-friction equation used to calculate the horizontal shear capacity of the bottom flange-to-web interface was calibrated using push-off specimens. A typical push-off specimen is pictured in Figure 7-26. Two boot-shaped sections are connected along a critical slip plane, the shear capacity of which is found through load-testing.

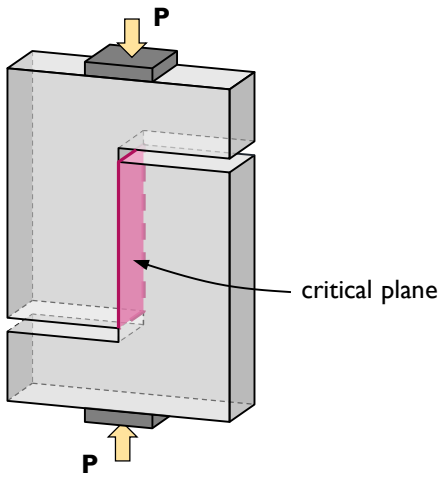

Figure 7-26: Typical push-off specimen as described in literature.

A series of modified push-off specimens were designed, fabricated, and tested. These specimens were designed to better represent the geometry of the Texas U-Beam bottom flange-to-web interface. Of particular interest was the lack of symmetry in the U-Beam concrete and reinforcement placement as compared to an I-Beam and a typical push-off specimen (Figure 7-27). In the I-Beam, there are two reinforcing bars crossing the bottom flange-to-web interface. When the bars are stressed, following the shear-friction theory, the resulting clamping force is evenly distributed across the width of the web. In the U-Beam, a single reinforcing bar placed off center crosses the bottom flange-to-web interface. The resulting clamping force is concentrated one side of the web.

Similarly, the bottom flange in the I-Beam is symmetric on both sides of the web, whereas the bottom flange of the U-Beam exists only towards the inside of the web.

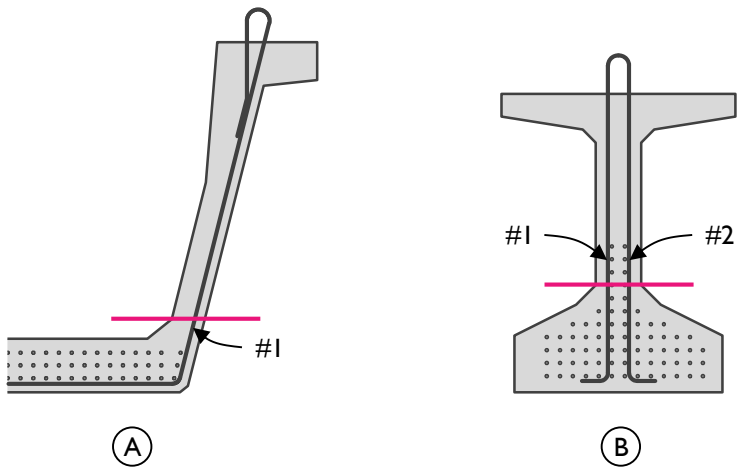

Figure 7-27: (A) Typical U-Beam and (B) I-Beam bottom flange-to-web interface and reinforcing.

The critical interface of push-off specimens meant to highlight the reinforcement layout of a U-Beam and an I-Beam are given in Figure 7-28. The I-Beam reinforcement is symmetric and similar to the specimens reported in the literature. Specimens like these were used to calibrate the shear-friction equation. The U-Beam reinforcement, with just one reinforcing bar crossing the shear plane, does not resemble previously tested specimens.

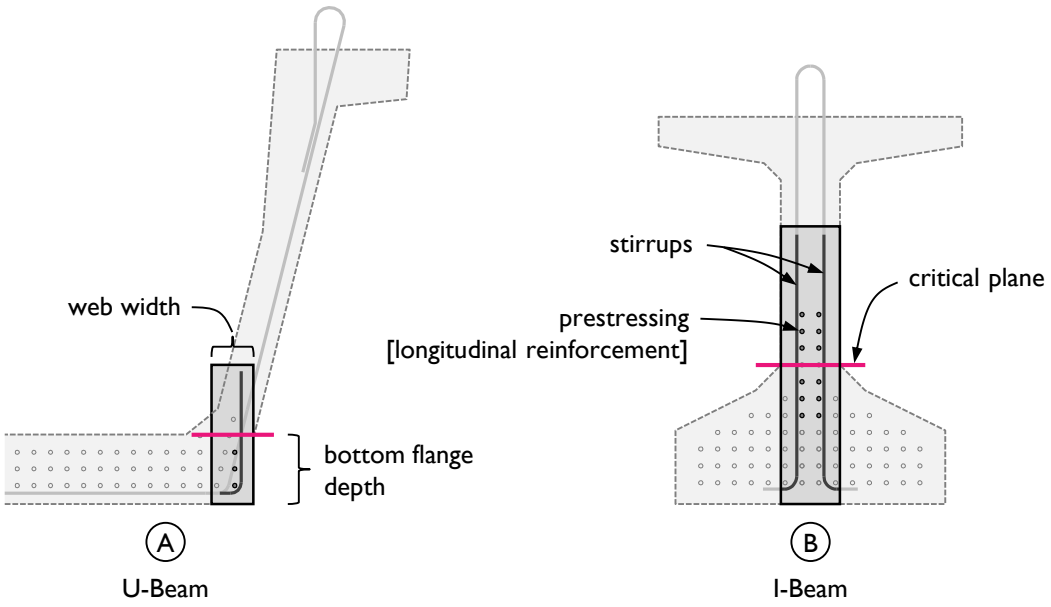

Figure 7-28: Critical interface of push-off specimens based on the reinforcement of (A) a standard Texas U-Beam and (B) an I-Beam (Tx 46).

7.8.2.1 Specimen Design

The modified push-off specimens fabricated and tested were designed such that the critical interface replicated the bottom flange-to-web interface of a Texas U-Beam. The design began by envisioning cutting a section of the interface from a U-Beam (Figure 7-29 Step 1). For simplicity, the sloped web and the chamfer were ignored (Step 2), resulting in an L-shaped specimen when viewed in cross section. As the load frame available to test the specimens required a vertical application of load, the section was rotated 90° (Step 3) prior to the addition of concrete caps (Step 4). The concrete caps isolate the critical interface and allow for a purely-shear application of load.

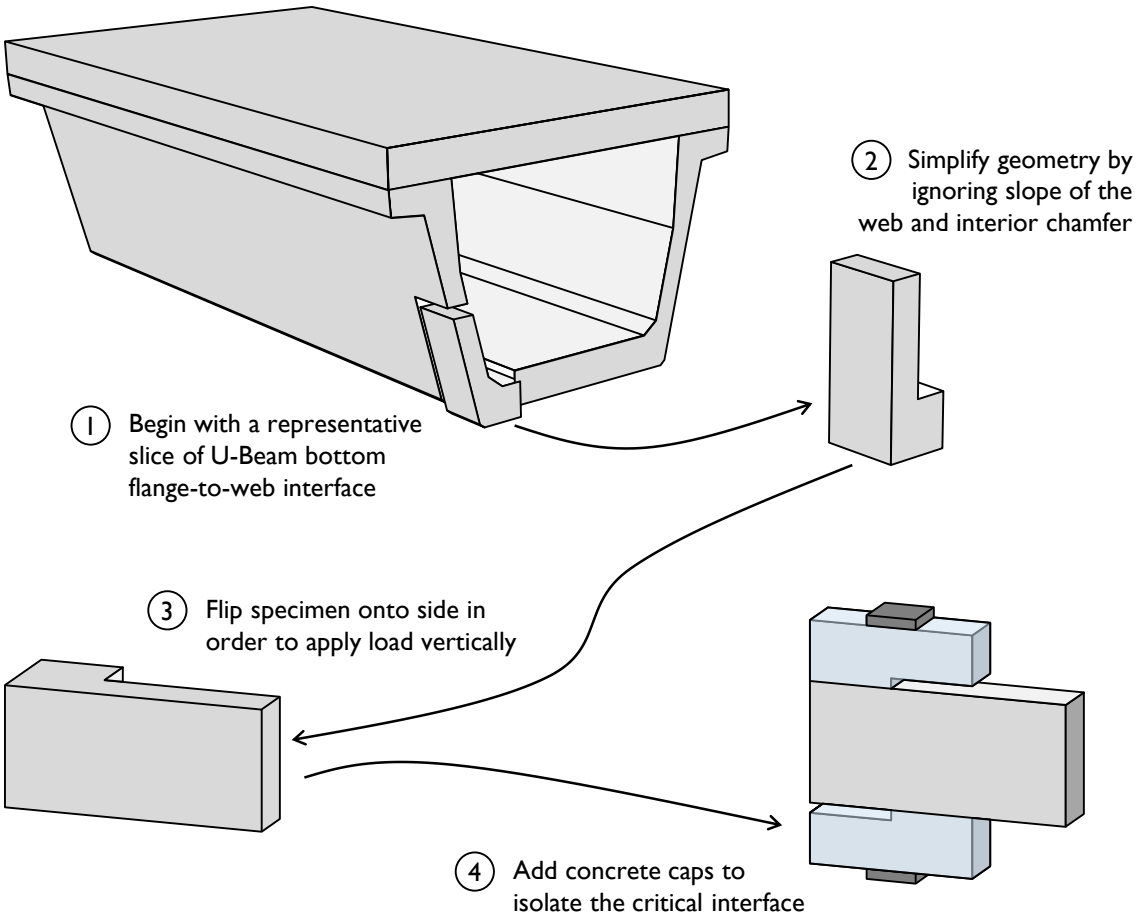

Figure 7-29: Steps taken to design the modified push-off specimens used.

Dimensions of the modified push-off specimen are given in Figure 7-30. The dimensions were chosen to match the critical dimensions of the Texas U-Beam web and bottom flange (5 in. web walls meeting an 8.25 in. bottom flange), with the shear area being tested representing a linear foot of U-Beam bottom flange-to-web. Three #4 reinforcing bars were used in each specimen, spaced at 4 in. To ease construction, the bars rested on two points of the formwork during concrete placement. Three-dimensional views of the specimen from each corner are given in Figure 7-31.

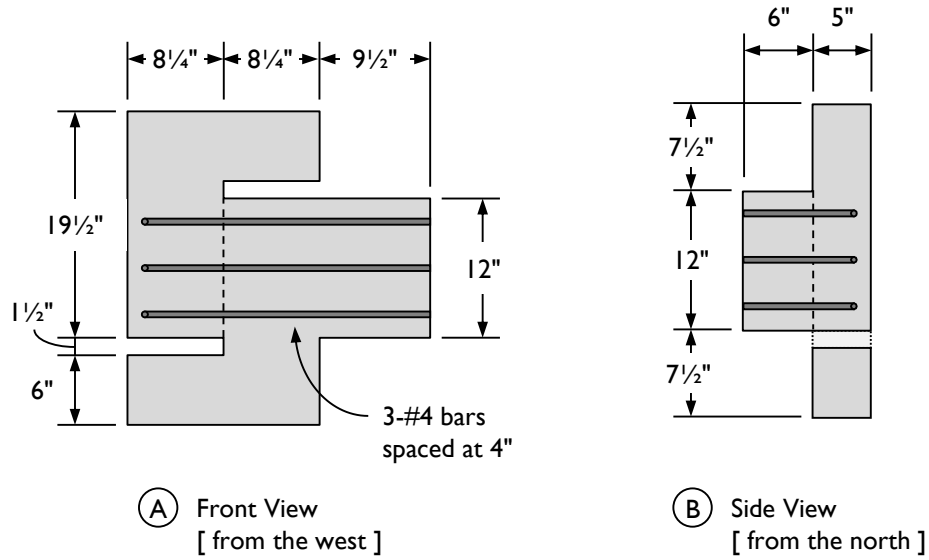

Figure 7-30: Dimensions and interface reinforcing bar locations in modified push-off specimens.

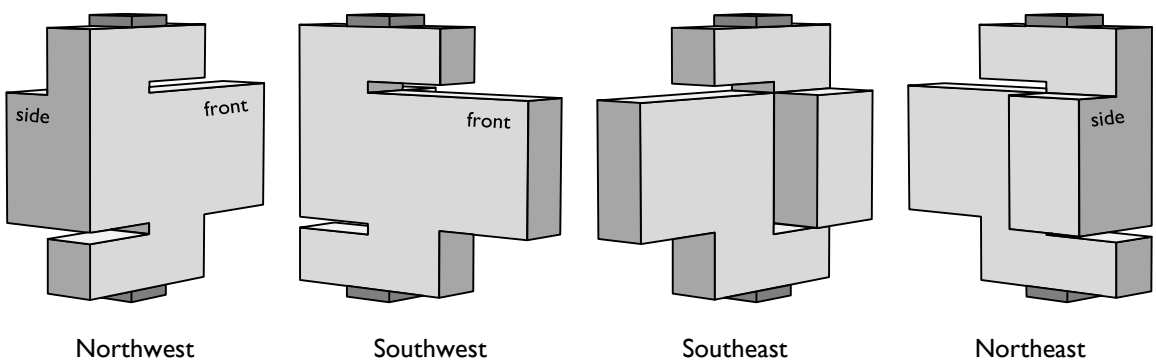

Figure 7-31: Modified push-off specimen viewed from four corners.

The tested area nominally measured 12 in. by 5 in. and contained three #4 reinforcing bars. Using the AASHTO shear-friction equation for a vertically-aligned interface (Equation 7-8 of this dissertation), the theoretical capacity of the interface of these push-off specimens was found to be 50.4 kip:

$$V_{ni} = \mu\left(A_{vf} f_y + P_c\right) \qquad \textbf{Equation 7-8}$$

$$V_n = 1.4[(3)(0.2\text{in.}^2)(60\text{ksi}) + 0\text{kip}]$$

$V_n = 50.4\text{kip}$

The reinforcing bars used in the push-off specimens were placed either in the center of the 5 in. thickness ("centered reinforcement" specimens) or to one side as is the case in the Texas U-Beam ("offset reinforcement" specimens), as shown in Figure 7-32 (the specimen has been cut horizontally to show the reinforcement crossing the critical interface). In the former case, the cover on the reinforcing bar was 2.25 in. in each direction; in the latter, the cover was 1.0 in. on the outside and 3.5 in. on the inside.

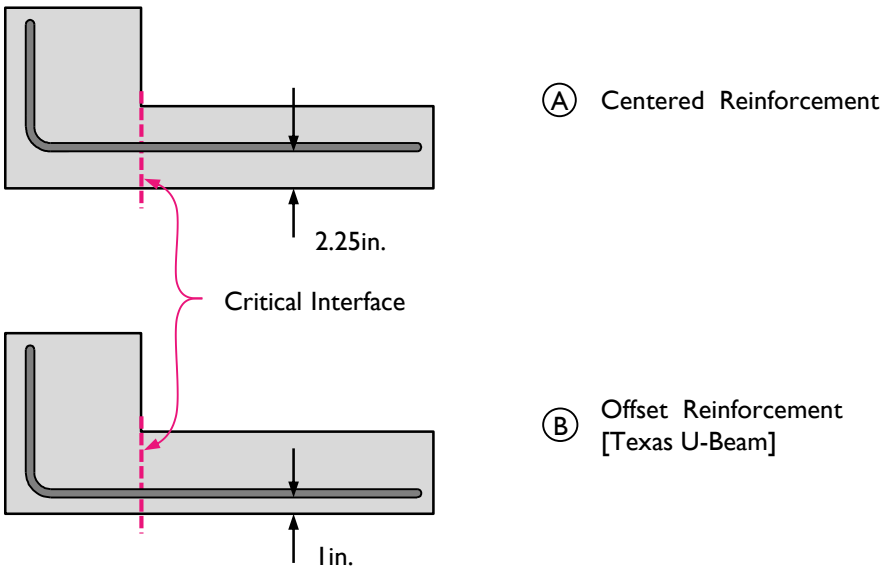

Figure 7-32: Placement of reinforcing bars crossing critical plane in modified push-off specimens.

7.8.2.2 Results

Four push-off specimens were tested, two with the reinforcing bars centered in the critical interface and two with the reinforcing bars offset as in the Texas U-Beam. The failure loads are presented in Table 7-11, with comparisons to the calculated capacity. Also provided is the ratio of the failure load in the offset specimen to the failure load in the centered specimen for each series of tests. The measured strength of the centered specimens was significantly higher than the offset specimens.

Table 7-11: Summary of modified push-off specimen results.

		Centered	Offset	Ratio: $\frac{\text{Offset}}{\text{Centered}}$
Series 1	Measured Value	67.4 kip	54.7 kip	0.81
	Ratio to Calculated	1.34	1.08	
Series 2	Measured Value	73.2 kip	60.1 kip	0.82
	Ratio to Calculated	1.45	1.19	
Average Ratio to Calculated		1.39	1.14	

7.8.3 Explanation of Behavior

The difference in capacity of the specimens with centered reinforcing bars versus offset reinforcing bars can be understood through further consideration of the shear friction theory. The original theory is presented considering an interface in elevation view (Figure 7-33); from this direction, an I-Beam and a U-Beam are essentially identical. The same interface considered in cross section is markedly different (Figure 7-34). In the I-Beam specimen with distributed reinforcement, as the interface opens, the reinforcement evenly applies a clamping force, maintaining some contact between the surfaces. In the U-Beam specimen with asymmetric reinforcing bar placement, the opening of the interface is not counterbalanced with reinforcement on one side, allowing the two surfaces to lose contact, removing any benefit of cohesion or aggregate interlock.

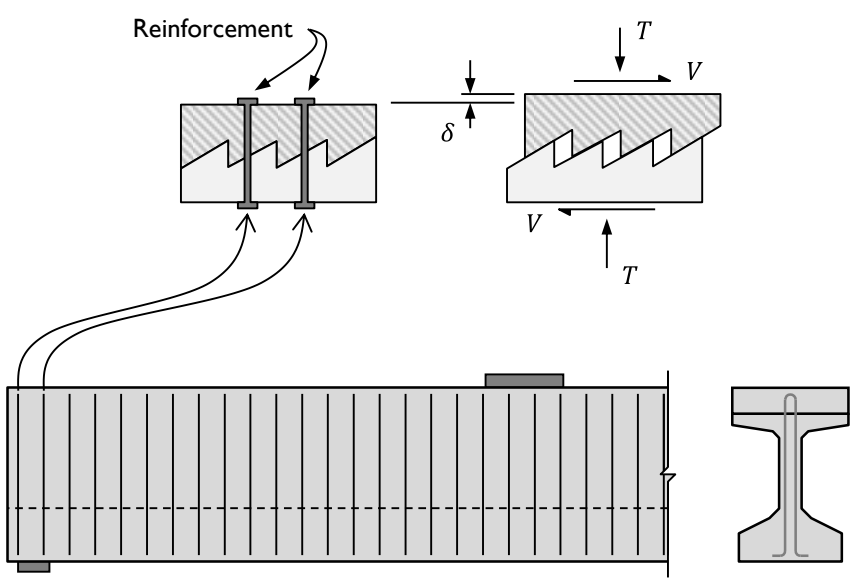

Figure 7-33: Elevation view of a beam and the shear-friction model.

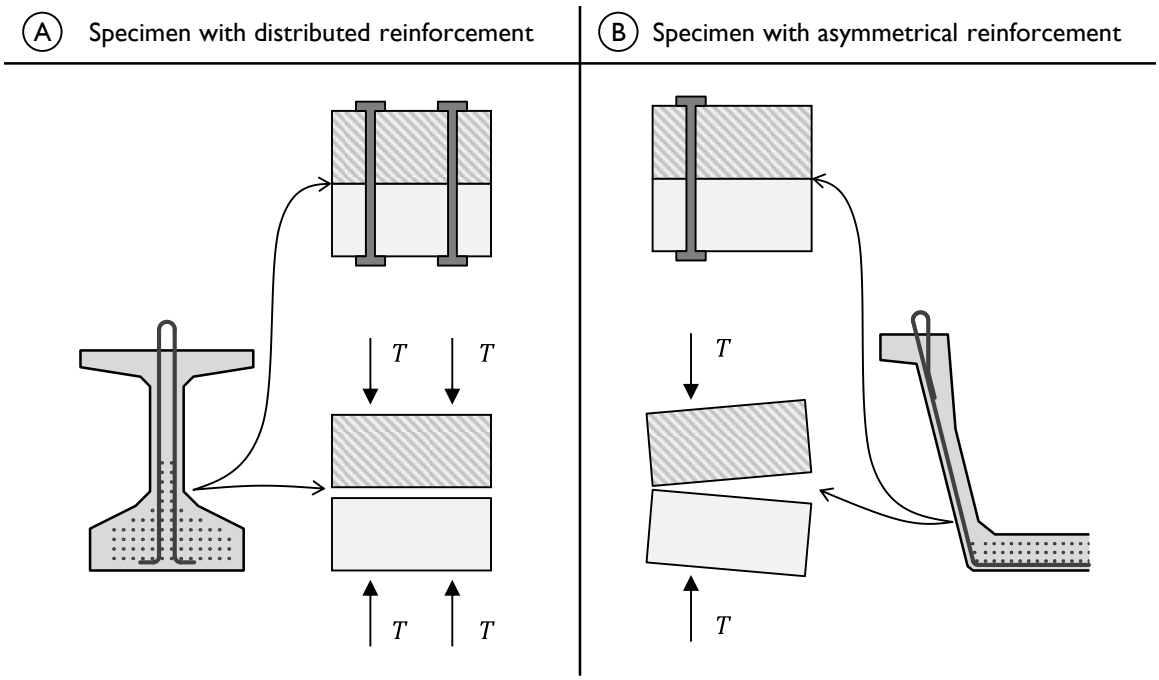

Figure 7-34: Cross-sectional view of shear-friction specimens with (A) distributed and (B) asymmetrical reinforcement.

The theoretical behavior shown in Figure 7-34(B) was observed during testing of the modified push-off specimens. A picture of one offset reinforcement specimen is given in Figure 7-35; the opening of the interface in one direction can be seen. This behavior also correlates well with observations from U-Beam testing, in which a large horizontal crack was visible at the bottom flange-to-web interface on the inside of each test specimen that failed in horizontal shear, but a singular horizontal crack was infrequently visible on the exterior side of the interface.

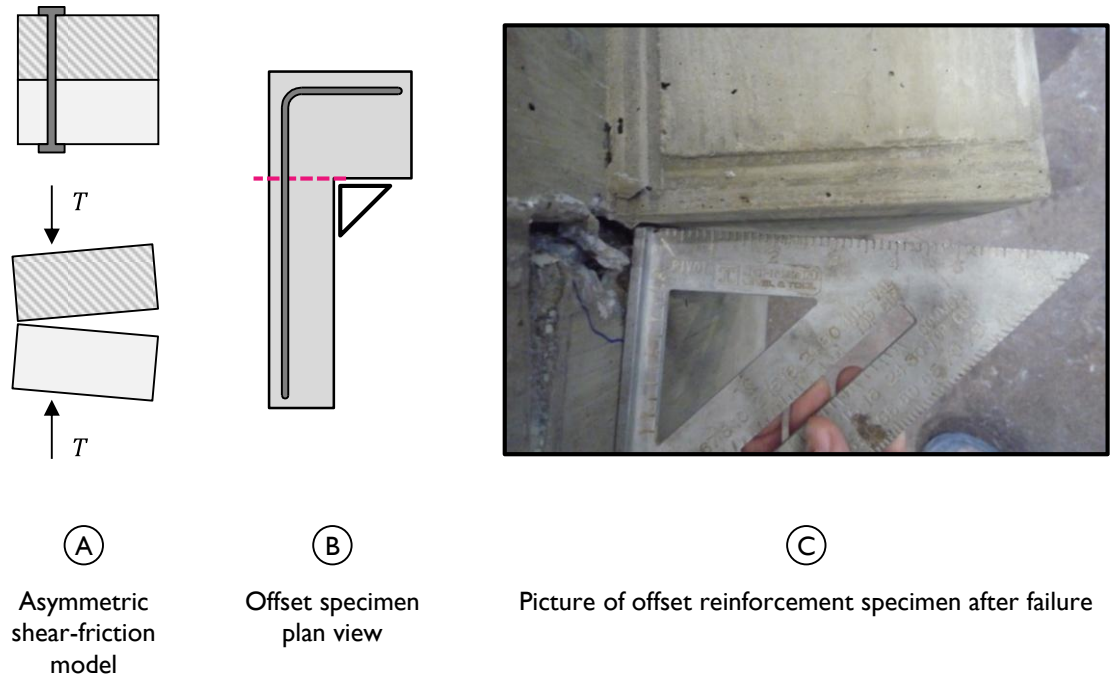

Figure 7-35: Observations of asymmetric opening of shear-friction interface.

7.8.4 Application of Findings

The results of the push-off specimen tests provide two important observations regarding U-Beam horizontal shear behavior:

1. When ignoring the effects of cohesion as is appropriate for a vertically-aligned specimen, the AASHTO shear-friction equation provide a conservative estimation for the shear strength of a specimen with geometric characteristics similar to the Texas U-Beam (average V_{test}/V_{calc} was 1.39 for the centered specimens and 1.14 for the offset specimens).
2. The location of reinforcing bars within the cross section, with regards to symmetry and cover thickness, influences the strength of the specimen (average $V_{offset}/V_{centered}$ was 0.82).

Given these observations, it is fair to conclude that the horizontal shear capacity equation, based on the AASHTO shear-friction equation, overestimates the horizontal shear strength of the Texas U-Beam bottom flange-to-web interface. This conclusion agrees

with the results of the horizontal shear calculations presented in Section 7.8.1, in which horizontal shear distress was not expected per calculation, but was observed.

Based on these results, a beam shape / reinforcement detailing factor, k_d, was set at 0.8 for the standard U-Beams with bars placed eccentrically in the shear plane. For the U-Beams fabricated with reinforcement placed more evenly across the web (B4S, B5N, and B6S), a k_d of 1.0 can be used. The U-Beam value was determined through comparison of the offset specimen failure shears to the centered specimen failure shears. When used in the horizontal shear evaluation process, the ratio of demand to capacity matches expectation, as shown in Figure 7-36.

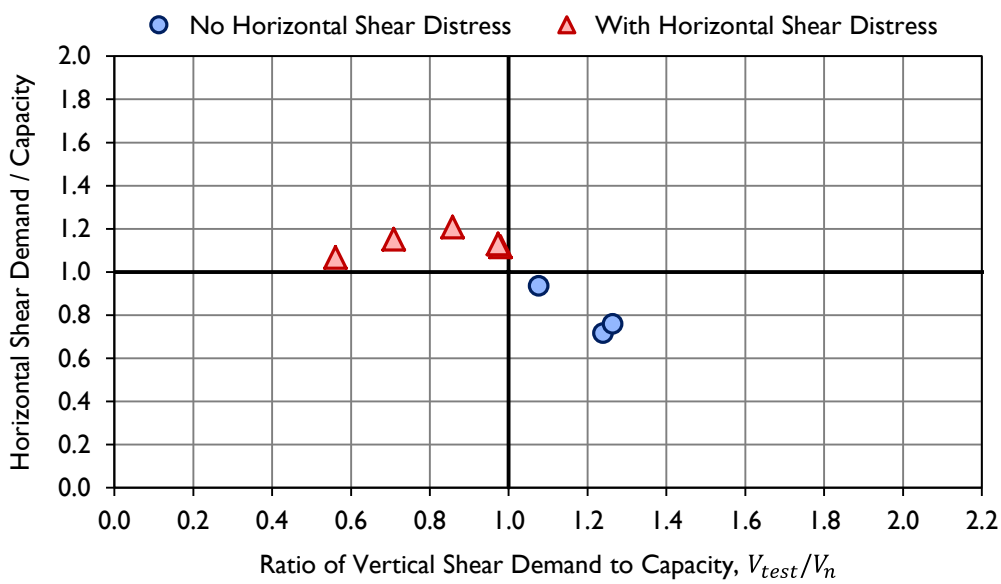

Figure 7-36: Summary of comparison between horizontal and vertical shear demand and capacity for Texas U-Beams, with correction factor in horizontal shear capacity calculation.

The average horizontal shear ratios for the two data sets (those with horizontal shear distress and those without) using the capacity equation with and without the reduction factor are given in Table 7-12. Two observations stand out from these statistics. First, the average horizontal shear ratio in each data set are markedly different when the reduction factor is included. Second, the average for each data set is on the correct side of the equality line – the expectation of horizontal shear distress matched

observations. Looking beyond the average to the individual data points, each data point falls as expected given the observations in the laboratory.

Table 7-12: Summary of average horizontal shear ratios using original and modified equations.

		Original Calculation	With Reduction Factor
Average horizontal shear demand / capacity in test specimens:	WITH horizontal shear distress	0.91	1.13
	WITHOUT horizontal shear distress	0.80	0.80

The HSR-SPR plot made from all tests in the Horizontal Shear Evaluation Database (including the eight U-Beams) is reproduced in Figure 7-37. With the inclusion of the k_d factor, the U-Beam data fall as expected.

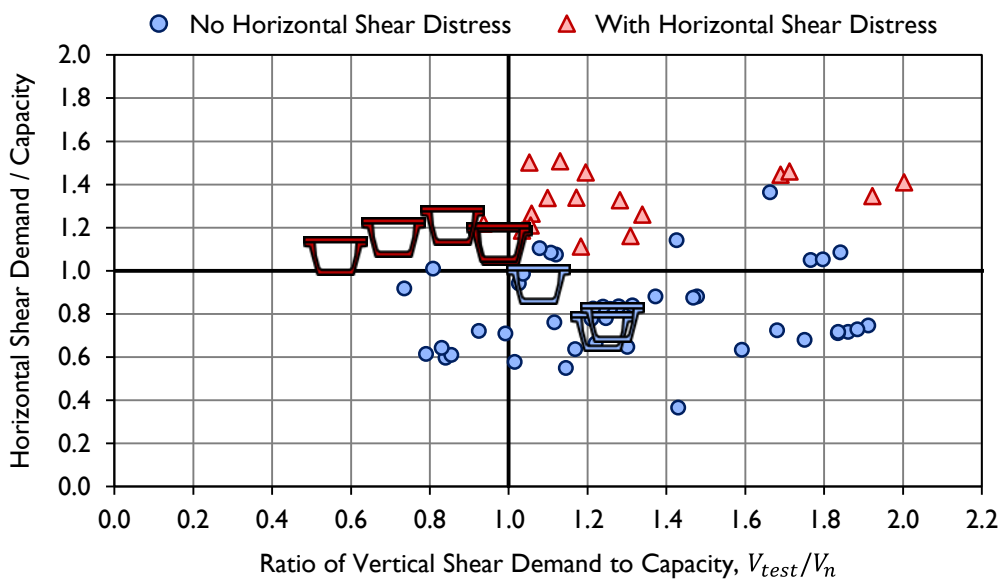

Figure 7-37: Ratio of horizontal shear demand to capacity for all points in the HSED.

Further research on the effect of cover, uneven distribution of reinforcing bars, and asymmetrical concrete sections could provide further understanding of why the Texas U-Beam does not behave similarly to other prestressed concrete I- and Box-Beams. Without further study, the use of an 0.8 reduction factor in the calculation for capacity of U-Beams with eccentrically-placed reinforcement results in conservative calculations for horizontal shear strength.

7.9 RECOMMENDATIONS FOR USE IN DESIGN

It is recommended that the method for calculating horizontal shear demand and capacity be performed as a check after a typical sectional shear analysis is completed. If horizontal shear is found to control capacity, modifications to the design should be made that will decrease the likelihood of this undesirable failure mode occurring.

The basic steps for checking horizontal shear capacity against demand during the design process are summarized here.

1. Calculate Vertical Shear Capacity

   A typical vertical shear capacity plot is shown in Figure 7-38. At each point of reinforcing bar change (located a distance labeled x_1, x_2, x_3, x_4, and x_5 from the end of the beam), the calculated capacity drops with the decrease in amount of reinforcement per unit length.

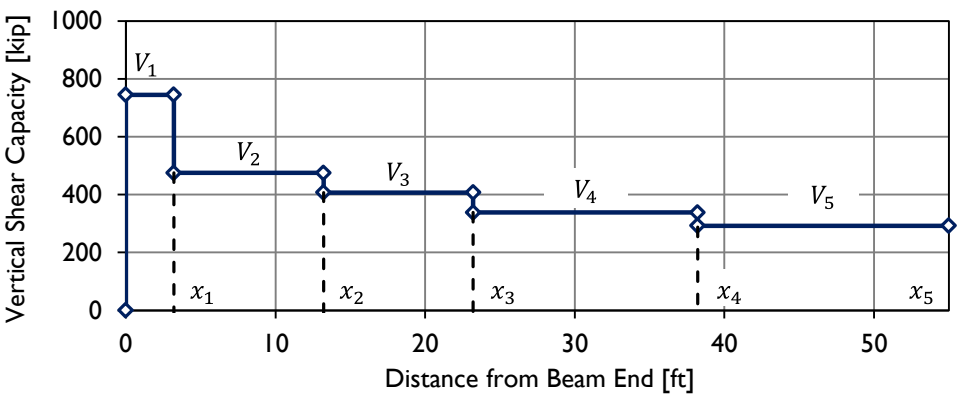

Figure 7-38: Typical vertical shear capacity plot.

2. Calculate Horizontal Shear Demand

   Equation 7-12 and 7-13 can be combined to form the following equation for use in a design beam:

$$V_{u_{hs}} = \left(\frac{V_n}{b_w d}\right) b_w l \qquad \textbf{Equation 7-16}$$

where

V_n = calculated vertical shear capacity [kip]

l = distance from centerline of bearing pad to furthest point where V_n applies

From the example vertical shear capacity plot presented above, Equation 7-16 is used five times, to calculate the demand at beam end due to a shear V_1 located a distance x_1 from beam end, V_2 at a distance x_2 from beam end, and so on through midspan (V_5 at x_5).

3. <u>Calculate Horizontal Shear Capacity</u>

   Horizontal shear capacity is calculated across regions of constant geometry and reinforcing bar spacing. These regions will correspond with constant calculated vertical shear capacity; horizontal shear capacity should be calculated from beam end to point x_1, from x_1 to x_2, and on through midspan. The capacity at any point is equal to the sum of the capacity from beam end to that point:

$$V_{ni} = \sum_{a=x_1}^{a=x_i} V_{na} \qquad \textbf{Equation 7-17}$$

   The first region of calculation for horizontal shear capacity must also consider the reduction in capacity due to the stresses induced at prestress transfer.

4. <u>Evaluate Likelihood of Horizontal Shear Failure</u>

   Once horizontal shear demand and capacity have each been found, the values are compared to determine if horizontal shear failure is likely. If, at any calculation point, the demand caused by the applied shear is less than the capacity of the beam to that point, the Horizontal Shear Ratio will exceed 1.0 and horizontal shear failure is likely.

By following the steps outlined here, a designer can confirm that the vertical shear failure expected to cause shear failure will not induce a horizontal shear force in the bottom flange-to-web interface that exceeds the horizontal shear capacity of the section. Modifications to the design – like the addition of reinforcing bars or an end block – should be taken to increase horizontal shear strength in cases where vertical shear is not the limiting case.

7.10 SUMMARY

A method for calculating the horizontal shear demand on and the horizontal shear strength of the bottom flange-to-web interface of prestressed concrete beams was presented in this chapter. A summary of the method is given here.

The horizontal shear demand is caused by bending of the beam under vertically applied loads. The magnitude of the demand can be found by estimating the horizontal shear stresses on the interface using the average shear stress through the depth of the member. The shear stress is applied over the area from centerline of bearing pad to the Ultimate Evaluation Point near the point of loading.

It is recommended to calculate horizontal shear capacity following the shear friction equation from the AASHTO LRFD Bridge Design Specifications, with an additional term that accounts for stresses induced in the reinforcing bars at prestress transfer and a reduction factor related to the beam shape and reinforcement detailing. The original AASHTO equation on which the recommended horizontal shear calculation is based was derived from the theories of shear friction and calibrated using the results of empirical testing.

This horizontal shear evaluation method was verified using the results from a series of prestressed beam shear tests from the literature. The Horizontal Shear Ratio, defined as the ratio of horizontal shear demand to capacity, was used as a metric to evaluate the accuracy of the calculation methods. An HSR greater than 1.0 indicates the demand exceeds the capacity, and a horizontal shear failure is expected. The recommended method accurately predicts whether horizontal shear damage is expected, with all inaccuracies being conservative (i.e., horizontal shear damage expected but not observed).

A method for using these calculations as a check in design was given. It is not recommended to allow horizontal shear to control the failure of a beam, as it is a brittle failure mode that has been studied much less than typical vertical shear. However, with the recommended calculation method, a designer can feel confident that horizontal shear failure will not occur at a load below the calculated vertical shear strength of the beam.

CHAPTER 8
Conclusions and Recommendations

8.1 TEXAS U-BEAMS

The Texas U-Beams were introduced into the TxDOT bridge standards in 1998, and have been heavily used across the state in the years since. The prestressed concrete beams, meant to replace two AASHTO Type IV beams in high-visibility interchanges, had not been load-tested prior to the start of this study.

8.2 PROJECT MOTIVATION

The major goals of this project were to establish the response of the Texas U-Beam (a) to prestressing forces at prestress transfer and (b) under shear-critical loads. Codified equations exist to estimate the stresses induced in reinforcing bars at prestress transfer, and to estimate the shear capacity of the beam. These equations have been shown to be conservative when compared to results from the literature (Dunkman, 2009; Nakamura, 2011).

The majority of tests in the literature, however, were conducted on small rectangular and I-shaped beams. The equations were generally calibrated using these same small specimens with simple geometry. The Texas U-Beam, massive in size, typically heavily prestressed, and with unusual geometry does not resemble these beams. Prior to performing a full investigation of the behavior of the beam, it was not clear whether the behavior of the Texas U-Beam would resemble that seen in the simpler beams present in the literature.

To highlight the difference between the Texas U-Beam and previously-tested beams, consider shear area ($b_w d$). The University of Texas Prestressed Concrete Shear Database (Nakamura, 2011) contains 1688 shear tests from the literature, from 99 sources, reported between 1954 and 2010. The largest shear area reported was 543 in.^{2}. The standard Texas U-Beam has a shear area of 605 in.^{2}. The modified U-Beam tested in

this program (Beam 4) had a shear area of 940 in.^{2}. While the measured shear capacity of specimens in the literature generally exceeded the capacity calculated following existing design equations, the appropriateness of the equation had never been confirmed for a beam the size of the Texas U-Beam.

Similar observations can be made when comparing data from the literature taken at prestress transfer. Dunkman (2009) reported on fifty-three test specimens containing internal instrumentation on reinforcing bars. Of these beams, forty-seven were I-shaped and six were inverted-Ts. While some specimens were as deep or deeper than the U-Beam, none contained two webs. The prestressing force applied to these beams was less than 2000 kip. A standard U-Beam with three full rows of fully-stressed 0.5-in. prestressing strands will be loaded with over 2300 kip of prestressing force. The beams monitored in this program were loaded up to 2400 kip of force at prestress transfer.

The tests reported in this dissertation expand the extent of information available in the literature. The test specimens are some of the biggest and most heavily prestressed beams ever tested, yet are similar to beams in service across the state of Texas. As more U-Beams are constructed in Texas and the design is used in exact or modified form in other states, the need for confidence in the appropriateness of the design equations grows.

8.3 PROJECT SUMMARY

The goals of this project were met through the fabrication of eight full-scale Texas U54 prestressed concrete beams. Eight end-regions were instrumented internally and monitored at prestress transfer; eleven end regions were load-tested.

In Phase I of shear testing, six tests were performed on beams containing standard reinforcement; in five of these tests, weakness of the bottom flange-to-web interface initiated a horizontal shear failure at loads below the calculated vertical shear capacity. To begin Phase II, two beams were fabricated containing three modified reinforcement and geometric designs, with the goal of strengthening the interface to a point where the calculated shear capacity could be met. Two of the end regions were sufficiently strengthened: horizontal shear damage was not seen, and the failures occurred at shears

exceeding the calculated shear capacities. The best features of each were combined into a recommended new standard design. The experimental study concluded with the implementation of the recommended design in two test specimens, one squared and one skewed to 45°. The vertical shear capacity of these beam test regions exceeded calculated capacity (found using the AASHTO General Procedure) by 27 and 65%.

Parallel to the experimental study, a method was formulated to approximate the horizontal shear demand on and horizontal shear strength of the bottom flange-to-web interface of prestressed concrete girders. The method was verified using sixty-one tests from the literature, as well as eight U-Beam tests.

8.4 RECOMMENDED NEW STANDARD DESIGN

When testing modifications to the U-Beam standard design, it was desired that the new design be constructable and allow web-shear failure to occur prior to a horizontal shear failure, and at loads above the calculated vertical shear capacity. The major changes successfully implemented in Beams 6 and 7 and recommended for use in the standard are summarized here. These changes are highlighted in Figures 7-1 and 7-2, with side-by-side comparisons of the existing and recommended designs.

- Stirrups

  Position #4 R-bars at 4 in. from beam end to 8'-3" (an increase of two feet).

- Supplementary Steel

  Add two #5 L-bars in each web at each R-bar location from beam end to 8'-3".

- Confinement

  Add #4 C-bars, paired with R-bars, from beam end to 8'-3".

- End Blocks

  Increase the range of lengths for a standard end block from [1'-6" to 2'-0"] to [2'-6" to 3'-0"] for beams skewed 0 to 30°. For beams skewed beyond 30°, set the end block length range to [3'-0" to 3'-6"]. Lengthen the legs of bars D and DS and add bars DE. Include a second plane of bars F.

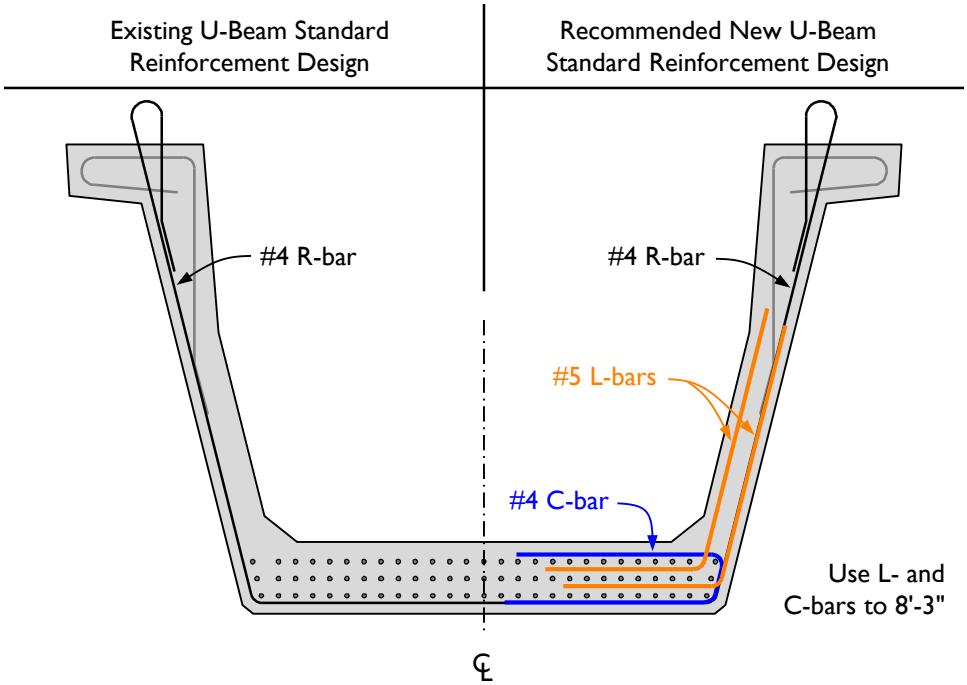

Figure 8-1: Existing and recommended U-Beam standard reinforcement.

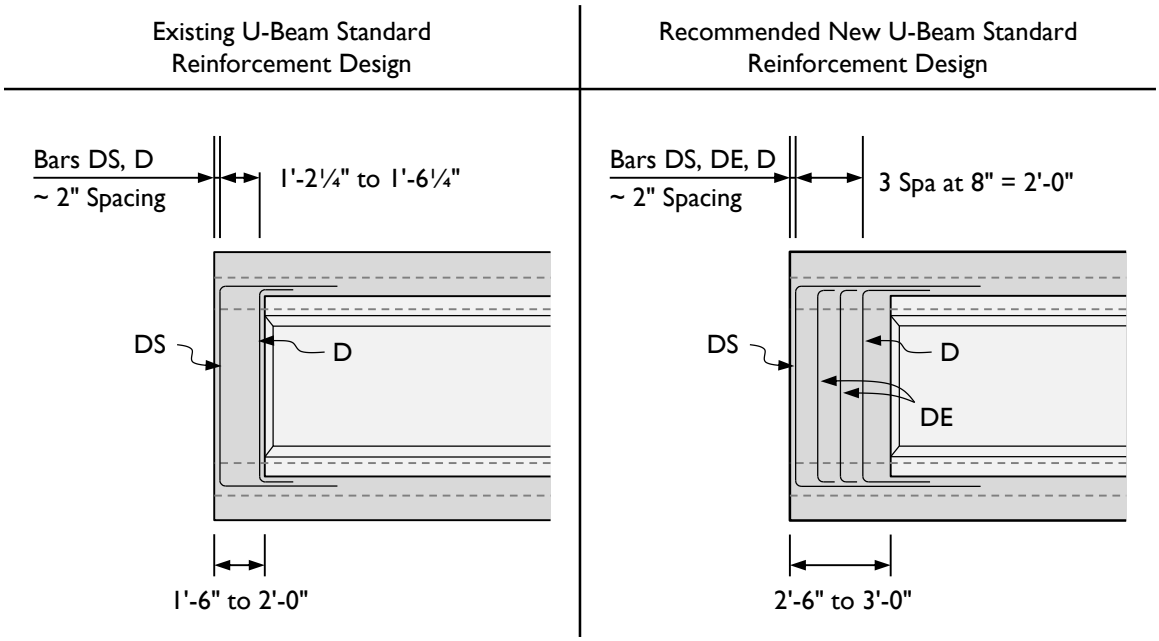

Figure 8-2: Existing and recommended U-Beam end-block geometry and reinforcement.

The difference in reinforcement crossing the bottom flange-to-web interface in the current standard and the recommended new standard is shown in Figure 8-3. While the current design contains 1% vertical bottom flange-to-web interface reinforcement away

from the end block, the new design would contain 4%. This amount of steel is much closer to that seen in the end region of the Tx Girder (6%), a beam seen to fail in horizontal shear, but only after surpassing the calculated vertical shear capacity.

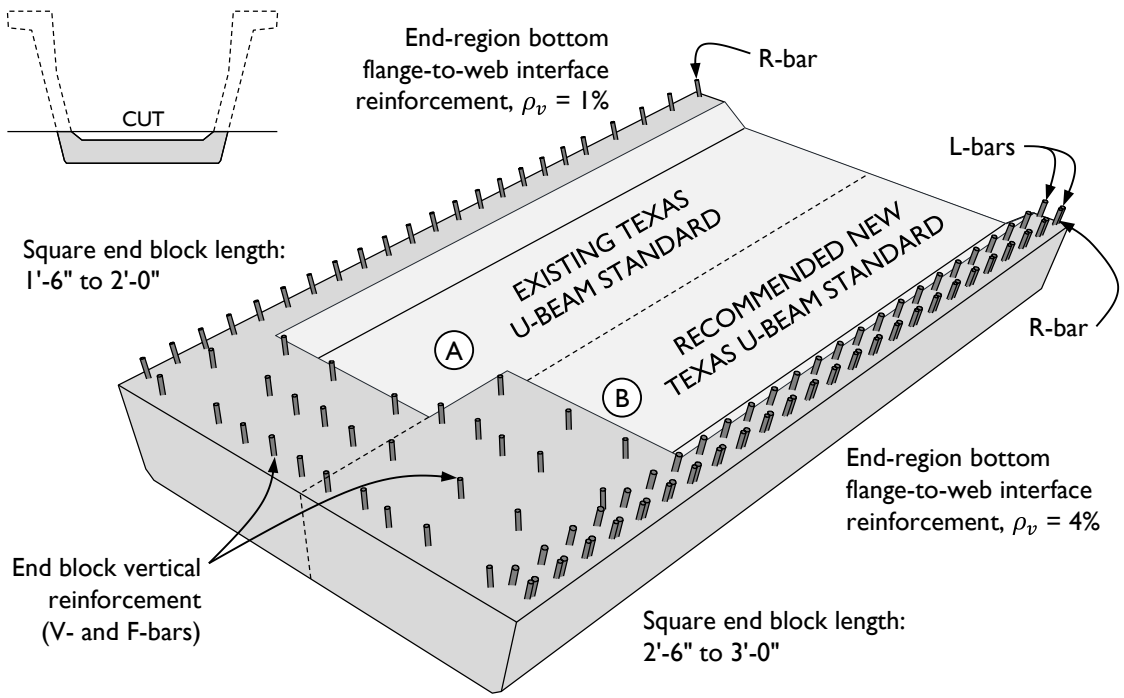

Figure 8-3: (A) Existing bottom flange-to-web interface reinforcement and (B) recommended new reinforcement.

8.5 CONCLUSIONS

The conclusions from this study are broken into three sections, reflecting the different major aspects of study pursued.

8.5.1 Behavior at Prestress Transfer

Eight end-regions were instrumented and studied at prestress transfer. The magnitude and extent of induced stresses in reinforcing bars and crack size and location were recorded. The following conclusions were drawn:

- The current standard end-block and web reinforcement used in the Texas U-Beam is sufficient for controlling stresses and cracking at prestress transfer.

- Debonding of strands at the end of the beam, as is common practice to reduce top- and bottom-fiber stresses at transfer, significantly reduced transverse bar stresses at beam end.
- No vertically-oriented cracks were observed on the end face of the beams, indicating transverse stresses across the width of the beam were small.
- Negligible stresses were induced in the beams beyond 18 in. from beam end ($h/3$). No significant stresses were measured in the bars expected to be stressed most heavily during shear testing.

8.5.2 Vertical Shear Performance

A total of eleven load tests were performed, resulting in five horizontal shear failures, two flexure-shear failures, two web-crushing failures, and one combined web-crushing / horizontal shear failure. One test region was not loaded to failure. The following conclusions were made from the collected data and observations of behavior.

- The existing Texas U-Beam standard design has a critical weakness along the bottom flange-to-web interface that can control failure and may occur at loads well below the calculated shear capacity. The strength can be increased using additional reinforcing bars across the interface and by lengthening the beam end block.
- Loads applied above the webs of the Texas U-Beam are distributed to the two webs evenly in square-ended beams. In beams with one end square and one end skewed to the maximum allowed, the shorter web took 60% of the load in the skewed end; at the square end, loads were distributed evenly.
- Despite the physical separation that exists between the webs of the Texas U-Beam, the assumption that the two webs work as one is acceptable for use in shear capacity calculations, even in beam ends with extreme skew.
- Bearing condition influenced the anchorage of the prestressing strands, with strands closest to the webs being better anchored at the beam end seated on two bearing pads. It was concluded that given the distance from the bearing

pad to the webs, a centrally-placed bearing pad resulted in a more critical state of loading than two smaller bearing pads.

- The four beams that failed in typical web-shear modes did so at loads exceeding the calculated capacity found following three vertical shear capacity calculation methods: ACI Detailed Method (2008), AASHTO General Procedure (2010), and AASHTO Segmental Procedure (2010). The level of conservatism seen in these three beam tests was similar to that seen in 170 tests previously reported in the literature and summarized by Nakamura (2011). These test-regions, each seated on a single bearing pad and one skewed to the maximum allowed by TxDOT, are considered to encompass the worst cases with regard to load distribution and shear capacity.
- Diagonal cracking was not observed in any tested U-Beam at loads below 20% of the failure capacity. Crack widths of 0.010 in. corresponded to loads of approximately 40% of the capacity. Diagonal cracks 0.030 in. wide were seen at loads within 10% of the capacity.
- No influence from stresses induced at prestress transfer was seen on the vertical shear strength.

8.5.3 Horizontal Shear Evaluation

A method for evaluating the likelihood of a horizontal shear failure was presented. It is recommended that this method be used as a check to confirm that the vertical shear capacity can be met prior to horizontal shear failure occurring. Conclusions from the study on horizontal shear in prestressed beams are given here.

- Especially in heavily-prestressed beams without supplementary steel (L-bars in Figure 8-1) in the end-region, horizontal shear failure can occur at loads below the calculated vertical shear capacity.
- The magnitude of horizontal shear stress at the bottom flange-to-web interface can be approximated using the average vertical shear stress in the section. The demand at beam end is calculated as:

$$V_{u_{hs}} = v_{hs} b_w l_{crit}$$ **Equation 8-1**

where

$V_{u_{hs}}$ = horizontal shear demand [kip]

v_{hs} = horizontal shear stress, equal to average vertical stress [kip]

b_w = web width [in.]

l_{crit} = distance from centerline of support to the point of interest [in.]

- The horizontal shear capacity of the bottom flange-to-web interface can be approximated following the equations for shear friction, with two reduction factors: first, prestress transfer must be considered, as the available capacity of the reinforcing bars decreases. Second, bar placement in the shear plane must be considered, as bars placed off-center do not clamp the sections together as evenly or as effectively as symmetrically-placed bars. The equation for capacity is:

$$V_{ni} = k_d\left[cA_{cv} + \mu\left(A_{vf} f_y - 0.04 P_{PS}\right)\right]$$ **Equation 8-2**

where

V_{ni} = horizontal shear capacity [kip]

k_d = factor related to reinforcement detailing and beam geometry, equal to 0.8 for U-Beams with reinforcement following the existing standard and 1.0 for I-Beams, Box-Beams, and U-Beams with reinforcement well-distributed as recommended in this dissertation.

c = cohesion factor, as specified in Article 5.8.4.3 of AASHTO LRFD (2010) [ksi]

A_{cv} = area of concrete considered to be engaged in interface shear transfer [in.^{2}]

μ = friction factor, as specified in Article 5.8.4.3 of AASHTO LRFD (2010)

A_{vf} = area of interface shear reinforcement crossing the shear plane within the area A_{cv} [in.^{2}]

f_y = specified yield strength of reinforcement [ksi], limited to 60 ksi

P_{PS} = force of prestressing transferred to the beam within the region of interest [kip]

8.6 RECOMMENDATIONS FOR FURTHER STUDY

Two recommendations for further study are presented here.

8.6.1 Existing U-Beam Analysis and Retrofit

The shear tests performed in this study uncovered a weakness in the standard Texas U-Beam. The strength of the bottom flange-to-web interface was insufficient and the beams failed at shears below the calculated vertical shear capacity. A recommended new standard design has been proposed.

The current U-Beam design has been in the TxDOT bridge standards since 2006, with a design containing less reinforcement first introduced in 1998. The beam has been used in bridges across the state since. These in-service bridges contain the same detailing that was found to be insufficient during the laboratory tests presented here. A study of these existing bridge beams is warranted to determine the likelihood of a horizontal shear failure occurring at loads below the expected capacity. In cases where horizontal shear failure is expected to control behavior, a strengthening system should be tested and installed to allow a typical shear failure mode to occur first.

Even with further understanding of the horizontal shear failure mode, it is not recommended to use a design in which horizontal shear is expected to control behavior. To that end, it has been confirmed that Texas U-Beams fabricated containing the recommended new standard reinforcing bars will not fail in horizontal shear prior to surpassing the calculated vertical shear capacity. The same cannot be said for U-Beams containing reinforcement following the existing standard design.

8.6.2 Effect of Reinforcement Position on Shear-Friction Strength

To better understand the derivation of the shear-friction equation, and understand why its use overestimated capacity for horizontal shear strength in U-Beams, an examination of the literature was performed. The specimens reported contained

reinforcement distributed evenly across the shear plane, typically consisting of two-legged closed stirrups. This reinforcement geometry is similar to that seen at the bottom flange-to-web interface of an I-Beam. The eccentric placement of reinforcement as can be seen at the bottom flange-to-web interface of the U-Beam had not been studied.

A total of four push-off specimens were tested with a single layer of reinforcement passing through the shear plane. In two of the specimens, the bars were placed centered in the shear plane; in the other two, the bars were offset towards one side. The measured capacity of the specimens with offset bars was approximately 80% that of the specimens with centered bars. Including a reduction factor of 0.8 for the U-Beams fabricated with eccentric reinforcement crossing the bottom flange-to-web interface (beams containing only R-bars) resulted in conservative and accurate evaluations of horizontal shear strength.

A more extensive study of the effect of eccentric reinforcement on shear-friction strength would continue to fill the gap in existing knowledge. It is possible that asymmetric concrete geometry could affect strength as well. The tests performed during this study were tailored towards better understanding the behavior of a specific beam geometry; a comprehensive study could prove useful in horizontal shear strength calculations for other prestressed beam shapes, but also in other structures in which the shear-friction equations are commonly used, including corbels and beam-to-wall connections.

APPENDIX A

U-Beam Information and Drawings

A.1 2006 PRESTRESSED CONCRETE U-BEAMS

Five sheets from the TxDOT Bridge Standards are provided on the following pages. These standard drawings were downloaded from the Texas Department of Transportation bridge standard website (http://www.dot.state.tx.us/insdtdot/orgchart/cmd/cserve/standard/bridge-e.htm).

- ubstde01.dgn: Prestressed Concrete U-Beam Details, Sheet 1 of 3
  Contains plan, elevation, and typical section views for U40 and U54 beams.
- ubstde01.dgn: Prestressed Concrete U-Beam Details, Sheet 3 of 3
  Contains end-region details and section views for straight and skewed beams.
- ubstde01.dgn: Prestressed Concrete U-Beam Details, Sheet 3 of 3
  Contains reinforcing bar shapes and geometries.
- ubstde02.dgn: Elastomeric Beamring and Bearing Seat Details -- Prestressed Concrete U-Beams
  Contains details of standard beam support system.
- ubstde04.dgn: Prestressed Concrete U-Beams (Design Data)
  Contains prestressed strand positions and general notes on the beam standard.

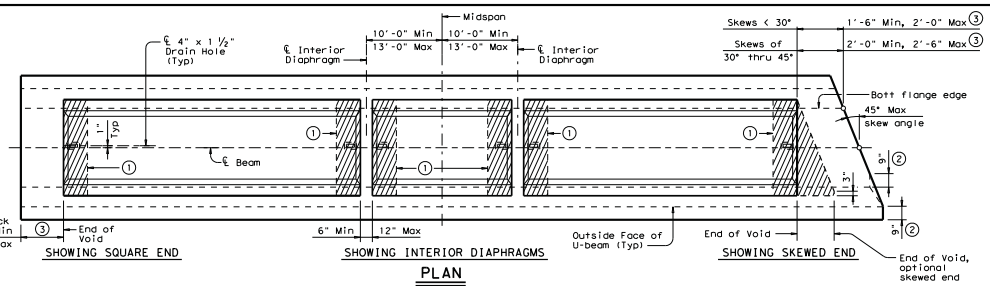

SHOWING SQUARE END — SHOWING INTERIOR DIAPHRAGMS — SHOWING SKEWED END

PLAN

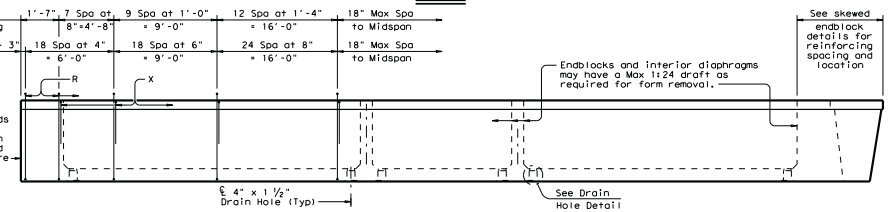

SHOWING SQUARE END — SHOWING INTERIOR DIAPHRAGMS — SHOWING SKEWED END

ELEVATION

1. Polystyrene may be used at ends of inside forms (12" maximum in length except at optional skewed ends) and left in place. Offset drain holes if not removing polystyrene.
2. For skews greater than 15 degrees, breakback both top and bottom flanges 9" as shown. Provide a smooth transition between top and bottom flange breakbacks. Adjust reinforcement as necessary to maintain minimum clear cover.
3. Minimum and maximum endblock dimensions apply throughout the endblock depth. This dimension control applies to the narrowest portion of endblocks at skewed beam ends.
4. Required for beams that will support cantilevered slab overhang formwork and exterior beams only.
5. Optional Bar U for beams requiring Bars P.
6. 5 ½" for normal Bars R.
   5 ½" - 6 ½" Max for Bars R at skewed beam ends.
7. Provide Bars E (#5 x 15'-0") at beam ends.

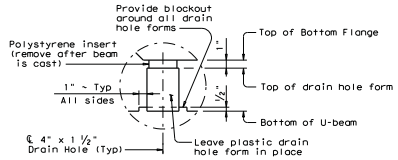

DRAIN HOLE DETAIL

Provide ¼" clear between strands and drain hole form.

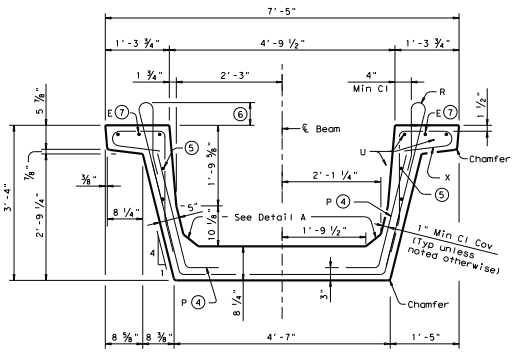

TYPICAL SECTION - U40

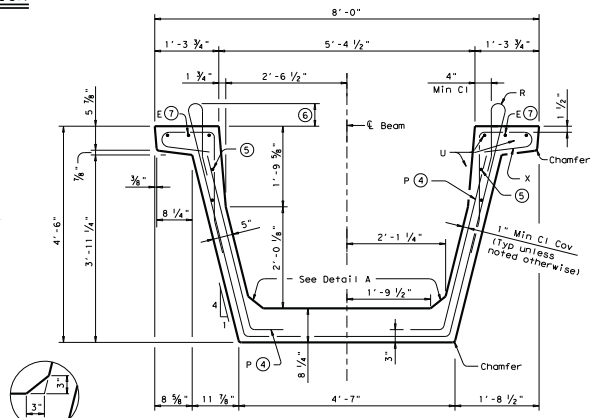

TYPICAL SECTION - U54

DETAIL A

TABLE OF BEAM SECTION PROPERTIES

Beam Type	Y_t (in.)	Y_b (in.)	Area (in.²)	I (in.⁴)	Weight (plf)⑧
U40	23.66	16.30	979.9	183,108	1021
U54	31.58	22.36	1120.0	403,020	1167

⑧ Weights shown assume a concrete density of 150 pcf and are for the typical section only. These weights do not include weight of diaphragms or endblocks.

HL93 LOADING — SHEET 1 OF 3

Texas Department of Transportation
Bridge Division

PRESTRESSED CONCRETE U-BEAM DETAILS

UBD

FILE: ubsta01.dgn	DN: TxDOT	CK: TxDOT	DW: TxDOT	CK: TxDOT
©TxDOT July 2006	DISTRICT	FEDERAL AID PROJECT		SHEET
REVISIONS	COUNTY	CONTROL	SECT	JOB	HIGHWAY

DISCLAIMER:
The use of this standard is governed by the "Texas Engineering Practice Act". No warranty of any kind is made by TxDOT for any purpose whatsoever. TxDOT disclaims the suitability of this standard for any purpose other than its use. TxDOT assumes no responsibility for incorrect results or damages resulting from its use.

LEVELS DISPLAYED
PATH:

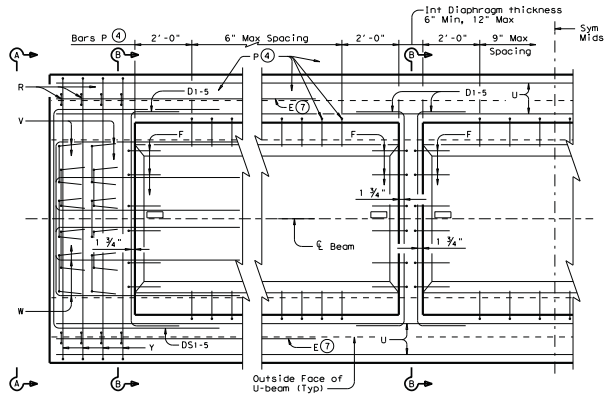

SHOWING SQUARE END

SHOWING INTERIOR DIAPHRAGM

PLAN

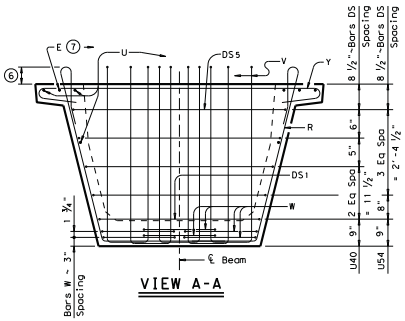

VIEW A-A

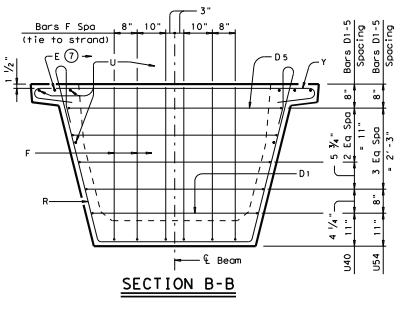

SECTION B-B

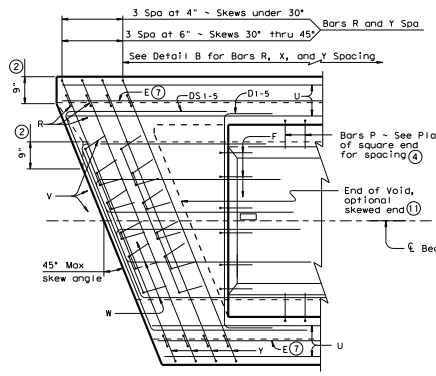

PLAN ~ SKEWED END

(Skews thru 45°)

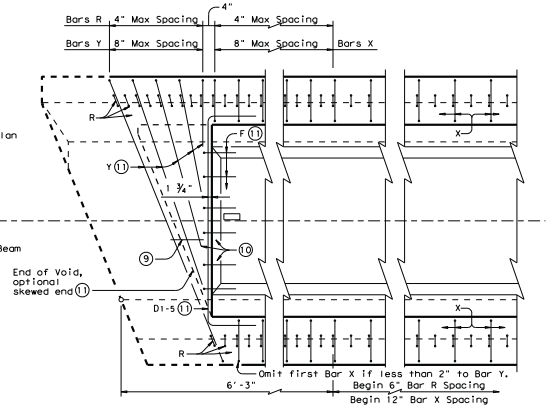

DETAIL B

(Bars DS, E, P, U, V and W not shown for clarity)

(2) For skews greater than 15 degrees, breakback both top and bottom flanges 9" as shown. Provide a smooth transition between top and bottom flange breakbacks. Adjust reinforcement as necessary to maintain minimum clear cover.

(4) Required for beams that will support cantilevered slab overhang formwork and exterior beams only.

(6) 5 ½" for normal Bars R.
5 ½" - 6 ½" Max for Bars R at skewed beam ends.

(7) Provide Bars E (#5 x 15'-0") at beam ends.

(9) Add support bars for Bars Y as necessary.

(10) Cut Bars Y and Bars R as necessary to provide 2" clear between adjacent bars.

(11) When fabricating beams using the optional skewed end, replace Bars Y that are shown to be cut with Bars X, adjust location of Bars F, and adjust Bars D1-5 in shape and location. Shop drawings must show details used.

DISCLAIMER:
The use of this standard is governed by the "Texas Engineering Practice Act". No warranty of any kind is made by TxDOT for any purpose whatsoever. TxDOT assumes no responsibility for the accuracy of this standard or for any other formats or for incorrect results or damages resulting from its use.

LEVELS DISPLAYED

PATH:

HL93 LOADING — SHEET 2 OF 3

Texas Department of Transportation
Bridge Division

PRESTRESSED CONCRETE U-BEAM DETAILS

UBD

FILE: ubsta01.dgn	DN: TxDOT	CK: TxDOT	DW: TxDOT	CK: TxDOT
©TxDOT July 2006	DISTRICT	FEDERAL AID PROJECT		SHEET
REVISIONS				
	COUNTY	CONTROL	SECT	JOB	HIGHWAY

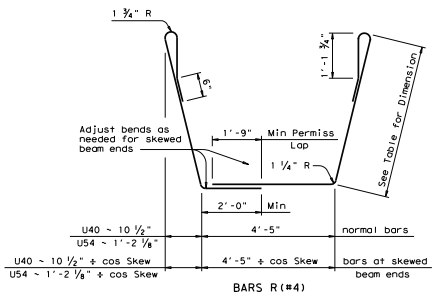

BARS R(#4)

BAR R DIMENSION		
Skew Angle	Beam Type	
	U40	U54
0° thru 15°	3'-9 ¼"	4'-11 ½"
15° thru 30°	3'-9 ½"	5'-0"
30° thru 45°	3'-10 ¼"	5'-1"

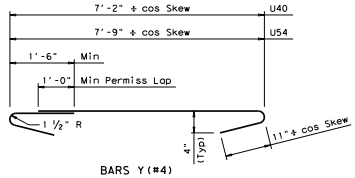

BARS Y(#4)

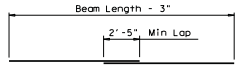

BARS U(#5)

Bars U may be placed with multiple segments, provided no segment is less than 10 ft in length and 40 ft Min C-C splices.

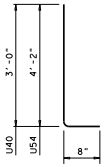

BARS F(#4)

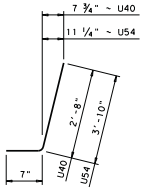

BARS P(#4)

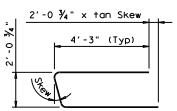

BARS W(#4)

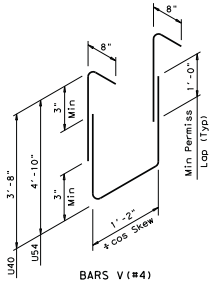

BARS V(#4)
(ISOMETRIC VIEW)

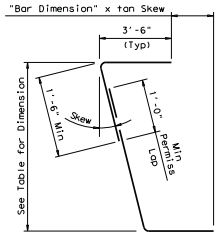

BARS DS1-5 (#4)

BAR DS DIMENSION		
Bar	Beam Type	
	U40	U54
DS1	4'-8"	4'-8"
DS2	4'-11"	5'-0"
DS3	5'-2"	5'-5"
DS4	5'-4 ¼"	5'-9 ½"
DS5	5'-6 ½"	6'-1 ¼"

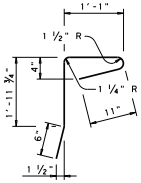

BARS X(#4)

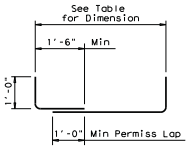

BARS D1-5 (#4)

BAR D DIMENSION		
Bar	Beam Type	
	U40	U54
D1	4'-9"	4'-9"
D2	4'-11¼"	5'-1"
D3	5'-2"	5'-5 ½"
D4	5'-4"	5'-10"
D5	5'-6 ½"	6'-1 ¼"

GENERAL NOTES:

Designed according to AASHTO LRFD Specifications.

Details are provided for skew angles up to 45 degrees.

Concrete must be Class H. Use Class H (HPC) if required elsewhere in plans.

All reinforcing steel must be Grade 60. An equal area of welded wire reinforcement, conforming to ASTM A 497, may be substituted for Bars R, P, X and Y.

Reinforcing steel dimensions and bend radii are shown to bar centerlines.

Provide a minimum of 1" clear cover to all reinforcing steel unless shown otherwise.

Chamfer all acute corners for skews over 20 degrees. Provide ¾" chamfer or 1 ⅜" radius at all corners noted to require a chamfer.

Horizontal form joints on exterior forms are not permitted.

Shop drawings can be prepared with horizontal skews rounded to nearest ¼ degree and beam end vertical batter rounded to the nearest ¼". These shop drawing tolerances are in addition to the fabrication tolerances listed in Item 424, "Precast Concrete Structures (Fabrication)".

DISCLAIMER:
The use of this standard is governed by the "Texas Engineering Practice Act". No warranty of any kind is made by TxDOT for any purpose whatsoever. TxDOT disclaims the suitability of this standard for any purpose other than that for which it is created. TxDOT assumes no responsibility for incorrect results or damages resulting from its use.

HL93 LOADING — SHEET 3 OF 3

Texas Department of Transportation
Bridge Division

PRESTRESSED CONCRETE U-BEAM DETAILS

UBD

FILE: ubsta01.dgn	DN: TxDOT	CK: TxDOT	DW: TxDOT	CK: TxDOT
©TxDOT July 2006	DISTRICT	FEDERAL AID PROJECT		SHEET
REVISIONS				
	COUNTY	CONTROL	SECT	JOB	HIGHWAY

PATH:
LEVELS DISPLAYED

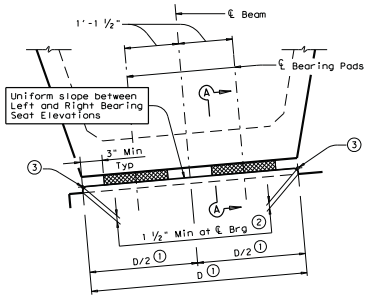

BEARING SEAT DETAIL

Looking up-station with two-pad condition.

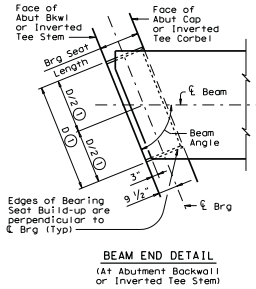

BEAM END DETAIL
(At Abutment Backwall or Inverted Tee Stem)

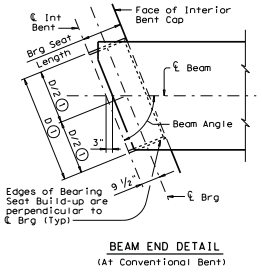

BEAM END DETAIL
(At Conventional Bent)

BEARING DIMENSIONS

BEARING SEAT DIMENSION "D" 4	
BEAM ANGLE	"D"
75° + thru 90°	4'-6"
60° + thru 75°	5'-0"
45° thru 60°	5'-6"

1. Measured along ℄ of Bearing.
2. Reinforce bearing seat build-ups greater than 3" high with #4 bars at 12" Max Spa as per Item 420, "Concrete Structures".
3. See Estimated Quantities and Bearing Seat Elevations sheet for right and left elevations and locations.
4. Unless noted otherwise in the plans.
5. Locate permanent mark here.
6. Fabricated pad top surface slope must not vary from plan bearing pad taper by more than $\left(\frac{0.0625"}{\text{Length}}\right)$(IN/IN).
7. Place 0.105" thick steel laminates parallel to the bottom surface of the pad, except the top laminate(s) may be sloped to satisfy maximum and minimum thickness criteria for tapered elastomeric layers.
8. Indicate BEARING TYPE on all pads. For tapered pads, locate BEARING TYPE on the high side. The Fabricator must include the value of "N" (amount of taper in ⅛" increments) in this mark.
   Examples: N=0, (for 0" taper)
   N=1, (for ⅛" taper)
   N=2, (for ¼" taper)
   (etc.)

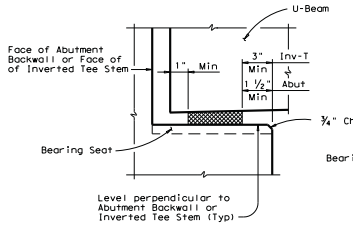

AT ABUTMENT OR INVERTED TEE BENT

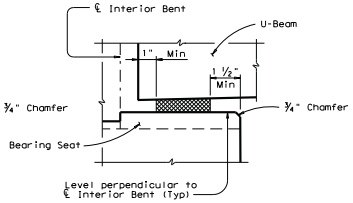

AT CONVENTIONAL BENT

SECTION A-A

GENERAL NOTES:
Shop drawings for approval are required.
Finish Bearing Surface with a wood float finish. Bearing Surface must be clean and free of all loose material before placing Bearing Pads.
For Transition Bents with backwall, the beams and elastomeric bearing pads must receive the same treatment as shown for Abutments.
See Bearing Pad Taper Report sheet for Fabricator's Report of bearing pad taper.
A bearing layout which identifies location and orientation of all bearings will be developed by the bearing fabricator. Permanently mark each bearing in accordance with the bearing layout. Provide a copy of the bearing layout to the Engineer.
Cost of furnishing and installing elastomeric bearings is included in unit price bid for "Prestressed Concrete U-Beams".

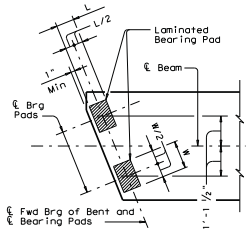

TWO-PAD DETAIL
Type U2-"N" Bearing

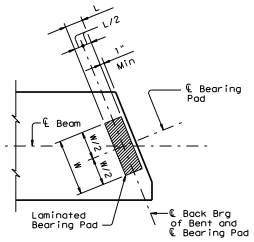

ONE-PAD DETAIL
Type U1-"N" Bearing

BEARING PAD DETAILS

Place one bearing at forward station beam end.
Place two bearings at back station beam end.

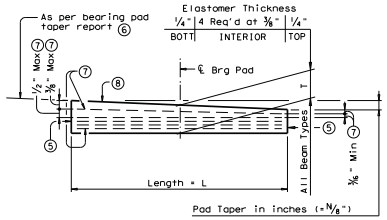

LAMINATED BEARING PAD

(50 DUROMETER)

TABLE OF ELASTOMERIC BEARING PAD DIMENSIONS (ALL U-BEAM TYPES)					
One-Pad (Ty U1-"N") 8			Two-Pad (Ty U2-"N") 8		
W	L	T	W	L	T
32"	9"	2 ½"	16"	9"	2 ½"

Note: The use of Polyisoprene (natural rubber) for the manufacture of bearing pads is not permitted.

HL93 LOADING

Texas Department of Transportation
Bridge Division

ELASTOMERIC BEARING AND BEARING SEAT DETAILS
PRESTR CONC U-BEAMS

UBEB

FILE: ubsta02.dgn	DN: TxDOT	CK: TxDOT	DW: TxDOT	CK: TxDOT
©TxDOT July 2006	DISTRICT	FEDERAL AID PROJECT		SHEET
REVISIONS				
	COUNTY	CONTROL	SECT	JOB	HIGHWAY

DISCLAIMER:
The use of this standard is governed by the "Texas Engineering Practice Act". No warranty of any kind is made by TxDOT for any purpose whatsoever. TxDOT disclaims the suitability of this standard for any purpose on any other formats or for incorrect results or damages resulting from its use.

LEGEND:
PATH:

STRUCTURE	DESIGNED BEAMS (STRAIGHT STRANDS)																							OPTIONAL DESIGN			
	SPAN NO.	BEAM NO.	BEAM TYPE	PRESTRESSING STRANDS							DEBONDED STRAND PATTERN PER ROW											CONCRETE		DESIGN LOAD COMP STRESS (TOP ℄) (SERV I) fct(ksi)	DESIGN LOAD TENSILE STRESS (BOTT ℄) (SERV III) fcb(ksi)	REQUIRED MINIMUM ULTIMATE MOMENT CAPACITY (STRGTH I) (ft-kips)	LIVE LOAD DISTRIB FACTOR ①
				STRAND PATTERN NO.	TOTAL NO.	SIZE (in)	STRGTH fpu (ksi)	"e" ℄ (in)	"e" END (in)	TOT NO. DEB	DIST FROM BOTTOM (in)	NO. OF STRANDS TOTAL	NO. OF STRANDS DE-BONDED	NUMBER OF STRANDS DEBONDED TO (ft from end) 3	6	9	12	15					MINIMUM RELEASE STRGTH f'ci (ksi)	MINIMUM 28 DAY COMP STRGTH f'c (ksi)				

TYPE U54

TYPE U40

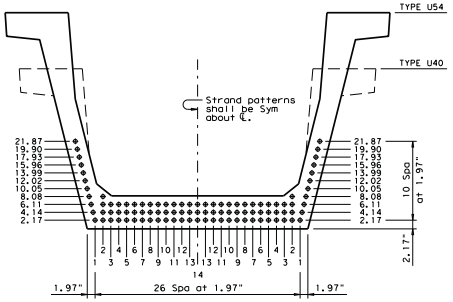

TxDOT TYPE U54 & TYPE U40 BMS

GENERAL NOTES:

Designed in accordance with AASHTO LRFD Specifications.

All concrete must be Class H. Use Class H (HPC) if required elsewhere in plans. All reinforcing bars shall be Grade 60.

When shown on this sheet, the Fabricator has the option of furnishing either the designed beam or an approved optional beam design. All optional design submittals and shop drawings must be signed, sealed and dated by a registered Professional Engineer.

Optional designs must have a calculated residual camber equal to or greater than that of the designed beam.

Prestress losses for the designed beams have been calculated for a relative humidity of percent. Optional designs must likewise conform.

Locate strands for the designed beam as low as possible on the 1.97" grid system. Fill row "2.17", then row "4.14", then row "6.11", etc., beginning each row in the "1" position and, distributing uniformly as practical, working inward until the required number of strands is reached. All strands, including those in the web, must be adequately tied to reinforcing steel, bar supports, or other devices to prevent displacement during concrete placement.

Do not debond strands in position "1". Distribute debonded strands equally about the vertical centerline. Debonded lengths must decrease working inward, with debonding staggered in each row.

Encase debonded strands in plastic tubing along entire debonded length, and seal ends of tubing with waterproof tape. Split plastic tubing may be used provided the seam of the tubing is sufficiently sealed with waterproof tape to prohibit grout infiltration. Wrapping of strands with tape to provide debonding is not permitted.

Full-length debonded strands are not permitted in strand positions 1 and 2. If placing concrete in two stages, double wrap all full-length debonded strands in row "2.17" and internal vibrator diameter cannot exceed 1 1/8" diameter for first stage. Full-length debonding must comply with Item 426.4.F.4.

Strands for the designed beam must be low relaxation strands pretensioned to 75 percent of fpu each.

The grid pattern for the strands is based on exact conversions from a metric grid spacing of 50mm.

① Portion of full HL 93

HL93 LOADING

Texas Department of Transportation
Bridge Division

PRESTRESSED CONCRETE U-BEAMS
(DESIGN DATA)

UBND

FILE: ubstde04.dgn	DN: TxDOT	CK: TxDOT	DW: TxDOT	CK: TxDOT
©TxDOT July 2006	DISTRICT	FEDERAL AID PROJECT		SHEET
REVISIONS	COUNTY	CONTROL	SECT	JOB	HIGHWAY

DISCLAIMER:
The use of this standard is governed by the Texas Engineering Practice Act. No warranty of any kind is made by TxDOT for any purpose whatsoever. TxDOT does not assume responsibility or liability for damages or other formats or for incorrect results or damages resulting from its use.

LEVELS DISPLAYED

ACC:

A.2 1998 EDITION OF U-BEAM STANDARDS

Two sheets from the 1998 TxDOT bridge standards are provided on the following pages:

- ubstd001.dgn: Prestressed Concrete U-Beam Details, Sheet 1 of 2

  Contains typical section and reinforcing bar shapes and geometries for the U40 and U54 beams.
- ubstd001.dgn: Prestressed Concrete U-Beam Details, Sheet 2 of 2

  Contains an elevation view, plan views of the end-regions of a skewed and a square beam, and section views in the end blocks.

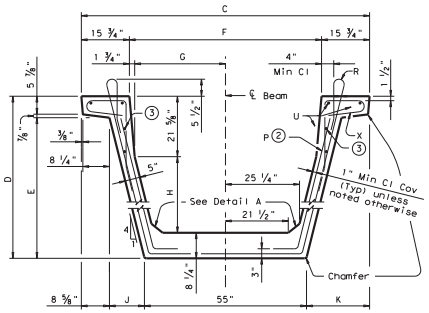

TYPICAL SECTION

② Required for exterior beams only.
③ Optional Bar U for exterior beams only.

DETAIL A

BAR DIMENSION		
Bar	Beam Type	
	U40	U54
DS1	4'-8"	4'-8"
DS2	4'-11"	5'-0"
DS3	5'-2"	5'-5"
DS4	5'-4 ¼"	5'-9 ½"
DS5	5'-6 ½"	6'-1 ¼"

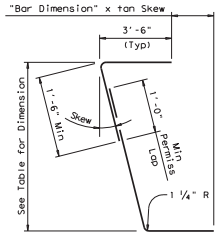

BARS DS1-5 (#4)

BAR DIMENSION		
Bar	Beam Type	
	U40	U54
D1	4'-9"	4'-9"
D2	4'-11¼"	5'-1"
D3	5'-2"	5'-5 ½"
D4	5'-4"	5'-10"
D5	5'-6 ½"	6'-1 ¼"

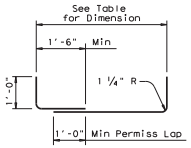

BARS D1-5 (#4)

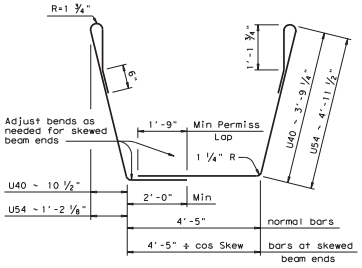

BARS R(#4)

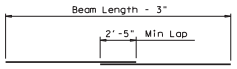

BARS U(#5)

Bars U may be placed with multiple segments, provided no segment is less than 10 ft in length and 40 ft min C-C splices.

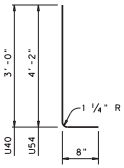

BARS F(#4)

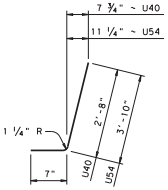

BARS P(#4)

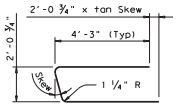

BARS W1(#4)

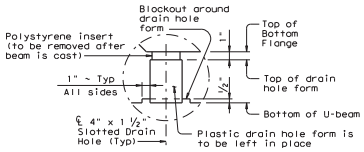

DRAIN HOLE DETAIL

Blockout to be used at all drain hole locations.

At all interior diaphragm locations, strands shall have ¼" clear cover to edge of drain hole form.

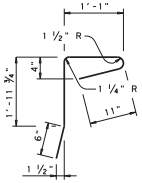

BARS X(#4)

BEAM DIMENSIONS AND SECTION PROPERTIES

Beam Type	C (in.)	D (in.)	E (in.)	F (in.)	G (in.)	H (in.)	J (in.)	K (in.)	Y_t (in.)	Y_b (in.)	Area (in.2)	I (in.4)	Weight (plf)①
U40	89	40	33 ¼	57 ½	27	10 ⅛	8 ⅜	17	23.66	16.30	979.9	183,108	1021
U54	96	54	47 ¼	64 ½	30 ½	24 ⅛	11 ⅞	20 ½	31.58	22.36	1120.0	403,020	1167

① Weights shown assume a concrete density of 150 pcf and are for the typical section only. These weights do not include weight of diaphragms or endblocks.

BEAM TOLERANCES
(Deviation from planned dimensions)

Type	Tolerance	Maximum
Horizontal Alignment (upon release of stress)	± ⅛" per 10' of length	¾"
Horizontal Skew at Ends	± ⅛" per 1' of width	½"
Vertical Batter at Ends	± ⅛" per 1' of depth	½"

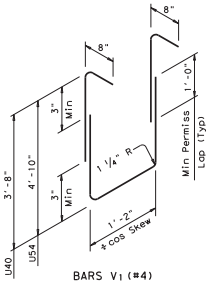

BARS V1(#4)
(ISOMETRIC VIEW)

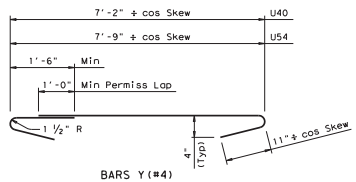

BARS Y(#4)

GENERAL NOTES :

All reinforcing steel shall be grade 60.

Reinforcing steel dimension and bend radii are shown to centerline of bars.

Reinforcing steel shall have 1" min clear cover unless noted otherwise.

All acute corners shall be chamfered for Skews greater than 20 Degrees. Any corner of the beam noted with "chamfer" shall be chamfered ¾" or rounded to a 1 ⅜" radius. Optional chamfers, if used shall likewise conform.

Horizontal form joints (seams) will not be permitted.

The beam section dimensions in inches are approximate values converted from the metric beam section dimesions shown on the UBA(M) sheets. The beam section properties are exact conversions of the metric beam section properties shown on the UBA(M) sheets. New forms for U-Beams should be fabricated to the metric dimensions shown on the UBA(M) sheets.

An equal area of welded wire fabric may be substituted for Bars R, P, X and Y.

Shop drawings may be prepared with horizontal skews rounded to the nearest ¼ degree and batter rounded to the nearest ¼ inch. These design tolerances are in addition to the fabrication tolerances.

Fabrication tolerances shall be as required for Box Beams under the Item, "Precast Concrete Structures (Fabrication)", except that the horizontal alignment, horizontal skew, and vertical batter shall be as shown above in table labeled "Beam Tolerances".

See Bridge Layout and Clearance Sign Bracket sheets for location of anchors in exterior beam for clearance sign bracket.

HS20 LOADING — SHEET 1 OF 2

Texas Department of Transportation
Design Division (Bridge)

PRESTRESSED CONCRETE U-BEAM DETAILS

UBA

FILE: ubstd001.dgn	DN: TxDOT	CK: TxDOT	DW: BBH	CK: TGA	STD: BS39
© TxDOT March 1998	DIST	FED REG	FEDERAL AID PROJECT #		SHEET
REVISIONS		6			BS39
	COUNTY		CONTROL	SECT	JOB	HIGHWAY

DISCLAIMER:
The use of this standard is governed by the "Texas Engineering Practice Act". No warranty of any kind is made by TxDOT for any purpose whatsoever. TxDOT disclaims any responsibility for the conversion of this standard to other formats or for incorrect results or damages resulting from its use.

LOGOS BIRGATED
ACC: (LV=1,2 for English)
1 2

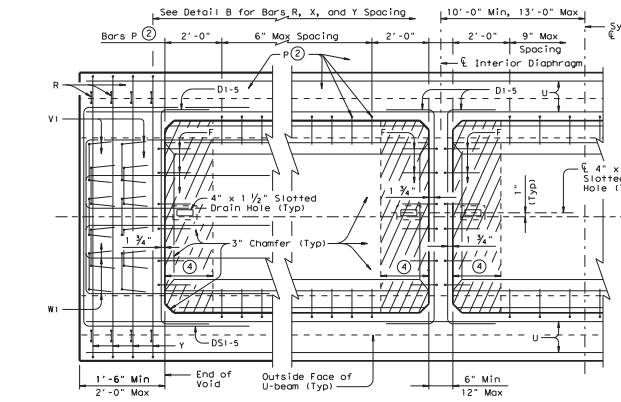

SHOWING SQUARE ENDBLOCK SHOWING INTERIOR DIAPHRAGM

PLAN

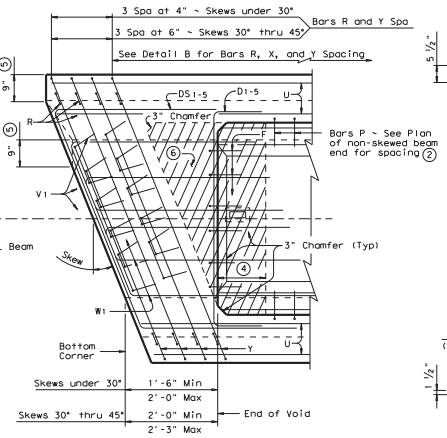

PLAN ~ SKEWED ENDBLOCK

(Skews thru 45°)

④ 12" max of inside non-skewed form at the endblock and at interior diaphragms may be replaced with polystyrene. Polystyrene may be left in place. The inside skewed form at the endblock may also be replaced in the skewed area with polystyrene, provided Bars F and D are modified accordingly, and the polystyrene is left in place to act as slab form. Drain holes shall be offset by the width of polystyrene.

⑤ For Skews greater than 15 Degrees, top flange and bottom flange shall have 9" breakback, with smooth transition from top flange to bottom flange. Adjust shape of Bars W1 as necessary to maintain 1" min clear cover to face of breakback.

⑥ Fabricator has the option of using polystyrene to form the cross-hatched area as shown. If this option is used, Bars R shall be as shown in Detail B. Only Bars Y shown as being cut in Detail B shall be omitted. Bars F shall be adjusted in location and Bars D1-5 shall be adjusted in shape and location for the skew. These details shall be shown on the shop plans for approval by the Engineer.

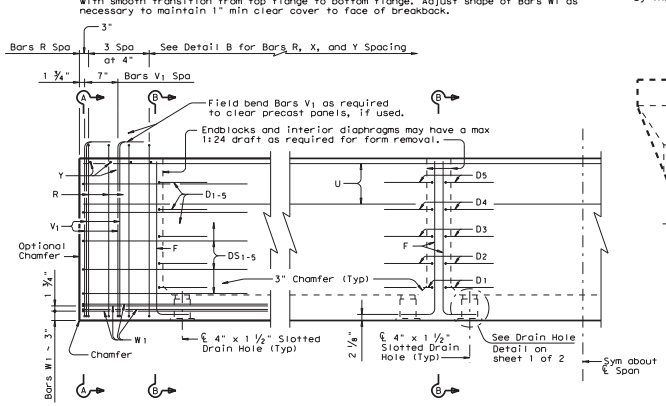

SHOWING ENDBLOCK SHOWING INTERIOR DIAPHRAGM

ELEVATION

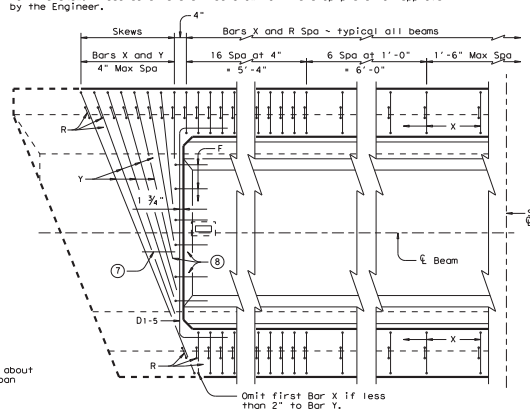

DETAIL B

(Bars U and P not shown for clarity)

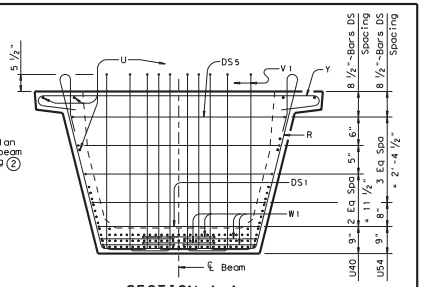

SECTION A-A

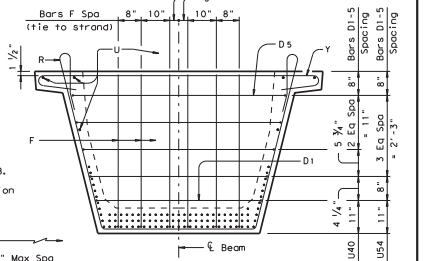

SECTION B-B

⑦ Add support bars for Bars Y as necessary.

⑧ Cut Bars Y and Bars R as required to obtain 1" min clear between bars.

HS20 LOADING SHEET 2 OF 2

Texas Department of Transportation
Design Division (Bridge)

PRESTRESSED CONCRETE U-BEAM DETAILS

UBA

FILE: ubstd001.dgn	DN: TxDOT	CK: TxDOT	DW: BWH	CK: TGA	STD: B539
© TxDOT March 1998	DIST	FED REG	FEDERAL AID PROJECT #		SHEET
REVISIONS		6			
	COUNTY		CONTROL	SECT	JOB	HIGHWAY

DISCLAIMER:
The use of this standard is governed by the "Texas Engineering Practice Act". No warranty of any kind is made by TxDOT for any purpose whatsoever. TxDOT disclaims the suitability of this standard for any purpose other than that for which it is specifically intended and assumes no liability for damages resulting from its use.

REVISIONS		
1	2	ACC: (LV=1.2 for English)

A.3 U-BEAM GEOMETRY

Seven of the eight U-Beams fabricated in this project used the standard cross-sectional geometry shown on page 251. The critical dimensions are not provided again here. The dimensions of the modified cross-section used in Beam 4 are given in Section A.10. The cross-sectional properties of the standard and modified sections used are given in Table A-1.

Table A-1: Standard and modified U54 beam section properties.

Beam Type	y_t [in.]	y_b [in.]	Area [in.^{2}]	I [in.^{4}]	Weight [kip/ft]	
					Main Span	End Block
Standard U54	31.58	22.36	1120	403,020	1.167	3.958
Modified U54	29.98	24.02	1380	464,790	1.438	3.958

A.4 U-BEAM REINFORCING BAR DETAILS

All reinforcing bars used in the beam drawings provided in Sections A.6 through A.9 (Beams 0, 1, 2, and 3) are as shown on page 3 of 3 of the 2006 TxDOT Prestressed Concrete U-Beam Details (pg 253). Phase II U-Beams (Beams 4, 5, 6, and 7) included many of these same standard reinforcing bars, but also bars that do not exist in the current standards or were modifications of bars in the standard. The details of these non-standard bars are provided in Figure A-1and Figure A-2.

Supplementary Web Reinforcing

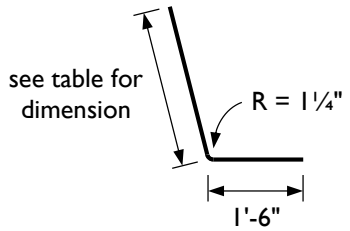

Beam	Bar Size	Dimension
0, 1, 2, 3	[not used]	
4	#5	2'-5"
5	#6	3'-10"
6, 7	#5	2'-5"

Confinement Reinforcing: [#4]

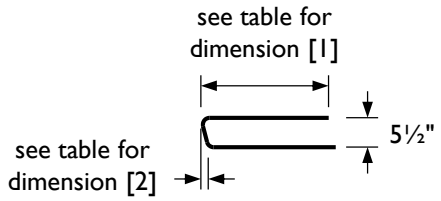

Beam	Dimension	
	[1]	[2]
0, 1, 2, 3	[not used]	
4	2'-0"	0"
5	3'-3"	$1^3/_8$"
6, 7	2'-0"	$1^3/_8$"

Figure A-1: Geometry of supplementary and confining reinforcement used in Beams 4, 5, 6, and 7.

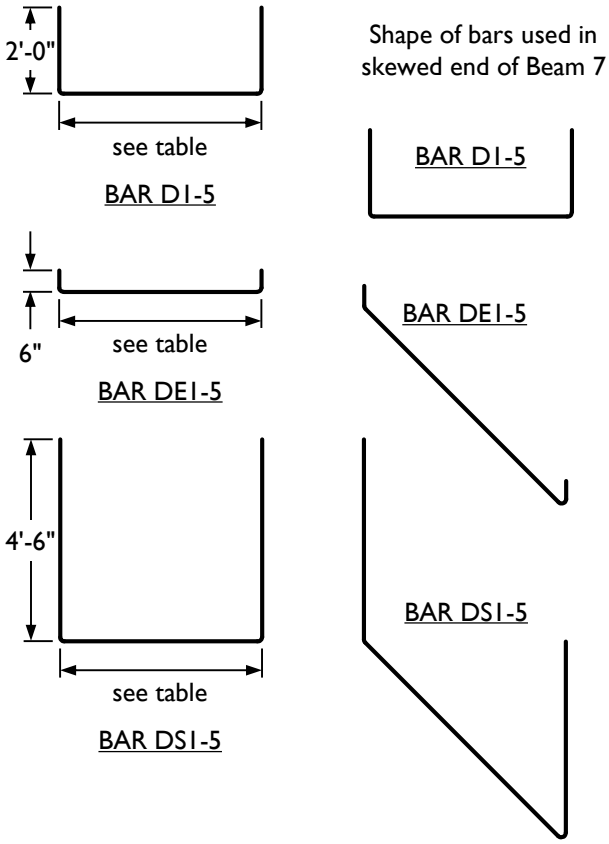

Bar Name	Dimension
D1, DE1	4'-7"
D2, DE2	4'-11½"
D3, DE3	5'-4"
D4, DE4	5'-8½"
D5, DE5	6'-0"

Bar Name	Dimension
DS1	4'-7"
DS2	4'-11½"
DS3	5'-4"
DS4	5'-8"
DS5	5'-11½"

Figure A-2: Modified end-block reinforcing bars used in Beams 6 and 7.

Elevation views for each beam are provided on the following pages, showing the positions of bars R, X, Y (standard reinforcement) and L and C bars (supplementary and confining reinforcement, respectively). As every bar is not marked in the elevation views, a key is given in Figure A-3, illustrating how each bar is drawn.

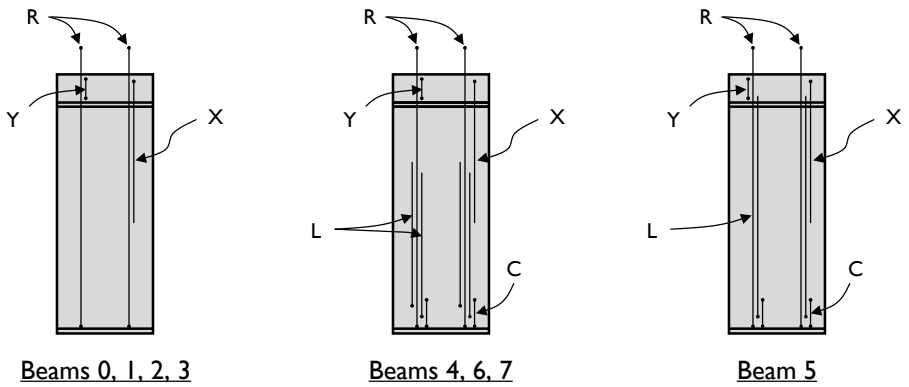

Figure A-3: Key showing reinforcing bar appearance in elevation view.

A.5 U-BEAM END BLOCK REINFORCEMENT

End block cross-sections and plan views for each beam fabricated in this study are provided in the following sections. The reinforcing bars placed in the end blocks of Beams 0, 1, 2 3, and 5 were as shown on page 2 of 3 of the 2006 TxDOT Prestressed Concrete U-Beam Details (pg 252). The end blocks of Beams 4, 6, and 7 contained slight modifications, as are shown in Sections A.10, A.12, and A.13. Unmarked dimensions should be assumed to be as shown in the TxDOT drawings.

A.6 BEAM 0 INFORMATION AND DRAWINGS

Beam 0 was fabricated with shear reinforcing bars spaced at 8 in. in the north end (B0N) and 18 in. in the south end (B0S). End block reinforcement was as drawn in the TxDOT standard drawings. The location of prestressing strands is shown in Figure A-4. A summary of information about the beam is given in Table A-2 and the beam drawings are shown in Figure A-5 and Figure A-6.

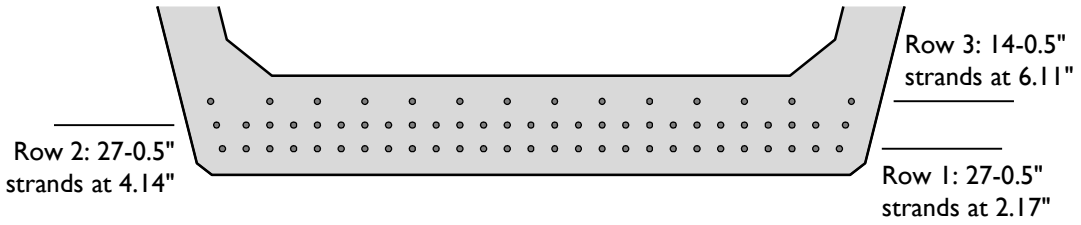

Figure A-4: Prestressing strand positions for Beam 0.

Table A-2: Summary of information about Beam 0.

BEAM 0 INFORMATION SUMMARY	North End	South End
GENERAL CHARACTERISTICS		
Beam test regions	B0N	B0S
Date of cast	29 January 2008	
Concrete mixture design designation	unknown (beam), III-A (deck)	
Fabrication location	Fabricator A	
End block geometry	square ext. square void 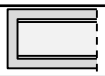	square ext. square void
Prestressing force	78 ½" strands at 202.5 ksi	
RELEASE MEASUREMENTS		
Strength at release, f'_{ci} (release factor[1])	[not known]	
Maximum release crack width	[not measured]	
Maximum stresses observed at release	[no data gathered]	
TEMPERATURE MEASUREMENTS		
Ambient temperature during cast and curing	50-77°F	
Maximum temperature during curing	[temperature data not recorded]	
Maximum temperature differential during curing	[temperature data not recorded]	
Maximum temperature at release point	[temperature data not recorded]	
SHEAR TESTING INFORMATION		
Shear test date	[not tested]	05 August 2008
28-day strength	[not recorded]	
Compressive strength at testing, f'_c		12.9 ksi
Deck compressive strength at testing, f'_{c_deck}		10.8 ksi
Reinforcing steel strength, f_y	60.0 ksi [assumed]	
Bearing condition during shear testing		two bearing pads
Shear span (span-to-depth ratio)		174 (3.0)
Failure shear		491 kip
Rebar spacing	8" for 14'-8"	18" for 15'-0"
Calculated shear capacity (AASHTO LRFD General Method)		472 kip
V_{test} / $V_{calculated}$ with given rebar spacing		1.04
Shear failure mode		web crushing
Horizontal shear demand		[not calculated]
Calculated horizontal shear capacity		[not calculated]
Horizontal shear performance ratio		[not calculated]

[1] Release factor is equal to the ratio of bottom fiber stress to concrete strength at time of transfer

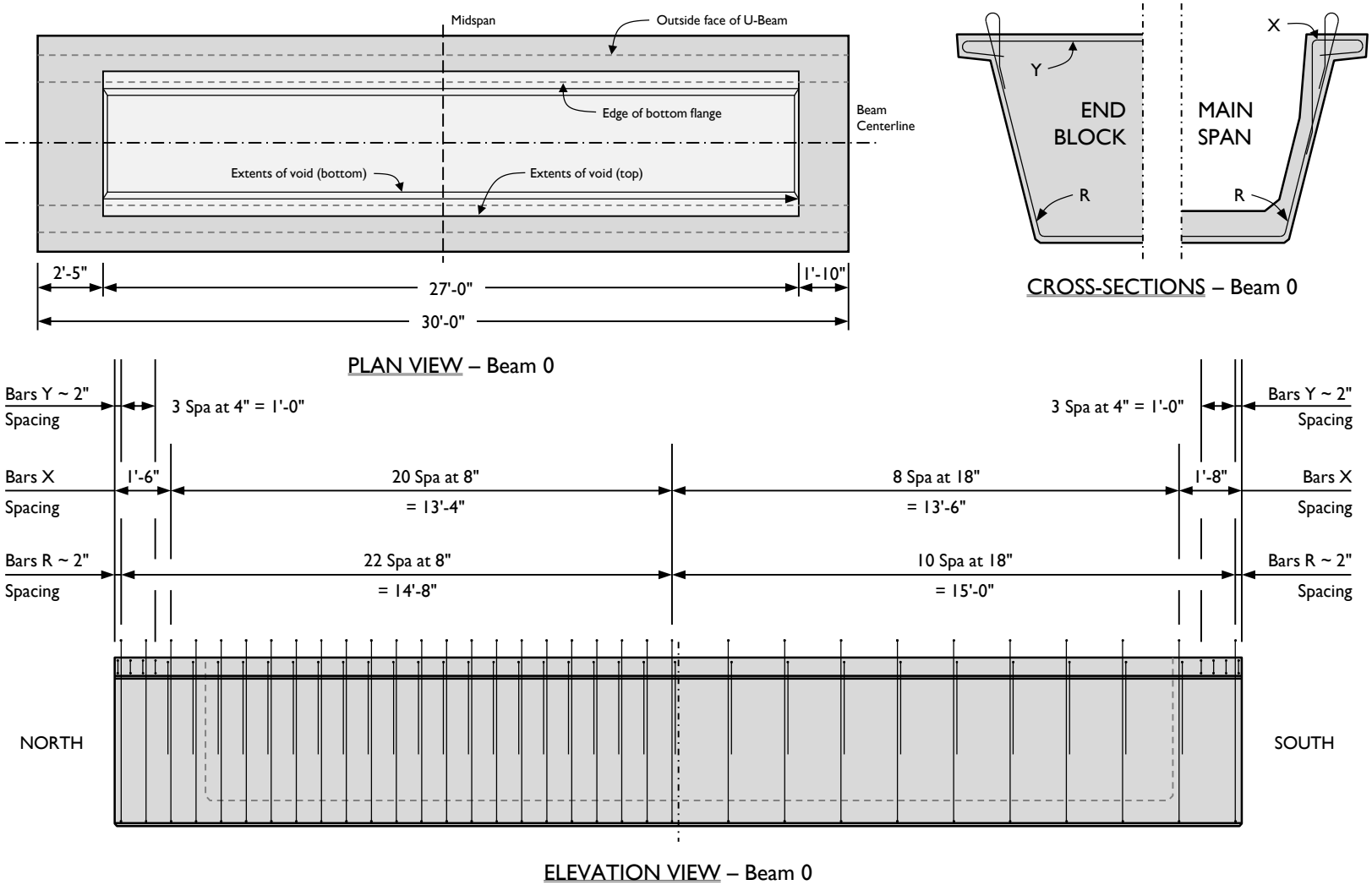

Figure A-5: Beam 0 plan view, elevation view, and standard sections.

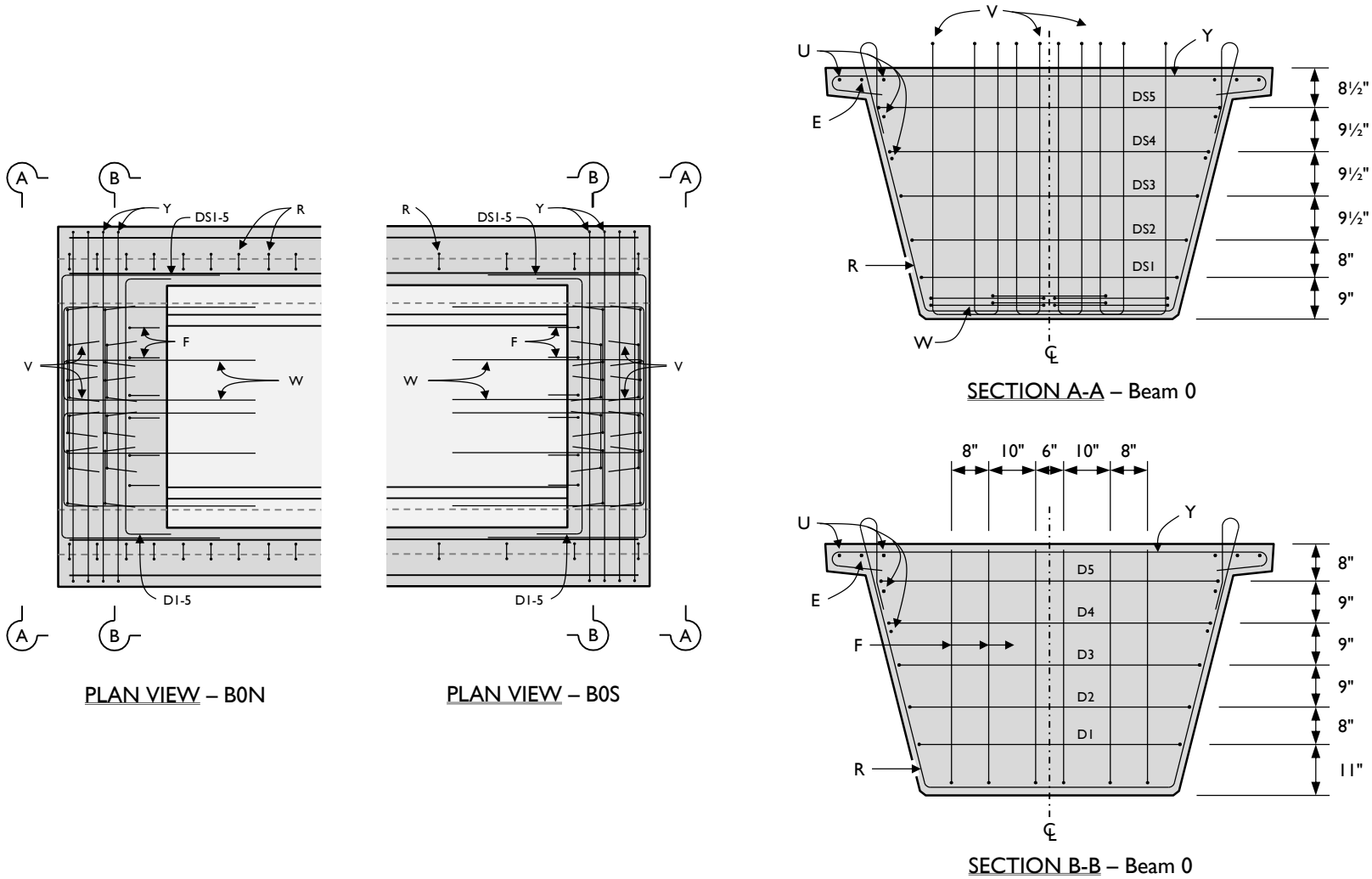

Figure A-6: Beam 0 end-region plan views and cross-sections.

A.7 BEAM 1 INFORMATION AND DRAWINGS

The reinforcement design of Beam 1 followed the TxDOT standard drawings. The beam was square at one end and skewed to 45° at the other. The void followed the optional skewed geometry given in the standard. End block reinforcement was as shown in the standard. It should be noted that at the skewed end, shear reinforcement spacing distances (i.e., at 4 in. for 6'-3") originated at the corner of the bottom flange on the short web.

The prestressing strands were positioned as shown in Figure A-7. A summary of information about the beam is given in Table A-3 and the beam drawings are shown in Figure A-8, Figure A-9, and Figure A-10.

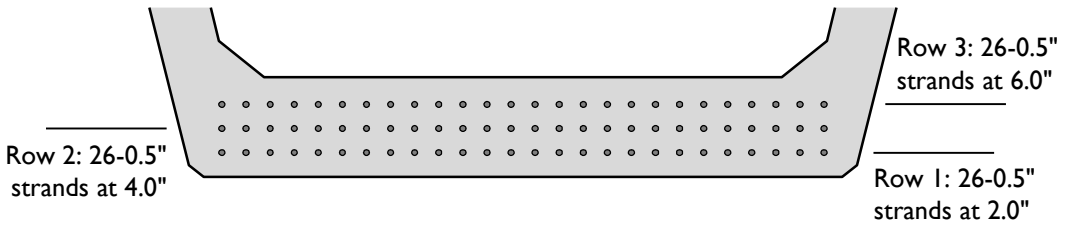

Figure A-7: Prestressing strand positions for Beam 1.

Table A-3: Summary of information about Beam 1.

BEAM 1 INFORMATION SUMMARY	North End		South End	
GENERAL CHARACTERISTICS				
Beam test regions	B1N		B1S	
Date of cast	18 November 2008			
Concrete mixture design designation	III-A (beam), I-F (deck)			
Fabrication location	Ferguson Structural Engineering Laboratory			
End block geometry	square ext. square void 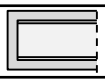		45° exterior 45° void 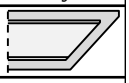	
Prestressing force	78 ½" strands at 202.5 ksi			
RELEASE MEASUREMENTS				
Strength at release, f'_{ci} (release factor[1])	6.4 ksi (0.66)			
Maximum release crack width	0.005 in.		0.020 in.	
Maximum stresses observed at release	18 ksi		24 ksi	
TEMPERATURE MEASUREMENTS				
Ambient temperature during cast and curing	71-77°F			
Maximum temperature during curing	137°F		139°F	
Maximum temperature differential during curing	38°F		28°F	
Maximum temperature at release point	115°F			
SHEAR TESTING INFORMATION				
Shear test date	08 January 2009		06 January 2009	
28-day strength	11.7 ksi			
Compressive strength at testing, f'_c	12.0 ksi		12.0 ksi	
Deck compressive strength at testing, f'_{c_deck}	10.5 ksi		10.5 ksi	
Reinforcing steel strength, f_y	65.8 ksi			
Bearing condition during shear testing	single bearing pad		two bearing pads	
Shear span (span-to-depth ratio)	152 (2.6)		154 (2.6)	
Failure shear	659 kip		612 kip	
Rebar spacing	4" for 6'-3"	6" for 11'-11"		4" for 6'-3"
Calculated shear capacity (AASHTO LRFD General Method)	930 kip	746 kip		929 kip
V_{test} / $V_{calculated}$ with given rebar spacing	0.71	0.89	0.82	0.66
Shear failure mode	horizontal shear		horizontal shear	
Horizontal shear demand	993 kip		[not calculated]	
Calculated horizontal shear capacity	862 kip		[not calculated]	
Horizontal shear performance ratio	1.15		[not calculated]	

[1] Release factor is equal to the ratio of bottom fiber stress to concrete strength at time of transfer

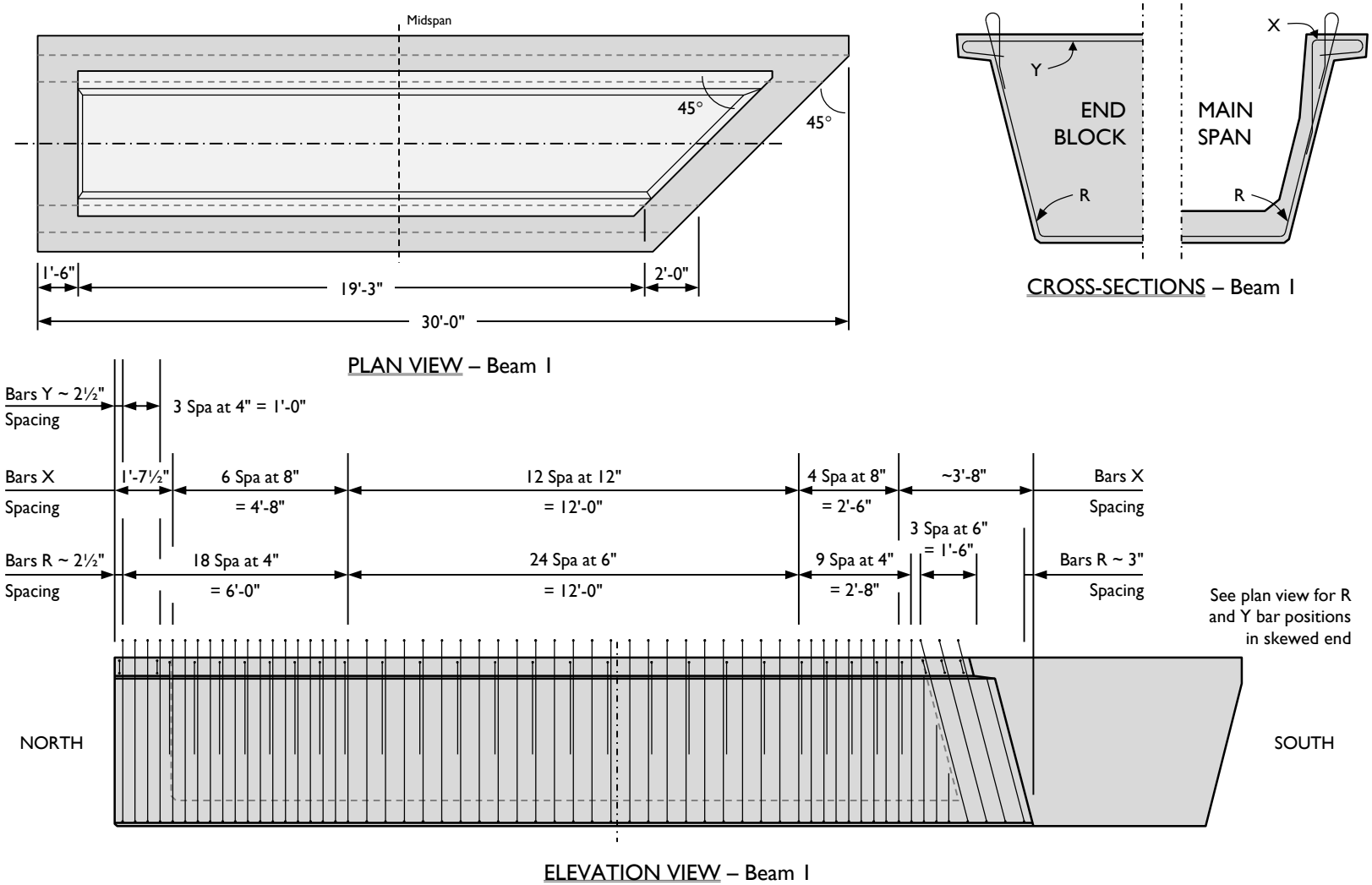

Figure A-8: Beam 1 plan view, elevation view, and standard sections.

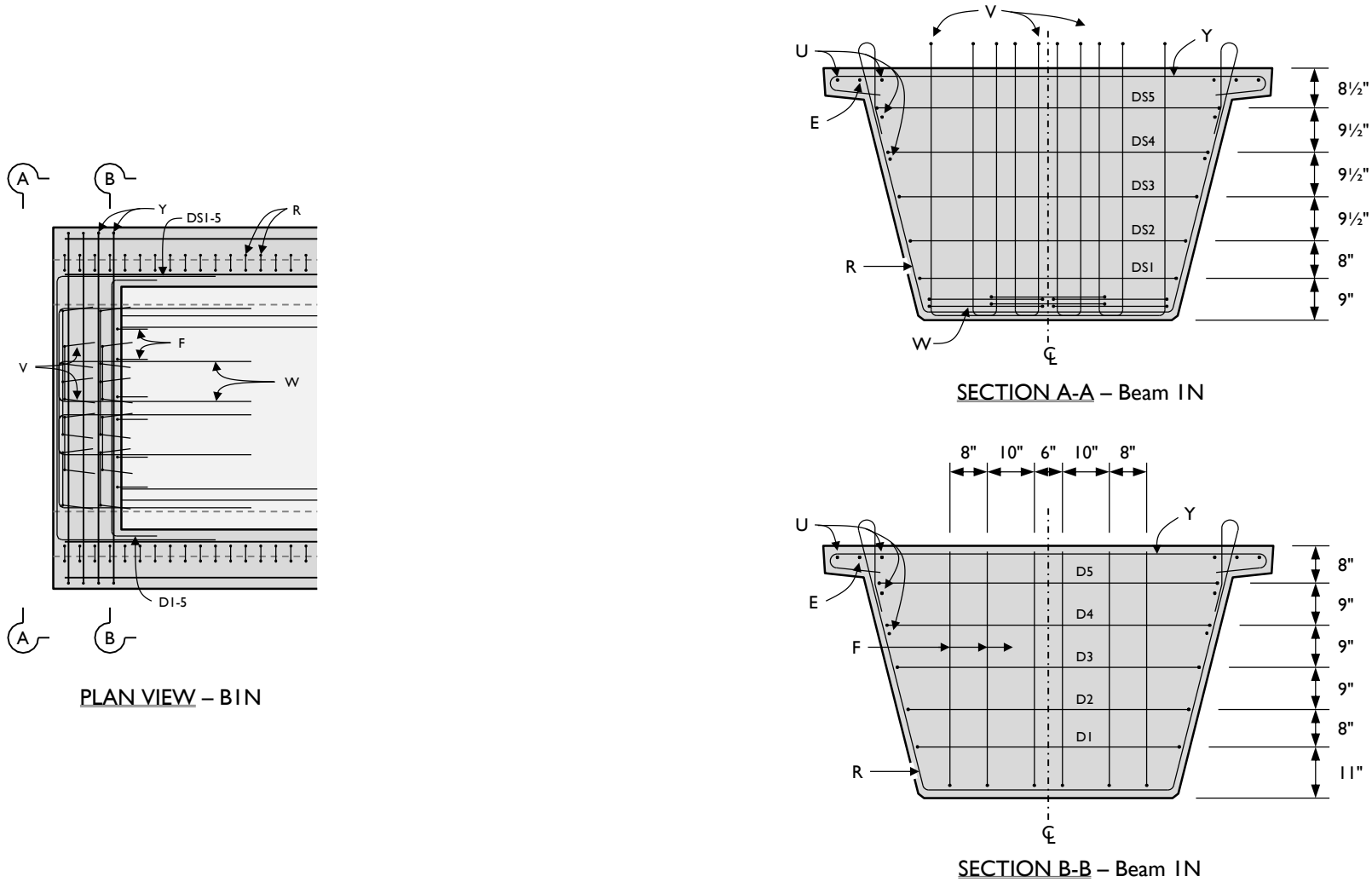

Figure A-9: Beam 1 north end-region plan view and cross-sections.

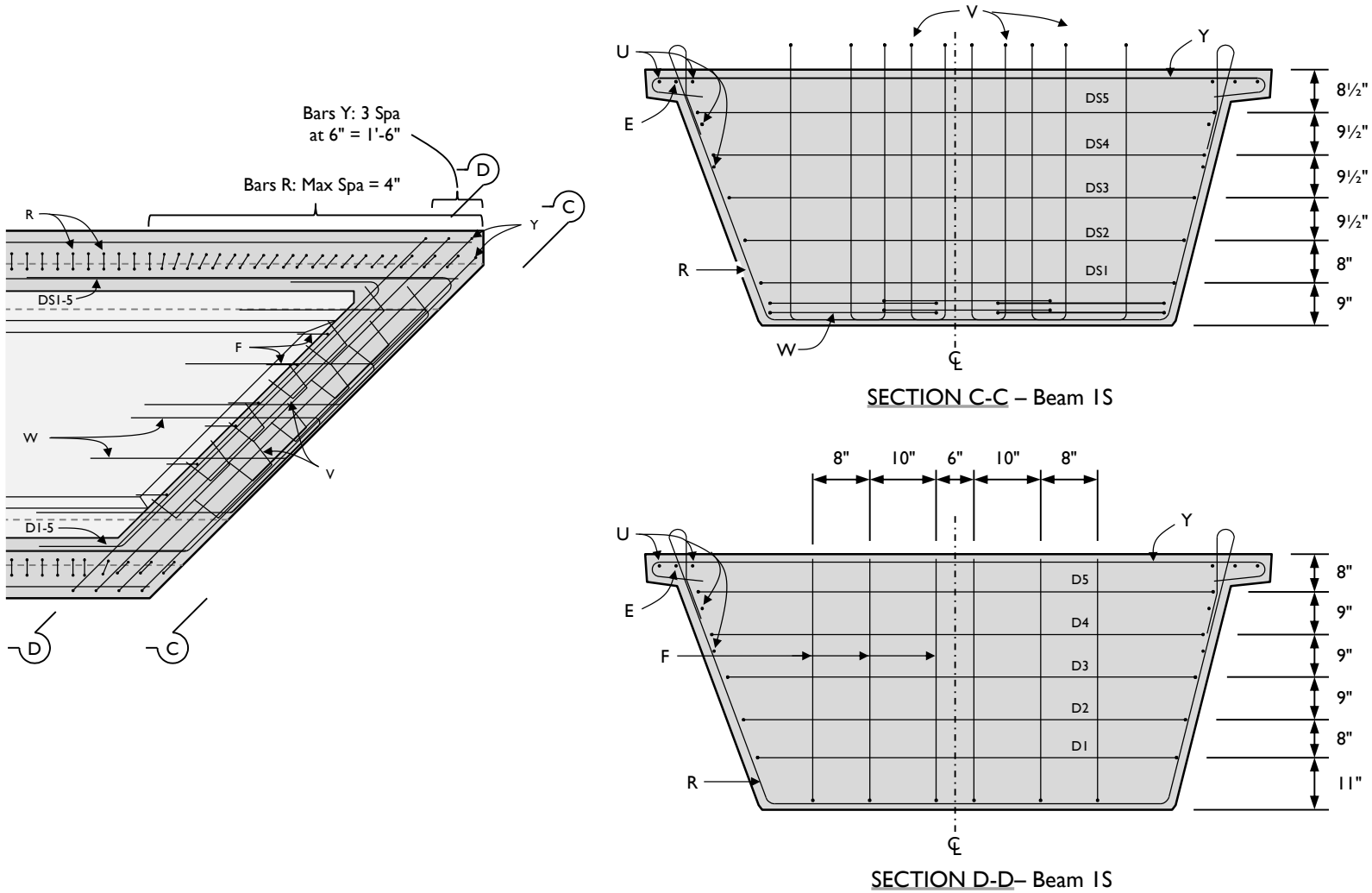

Figure A-10: Beam 1 south end-region plan view and cross-sections.

A.8 BEAM 2 INFORMATION AND DRAWINGS

The reinforcement design of Beam 2 followed the TxDOT standard drawings. The beam was square at one end and skewed to 45° at the other. The void was rectangular, resulting in a triangular end block at the skewed end. End block reinforcement was as shown in the standard. It should be noted that at the skewed end, shear reinforcement spacing distances (i.e., at 4 in. for 6'-3") originated at the corner of the bottom flange on the short web.

The prestressing strands were positioned as shown in Figure A-11. A summary of information about the beam is given in Table A-4 and the beam drawings are shown in Figure A-12, Figure A-13, and Figure A-14.

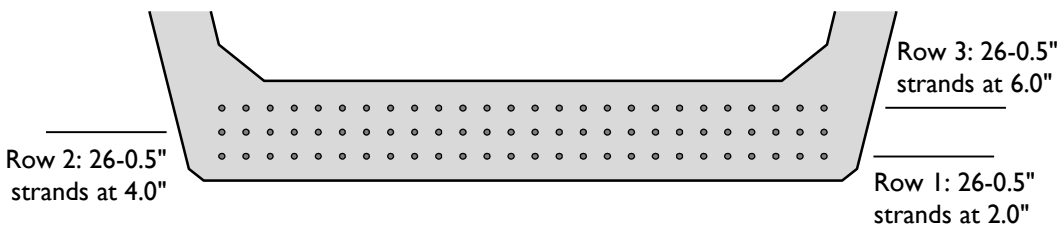

Figure A-11: Prestressing strand positions for Beam 2.

Table A-4: Summary of information about Beam 2.

BEAM 2 INFORMATION SUMMARY	North End		South End
GENERAL CHARACTERISTICS			
Beam test regions	B2N		B2S
Date of cast	26 February 2009		
Concrete mixture design designation	III-A (beam), I-F (deck)		
Fabrication location	Ferguson Structural Engineering Laboratory		
End block geometry	square ext. square void 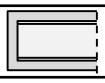		45° exterior square void 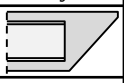
Prestressing force	78 ½" strands at 202.5 ksi		
RELEASE MEASUREMENTS			
Strength at release, f'_{ci} (release factor[1])	6.7 ksi (0.64)		
Maximum release crack width	0.005 in.		0.025 in.
Maximum stresses observed at release	22 ksi		30 ksi
TEMPERATURE MEASUREMENTS			
Ambient temperature during cast and curing	73-84°F		
Maximum temperature during curing	142°F		160°F
Maximum temperature differential during curing	34°F		55°F
Maximum temperature at release point	120°F		
SHEAR TESTING INFORMATION			
Shear test date	02 April 2009		[not tested]
28-day strength	10.3 ksi		
Compressive strength at testing, f'_c	11.5 ksi		
Deck compressive strength at testing, f'_{c_deck}	8.6 ksi		
Reinforcing steel strength, f_y	85.2 ksi		65.8 ksi
Bearing condition during shear testing	single bearing pad		
Shear span (span-to-depth ratio)	152 (2.6)		
Failure shear	610 kip		
Rebar spacing	4" for 6'-3"	6" for 11'-11"	
Calculated shear capacity (AASHTO LRFD General Method)	1087 kip	849 kip	
V_{test} / $V_{calculated}$ with given rebar spacing	0.56	0.72	
Shear failure mode	horizontal shear		
Horizontal shear demand	919 kip		
Calculated horizontal shear capacity	862 kip		
Horizontal shear performance ratio	1.07		

[1] Release factor is equal to the ratio of bottom fiber stress to concrete strength at time of transfer

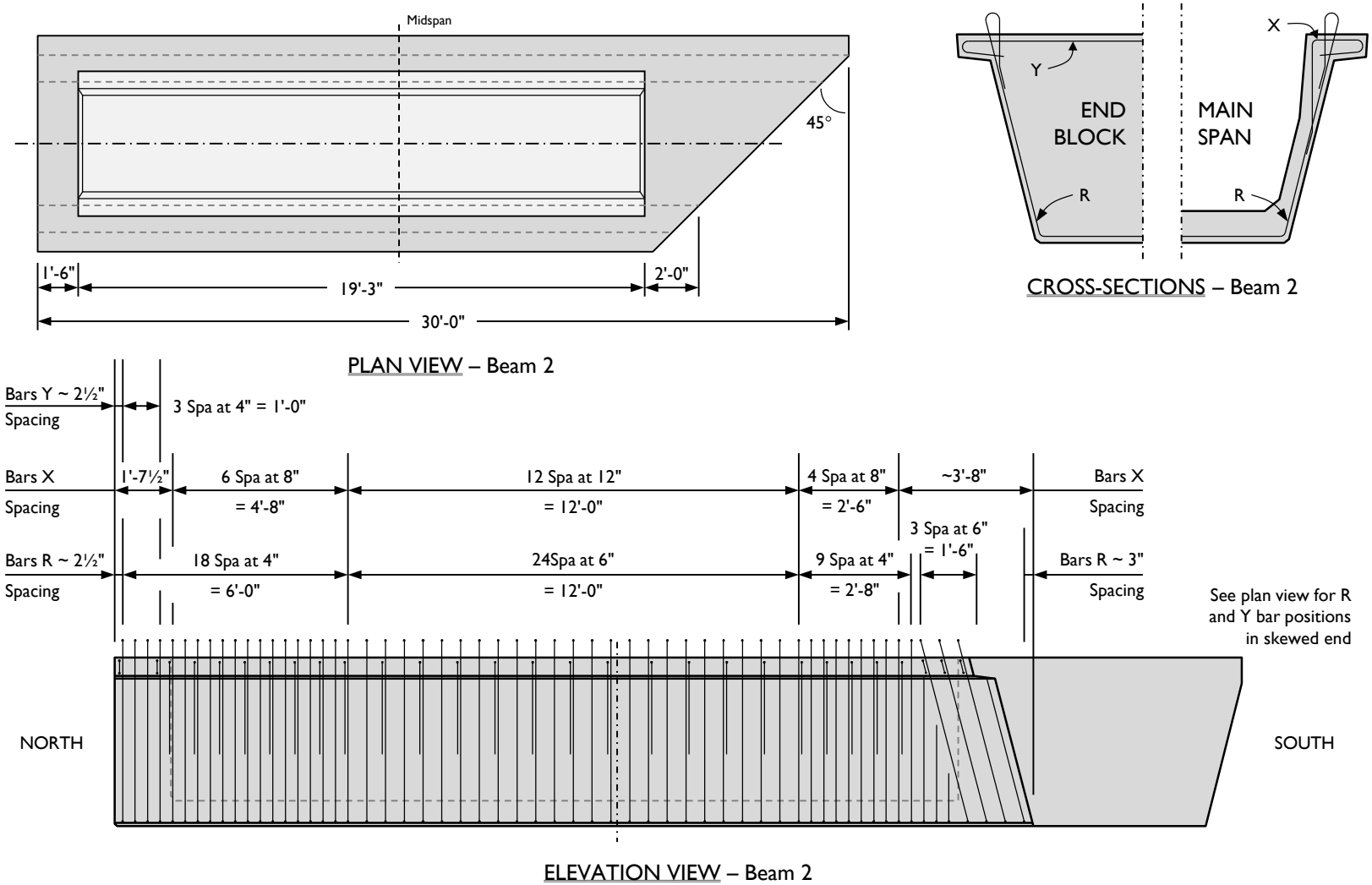

Figure A-12: Beam 2 plan view, elevation view, and standard sections.

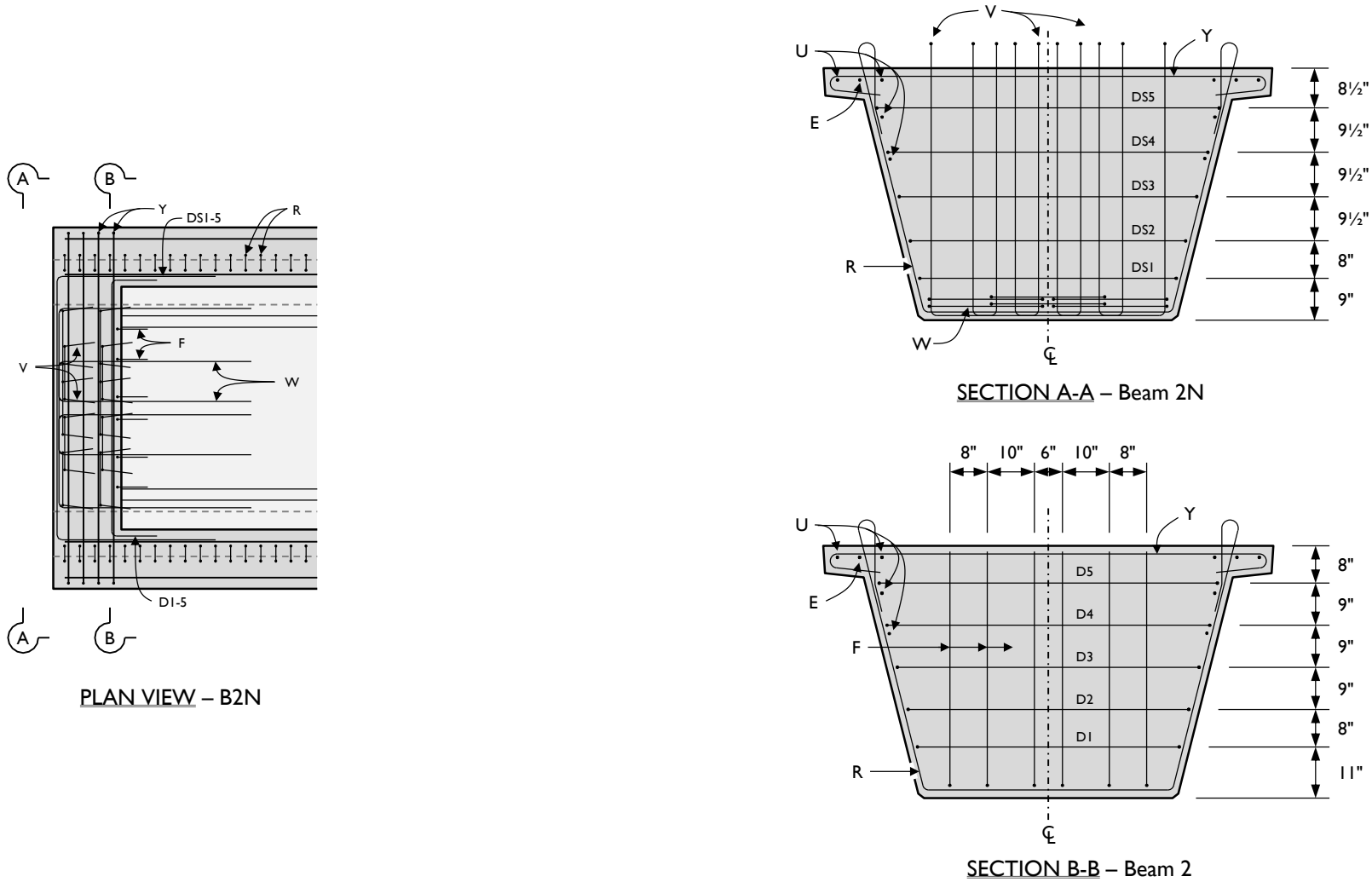

Figure A-13: Beam 2 north end-region plan view and north and south cross-sections.

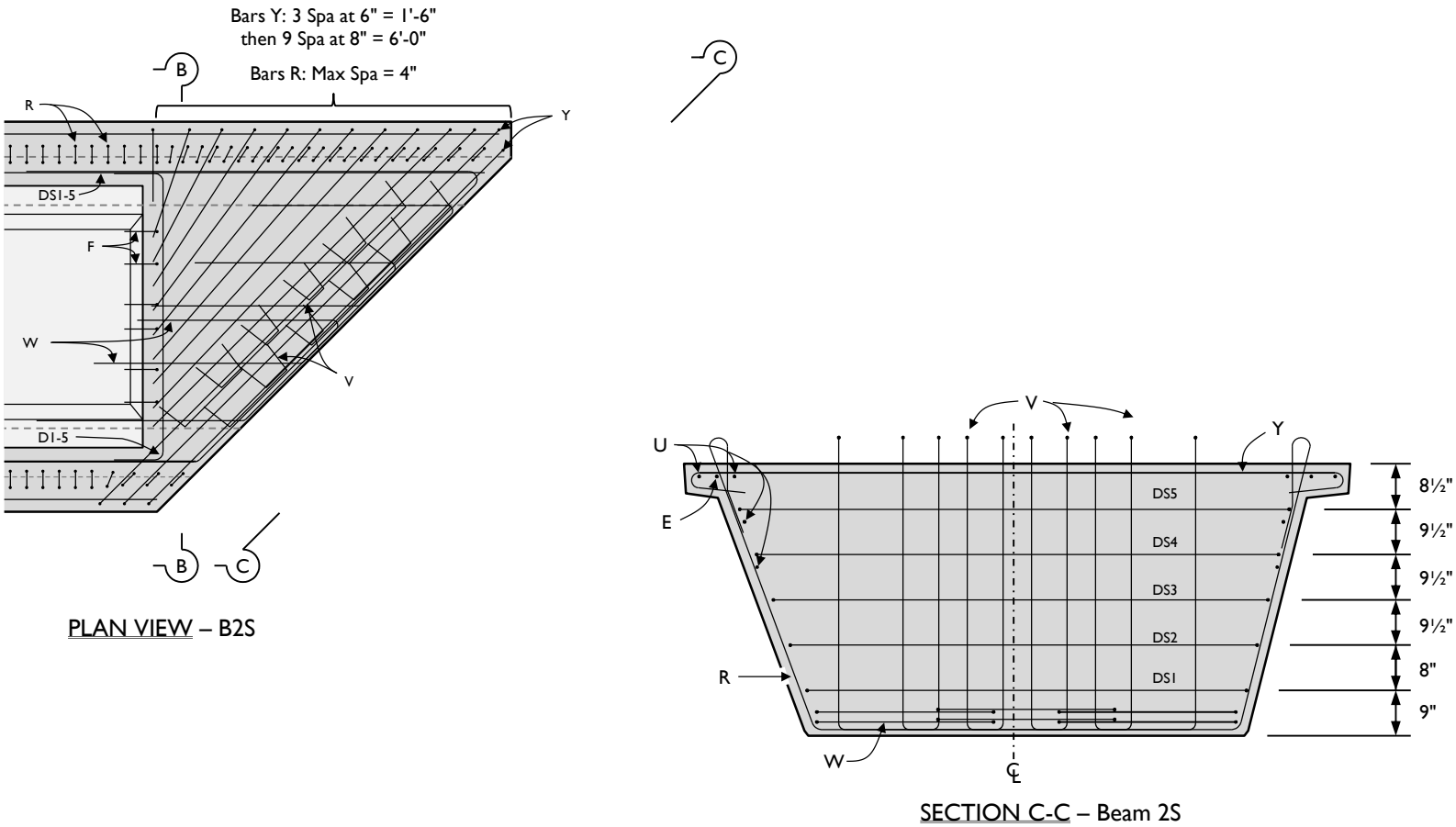

Figure A-14: Beam 2 south end region plan view and cross-sections

A.9 BEAM 3 INFORMATION AND DRAWINGS

The reinforcement design of Beam 3 followed the TxDOT standard drawings. The beam was square at both ends. The two ends were identical with respect to geometry, reinforcement, and prestressing. End block reinforcement was as shown in the standard. The prestressing strands were positioned as shown in Figure A-15, with the details of the debonding pattern provided in Table A-5 and Figure A-16. A summary of information about the beam is given in and the beam drawings are shown in Figure A-17 and Figure A-18.

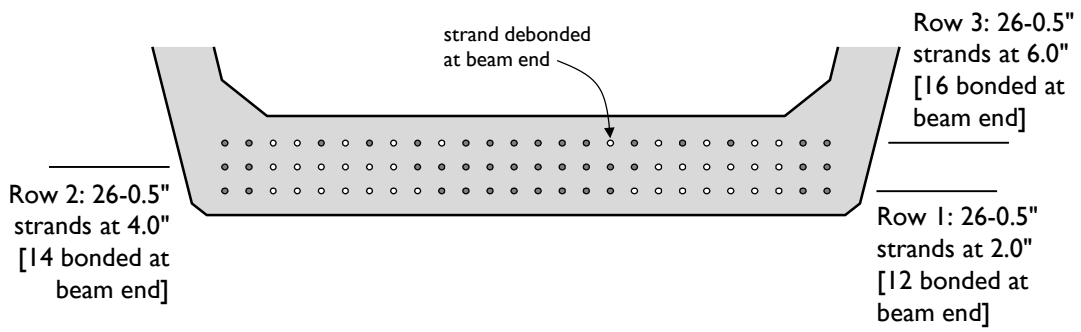

Figure A-15: Prestressing strand positions for Beam 3.

Table A-5: Details of debonding pattern used in Beam 3.

STRUCTURE	DEBONDED STRAND PATTERN PER ROW							
	DIST FROM BOTTOM (in.)	NO. OF STRANDS		NUMBER OF STRANDS DEBONDED TO (ft from end)				
		TOTAL	DE-BOND	3	6	9	12	15
UT U-Beam 3	2.0	26	14		4	4	4	2
	4.0	26	12		4	2	4	2
	6.0	26	10		2	2		6

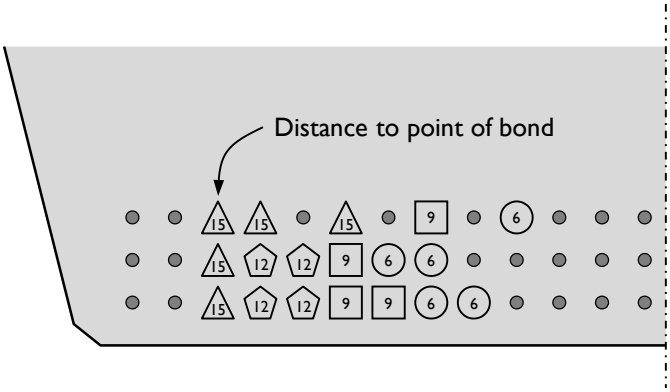

Figure A-16: Distance from beam end to point of bond for strands in Beam 3.

Table A-6: Summary of information about Beam 3.

BEAM 3 INFORMATION SUMMARY	North End		South End	
GENERAL CHARACTERISTICS				
Beam test regions	B3N		B3N	
Date of cast	26 February 2009			
Concrete mixture design designation	III-B (beam), I-F (deck)			
Fabrication location	Ferguson Structural Engineering Laboratory			
End block geometry	square ext. square void 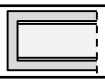		square ext. square void 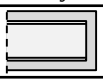	
Prestressing force	78 ½" strands at 202.5 ksi; 42 strands (56%) bonded at beam end			
RELEASE MEASUREMENTS				
Strength at release, f'_{ci} (release factor[1])	5.9 ksi (0.62)			
Maximum release crack width	no cracking observed			
Maximum stresses observed at release	6 ksi		4 ksi	
TEMPERATURE MEASUREMENTS				
Ambient temperature during cast and curing	93-105°F			
Maximum temperature during curing	165°F		184°F	
Maximum temperature differential during curing	52°F		47°F	
Maximum temperature at release point	139°F			
SHEAR TESTING INFORMATION				
Shear test date	17 August 2009		08 September 2009	
28-day strength	11.3 ksi			
Compressive strength at testing, f'_c	11.4 ksi		12.1 ksi	
Deck compressive strength at testing, f'_{c_deck}	9.2 ksi		10.7 ksi	
Reinforcing steel strength, f_y	65.3 ksi			
Bearing condition during shear testing	single bearing pad		two bearing pads	
Shear span (span-to-depth ratio)	154 (2.6)		154 (2.6)	
Failure shear	655 kip		663 kip	
Rebar spacing	4" for 6'-3"	6" for 17'-6"		4" for 6'-3"
Calculated shear capacity (AASHTO LRFD General Method)	680 kip	615 kip		680 kip
V_{test} / $V_{calculated}$ with given rebar spacing	0.96	1.07	1.08	0.97
Shear failure mode	horizontal shear		horizontal shear	
Horizontal shear demand	1012 kip		1025 kip	
Calculated horizontal shear capacity	907 kip			
Horizontal shear performance ratio	1.12		1.13	

[1] Release factor is equal to the ratio of bottom fiber stress to concrete strength at time of transfer

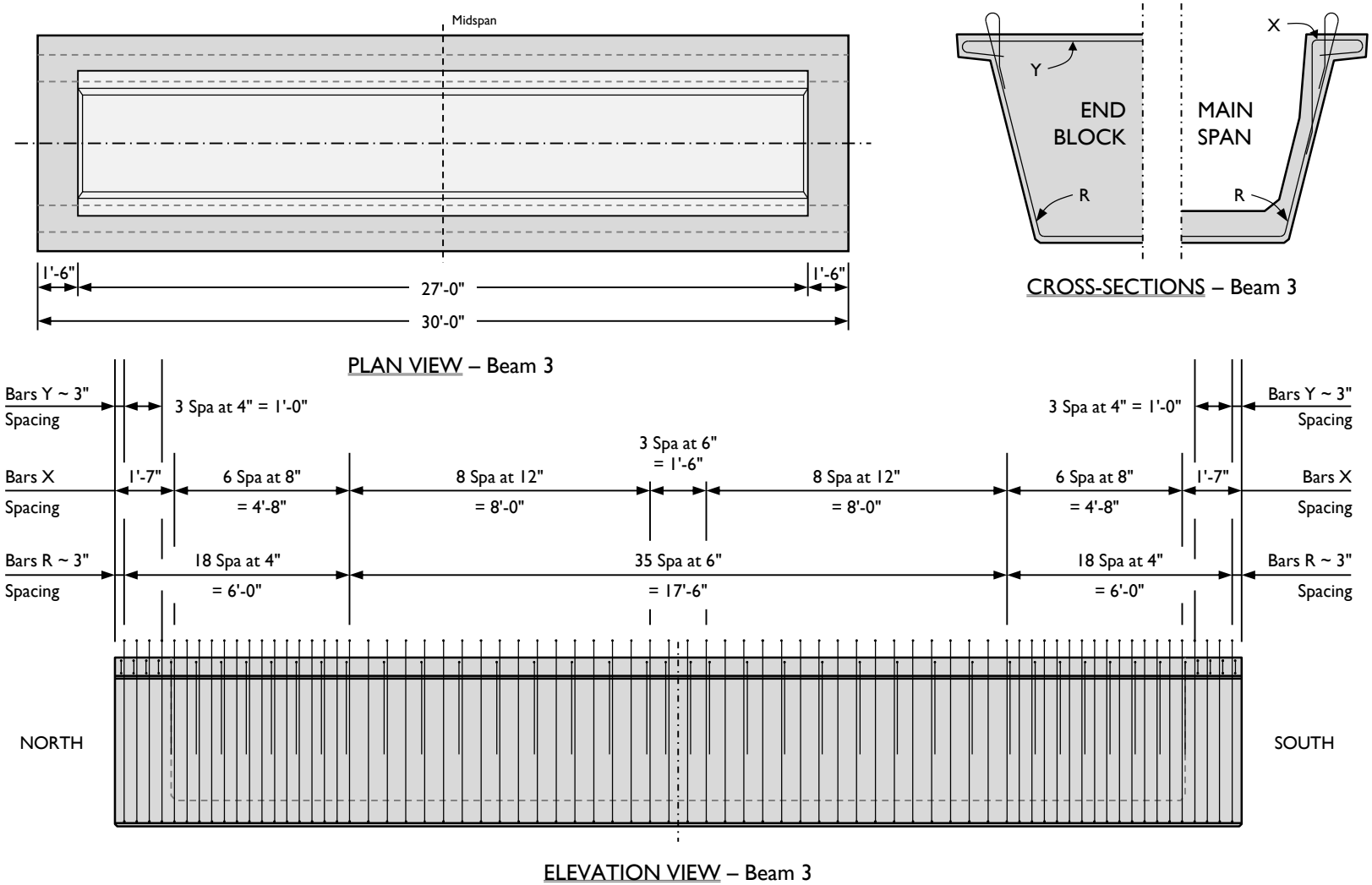

Figure A-17: Beam 3 plan view, elevation view, and standard sections.

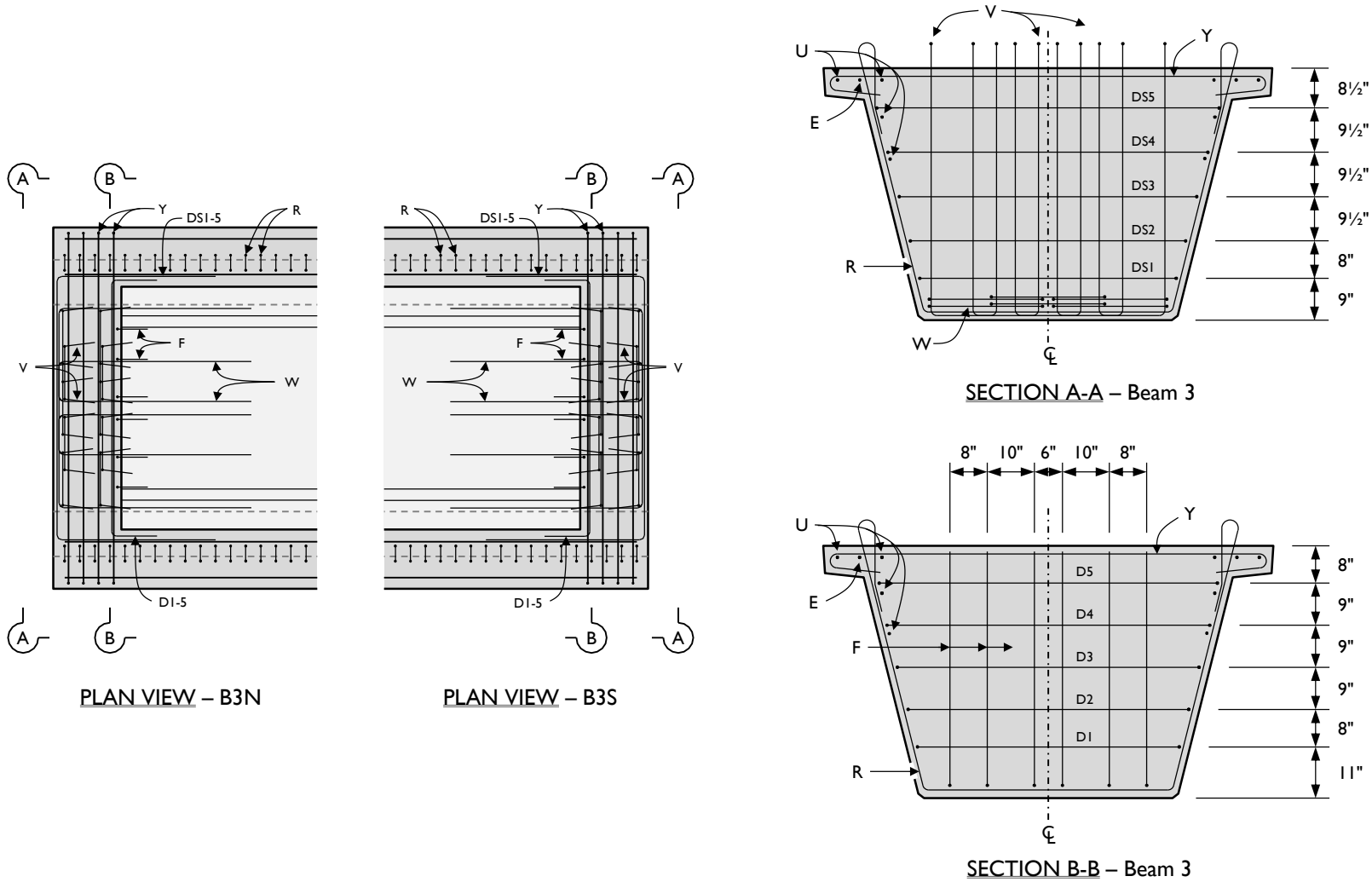

Figure A-18: Beam 3 end-region plan views and cross-sections.

A.10 BEAM 4 INFORMATION AND DRAWINGS

Beam 4 contained reinforcement and geometric changes to the standard design, as presented in Chapter 5. The beam was square at both ends. One end contained supplementary reinforcement while the other end contained only confining bars in addition to the standard bars. End block reinforcement was as shown in the standard. The prestressing strands were as shown in Figure A-19. A summary of information about the beam is given in Table A-7 and the beam drawings are shown in Figure A-20, Figure A-21, Figure A-22, and Figure A-23. The cross-sectional dimensions of the modified U-Beam are given in Figure A-24.

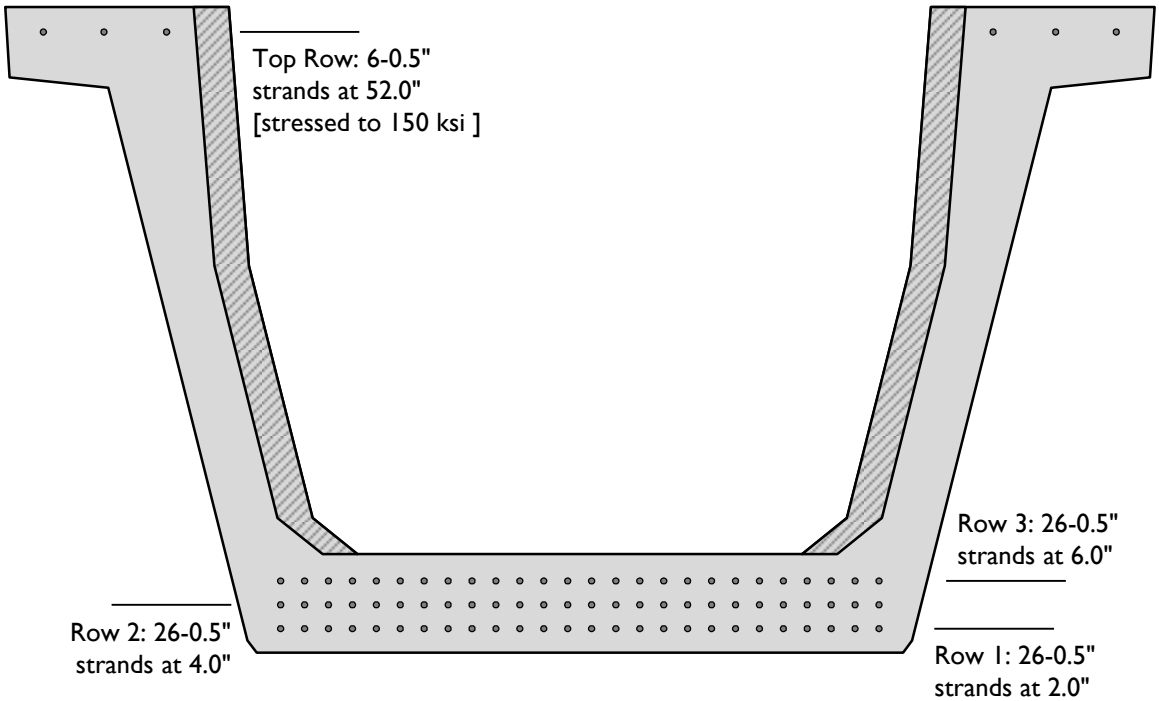

Figure A-19: Prestressing strand positions for Beam 4.

Table A-7: Summary of information about Beam 4.

BEAM 4 INFORMATION SUMMARY	North End			South End		
GENERAL CHARACTERISTICS						
Beam test regions	B4N			B4S		
Date of cast	27 October 2009					
Concrete mixture design designation	III-B (beam), I-F (deck)					
Fabrication location	Ferguson Structural Engineering Laboratory					
End block geometry	square ext. square void 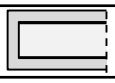			square ext. square void 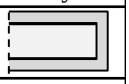		
Prestressing force	78 ½" strands at 202.5 ksi; 6 top flange strands at 150 ksi					
RELEASE MEASUREMENTS						
Strength at release, f'_{ci} (release factor[1])	6.4 ksi (0.66)					
Maximum release crack width	0.016 in.			0.013 in.		
Maximum stresses observed at release	16 ksi			30 ksi		
TEMPERATURE MEASUREMENTS						
Ambient temperature during cast and curing	62-78°F					
Maximum temperature during curing	131°F			139°F		
Maximum temperature differential during curing	45°F			34°F		
Maximum temperature at release point	112°F					
SHEAR TESTING INFORMATION						
Shear test date	07 January 2010			04 January 2010		
28-day strength	10.3 ksi					
Compressive strength at testing, f'_c	11.4 ksi			11.4 ksi		
Deck compressive strength at testing, f'_{c_deck}	7.5 ksi			7.5 ksi		
Reinforcing steel strength, f_y	63.0 ksi					
Bearing condition during shear testing	single bearing pad			single bearing pad		
Shear span (span-to-depth ratio)	154 (2.6)			154 (2.6)		
Failure shear	973 kip			test halted at 1191 kip		
Rebar spacing	3" for 5'-0"	4" for 5'-0"	6" for 10'-0"		4" for 5'-0"	3" for 5'-0"
Calculated shear capacity (AASHTO LRFD General Method)	1134 kip	1043 kip	871 kip		1043 kip	1134 kip
V_{test} / $V_{calculated}$ with given rebar spacing	0.86	0.93	1.12	1.37	1.14	1.05
Shear failure mode	horizontal shear and web crushing			not loaded to failure		
Horizontal shear demand	1499 kip			1834 kip		
Calculated horizontal shear capacity	1242 kip			2559 kip		
Horizontal shear performance ratio	1.21			0.72		

[1] Release factor is equal to the ratio of bottom fiber stress to concrete strength at time of transfer

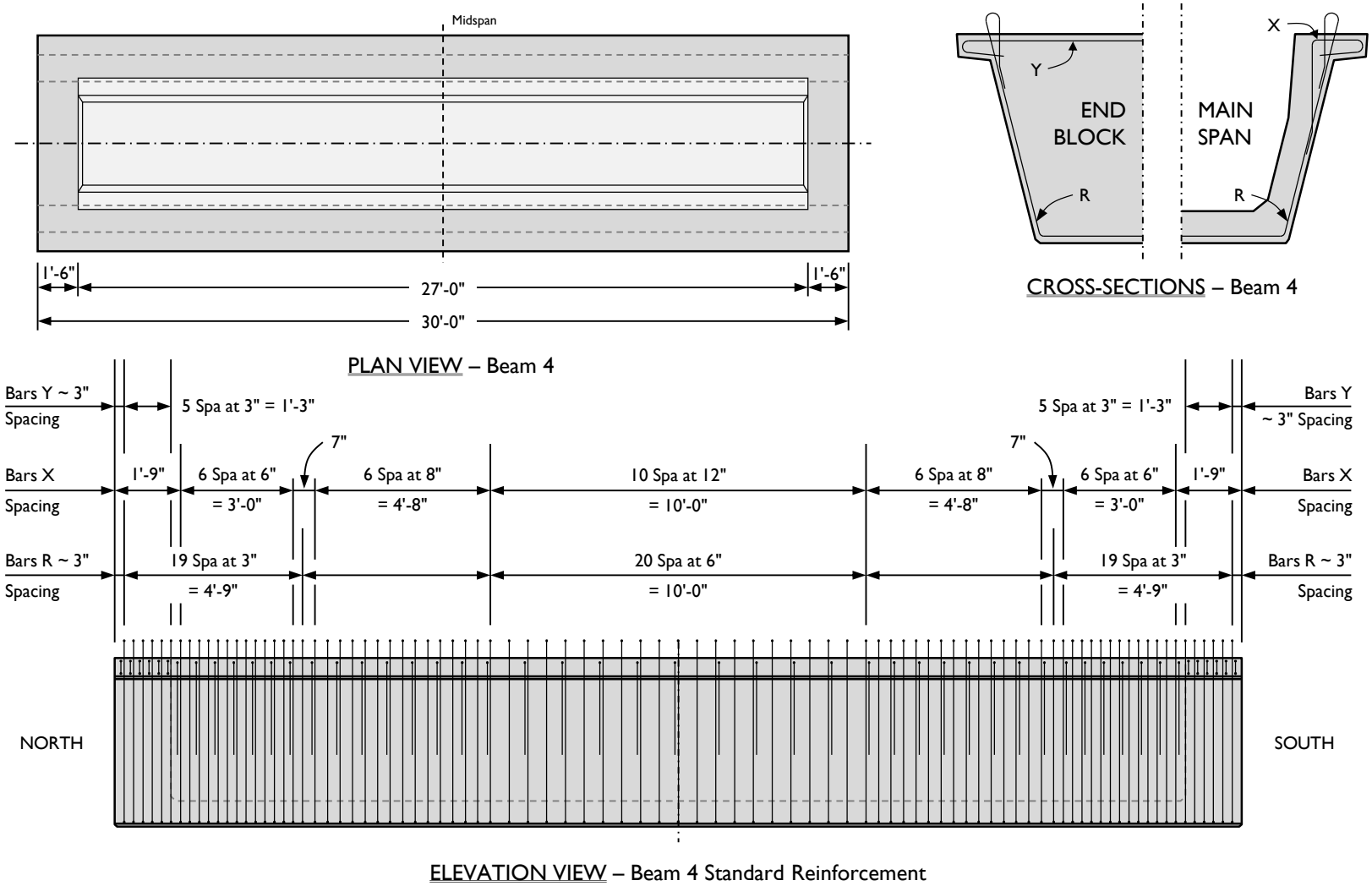

Figure A-20: Beam 4 plan view, elevation view, and sections showing standard reinforcement.

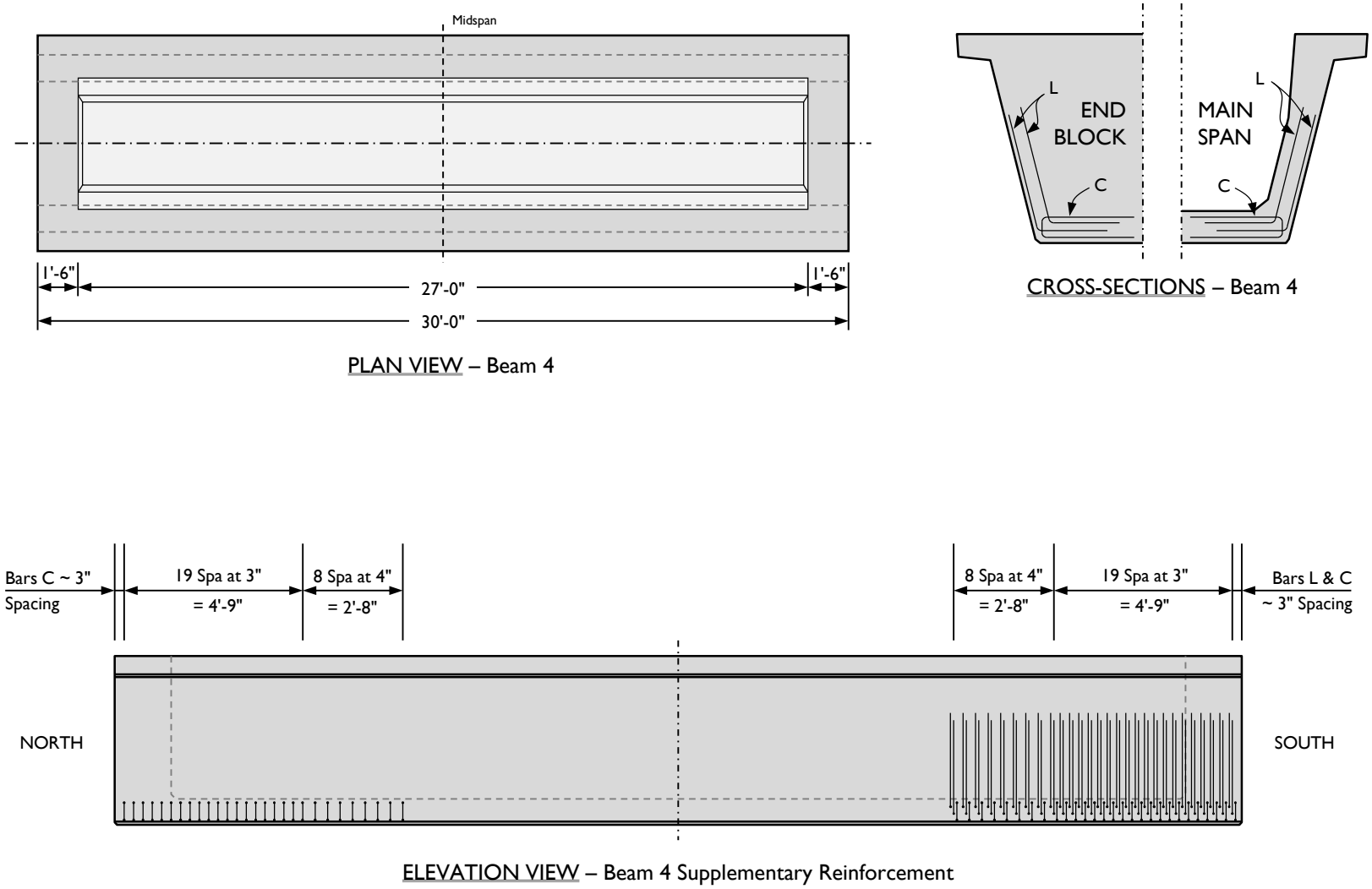

Figure A-21: Beam 4 plan view, elevation view, and sections showing supplementary reinforcement.

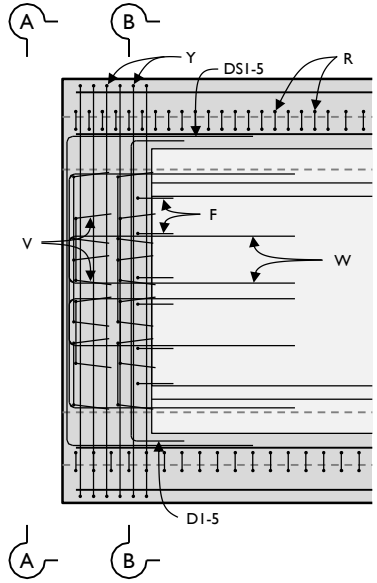

PLAN VIEW – B4N

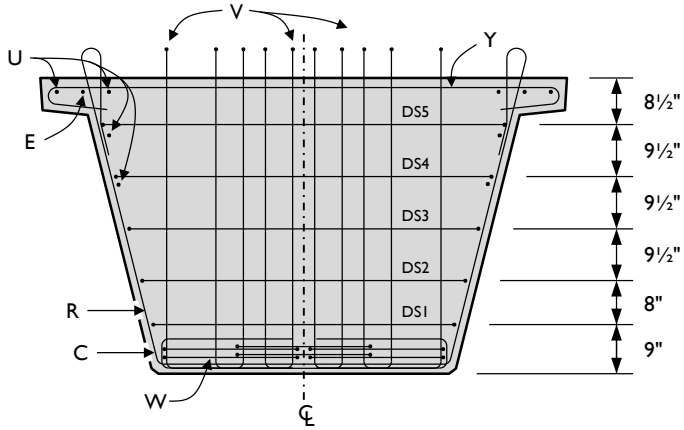

SECTION A-A – Beam 4N

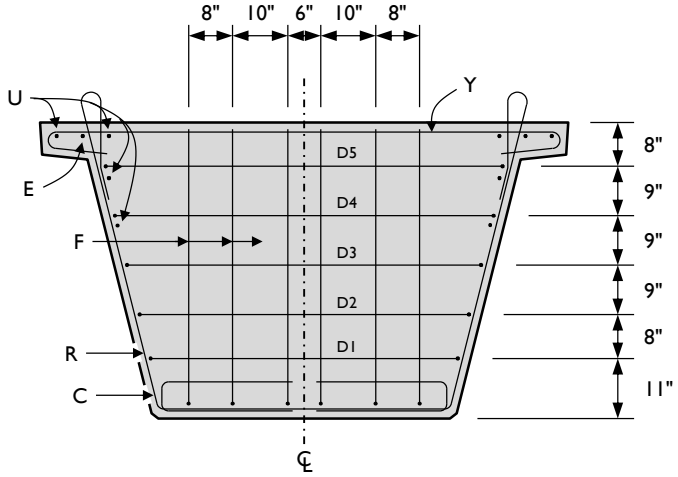

SECTION B-B – Beam 4N

Figure A-22: Beam 4 north end-region plan views and cross-sections.

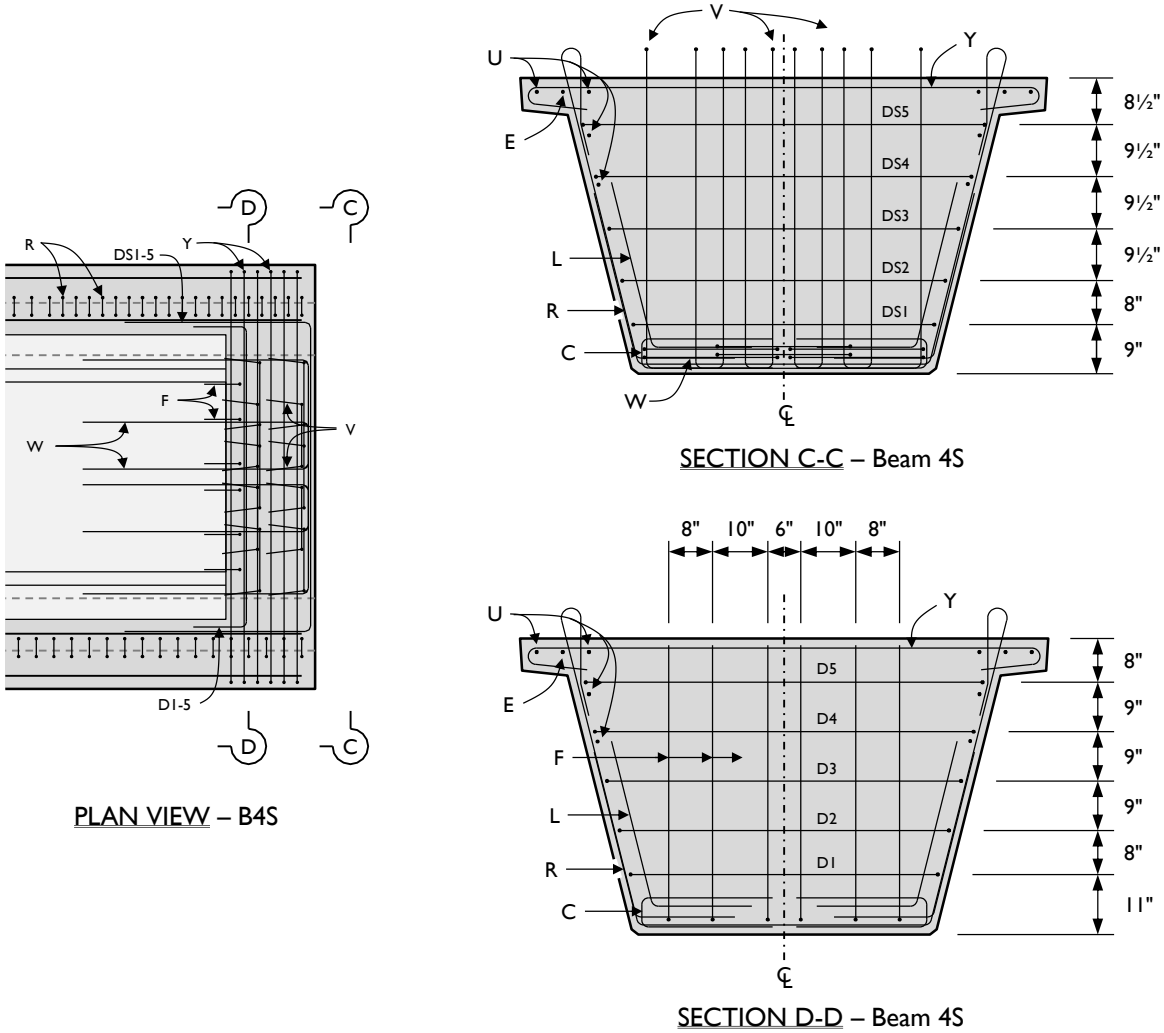

Figure A-23: Beam 4 south end region plan views and cross-sections.

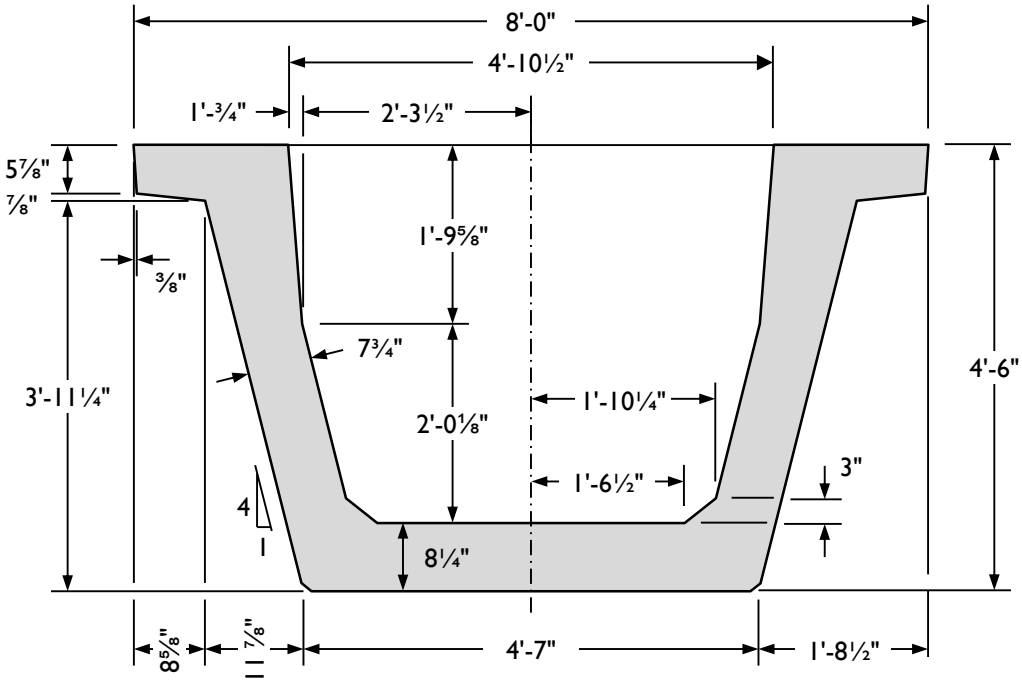

Figure A-24: Cross-sectional dimensions of the modified U-Beam used in Beam 4.

A.11 BEAM 5 INFORMATION AND DRAWINGS

The reinforcement design of Beam 5 contained modifications to the TxDOT standard, as were described in Chapter 5. The beam was square at both ends. The two ends were identical with respect to geometry, reinforcement, and prestressing. End block reinforcement was as shown in the standard. The prestressing strands were positioned as shown in Figure A-25. A summary of information about the beam is given in Table A-8 and the beam drawings are shown in Figure A-26, Figure A-27, and Figure A-28.

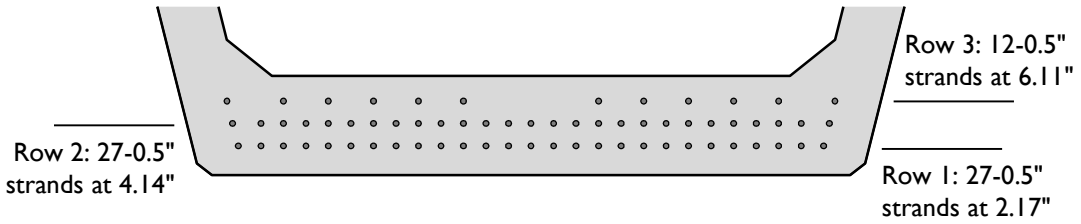

Figure A-25: Prestressing strand positions for Beam 5.

Table A-8: Summary of information about Beam 5.

BEAM 5 INFORMATION SUMMARY	North End		South End
GENERAL CHARACTERISTICS			
Beam test regions	B5N		B5S
Date of cast	17 November 2009		
Concrete mixture design designation	III-C (beam), I-G (deck)		
Fabrication location	Fabricator A		
End block geometry	square ext. square void 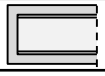		square ext. square void 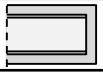
Prestressing force	66 ½" strands at 202.5 ksi		
RELEASE MEASUREMENTS			
Strength at release, f'_{ci} (release factor[1])	5.6 ksi (0.65)		
Maximum release crack width	0.005 in.		0.005 in.
Maximum stresses observed at release	[no data gathered]		
TEMPERATURE MEASUREMENTS			
Ambient temperature during cast and curing	39-68°F		
Maximum temperature during curing	[temperature data not recorded]		
Maximum temperature differential during curing	[temperature data not recorded]		
Maximum temperature at release point	[temperature data not recorded]		
SHEAR TESTING INFORMATION			
Shear test date	02 February 2010		[not tested]
28-day strength	12.4 ksi		
Compressive strength at testing, f'_c	13.2 ksi		
Deck compressive strength at testing, f'_{c_deck}	7.6 ksi		
Reinforcing steel strength, f_y	63.8 ksi		
Bearing condition during shear testing	single bearing pad		
Shear span (span-to-depth ratio)	154 (2.6)		
Failure shear	1031 kip		
Rebar spacing	4" for 8'-3"	6" for 13'-6"	4" for 8'-3"
Calculated shear capacity (AASHTO LRFD General Method)	1032 kip	925 kip	
V_{test} / $V_{calculated}$ with given rebar spacing	1.00	1.11	
Shear failure mode	flexure-shear		
Horizontal shear demand	1580 kip		
Calculated horizontal shear capacity	1691 kip		
Horizontal shear performance ratio	0.93		

[1] Release factor is equal to the ratio of bottom fiber stress to concrete strength at time of transfer

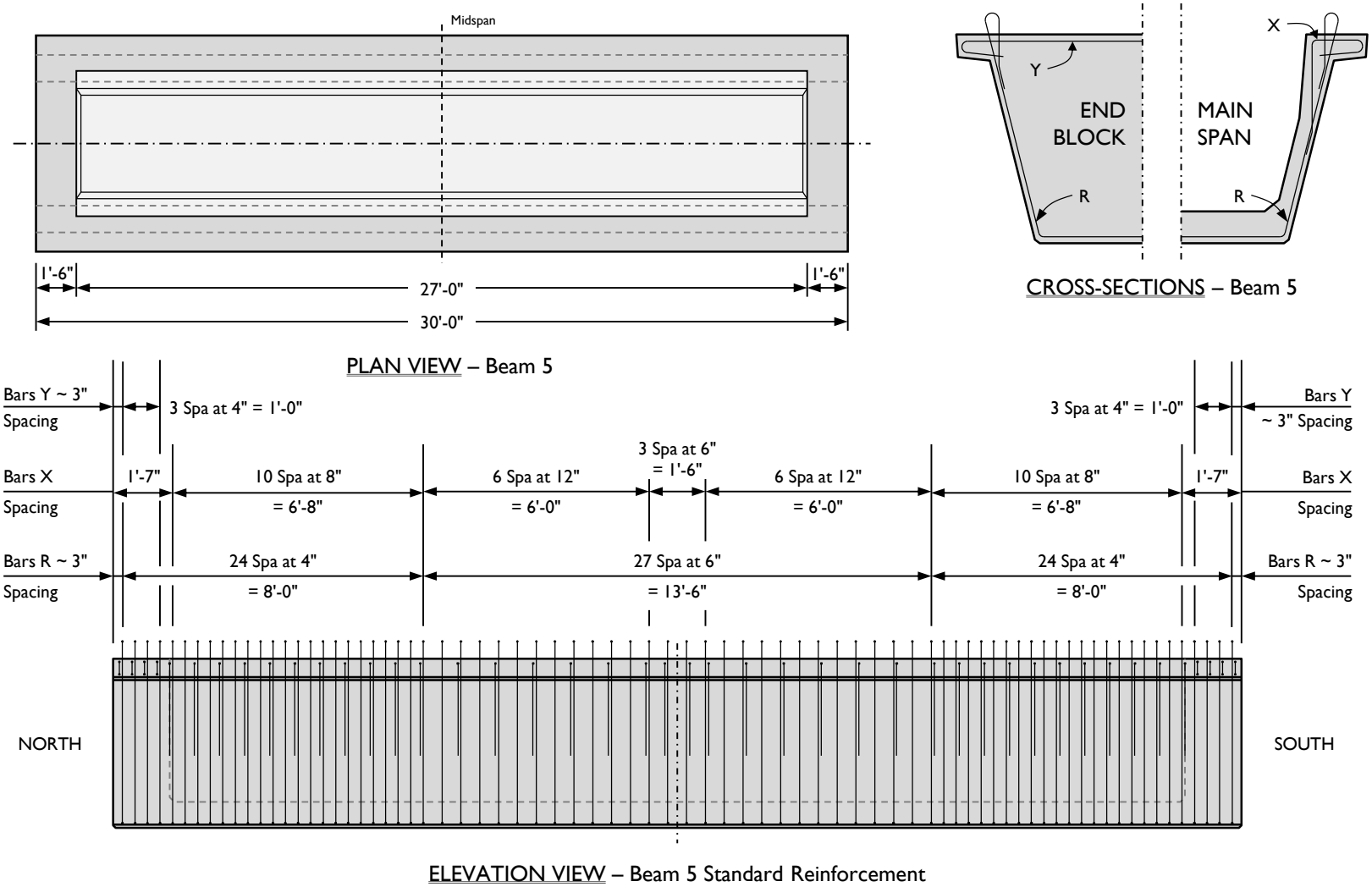

Figure A-26: Beam 5 plan view, elevation view, and sections showing standard reinforcement.

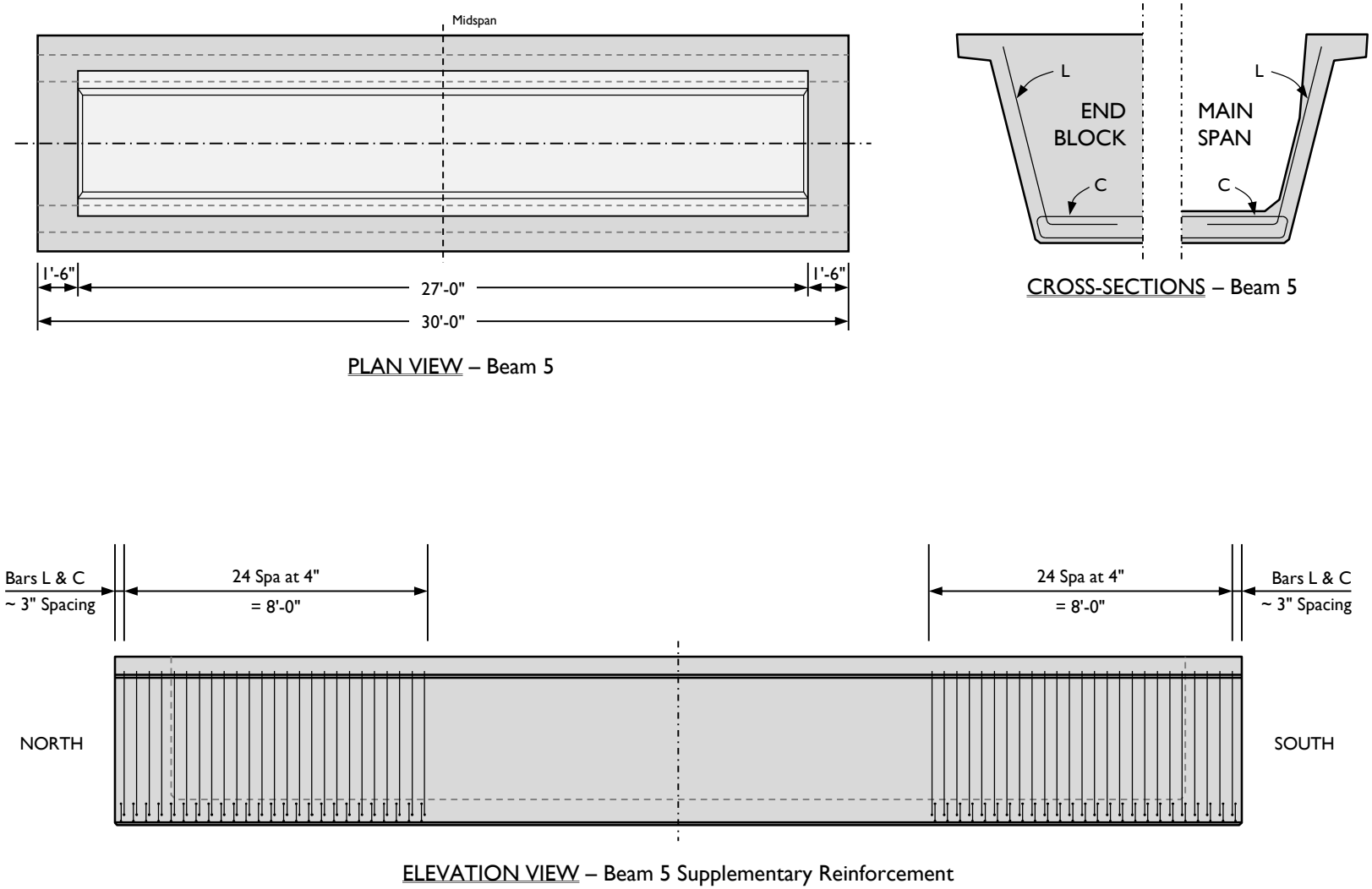

Figure A-27: Beam 5 plan view, elevation view, and sections showing supplementary reinforcement.

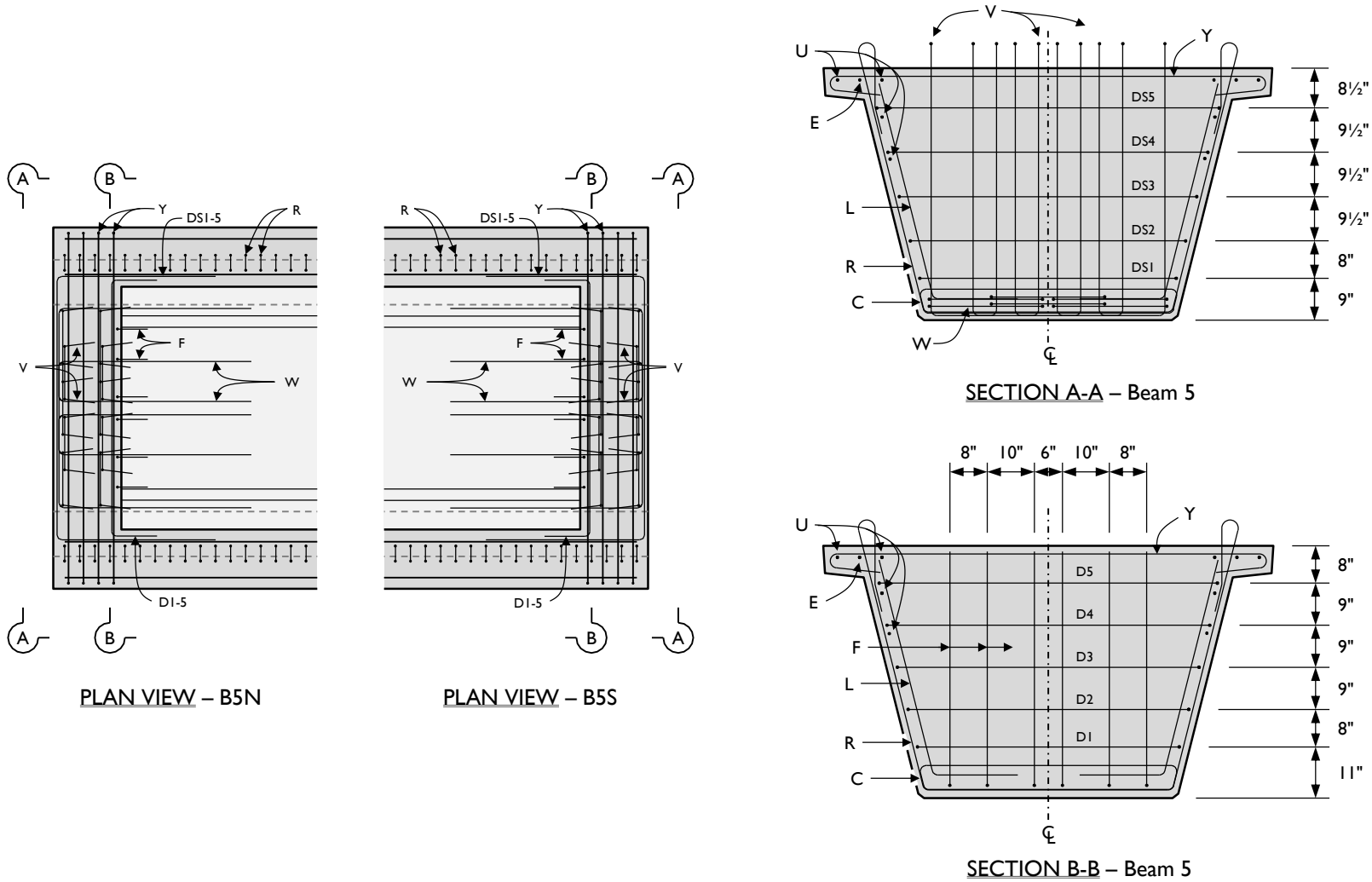

Figure A-28: Beam 5 end-region plan views and cross-sections.

A.12 BEAM 6 INFORMATION AND DRAWINGS

The reinforcement design of Beam 6 contained modifications to the TxDOT standard, as were described in Chapter 5. The beam was square at both ends. The two ends had slight differences with respect to geometry (end block length) and reinforcement. The prestressing was identical on the two ends, with the prestressing strands positioned as shown in Figure A-29. A summary of information about the beam is given in Table A-9 and the beam drawings are shown in Figure A-30, Figure A-31, and Figure A-32.

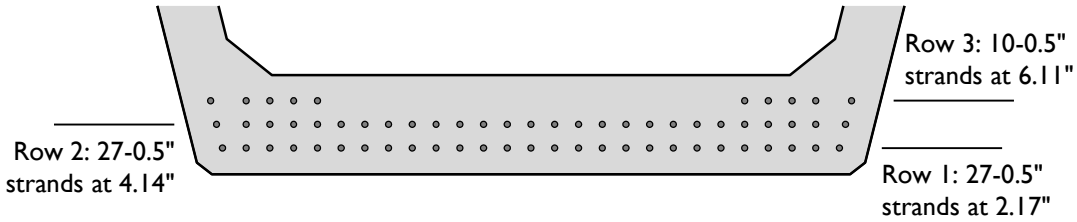

Figure A-29: Prestressing strand positions for Beam 6.

Table A-9: Summary of information about Beam 6.

BEAM 6 INFORMATION SUMMARY	North End		South End
GENERAL CHARACTERISTICS			
Beam test regions	B6N		B6S
Date of cast	11 November 2010		
Concrete mixture design designation	III-D (beam), I-H (deck)		
Fabrication location	Fabricator B		
End block geometry	square ext. square void 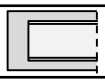		square ext. square void 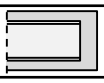
Prestressing force	64 ½" strands at 202.5 ksi		
RELEASE MEASUREMENTS			
Strength at release, f'_{ci} (release factor[1])	5.3 ksi (0.66)		
Maximum release crack width	0.007 in.		0.007 in.
Maximum stresses observed at release	[no data gathered]		
TEMPERATURE MEASUREMENTS			
Ambient temperature during cast and curing	65-84°F		
Maximum temperature during curing	[data not recorded]		163°F
Maximum temperature differential during curing	[data not recorded]		53°F
Maximum temperature at release point	[temperature data not recorded]		
SHEAR TESTING INFORMATION			
Shear test date	[not tested]		11 January 2011
28-day strength	11.4 ksi		
Compressive strength at testing, f'_c			12.0 ksi
Deck compressive strength at testing, f'_{c_deck}			10.7 ksi
Reinforcing steel strength, f_y			85.0 ksi
Bearing condition during shear testing			single bearing pad
Shear span (span-to-depth ratio)			154 (2.6)
Failure shear			1054 kip
Rebar spacing	4" for 8'-3"	6" for 13'-6"	4" for 8'-3"
Calculated shear capacity (AASHTO LRFD General Method)		832 kip	964 kip
V_{test} / $V_{calculated}$ with given rebar spacing		1.27	1.09
Shear failure mode			flexure-shear
Horizontal shear demand			1613 kip
Calculated horizontal shear capacity			2123 kip
Horizontal shear performance ratio			0.76

[1] Release factor is equal to the ratio of bottom fiber stress to concrete strength at time of transfer

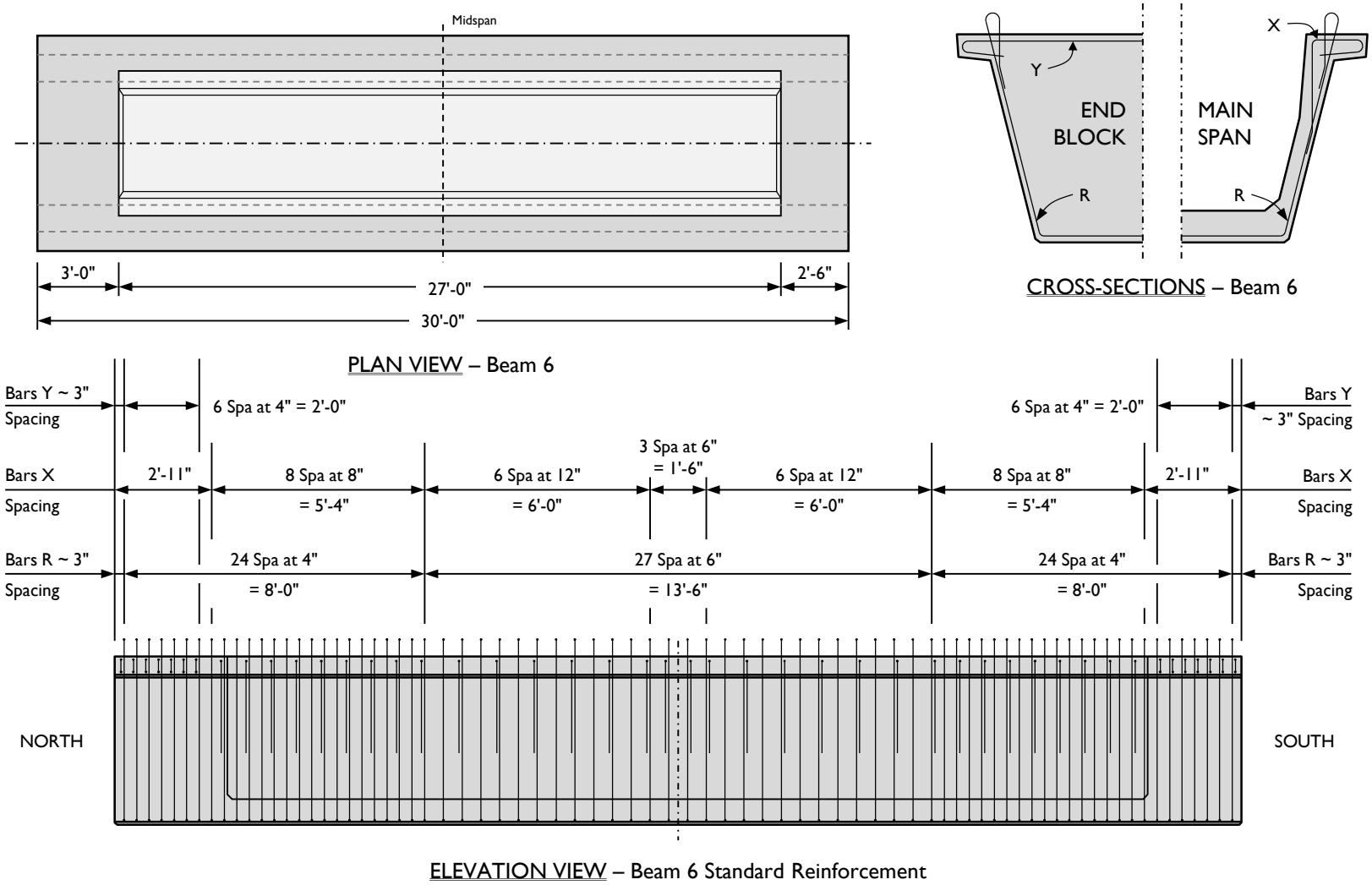

Figure A-30: Beam 6 plan view, elevation view, and sections showing standard reinforcement.

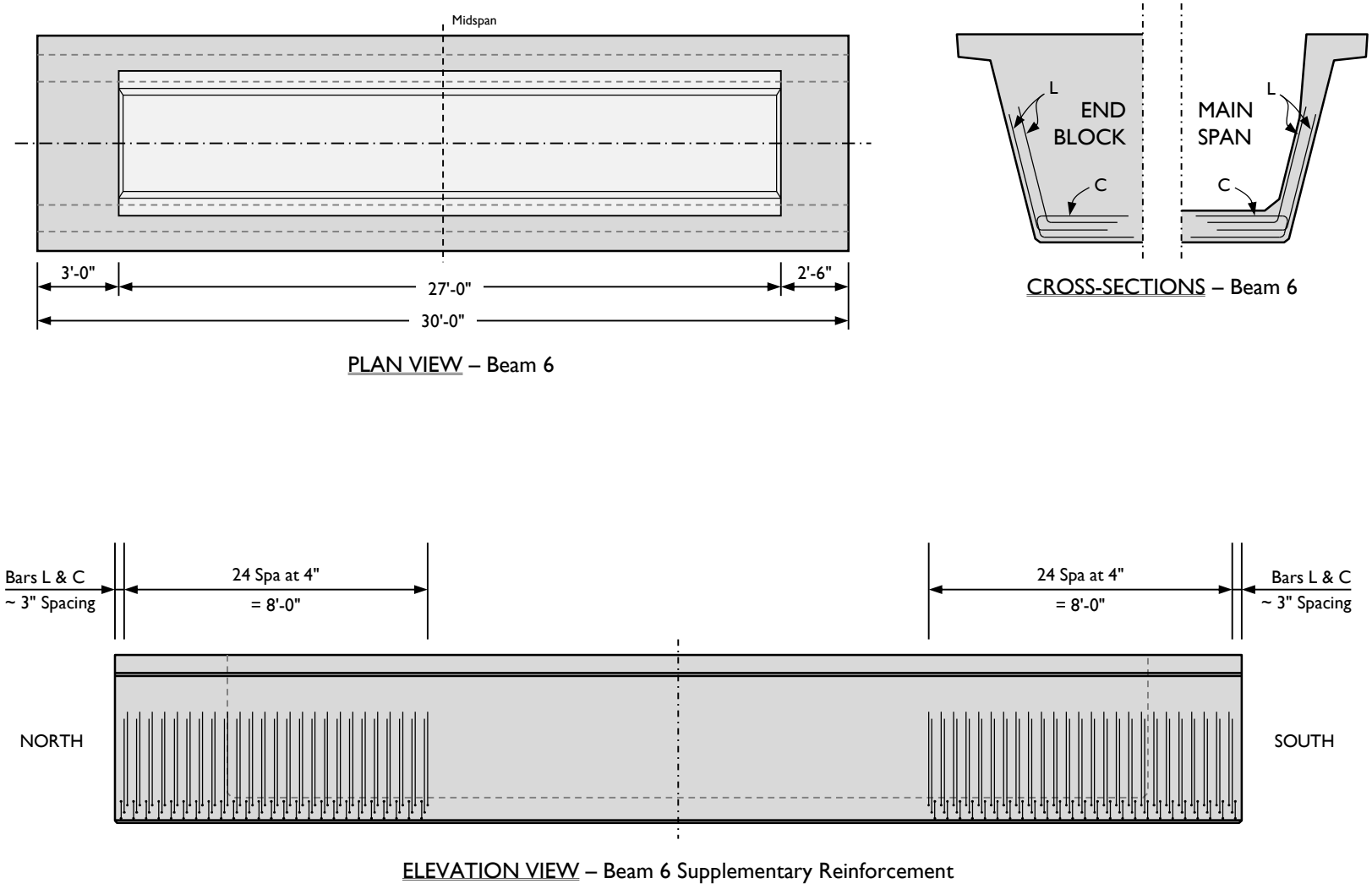

Figure A-31: Beam 6 plan view, elevation view, and sections showing supplementary reinforcement.

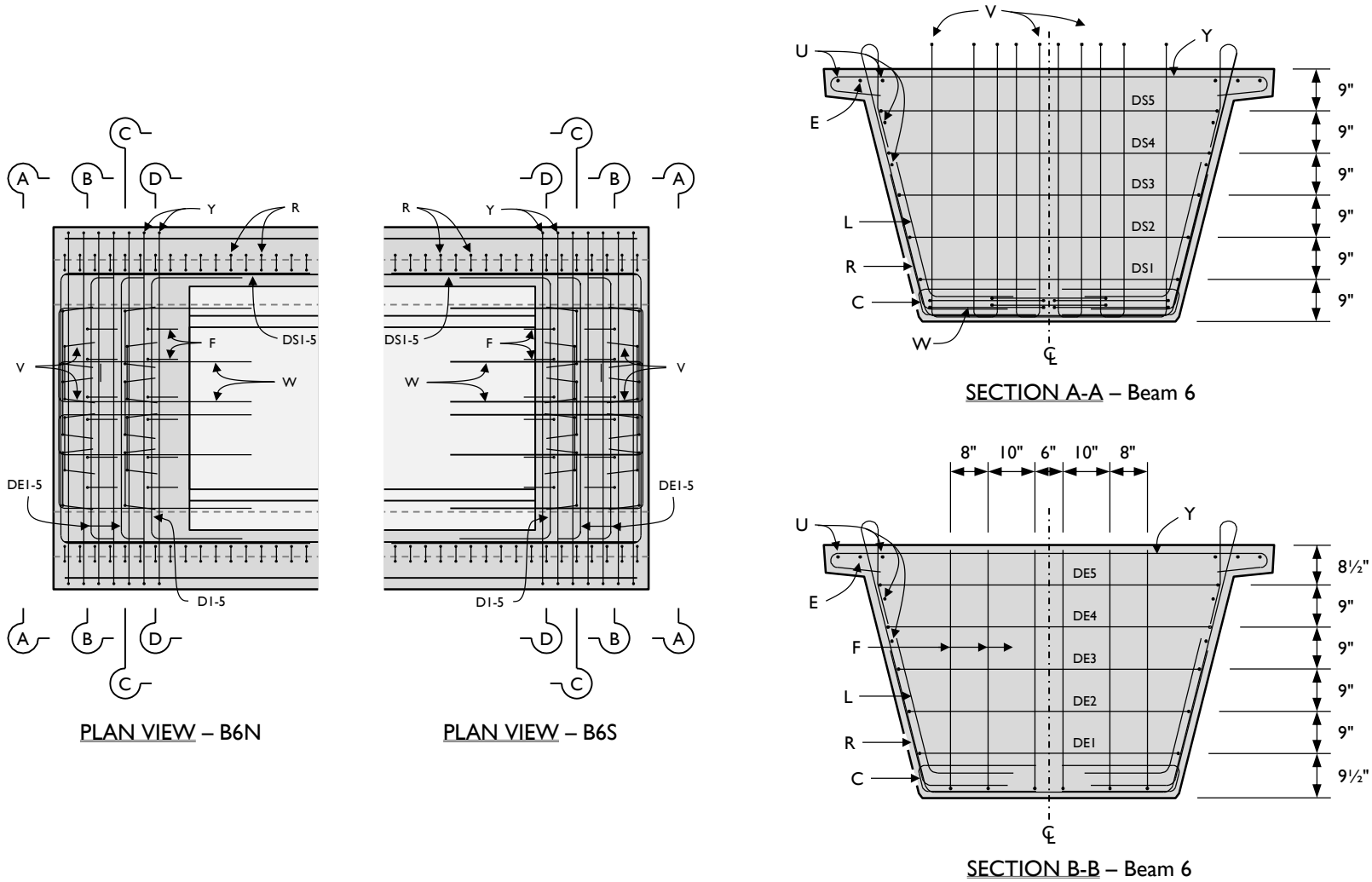

Figure A-32: Beam 6 end-region plan views and cross-sections (1 of 2).

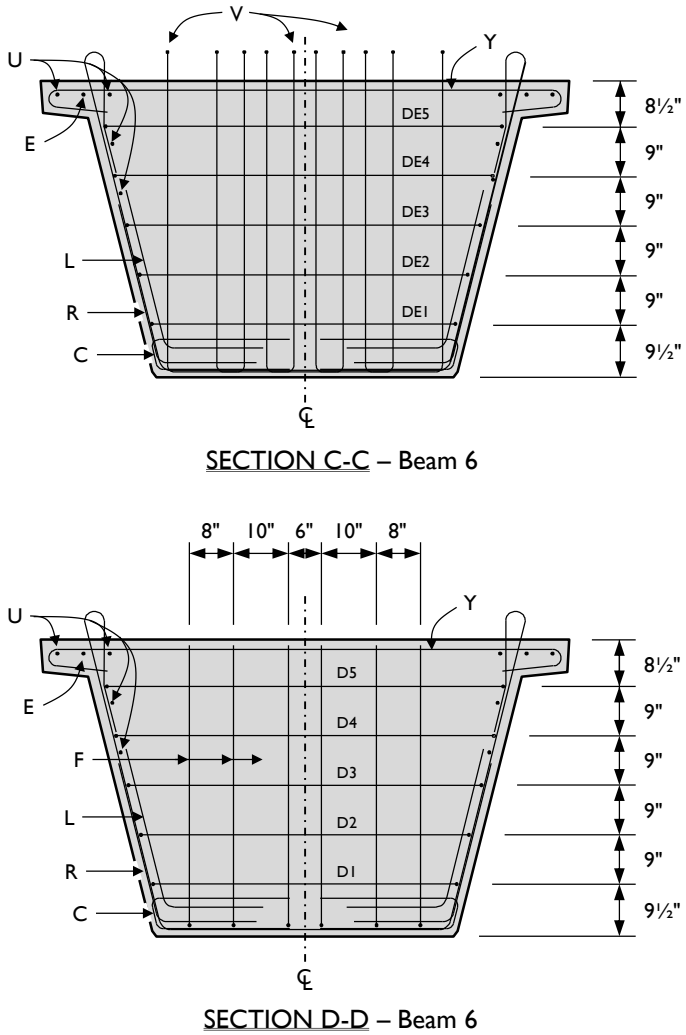

Figure A-32: Beam 6 end-region plan views and cross-sections (2 of 2).

A.13 BEAM 7 INFORMATION AND DRAWINGS

The reinforcement design of Beam 7 matched that of Beam 6, with several modifications to the TxDOT standard, as described in Chapter 5. The beam was square at one end and skewed to 45° at the other. The prestressing is shown in Figure A-33, with 58 0.6-in. diameter prestressing strands used. Five strands in the second row were debonded the full length of the beam (Table A-10). A summary of information about the beam is given in Table A-11 and the beam drawings are shown in Figure A-34, Figure A-35, Figure A-36, and Figure A-37.

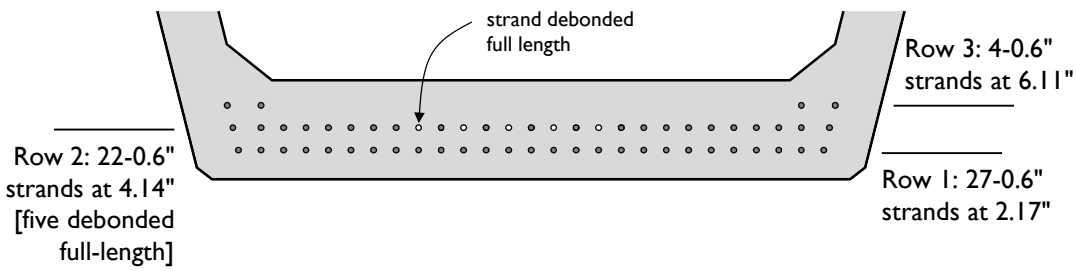

Figure A-33: Prestressing strand positions for Beam 7.

Table A-10: Details of debonding pattern used in Beam 7.

STRUCTURE	DEBONDED STRAND PATTERN PER ROW							
	DIST FROM BOTTOM (in.)	NO. OF STRANDS		NUMBER OF STRANDS DEBONDED TO (ft from end)				
		TOTAL	DE-BOND	3	6	9	12	Full-Length
UT U-Beam 7	2.17	27	0					
	4.14	27	5					5
	6.11	4	0					

Table A-11: Summary of information about Beam 7.

BEAM 7 INFORMATION SUMMARY	North End		South End
GENERAL CHARACTERISTICS			
Beam test regions	B7N		B7S
Date of cast	27 April 2011		
Concrete mixture design designation	III-E (beam), I-H (deck)		
Fabrication location	Fabricator C		
End block geometry	45° exterior square void 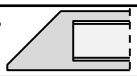		square ext. square void 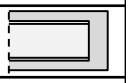
Prestressing force	58 0.6" strands at 202.5 ksi, 53 (91%) bonded at beam end		
RELEASE MEASUREMENTS			
Strength at release, f'_{ci} (release factor[1])	7.9 ksi (0.55)		
Maximum release crack width	0.013 in.		0.013 in.
Maximum stresses observed at release	[no data gathered]		
TEMPERATURE MEASUREMENTS			
Ambient temperature during cast and curing	70-97°F		
Maximum temperature during curing	[data not recorded]		
Maximum temperature differential during curing	[temperature data not recorded]		
Maximum temperature at release point	[temperature data not recorded]		
SHEAR TESTING INFORMATION			
Shear test date	25 May 2011		[not tested]
28-day strength	12.4 ksi		
Compressive strength at testing, f'_c	12.4 ksi		
Deck compressive strength at testing, f'_{c_deck}	9.6 ksi		
Reinforcing steel strength, f_y	62.5 ksi		
Bearing condition during shear testing	single bearing pad		
Shear span (span-to-depth ratio)	154 (2.6)		
Failure shear	1210 kip		
Rebar spacing	4" for 8'-3"	6" for 13'-6"	4" for 8'-3"
Calculated shear capacity (AASHTO LRFD General Method)	913 kip	735 kip	
V_{test} / $V_{calculated}$ with given rebar spacing	1.33	1.65	
Shear failure mode	web crushing		
Horizontal shear demand	1841 kip		
Calculated horizontal shear capacity	2420 kip		
Horizontal shear performance ratio	0.76		

[1] Release factor is equal to the ratio of bottom fiber stress to concrete strength at time of transfer

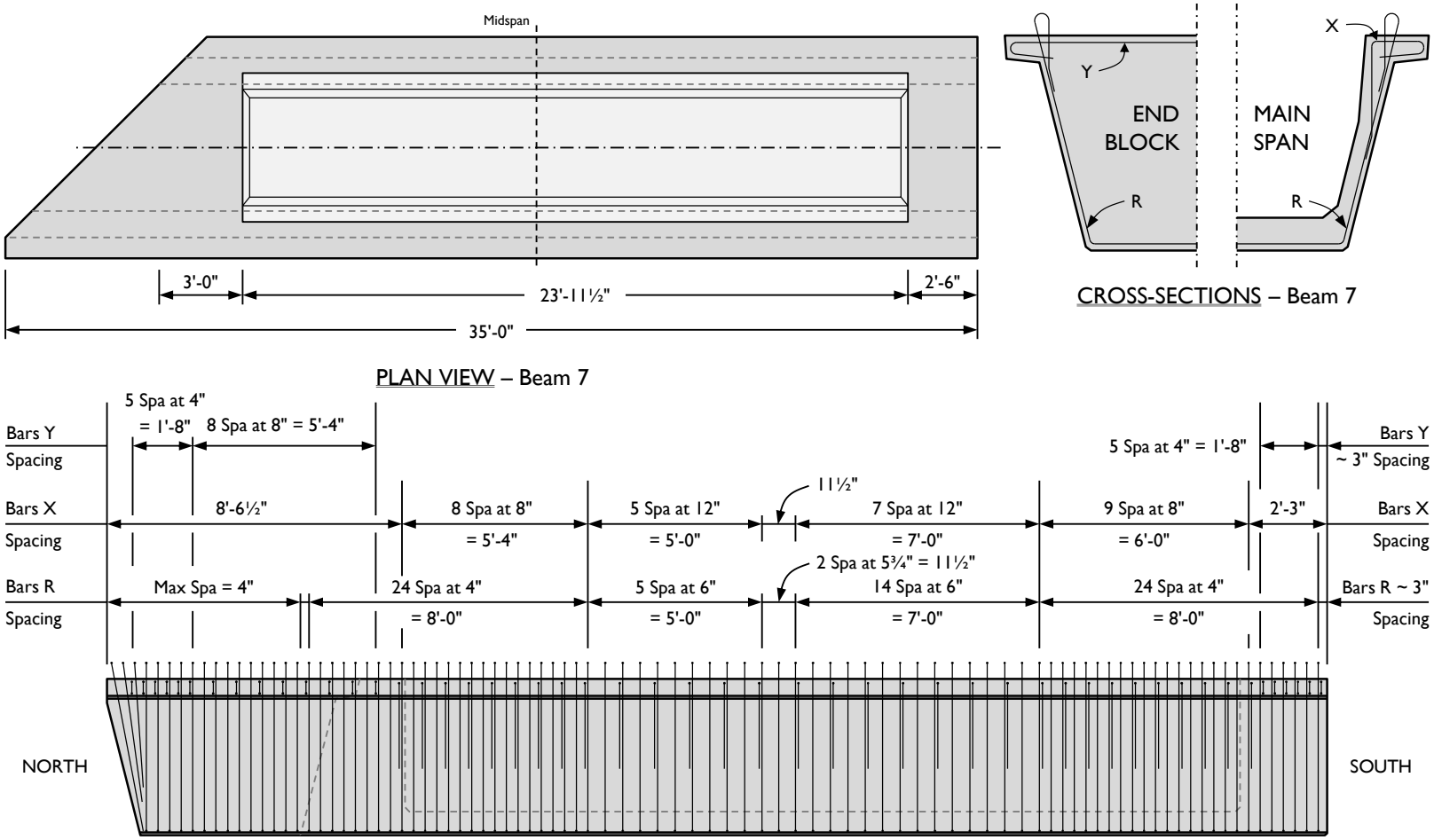

Figure A-34: Beam 7 plan view, elevation view, and sections showing standard reinforcement.

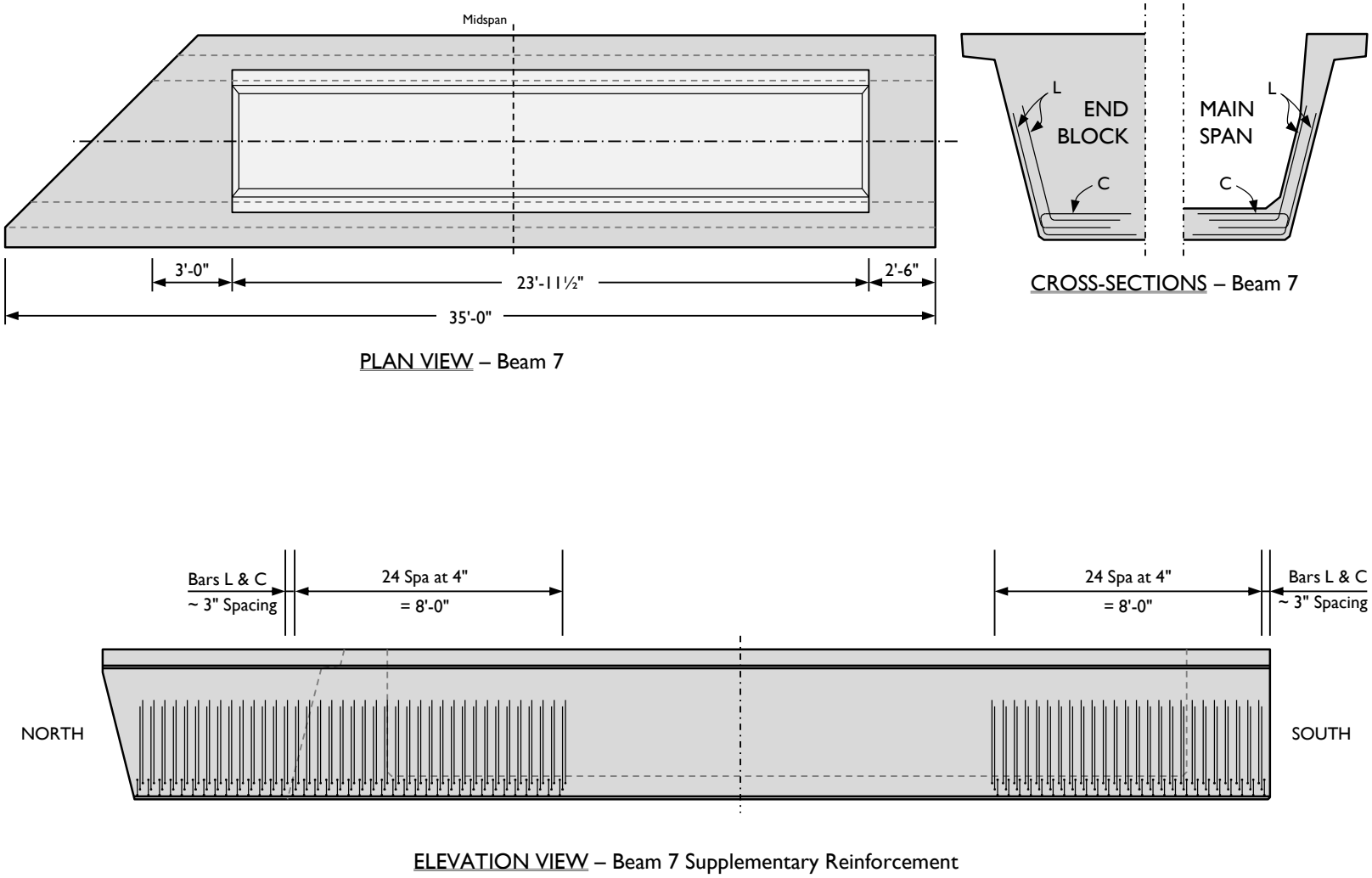

Figure A-35: Beam 7 plan view, elevation view, and sections showing supplementary reinforcement.

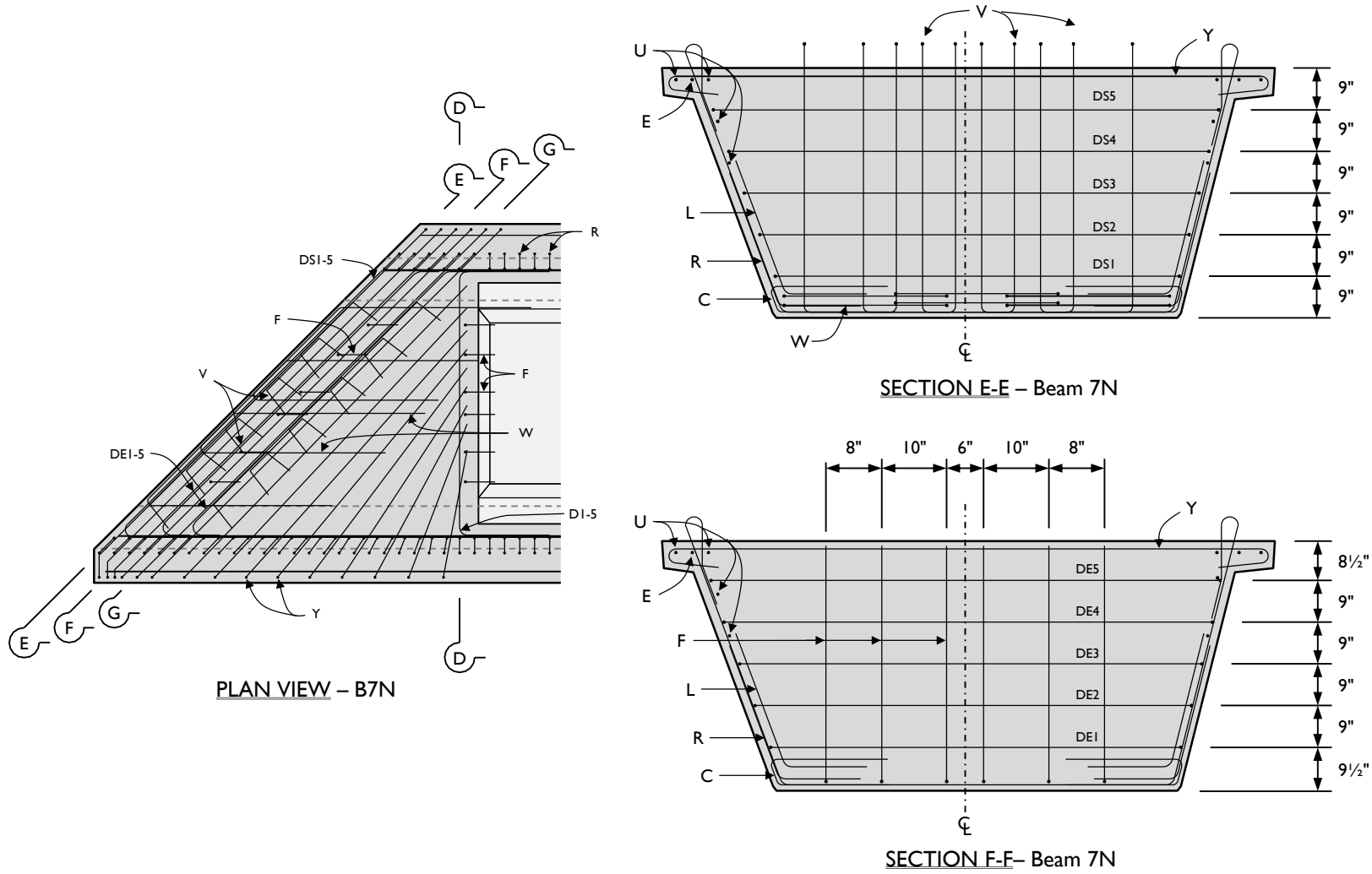

Figure A-36: Beam 7 north end-region plan views and cross-sections (1 of 2).

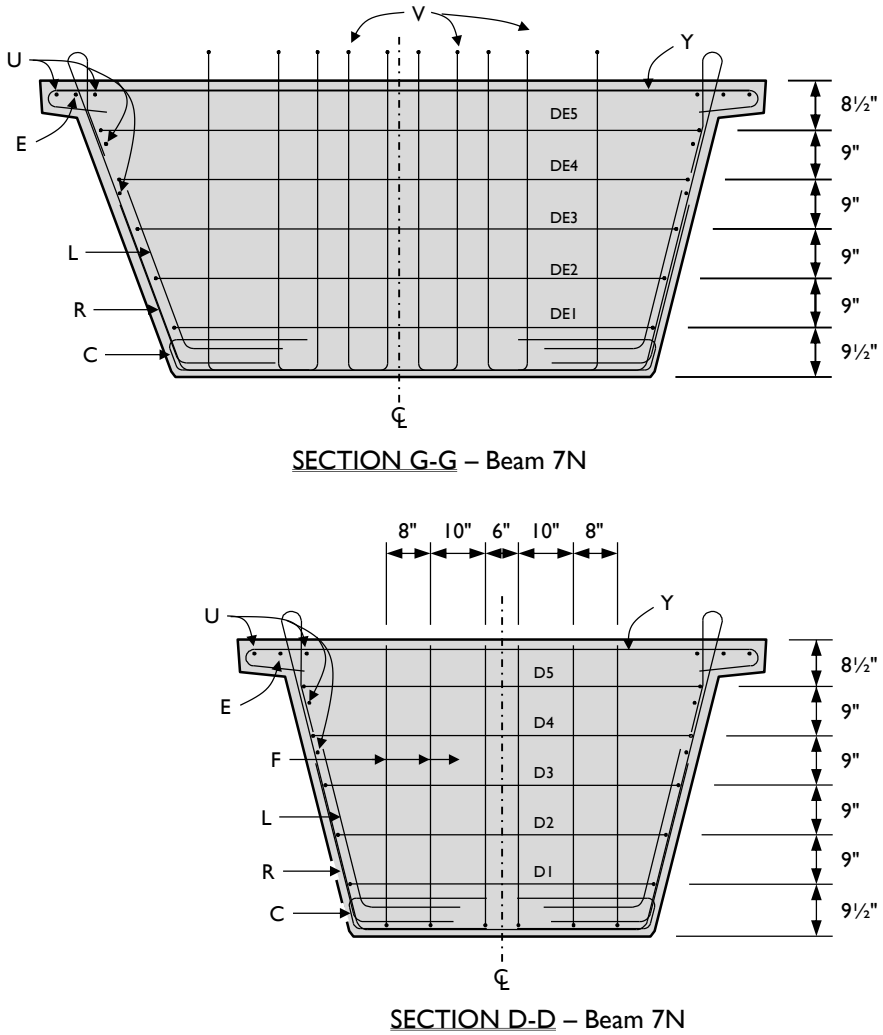

Figure A-36: Beam 7 north end-region plan views and cross-sections (2 of 2).

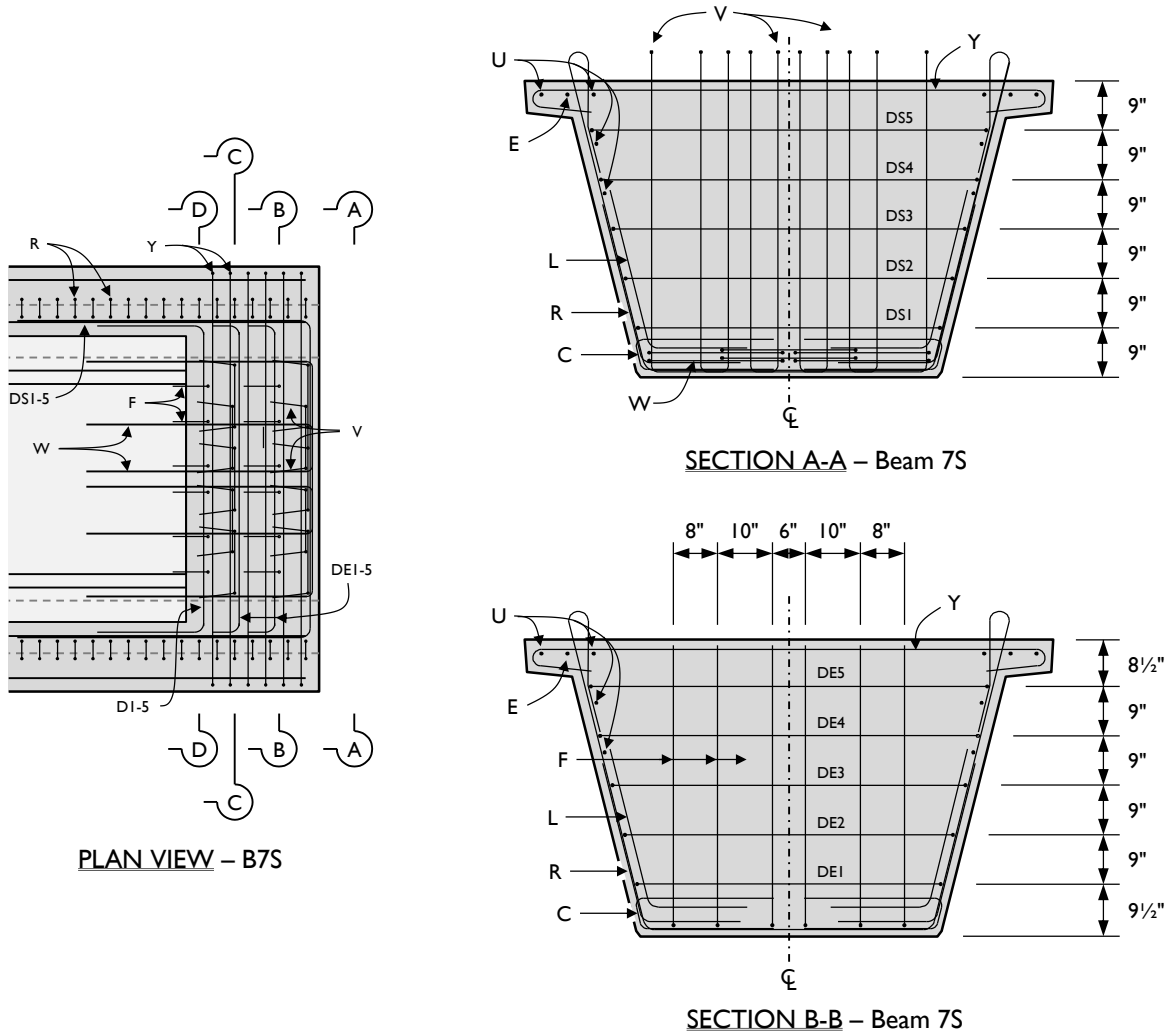

Figure A-37: Beam 7 south end-region plan views and cross-sections (1 of 2).

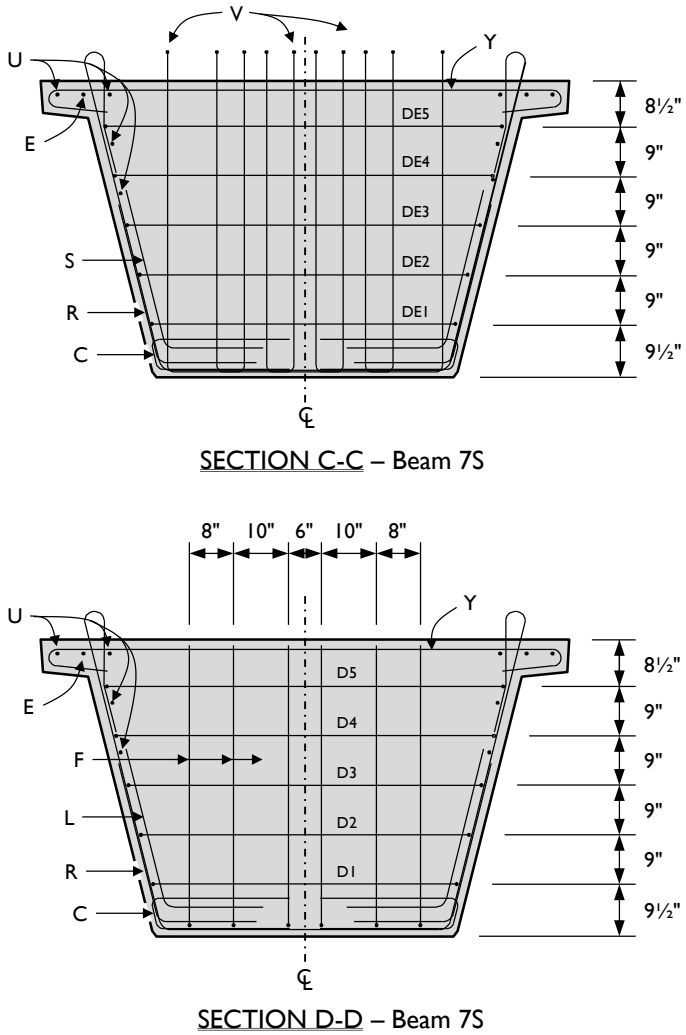

Figure A-37: Beam 7 south end-region plan views and cross-sections (2 of 2).

APPENDIX B
Collected Data

B.1 OVERVIEW

Within Chapter 6, the collected data were often shown en masse (without differentiation regarding test specifics) or singularly (as an example of typical behavior). These reductions in presented data highlighted differences or trends and allowed the rationale behind conclusions to be seen. All collected data are presented in this chapter, split apart by beam or beam test. Each graph corresponds with a graph presented in Chapter 6, with clear explanation of the origin of each data point. Seven data sets are presented: (i) reinforcing bars stresses measured at prestress transfer, (ii) concrete temperatures measured during curing, and (iii) web distortion, (iv) load distribution, (v) maximum crack widths, (vi) vertical strain in web walls, and (vii) strain in reinforcing bars, each measured during shear testing.

B.2 END-REGION STRESSES AT PRESTRESS TRANSFER

Strains measured in reinforcing bars at prestress transfer were transformed into stresses using an assumed modulus of elasticity for the steel of 29,000 ksi. The "measured" stresses in each end region of the four monitored beams are presented in the following four figures, along with the cracks observed after transfer.

The diameter of the circles is indicative of the magnitude of the stress seen in the bar at that location. The color of the circle indicates the stress range: a blue circle was used for stresses less than 10 ksi; a green circle for stresses between 10 and 20 ksi. A red circle was used when measured bar stresses exceeded 20 ksi.

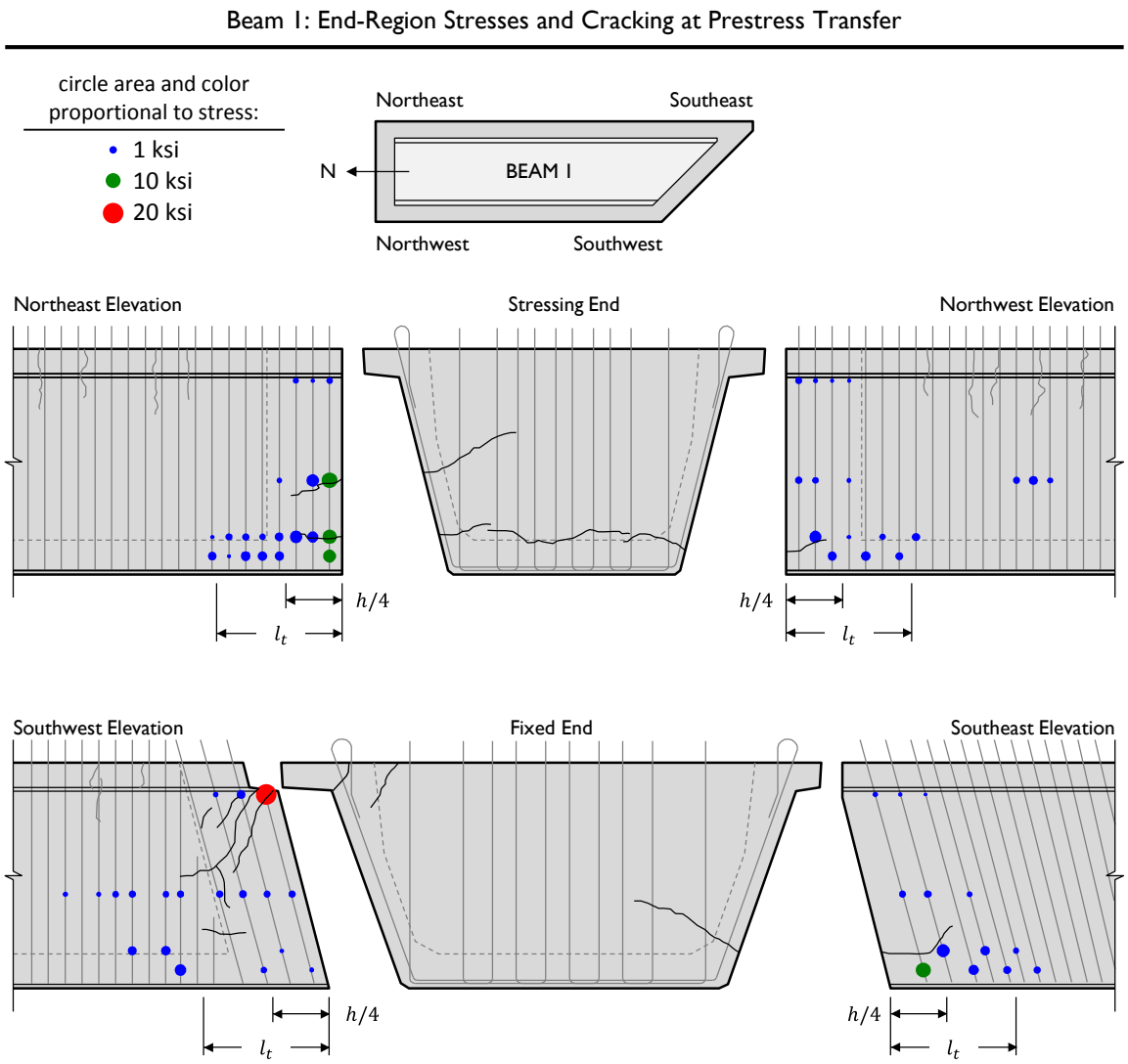

Figure B-1: Magnitude and location of cracking and stresses induced in reinforcement at prestress transfer for Beam 1.

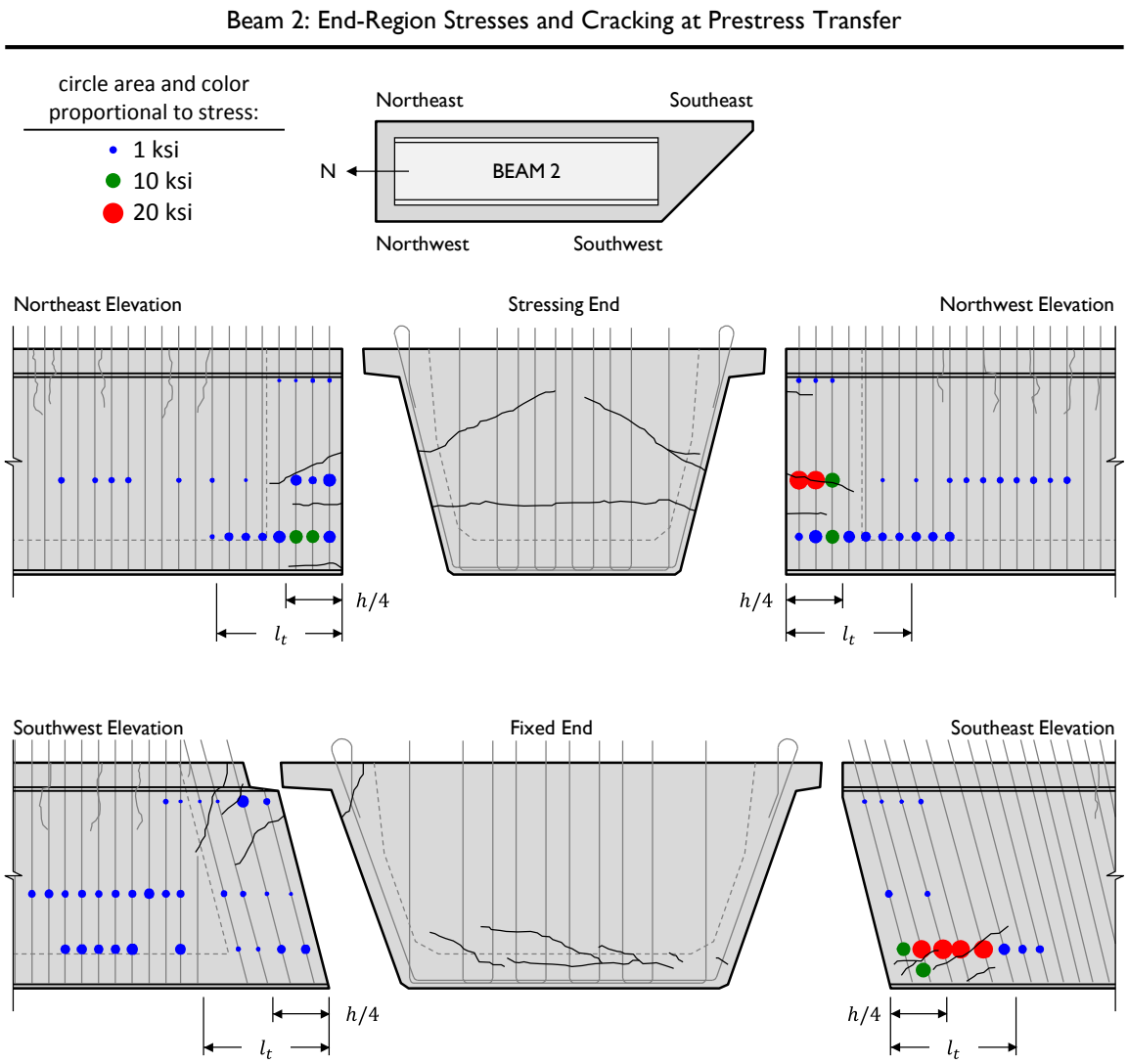

Figure B-2: Magnitude and location of cracking and stresses induced in reinforcement at prestress transfer for Beam 2.

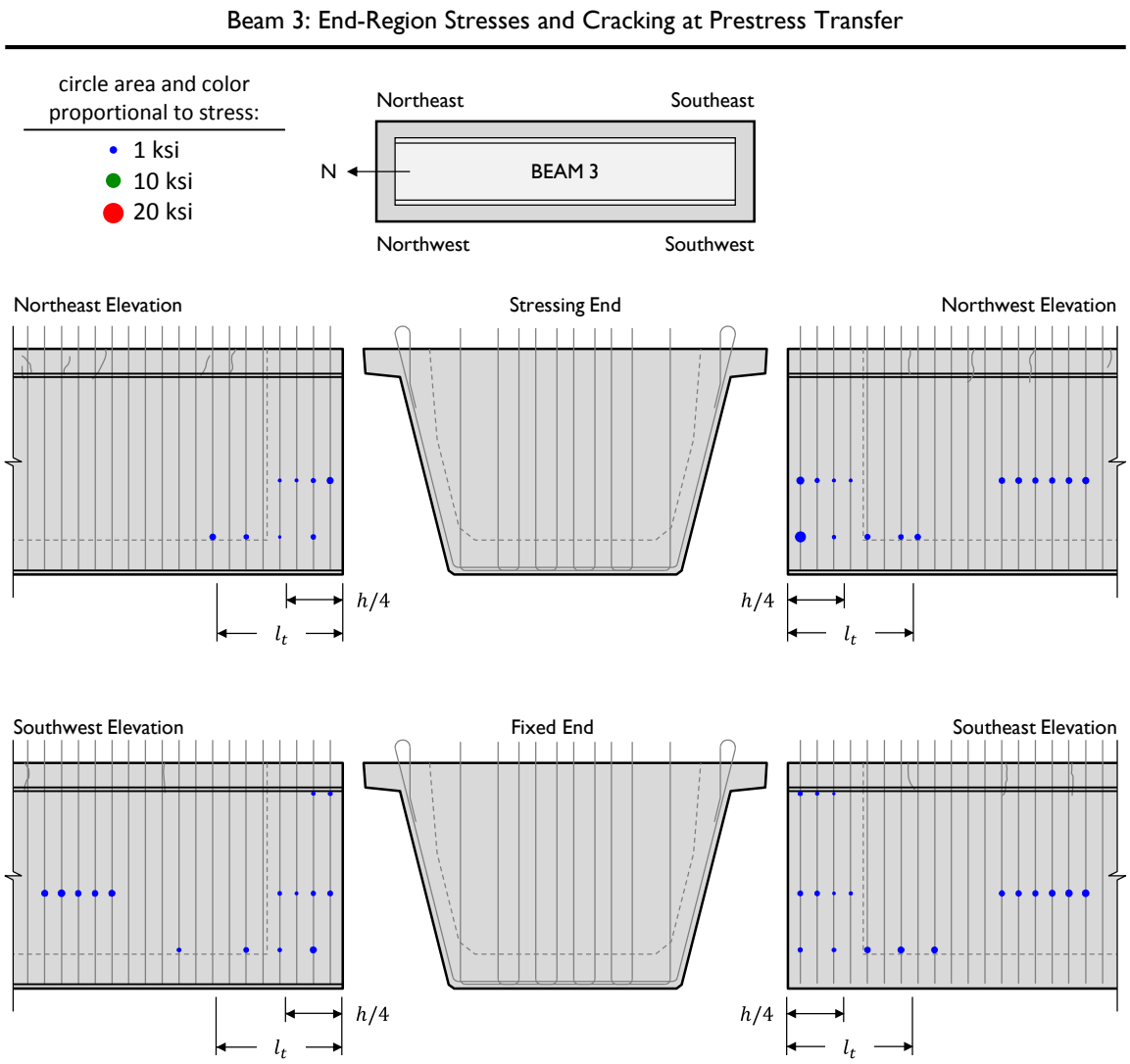

Figure B-3: Magnitude and location of cracking and stresses induced in reinforcement at prestress transfer for Beam 3.

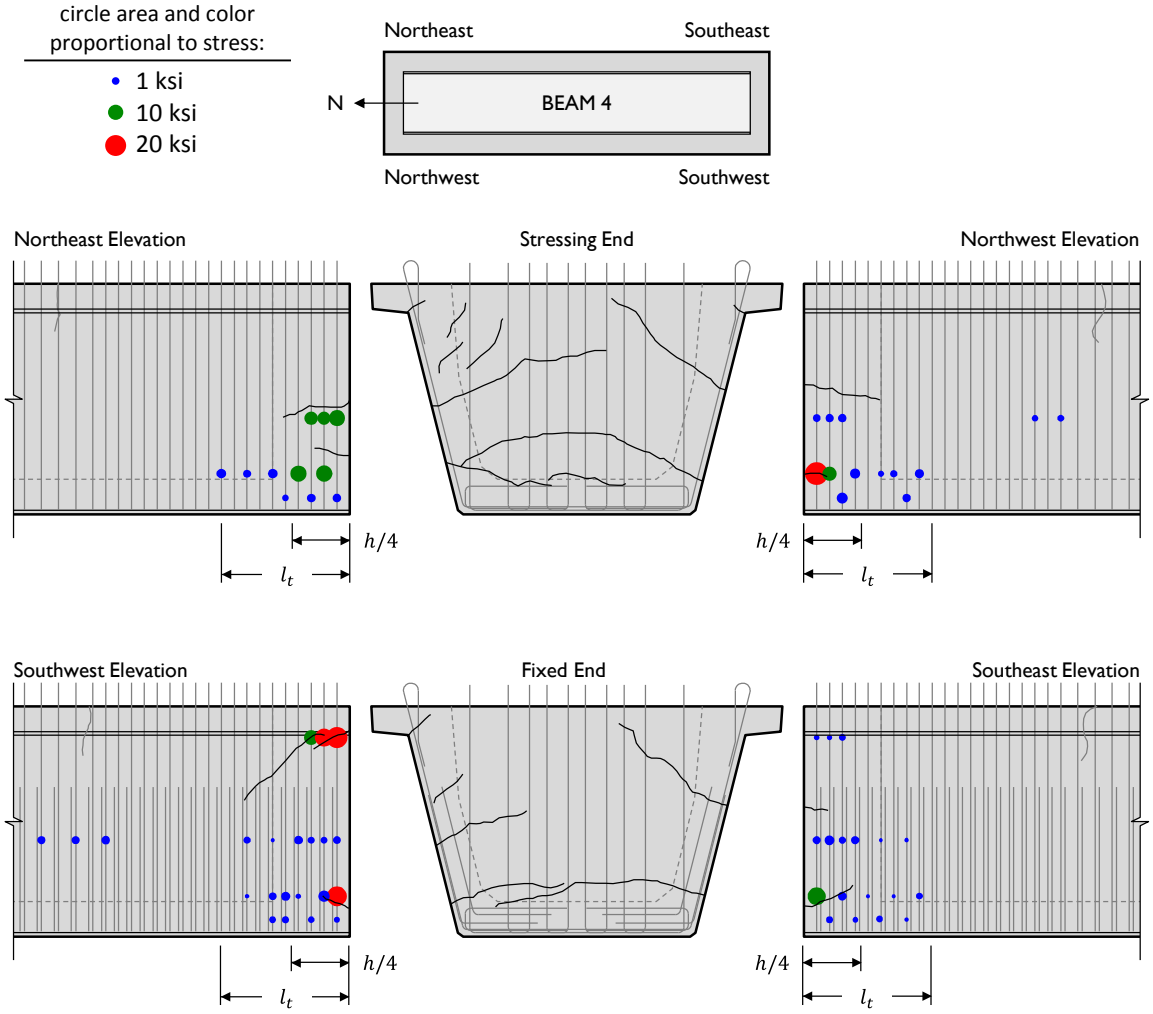

Figure B-4: Magnitude and location of cracking and stresses induced in reinforcement at prestress transfer for Beam 4.

B.3 CURING TEMPERATURES

The range of temperatures of the concrete in the end blocks of five beams were measured and are shown at two points during the curing process in the following five tables. First, the temperature distribution at the time of maximum temperature is given, then the distribution at the time of maximum temperature differential. Maximum temperatures and differentials that are in excess of the TxDOT limits set in the Standard Specifications are written in red, bold text.

Table B-1: Temperature measurements in Beam 1 (cast October, 2008).

Temperature Measurement	Beam 1N [rectangular] 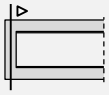	Beam 1S [45° skew] 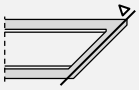
Maximum Temperature	137°F max 22 hours after cast 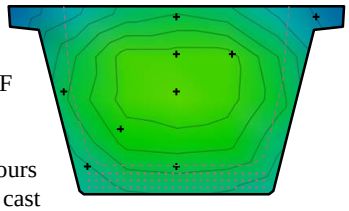	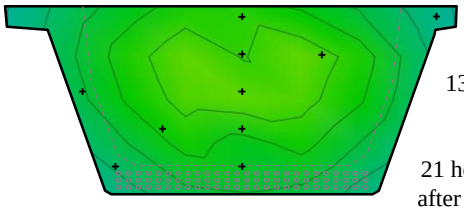 139°F max 21 hours after cast
Temperature Differential	**38**°F Δt_{max} 25 hours after cast 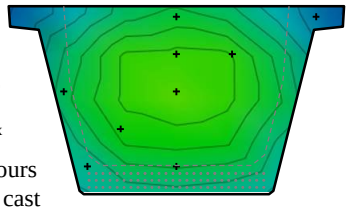	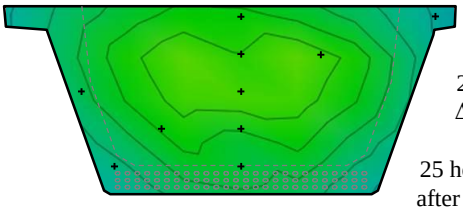 28°F Δt_{max} 25 hours after cast
Temperature Scale	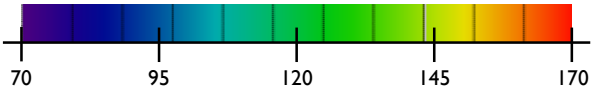	

Table B-2: Temperature measurements in Beam 2 (cast February, 2009).

Temperature Measurement	Beam 2N [rectangular] 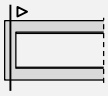	Beam 2S [45° skew] 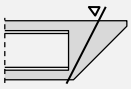
Maximum Temperature	142°F max 18 hours after cast 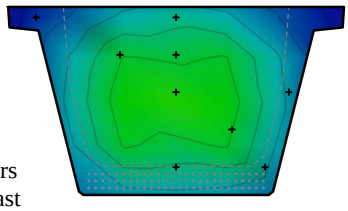	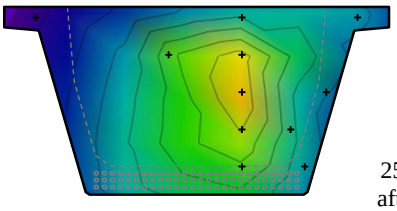 **160**°F max 25 hours after cast
Temperature Differential	**34**°F Δt_{max} 26 hours after cast 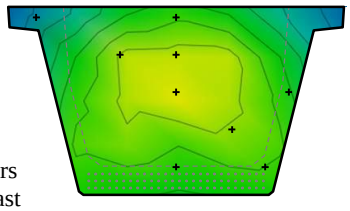	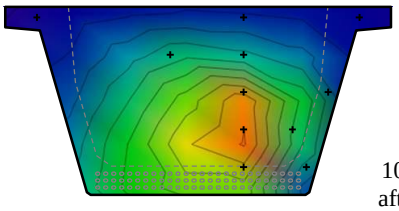 **55**°F Δt_{max} 10 hours after cast
Temperature Scale	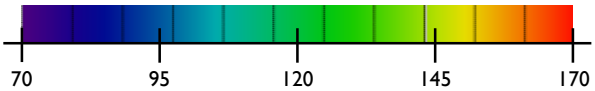	

Table B-3: Temperature measurements in Beam 3 (cast July, 2009).

Temperature Measurement	Beam 3N [rectangular] 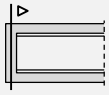	Beam 3S [rectangular] 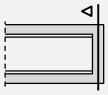
Maximum Temperature	165°F max 20 hours after cast 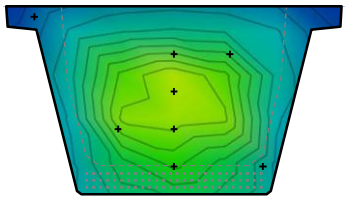	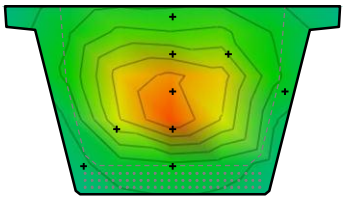 **184**°F max 21 hours after cast
Temperature Differential	**52**°F Δt_{max} 23 hours after cast 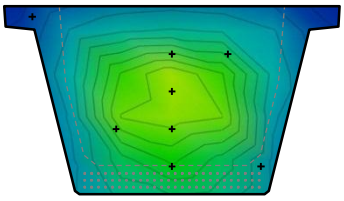	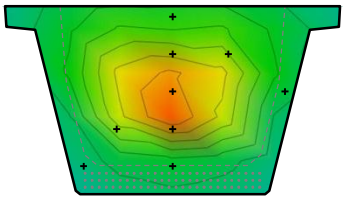 **47**°F Δt_{max} 23 hours after cast
Temperature Scale	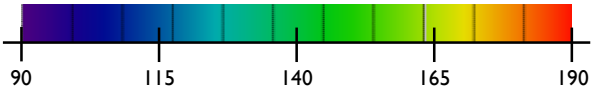	

Table B-4: Temperature measurements in Beam 4 (cast October, 2009).

Temperature Measurement	Beam 4N [no skew] 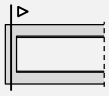	Beam 4S [no skew] 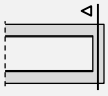
Maximum Temperature	131°F max 24 hours after cast 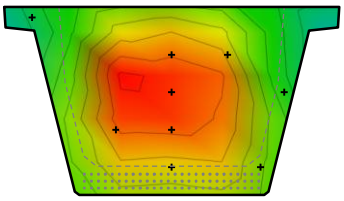	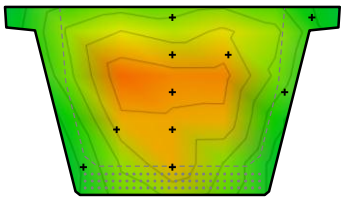 139°F max 29 hours after cast
Temperature Differential	**45**°F Δt_{max} 34 hours after cast 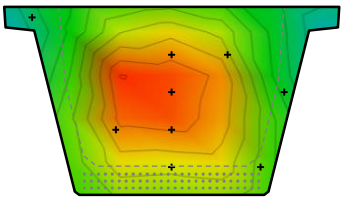	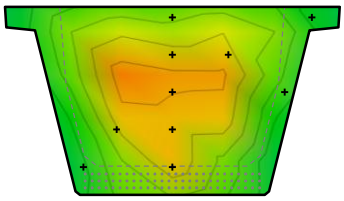 34°F Δt_{max} 27 hours after cast
Temperature Scale	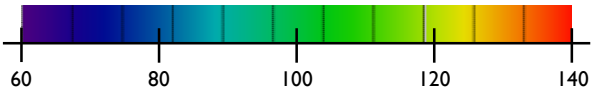	

Table B-5: Temperature measurements in Beam 6 (cast November, 2010).

Temperature Measurement	Beam 6S [no skew] 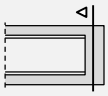
Maximum Temperature	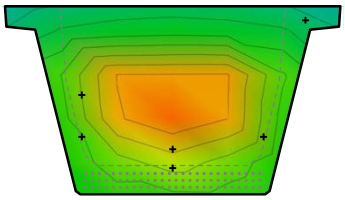 164°F max 15 hours after cast
Temperature Differential	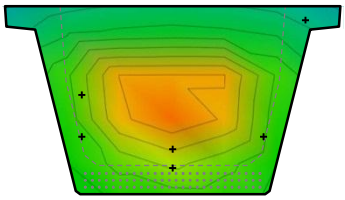 **53**°F ΔT_{max} hours after cast
Temperature Scale	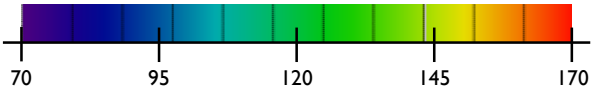

B.4 WEB DISTORTION

The distortion of the webs of six of the load-tested U-Beam end regions was measured using three linear potentiometers mounted on the web walls between load point and the bearing. The distortion was calculated following the equation provided in Chapter 6. The remaining five end-regions either were tested without the use of this instrumentation, or had errors occur during data collection, rendering the information useless.

The distortion found through the loading of these six test regions are given in the following four plots. When appropriate (i.e., when the test region failed in a typical web-shear mode), a horizontal line indicating the capacity of the test region is also plotted. The capacity was found using the AASHTO General Procedure (2010).

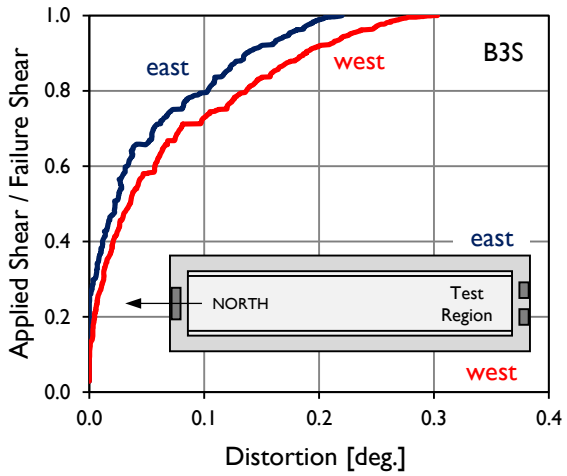

Figure B-5: Distortion measured in the webs during loading of test specimen B3S.

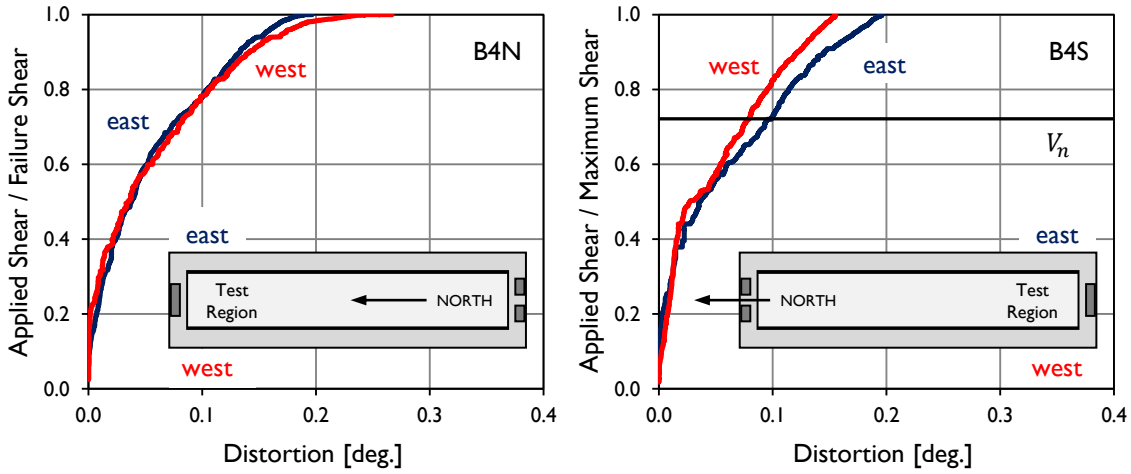

Figure B-6: Distortion measured in the webs during loading of test specimens B4N and B4S.

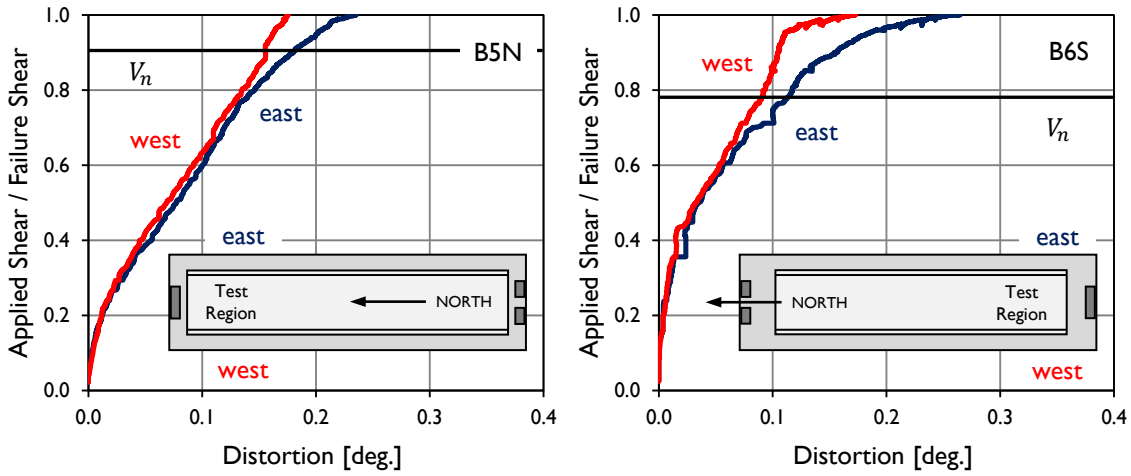

Figure B-7: Distortion measured in the webs during loading of test specimens B5N and B6S.

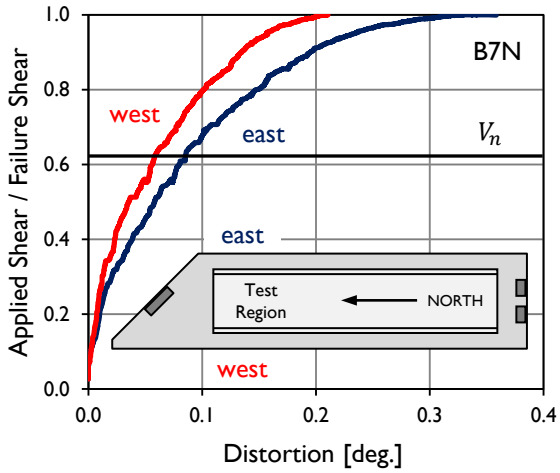

Figure B-8: Distortion measured in the webs during loading of test specimen B7N.

B.5 LOAD DISTRIBUTION

Texas U-Beams are supported on three bearing pads: one central pad (measuring 32 in. wide) at one end and two smaller pads (16 in. wide) at the other. This bearing configuration provides more stability than the two pads used for I-Beams, which are much narrower. During shear testing, support reactions were measured using load cells placed beneath the bearing pads, as was described in Chapter 3. The loads measured at end of the beam resting on two bearing pads were believed to be adequate estimations of the load in the respective webs (Figure B-9(A)); the same assumption was not made for load cells positioned underneath a single bearing pad (Figure B-9(B)).

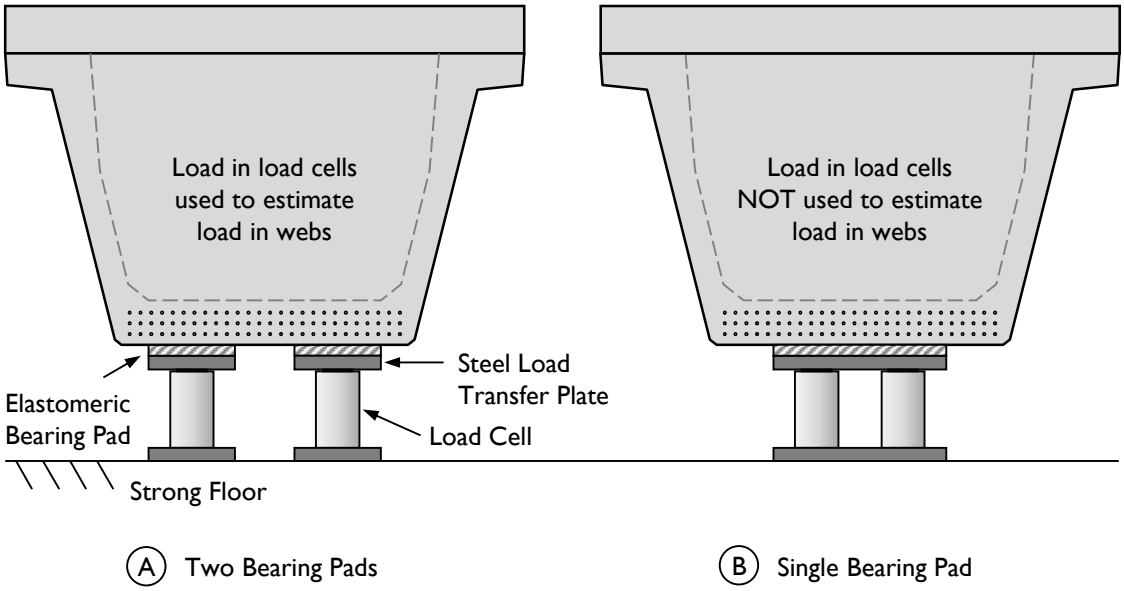

Figure B-9: Bearing conditions used in U-Beam load tests.

The division of load between the two webs was estimated by calculating the ratio of load in one load cell to the total load carried by that end. For consistency, the load cell under the west side of the beam was used as the reference point (in skewed Beams 1 and 2, the west side is the shorter side of the skew; in Beam 7, the west side is the longer side of the skew). As the test region was most frequently supported on a single bearing pad, much of the presented data was collected from the opposite end of the beam.

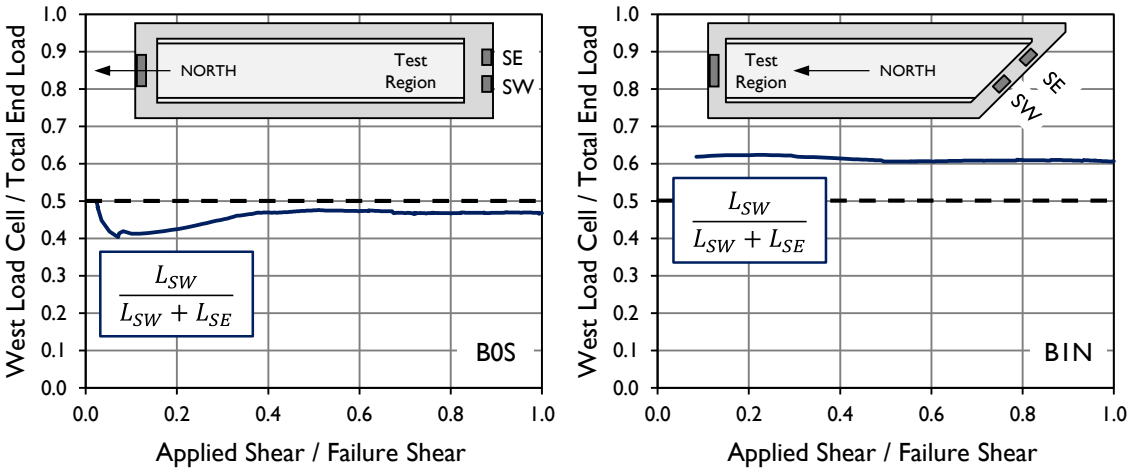

Figure B-10: Distribution of load into two bearing pads during testing of specimens B0S and B1N.

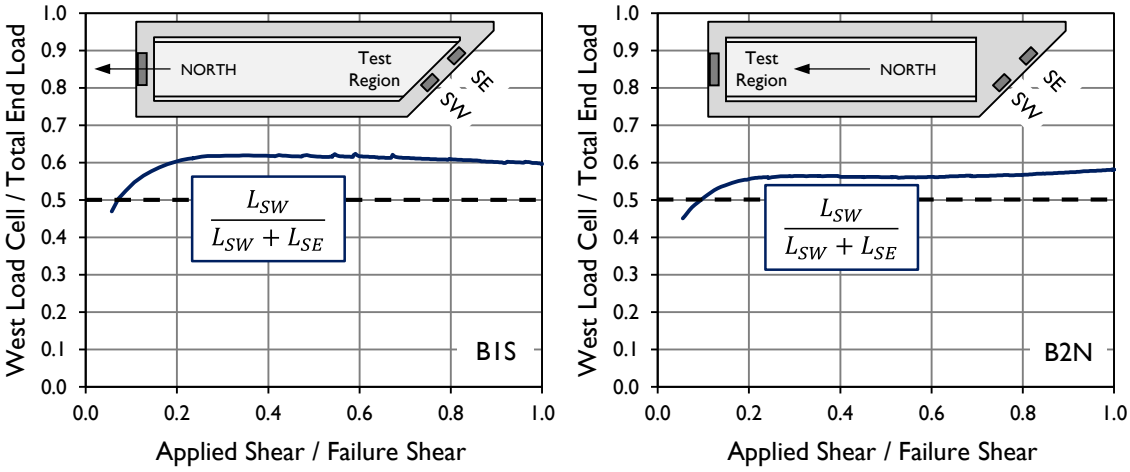

Figure B-11: Distribution of load into two bearing pads during testing of specimens B1S and B2N.

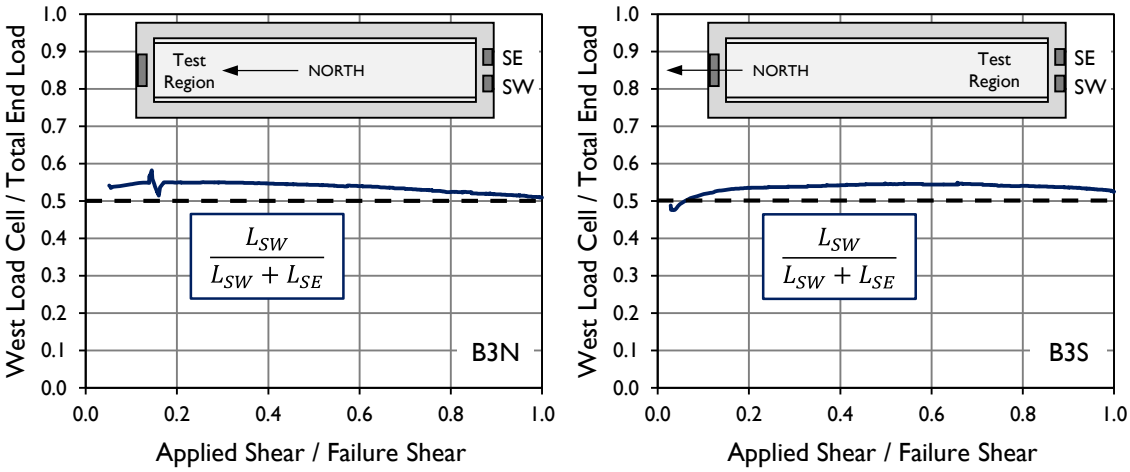

Figure B-12: Distribution of load into two bearing pads during testing of specimens B3N and B3S.

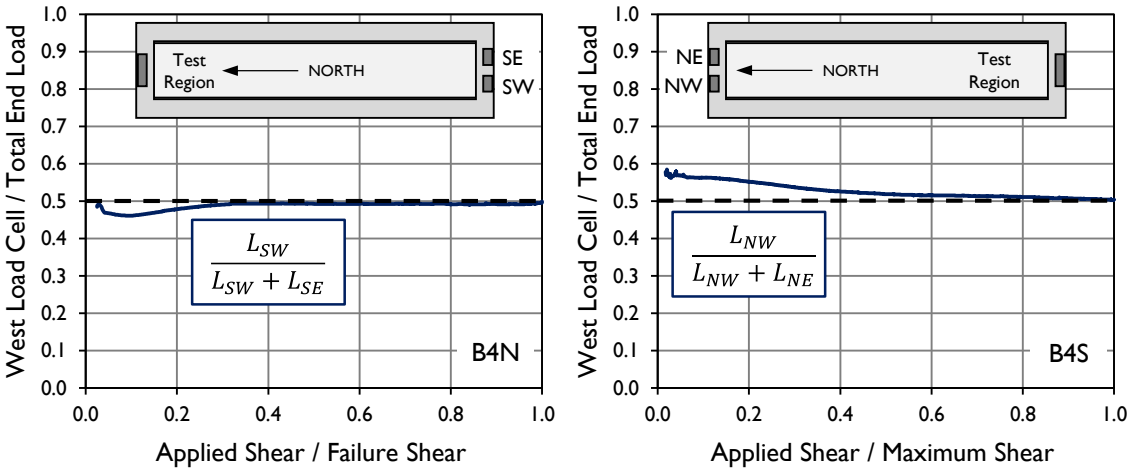

Figure B-13: Distribution of load into two bearing pads during testing of specimens B4N and B4S.

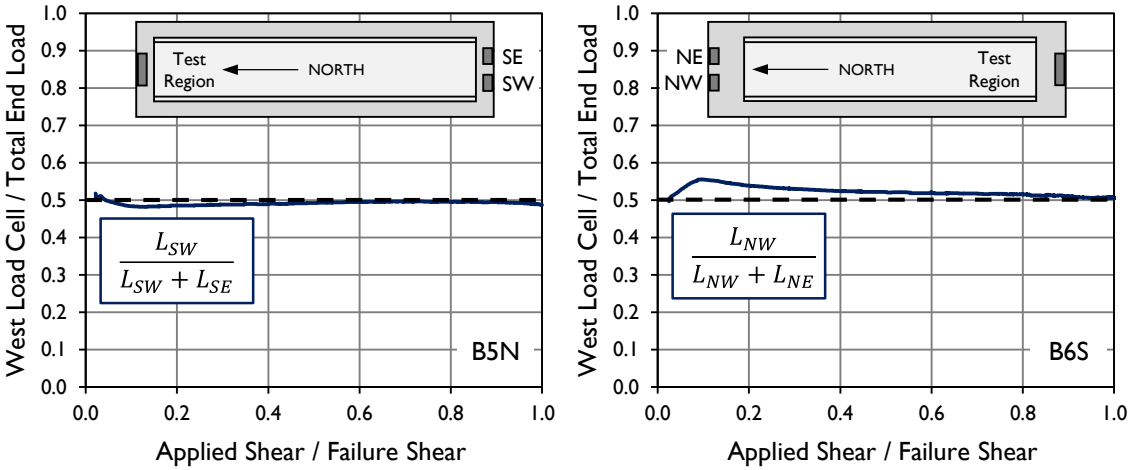

Figure B-14: Distribution of load into two bearing pads during testing of specimens B5N and B6S.

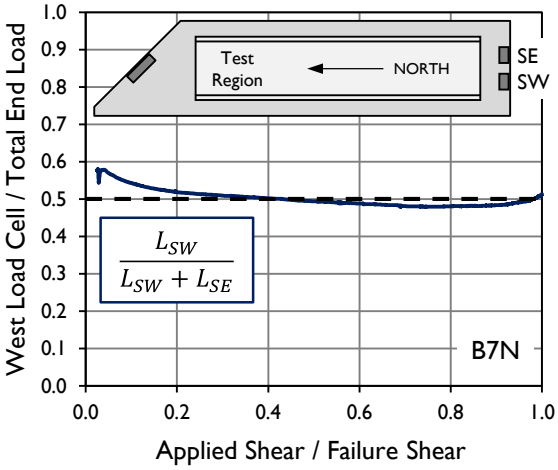

Figure B-15: Distribution of load into two bearing pads during testing of specimen B7N.

B.6 SHEAR TEST CRACKS

During shear testing, cracks were marked on the beams as they formed. The cracks seen at several load steps for each test specimen are provided in the following eleven figures. Included are the cracks present prior to testing, the first diagonal cracks observed, cracks seen at calculated shear capacity (when reached), and the damage associated with failure, as well as one additional intermediate load step.

For each load step, the ratio of applied load (V) to calculated capacity (V_n) and to failure shear (V_{test}) are presented. Shear capacity was calculated following the General Procedure found in the AASHTO LRFD Specifications (2010). Maximum crack widths measured at each presented point in the loading are also provided.

B0S: web-crushing failure at V_{test} = 491 kip; V_n = 472 kip; V_{test}/V_n = 1.04

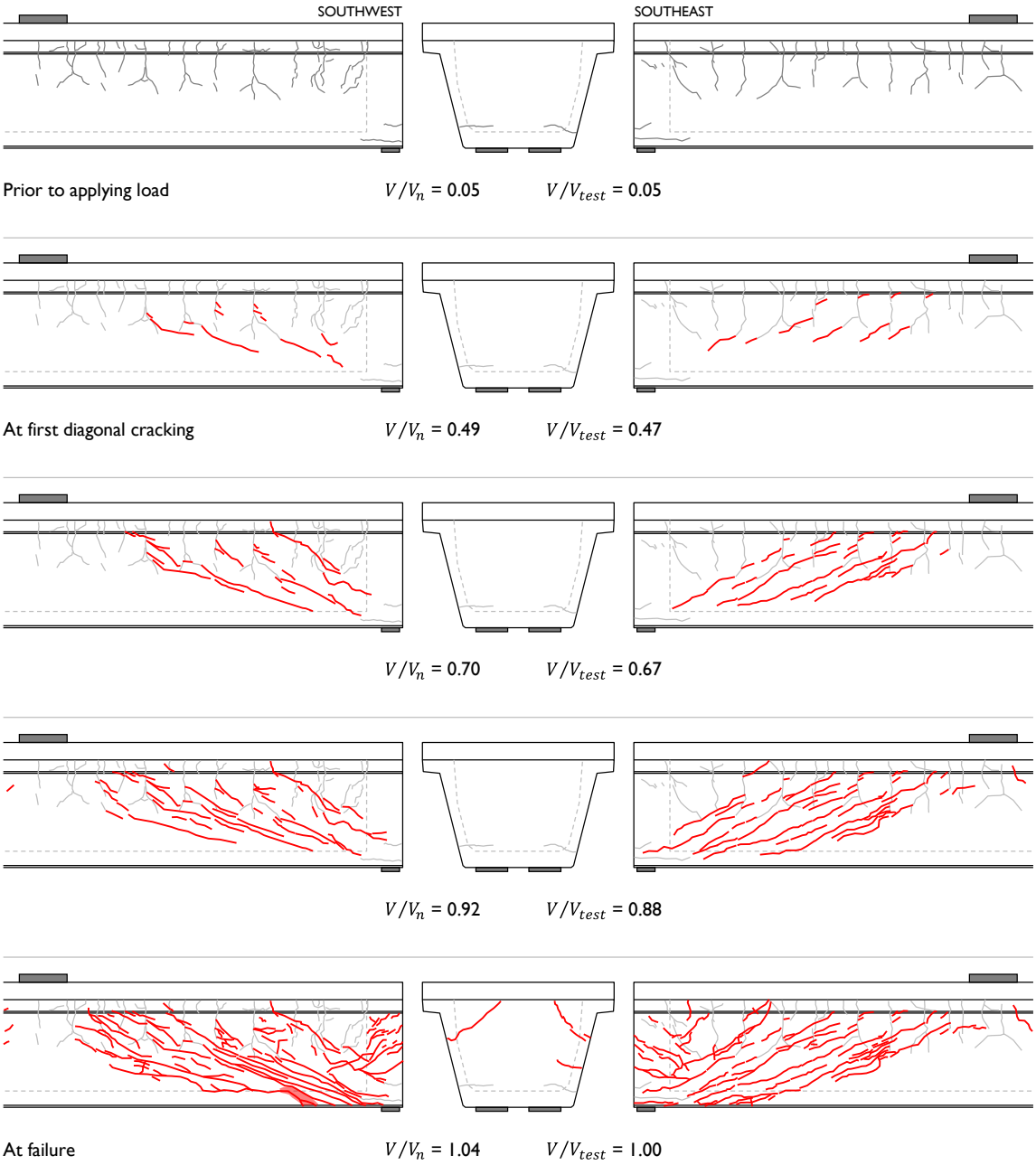

Figure B-16: Cracks observed during testing of specimen B0S.

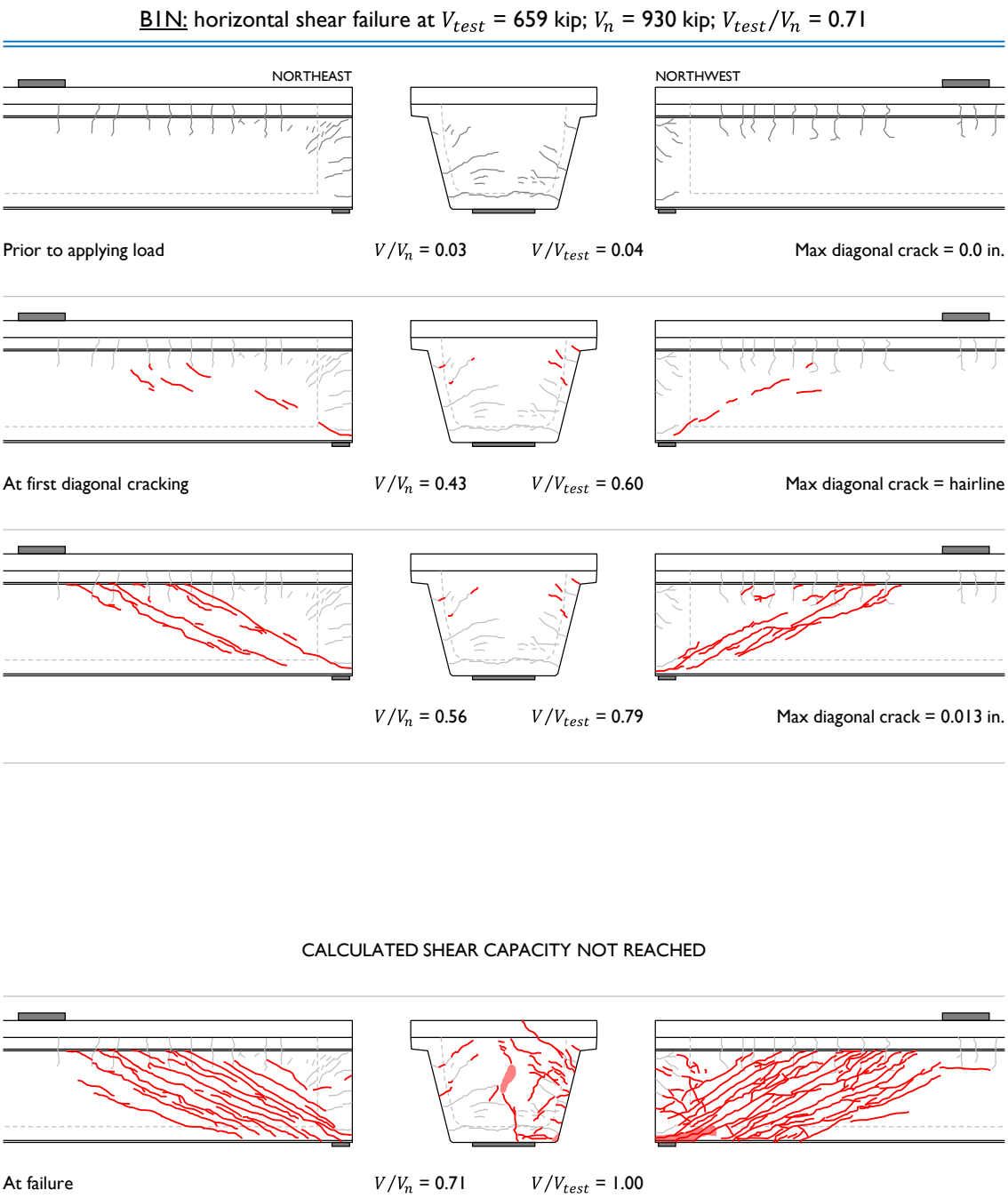

Figure B-17: Cracks observed during testing of specimen B1N.

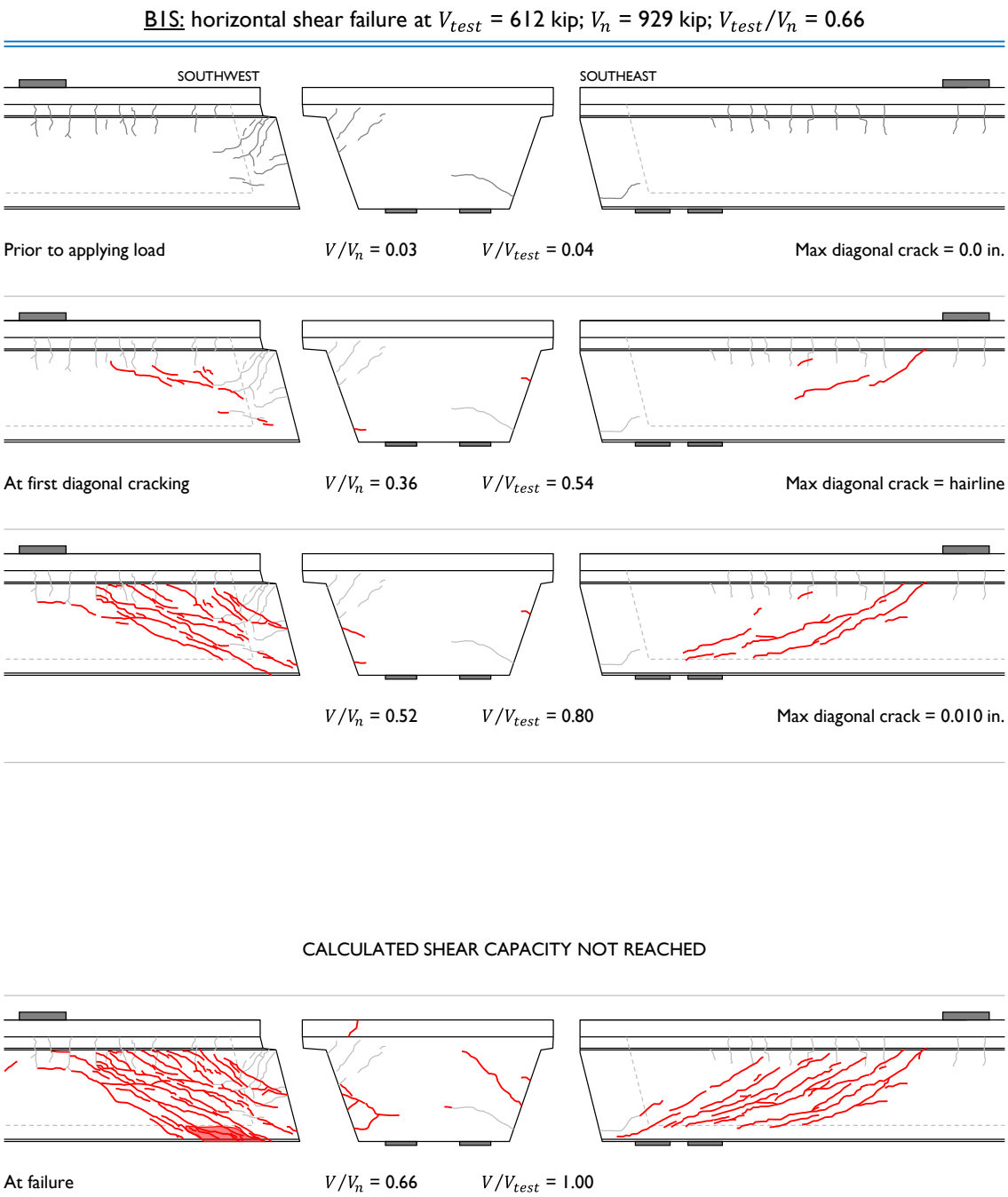

Figure B-18: Cracks observed during testing of specimen B1S.

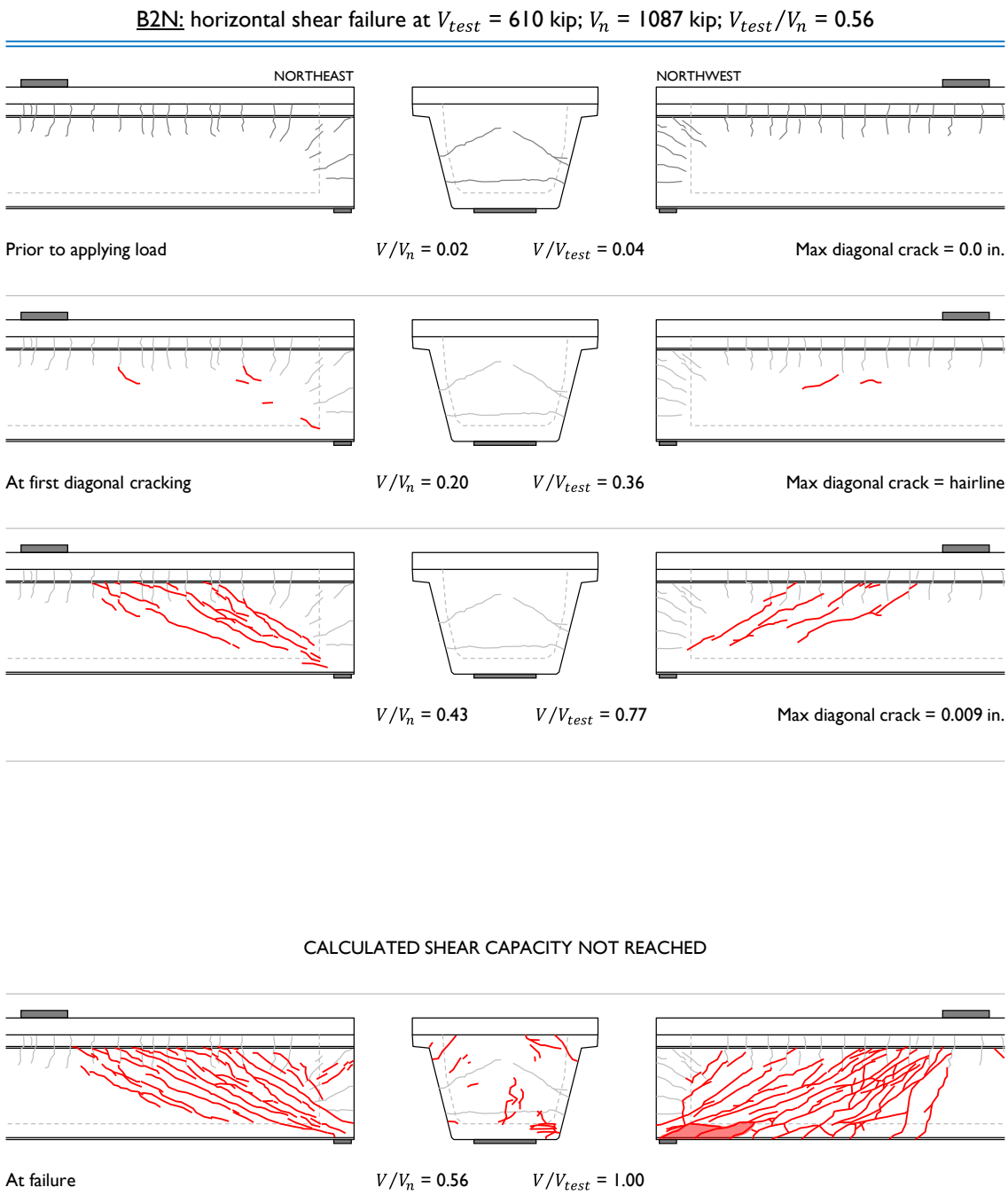

Figure B-19: Cracks observed during testing of specimen B2N.

B3N: horizontal shear failure at V_{test} = 655 kip; V_n = 679 kip; V_{test}/V_n = 0.96

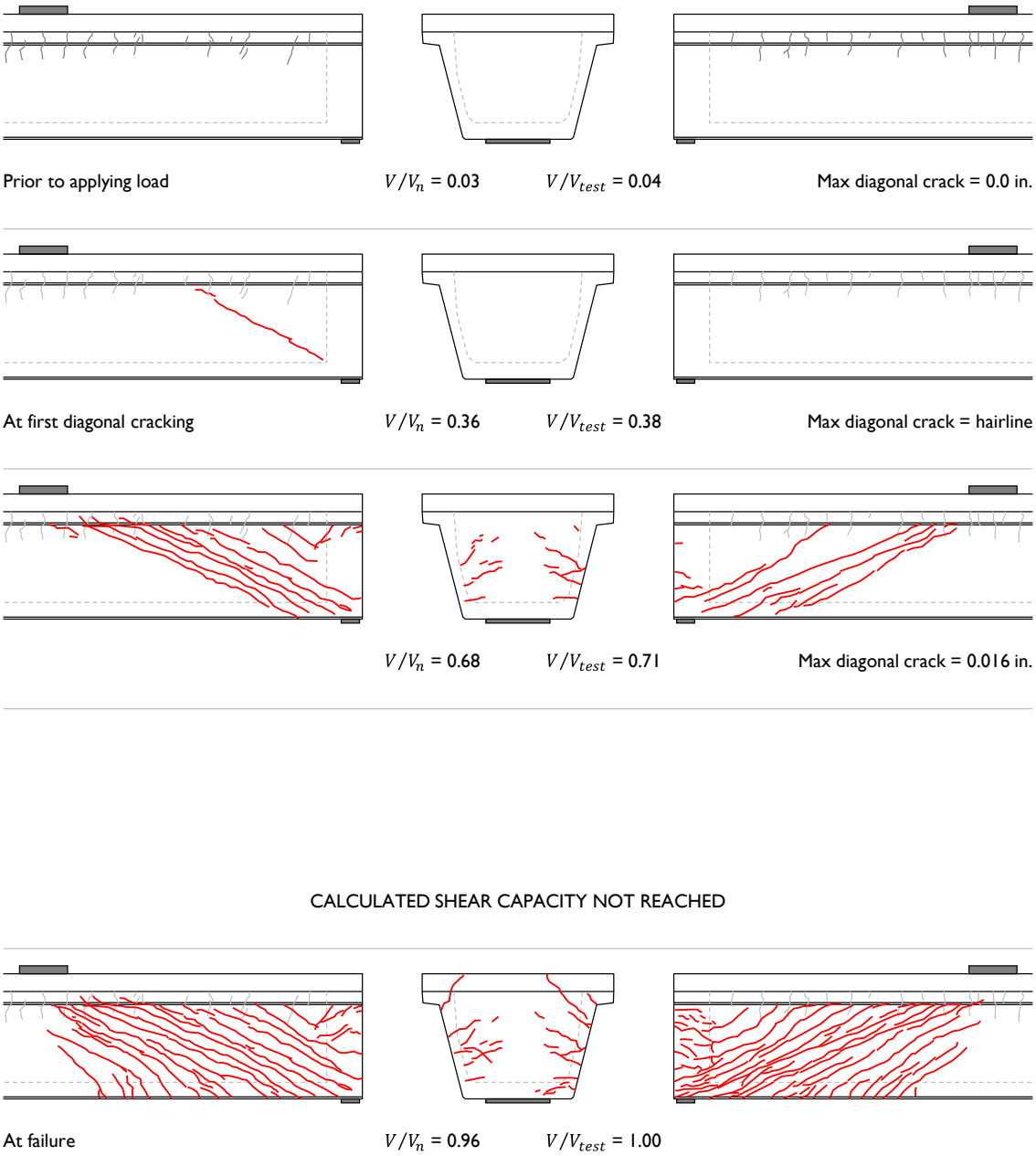

Figure B-20: Cracks observed during testing of specimen B3N.

B3S: horizontal shear failure at V_{test} = 663 kip; V_n = 681 kip; V_{test}/V_n = 0.97

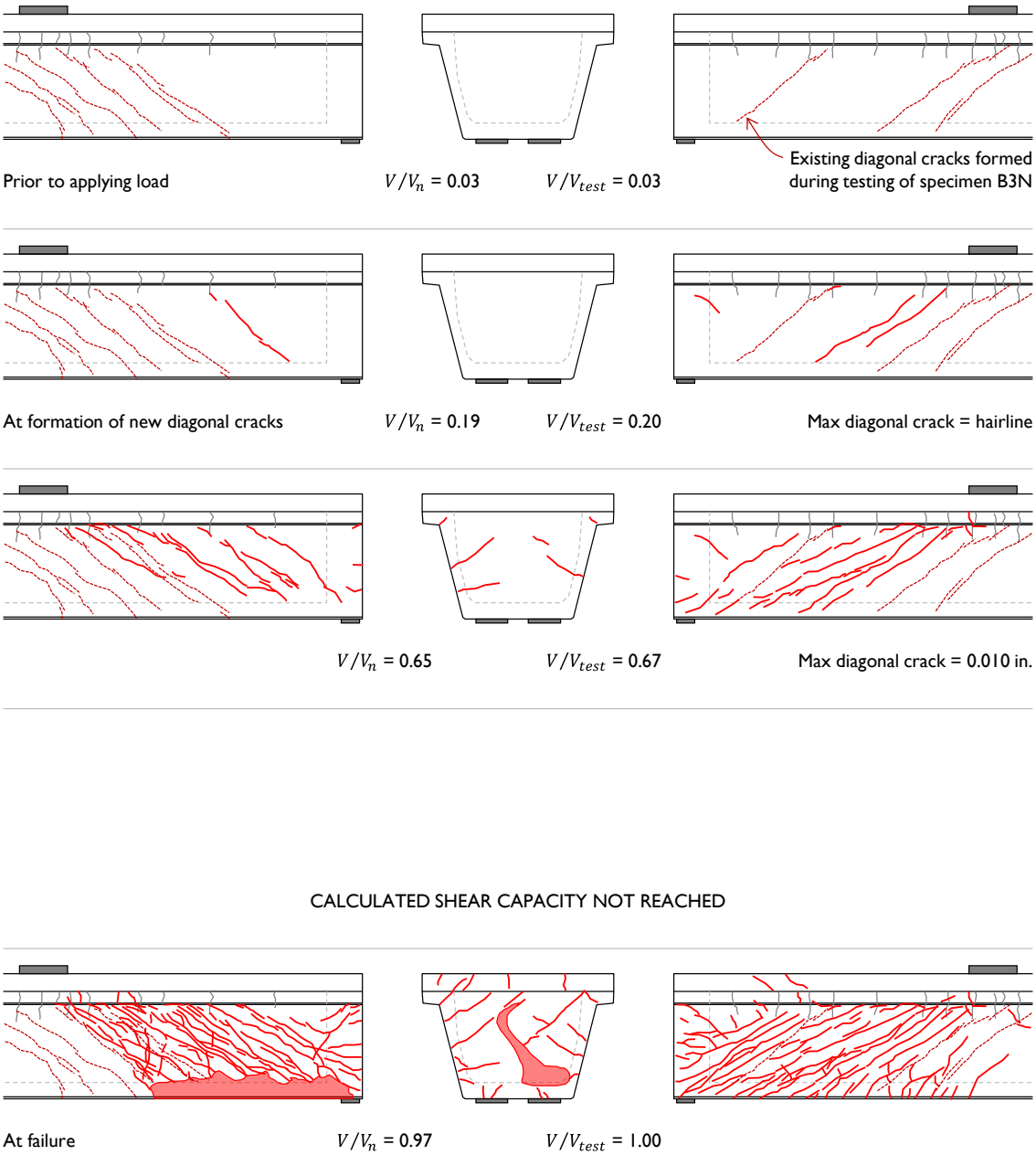

Figure B-21: Cracks observed during testing of specimen B3S.

B4N: horizontal shear failure at V_{test} = 973 kip; V_n = 1134 kip; V_{test}/V_n = 0.86

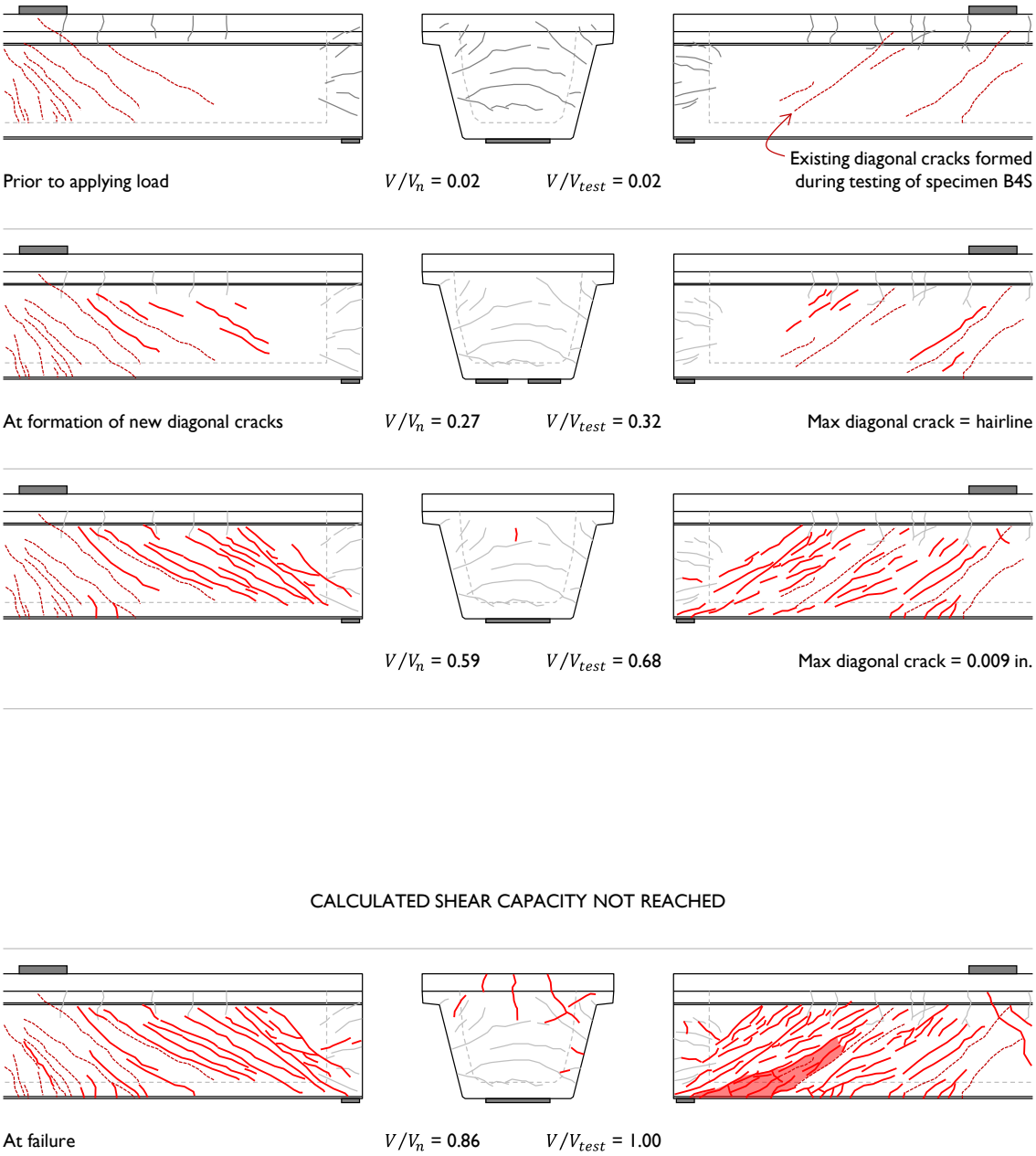

Figure B-22: Cracks observed during testing of specimen B4N.

B4S: not loaded to failure; V_{max} = 1191 kip; V_n = 871 kip; V_{max}/V_n = 1.37

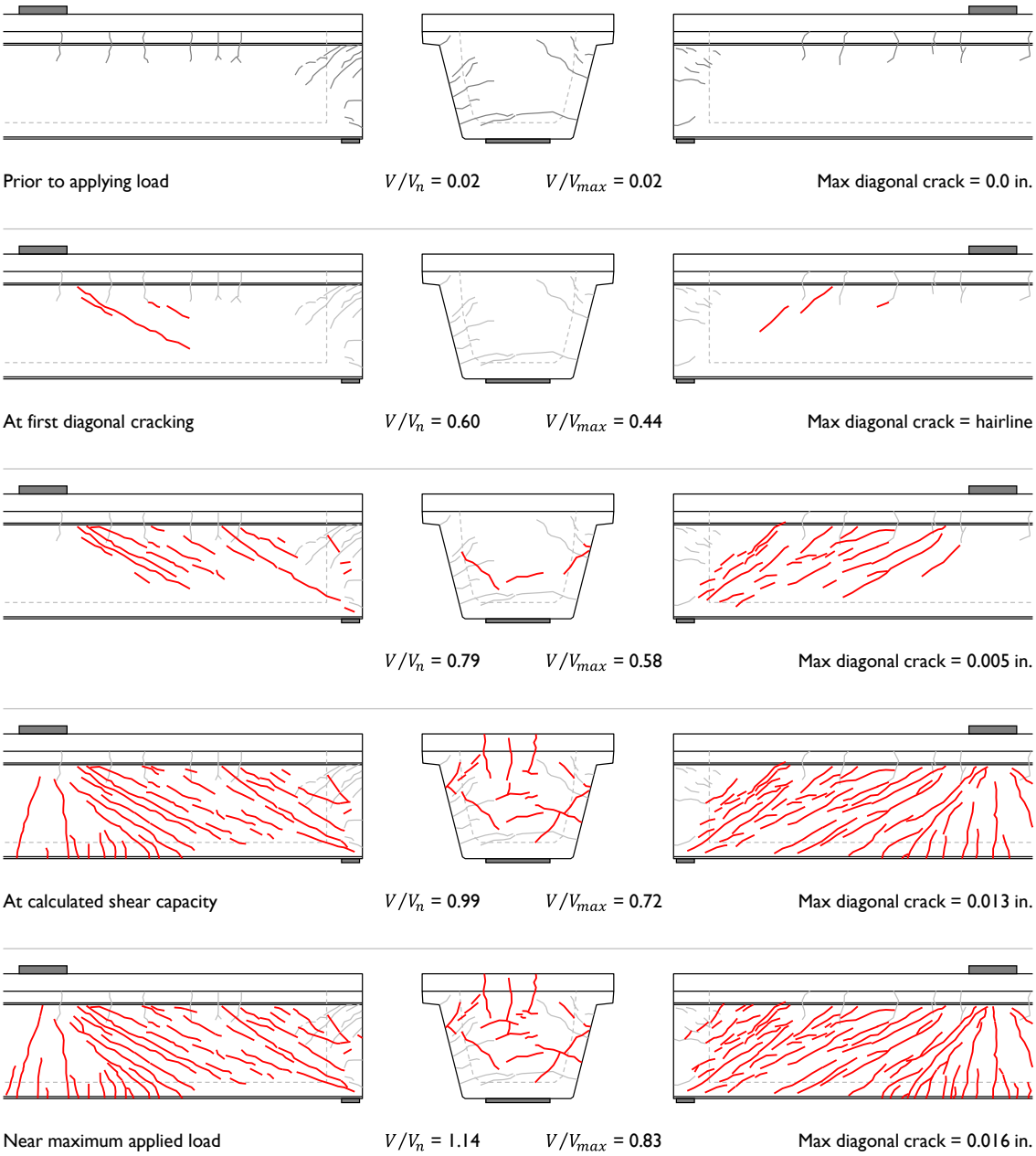

Figure B-23: Cracks observed during testing of specimen B4S.

B5N: flexure-shear failure at V_{test} = 1031 kip; V_n = 925 kip; V_{test}/V_n = 1.11

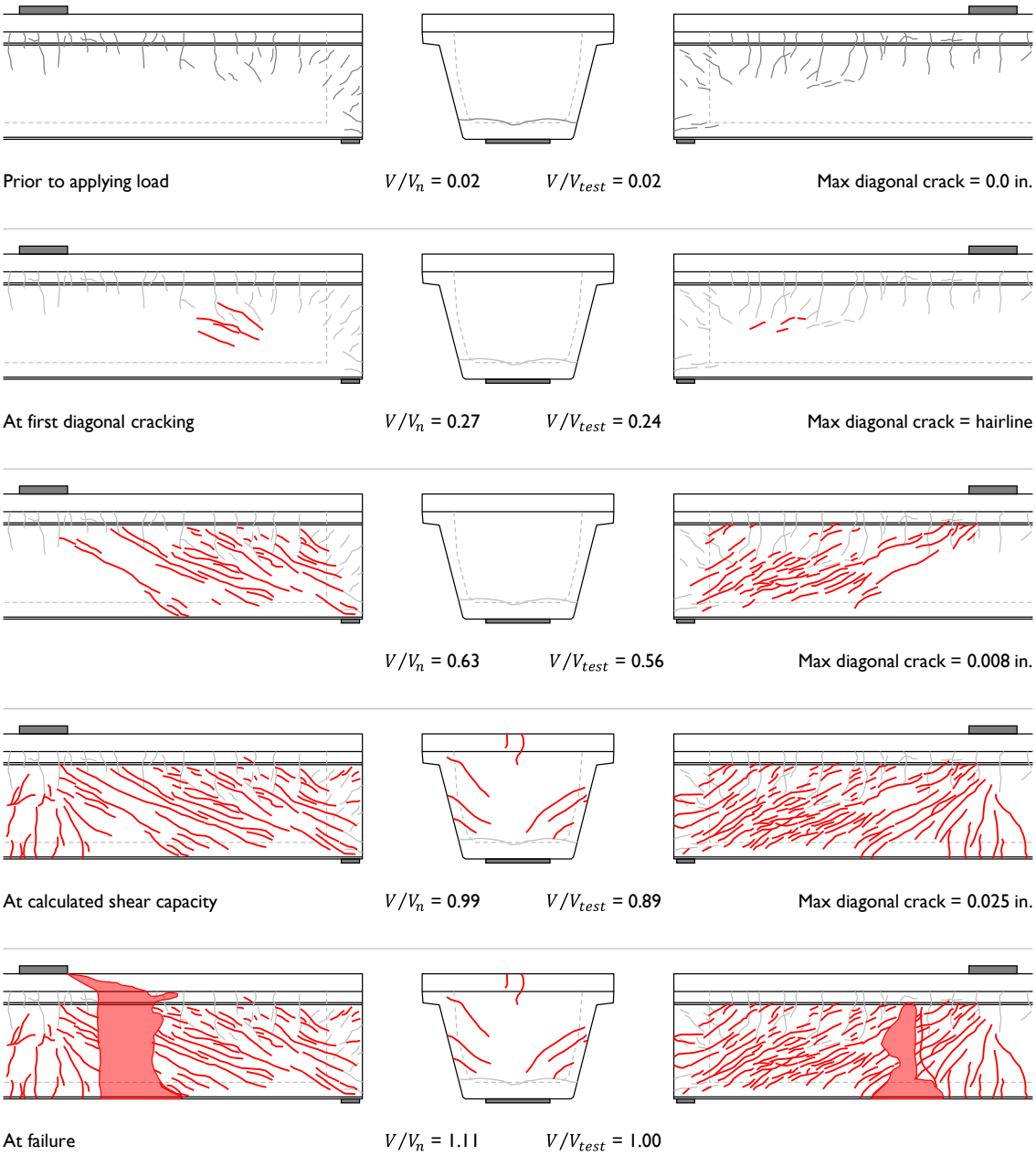

Figure B-24: Cracks observed during testing of specimen B5N.

B6S: flexure-shear failure at V_{test} = 1054 kip; V_n = 833 kip; V_{test}/V_n = 1.27

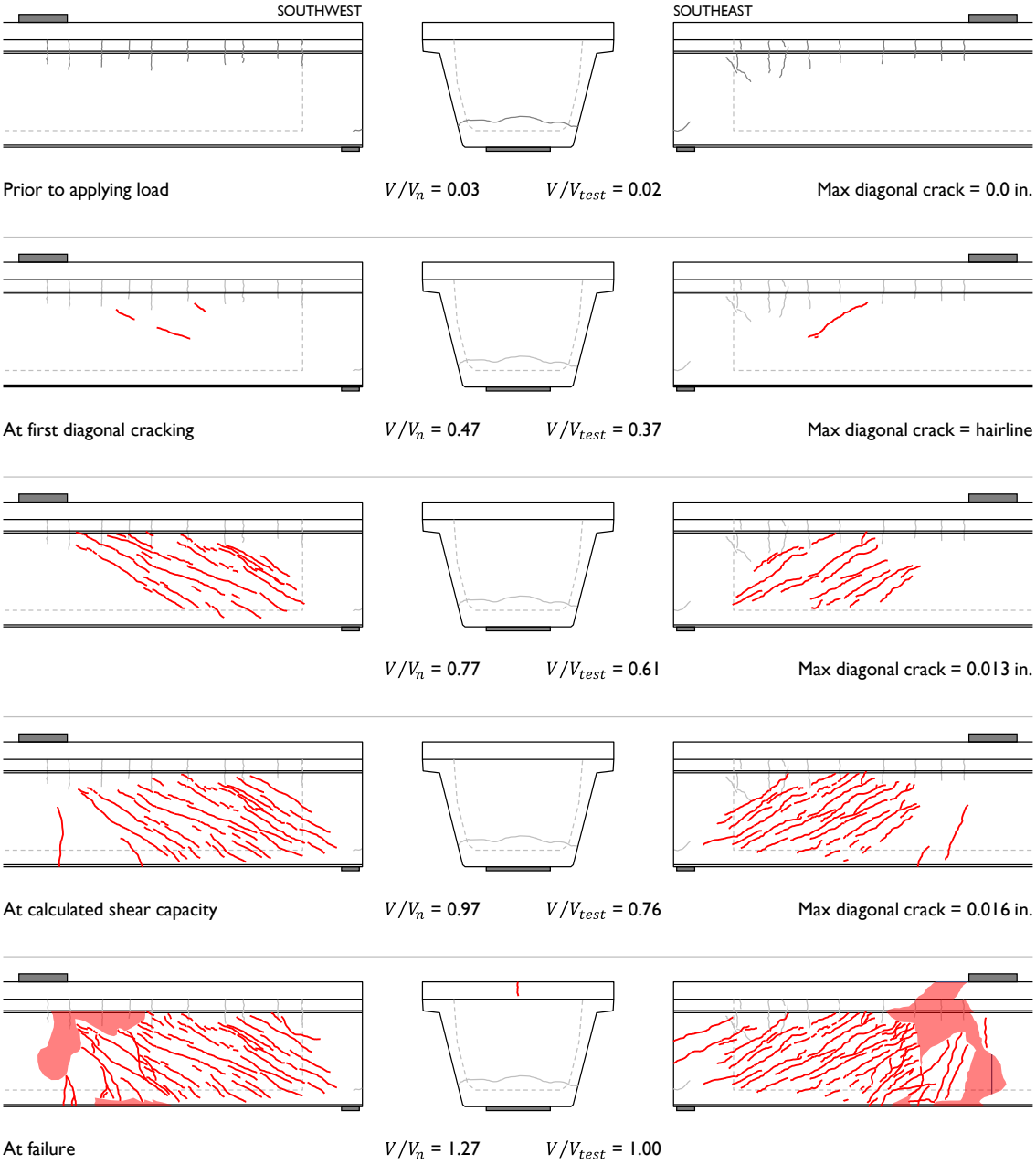

Figure B-25: Cracks observed during testing of specimen B6S.

B7N: web-crushing at V_{test} = 1209 kip; V_n = 735 kip; V_{test}/V_n = 1.65

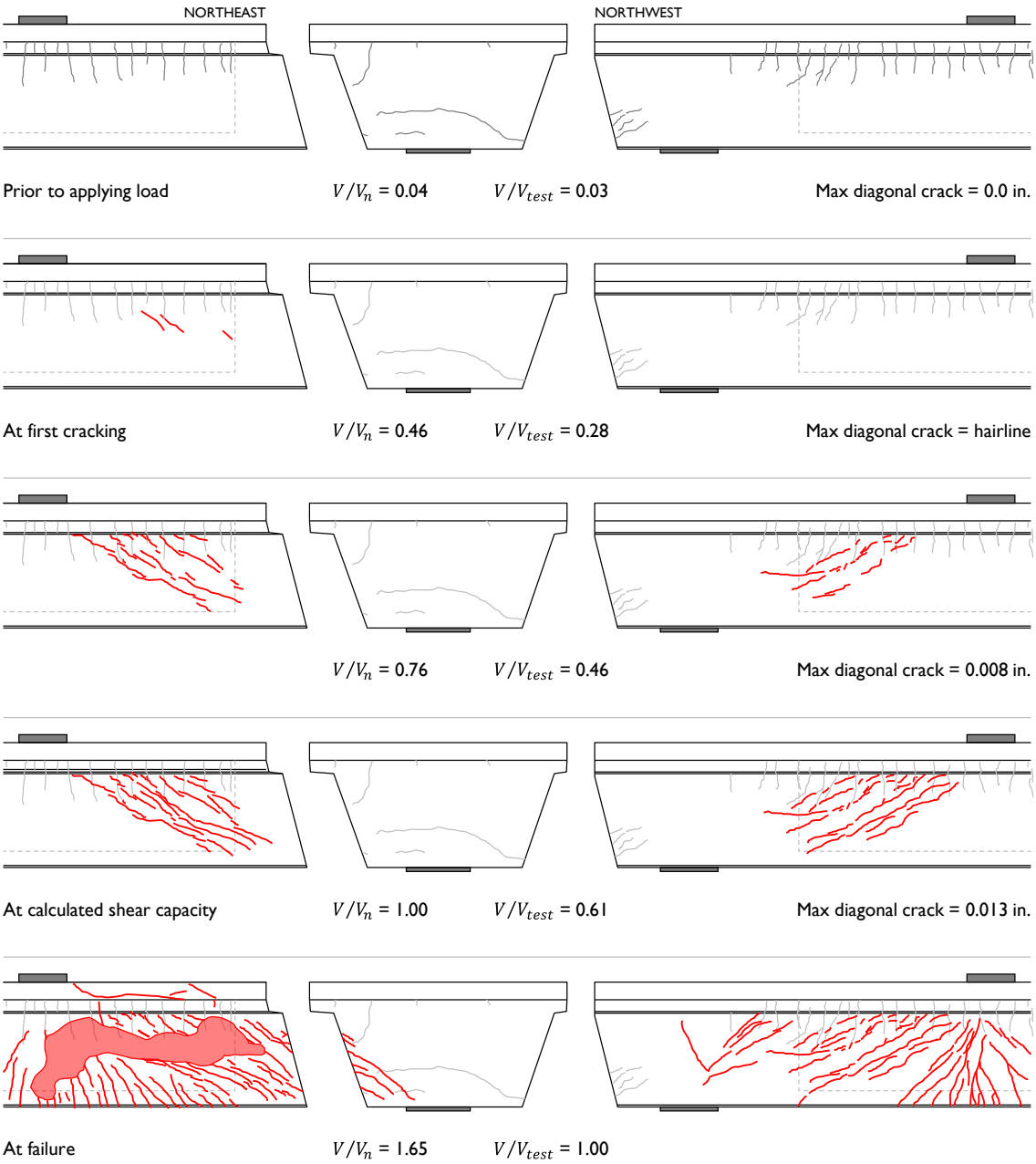

Figure B-26: Cracks observed during testing of specimen B7N.

B.7 MAXIMUM CRACK WIDTHS

Maximum measured crack widths from the eleven shear test regions are presented in the following six figures. No crack width data was gathered from specimen B0S. Crack widths were measured more frequently in later tests as the importance of having a metric for evaluating in-service beams increased, given the horizontal shear failures observed. Offsetting the load from the midpoint of the centerline (as became standard practice with Beam 3) also aided in data collection as each end of the beam could be studied individually, as opposed to simultaneously.

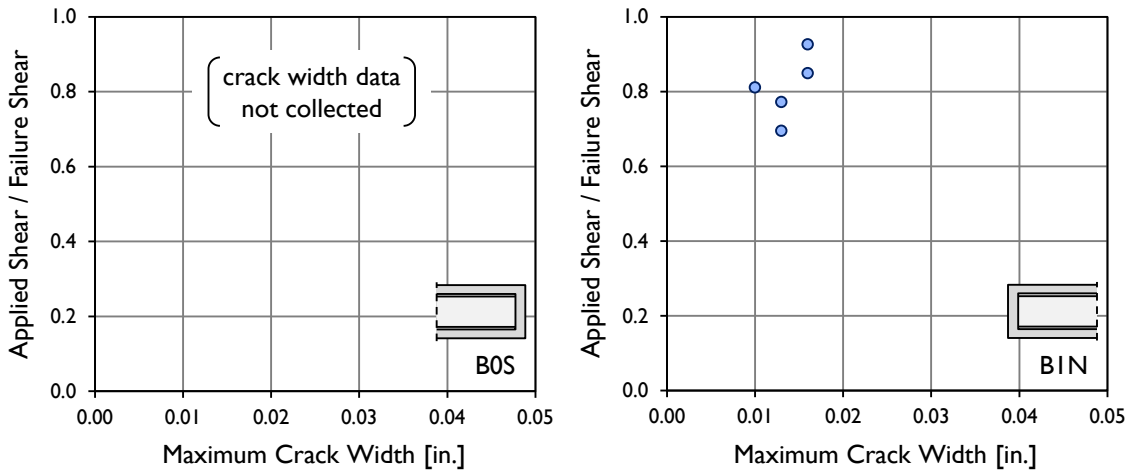

Figure B-27: Maximum crack widths measured in test specimens B0S and B1N.

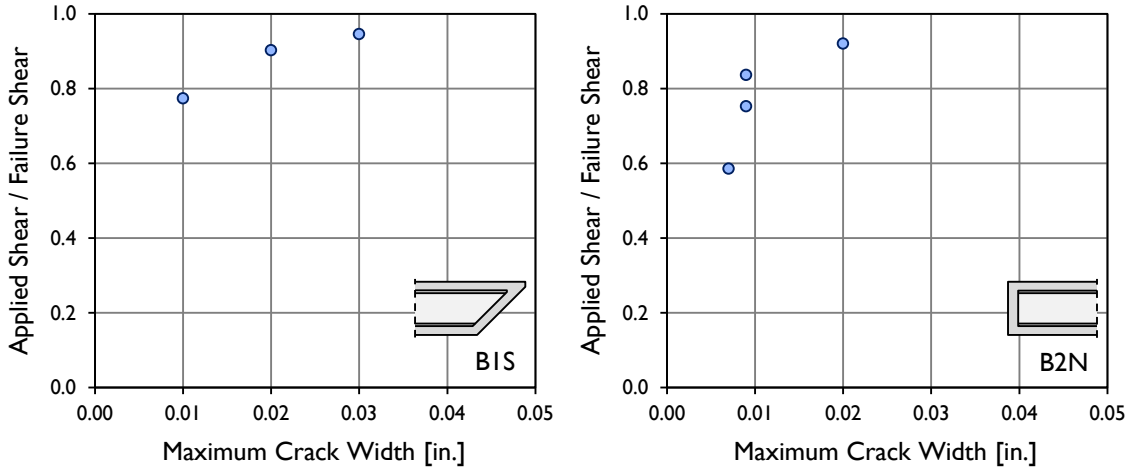

Figure B-28:Maximum crack widths measured in test specimens B1S and B2N.

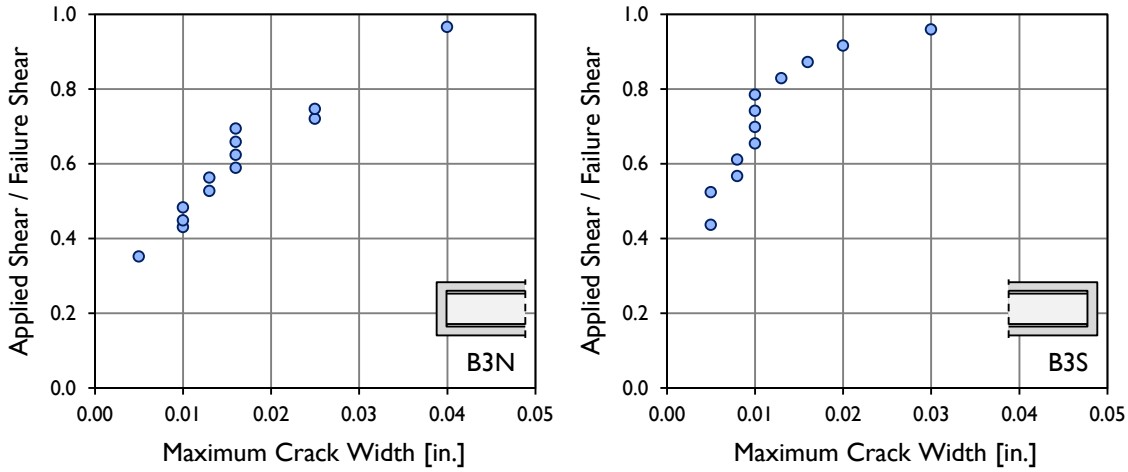

Figure B-29: Maximum crack widths measured in test specimens B3N and B3S.

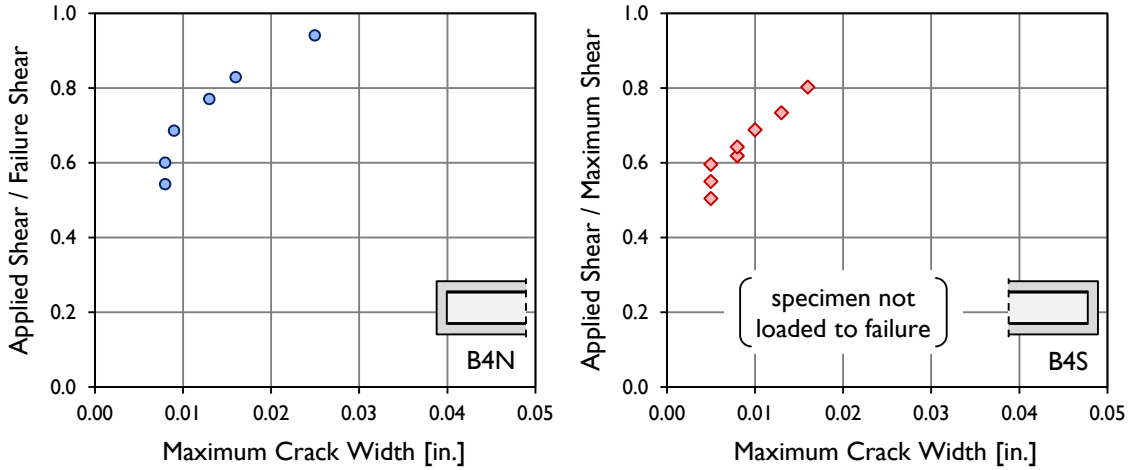

Figure B-30: Maximum crack widths measured in test specimens B4N and B4S.

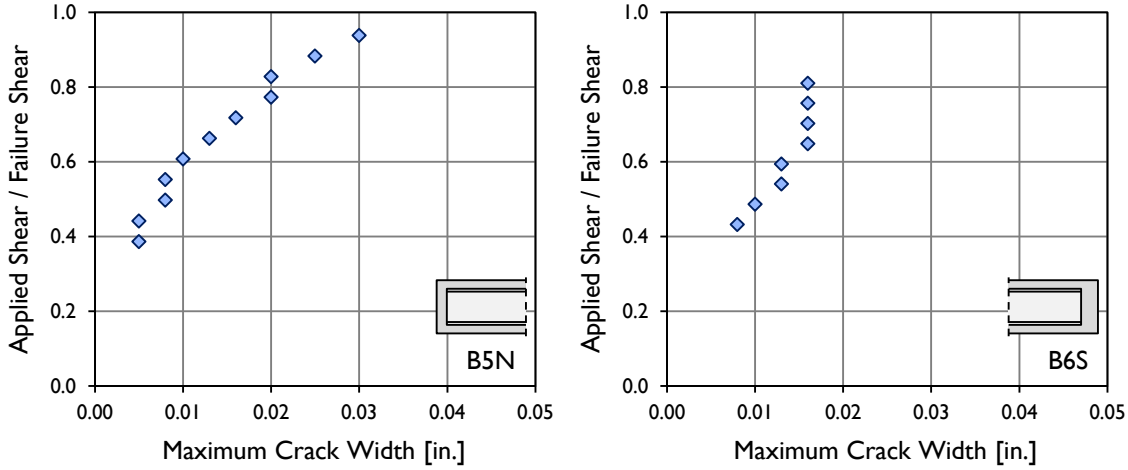

Figure B-31: Maximum crack widths measured in test specimens B5N and B6S.

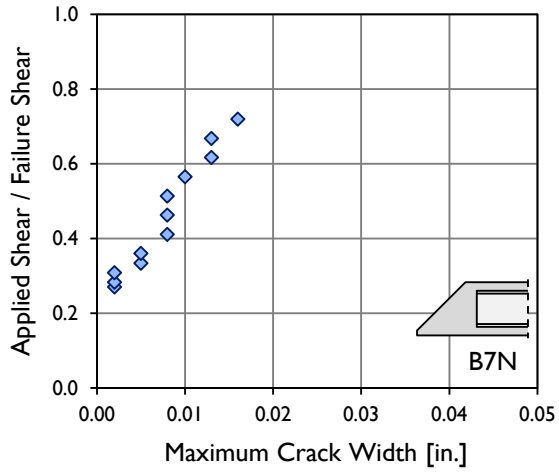

Figure B-32: Maximum crack widths measured in test specimen B7N.

B.8 VERTICAL STRAIN IN WEBS

The overall vertical strain in each web was measured between load point and support using linear potentiometers during six of the shear load tests (Figure B-33). Errors in data acquisition prevented the collection of strain data during testing of the other five beam ends.

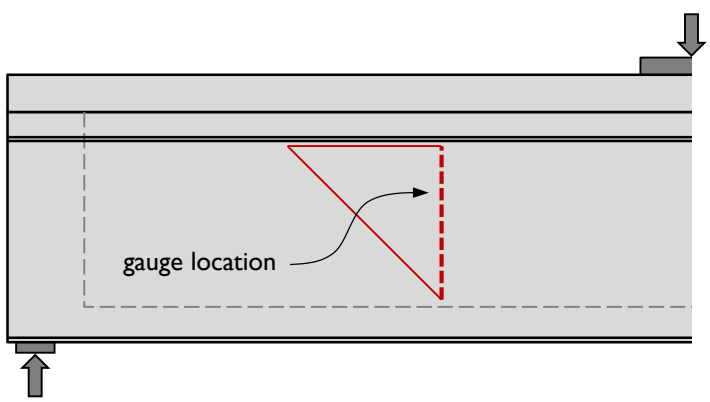

Figure B-33: Location of linear potentiometer used to measure vertical strain during loading.

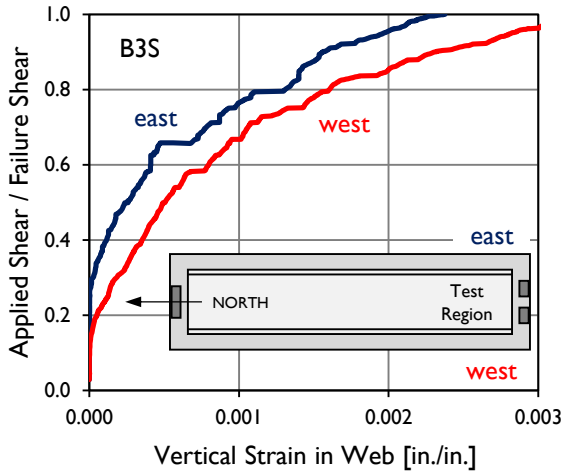

Figure B-34: Vertical strains measured in the webs of test specimen B3S during loading.

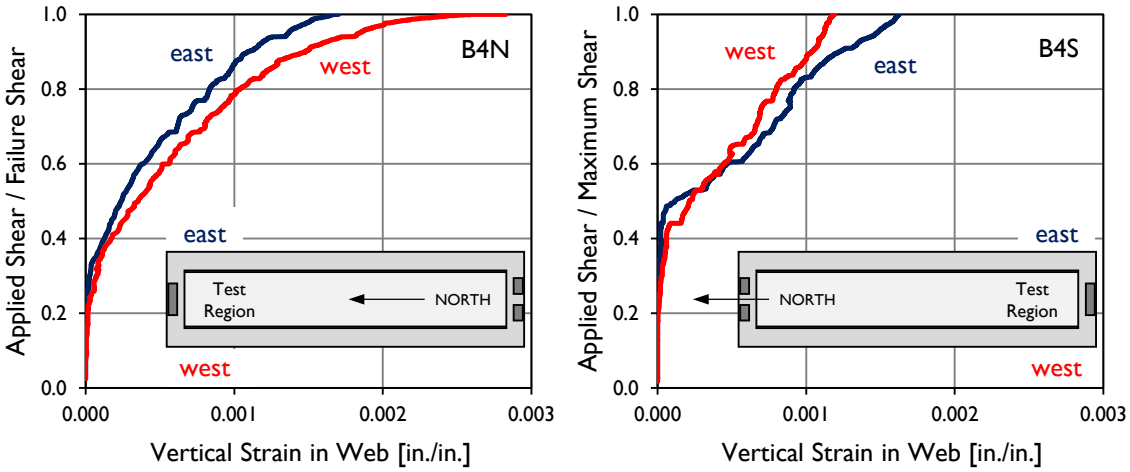

Figure B-35: Vertical strains measured in the webs of test specimens B4N and B4S during loading.

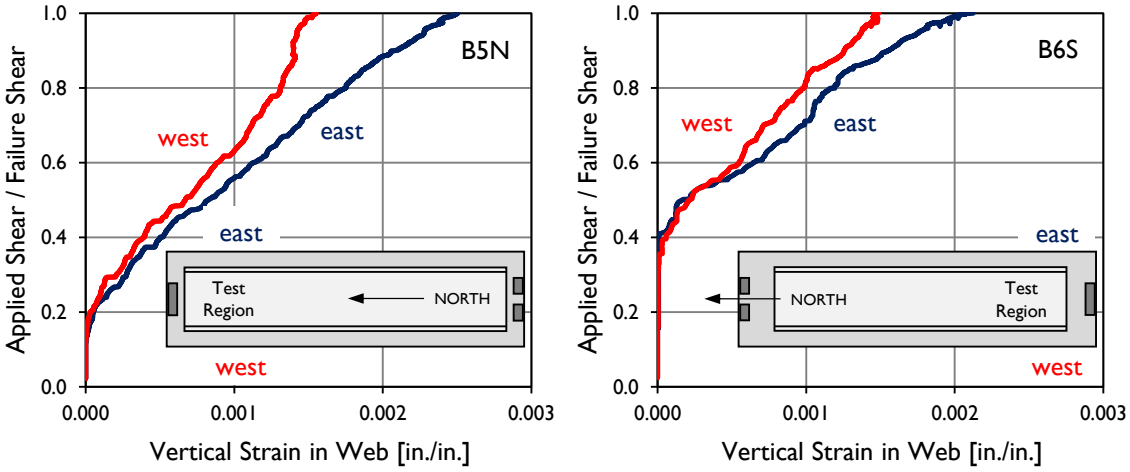

Figure B-36: Vertical strains measured in the webs of test specimens B5N and B6S during loading.

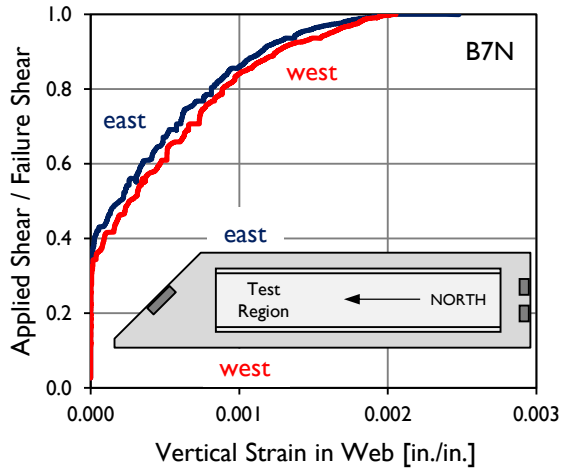

Figure B-37: Vertical strains measured in the webs of test specimen B7N during loading.

B.9 STRAIN IN REINFORCING BARS

Strains in reinforcing bars located near beam end and in the middle of the shear span were monitored during the application of load. The collected data are provided in the following six figures. The data from B1S, the one skewed specimen that was both instrumented and loaded to failure, are not presented as no data was collected outside of the skewed region (equal to $x < 0$ in. for the other end regions). The data collected from specimen B2N was lost due to a malfunction of the data acquisition system.

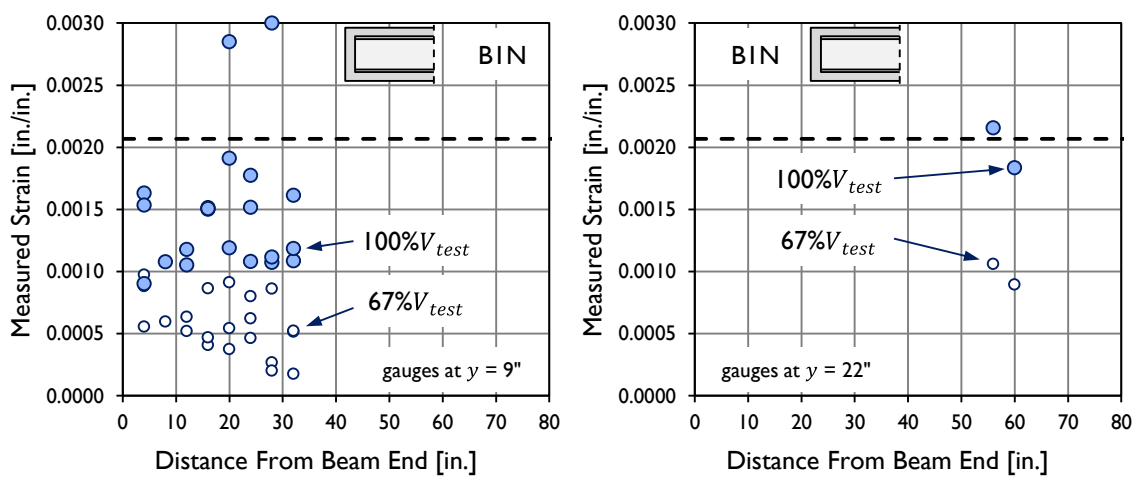

Figure B-38: Strain measured in reinforcing bars during load-testing of specimen B1N.

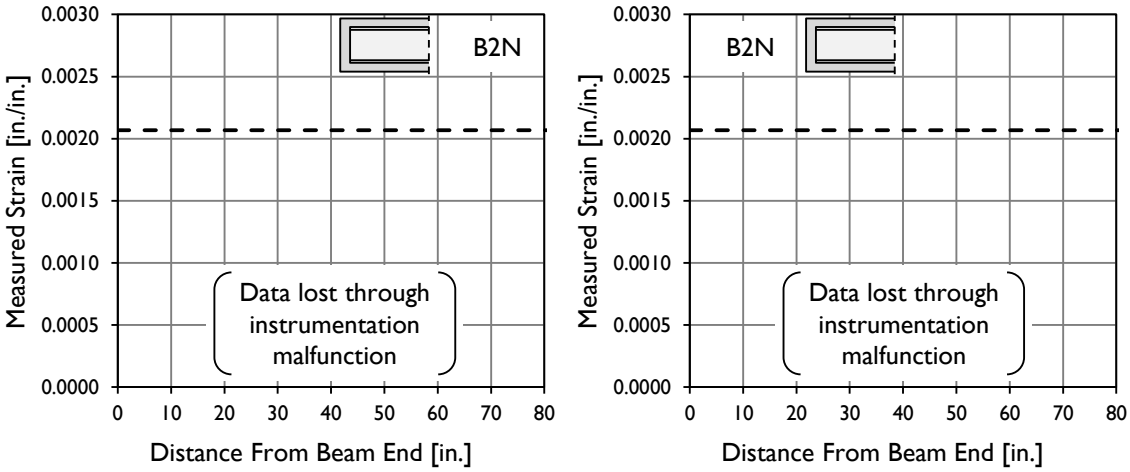

Figure B-39: Strain measured in reinforcing bars during load-testing of specimen B2N.

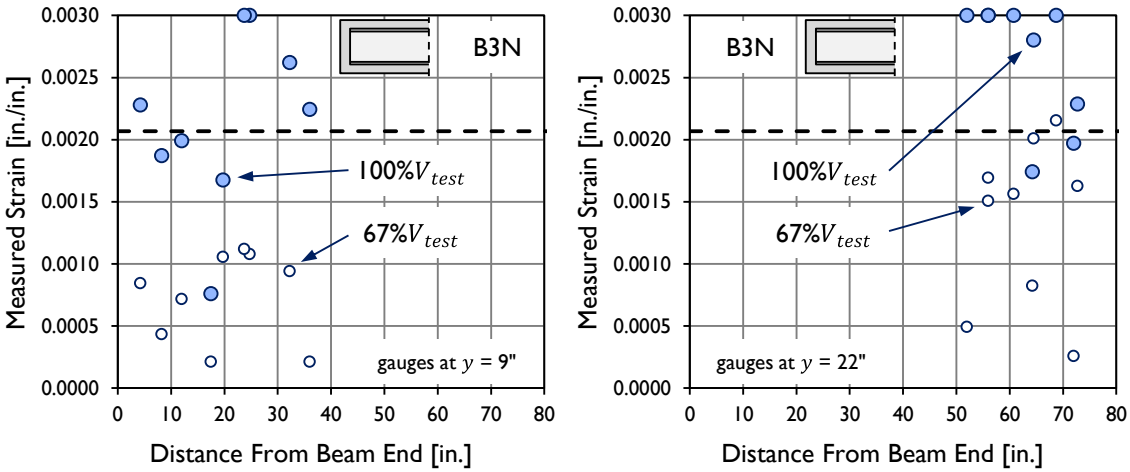

Figure B-40: Strain measured in reinforcing bars during load-testing of specimen B3N.

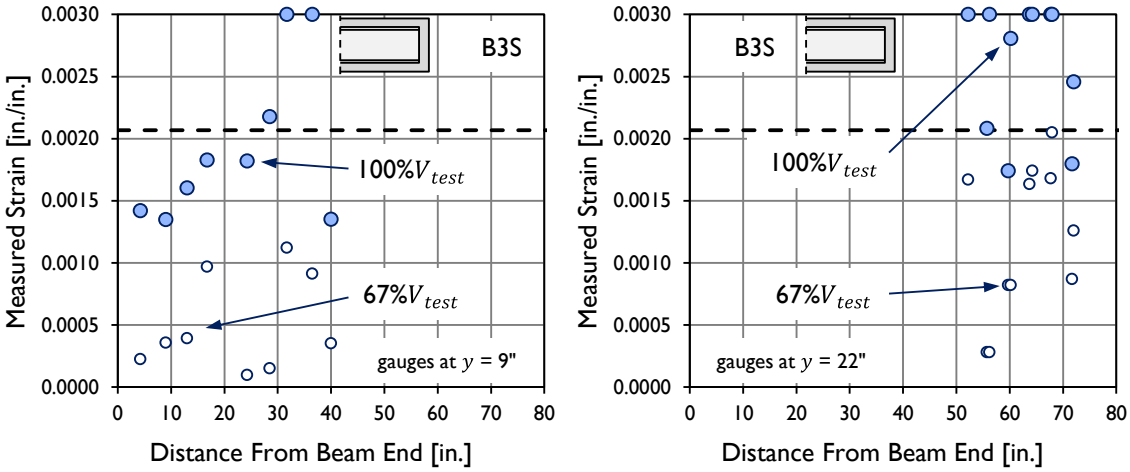

Figure B-41: Strain measured in reinforcing bars during load-testing of specimen B3S.

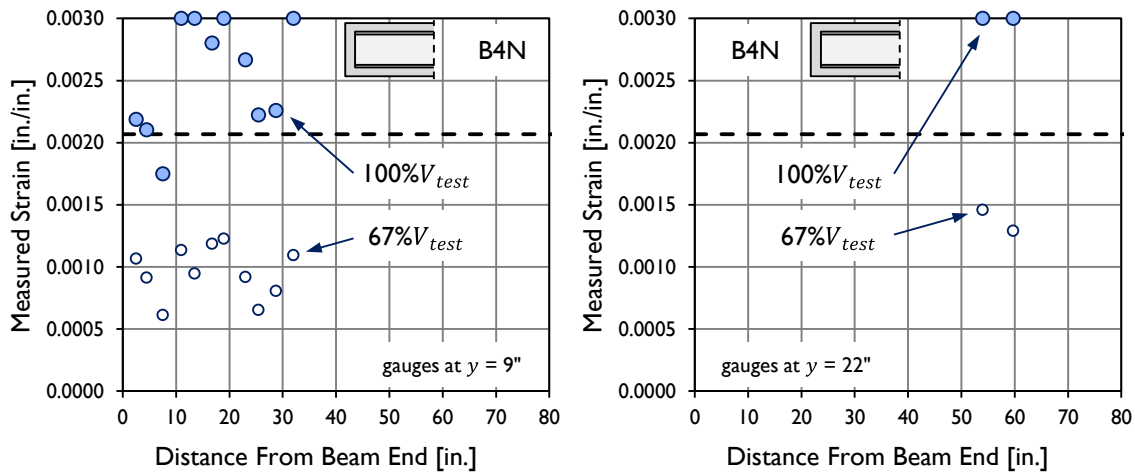

Figure B-42: Strain measured in reinforcing bars during load-testing of specimen B4N.

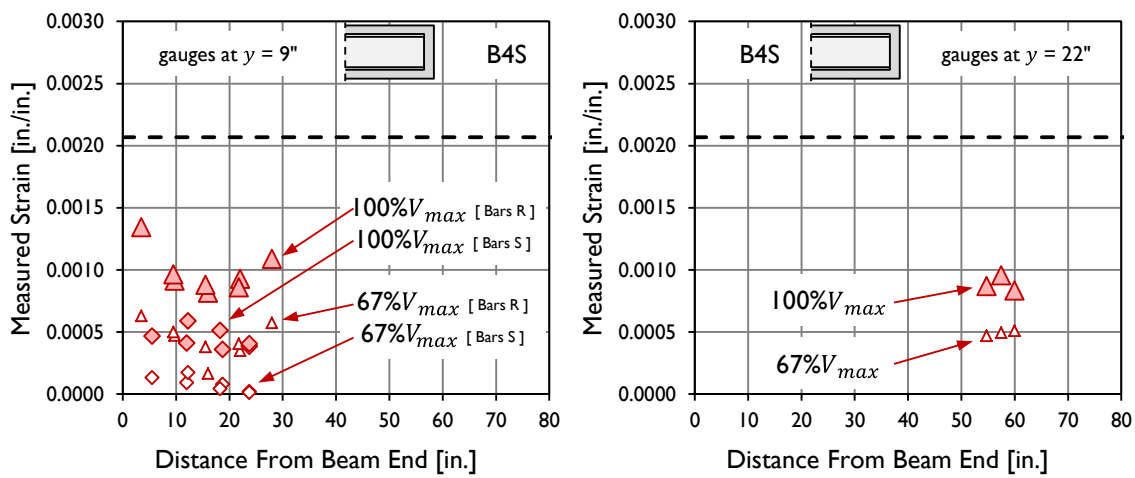

Figure B-43: Strain measured in reinforcing bars during load-testing of specimen B4S.

B.10 SHEAR-DEFLECTION PLOTS

Shear-deflection plots are provided for each of the eleven shear tests performed. Deflection was measured at six points: directly under the load point (east and west sides) and at the longitudinal centerline of the bearing pads (northeast, northwest, southeast, and southwest corners). The plotted deflection is the average of the load point deflections minus the average rigid body motion associated with bearing pad compression:

$$\Delta_{avg} = 0.5(\Delta_{LE} + \Delta_{LW}) - 0.25(\Delta_{NE} + \Delta_{NW} + \Delta_{SE} + \Delta_{SW}) \qquad \textbf{Equation B-1}$$

where

Δ_{avg} = overall deflection measured at the load point [in.]

Δ_{LE} = deflection measured on the east side of the beam at the load point [in.]

Δ_{LW} = deflection measured on the west side of the beam at the load point [in.]

Δ_{NE} = deflection measured on the east side of the beam at the north support [in.]

Δ_{NW} = deflection measured on the west side of the beam at the north support [in.]

Δ_{SE} = deflection measured on the east side of the beam at the south support [in.]

Δ_{SW} = deflection measured on the west side of the beam at the south support [in.]

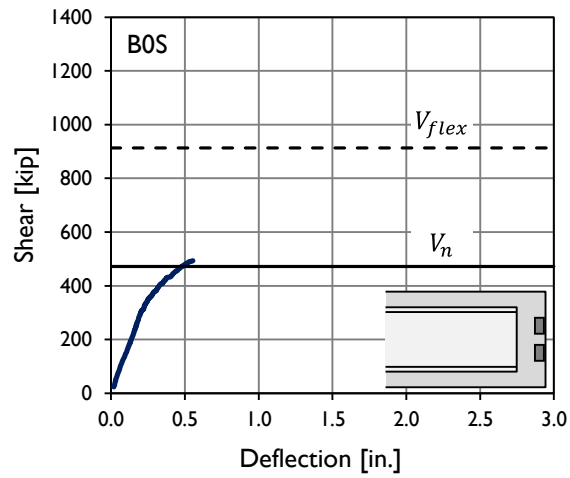

Figure B-44: Shear-deflection plot for specimen B0S.

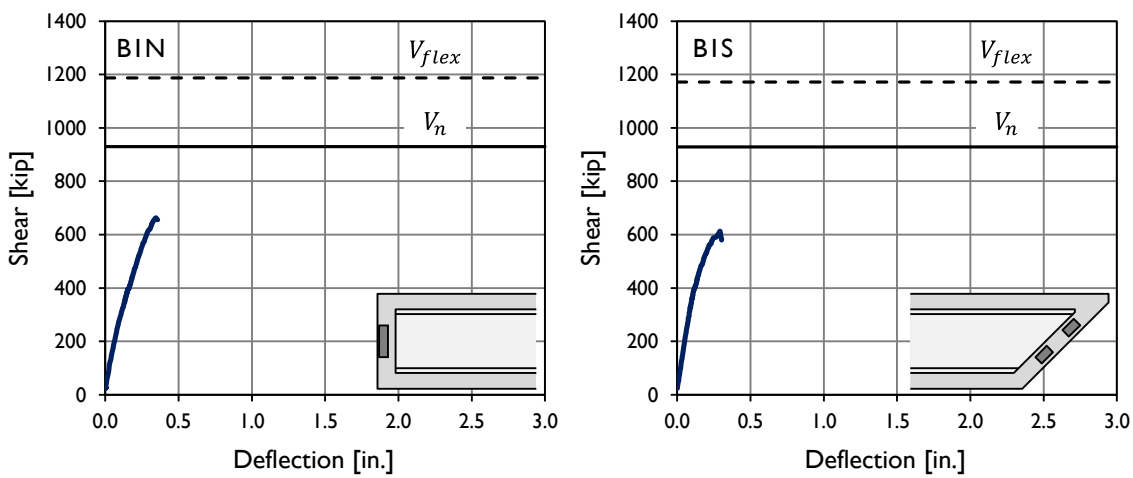

Figure B-45: Shear-deflection plot for specimens B1N and B1S.

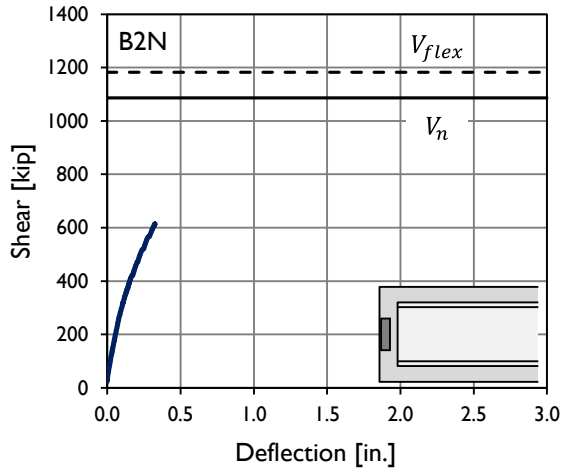

Figure B-46: Shear-deflection plot for specimens B2N.

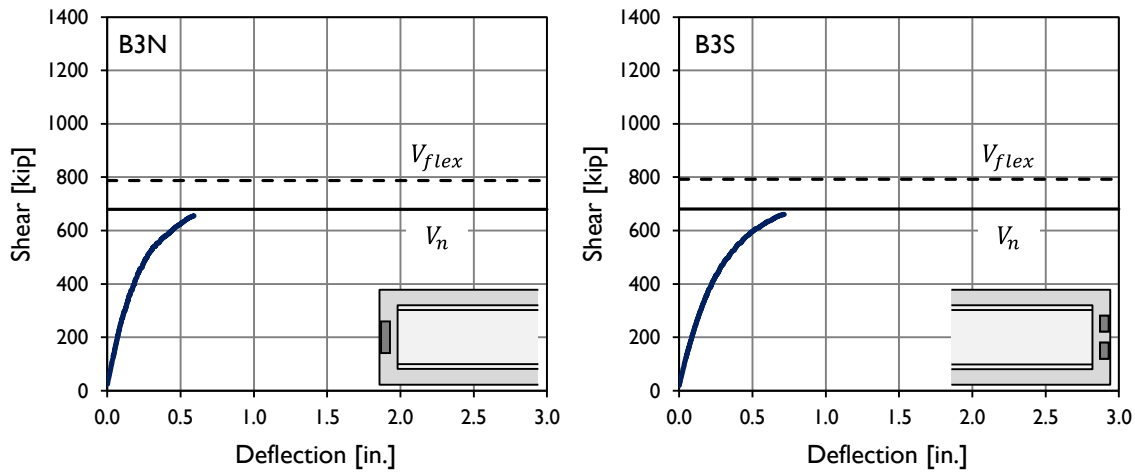

Figure B-47: Shear-deflection plot for specimens B3N and B3S.

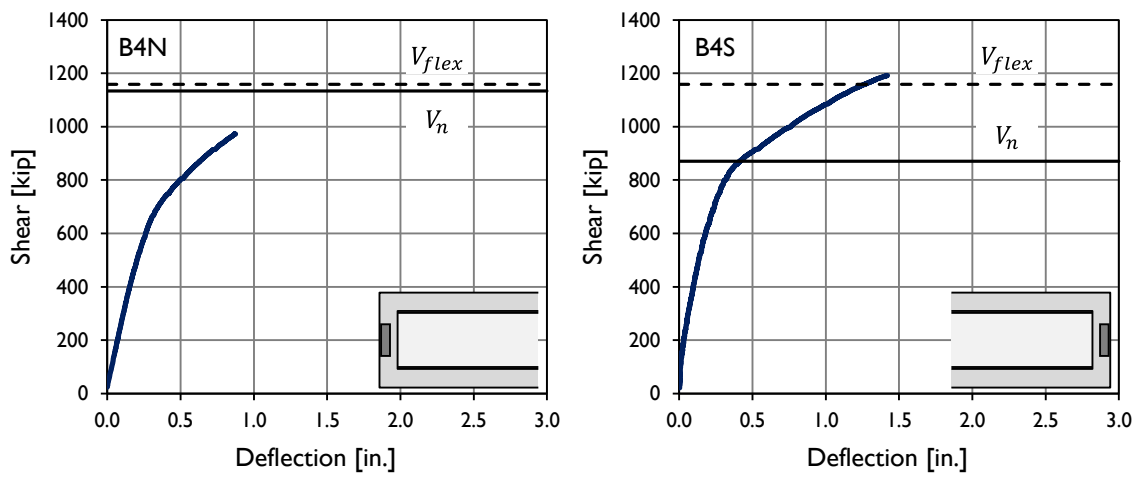

Figure B-48: Shear-deflection plot for specimens B4N and B4S.

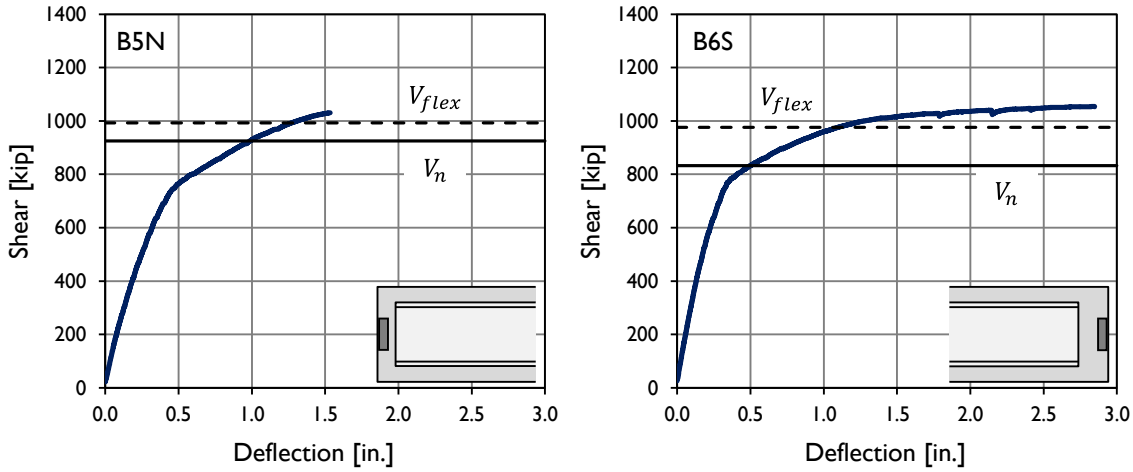

Figure B-49: Shear-deflection plot for specimens B5N and B6S.

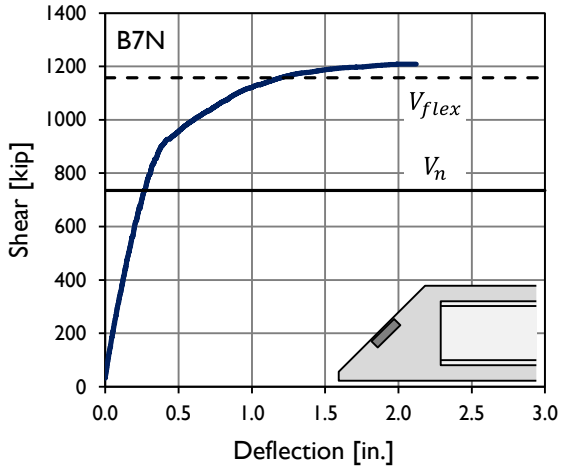

Figure B-50: Shear-deflection plot for specimens B7N.

APPENDIX C
Horizontal Shear Evaluation Database

C.1 INTRODUCTION

At the conclusion of the study on Texas U-Beams, seven of the test specimens were added to the Horizontal Shear Database. The details necessary for horizontal shear demand and capacity calculations for these beams and the other beams in the HSED are provided in this appendix through a series of tables and figures. General information about each test specimen is given in the first table (Table C-1). The parameters necessary for horizontal shear demand calculations can be found in Table C-2. The additional parameters necessary for horizontal shear capacity calculations are in Table C-3.

After these tables are a series of tables and figures showing the reinforcing bar shapes and positions used in calculations and summarized in Table C-3. Additional information about the specimens in the HSED can be found in the original source documents, which are summarized in Table C-18.

C.2 NOTATIONS

The following list of notations was used in the tables in this section:

a = shear span [in.]

A_{cv} = area of concrete within the region of interest [in.^{2}]

A_{eb} = additional area able to resist horizontal shear gained from the end block [in.^{2}]

A_{vf} = area of steel oriented perpendicular to the shear plane in the region of interest [in.^{2}]

Beam Type = cross-section type (e.g., AASHTO Type II, U54, Tx70). Inclusion of "-D" indicates the beam had a composite deck.

b_w = web width [in.]

d	=	depth from compressive fiber to centroid of tensile prestressing [in.]
h	=	total height of the test specimen [in.]
HS	=	binary reference to whether horizontal shear distress was seen at failure of the test section
f_c'	=	compressive strength of concrete [ksi]
f_{PS}	=	stress due to prestressing at the centroid of the section [ksi]
f_y	=	yield strength of primary vertical reinforcement [ksi]
l	=	length of the region of interest [in.]
l_{LP}	=	length of the load plate [in.]
l_{UEP}	=	length from beam end to the Ultimate Evaluation Point [in.]
oh	=	beam overhang, measured from centerline of bearing pad to beam end [in.]
P_{PS}	=	effective prestress force, after consideration of losses [kip]
Specimen ID	=	specimen name as provided in the original reference
Total V_{ni}	=	horizontal shear capacity from beam end to the UEP [kip]
$V_{u_{hs}}$	=	horizontal shear demand on the critical interface due to the load V_{test}
V_{ni}	=	horizontal shear capacity of the region of interest, considering limiting cases [kip]
V_{test}	=	failure shear [kip]
$\frac{V_{test}}{V_n}$	=	ratio of failure shear to capacity, calculated using the AASHTO General Procedure
With EB	=	binary reference to whether the beam contained an end block
y_{crit}	=	distance from tensile fiber to critical interface, generally defined as the bottom flange-to-web interface [in.]
$\rho_v f_y$	=	reinforcement ratio of primary shear reinforcement [ksi]

C.3 TABLE OF GENERAL PROPERTIES

Table C-1: General properties of beams in the Horizontal Shear Evaluation Database (Page 1 of 3).

Specimen ID	Beam Type	HS?	f'_c [ksi.]	f_y [ksi]	With EB?	A_{eb} [in.^{2}]	P_{PS} [kip]	f_{PS} [ksi]	$\frac{a}{d}$	$\rho_v f_y$ [psi]
Hovell (2011)										
B1N	U54-D	yes	11.9	65.8	yes	162	1874	1.67	2.62	658
B2N	U54-D	yes	11.5	85.2	yes	162	1874	1.67	2.62	852
B3N	U54-D	yes	11.4	65.3	yes	162	1009	0.90	2.63	653
B3S	U54-D	yes	12.1	65.3	yes	162	1009	0.90	2.63	653
B4N	U54-D	yes	11.4	63.0	yes	162	1874	1.36	2.62	525
B4S	U54-D	no	11.4	63.0	yes	162	1874	1.36	2.62	263
B5N	U54-D	no	13.2	65.0	yes	162	1585	1.42	2.61	1008
B6S	U54-D	no	12.0	85.0	yes	450	1537	1.37	2.60	567
Alshegeir & Ramirez (1992)										
Type I-4A-S	Type I	no	8.8	52.0	no		245	0.89	2.35	193
Type II-1A-N	Type II	no	9.0	52.0	no		360	0.97	2.16	165
Type I-3A-N	Type I	no	8.8	46.0	no		241	0.87	2.35	141
Avendaño (2011)										
BB-01Q	4B28	no	11.3	60.0	yes	128	558	0.82	2.96	120
BB-02Q	4B28	no	11.3	60.0	yes	128	558	0.82	2.96	120
BB-03Q	4B28	no	11.2	60.0	yes	128	558	0.82	2.96	120
BB-04Q	4B28	no	10.7	60.0	yes	128	558	0.82	2.96	120
BB-05Q	4B28	no	10.9	60.0	yes	128	558	0.82	2.96	120
5B40-1-Q	5B40	no	11.8	65.0	yes	128	1826	1.75	2.83	433
5B40-2-Q	5B40	yes	9.4	65.0	yes	128	1826	1.75	2.83	433
5B40-3-Q	5B40	yes	11.7	65.0	yes	128	1826	1.75	2.83	433
5B40-4-Q	5B40	yes	10.0	65.0	yes	128	1826	1.75	2.83	433
5B40-X-QS	5XB40-D	no	10.5	65.0	yes	128	1585	1.31	2.78	333
Avendaño & Bayrak (2008)										
Tx28-I-L	Tx28	yes	13.8	60.0	no		1232	2.11	2.97	286
Tx28-I-D	Tx28	yes	13.8	60.0	no		1232	2.11	2.97	286
Tx28-II-L	Tx28	yes	11.4	75.0	no		1232	2.11	3.82	352
Tx28-II-D	Tx28	yes	11.4	75.0	no		1232	2.11	3.82	352
Avendaño, et al. (unpublished)										
Tx70-N	Tx70	yes	11.8	60.0	no		1763	1.83	2.68	429
Tx46-N	Tx46	yes	13.2	75.0	no		1492	1.96	2.67	704
Tx46-S	Tx46	yes	13.2	75.0	no		1492	1.96	2.67	704
Hamilton, Llanos, & Ross (2009)										
B1U4	Type III	no	5.6	56.7	no		694	1.24	4.53	180
B4U4	Type III	no	5.6	56.7	no		694	1.24	4.53	180

Table C-1: General properties of beams in the Horizontal Shear Evaluation Database (Page 2 of 3).

Specimen ID	Beam Type	HS?	f'_c [ksi.]	f_y [ksi]	With EB?	A_{eb} [in.^{2}]	P_{PS} [kip]	f_{PS} [ksi]	$\frac{a}{d}$	$\rho_v f_y$ [psi]
Hawkins & Kuchma (2007)										
G1E	BT-63-D	yes	12.1	70.0	no		1109	1.56		389
G1W	BT-63-D	yes	12.1	70.0	no		1109	1.56		389
G2E	BT-63-D	yes	12.6	79.3	no		1239	1.74		745
G2W	BT-63-D	yes	12.6	79.3	no		1239	1.74		745
G3E	BT-63-D	yes	15.9	67.8	no		1412	1.98		565
G3W	BT-63-D	yes	15.9	67.8	no		1412	1.98		565
G5E	BT-63-D	yes	17.8	92.2	no		898	1.26		169
Heckmann & Bayrak (2008)										
CB-70-1	Type C	no	12.1	60.0	no		665	1.34	2.07	143
CB-70-4	Type C	no	12.4	60.0	no		649	1.31	2.07	143
CB-70-5	Type C	no	12.5	60.0	no		645	1.30	2.07	143
CB-70-6	Type C	no	12.8	60.0	no		636	1.29	2.07	143
CB-60-1	Type C	no	12.3	60.0	no		666	1.35	2.07	143
CB-60-2	Type C	no	12.7	60.0	no		667	1.35	2.07	143
Labonte & Hamilton (2005)										
S1-STDS	Type II	no	7.5	60.0	no		263	0.71	2.25	129
Natio, Parent, & Brunn (2005)										
HESC B1	PCEF-45	no	9.2	65.8	no		618	0.83	2.21	1253
Ramirez & Aguilar (2005)										
13.3-5.1-326P	Type I	no	13.3	85.0	no		263	0.95	3.68	315
16.2-5.1-326P	Type I	no	16.2	85.0	no		263	0.95	3.72	315
Runzell, Shield, & French (2007)										
I	MnType54-D	no	10.1	67.3	no		824	1.04	2.97	160
II	MnType54-D	no	10.1	67.3	no		824	1.04	3.51	160
Shahawy & Batchelor (1996)										
A0-00-R-N	Type II-D	no	6.0	60.0	no		376	1.02	2.17	375
A0-00-R-S	Type II-D	no	6.0	60.0	no		376	1.02	2.17	375
A1-00-R/2-N	Type II-D	no	6.0	60.0	no		376	1.02	2.60	125
A1-00-R/2-S	Type II-D	no	6.0	60.0	no		376	1.02	3.16	125
A1-00-R-N	Type II-D	no	6.0	60.0	no		376	1.02	2.60	250
A1-00-3R/2-N	Type II-D	no	6.0	60.0	no		376	1.02	2.60	375
B0-00-R-N	Type II-D	no	6.0	60.0	no		353	0.96	2.58	250
B0-00-R-S	Type II-D	no	6.0	60.0	no		353	0.96	3.14	250

Table C-1: General properties of beams in the Horizontal Shear Evaluation Database (Page 3 of 3).

Specimen ID	Beam Type	HS?	f'_c [ksi.]	f_y [ksi]	With EB?	A_{eb} [in.^{2}]	P_{PS} [kip]	f_{PS} [ksi]	$\frac{a}{d}$	$\rho_v f_y$ [psi]
Tawfiq (1995)										
R8N	Type II-D	no	8.2	60.0	no		422	1.14	2.68	500
R10N	Type II-D	no	10.1	60.0	no		422	1.14	2.68	500
R12N	Type II-D	no	11.0	60.0	no		422	1.14	2.68	500
2R8N	Type II-D	no	8.1	60.0	no		422	1.14	2.68	1000
2R10N	Type II-D	no	9.9	60.0	no		422	1.14	2.68	1000
2R12N	Type II-D	no	11.0	60.0	no		422	1.14	2.68	1000
R8S	Type II-D	no	8.2	60.0	no		422	1.14	2.26	500
R10S	Type II-D	no	10.1	60.0	no		422	1.14	2.26	500
R12S	Type II-D	no	11.0	60.0	no		422	1.14	2.26	500
2R8S	Type II-D	no	8.1	60.0	no		422	1.14	2.26	1000
2R10S	Type II-D	no	9.9	60.0	no		422	1.14	2.26	1000
2R12S	Type II-D	no	11.0	60.0	no		422	1.14	2.26	1000

C.4 TABLE OF DATA FOR DEMAND CALCULATIONS

Table C-2: Parameters for horizontal shear demand calculation (Page 1 of 3).

Specimen ID	V_{test} [kip]	$\frac{V_{test}}{V_n}$	b_w [in.]	d [in.]	a [in.]	oh [in.]	l_{LP} [in.]	h [in.]	y_{crit} [in.]	l_{UEP} [in.]	$V_{u_{hs}}$ [kip]
Hovell (2011)											
B1N	659.0	0.71	10.0	58.8	154	6.0	24.0	62.75	11.25	94.5	1015
B2N	610.0	0.56	10.0	58.8	154	6.0	24.0	62.75	11.25	94.5	940
B3N	655.0	0.98	10.0	58.6	154	6.0	24.0	62.75	11.25	96.5	1012
B3S	663.0	0.97	10.0	58.6	154	6.0	24.0	62.75	11.25	96.5	1025
B4N	973.0	0.86	16.0	58.8	154	6.0	24.0	62.75	11.25	96.5	1499
B4S	1190.9	1.24	16.0	58.8	154	6.0	24.0	62.75	11.25	96.5	1834
B5N	1031.0	1.08	10.0	59.1	154	6.0	24.0	62.75	11.25	96.5	1580
B6S	1053.8	1.26	10.0	59.1	154	6.0	24.0	62.75	11.25	96.5	1613
Alshegeir & Ramirez (1992)											
Type I-4A-S	161.5	1.43	6.0	25.5	60	60.0	9.0	28.0	10.0	97.5	238
Type II-1A-N	222.0	1.59	6.0	33.3	72	24.0	9.0	36.0	12.0	67.5	290
Type I-3A-N	113.0	1.15	6.0	25.5	60	18.0	9.0	28.0	10.0	55.5	166
Avendaño (2011)											
BB-01Q	244.1	1.48	10.0	24.4	72	9.0	10.8	28.0	10.0	57.6	487
BB-02Q	242.4	1.47	10.0	24.4	72	9.0	10.8	28.0	10.0	57.6	484
BB-03Q	290.5	1.77	10.0	24.4	72	9.0	10.8	28.0	10.0	57.6	580
BB-04Q	291.3	1.80	10.0	24.4	72	9.0	10.8	28.0	10.0	57.6	581
BB-05Q	300.6	1.84	10.0	24.4	72	9.0	10.8	28.0	10.0	57.6	600
5B40-1-Q	438.1	1.03	10.0	31.8	90	4.5	24.0	40.0	22.0	64.5	828
5B40-2-Q	543.6	1.31	10.0	31.8	90	6.0	24.0	40.0	22.0	66.0	1027
5B40-3-Q	521.0	1.18	10.0	31.8	90	6.0	24.0	40.0	22.0	66.0	984
5B40-4-Q	589.8	1.34	10.0	31.8	90	6.0	24.0	40.0	22.0	66.0	1114
5B40-X-QS	675.0	1.12	13.0	43.2	120	6.0	24.0	48.0	22.0	88.0	0
Avendaño & Bayrak (2008)											
Tx28-I-L	400.1	1.92	7.0	28.3	84	12.0	6.0	36.0	14.5	71.5	842
Tx28-I-D	416.8	2.00	7.0	28.3	84	12.0	6.0	36.0	14.5	71.5	877
Tx28-II-L	370.5	1.69	7.0	28.3	108	12.0	6.0	36.0	14.5	95.5	1094
Tx28-II-D	375.4	1.71	7.0	28.3	108	12.0	6.0	36.0	14.5	95.5	1108
Avendaño, et al. (unpublished)											
Tx70-N	772.8	1.28	7.0	66.2	178	9.0	24.0	78.0	16.5	113.0	1214
Tx46-N	575.1	1.06	7.0	45.0	120	9.0	24.0	54.0	16.5	79.5	901
Tx46-S	573.7	1.06	7.0	45.0	120	9.0	24.0	54.0	16.5	79.5	899
Hamilton, Llanos, & Ross (2009)											
B1U4	180.0	0.74	7.0	43.2	196	5.5	10.0	52.0	14.5	158.5	638
B4U4	198.0	0.81	7.0	43.2	196	5.5	10.0	52.0	14.5	158.5	702

Table C-2: Parameters for horizontal shear demand calculation (Page 2 of 3).

Specimen ID	V_{test} [kip]	$\frac{V_{test}}{V_n}$	b_w [in.]	d [in.]	a [in.]	oh [in.]	l_{LP} [in.]	h [in.]	y_{crit} [in.]	l_{UEP} [in.]	$V_{u_{hs}}$ [kip]
Hawkins & Kuchma (2007)											
G1E	485[1]	1.03	6.0	65.2	76	12.0		73.0	10.5	162	1101
G1W	574[1]	1.13	6.0	63.4	71	12.0		73.0	10.5	162	1399
G2E	653[1]	0.94	6.0	64.8	68	12.0		73.0	10.5	150	1362
G2W	765[1]	1.05	6.0	64.8	63	12.0		73.0	10.5	150	1678
G3E	672[1]	1.10	6.0	65.2	74	12.0		73.0	10.5	162	1511
G3W	731[1]	1.20	6.0	65.2	74	12.0		73.0	10.5	162	1644
G5E	428[1]	1.17	6.0	70.0	83	12.0		73.0	10.5	126	764
Heckmann & Bayrak (2008)											
CB-70-1	358.5	1.86	7.0	34.8	72	51.0	9.0	40.0	14.5	93.0	433
CB-70-4	355.8	1.84	7.0	34.8	72	51.0	9.0	40.0	14.5	93.0	430
CB-70-5	339.9	1.75	7.0	34.8	72	51.0	9.0	40.0	14.5	93.0	411
CB-70-6	373.5	1.91	7.0	34.8	72	51.0	9.0	40.0	14.5	93.0	451
CB-60-1	364.6	1.88	7.0	34.8	72	51.0	9.0	40.0	14.5	93.0	440
CB-60-2	358.5	1.84	7.0	34.8	72	51.0	9.0	40.0	14.5	93.0	433
Labonte & Hamilton (2005)											
S1-STDS	191.2	1.68	6.0	32.0	72	18.0		36.0	12.0	66.0	287
Natio, Parent, & Brunn (2005)											
HESC B1	488.8	1.04	7.0	41.8	92	8.0		45.0	13.5	68.7	711
Ramirez & Aguilar (2005)											
13.3-5.1-326P	179.9	1.43	6.0	25.0	92	36.0	8.0	28.0	10.0	106.0	504
16.2-5.1-326P	214.9	1.66	6.0	25.0	92	36.0	8.0	28.0	10.0	106.0	602
Runzell, Shield, & French (2007)											
I	383.1	1.11	8.0	58.6	174	12.0		63.0	17.0	140.0	836
II	320.3	1.08	8.0	49.6	174	12.0		54.0	17.0	149.0	884
Shahawy & Batchelor (1996)											
A0-00-R-N	313.0	1.37	6.0	39.3	85	6.0		44.0	12.0	59.0	423
A0-00-R-S	276.0	1.21	6.0	39.3	85	6.0		44.0	12.0	59.0	373
A1-00-R/2-N	166.0	1.25	6.0	39.3	102	6.0		44.0	12.0	76.0	296
A1-00-R/2-S	173.0	1.31	6.0	39.3	124	6.0		44.0	12.0	98.0	406
A1-00-R-N	210.0	1.17	6.0	39.3	102	6.0		44.0	12.0	76.0	375
A1-00-3R/2-N	207.0	1.02	6.0	39.3	102	6.0		44.0	12.0	76.0	369
B0-00-R-N	220.0	1.22	6.0	39.5	102	6.0		44.0	12.0	76.0	390
B0-00-R-S	206.0	1.30	6.0	39.5	124	6.0		44.0	12.0	98.0	479

[1] Tested under a distributed load

Table C-2: Parameters for horizontal shear demand calculation (Page 3 of 3).

Specimen ID	V_{test} [kip]	$\frac{V_{test}}{V_n}$	b_w [in.]	d [in.]	a [in.]	oh [in.]	l_{LP} [in.]	h [in.]	y_{crit} [in.]	l_{UEP} [in.]	$V_{u_{hs}}$ [kip]
Tawfiq (1995)											
R8N	275.0	1.26	6.0	40.3	108	6.0		44.0	12.0	82.0	519
R10N	281.0	1.28	6.0	40.3	108	6.0		44.0	12.0	82.0	531
R12N	277.0	1.26	6.0	40.3	108	6.0		44.0	12.0	82.0	523
2R8N	233.0	0.84	6.0	40.3	108	6.0		44.0	12.0	82.0	440
2R10N	238.0	0.85	6.0	40.3	108	6.0		44.0	12.0	82.0	449
2R12N	277.0	0.99	6.0	40.3	108	6.0		44.0	12.0	82.0	523
R8S	300.0	1.24	6.0	40.3	91	6.0		44.0	12.0	65.0	440
R10S	297.0	1.21	6.0	40.3	91	6.0		44.0	12.0	65.0	435
R12S	274.0	1.12	6.0	40.3	91	6.0		44.0	12.0	65.0	402
2R8S	254.0	0.83	6.0	40.3	91	6.0		44.0	12.0	65.0	372
2R10S	243.0	0.79	6.0	40.3	91	6.0		44.0	12.0	65.0	356
2R12S	285.0	0.92	6.0	40.3	91	6.0		44.0	12.0	65.0	418

C.5 TABLE OF DATA FOR CAPACITY CALCULATIONS

Table C-3: Parameters for horizontal shear capacity calculation (Page 1 of 3).

Specimen ID	k_d	Transfer Region, l = 36"			Region Two				Region Three				Total V_{ni} [kip]
		A_{cv} [in.^{2}]	A_{vf} [in.^{2}]	V_{ni} [kip]	l [in.]	A_{cv} [in.^{2}]	A_{vf} [in.^{2}]	V_{ni} [kip]	l [in.]	A_{cv} [in.^{2}]	A_{vf} [in.^{2}]	V_{ni} [kip]	
Hovell (2011)													
B1N	0.8	522	3.60	325	39.0	390	4.00	394	21.5	215	1.20	149	868
B2N	0.8	522	3.60	325	39.0	390	4.00	394	21.5	215	1.20	149	868
B3N	0.8	522	3.60	364	39.0	390	4.00	394	21.5	215	1.20	149	907
B3S	0.8	522	3.60	364	39.0	390	4.00	394	21.5	215	1.20	149	907
B4N	0.8	738	4.80	475	54.0	864	6.00	680	6.5	104	0.80	87	1242
B4S	1.0	738	27.1	1107	54.0	864	33.9	1296	6.5	104	2.66	156	2559
B5N	1.0	522	13.5	783	60.5	605	22.5	908	0	0	0	0	1691
B6S	1.0	810	14.8	1215	60.5	605	24.6	908	0	0	0	0	2123
Alshegeir & Ramirez (1992)													
Type I-4A-S	1.0	216	3.72	324	61.5	369	2.44	325	0	0	0	0	649
Type II-1A-N	1.0	216	3.72	324	31.5	189	0.80	134	0	0	0	0	458
Type I-3A-N	1.0	216	2.44	230	19.5	117	0.40	73	0	0	0	0	303
Avendaño (2011)													
BB-01Q	1.0	488	3.20	441	21.6	216	0.40	120	0	0	0	0	561
BB-02Q	1.0	488	3.20	441	21.6	216	0.40	120	0	0	0	0	561
BB-03Q	1.0	488	3.20	441	21.6	216	0.40	120	0	0	0	0	561
BB-04Q	1.0	488	3.20	441	21.6	216	0.40	120	0	0	0	0	561
BB-05Q	1.0	488	3.20	441	21.6	216	0.40	120	0	0	0	0	561
5B40-1-Q	1.0	488	4.80	504	28.5	285	3.20	389	0	0	0	0	887
5B40-2-Q	1.0	488	4.80	504	30.0	300	3.20	389	0	0	0	0	893
5B40-3-Q	1.0	488	4.80	504	30.0	300	3.20	389	0	0	0	0	893
5B40-4-Q	1.0	488	4.80	504	30.0	300	3.20	389	0	0	0	0	893
5XB40-S	1.0	596	4.80	561	26.0	338	2.40	337	26.0	338	2.0	303	1201
Avendaño & Bayrak (2008)													
Tx28-I-L	1.0	252	5.76	378	10.5	74	1.20	110	25.0	175	0.80	137	625
Tx28-I-D	1.0	252	5.36	378	14.5	102	1.60	152	21.0	147	0.40	92	623
Tx28-II-L	1.0	252	5.36	378	14.5	102	1.60	152	45.0	315	1.20	227	757
Tx28-II-D	1.0	252	5.76	378	10.5	74	1.20	110	49.0	343	1.60	272	760
Avendaño, et al. (unpublished)													
Tx70-N	1.0	252	10.1	378	2.5	18	0.40	26	74.5	522	3.60	511	915
Tx46-N	1.0	252	7.46	378	10.5	74	1.18	110	33.0	231	1.58	225	713
Tx46-S	1.0	252	6.19	378	14.5	102	1.58	152	29.0	203	1.58	214	744
Hamilton, Llanos, & Ross (2009)													
B1U4	1.0	252	2.26	241	6.0	42	0.20	33	117	816	1.20	421	695
B4U4	1.0	252	2.26	241	6.0	42	0.20	33	117	816	1.20	421	695

Table C-3: Parameters for horizontal shear capacity calculation (Page 2 of 3).

Specimen ID	k_d	Transfer Region, l = 36"			Region Two				Region Three				Total V_{ni} [kip]
		A_{cv} [in.^{2}]	A_{vf} [in.^{2}]	V_{ni} [kip]	l [in.]	A_{cv} [in.^{2}]	A_{vf} [in.^{2}]	V_{ni} [kip]	l [in.]	A_{cv} [in.^{2}]	A_{vf} [in.^{2}]	V_{ni} [kip]	
Hawkins & Kuchma (2007)													
G1W	1.0	216	4.92	324	120	720	3.60	590	6	36	0	14	929
G1E	1.0	216	4.96	324	120	720	3.60	590	6	36	0	14	929
G2E	1.0	216	4.96	324	108	648	6.20	780	6	36	0	14	1118
G2W	1.0	216	5.44	324	108	648	6.20	780	6	36	0	14	1118
G3E	1.0	216	5.44	324	120	720	6.00	792	6	36	0	14	1130
G3W	1.0	216	5.44	324	120	720	6.00	792	6	36	0	14	1130
G5E	1.0	216	2.92	281	120	720	6.00	792	0	0	0	0	571
Heckmann & Bayrak (2008)													
CB-70-1	1.0	252	9.04	378	57.0	399	0.80	227	0	0	0	0	605
CB-70-4	1.0	252	9.04	378	57.0	399	0.80	227	0	0	0	0	605
CB-70-5	1.0	252	9.04	378	57.0	399	0.80	227	0	0	0	0	605
CB-70-6	1.0	252	9.04	378	57.0	399	0.80	227	0	0	0	0	605
CB-60-1	1.0	252	9.04	378	57.0	399	0.80	227	0	0	0	0	605
CB-60-2	1.0	252	9.04	378	57.0	399	0.80	227	0	0	0	0	605
Labonte & Hamilton (2005)													
S1-STDS	1.0	216	4.03	324	30.0	180	0	72	0	0	0	0	396
Naito, Parent, & Brunn (2005)													
HESC B1	1.0	252	5.11	378	32.7	229	4.00	343	0	0	0	0	721
Ramirez & Aguilar (2005)													
12.3-5.1-326P	1.0	216	0.80	139	70.0	420	1.60	302	0	0	0	0	441
16.2-5.1-326P	1.0	216	0.80	139	70.0	420	1.60	302	0	0	0	0	441
Runzell, Shield, & French (2007)													
I	1.0	288	2.40	271	101	808	2.00	491	0	0	0	0	762
II	1.0	288	2.40	271	110	880	2.00	520	0	0	0	0	791
Shahawy, Robinson, Batchelor (1993)													
A0-00-R-N	1.0	216	3.20	324	18.0	108	1.20	144	5.0	30	0	12	480
A0-00-R-S	1.0	216	3.20	324	18.0	108	1.20	144	5.0	30	0	12	480
A1-00-R/2-N	1.0	216	1.60	200	18.0	108	0.60	94	22.0	132	0.40	86	380
A1-00-R/2-S	1.0	216	1.60	200	18.0	108	0.60	94	44.0	264	1.00	190	483
A1-00-R-N	1.0	216	3.20	324	18.0	108	1.20	144	22.0	132	0.80	120	588
A1-00-3R/2-N	1.0	216	4.80	324	18.0	108	1.80	162	22.0	132	1.20	154	640
B0-00-R-N	1.0	216	3.20	324	18.0	108	1.20	144	22.0	132	0.80	120	588
B0-00-R-S	1.0	216	3.20	324	18.0	108	1.20	144	44.0	264	2.00	274	742

Table C-3: Parameters for horizontal shear capacity calculation (Page 3 of 3).

Specimen ID	k_d	Transfer Region, l = 36"			Region Two				Region Three				Total V_{ni} [kip]
		A_{cv} [in.^{2}]	A_{vf} [in.^{2}]	V_{ni} [kip]	l [in.]	A_{cv} [in.^{2}]	A_{vf} [in.^{2}]	V_{ni} [kip]	l [in.]	A_{cv} [in.^{2}]	A_{vf} [in.^{2}]	V_{ni} [kip]	
Tawfiq (1995)													
R8N	1.0	216	3.20	324	18.0	108	1.20	144	28.0	168	1.20	168	636
R10N	1.0	216	3.20	324	18.0	108	1.20	144	28.0	168	1.20	168	636
R12N	1.0	216	3.20	324	18.0	108	1.20	144	28.0	168	1.20	168	636
2R8N	1.0	216	4.80	324	18.0	108	2.40	162	28.0	168	2.80	252	738
2R10N	1.0	216	4.80	324	18.0	108	2.40	162	28.0	168	2.80	252	738
2R12N	1.0	216	4.80	324	18.0	108	2.40	162	28.0	168	2.80	252	738
R8S	1.0	216	3.20	324	18.0	108	1.20	144	11.0	66	0.40	60	528
R10S	1.0	216	3.20	324	18.0	108	1.20	144	11.0	66	0.40	60	528
R12S	1.0	216	3.20	324	18.0	108	1.20	144	11.0	66	0.40	60	528
2R8S	1.0	216	4.80	324	18.0	108	2.40	162	11.0	66	0.80	94	580
2R10S	1.0	216	4.80	324	18.0	108	2.40	162	11.0	66	0.80	94	580
2R12S	1.0	216	4.80	324	18.0	108	2.40	162	11.0	66	0.80	94	580

C.6 REINFORCING BAR LOCATIONS

The reinforcing bar locations, as gathered from the source documents, that were used in the horizontal shear capacity calculations are presented in the following sections. The location of bars included in the transfer zone are written in red. When available in the original research document, bar shapes and position in the cross-section are also provided. The reinforcing bar layout for every beam within a research program is not necessarily drawn.

C.6.1 Texas U-Beams: Hovell (2011)

Eight test specimens were added to the HSED upon completion of the U-Beam study presented in this dissertation. The full beam drawings can be found in Appendix A. Provided in Table C-4 are the locations of reinforcing bars used in horizontal shear capacity calculations for the beams. A simplified drawing of one test specimen (B6S) is also given. Bars positioned less than 36.0 in. from beam end were considered to be in the transfer region. The two skewed test regions were not included in this study.

Table C-4: Reinforcing bar locations in specimens tested by Hovell (2011).

Specimen ID	l_{UEP} [in.]	Bar Name	No. & Size	Locations [in. from end]								
Hovell (2011)												
B1N	96.5	R	2-#4	3.0	7.0	11.0	15.0	19.0	23.0	27.0	31.0	35.0
				39.0	43.0	47.0	51.0	55.0	59.0	63.0	67.0	71.0
				75.0	81.0	87.0	93.0					
B2N	96.5	R	2-#4	3.0	7.0	11.0	15.0	19.0	23.0	27.0	31.0	35.0
				39.0	43.0	47.0	51.0	55.0	59.0	63.0	67.0	71.0
				75.0	81.0	87.0	93.0					
B3N	96.5	R	2-#4	3.0	7.0	11.0	15.0	19.0	23.0	27.0	31.0	35.0
				39.0	43.0	47.0	51.0	55.0	59.0	63.0	67.0	71.0
				75.0	81.0	87.0	93.0					
B3S	96.5	R	2-#4	3.0	7.0	11.0	15.0	19.0	23.0	27.0	31.0	35.0
				39.0	43.0	47.0	51.0	55.0	59.0	63.0	67.0	71.0
				75.0	81.0	87.0	93.0					
B4N	96.5	R	2-#4	3.0	6.0	9.0	12.0	15.0	18.0	21.0	24.0	27.0
				30.0	33.0	36.0	39.0	42.0	45.0	48.0	51.0	54.0
				57.0	60.0	64.0	68.0	72.0	76.0	80.0	84.0	88.0
				92.0	96.0							
B4S	96.5	R L	2-#4 6-#5	3.0	6.0	9.0	12.0	15.0	18.0	21.0	24.0	27.0
				30.0	33.0	36.0	39.0	42.0	45.0	48.0	51.0	54.0
				57.0	60.0	64.0	68.0	72.0	76.0	80.0	84.0	88.0
				92.0	96.0							
B5N	96.5	R L	2-#5 2-#6	3.0	7.0	11.0	15.0	19.0	23.0	27.0	31.0	35.0
				39.0	43.0	47.0	51.0	55.0	59.0	63.0	67.0	71.0
				75.0	79.0	83.0	87.0	91.0	95.0			
B6S	96.5	R L	2-#4 4-#5	3.0	7.0	11.0	15.0	19.0	23.0	27.0	31.0	35.0
				39.0	43.0	47.0	51.0	55.0	59.0	63.0	67.0	71.0
				75.0	79.0	83.0	87.0	91.0	95.0			

B6S

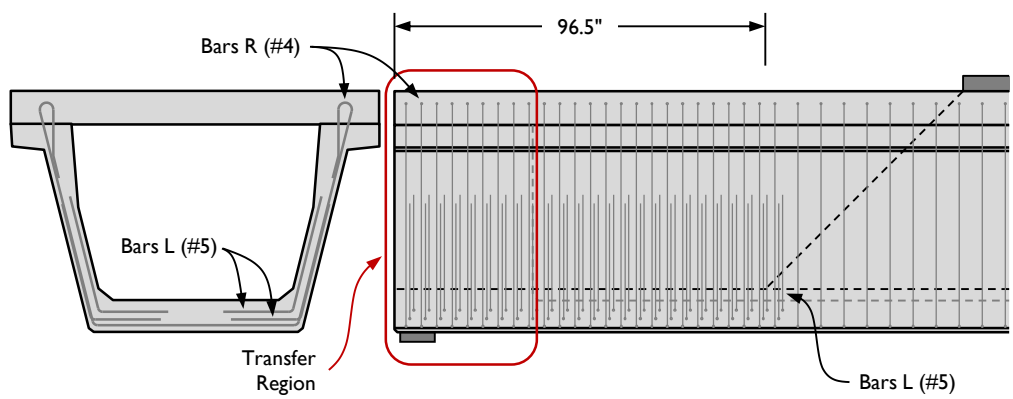

C.6.2 Alshegeir & Ramirez (1992)

Three specimens tested by Alshegeir and Ramirez were included in the HSED. Included are two AASHTO Type I beams and one AASHTO Type II beam. The details of the reinforcing bar layout in this beams are provided in Table C-5. Bars located within 36.0 in. from beam end were considered to be in the transfer region, and are written in red.

Table C-5: Reinforcing bar locations in specimens tested by Alshegeir and Ramirez (1992) (1 of 3).

Specimen ID	l_{UEP} [in.]	Bar Name	No. & Size	Locations [in. from end]								
Alshegeir & Ramirez (1992)												
Type I-4A-S	97.5		4-#5	6.0	9.0	27.0	45.0					
			2-#4	66.0	75.0	93.0						

TypeI-4A

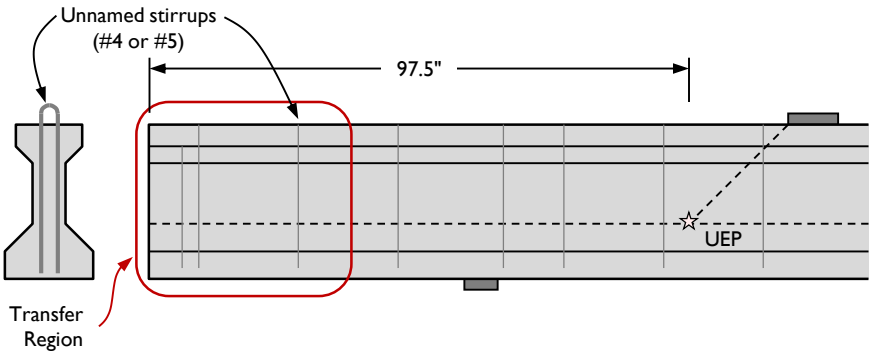

Table C-5: Reinforcing bar locations in specimens tested by Alshegeir and Ramirez (1992) (2 of 3).

Specimen ID	l_{UEP} [in.]	Bar Name	No. & Size	Locations [in. from end]								
Alshegeir & Ramirez (1992)												
Type II-1A-N	67.5		4-#5	6.0	9.0	12.0						
			2-#4	37.5	58.5							

TypeII-1A

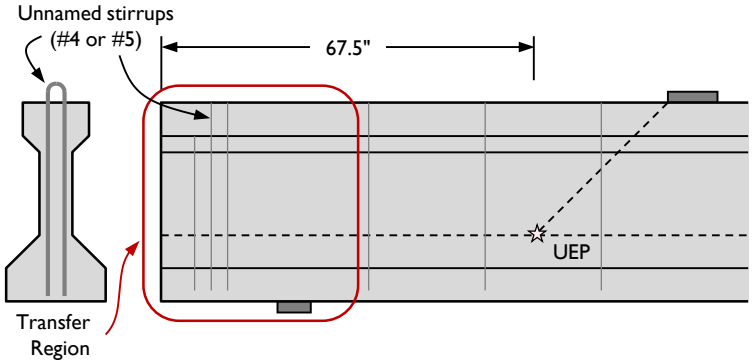

Table C-5: Reinforcing bar locations in specimens tested by Alshegeir and Ramirez (1992) (3 of 3).

Specimen ID	l_{UEP} [in.]	Bar Name	No. & Size	Locations [in. from end]								
Alshegeir & Ramirez (1992)												
Type I-3A-N	55.5		4-#5	6.0								
			2-#4	12.0	24.0	36.0	48.0					

TypeI-3A

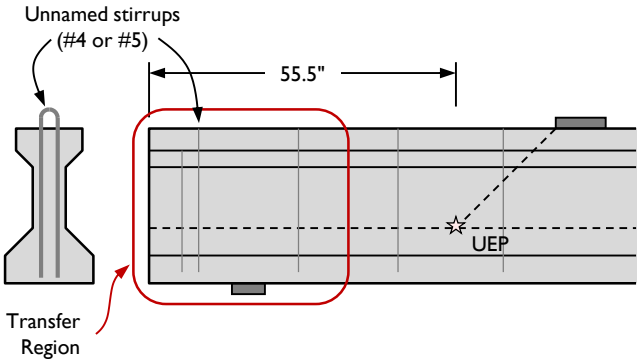

C.6.3 Avendaño (2011)

Five 4B28 Box-Beam tests, four 5B40 Box-Beam tests, and one 5XB40 (with deck) Box-Beam test reported by Avendaño are included in the HSED. Several of the larger of these beams showed signs of horizontal shear distress at failure, but that failure mode was not concluded to be governing behavior. The general reinforcing bar shapes and exact reinforcing bar locations are given in Table C-6.

Table C-6: Reinforcing bar locations in specimens tested by Avendaño (2011) (1 of 3).

Specimen ID	l_{UEP} [in.]	Bar Name	No. & Size	Locations [in. from end]								
Avendaño (2011)												
BB-01Q	57.6	U	2-#4	2.3	6.4	10.5	14.0	34.0	54.0			
		N	2-#4	2.3	6.4	10.5						
BB-02Q	57.6	U	2-#4	2.3	6.4	10.5	14.0	34.0	54.0			
		N	2-#4	2.3	6.4	10.5						
BB-03Q	57.6	U	2-#4	2.3	6.4	10.5	14.0	34.0	54.0			
		N	2-#4	2.3	6.4	10.5						
BB-04Q	57.6	U	2-#4	2.3	6.4	10.5	14.0	34.0	54.0			
		N	2-#4	2.3	6.4	10.5						
BB-05Q	57.6	U	2-#4	2.3	6.4	10.5	14.0	34.0	54.0			
		N	2-#4	2.3	6.4	10.5						

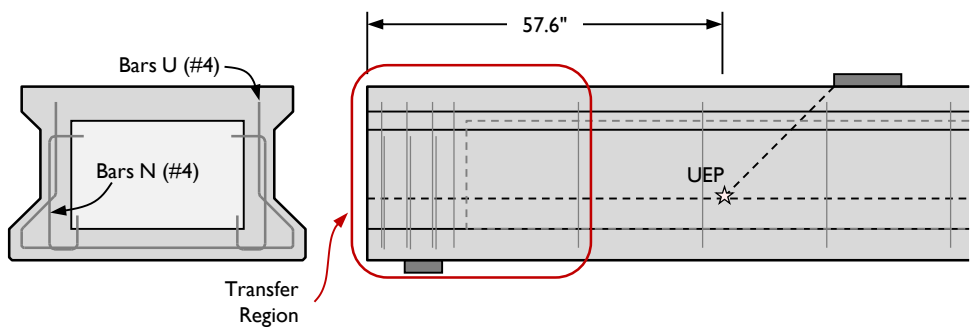

Table C-6: Reinforcing bar locations in specimens tested by Avendaño (2011) (2 of 3)

Specimen ID	l_{UEP} [in.]	Bar Name	No. & Size	Locations [in. from end]								
Avendaño (2011)												
5B40-1-Q	64.5	C	2-#4	2.3	6.4	10.5	14.0	20.0	26.0	32.0	38.0	44.0
				50.0	56.0	62.0						
		U	2-#4	2.3	6.4	10.5	14.0	26.0	38.0	50.0	62.0	
		N	2-#4	2.3	6.4	10.5						
5B40-2-Q	66.0	C	2-#4	2.3	6.4	10.5	14.0	20.0	26.0	32.0	38.0	44.0
				50.0	56.0	62.0						
		U	2-#4	2.3	6.4	10.5	14.0	26.0	38.0	50.0	62.0	
		N	2-#4	2.3	6.4	10.5						
5B40-3-Q	66.0	C	2-#4	2.3	6.4	10.5	14.0	20.0	26.0	32.0	38.0	44.0
				50.0	56.0	62.0						
		U	2-#4	2.3	6.4	10.5	14.0	26.0	38.0	50.0	62.0	
		N	2-#4	2.3	6.4	10.5						
5B40-4-Q	66.0	C	2-#4	2.3	6.4	10.5	14.0	20.0	26.0	32.0	38.0	44.0
				50.0	56.0	62.0						
		U	2-#4	2.3	6.4	10.5	14.0	26.0	38.0	50.0	62.0	
		N	2-#4	2.3	6.4	10.5						

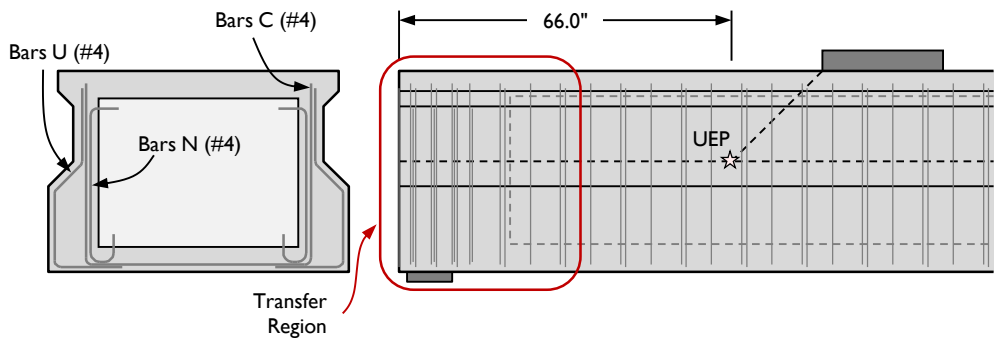

Table C-6: Reinforcing bar locations in specimens tested by Avendaño (2011) (3 of 3)

Specimen ID	l_{UEP} [in.]	Bar Name	No. & Size	Locations [in. from end]								
Avendaño (2011)												
5XB40-S	88.0	R	2-#4	2.3	6.3	10.3	14.3	18.3	22.3	26.3	30.3	34.3
				38.3	42.3	46.3	50.3	54.3	58.3	62.3	68.3	74.3
				80.3	86.3							
		N	2-#4	2.8	6.8	10.8						

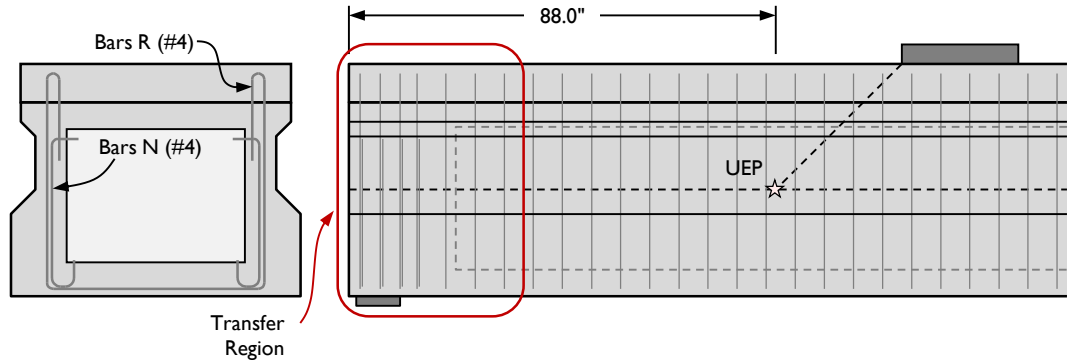

C.6.4 Avendaño & Bayrak (2008)

Four Texas Tx28 I-Beams load-tested by Avendaño and Bayrak (2008) were included in the HSED. All four of these beams failed by sliding of the web relative to the bottom flange, with relatively little distress in the webs of the beams. The reinforcing bars locations are given in Table C-7; those located within 36.0 in. from beam end were considered to be in the transfer zone.

Table C-7: Reinforcing bar locations in specimens tested by Avendaño and Bayrak (2008).

Specimen ID	l_{UEP} [in.]	Bar Name	No. & Size	Locations [in. from end]								
Avendaño and Bayrak (2008)												
Tx28-I-L	71.5	R	2-#4	2.5	5.5	8.5	11.5	14.5	18.5	22.5	26.5	30.5
				34.5	38.5	42.5	46.5	58.5	70.5			
		S	2-#6	2.5	5.5							
Tx28-I-D	71.5	R	2-#4	2.5	6.5	10.5	14.5	18.5	22.5	26.5	30.5	34.5
				38.5	42.5	46.5	50.5	62.5				
		S	2-#6	2.5	6.5							
Tx28-II-L	95.5	R	2-#4	2.5	6.5	10.5	14.5	18.5	22.5	26.5	30.5	34.5
				38.5	42.5	46.5	50.5	62.5				
		S	2-#6	2.5	6.5							
Tx28-II-D	95.5	R	2-#4	2.5	5.5	8.5	11.5	14.5	18.5	22.5	26.5	30.5
				34.5	38.5	42.5	46.5	58.5	70.5	82.5	94.5	
		S	2-#6	2.5	5.5							

Tx28-I-L and Tx28-II-D

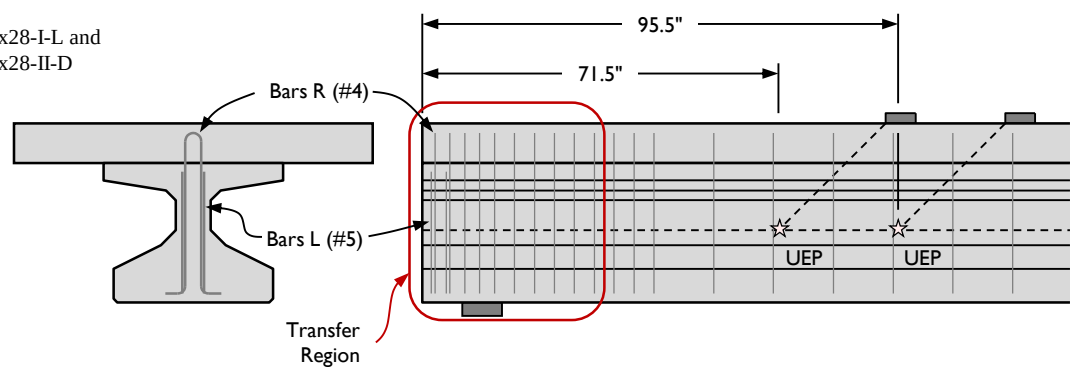

C.6.5 Avendaño, et al. (unpublished)

Three Texas Tx Girders (one Tx70 and both ends of a Tx46) were tested in 2010 by author of this dissertation and others. The data from these tests were included in the HSED, as horizontal shear failure controlled in all three tests. The results of this study are expected to be published soon. The reinforcing bar locations are given in Table C-8;

bars marked in red (within 36.0 in. from beam end) were included in transfer region calculations.

Table C-8: Reinforcing bar locations in specimens tested by Avendaño, et al. (unpublished).

Specimen ID	l_{UEP} [in.]	Bar Name	No. & Size	Locations [in. from end]								
Avendaño, et al. (unpublished)												
Tx70-N	113.0	R	2-#4	2.5	5.5	8.5	11.5	14.5	17.5	20.5	23.5	26.5
				29.5	32.5	35.5	38.5	46.5	54.5	62.5	70.5	78.5
				86.5	94.5	103	111					
		S	2-#6	4.0	7.0	10.0	13.0	16.0	19.0			

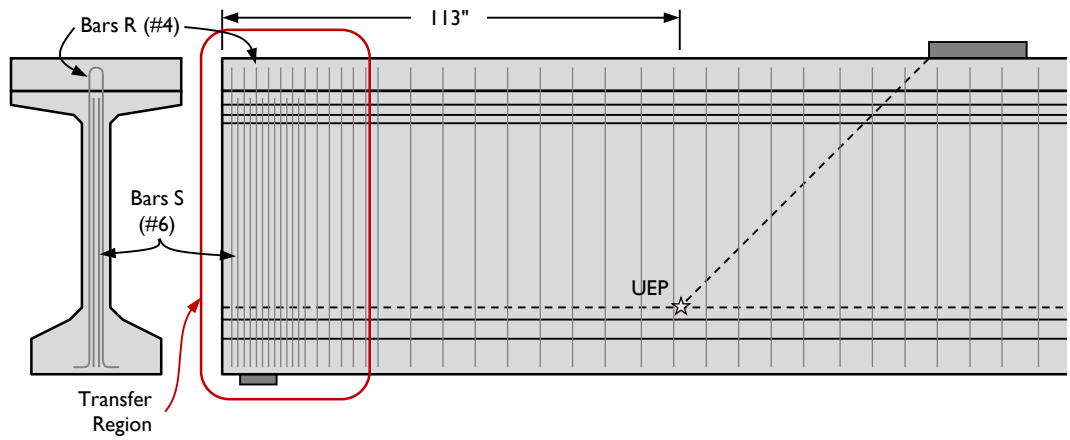

Tx46-N	79.5	R	2-#4	2.5	5.5	8.5	11.5	14.5	18.5	22.5	26.5	30.5
				34.5	38.5	42.5	46.5	52.5	58.5	64.5	70.5	
		S	2-#6	2.5	5.5	8.5	11.5					
Tx46-S	79.5	R	2-#4	2.5	6.5	10.5	14.5	18.5	22.5	26.5	30.5	34.5
				38.5	42.5	46.5	50.5	56.5	62.5	68.5	74.5	
		S	2-#6	2.5	6.5	10.5						

Tx46-S

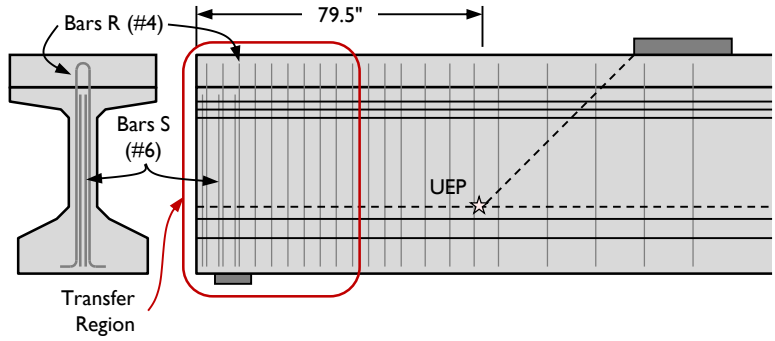

C.6.6 Hamilton, Llanos, & Ross (2009)

Two Type III beams tested by Hamilton, Llanos, and Ross were included in the HSED. The details of the reinforcing bars included in horizontal shear capacity calculations are given in Table C-9. Bars positioned within 36.0 in. of beam end were considered to be in the transfer region.

Table C-9: Reinforcing bar locations in specimens tested by Hamilton, Llanos, and Ross (2009).

Specimen ID	l_{UEP} [in.]	Bar Name	No. & Size	Locations [in. from end]								
Hamilton, Llanos, & Ross (2009)												
B1U4	158.5	K2	1-#5	2.0	10.0	20.0						
		Z2	1-#5	6.0	14.0	26.0						
		K1	1-#4	32.0	44.0	62.0	80.0	98.0	116	134	152	
		Z1	1-#4	38.0	50.0							
B4U4	158.5	K2	1-#5	2.0	10.0	20.0						
		Z2	1-#5	6.0	14.0	26.0						
		K1	1-#4	32.0	44.0	62.0	80.0	98.0	116	134	152	
		Z1	1-#4	38.0	50.0							

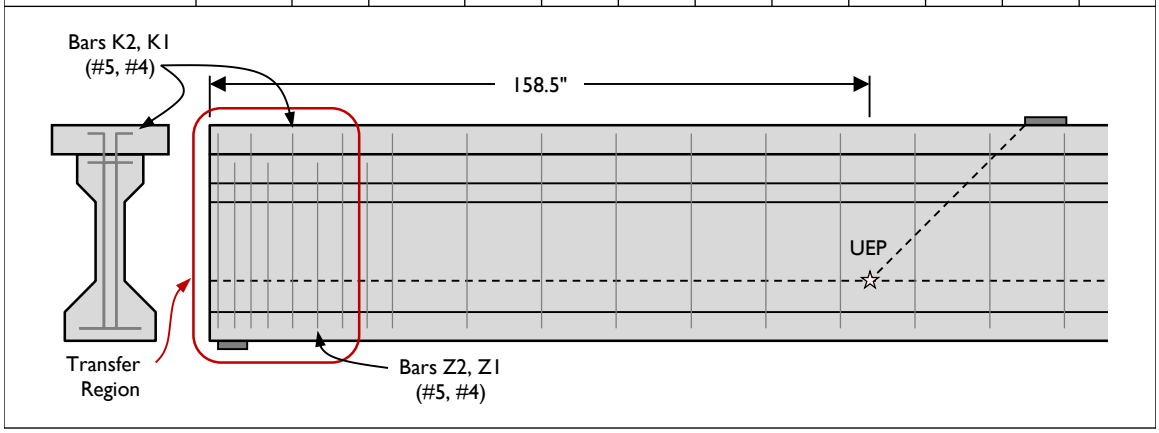

C.6.7 Hawkins & Kuchma (2007)

The beams tested by Hawkins and Kuchma were the only ones included in the database loaded with a continuous or spread load. Finding the Ultimate Evaluation Point was more complicated than for beams loaded at a single point.

For these beams, horizontal shear demand and capacity were calculated at 6 to 12 in. intervals from beam end to midspan. The two were compared and the reported data reflects the data from the worst evaluation point along the length (at which the ratio of

demand to capacity was the highest). The reinforcing bars locations given in Table C-10 include the bars located between beam end and this worst-case point.

Table C-10: Reinforcing bar locations in specimens tested by Hawkins and Kuchma (2007).

Specimen ID	l_{UEP} [in.]	Bar	Size	Locations [in. from end]								
Hawkins and Kuchma (2007)												
G1W	162	R2	2-#5	2.0	4.0	6.0	8.0	10.0	12.0			
		R1	2-#4	24.0	36.0	48.0	60.0	72.0	84.0	96.0	108	120
				132	144	156						
G1E	162	R2	2-#5	2.0	4.0	6.0	8.0	10.0	12.0			
		R1	2-#4	24.0	36.0	48.0	60.0	72.0	84.0	96.0	108	120
				132	144	156						
G2W	150	R2	2-#5	2.0	4.0	6.0	8.0	10.0	12.0	23.0	34.0	45.0
				56.0	67.0	78.0	89.0	100	111	122	133	144
G2E	150	R2	2-#5	2.0	4.0	6.0	8.0	10.0	12.0	23.0	34.0	45.0
				56.0	67.0	78.0	89.0	100	111	122	133	144
G3W	162	R2	2-#5	2.0	4.0	6.0	8.0	10.0	12.0			
		R1	2-#4	20.0	28.0	36.0	44.0	54.0	60.0	68.0	76.0	84.0
				92.0	100	108	116	124	132	140	148	156
G3E	162	R2	2-#5	2.0	4.0	6.0	8.0	10.0	12.0			
		R1	2-#4	20.0	28.0	36.0	44.0	54.0	60.0	68.0	76.0	84.0
				92.0	100	108	116	124	132	140	148	156
G5E	126	R2	2-#5	2.0	4.5	7.0	9.5					
		R6	2-#3	12.0	32.0	52.0	72.0	92.0	112			

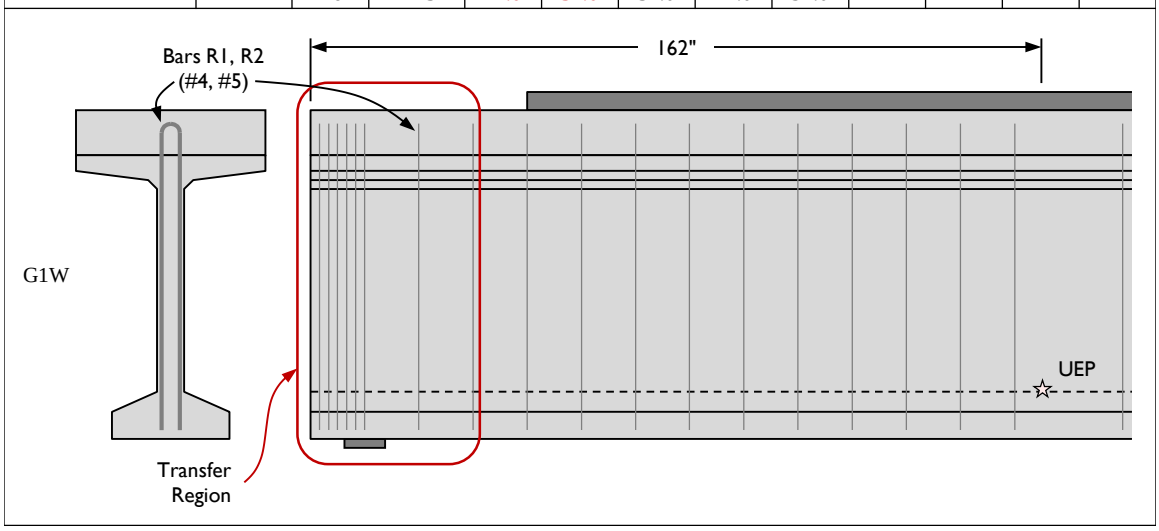

C.6.8 Heckmann & Bayrak (2008)

Six test specimens from Heckmann and Bayrak (2008) were included in the HSED. Provided in Table C-11 are the locations of reinforcing bars used in horizontal

shear capacity calculations. Bars positioned less than 36.0 in. from beam end (written in red) were considered to be in the transfer region.

Table C-11: Reinforcing bar locations in specimens tested by Heckmann and Bayrak (2008).

Specimen ID	l_{UEP} [in.]	Bar Name	No. & Size	Locations [in. from end]								
Heckmann & Bayrak (2008)												
CB-70-1	93.0	Y	2-#6	1.5								
		S	2-#5	4.0	8.0	12.0	16.0	20.0	24.0	28.0	32.0	
		R	2-#4	6.0	10.0	14.0	18.0	22.0	26.0	30.0	34.0	58.0
				82.0								
CB-70-4	93.0	Y	2-#6	1.5								
		S	2-#5	4.0	8.0	12.0	16.0	20.0	24.0	28.0	32.0	
		R	2-#4	6.0	10.0	14.0	18.0	22.0	26.0	30.0	34.0	58.0
				82.0								
CB-70-5	93.0	Y	2-#6	1.5								
		S	2-#5	4.0	8.0	12.0	16.0	20.0	24.0	28.0	32.0	
		R	2-#4	6.0	10.0	14.0	18.0	22.0	26.0	30.0	34.0	58.0
				82.0								
CB-70-6	93.0	Y	2-#6	1.5								
		S	2-#5	4.0	8.0	12.0	16.0	20.0	24.0	28.0	32.0	
		R	2-#4	6.0	10.0	14.0	18.0	22.0	26.0	30.0	34.0	58.0
				82.0								
CB-60-1	93.0	Y	2-#6	1.5								
		S	2-#5	4.0	8.0	12.0	16.0	20.0	24.0	28.0	32.0	
		R	2-#4	6.0	10.0	14.0	18.0	22.0	26.0	30.0	34.0	58.0
				82.0								
CB-60-2	93.0	Y	2-#6	1.5								
		S	2-#5	4.0	8.0	12.0	16.0	20.0	24.0	28.0	32.0	
		R	2-#4	6.0	10.0	14.0	18.0	22.0	26.0	30.0	34.0	58.0
				82.0								

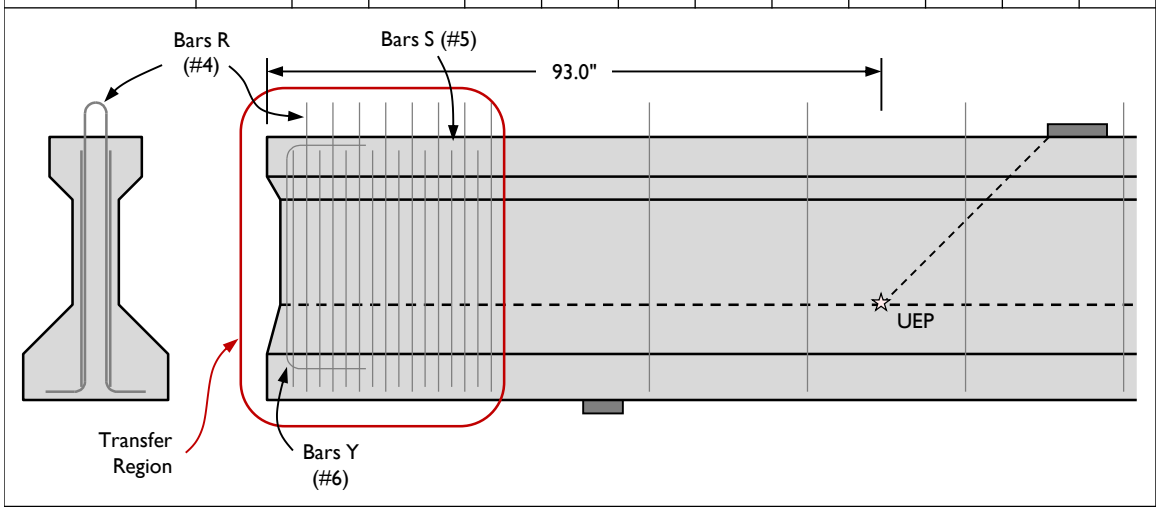

C.6.9 Labonte & Hamilton (2005)

One Type III beam tested by Labonte and Hamilton was included in the HSED. No signs of horizontal shear distress were seen at failure of this beam. The reinforcing bar locations are given in Table C-12.

Table C-12: Reinforcing bar locations in specimens tested by Labonte and Hamilton (2005).

Specimen ID	l_{UEP} [in.]	Bar Name	No. & Size	Locations [in. from end]								
Labonte & Hamilton (2005)												
S1-STDS	66.0		2-#5	3.0	6.0	9.0	12.0	15.0				
			#5	21.0	27.0	33.0						

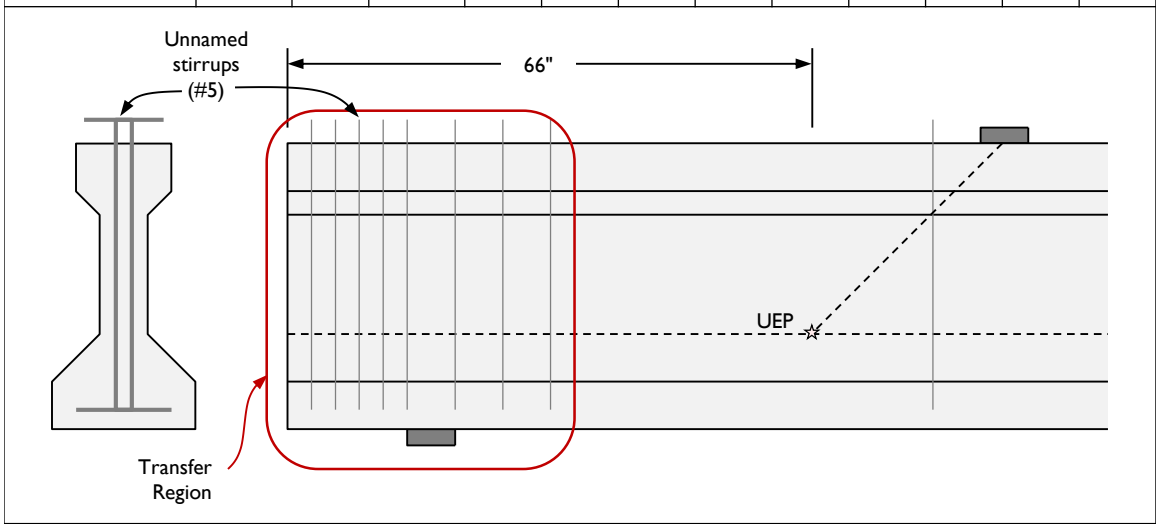

C.6.10 Naito, Parent, & Brunn (2005)

One PCEF-45 beam tested by Naito, Parent, and Brunn was included in the HSED. This beam failed with no signs of horizontal shear distress. The reinforcing bar locations used in horizontal shear capacity calculations for the beam are provided in Table C-13. The bars located within 36.0 in. from beam end (written in red) were considered to be part of the transfer region.

Table C-13: Reinforcing bar locations in specimens tested by Naito, Parent, and Brunn (2005).

Specimen ID	l_{UEP} [in.]	Bar Name	No. & Size	Locations [in. from end]								
Naito, Parent, & Brunn (2005)												
HESC B1	68.7	A160	#5	3.0								
		A110	2-#4	3.0	6.0	9.0	12.0	15.0	18.0	21.0	24.0	27.0
				30.0	33.0	36.0	39.0	42.0	45.0	48.0	51.0	54.0
				57.0	60.0	63.0	66.0					

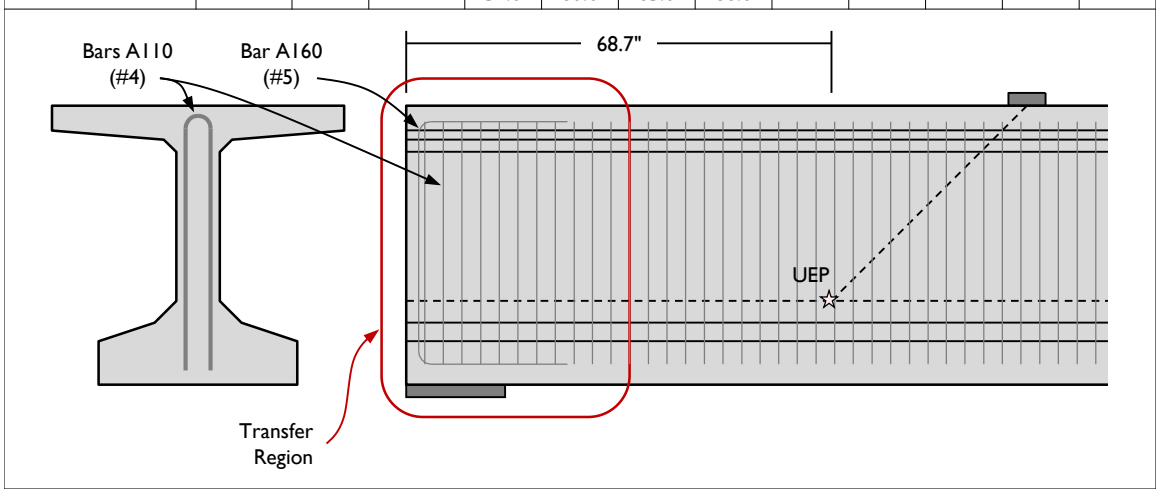

C.6.11 Ramirez & Aguilar (2005)

Two Type II beams tested by Ramirez and Aguilar were included in the HSED. These beams showed no signs of horizontal shear distress at failure. The reinforcing bar locations used in capacity calculations for these beams are given in Table C-14, with the bars located within the transfer region highlighted.

Table C-14: Reinforcing bar locations in specimens tested by Ramirez and Aguilar (2005).

Specimen ID	l_{UEP} [in.]	Bar Name	No. & Size	Locations [in. from end]								
Ramirez & Aguilar (2005)												
12.3-5.1-326P	106.0		2-#4	2.0	20.0	38.0	56.0	74.0	92.0			
16.2-5.1-326P	106.0		2-#4	2.0	20.0	38.0	56.0	74.0	92.0			

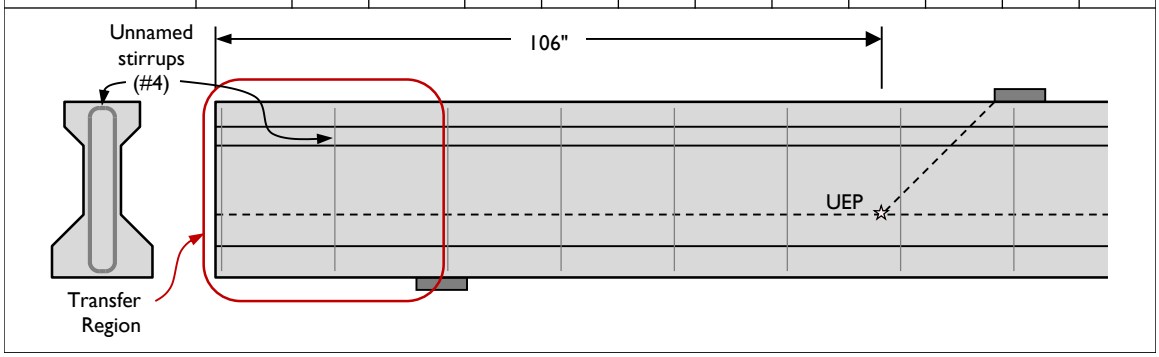

C.6.12 Runzell, Shield, and French (2007)

Two Minnesota Type54 specimens (one decked, one not decked) tested by Runzell, Shield, and French were included in the HSED. The locations of the reinforcing bars used in horizontal shear capacity calculations for these beams are given in Table C-15. The bar locations marked in red are considered to be within the transfer region, within 36.0 in. from beam end.

Table C-15: Reinforcing bar locations in specimens tested by Runzell, Shield, and French (2007).

Specimen ID	l_{UEP} [in.]	Bar Name	No. & Size	Locations [in. from end]								
Runzell, Shield, & French (2007)												
I	137.0		2-#4	5.0	8.0	11.0	14.0	19.0	24.0	45.0	66.0	87.0
				108	129							
				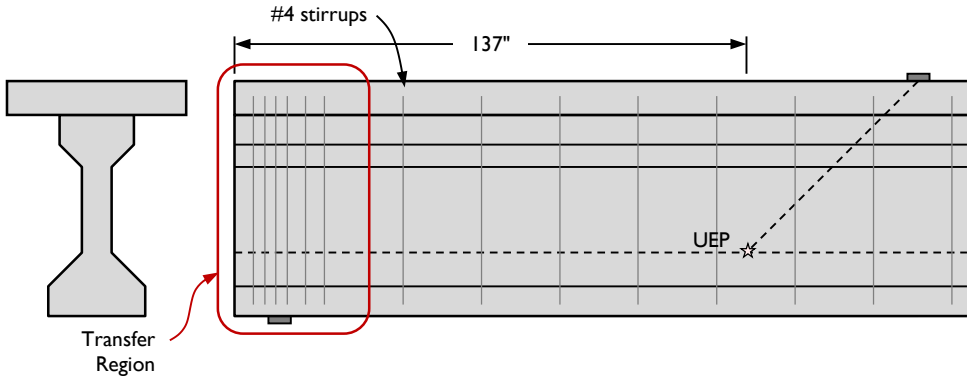								
II	146.0		2-#4	5.0	8.0	11.0	14.0	19.0	24.0	45.0	66.0	87.0
				108	129							
				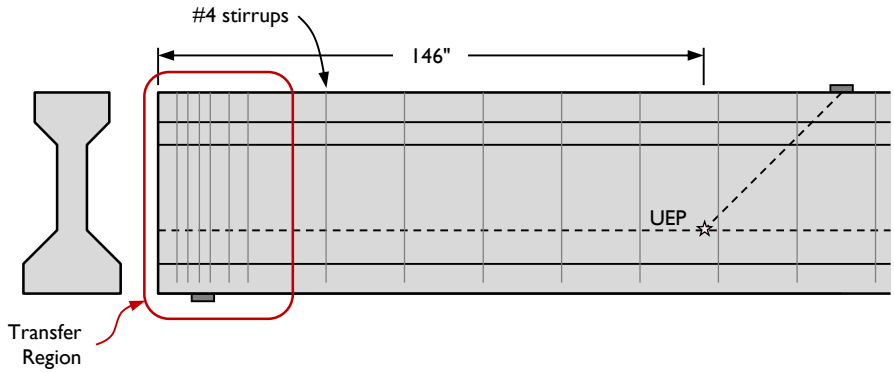								

C.6.13 Shahawy, Robinson, and Batchelor (1993)

Eight test specimens in the HSED are from Shahawy, Robinson, and Batchelor (1993). A summary of the reinforcing bars considered in capacity calculations are given in Table C-16. Bars positioned less than 36.0 in. from beam end (written in red) were considered to be in the transfer region.

Table C-16: Reinforcing bar locations in specimens tested by Shahawy, Robinson, and Batchelor (1993).

Specimen ID	l_{UEP} [in.]	Bar Name	No. & Size	Locations [in. from end]								
Shahawy, Robinson, Batchelor (1993)												
A0-00-R-N	59.0	C	2-#4	3.0	6.0	9.0	12.0	18.0	24.0	30.0	36.0	42.0
				48.0	54.0							
A0-00-R-S	59.0	C	2-#4	3.0	6.0	9.0	12.0	18.0	24.0	30.0	36.0	42.0
				48.0	54.0							
A1-00-R/2-N	76.0	C	#4	3.0	6.0	9.0	12.0	18.0	24.0	30.0	36.0	42.0
				48.0	54.0	62.0	70.0					
A1-00-R/2-S	98.0	C	#4	3.0	6.0	9.0	12.0	18.0	24.0	30.0	36.0	42.0
				48.0	54.0	62.0	70.0	78.0	86.0	94.0		
A1-00-R-N	76.0	C	#4	3.0	6.0	9.0	12.0	18.0	24.0	30.0	36.0	42.0
				48.0	54.0	62.0	70.0					
A1-00-3R/2-N	76.0	C	3-#4	3.0	6.0	9.0	12.0	18.0	24.0	30.0	36.0	42.0
				48.0	54.0	62.0	70.0					
B0-00-R-N	76.0	C	#4	3.0	6.0	9.0	12.0	18.0	24.0	30.0	36.0	42.0
				48.0	54.0	62.0	70.0					
B0-00-R-S	98.0	C	2-#4	3.0	6.0	9.0	12.0	18.0	24.0	30.0	36.0	42.0
				48.0	54.0	62.0	70.0	78.0	86.0	94.0		

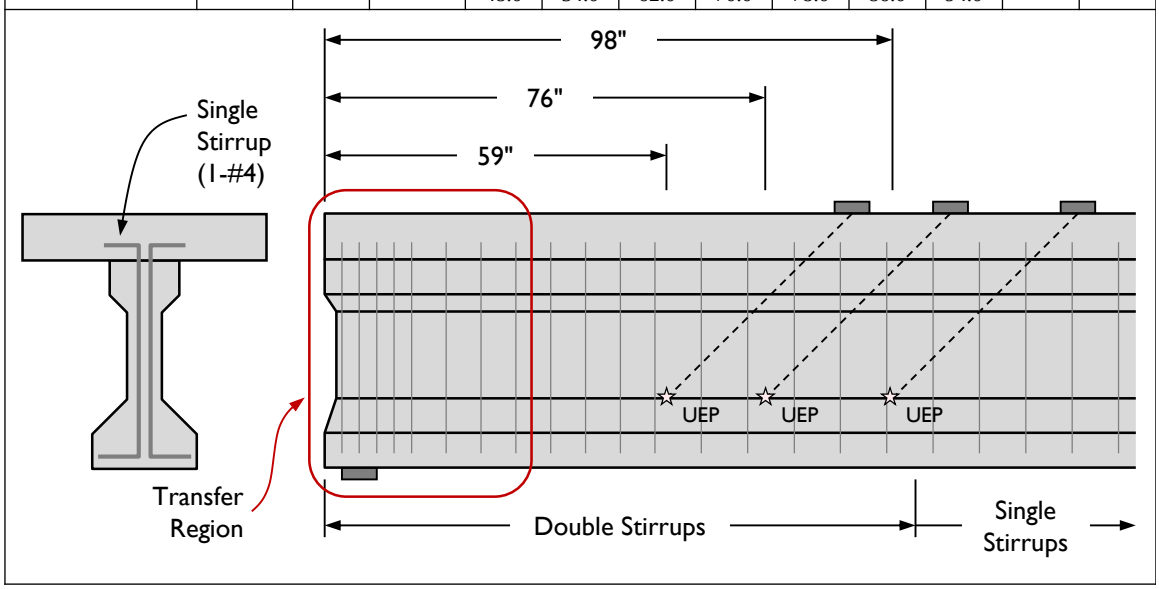

C.6.14 Tawfiq (1995)

Twelve specimens tested by Tawfiq were included in the HSED. The details of the reinforcing steel in these beams are summarized in Table C-17. Bar locations written in red are considered to be in the transfer region (less than 36.0 in. from beam end).

Table C-17: Reinforcing bar locations in specimens tested by Tawfiq (1995).

Specimen ID	l_{UEP} [in.]	Bar Name	No. & Size	Locations [in. from end]								
Tawfiq (1995)												
R8N	82.0		2-#4	3.0	6.0	9.0	12.0	18.0	24.0	30.0	36.0	42.0
				48.0	54.0	62.0	70.0	78.0				
R10N	82.0		2-#4	3.0	6.0	9.0	12.0	18.0	24.0	30.0	36.0	42.0
				48.0	54.0	62.0	70.0	78.0				
R12N	82.0		2-#4	3.0	6.0	9.0	12.0	18.0	24.0	30.0	36.0	42.0
				48.0	54.0	62.0	70.0	78.0				
2R8N	82.0		2-#4	3.0	6.0	9.0	12.0	15.0	18.0	21.0	24.0	27.0
				30.0	33.0	36.0	39.0	42.0	45.0	48.0	51.0	54.0
				58.0	62.0	66.0	70.0	74.0	78.0	82.0		
2R10N	82.0		2-#4	3.0	6.0	9.0	12.0	15.0	18.0	21.0	24.0	27.0
				30.0	33.0	36.0	39.0	42.0	45.0	48.0	51.0	54.0
				58.0	62.0	66.0	70.0	74.0	78.0	82.0		
2R12N	82.0		2-#4	3.0	6.0	9.0	12.0	15.0	18.0	21.0	24.0	27.0
				30.0	33.0	36.0	39.0	42.0	45.0	48.0	51.0	54.0
				58.0	62.0	66.0	70.0	74.0	78.0	82.0		

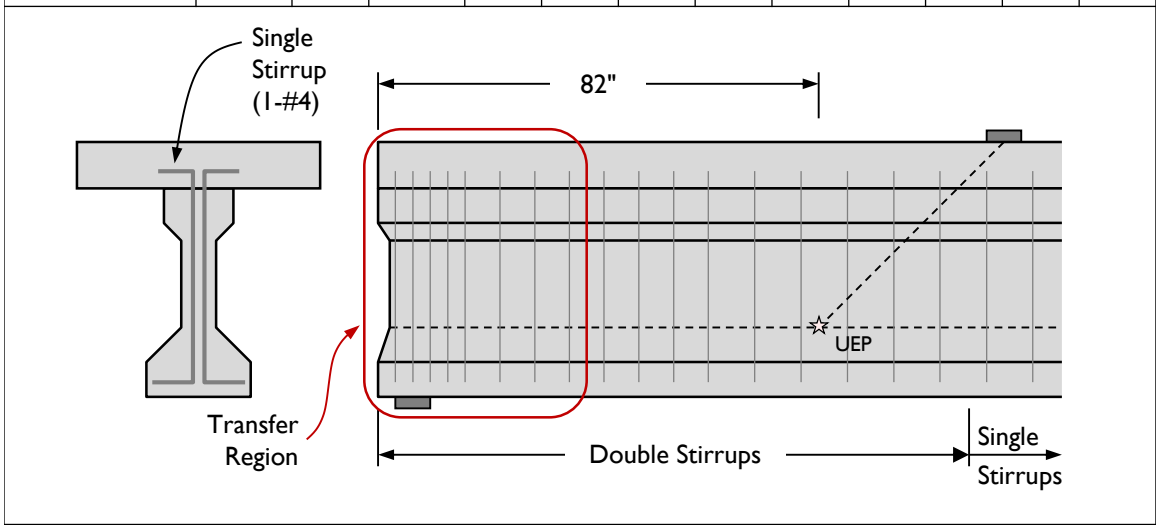

Table C-17: Reinforcing bar locations in specimens tested by Tawfiq (1995) (2 of 2).

Specimen ID	l_{UEP} [in.]	Bar Name	No. & Size	Locations [in. from end]								
Tawfiq (1995)												
R8S	65.0		2-#4	3.0	6.0	9.0	12.0	18.0	24.0	30.0	36.0	42.0
				48.0	54.0	62.0						
R10S	65.0		2-#4	3.0	6.0	9.0	12.0	18.0	24.0	30.0	36.0	42.0
				48.0	54.0	62.0						
R12S	65.0		2-#4	3.0	6.0	9.0	12.0	18.0	24.0	30.0	36.0	42.0
				48.0	54.0	62.0						
2R8S	65.0		2-#4	3.0	6.0	9.0	12.0	15.0	18.0	21.0	24.0	27.0
				30.0	33.0	36.0	39.0	42.0	45.0	48.0	51.0	54.0
				58.0	62.0							
2R10S	65.0		2-#4	3.0	6.0	9.0	12.0	15.0	18.0	21.0	24.0	27.0
				30.0	33.0	36.0	39.0	42.0	45.0	48.0	51.0	54.0
				58.0	62.0							
2R12S	65.0		2-#4	3.0	6.0	9.0	12.0	15.0	18.0	21.0	24.0	27.0
				30.0	33.0	36.0	39.0	42.0	45.0	48.0	51.0	54.0
				58.0	62.0							

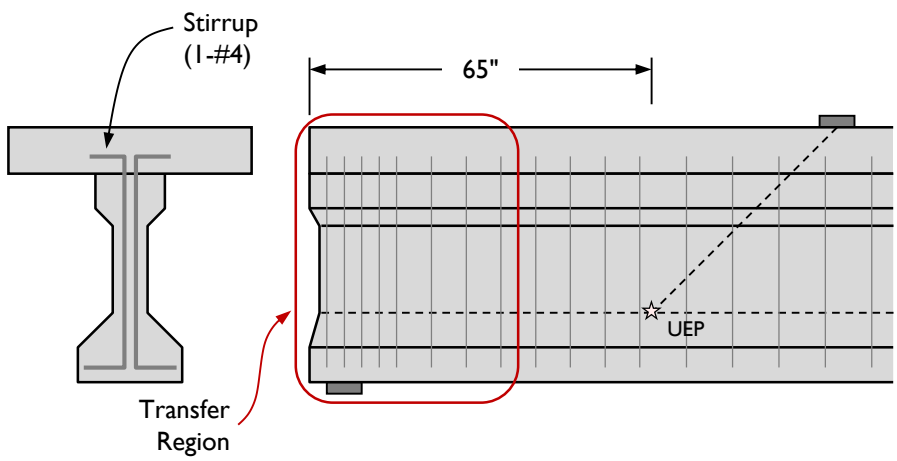

C.7 REFERENCES FOR HSED DATA POINTS

The author names, paper title, and year of publication for the fourteen references with tests included in the HSED are given in Table C-18. The full reference information can be found in the reference list of this dissertation.

Table C-18: Author names, titles, and publication years for references included in the HSED.

Ref. No.	Year	Authors	Title
1	1992	Alshegeir & Ramirez	Strut-Tie Approach in Pretensioned Deep Beams
2	2008	Avendaño & Bayrak	Shear Strength and Behavior of Prestressed Concrete Beams
3	2009	Hamilton, Llanos, & Ross	Shear Performance of Existing Prestressed Concrete Bridge Girders
4	2007	Hawkins & Kuchma	Application of LRFD Bridge Design Specifications to High-Strength Structural Concrete: Shear Provisions
5	2008	Heckmann & Bayrak	Effects of Increasing the Allowable Compressive Stress at Release on the Shear Strength of Prestressed Concrete Girders
6	2011	Avendaño	To be published, Fall 2011
7	2005	Labonte & Hamilton	Self-Consolidating Concrete (SCC) Structural Investigation
8	2005	Naito, Parent, Brunn, & Tate	Comparative Performance of High Early Strength and Self Consolidating Concrete for Use in Precast Bridge Beam Construction – Final Report
9	2005	Ramirez & Aguilar	Shear Reinforcement Requirements for High-Strength Concrete Bridge Girders
10	2007	Runzell, Shield, & French	Shear Capacity of Prestressed Concrete Beams
11	1993	Shahawy, Robinson, & Batchelor	An Investigation of Shear Strength of Prestressed Concrete AASHTO Type II Girders
12	1995	Tawfiq	Cracking and Shear Capacity of High Strength Concrete Girders
13	2011	Avendaño, et al.	Unpublished
14	2011	Hovell	Structural Performance of Texas U-Beams at Prestress Transfer and Under Shear-Critical Loads

APPENDIX D
Vertical Shear Capacity Calculations

D.1 NOTATION

The symbols used in the calculation summary tables presented here are as in the vertical shear capacity calculation methods presented in Chapter 2. The meaning of these variables is repeated here for reference.

A_{ct} = area of concrete in tension [in.^{2}]

A_v = area of vertical shear reinforcement at spacing s [in.^{2}]

A_{ps} = area of prestressing steel on the flexural tension side of the member [in.^{2}]

b_w = web width [in.]

b_v = effective web width [in.]

d = distance from extreme compression fiber to centroid of longitudinal tension reinforcement [in.]

d_p = distance from extreme compression fiber to centroid of prestressing steel [in.]

d_v = effective shear depth [in.]

E_c = modulus of elasticity of concrete [ksi]

E_p = modulus of elasticity of prestressing tendons [ksi]

f_c' = compressive strength of concrete [ksi]

f_{pc} = compressive stress in concrete at centroid of cross-section resisting externally applied loads [psi]

f_{po} = locked-in stress differential between prestressing strands and the surrounding concrete [ksi]

f_y = yield strength of transverse reinforcement [ksi]

f_{yt} = yield strength of transverse reinforcement [ksi]

K	=	stress variable used in AASHTO Segmental Procedure
Max V_n	=	maximum value for shear strength; equal to $0.25f_c'b_vd_v$ when using the AASHTO General Procedure and $12\sqrt{f_c'}b_vd_v$ when using the AASHTO Segmental Procedure.
M_{cre}	=	moment causing flexural cracking at section due to externally applied loads [kip-in.]
M_{max}	=	maximum factored moment at section due to externally applied loads [kip-in.]
M_u	=	factored moment [kip-in.]
s	=	center-to-center spacing of reinforcement [in.]
V_c	=	nominal shear strength provided by concrete [kip]
V_{ci}	=	flexure-shear cracking shear strength [kip]
V_{cw}	=	diagonal web-cracking shear strength [kip]
V_d	=	shear force at section due to unfactored dead load [kip]
V_i	=	factored shear force at section due to externally applied loads occurring simultaneously with M_{max} [kip]
V_n	=	nominal shear strength [kip]
V_s	=	nominal shear strength provided by shear reinforcement [kip]
V_u	=	factored shear force [kip]
β	=	factor indicating ability of diagonally cracked concrete to transmit tension and shear
ε_s	=	longitudinal strain [in./in.]
θ	=	angle of inclination of diagonal compressive stresses [°]

D.2 ACI DETAILED METHOD (2008)

		f_c' [ksi]	b_w [in.]	d_p [in.]	V_d [kip]	$\frac{V_i M_{cre}}{M_{max}}$ [kip]	V_{ci} [kip]	f_{pc} [psi]	V_{cw} [kip]	A_v [in.^{2}]	f_{yt} [ksi]	d [in.]	s [in.]	V_s [kip]	V_n [kip]
B0N	All	12.9	10.0	59.0	15.6	712	768	448	314	0.4	60	15.6	18.0	79	392
B1N	End	12.0	10.0	58.8	15.5	957	1011	521	317	0.4	66	15.5	4.0	387	703
	Mid	12.0	10.0	58.8	15.5	957	1011	521	317	0.4	66	15.5	6.0	258	574
B1S	End	12.0	10.0	58.8	15.0	942	995	521	317	0.4	66	15.0	4.0	387	703
	Mid	12.0	10.0	58.8	15.0	942	995	521	317	0.4	66	15.0	6.0	258	574
B2N	End	11.5	10.0	58.8	15.5	946	999	581	323	0.4	85	15.5	4.0	501	823
	Mid	11.5	10.0	58.8	15.5	946	999	581	323	0.4	85	15.5	6.0	334	656
B3N	End	11.3	10.0	58.6	20.1	525	582	302	271	0.4	65	20.1	4.0	382	653
	Mid	11.3	10.0	58.6	20.1	525	582	302	271	0.4	65	20.1	6.0	255	526
B3S	End	12.1	10.0	58.6	20.1	534	593	270	273	0.4	65	20.1	4.0	382	655
	Mid	12.1	10.0	58.6	20.1	534	593	270	273	0.4	65	20.1	6.0	255	528
B4N	End	11.4	16.0	58.8	20.1	875	955	730	558	0.4	63	20.1	3.0	494	1051
	Int	11.4	16.0	58.8	20.1	875	955	730	558	0.4	63	20.1	4.0	370	928
	Mid	11.4	16.0	58.8	20.1	875	955	730	558	0.4	63	20.1	6.0	247	804
B4S	End	11.4	16.0	58.8	20.1	875	955	730	558	0.4	63	20.1	3.0	494	1051
	Int	11.4	16.0	58.8	20.1	875	955	730	558	0.4	63	20.1	4.0	370	928
	Mid	11.4	16.0	58.8	20.1	875	955	730	558	0.4	63	20.1	6.0	247	804
B5N	End	13.2	10.0	59.1	20.2	789	850	546	335	0.62	64	20.2	4.0	543	878
	Mid	13.2	10.0	59.1	20.2	789	850	546	335	0.62	64	20.2	6.0	389	724
B6S	End	12.0	10.0	59.1	20.2	787	846	394	297	0.4	85	20.2	4.0	503	800
	Mid	12.0	10.0	59.1	20.2	787	846	394	297	0.4	85	20.2	6.0	335	632
B7N	End	12.5	10.0	59.5	22.5	925	987	514	324	0.4	63	22.5	4.0	372	696
	Mid	12.5	10.0	59.5	22.5	925	987	514	324	0.4	63	22.5	6.0	248	572

D.3 AASHTO LRFD General Procedure (2010)

		f_c' [ksi]	b_v [in.]	d_v [in.]	M_u [kip-in.]	V_u [kip]	A_{ps} [in.^{2}]	f_{po} [ksi]	E_p [ksi]	E_c [ksi]	A_{ct} [in.^{2}]	ε_s [in./in.] $\times 10^3$	β	V_c [kip]	A_v [in.^{2}]	f_y [ksi]	$\cot\theta$	s [in.]	V_s [kip]	Max V_n [kip]	V_n [kip]
B0N	All	12.9	10.0	53.1	36,927	424	10.4	203	28,500	6474	717.5	-0.2	5.6	340	0.40	60.0	1.9	18.0	131	1712	472
B1N	End	12.0	10.0	52.9	63,579	837	11.9	203	28,500	6234	717.5	-0.1	5.1	294	0.40	65.8	1.8	4.0	635	1581	929
	Mid	12.0	10.0	52.9	50,916	670	11.9	203	28,500	6234	717.5	-0.2	5.5	316	0.40	65.8	1.8	6.0	428	1581	744
B1S	End	12.0	10.0	52.9	64,351	836	11.9	203	28,500	6234	717.5	-0.1	5.1	294	0.40	65.8	1.8	4.0	635	1581	929
	Mid	12.0	10.0	52.9	51,533	669	11.9	203	28,500	6234	717.5	-0.2	5.5	315	0.40	65.8	1.8	6.0	428	1581	744
B2N	End	11.5	10.0	52.9	74,330	978	11.9	203	28,500	6107	717.5	0.0	4.8	273	0.40	85.2	1.8	4.0	814	1518	1087
	Mid	11.5	10.0	52.9	58,075	764	11.9	203	28,500	6107	717.5	-0.1	5.3	298	0.40	85.2	1.8	6.0	551	1518	849
B3N	End	11.3	10.0	52.7	47,056	611	6.4	203	28,500	6062	717.5	1.1	2.6	147	0.40	65.3	1.5	4.0	532	1490	679
	Mid	11.3	10.0	52.7	42,506	552	6.4	203	28,500	6062	717.5	0.3	3.9	218	0.40	65.3	1.7	6.0	396	1490	613
B3S	End	12.1	10.0	52.7	47,190	613	6.4	203	28,500	6270	717.5	1.1	2.6	151	0.40	65.3	1.5	4.0	530	1594	681
	Mid	12.1	10.0	52.7	42,663	554	6.4	203	28,500	6270	717.5	0.3	3.8	222	0.40	65.3	1.7	6.0	394	1594	616
B4N	End	11.4	16.0	52.9	78,576	1020	11.9	203	28,500	6097	856	0.3	4.0	362	0.40	63.0	1.7	3.0	772	2420	1134
	Int	11.4	16.0	52.9	72,298	939	11.9	203	28,500	6097	856	0.0	4.9	441	0.40	63.0	1.8	4.0	603	2420	1043
	Mid	11.4	16.0	52.9	60,337	784	11.9	203	28,500	6097	856	-0.1	5.1	465	0.40	63.0	1.8	6.0	406	2420	871
B4S	End	11.4	16.0	52.9	78,576	1020	11.9	203	28,500	6097	856	0.3	4.0	362	0.40	63.0	1.7	3.0	772	2420	1134
	Int	11.4	16.0	52.9	72,298	939	11.9	203	28,500	6097	856	0.0	4.9	441	0.40	63.0	1.8	4.0	603	2420	1043
	Mid	11.4	16.0	52.9	60,337	784	11.9	203	28,500	6097	856	-0.1	5.1	465	0.40	63.0	1.8	6.0	406	2420	871
B5N	End	13.2	10.0	53.2	71,487	928	10.1	203	28,500	6556	717.5	0.8	3.0	184	0.62	63.8	1.6	4.0	848	1758	1032
	Mid	13.2	10.0	53.2	64,121	833	10.1	203	28,500	6556	717.5	0.0	4.8	293	0.62	63.8	1.8	6.0	632	1758	925
B6S	End	12.0	10.0	53.2	66,794	867	9.8	203	28,500	6249	717.5	0.5	3.5	204	0.40	85.0	1.7	4.0	760	1599	964
	Mid	12.0	10.0	53.2	57,732	750	9.8	203	28,500	6249	717.5	0.0	4.9	287	0.40	85.0	1.8	6.0	547	1599	833
B7N	End	12.5	10.0	53.5	63,261	822	11.7	203	28,500	6360	717.5	-0.1	5.1	303	0.40	62.5	1.8	4.0	610	1666	913
	Mid	12.5	10.0	53.5	50,923	661	11.7	203	28,500	6360	717.5	-0.2	5.4	324	0.40	62.5	1.8	6.0	411	1666	735

D.4 AASHTO LRFD SEGMENTAL PROCEDURE (2010)

		f_c' [ksi]	b_v [in.]	d_v [in.]	f_{pc} [ksi]	K	V_c [kip]	A_v [in.^{2}]	f_y [ksi]	s [in.]	V_s [kip]	Max V_n [kip]	V_n [kip]
B0N	All	12.9	10.0	59.0	0.448	1.72	231	0.40	60.0	18.0	79	803	310
B1N	End	12.0	10.0	58.8	0.521	1.84	236	0.40	65.8	4.0	387	770	623
	Mid	12.0	10.0	58.8	0.521	1.84	236	0.40	65.8	6.0	258	770	494
B1S	End	12.0	10.0	58.8	0.521	1.84	236	0.40	65.8	4.0	387	770	623
	Mid	12.0	10.0	58.8	0.521	1.84	236	0.40	65.8	6.0	258	770	494
B2N	End	11.5	10.0	58.8	0.581	1.93	243	0.40	85.2	4.0	501	754	743
	Mid	11.5	10.0	58.8	0.581	1.93	243	0.40	85.2	6.0	334	754	576
B3N	End	11.3	10.0	58.6	0.302	1.56	194	0.40	65.3	4.0	382	746	576
	Mid	11.3	10.0	58.6	0.302	1.56	194	0.40	65.3	6.0	255	746	449
B3S	End	12.1	10.0	58.6	0.270	1.49	192	0.40	65.3	4.0	382	772	574
	Mid	12.1	10.0	58.6	0.270	1.49	192	0.40	65.3	6.0	255	772	447
B4N	End	11.4	16.0	58.8	0.730	2.10	422	0.40	63.0	3.0	494	1205	916
	Int	11.4	16.0	58.8	0.730	2.10	422	0.40	63.0	4.0	370	1205	793
	Mid	11.4	16.0	58.8	0.730	2.10	422	0.40	63.0	6.0	247	1205	669
B4S	End	11.4	16.0	58.8	0.730	2.10	422	0.40	63.0	3.0	494	1205	916
	Int	11.4	16.0	58.8	0.730	2.10	422	0.40	63.0	4.0	370	1205	793
	Mid	11.4	16.0	58.8	0.730	2.10	422	0.40	63.0	6.0	247	1205	669
B5N	End	13.2	10.0	59.1	0.546	1.84	250	0.62	63.8	4.0	584	814	814
	Mid	13.2	10.0	59.1	0.546	1.84	250	0.62	63.8	6.0	389	814	639
B6S	End	12.0	10.0	59.1	0.394	1.67	217	0.40	85.0	4.0	503	777	720
	Mid	12.0	10.0	59.1	0.394	1.67	217	0.40	85.0	6.0	335	777	552
B7N	End	12.5	10.0	59.5	0.514	1.82	241	0.40	62.5	4.0	372	795	613
	Mid	12.5	10.0	59.5	0.514	1.82	241	0.40	62.5	6.0	248	795	489

APPENDIX E

Three-Dimensional U-Beam Model

[scissors, tape, and some assembly required]

E.1 INSTRUCTIONS

The geometry of the U-Beams fabricated in the course of this project can be hard to visualize, especially when the beam was skewed. To aid in visualization, printable rectangular and skewed U-Beam models are given Figures E-1 and E-2. Through simple cutting and folding, three-dimensional models of two beams can be made.

To assemble, cut along the solid black lines and fold along the dotted gray lines. Secure end faces to webs using tape. The beams can be assembled with the reinforcement, void shape, and bearing conditions visible on the inside or outside of the beam.

Reinforcing bars (solid gray lines) and the void (dashed gray line) in Figure E-1 are shown following the existing standard details (as used in Beams 1, 2, and 3). Reinforcing bars and the void in Figure E-2 are shown following the recommended new design (as used in Beams 6 and 7).

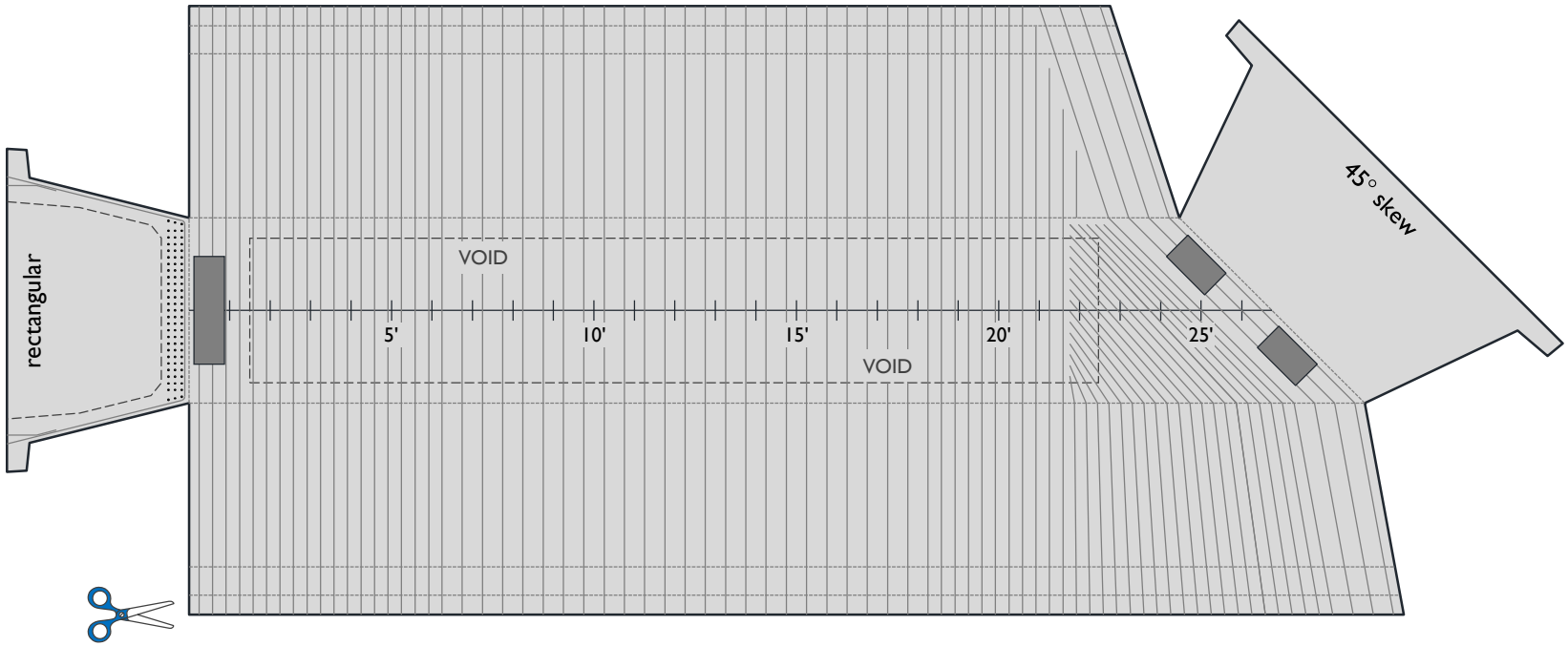

Instructions:

1. Cut along solid black lines [——]
2. Fold on dashed gray lines [- - - - -]

Figure E-1: Model of 30-ft Texas U54 with detailing matching current standard.

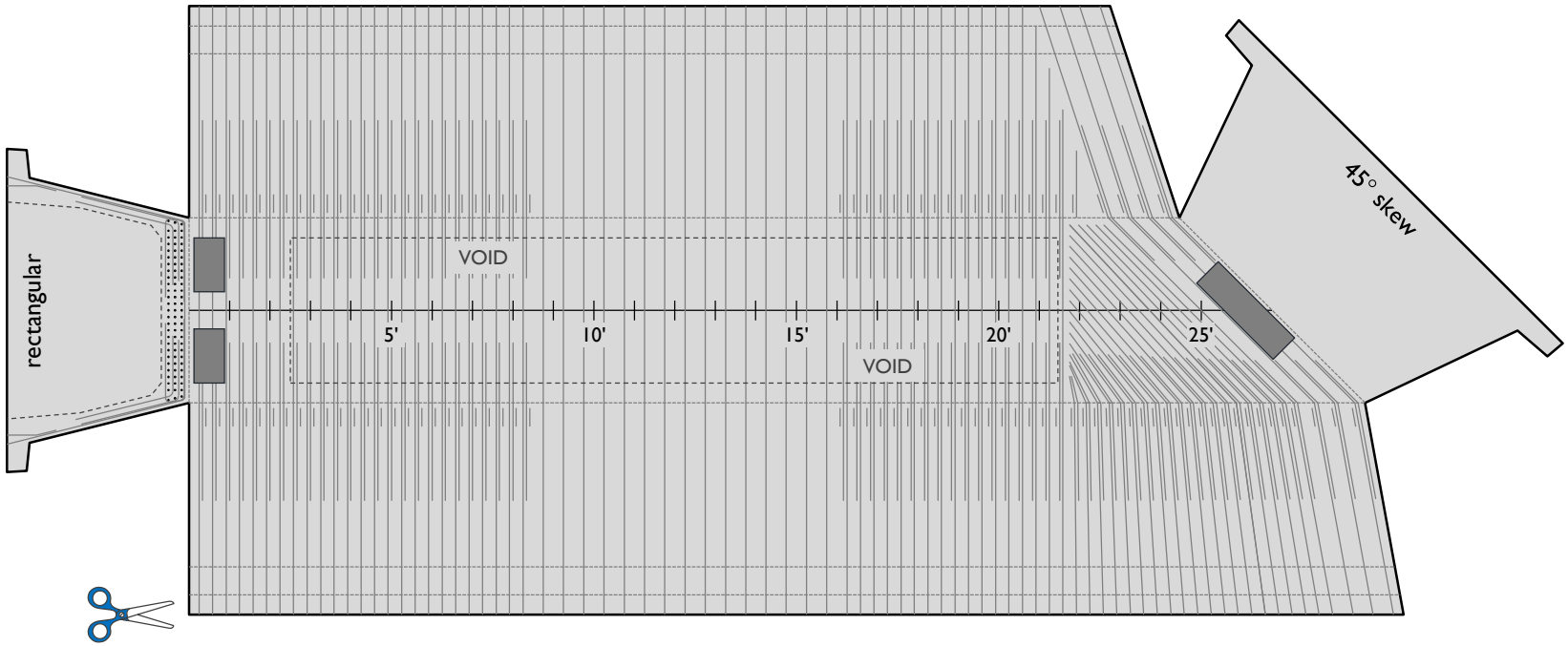

Instructions:

1. Cut along solid black lines [——]
2. Fold on dashed gray lines [- - - - - -]

Figure E-2 Model of 30-ft Texas U54 with detailing following recommended design.

REFERENCES

Alshegeir, A. and J.A. Ramirez (1992). "Strut-Tie Approach in Pretensioned Deep Beams." *ACI Structural Journal*, Vol. 89, No. 3, pp. 296-304.

American Association of State Highway and Transportation Officials (AASHTO) (2007). "AASHTO LRFD Bridge Design Specifications: Customary Units." 4th Edition. Washington, DC.

American Association of State Highway and Transportation Officials (AASHTO) (2008). "2008 Interim Revisions: AASHTO LRFD Bridge Design Specifications: Customary Units." 4th Edition. Washington, DC.

American Association of State Highway and Transportation Officials (AASHTO) (2009). "2009 Interim Revisions: AASHTO LRFD Bridge Design Specifications: Customary Units." 4th Edition. Washington, DC.

American Association of State Highway and Transportation Officials (AASHTO) (2010). "2010 Interim Revisions: AASHTO LRFD Bridge Design Specifications: Customary Units." 4th Edition. Washington, DC.

American Concrete Institute (ACI) Committee 318 (1963). "Building Code Requirements for Structural Concrete and Commentary." *American Concrete Institute*, Farmington Hills, MI.

American Concrete Institute (ACI) Committee 318 (2008). "Building Code Requirements for Structural Concrete (ACI 318-08) and Commentary." *American Concrete Institute*, Farmington Hills, MI.

Avendaño (2011). PhD research in progress. Dissertation publication expected within 2011.

Avendaño, A.R. and O. Bayrak (2008). "Shear Strength and Behavior of Prestressed Concrete Beams." *Report No. IAC-88-5DD1A003-3*, Center for Transportation Research, The University of Texas at Austin, Austin, TX.

Avendaño, A.R., Hovell, C.G., Nakamura, E., O'Callaghan, M.R., and O. Bayrak (unpublished). "Shear Behavior of the New Family of Texas Prestressed Concrete Girders."

Barnes, R.W., Burns, N.H., and M.E. Kreger (1999). "Development Length of 0.6-Inch Prestressing Strand in Standard I-Shape Pretensioned Concrete Beams." *Report No. FHWA/TX-02/1388-1*, Center for Transportation Research, The University of Texas at Austin, Austin, TX.

Barrios, A.O. (1994). "Behavior of High Strength Concrete Pretensioned Girders During Transfer of Prestressing Forces." MSE Thesis, The University of Texas at Austin, Austin, TX.

Bass, R.A., Carrasquillo, R.L., and J.O. Jirsa (1989). "Shear Transfer Across New and Existing Concrete Interfaces." *ACI Structural Journal*, Vol. 86, No. 4, pp. 383-393.

Bauer, S., Cornell, B., Figurski, D., Ley, T., Miralles, J., and K.J. Folliard (2001). "Alkali-Silica Reaction and Delayed Ettringite Formation in Concrete: A Literature Review." *Report No. 0-4085-1*, Center for Transportation Research, The University of Texas at Austin, Austin, TX.

Bennett, E.W. and B.M.A. Balasooriya (1971). "Shear Strength of Prestressed Beams With Thin Webs Failing in Inclined Compression." *ACI Journal*, No. 68, No. 3, pp. 204-212.

Bentz, E.C., Vecchio, F.J., and M.P. Collins (2006). "The Simplified Modified Compression Field Theory for Calculating the Shear Strength of Reinforced Concrete Elements." *ACI Structural Journal*, Vol. 103, No. 4, pp. 614-624.

Birkeland, P.W., and H.W. Birkeland (1966). "Connections in Precast Concrete Construction." *Journal of the American Concrete Institute*, Vol. 63, No. 3, pp. 345-368.

Bruce, B., Russell, H., and J. Roller (2005). "Fatigue and Shear Behavior of HPC Bulb-Tee Girders." *Report No. FHWA/LA.05/395*, Tulane University, New Orleans, LA.

Canadian Standards Association (CSA) (2010). "CSA-A23.3-04, Design of Concrete Structures." 5th Edition, published in 2004, reaffirmed in 2010. *Canadian Standards Association*, Ontario, Canada.

Crispino, E.D. (2007). "Anchorage Zone Design for Pretensioned Bulb-Tee Bridge Girders in Virginia." Thesis, Virginia Polytechnic Institute and State University, Blacksburg, VA.

Dunkman, D.A. (2009). "Bursting and Spalling in Pretensioned U-Beams." MSE Thesis, The University of Texas at Austin, Austin, TX.

Elzanaty, A.H., Nilson, A.H., and F.O. Slate (1986). "Shear Capacity of Prestressed Concrete Beams Using High-Strength Concrete." *ACI Journal*, Vol. 83, No. 2, pp. 359-368.

Geren, K.L., and M.K. Tadros (1994). "The NU Precast/Prestressed Concrete Bridge I-Girder Series." *PCI Journal*, Vol. 39, No. 3, pp. 26-39.

Gross, S.P. (1998). "Field Performance of Prestressed High Performance Concrete Highway Bridges in Texas." PhD Dissertation, The University of Texas at Austin, Austin, TX.

Gross, S.P., and N.H. Burns (2000). "Field Performance of Prestressed High Performance Concrete Highway Bridges in Texas." *Report No. FHWA/TX-05/9-580/589-2*, Center for Transportation Research, The University of Texas at Austin, Austin, TX.

Guyon, Y. (1953). *Prestressed Concrete, Vol. 1*. Contractors Record Ltd, London, Great Britain, and John Wiley & Sons, Inc., New York, NY.

Hamilton III, H.R., Llanos, G., and B.E. Ross (2008). "Shear Performance of Existing Prestressed Concrete Bridge Girders." *Report No. BD 545-56*, University of Florida, Gainesville, FL.

Hansen, N.W. (1960). "Precast-Prestressed Concrete Bridges. 2—Horizontal Shear Connections." *Journal, PCA Development Bulletin D35*, PCA Research and Development Laboratories, Vol. 2, No. 2, pp. 38-58.

Hawkins, N.M., and D.A. Kuchma (2007). "Application of LRFD Bridge Design Specifications to High-Strength Structural Concrete: Shear Provisions." *NCHRP Report 579*, Transportation Research Board, National Research Council, Washington, D.C.

Heckmann, C.P. (2008). "Effects of Increasing the Allowable Compressive Stress at Release on the Shear Strength of Prestressed Concrete Girders." MS Thesis, The University of Texas at Austin, Austin, TX.

Heckmann, C.P. and O. Bayrak (2008). "Effects of Increasing the Allowable Compressive Stress at Release on the Shear Strength of Prestressed Concrete Girders." *Report No. 0-5197-3*, Center for Transportation Research, The University of Texas at Austin, Austin, TX.

Hermansen, B.R. and J. Cowan (1974). "Modified Shear-Friction Theory for Bracket Design." *ACI Journal*, Vol. 71, No. 2, pp. 55-60.

Hibbeler, R.C. (2003). *Mechanics of Materials, Fifth Edition*, Pearson Education, Inc., Upper Saddle River, NJ.

Hofbeck, J.A., Ibrahim, I.O., and A.H. Mattock (1969). "Shear Transfer in Reinforced Concrete." *ACI Journal*, Vol. 66, No. 2, pp. 119-128.

Holt, J. (2010). Personal communication.

Huang, D. and M. Shahawy (2005). "Analysis of Tensile Stresses in Transfer Zone of Prestressed Concrete U-Beams." *Transportation Research Record*, No. 1928, pp. 134-141.

Itani, R.Y. and R.L. Galbraith (1986). "Design of Prestressed Concrete Girders Without End Blocks." *WSDOT Report WA-RD 81*, Washington State Transportation Center, Pullman, WA.

Kahn, L.F. and A.D. Mitchell (2002). "Shear Friction Tests with High-Strength Concrete." *ACI Structural Journal*, Vol. 99, No. 1, pp. 98-103.

Kahn, L.F. and Slapkus, A. (2004). "Interface Shear in High Strength Composite T-Beams." *PCI Journal*, Vol. 49, No. 4, pp. 102-110.

Kupfer, H., Hilsdorf, H.K., and H. Rusch (1969). "Behavior of Concrete Under Biaxial Stress." *ACI Journal*, Vol. 66, No. 8, pp. 656-666.

Labonte, T. and H.R. Hamilton III (2005). "Self-Consolidating Concrete (SCC) Structural Investigation." *Report No. BD 545, RPWO# 21*, University of Florida, Gainesville, FL.

Larson, N.A., Wang, T.-W., Bindrich, B.V., Bayrak, O., and J.O. Jirsa (2010). "Structural Performance of ASR/DEF Damaged Prestressed Concrete Trapezoidal Box Beams with Dapped Ends." *Report No. 12-8XXIA007*, Center for Transportation Research, The University of Texas at Austin, Austin, TX.

Loov, R.E. and A.K. Patnaik (1994). "Horizontal Shear Strength of Composite Concrete Beams with a Rough Interface." *PCI Journal*, No. 1, pp. 48-69.

Ma, Z., Tadros, M.K., and Baishya, M. (2000). "Shear Behavior of Pretensioned High-Strength Concrete I-Girders." *ACI Structural Journal*, Vol. 97, No. 1, pp. 185-192.

Marshall, W.T., and A.H. Mattock (1962). "Control of Horizontal Cracking in the Ends of Pretensioned Prestressed Concrete Girders." *PCI Journal*, Vol. 7, No. 10, pp. 56-75.

Mast, R.F. (1968). "Auxiliary Reinforcement in Concrete Connections." *ASCE Journal of the Structural Division*, Vol. 94, No. ST 6, pp. 1485-1504.

Mattock, A.H. (2001). "Shear Friction and High-Strength Concrete." *ACI Structural Journal*, Vol. 98, No. 1, pp. 50-59.

Mattock, A.H., and N.M. Hawkins (1972). "Shear Transfer in Reinforced Concrete – Recent Research." *PCI Journal*, Vol. 17, No. 2, pp. 55-75.

Mattock, A.H., Johal, L., and H.C. Chow (1975). "Shear Transfer in Reinforced Concrete with Moment or Tension Acting Across the Shear Plane." *PCI Journal*, Vol. 20, No. 4, pp. 76-93.

Mattock, A.H., Li, W.K., and T.C. Wang (1976). "Shear Transfer in Lightweight Reinforced Concrete." *PCI Journal*, Vol. 21, No. 1, pp. 20-39.

Moore, A.M. (2010). "Shear Behavior of Prestressed Concrete U-Beams." MSE Thesis, The University of Texas at Austin, Austin, TX.

Myers, J.J., and R.L. Carrasquillo (1998). "Production and Quality Control of High Performance Concrete in Texas Bridge Structures." *Report No. FHWA/TX-05/9-580/589-1*, Center for Transportation Research, The University of Texas at Austin, Austin, TX.

Nagle, T.J. and D.A. Kuchma (2007). "Nontraditional Limitations on the Shear Capacity of Prestressed Concrete Girders." *NSEL Report Series, Report No. NSEL-003*. University of Illinois at Urbana-Champaign.

Naito, C.J., Brunn, G., Parent, G., and T. Tate (2005). "Comparative Performance of High Early Strength and Self Consolidating Concrete for Use in Precast Bridge Beam Construction – Final Report." *ATLSS Report No. 05-03*, National Center for Engineering Research on Advanced Technology for Large Structural Systems, Bethlehem, PA.

Naito, C.J., Parent, G., and G. Brunn (2006). "Performance of Bulb-Tee Girders Made with Self-Consolidating Concrete." *PCI Journal*, Vol. 51, No. 6, pp. 72-85.

Nakamura, E. (2011). "Shear Database for Prestressed Concrete Members." MSE Thesis, The University of Texas at Austin, Austin, TX.

Nilson, A.H. (1987). *Design of Prestressed Concrete*, John Wiley & Sons, Inc., New York, NY.

O'Callaghan, M.R. (2007). "Tensile Stresses in the End Regions of Pretensioned I-Beams at Release." MSE Thesis, The University of Texas at Austin, Austin, TX.

O'Callaghan, M.R. and O. Bayrak (2007). "Tensile Stresses in the End Regions of Pretensioned I-Beams at Release." *Report No. IAC-88-5DD1A003-1*, Center for Transportation Research, The University of Texas at Austin, Austin, TX.

Ralls, M.L, Ybanez, L., and J.J. Panak (1993). "The New Texas U-Beam Bridges: An Aesthetic and Economical Design Solution." *PCI Journal*, Vol. 38, No. 5, pp. 20-29.

Ramirez, J.A., and G. Aguilar (2005). "Shear Reinforcement Requirements for High-Strength Concrete Bridge Girders." *Report No. FHWA/IN/JTRP-2005/19*, Purdue University, West Lafayette, IN.

Ramirez, J.A. and J.E. Breen (1983). "Review of Design Procedures for Shear and Torsion in Reinforced and Prestressed Concrete." *Report No. FHWA/TX-84/26+248-2*, Center for Transportation Research, The University of Texas at Austin, Austin, TX.

Ramirez, J.A. and J.E. Breen (1983). "Experimental Verification of Design Procedures for Shear and Torsion in Reinforced and Prestressed Concrete." *Report No. FHWA/TX-84/37+248-3*, Center for Transportation Research, The University of Texas at Austin, Austin, TX.

Ramirez, J.A. and J.E. Breen (1983). "Proposed Design Procedures for Shear and Torsion in Reinforced and Prestressed Concrete." *Report No. FHWA/TX-84/38+248-4F*, Center for Transportation Research, The University of Texas at Austin, Austin, TX.

Ramirez, J.A. and J.E. Breen (1991). "Evaluation of a Modified Truss-Model Approach for Beams in Shear." *ACI Structural Journal*, Vol. 88, No. 5, pp. 562-571.

Ritter, W. (1899) "Die Bauweise Hennebique (The Hennebique System)." *Schweizerische Bauzeitung*, Bd. XXXIII, No. 7, Zurich, Switzerland.

Runzell, B., Shield, C., and C.W. French (2007). "Shear Capacity of Prestressed Concrete Beams." *Report No. MN/RC 2007-47*, University of Minnesota, Minneapolis, MN.

Saemann, J.C. and G.W. Washa (1964). "Horizontal Shear Connections Between Precast Beams and Cast-in-Place Slabs." *Journal of the American Concrete Institute*, Vol. 61, No. 11, pp. 1383-1408.

Schnittker, B. (2008). "Allowable Compressive Stress at Prestress Transfer." MSE Thesis, The University of Texas at Austin, Austin, TX.

Schnittker, B., and O. Bayrak (2008). "Allowable Compressive Stress at Prestress Transfer." *Report No. 0-5197-4*, Center for Transportation Research, The University of Texas at Austin, Austin, TX.

Shahawy, M.A. and B. deV. Batchelor (1996). "Shear Behavior of Full-Scale Prestressed Concrete Girders: Comparison Between AASHTO Specifications and LRFD Code." *PCI Journal*, Vol. 41, No. 3, pp. 48-62.

Shahawy, M.A., Robinson, B., and B. deV. Batchelor (1993). "An Investigation of Shear Strength of Prestressed Concrete AASHTO Type II Girders." Structures Research Center Report, Florida Department of Transportation, Tallahassee, FL.

Tawfiq, K.S. (1995). "Cracking and Shear Capacity of High Strength Concrete Girders." *Report No. FL/DOT/RMC/612(1)-4269*, FAMU/FSU College of Engineering, Tallahassee, FL.

Texas Department of Transportation (TxDOT) (1998). Bridge Division Standard Drawings: Prestressed Concrete U-Beam Details. www.dot.state.tx.us, Austin, TX.

Texas Department of Transportation (TxDOT) (2004). "Standard Specifications for Construction and Maintenance of Highways, Streets, and Bridges." Texas Department of Transportation, Austin, TX.

Texas Department of Transportation (TxDOT) (2005). Bridge Division Standard Drawings: English Prestressed Concrete I-Beam Standards. www.dot.state.tx.us, Austin, TX.

Texas Department of Transportation (TxDOT) (2006). Bridge Division Standard Drawings: English Prestressed Concrete U-Beam Standards. www.dot.state.tx.us, Austin, TX.

Texas Department of Transportation (TxDOT) (2006). Bridge Division Standard Drawings: English Prestressed Concrete Box Beam Standards. www.dot.state.tx.us, Austin, TX.

Texas Department of Transportation (TxDOT) (2009). Bridge Division Standard Drawings: English Prestressed Concrete I-Girder Standards. Revised 2010. www.dot.state.tx.us, Austin, TX.

Texas Department of Transportation (TxDOT) (2011). Bridge Division Standard Drawings: English Prestressed Concrete X-Beam Standards. www.dot.state.tx.us, Austin, TX.

Texas Department of Transportation (TxDOT) Project Monitoring Committee (2010). Response to Interim Report for Project 0-5893.

Tuan, C.Y., Yehia, S.A., Jongpitaksseel, N., and M.K. Tadros (2004). "End Zone Reinforcement for Pretensioned Concrete Girders." *PCI Journal*, Vol. 49, No. 3, pp. 68-82.

Valluvan, R., Kreger, M.E., and J.O. Jirsa (1999). "Evaluation of ACI 318-95 Shear-Friction Provisions." *ACI Structural Journal*, Vol. 96, No. 4, pp. 473-481.

Van Landuyt, D. (2009). Personal communication.

Vecchio, F.J. and M.P. Collins (1986). "The Modified Compression-Field Theory for Reinforced Concrete Elements Subjected to Shear." *ACI Journal*, Vol. 83, No. 2, pp. 219-231.

Vecchio, F.J. and M.P. Collins (1988). "Predicting the Response of Reinforced Concrete Beams Subjected to Shear Using Modified Compression Field Theory." *ACI Structural Journal*, Vol. 85, No. 3, pp. 258-268.

Walraven, J., Frenay, J., and A. Pruijssers (1987). "Influence of Concrete Strength and Load History on the Shear Friction Capacity of Concrete Members." *PCI Journal*, Vol. 32, No. 1, pp. 66-84.

Walraven, J. and J. Stroband (1994). "Shear Friction in High-Strength Concrete." *SP-149 High Performance Concrete*, American Concrete Institute, Farmington Hills, MI, pp. 311-330.

VITA

Catherine Grace Hovell grew up in Darien, Connecticut with her parents, Peter and Meg, and her brother, John. She received a Bachelor's of Science in Civil Engineering from the University of Virginia in 2005. After graduation, she came to the University of Texas at Austin to work as a Graduate Research Assistant at the Phil M. Ferguson Structural Engineering Laboratory. She received a Master's of Science in Engineering in 2007, with a thesis on the analysis of structural redundancy of a steel trapezoidal box girder bridge. Her PhD was completed in 2011. Catherine left the academic world to design iconic, large-scale bridges within the United States and across the world.

Permanent Address:

cghovell@gmail.com

This dissertation was typed by the author.